POST-TRANSCRIPTIONAL REGULATION OF IMMUNE RESPONSES

EDITED BY: Manuel Daniel Díaz-Muñoz, Osamu Takeuchi and Simon Fillatreau

PUBLISHED IN: Frontiers in Immunology

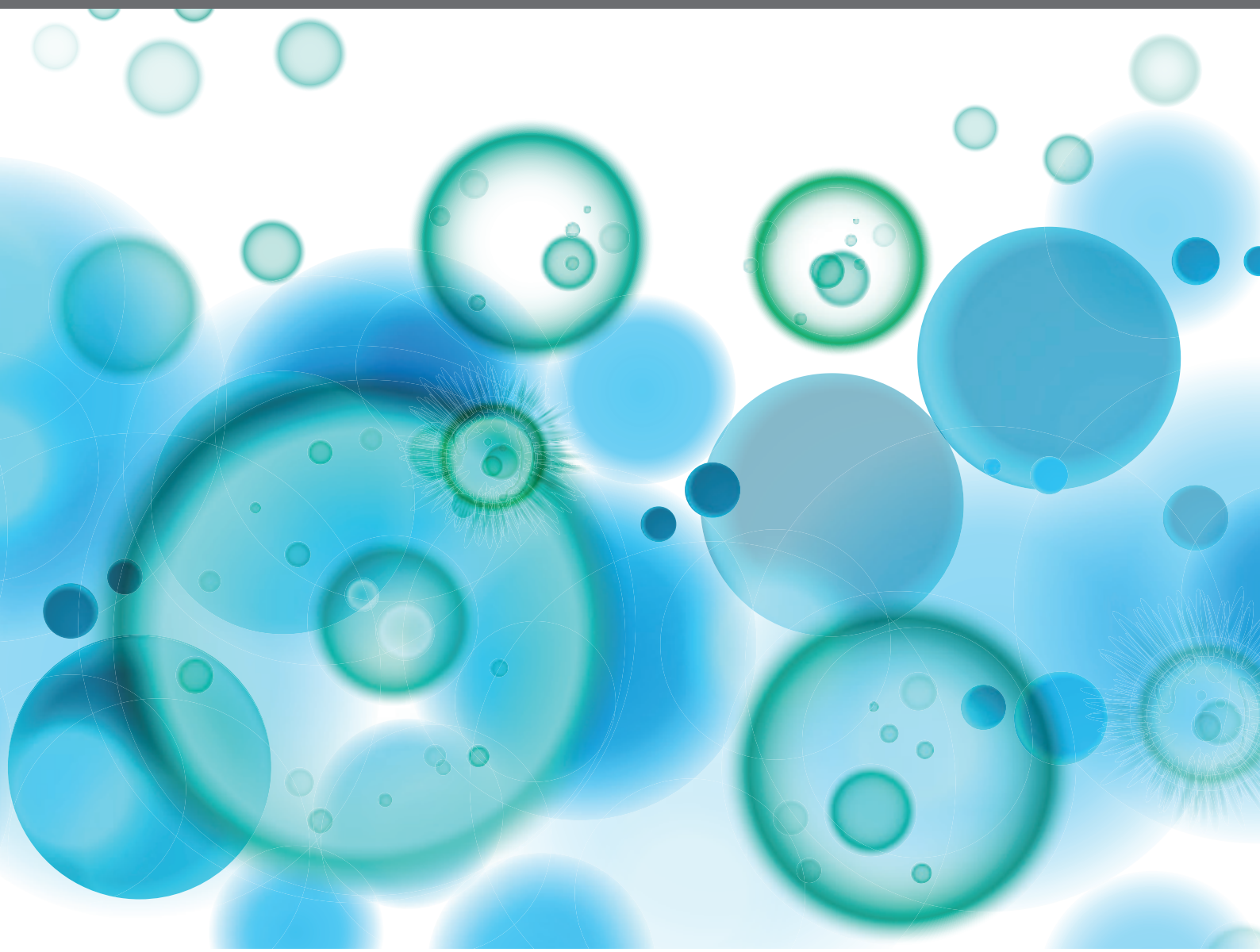

frontiers Research Topics

ISSN 1664-8714
ISBN 978-2-83250-635-6
DOI 10.3389/978-2-83250-635-6

About Frontiers

Frontiers is more than just an open-access publisher of scholarly articles: it is a pioneering approach to the world of academia, radically improving the way scholarly research is managed. The grand vision of Frontiers is a world where all people have an equal opportunity to seek, share and generate knowledge. Frontiers provides immediate and permanent online open access to all its publications, but this alone is not enough to realize our grand goals.

Frontiers Journal Series

The Frontiers Journal Series is a multi-tier and interdisciplinary set of open-access, online journals, promising a paradigm shift from the current review, selection and dissemination processes in academic publishing. All Frontiers journals are driven by researchers for researchers; therefore, they constitute a service to the scholarly community. At the same time, the Frontiers Journal Series operates on a revolutionary invention, the tiered publishing system, initially addressing specific communities of scholars, and gradually climbing up to broader public understanding, thus serving the interests of the lay society, too.

Dedication to Quality

Each Frontiers article is a landmark of the highest quality, thanks to genuinely collaborative interactions between authors and review editors, who include some of the world's best academicians. Research must be certified by peers before entering a stream of knowledge that may eventually reach the public - and shape society; therefore, Frontiers only applies the most rigorous and unbiased reviews.
Frontiers revolutionizes research publishing by freely delivering the most outstanding research, evaluated with no bias from both the academic and social point of view. By applying the most advanced information technologies, Frontiers is catapulting scholarly publishing into a new generation.

What are Frontiers Research Topics?

Frontiers Research Topics are very popular trademarks of the Frontiers Journals Series: they are collections of at least ten articles, all centered on a particular subject. With their unique mix of varied contributions from Original Research to Review Articles, Frontiers Research Topics unify the most influential researchers, the latest key findings and historical advances in a hot research area! Find out more on how to host your own Frontiers Research Topic or contribute to one as an author by contacting the Frontiers Editorial Office: frontiersin.org/about/contact

POST-TRANSCRIPTIONAL REGULATION OF IMMUNE RESPONSES

Topic Editors:
Manuel Daniel Díaz-Muñoz, INSERM UMR1291 Institut Toulousain des Maladies Infectieuses et Inflammatoires, France
Osamu Takeuchi, Kyoto University, Japan
Simon Fillatreau, Université Paris Cité, France

Citation: Díaz-Muñoz, M. D., Takeuchi, O., Fillatreau, S., eds. (2022). Post-Transcriptional Regulation of Immune Responses. Lausanne: Frontiers Media SA. doi: 10.3389/978-2-83250-635-6

Table of Contents

frontiers in Immunology

MINI REVIEW
published: 01 July 2021
doi: 10.3389/fimmu.2021.711633

Post-Transcriptional Regulation of Immune Responses and Inflammatory Diseases by RNA-Binding ZFP36 Family Proteins

Sohei Makita[1], *Hiroaki Takatori*[1,2*] *and Hiroshi Nakajima*[1*]

[1] Department of Allergy and Clinical Immunology, Graduate School of Medicine, Chiba University, Chiba, Japan,
[2] Department of Rheumatology, Hamamatsu Medical Center, Hamamatsu, Japan

Post-transcriptional regulation is involved in the regulation of many inflammatory genes. Zinc finger protein 36 (ZFP36) family proteins are RNA-binding proteins involved in messenger RNA (mRNA) metabolism pathways. The ZFP36 family is composed of ZFP36 (also known as tristetraprolin, TTP), ZFP36L1, ZFP36L2, and ZFP36L3 (only in rodents). The ZFP36 family proteins contain two tandemly repeated CCCH-type zinc-finger motifs, bind to adenine uridine-rich elements in the 3'-untranslated regions (3' UTR) of specific mRNA, and lead to target mRNA decay. Although the ZFP36 family members are structurally similar, they are known to play distinct functions and regulate different target mRNAs, probably due to their cell-type-specific expression patterns. For instance, ZFP36 has been well-known to function as an anti-inflammatory modulator in murine models of systemic inflammatory diseases by down-regulating the production of various pro-inflammatory cytokines, including TNF-α. Meanwhile, ZFP36L1 is required for the maintenance of the marginal-zone B cell compartment. Recently, we found that ZFP36L2 reduces the expression of *Ikzf2* (encoding HELIOS) and suppresses regulatory T cell function. This review summarizes the current understanding of the post-transcriptional regulation of immunological responses and inflammatory diseases by RNA-binding ZFP36 family proteins.

Keywords: tristetraprolin, zinc finger protein 36, zinc finger protein 36-like 1, zinc finger protein 36-like 2, RNA-binding protein, untranslated region, AU-rich element

OPEN ACCESS

Edited by:
Osamu Takeuchi,
Kyoto University, Japan

Reviewed by:
Taishin Akiyama,
RIKEN Yokohama, Japan
Ceren Ciraci,
Istanbul Technical University, Turkey

***Correspondence:**
Hiroaki Takatori
takatorih@faculty.chiba-u.jp
Hiroshi Nakajima
nakajimh@faculty.chiba-u.jp

Specialty section:
This article was submitted to Molecular Innate Immunity, a section of the journal Frontiers in Immunology

Received: *18 May 2021*
Accepted: *17 June 2021*
Published: *01 July 2021*

Citation:
Makita S, Takatori H and Nakajima H (2021) Post-Transcriptional Regulation of Immune Responses and Inflammatory Diseases by RNA-Binding ZFP36 Family Proteins. Front. Immunol. 12:711633. doi: 10.3389/fimmu.2021.711633

INTRODUCTION

For many years, the importance of post-transcriptional regulation of mRNAs has not been fully recognized in the immune system. However, with the advance in functional analyses of RNA-binding proteins (RBPs), the importance of post-transcriptional regulation in immune system regulation has come to the fore. RBPs are critical effectors of gene expression of many genes and form regulatory networks to maintain cell homeostasis. RBPs recognize target RNA with the RNA-recognition domain (1). RBPs also have binding domains with other proteins, and these interactions enable them to fulfill their regulatory functions (2).

Recent analyses have shown that RBPs are remarkably involved in regulating various cell type-specific functions (3). Among RBPs, ZFP36 family proteins including ZFP36, known as tristetraprolin (TTP), are characterized by the presence of one or more CCCH-type zinc finger domain(s) that contain three cysteines (C) and one histidine (H) residues. ZFP36 family proteins bind to adenylate-uridylate-rich elements (AREs) in the 3'-untranslated region (3' UTR) of a target mRNA, leading to the decay of the mRNA (4). Although the ZFP36 family members are structurally similar, they play different roles and regulate different target mRNAs, probably due to their cell type-specific expression patterns (5). For instance, ZFP36 plays a significant role in regulating immune responses and inflammatory diseases by inhibiting the production of various inflammatory cytokines such as TNF-α in macrophages (6).

ZFP36L1 is known to be required for the maintenance of the marginal zone B cell compartment by limiting the expression of the transcription factors such as Kruppel-like factor 2 (KLF2) and interferon regulatory factor 8 (IRF8) (7). We have recently reported that ZFP36L2 down-regulates the expression of *Ikzf2* (encoding HELIOS) and suppresses the function of induced regulatory T cells (iTregs) (8). In this review, we discuss our current understanding of post-transcriptional regulation in immune responses by RNA-binding ZFP36 family proteins. We also discuss the control of those protein expressions as potential therapeutic strategies for human inflammatory diseases.

RNA-BINDING PROTEINS ARE INVOLVED IN POST-TRANSCRIPTIONAL REGULATION

RBPs recognize cis-elements or specific structures in the 5' UTR, 3' UTR, or intron of mRNA at each step of RNA metabolism (9). Adenylate-uridylate-rich elements (AU-rich elements; AREs) characterized by AUUUA nucleotide repeats are present in the 3' UTRs of many cytokines, chemokines, and proto-oncogenes (3), and ARE-binding RBPs, including ZFP36, human antigen R (HuR)/ELAVL1, AU-rich RNA binding factor 1 (AUF1), T-cell interleukin-1 (TIA-1)/TIA-associated protein (TIAR), and KH-type splicing regulatory protein (KSRP), regulate the degradation and translation of target mRNA (3). In contrast, several other RBPs such as Roquin, regulatory RNase (Regnase), and AT-rich interactive domain-containing protein 5a (Arid5a) recognize the stem-loop structure of the 3' UTR (3). Thus, RBPs can interact with specific RNA sequences and structures and interact with them to regulate target mRNAs positively or negatively (3).

ZFP36 FAMILY MEMBERS ARE CRITICAL FOR POST-TRANSCRIPTIONAL REGULATION

ZFP36 family is composed of three proteins (ZFP36 (TTP), ZFP36L1, and ZFP36L2) in humans and most other mammals, while the fourth subtype, ZFP36L3, is expressed in the yolk sac and placenta of rodents (10). The ZFP36 family members are known to have three essential domains: An N-terminal nuclear export sequence (NES), a central tandem Cys-Cys-Cys-His (CCCH) zinc finger domain, and a C-terminal CNOT1 binding domain (9). Although ZFP36 family members are structurally similar to each other, each ZFP36 family member is thought to have different functions, as it has been shown in both immune and non-immune cells that each ZFP36 family member is expressed in different cell-type and is differently controlled upon stimulation (8, 11).

Among ZFP36 family members, the molecular mechanisms of the post-transcriptional regulation are most intensively investigated for ZFP36 (9). The C-terminal motif of ZFP36 binds directly to the central domain of CNOT1, which is the core subunit of the CCR4-NOT complex, and the ZFP36-CCR4-NOT complex plays a crucial role in ZFP36-mediated deadenylation of target mRNAs (12). The deadenylation is thought to be important for rapid mRNA degradation and to be induced in small nests of the cytoplasm (called processing bodies) containing many enzymes (13). Under stress conditions, ZFP36-bound mRNAs are recruited to stress granules, and the translation repressor, TIA-1, prevents translation in stress granules (14). In addition, ZFP36 has been shown to facilitate the degradation of selected mRNAs by transporting them from stress granules to processing bodies (15, 16). Taken together, although the precise mechanism of mRNA turnover by ZFP36 is still unclear, various factors such as the CCR4-NOT complex seem to be essential for the regulation of ZFP36-mediated decay of mRNAs (**Figure 1**).

REGULATION OF THE EXPRESSION AND FUNCTION OF ZFP36

With respect to the molecular mechanisms to regulate ZFP36 expression, it has been shown that ZFP36 autoregulates its expression *via* interaction with AREs in 3' UTR of its mRNA (17). Experimental deletion of ARE from *Zfp36* mRNA has been shown to free ZFP36 from autoinhibition or repression by other ARE-binding proteins and increase the abundance of ZFP36 (18). Regarding the second mechanism to regulate ZFP36 function, phosphorylation is reported to be involved in the stabilization and inactivation of ZFP36. ZFP36 is phosphorylated by multiple kinases such as ERK, p38 MAPK, JNK, and AKT (19). MAPK-activated protein kinase 2 (MK2) is activated by p38 MAPK and phosphorylates ZFP36 at two serine residues (S60 and S186 in humans, and S52 and S178 in mice) (20, 21). Phosphorylated ZFP36 is more stable than unphosphorylated ZFP36, and the phosphorylated ZFP36 accumulates until p38 MAPK activity is reduced (22, 23). Moreover, the phosphorylation of ZFP36 promotes its binding to 14-3-3 proteins, and the resultant ZFP36-14-3-3 complex does not recruit the CNOT deadenylase complex (21, 22). Therefore, phosphorylated ZFP36 seems to lose its ability to degrade mRNA.

Dual-specificity phosphatase 1 (DUSP1) is known to dephosphorylate and inactivate MAPK superfamily members

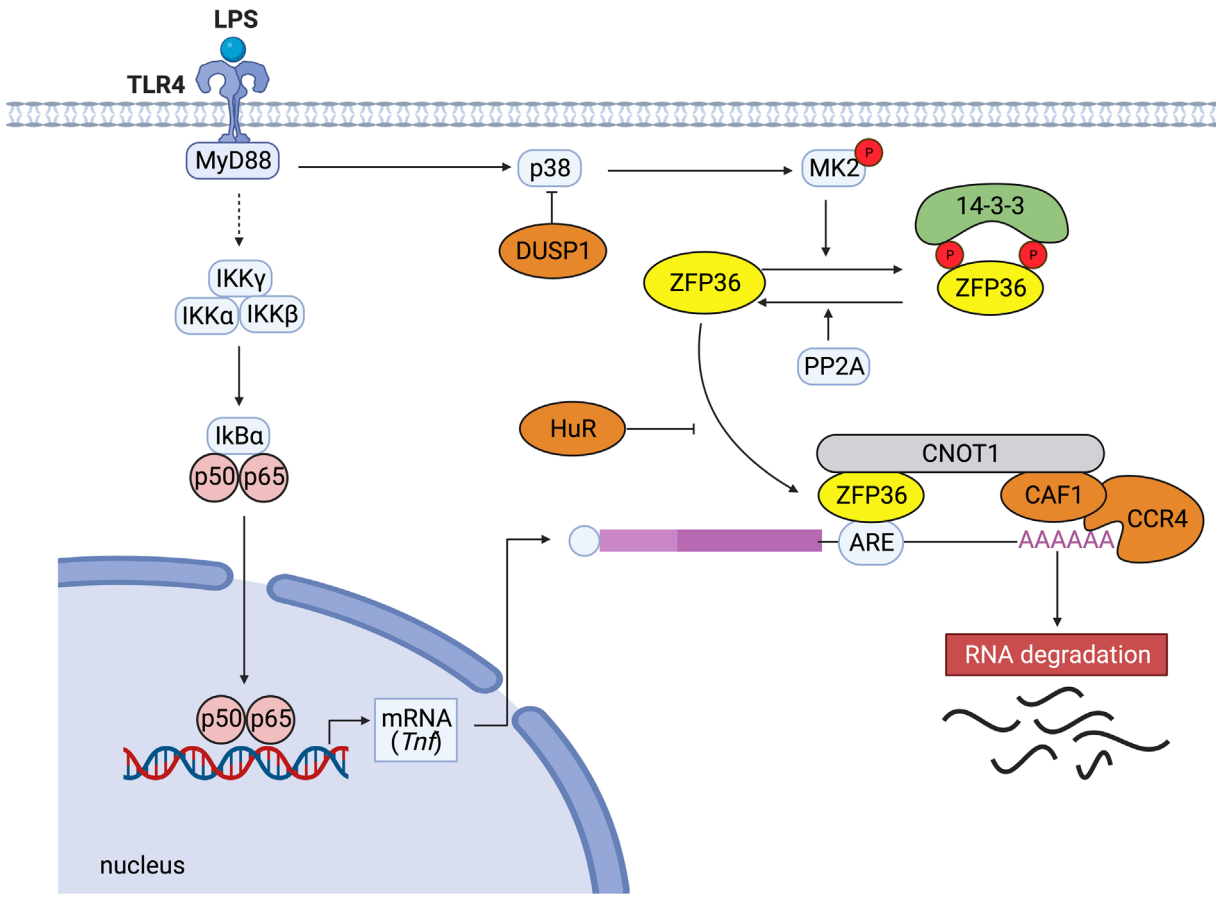

FIGURE 1 | Typical post-transcriptional regulation by ZFP36. When LPS activates TLR4, the downstream NF-κB kinase (IKK) complexes (IKKγ, IKKα, IKKβ) are activated. Subsequently, IκBα is phosphorylated and degraded. The released NF-κB migrates to the nucleus and activates the expression of genes such as TNF. ZFP36 binds to the ARE in the 3' UTR of *Tnf* mRNA and promotes the decay of the target mRNA by recruiting the CCR4-CAF1-CNOT1 complex. ZFP36 binds directly to the central domain of CNOT1, the core subunit of the CCR4-NOT complex. Conversely, the binding of stabilizing proteins such as human antigen R (HuR) that compete with destabilizing factors inhibits ARE-mediated RNA degradation. p38 MAPK activates MK2, which phosphorylates two serine residues of ZFP36 (S60 and S186 in humans, S52 and S178 in mice). Dual-specificity phosphatase DUSP1 dephosphorylates p38 MAPK. Phosphorylation of ZFP36 promotes its binding to 14-3-3 proteins, resulting in stabilization of target mRNAs. Serine/threonine PP2A dephosphorylates ZFP36 and releases 14-3-3 proteins from ZFP36.

such as JNKs, p38a, and p38b MAPKs, and then DUSP1 and ZFP36 cooperate to regulate inflammation (23). The loss of DUSP1 leads to ZFP36 phosphorylation and accumulation of inactive ZFP36, and the production of TNF-α and IL-10 is enhanced in Dusp1-deficient bone marrow-derived macrophages (23). Moreover, protein phosphatase 2A (PP2A) activation has been shown to induce dephosphorylation and activation of ZFP36 (21).

In terms of the other mechanisms preventing ZFP36 function, HuR competes with ZFP36 for the AREs in the 3' UTR of *Il6* mRNA and stabilizes it (24). In addition, ZFP36 is polyubiquitinated by TNF receptor-associated factor 2 (TRAF2), and the polyubiquitination appears to be specifically necessary for its function for JNK activation (25). These studies suggest that multiple mechanisms in immune responses regulate the expression and function of ZFP36, and various kinases affect the activation and stability of ZFP36 in response to different environmental cues (**Figure 1**).

ZFP36 CONTROLS VARIOUS IMMUNE RESPONSES

It is well known that mRNAs encoding cytokines such as TNF-α have short half-lives and decay *via* AREs (26). ZFP36 down-regulates TNF-α production by directly binding to the ARE in the 3' UTR of *Tnf* mRNA and promoting *Tnf* mRNA decay by recruiting the CCR4-NOT deadenylase complex (6). Meanwhile, ZFP36 expression is induced by TNF-α-mediated signaling. Thus, ZFP36 acts as one component of a negative feedback loop that regulates TNF-α production by destabilizing *Tnf*

mRNA (27). In accordance with this finding, ZFP36-deficient mice develop a complex syndrome of inflammatory arthritis, dermatitis, cachexia, autoimmunity, and bone marrow hyperplasia, which resemble the phenotypes due to excessive TNF-α production *in vivo* just like the phenomena observed in TNF-transgenic mice (28, 29).

Not only TNF-α but also IL-6 is well-known to be a multifunctional pro-inflammatory cytokine that plays a critical role in various diseases, and its expression is tightly regulated at both the transcriptional and post-transcriptional levels (4). There are five AREs in the 3' UTR of murine *Il6* mRNA, and ZFP36 is shown to bind to ARE2, ARE3, and ARE4 in the 3' UTR region to promote *Il6* mRNA degradation (30).

Surprisingly, the mRNA of IL-10, which is one of the representative anti-inflammatory cytokines, was also identified as a target of ZFP36. Consistent with studies regarding TNF-α and IL-6, *Il10* mRNA degradation was induced by the binding of ZFP36 to ARE in its 3' UTR (31). Furthermore, IL-10 induces the ZFP36 expression in macrophages by activating STAT3 (32). Thus, IL-10-mediated ZFP36 induction seems a part of the negative feedback loop to regulate IL-10 production to terminate anti-inflammatory signals. Interestingly, Schaljo et al. have reported that IL-10 reduces TNF-α expression in LPS-activated bone marrow-derived murine macrophages in part through the induction of ZFP36 (33). Together, it is suggested that ZFP36-mediated post-transcriptional regulatory mechanisms control both the initiation and resolution of inflammatory responses in multiple mechanisms.

With respect to the roles of ZFP36 in T cell-mediated immune responses, Moore et al. have recently shown that using a lymphocytic choriomeningitis virus (LCMV) infection model, virus-specific expansion and recession of T cells is accelerated, and LCMV clearance is enhanced by the absence of ZFP36 (34), suggesting that ZFP36 restrains T cells and slows down the immune responses.

Taken together, ZFP36 regulates immune responses in various immune cells through many mechanisms.

THE ROLES OF ZFP36L1 AND ZFP36L2 IN IMMUNE RESPONSES

Similar to ZFP36, ZFP36L1 interacts with AREs in the 3' UTR of mRNAs to attenuate the expression of the corresponding genes (35). Regarding the role of ZFP36L1 in post-transcriptional regulation, it has recently been demonstrated that ZFP36L1 expressed in B cells has an essential function in maintaining a population of marginal zone B cells by limiting the expression of KLF2 and IRF8 (7). Although the precise roles of ZFP36L1 in germinal center responses and immune memory remain unclear, it has been reported that ZFP36L1 expressed in B cells promotes the migration of antibody-secreting cells from secondary lymphoid organs to survival niches in the bone marrow by restricting the expression of G protein-coupled receptor kinase 2 (GRK2) and integrin chains α4 and β1, facilitating the long-term establishment of antibody-secreting cells (36).

In developing B cells, because the expression of recombination activating gene 2 (RAG2) protein is restricted to the G0-G1 phase of the cell cycle (37–39), quiescence is essential for promoting variable-diversity-joining (VDJ) recombination. Recently, Galloway et al. have shown that in developing B cells, both ZFP36L1 and ZFP36L2 are important for maintaining quiescence before expressing pre-B cell receptor (pre-BCR) and for the re-establishment of quiescence after expansion by the pre-BCR (40). Importantly, double-deficiency of ZFP36L1 and ZFP36L2 in T-cell lineage in mice causes the arrest of thymopoiesis at the double-negative stage and develops T cell acute lymphoblastic leukemia (T-ALL) due to aberrant activation of Notch signaling (41). In contrast, the single deletion of ZFP36L1 or ZFP36L2 in T-cell lineage does not result in T-ALL (41). These findings suggest that ZFP36L1 and ZFP36L2 play both redundant and non-redundant roles in lymphocyte differentiation.

How ZFP36L2 alters the function of T cells is not fully understood yet. We have recently shown that ZFP36L2 is highly expressed in naive $CD4^+$ T cells, and ZFP36L2 expression in $CD4^+$ T cells is rapidly reduced by the stimulation *via* the T cell receptor (8). In addition, we found that ZFP36L2 expression levels in iTregs are significantly lower than those in naive $CD4^+$ T cells (8). Moreover, we found that ZFP36L2 directly binds to AREs in 3' UTR of *Ikzf2* mRNA, resulting in its degradation of *Ikzf2* mRNA and down-regulation of iTreg function (**Figure 2**) (8). These results indicate that ZFP36L2 also promotes post-transcriptional regulation of immune responses and regulates immune cell function.

CLINICAL IMPLICATION OF ZFP36 FAMILY PROTEINS IN HUMAN INFLAMMATORY DISEASES

Genome-wide association studies (GWAS) have highlighted the association of *ZFP36* family members with pathogenic mechanisms in various autoimmune diseases. Twenty-eight single-nucleotide polymorphisms (SNPs) in the *ZFP36* gene were found in patients with autoimmune disorders such as rheumatoid arthritis (RA), psoriasis, multiple sclerosis (MS), and juvenile idiopathic arthritis (JIA) (42).

Interestingly, one SNP called *ZFP36**8 variant has been shown to be significantly associated with RA in African Americans (42). Suzuki et al. have reported that compared with AA/AG genotypes, GG genotype in *ZFP36* promoter region SNP, in which promoter activity is lower than that with AA/AG genotypes, is associated with age at onset, duration, disease progression, and infliximab usage in Japanese RA patients (43).

It is not yet clear how ZFP36 is involved in the pathogenesis of human diseases. It has been reported that ZFP36 is highly expressed in synovial tissues of RA patients and inflamed mucosal tissues of inflammatory bowel disease (IBD) (44–46). In the rheumatoid synovium, ZFP36 is detected in macrophages, vascular endothelial cells, and fibroblasts (45). Interestingly, *ZFP36/TNF* gene expression ratio in synovial tissues correlates inversely with CRP (44). These findings suggest that

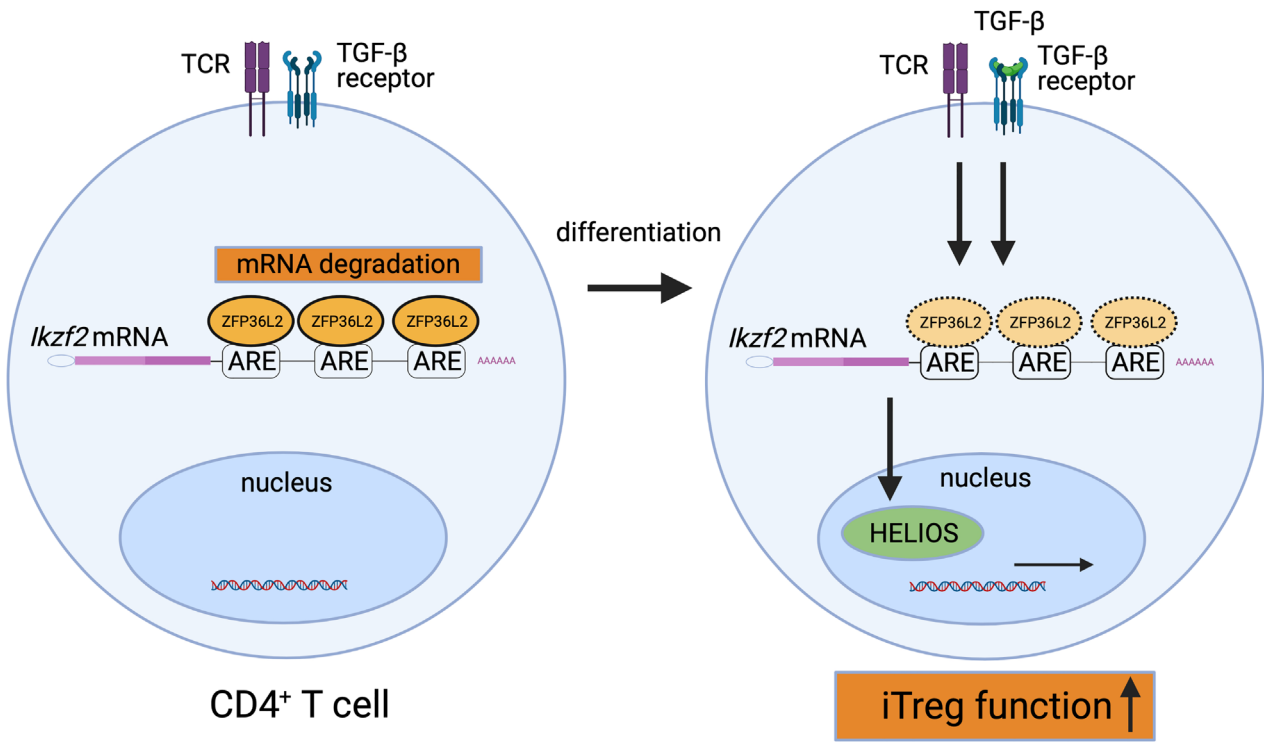

FIGURE 2 | Suppression of HELIOS expression by ZFP36L2. ZFP36L2 is highly expressed in naïve CD4$^+$ T cells and can degrade *Ikzf2* mRNAs by binding ARE in the 3' UTR. Upon TCR stimulation, ZFP36L2 expression is rapidly reduced. Consequently, the transcribed *Ikzf2* mRNA is stabilized, HELIOS is firmly produced, CD4$^+$ T cells differentiate and mature into iTregs possessing sufficient suppressive capacity.

inappropriate TTP production in response to increased TNF-α may be one factor that contributes to the pathogenesis of RA.

GWAS have also revealed that the *ZFP36L1* region is significantly associated with RA, JIA, Crohn's disease, celiac disease, and type 1 diabetes (47, 48). In addition, *ZFP36L2* is identified as a susceptibility gene of MS, and its expression is decreased in MS patients compared to healthy subjects (49). Similarly, gene expression levels of *ZFP36L2* in peripheral blood mononuclear cells are significantly lower in SLE patients than those in healthy controls (50). Therefore, the variants of *ZFP36, ZFP36L1, and ZFP36L2* or dysregulation of those expressions may be involved in developing various inflammatory diseases in humans.

Regarding the association with allergic diseases, a comprehensive transcriptome analysis has shown that *ZFP36* expression in peripheral blood leucocytes is lower in persistent asthma children than in healthy children (51), suggesting that the reduction of *ZFP36* gene expression may be associated with asthma in children. Moreover, Leigh et al. have reported that budesonide inhalation induces various gene expressions including *ZFP36* in bronchial tissues and whole blood cells in healthy subjects (52), indicating that inhaled corticosteroids may provide anti-inflammatory effects by inducing *ZFP36* expression in both immune cells and non-immune cells. On the other hand, the expression of *ZFP36L1* in bronchoalveolar lavage cells is higher in patients with steroid-resistant asthma than that in patients with steroid-sensitive asthma (53). Hansel et al. have reported that *ZFP36L2* expression in peripheral blood CD4$^+$ T cells is significantly higher in severe asthma patients than in mild asthma patients (54). Although further studies are required, these findings suggest that ZFP36 family proteins in immune cells and bronchial structural cells may contribute to the development of allergic airway inflammation and the sensitivity to inhaled corticosteroids.

CLINICAL POTENTIAL OF ZFP36 FAMILY PROTEINS IN INFLAMMATORY DISEASES

The forced expression of ZFP36 family proteins in peripheral tissues or immune cells could be novel therapeutic approaches for inflammatory diseases in humans (55). It has been reported that adenoviral overexpression of ZFP36 results in protection against bone loss and reduced inflammatory cell infiltration in experimental periodontitis in rats (56). Consistent with these findings, ZFP36-delta ARE mice, in which the stability of ZFP36 mRNA is enhanced by the deletion of a 136-base instability motif in the 3' UTR of *ZFP36* mRNA, show the increased levels of ZFP36 expression in tissues (57) and are protected from anti-type II collagen antibody-induced arthritis, imiquimod-induced dermatitis, and experimental autoimmune encephalomyelitis

(57). These findings suggest that sustained ZFP36 expression or activation is helpful in developing therapeutic strategies against inflammatory diseases.

As discussed in this review, the p38 MAPK pathway inactivates ZFP36 *via* the phosphorylation of two serine residues in mice and humans (20), while ZFP36 is dephosphorylated and activated by PP2A (58). Importantly, Ross et al. have reported that *in vivo* administration of PP2A agonists such as COG1410 (an apolipoprotein E peptide mimetic) or AAL(s) (a lipid derivative of the immunosuppressant FTY720 (Fingolimod)) activates ZFP36 through the dephosphorylation and ameliorates experimental murine arthritis models (45). Although the precise roles of ZFP36L2 in T cell function and inflammatory diseases remain to be elucidated, we have reported that ZFP36L2 reduces HELIOS expression in iTregs and suppresses iTreg function (**Figure 2**) (8). Thus, the reduction of ZFP36L2 expression in iTregs could be an attractive strategy for developing adoptive antigen-specific iTreg therapy.

CONCLUDING REMARKS

RBPs, including ZFP36 family proteins, are essential for post-transcriptional regulation in RNA metabolism. Recent studies have uncovered that gene polymorphism of ZFP36 family members is associated with various autoimmune diseases and that the dysregulation of stabilization or inactivation by phosphorylation of ZFP36 family proteins could be involved in the pathogenesis of inflammatory diseases. However, it remains to be elucidated if there is functional redundancy and interaction among these family molecules for post-transcriptional regulation of immune responses. Therefore, a better understanding of the post-transcriptional processes mediated by each of the ZFP36 family members will be necessary to develop a novel therapeutic strategy for chronic inflammatory diseases.

AUTHOR CONTRIBUTIONS

SM, HT, and HN planned and wrote the MS. All authors contributed to the article and approved the submitted version.

FUNDING

This work was supported in part by Grants-in-Aids for Scientific research from the Ministry of Education, Culture, Sports, Science and Technology (MEXT), LGS (Leading Graduate School at Chiba University) Program, Global Prominent Research (Chiba University), Takeda Science Foundation, and GSK Japan Research Grant.

REFERENCES

1. Castello A, Fischer B, Eichelbaum K, Horos R, Beckmann BM, Strein C, et al. Insights Into RNA Biology From an Atlas of Mammalian mRNA-Binding Proteins. *Cell* (2012) 149(6):1393–406. doi: 10.1016/j.cell.2012.04.031
2. Lunde BM, Moore C, Varani G. RNA-Binding Proteins: Modular Design for Efficient Function. *Nat Rev Mol Cell Biol* (2007) 8(6):479–90. doi: 10.1038/nrm2178
3. Akira S, Maeda K. Control of RNA Stability in Immunity. *Annu Rev Immunol* (2021) 39:481–509. doi: 10.1146/annurev-immunol-101819-075147
4. Fu M, Blackshear PJ. RNA-Binding Proteins in Immune Regulation: A Focus on CCCH Zinc Finger Proteins. *Nat Rev Immunol* (2017) 17(2):130–43. doi: 10.1038/nri.2016.129
5. Turner M, Diaz-Munoz MD. RNA-Binding Proteins Control Gene Expression and Cell Fate in the Immune System. *Nat Immunol* (2018) 19(2):120–9. doi: 10.1038/s41590-017-0028-4
6. Lai WS, Carballo E, Strum JR, Kennington EA, Phillips RS, Blackshear PJ. Evidence That Tristetraprolin Binds to AU-Rich Elements and Promotes the Deadenylation and Destabilization of Tumor Necrosis Factor Alpha mRNA. *Mol Cell Biol* (1999) 19(6):4311–23. doi: 10.1128/MCB.19.6.4311
7. Newman R, Ahlfors H, Saveliev A, Galloway A, Hodson DJ, Williams R, et al. Maintenance of the Marginal-Zone B Cell Compartment Specifically Requires the RNA-Binding Protein ZFP36L1. *Nat Immunol* (2017) 18(6):683–93. doi: 10.1038/ni.3724
8. Makita S, Takatori H, Iwata A, Tanaka S, Furuta S, Ikeda K, et al. RNA-Binding Protein ZFP36L2 Downregulates Helios Expression and Suppresses the Function of Regulatory T Cells. *Front Immunol* (2020) 11:1291. doi: 10.3389/fimmu.2020.01291
9. Kafasla P, Skliris A, Kontoyiannis DL. Post-Transcriptional Coordination of Immunological Responses by RNA-Binding Proteins. *Nat Immunol* (2014) 15(6):492–502. doi: 10.1038/ni.2884
10. Stumpo DJ, Trempus CS, Tucker CJ, Huang W, Li L, Kluckman K, et al. Deficiency of the Placenta- and Yolk Sac-Specific Tristetraprolin Family Member ZFP36L3 Identifies Likely mRNA Targets and an Unexpected Link to Placental Iron Metabolism. *Development* (2016) 143(8):1424–33. doi: 10.1242/dev.130369
11. Hacker C, Valchanova R, Adams S, Munz B. ZFP36L1 is Regulated by Growth Factors and Cytokines in Keratinocytes and Influences Their VEGF Production. *Growth Factors* (2010) 28(3):178–90. doi: 10.3109/08977190903578660
12. Fabian MR, Frank F, Rouya C, Siddiqui N, Lai WS, Karetnikov A, et al. Structural Basis for the Recruitment of the Human CCR4-NOT Deadenylase Complex by Tristetraprolin. *Nat Struct Mol Biol* (2013) 20(6):735–9. doi: 10.1038/nsmb.2572
13. Anderson P, Kedersha N. RNA Granules: Post-Transcriptional and Epigenetic Modulators of Gene Expression. *Nat Rev Mol Cell Biol* (2009) 10(6):430–6. doi: 10.1038/nrm2694
14. Protter DSW, Parker R. Principles and Properties of Stress Granules. *Trends Cell Biol* (2016) 26(9):668–79. doi: 10.1016/j.tcb.2016.05.004
15. Phillips K, Kedersha N, Shen L, Blackshear PJ, Anderson P. Arthritis Suppressor Genes TIA-1 and TTP Dampen the Expression of Tumor Necrosis Factor Alpha, Cyclooxygenase 2, and Inflammatory Arthritis. *Proc Natl Acad Sci USA* (2004) 101(7):2011–6. doi: 10.1073/pnas.0400148101
16. Kedersha N, Stoecklin G, Ayodele M, Yacono P, Lykke-Andersen J, Fritzler MJ, et al. Stress Granules and Processing Bodies are Dynamically Linked Sites of mRNP Remodeling. *J Cell Biol* (2005) 169(6):871–84. doi: 10.1083/jcb.200502088
17. Brooks SA, Connolly JE, Rigby WF. The Role of mRNA Turnover in the Regulation of Tristetraprolin Expression: Evidence for an Extracellular Signal-Regulated Kinase-Specific, AU-Rich Element-Dependent, Autoregulatory Pathway. *J Immunol* (2004) 172(12):7263–71. doi: 10.4049/jimmunol.172.12.7263
18. Tang T, Scambler TE, Smallie T, Cunliffe HE, Ross EA, Rosner DR, et al. Macrophage Responses to Lipopolysaccharide are Modulated by a Feedback Loop Involving Prostaglandin E2, Dual Specificity Phosphatase 1 and Tristetraprolin. *Sci Rep* (2017) 7(1):4350. doi: 10.1038/s41598-017-04100-1
19. Clark AR, Dean JL. The Control of Inflammation *via* the Phosphorylation and Dephosphorylation of Tristetraprolin: A Tale of Two Phosphatases. *Biochem Soc Trans* (2016) 44(5):1321–37. doi: 10.1042/BST20160166
20. Chrestensen CA, Schroeder MJ, Shabanowitz J, Hunt DF, Pelo JW, Worthington MT, et al. MAPKAP Kinase 2 Phosphorylates Tristetraprolin on *In Vivo* Sites Including Ser178, a Site Required for 14-3-3 Binding. *J Biol Chem* (2004) 279(11):10176–84. doi: 10.1074/jbc.M310486200

21. Stoecklin G, Stubbs T, Kedersha N, Wax S, Rigby WF, Blackwell TK, et al. MK2-Induced Tristetraprolin:14-3-3 Complexes Prevent Stress Granule Association and ARE-mRNA Decay. *EMBO J* (2004) 23(6):1313–24. doi: 10.1038/sj.emboj.7600163
22. Tiedje C, Diaz-Munoz MD, Trulley P, Ahlfors H, Laass K, Blackshear PJ, et al. The RNA-Binding Protein TTP is a Global Post-Transcriptional Regulator of Feedback Control in Inflammation. *Nucleic Acids Res* (2016) 44(15):7418–40. doi: 10.1093/nar/gkw474
23. Smallie T, Ross EA, Ammit AJ, Cunliffe HE, Tang T, Rosner DR, et al. Dual-Specificity Phosphatase 1 and Tristetraprolin Cooperate To Regulate Macrophage Responses to Lipopolysaccharide. *J Immunol* (2015) 195 (1):277–88. doi: 10.4049/jimmunol.1402830
24. Shi JX, Su X, Xu J, Zhang WY, Shi Y. HuR Post-Transcriptionally Regulates TNF-Alpha-Induced IL-6 Expression in Human Pulmonary Microvascular Endothelial Cells Mainly *via* Tristetraprolin. *Respir Physiol Neurobiol* (2012) 181(2):154–61. doi: 10.1016/j.resp.2012.02.011
25. Resch U, Cuapio A, Sturtzel C, Hofer E, de Martin R, Holper-Schichl YM. Polyubiquitinated Tristetraprolin Protects From TNF-Induced, Caspase-Mediated Apoptosis. *J Biol Chem* (2014) 289(36):25088–100. doi: 10.1074/jbc.M114.563312
26. Kontoyiannis D, Pasparakis M, Pizarro TT, Cominelli F, Kollias G. Impaired on/Off Regulation of TNF Biosynthesis in Mice Lacking TNF AU-Rich Elements: Implications for Joint and Gut-Associated Immunopathologies. *Immunity* (1999) 10(3):387–98. doi: 10.1016/S1074-7613(00)80038-2
27. Carballo E, Lai WS, Blackshear PJ. Feedback Inhibition of Macrophage Tumor Necrosis Factor-Alpha Production by Tristetraprolin. *Science* (1998) 281 (5379):1001–5. doi: 10.1126/science.281.5379.1001
28. Taylor GA, Carballo E, Lee DM, Lai WS, Thompson MJ, Patel DD, et al. A Pathogenetic Role for TNF Alpha in the Syndrome of Cachexia, Arthritis, and Autoimmunity Resulting From Tristetraprolin (TTP) Deficiency. *Immunity* (1996) 4(5):445–54. doi: 10.1016/S1074-7613(00)80411-2
29. Carballo E, Blackshear PJ. Roles of Tumor Necrosis Factor-Alpha Receptor Subtypes in the Pathogenesis of the Tristetraprolin-Deficiency Syndrome. *Blood* (2001) 98(8):2389–95. doi: 10.1182/blood.V98.8.2389
30. Zhao W, Liu M, D'Silva NJ, Kirkwood KL. Tristetraprolin Regulates Interleukin-6 Expression Through P38 MAPK-Dependent Affinity Changes With mRNA 3' Untranslated Region. *J Interferon Cytokine Res* (2011) 31 (8):629–37. doi: 10.1089/jir.2010.0154
31. Stoecklin G, Tenenbaum SA, Mayo T, Chittur SV, George AD, Baroni TE, et al. Genome-Wide Analysis Identifies Interleukin-10 mRNA as Target of Tristetraprolin. *J Biol Chem* (2008) 283(17):11689–99. doi: 10.1074/jbc.M709657200
32. Gaba A, Grivennikov SI, Do MV, Stumpo DJ, Blackshear PJ, Karin M. Cutting Edge: IL-10-Mediated Tristetraprolin Induction is Part of a Feedback Loop That Controls Macrophage STAT3 Activation and Cytokine Production. *J Immunol* (2012) 189(5):2089–93. doi: 10.4049/jimmunol.1201126
33. Schaljo B, Kratochvill F, Gratz N, Sadzak I, Sauer I, Hammer M, et al. Tristetraprolin is Required for Full Anti-Inflammatory Response of Murine Macrophages to IL-10. *J Immunol* (2009) 183(2):1197–206. doi: 10.4049/jimmunol.0803883
34. Moore MJ, Blachere NE, Fak JJ, Park CY, Sawicka K, Parveen S, et al. ZFP36 RNA-Binding Proteins Restrain T Cell Activation and Anti-Viral Immunity. *Elife* (2018) 7:e33057. doi: 10.7554/eLife.33057
35. Brooks SA, Blackshear PJ. Tristetraprolin (TTP): Interactions With mRNA and Proteins, and Current Thoughts on Mechanisms of Action. *Biochim Biophys Acta* (2013) 1829(6-7):666–79. doi: 10.1016/j.bbagrm.2013.02.003
36. Saveliev A, Bell SE, Turner M. Efficient Homing of Antibody-Secreting Cells to the Bone Marrow Requires RNA-Binding Protein ZFP36L1. *J Exp Med* (2021) 218(3):e20200504. doi: 10.1084/jem.20200504
37. Zhang L, Reynolds TL, Shan X, Desiderio S. Coupling of V(D)J Recombination to the Cell Cycle Suppresses Genomic Instability and Lymphoid Tumorigenesis. *Immunity* (2011) 34(2):163–74. doi: 10.1016/j.immuni.2011.02.003
38. Johnson K, Chaumeil J, Micsinai M, Wang JM, Ramsey LB, Baracho GV, et al. IL-7 Functionally Segregates the Pro-B Cell Stage by Regulating Transcription of Recombination Mediators Across Cell Cycle. *J Immunol* (2012) 188 (12):6084–92. doi: 10.4049/jimmunol.1200368
39. Bendall SC, Davis KL, Amir e-A, Tadmor MD, Simonds EF, Chen TJ, et al. Single-Cell Trajectory Detection Uncovers Progression and Regulatory Coordination in Human B Cell Development. *Cell* (2014) 157(3):714–25. doi: 10.1016/j.cell.2014.04.005
40. Galloway A, Saveliev A, Lukasiak S, Hodson DJ, Bolland D, Balmanno K, et al. RNA-Binding Proteins ZFP36L1 and ZFP36L2 Promote Cell Quiescence. *Science* (2016) 352(6284):453–9. doi: 10.1126/science.aad5978
41. Hodson DJ, Janas ML, Galloway A, Bell SE, Andrews S, Li CM, et al. Deletion of the RNA-Binding Proteins ZFP36L1 and ZFP36L2 Leads to Perturbed Thymic Development and T Lymphoblastic Leukemia. *Nat Immunol* (2010) 11(8):717–24. doi: 10.1038/ni.1901
42. Carrick DM, Chulada P, Donn R, Fabris M, McNicholl J, Whitworth W, et al. Genetic Variations in ZFP36 and Their Possible Relationship to Autoimmune Diseases. *J Autoimmun* (2006) 26(3):182–96. doi: 10.1016/j.jaut.2006.01.004
43. Suzuki T, Tsutsumi A, Suzuki H, Suzuki E, Sugihara M, Muraki Y, et al. Tristetraprolin (TTP) Gene Polymorphisms in Patients With Rheumatoid Arthritis and Healthy Individuals. *Mod Rheumatol* (2008) 18(5):472–9. doi: 10.3109/s10165-008-0085-5
44. Tsutsumi A, Suzuki E, Adachi Y, Murata H, Goto D, Kojo S, et al. Expression of Tristetraprolin (G0S24) mRNA, a Regulator of Tumor Necrosis Factor-Alpha Production, in Synovial Tissues of Patients With Rheumatoid Arthritis. *J Rheumatol* (2004) 31(6):1044–9.
45. Ross EA, Naylor AJ, O'Neil JD, Crowley T, Ridley ML, Crowe J, et al. Treatment of Inflammatory Arthritis *via* Targeting of Tristetraprolin, a Master Regulator of Pro-Inflammatory Gene Expression. *Ann Rheum Dis* (2017) 76(3):612–9. doi: 10.1136/annrheumdis-2016-209424
46. Di Silvestre A, Lucafò M, Pugnetti L, Bramuzzo M, Stocco G, Barbi E, et al. Role of Tristetraprolin Phosphorylation in Paediatric Patients With Inflammatory Bowel Disease. *World J Gastroenterol* (2019) 25(39):5918–25. doi: 10.3748/wjg.v25.i39.5918
47. Hinks A, Cobb J, Marion MC, Prahalad S, Sudman M, Bowes J, et al. Dense Genotyping of Immune-Related Disease Regions Identifies 14 New Susceptibility Loci for Juvenile Idiopathic Arthritis. *Nat Genet* (2013) 45 (6):664–9. doi: 10.1038/ng.2614
48. Franke A, McGovern DP, Barrett JC, Wang K, Radford-Smith GL, Ahmad T, et al. Genome-Wide Meta-Analysis Increases to 71 the Number of Confirmed Crohn's Disease Susceptibility Loci. *Nat Genet* (2010) 42(12):1118–25. doi: 10.1038/ng.717
49. Parnell GP, Gatt PN, Krupa M, Nickles D, McKay FC, Schibeci SD, et al. The Autoimmune Disease-Associated Transcription Factors EOMES and TBX21 are Dysregulated in Multiple Sclerosis and Define a Molecular Subtype of Disease. *Clin Immunol* (2014) 151(1):16–24. doi: 10.1016/j.clim.2014.01.003
50. Mandel M, Gurevich M, Pauzner R, Kaminski N, Achiron A. Autoimmunity Gene Expression Portrait: Specific Signature That Intersects or Differentiates Between Multiple Sclerosis and Systemic Lupus Erythematosus. *Clin Exp Immunol* (2004) 138(1):164–70. doi: 10.1111/j.1365-2249.2004.02587.x
51. Persson H, Kwon AT, Ramilowski JA, Silberberg G, Soderhall C, Orsmark-Pietras C, et al. Transcriptome Analysis of Controlled and Therapy-Resistant Childhood Asthma Reveals Distinct Gene Expression Profiles. *J Allergy Clin Immunol* (2015) 136(3):638–48. doi: 10.1016/j.jaci.2015.02.026
52. Leigh R, Mostafa MM, King EM, Rider CF, Shah S, Dumonceaux C, et al. An Inhaled Dose of Budesonide Induces Genes Involved in Transcription and Signaling in the Human Airways: Enhancement of Anti- and Proinflammatory Effector Genes. *Pharmacol Res Perspect* (2016) 4(4):e00243. doi: 10.1002/prp2.243
53. Alrashoudi RH, Crane IJ, Wilson HM, Al-Alwan M, Alajez NM. Gene Expression Data Analysis Identifies Multiple Deregulated Pathways in Patients With Asthma. *Biosci Rep* (2018) 38(6):BSR20180548. doi: 10.1042/BSR20180548
54. Hansel NN, Hilmer SC, Georas SN, Cope LM, Guo J, Irizarry RA, et al. Oligonucleotide-Microarray Analysis of Peripheral-Blood Lymphocytes in Severe Asthma. *J Lab Clin Med* (2005) 145(5):263–74. doi: 10.1016/j.lab.2005.02.010
55. Patial S, Blackshear PJ. Tristetraprolin as a Therapeutic Target in Inflammatory Disease. *Trends Pharmacol Sci* (2016) 37(10):811–21. doi: 10.1016/j.tips.2016.07.002
56. Patil CS, Liu M, Zhao W, Coatney DD, Li F, VanTubergen EA, et al. Targeting mRNA Stability Arrests Inflammatory Bone Loss. *Mol Ther* (2008) 16 (10):1657–64. doi: 10.1038/mt.2008.163
57. Patial S, Curtis AD2nd, Lai WS, Stumpo DJ, Hill GD, Flake GP, et al. Enhanced Stability of Tristetraprolin mRNA Protects Mice Against Immune-Mediated Inflammatory Pathologies. *Proc Natl Acad Sci U S A* (2016) 113(7):1865–70. doi: 10.1073/pnas.1519906113
58. Sun L, Stoecklin G, Van Way S, Hinkovska-Galcheva V, Guo RF, Anderson P, et al. Tristetraprolin (TTP)-14-3-3 Complex Formation Protects TTP From Dephosphorylation by Protein Phosphatase 2a and Stabilizes Tumor Necrosis

Factor-Alpha mRNA. *J Biol Chem* (2007) 282(6):3766–77. doi: 10.1074/jbc.M607347200

Conflict of Interest: The authors declare that the research was conducted in the absence of any commercial or financial relationships that could be construed as a potential conflict of interest.

frontiers in Immunology

ORIGINAL RESEARCH
published: 06 July 2021
doi: 10.3389/fimmu.2021.685896

The Enhanced Immune Protection in Small Abalone *Haliotis diversicolor* Against a Secondary Infection With *Vibrio harveyi*

Tuo Yao[1], *Jie Lu*[1], *Changming Bai*[2], *Zhilv Xie*[1] *and Lingtong Ye*[3]*

[1] *Key Laboratory of South China Sea Fishery Resources Exploitation & Utilization, Ministry of Agriculture and Rural Affairs, South China Sea Fisheries Research Institute, Chinese Academy of Fishery Sciences, Guangzhou, China,* [2] *Key Laboratory of Maricultural Organism Disease Control, Ministry of Agriculture and Rural Affairs, Qingdao Key Laboratory of Mariculture Epidemiology and Biosecurity, Yellow Sea Fisheries Research Institute, Chinese Academy of Fishery Sciences, Qingdao, China,* [3] *Key Laboratory of Aquatic Product Processing, Ministry of Agriculture and Rural Affairs, South China Sea Fisheries Research Institute, Chinese Academy of Fishery Sciences, Guangzhou, China*

OPEN ACCESS

Edited by:
Osamu Takeuchi,
Kyoto University, Japan

Reviewed by:
Surya Pandey,
University of Chicago, United States
Xiaocui He,
La Jolla Institute for Immunology (LJI), United States

***Correspondence:**
Lingtong Ye
lingtong2753@126.com

Specialty section:
This article was submitted to Molecular Innate Immunity, a section of the journal Frontiers in Immunology

Received: *26 March 2021*
Accepted: *22 June 2021*
Published: *06 July 2021*

Citation:
Yao T, Lu J, Bai C, Xie Z and Ye L (2021) The Enhanced Immune Protection in Small Abalone Haliotis diversicolor Against a Secondary Infection With Vibrio harveyi. Front. Immunol. 12:685896. doi: 10.3389/fimmu.2021.685896

In recent years, more and more studies have shown that early pathogenic bacterial infection in invertebrates can enhance immunity and significantly reduce mortality when reinfected with the same pathogen. There are mechanisms to explain this phenomenon, but they are relatively few. In addition, dose-dependent primary infection is also associated with increased immunity. In the present study, the initial infection dose and mortality of abalone *Haliotis diversicolor* after reinfection with *Vibrio harveyi* were recorded, and the mechanism of immune enhancement was investigated by the transcriptomic response of abalone after two successive stimuli with *V. harveyi*. Priming with different concentrations of pathogen can enhance immunity; however, higher concentration is not always better. Compared with the first exposure, more genes were up-regulated after the second exposure. Among the commonly expressed genes, the immune related genes were significantly or persistently highly expressed after two infections and included pattern recognition receptors as well as immune effectors, such as toll-like receptors, perlucin 4, scavenger receptor class B-like protein, cytochrome P450 1B1-like, glutathione S-transferase 6, lysozyme and so on; in addition, these immune-related genes were mainly distributed in the pathways related to phagocytosis and calcium signaling. Among the specifically expressed genes, compared with the first infection, more genes were involved in the immune, metabolic and digestive pathways after the second infection, which would be more conducive to preventing the invasion of pathogens. This study outlined the mechanism of immune enhancement in abalone after secondary infection at the global molecular level, which is helpful for a comprehensive understanding of the mechanism of immune priming in invertebrates.

Keywords: *Haliotis diversicolor*, *Vibrio harveyi*, enhanced immune protection, secondary infection, immune priming

INTRODUCTION

More and more studies have shown that the innate immune system has a memory similar to the adaptive immune system, which endows the organism with a stronger and more effective resistance to reinfection, and can be found in a variety of organisms (1, 2). This characteristic is found in plants (3), bacteria (4, 5) and viruses (6). And, this phenomenon is defined in different terms depending on the species studied, for example "trained immunity" in vertebrates (7–9), "immune priming" in invertebrates (10, 11) and "Systemic Acquired Resistance" (SAR) in plants (12, 13). Based on molecular, immunological and evolutionary arguments, Netea et al. (9) proposed that innate immune memory is a primitive form of immune memory, while adaptive immune memory is an advanced form of immune memory. It is necessary to develop an immune memory as it is of great advantage in improving the organism's survival rate in an unfavorable environment.

Invertebrates include a wide variety of species, accounting for more than 95% of the animal kingdom (14). Invertebrate immunology has attracted more and more attention, and with the further study of invertebrate immune priming, some mechanisms have been identified. It is generally believed that improved resistance after reinfection is mainly related to the up-regulated expression of pattern recognition receptors (PRRs) and the enhancement of phagocytic activity. For example, fibrinogen-related proteins (FREPs) were over represented in the Vector Snail following a secondary challenge (15). Following re-exposure to the pathogen, C-lectins and peptidoglycan recognition protein-S1 were up-regulated in scallop (16, 17). Increased phagocytosis was found in silkworm (18), Drosophila (19) and Pacific oyster (20) after homologous exposure. In addition, other mechanisms such as DNA synthesis (21) and RNA methylation (22) have also been used to explain immune priming. Moreover, initial priming doses can affect the immune priming outcome. A positive correlation between increased resistance and priming dose was found in *Galleria mellonella* larvae (23). However, immune priming is not universal. Immune memory failed to be detected in damselflies (24) and ants (25).

Abalone is an important economic shellfish in China, and plays a pivotal role in the aquaculture of marine shellfish. Compared with 2018, production in 2019 increased by 9.85%; the annual growth rate far exceeds that of other farmed shellfish. Although abalone farming is generally on the rise in China, the frequent occurrence of disease has seriously affected the rapid development of abalone aquaculture. The cultivation and promotion of new varieties of abalone have promoted the revitalization and development of the abalone breeding industry to a certain extent, but diseases still occur from time to time 3–5 years after the breeding of new varieties. *Vibrio harveyi* is a Gram-negative bacterium, which is widely distributed in various waters and has high pathogenicity in abalone. In previous studies, we confirmed that improved survival rate could be obtained during re-infection when *Haliotis diversicolor* was primed with *V. harveyi*. However, it is not clear whether the initial priming dose is associated with increased resistance in re-infection. Although mechanisms of immune priming at the cytological level have been studied in abalone (26), molecular studies have not been reported. To fully understand the basis of innate immune memory generation, a global molecular approach is needed. The development of high-throughput sequencing technology has accelerated the study of non-model organisms and made it possible to investigate immune priming mechanisms at the overall molecular level.

In order to determine whether different infection doses affect resistance and address the mechanism of immune enhancement after abalone secondary infection, in this study, two different experiments were conducted. In the first experiment, *H. diversicolor* were exposed to different concentrations of *V. harveyi* in the first infection. However, the same concentration was used in the second infection to detect the relationship between the infection dose and immune resistance *via* survival rate changes. In the second experiment, we examined the alterations in mRNA expression of immune-related genes during one and two infections of abalone, respectively, using a transcriptomic approach. In this study, we hoped to understand the mechanism of improved immunity during re-infection.

MATERIALS AND METHODS

Abalone and Microbes

The abalone (mean shell length 41.35 ± 0.23 mm) used in this study were obtained from our aquaculture base in Jieyang, Guangdong Province, China. The animals were acclimated in experimental barrels with continuous oxygenation and a flow-through sea water supply for 2 weeks. Filtered seawater and salinity were maintained at 28°C and 30, respectively.

V. harveyi isolated from the hepatopancreas of moribund abalone, was used in these experiments. The bacteria were incubated in LB medium at 28°C for 20 h, and harvested by centrifugation at 7,000 × *g* at 25°C for 5 min. The pellet was resuspended in sterile sea water (SSW) which was filtered using a 0.2 μm Millipore filter, and the final concentration was adjusted according to experimental requirements.

Immune Challenge and Sample Collection

For observation of immune priming, the abalone received two immune challenges in total. A schematic diagram of the experimental design is shown in **Figure 1**. For the primary immune challenge, abalone were divided into five treatment groups designated as V_3, V_4, V_5, V_6 and V_7, and were injected with 50 μL of different concentrations of *V. harveyi* as follows: 1.42×10^3 CFU mL^{-1}, 1.42×10^4 CFU mL^{-1}, 1.42×10^5 CFU mL^{-1}, 1.42×10^6 CFU mL^{-1} and 1.42×10^7 CFU mL^{-1}, respectively. Abalone in a control group received an injection of 50 μL SSW as a control (designated the V_0 group). Fifteen days later, the secondary immune challenge was performed. Five treatment groups designated as V_{3+6}, V_{4+6}, V_{5+6}, V_{6+6} and V_{7+6}, corresponding to the five primary immune challenge groups were each injected with 50 μL *V. harveyi* at a concentration of 1.58×10^6 CFU mL^{-1} for the secondary immune challenge. In addition, the SSW group was divided into two subgroups, designated as V_{0+0} (receiving an injection of 50 μL SSW) and V_{0+6} (receiving an

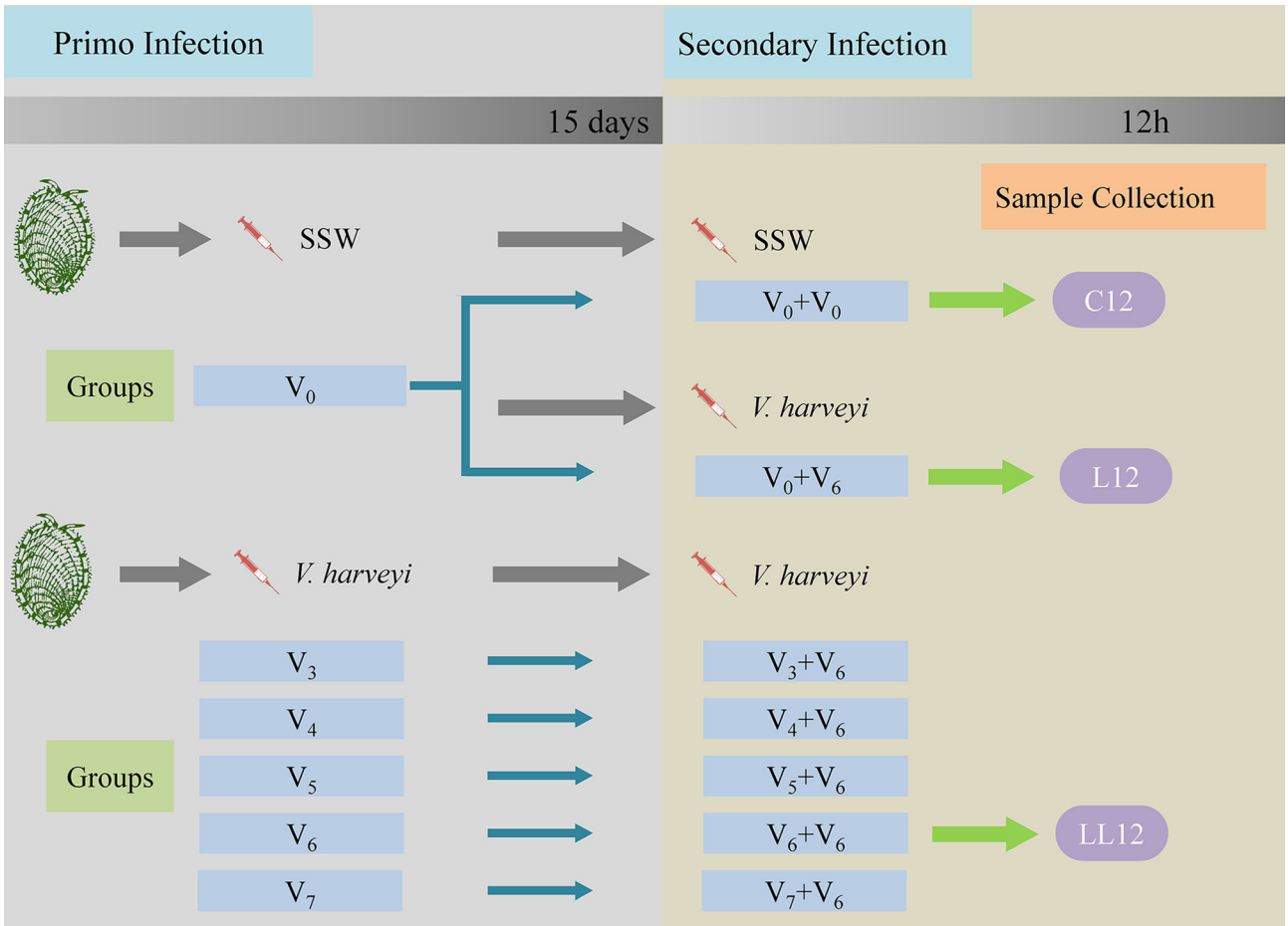

FIGURE 1 | Schematic diagram of the experimental design. Each experiment consisted of two successive infection challenges. For the primary immune challenge, abalone from the same batch were injected with either sterile sea water (SSW, group V_0) or different concentrations of *V. harveyi*: 1.42×10^3 CFU mL^{-1}, 1.42×10^4 CFU mL^{-1}, 1.42×10^5 CFU mL^{-1}, 1.42×10^6 CFU mL^{-1} and 1.42×10^7 CFU mL^{-1}, designated as V_3, V_4, V_5, V_6 and V_7, respectively. Fifteen days later, the five treatment groups and the V_0 group received an injection of *V. harveyi* at a concentration of 1.58×10^6 CFU mL^{-1} (designated as V_{3+6}, V_{4+6}, V_{5+6}, V_{6+6} V_{7+6} and V_{0+6}). The V_0 group was also injected with SSW as a control for the secondary infection (V_{0+0}). During each experimental infection, mortalities were monitored daily post-challenge. The abalone hepatopancreases were sampled 12 h after the second stimulation in the V_{0+0}, V_{0+6} and V_{6+6} groups, and named C12, L12 and LL12 groups, respectively. Gene expression levels in the hepatopancreas were then analyzed by transcriptomics.

injection of 50 μL *V. harveyi* at the concentration of 1.58×10^6 CFU mL^{-1}). During the first injection, 360 abalone were used in each group. During the second infection, 90 abalone in each group were used for mortality monitoring, and at least 30 abalone were used in each of the sampling groups. All experiments were performed in triplicate with abalone in 500 L plastic tanks. In these experiments, dead animals were removed in a timely manner to avoid affecting the water quality.

To study the correlation between initial infection dose and degree of protection, daily mortality rates in each group were monitored. To study the molecular mechanism of immune priming, the hepatopancreases of live abalone were randomly sampled at the time point of 12 h after the second stimulation from the V_{0+0}, V_{0+6} and V_{6+6} groups, and were named the C12, L12 and LL12 groups, respectively. A total of nine abalone were sacrificed in each group, and three hepatopancreases from each replicate were pooled together as one sample. These samples were immediately frozen in liquid nitrogen and stored separately at -80° C for subsequent transcriptome sequencing. The survival rate was calculated with a Kaplan-Meier estimate followed by a log-rank test in SPSS 25. Significant differences were set at $P < 0.05$.

RNA Extraction, Library Construction, and Sequencing

Total RNA was extracted using the TRIzol kit (Invitrogen, Carlsbad, CA, USA) according to the manufacturer's instructions. Total RNA samples were then digested with DNase I (Ambion, Thermo Scientific, Waltham, MA, USA) to remove potential genomic DNA contamination. RNA degradation and contamination were monitored in 1% agarose

gels. RNA quantity and integrity were measured using a NanoDrop 2000 spectrophotometer (ThermoFisher Scientific, Wilmington, DE, USA) and an Agilent 2100 Bioanalyzer (Agilent Technologies, Santa Clara, CA, USA), respectively. The resultant RNA samples were then used for RNA-seq.

The poly (A) mRNA was enriched using poly-T oligo-attached magnetic beads (Dynabeads; Invitrogen, Carlsbad, CA, USA) and then cleaved into fragments in the NEB proprietary fragmentation buffer. Following first strand and complementary strand synthesis, the resultant RNA was ligated with sequencing adapters. Then PCR amplification was performed to generate the RNA-seq library. The library preparations were sequenced on an Illumina Novaseq 6000 platform (Illumina, San Diego, CA, USA) and 150 bp paired-end reads were generated.

Bioinformatics Analysis

Clean reads were obtained from the raw reads (149,598,910, 148,942,646 and 165,147,008 reads in C12, L12 and LL12 groups, respectively) by removing adapter reads, unknown reads (with 'N' ratios > 10%), low quality reads (with quality value ≤ 20) and short reads (with length < 30 bp). After this processing, 148,180,604, 147,780,808 and 163,874,166 clean reads were obtained from the C12, L12 and LL12 groups, respectively (**Table 1**). The resultant reads were then assembled into a transcriptome using Trinity software with default settings (27). BlastX was used to obtain functional annotation of all expressed genes, by comparing with six databases, including the NCBI nonredundant protein (NR), Swiss-Prot, Protein family (Pfam), Gene Ontology (GO), Cluster of Orthologous Groups (COG) and Kyoto Encyclopedia of Genes and Genome (KEGG) databases, with a cut-off E-value of < 10^{-5}. GO annotations were analyzed with the Blast2GO program (28) utilizing default parameters. After treatment, the mapping rates ranged from 56.34% to 59.68% for all groups (**Table 1**). The expression abundance of *H. diversicolor* was calculated using RSEM software (29) and gene expression levels were measured using the FPKM (Fragments Per Kilobase of transcript per Million fragments) method. Differentially expressed genes (DEGs) in the different groups were detected using the DESeq package (30). Significant differential expression was defined by setting absolute $\log_2$Flodchange > 1 and FDR (false discovery rate) p-value (q-value) < 0.05 as the threshold. Finally, the obtained DEGs were included in the GO and KEGG enrichment analysis, based on the Hypergeometric distribution model.

Gene Expression Validation

Twelve DEGs, including toll-like receptor (TLR), TLR2, TLR8, scavenger receptor class B-like protein (SR-BI), X-box binding protein (XBP), cathepsin B (CatB), tumor necrosis factor ligand superfamily member 6-like (TNFSF6), legumain (Lgmn), Zinc transporter ZIP10 (ZIP10), peptidoglycan-recognition protein SC2 isoform X1 (PGRP-SC2), pannexin 5 (Px5) and tumor necrosis factor ligand superfamily member 6 isoform X2 (TNFSF6-X2) were selected to validate Illumina sequencing data by real-time qRT-PCR analysis, and qPCR was performed on different individuals exposed to the same conditions. All primers were acquired with Primer Premier 5.0 based on the reference transcriptome sequences and β-actin was selected as the reference gene (**Table 2**). RNA preparation was carried out as above. The first strand cDNA was synthesized from approximately 1 μg of total RNA using the PrimeScript™ RT Reagent Kit (Takara, Dalian, China) in a 20 μL reaction system following the manufacturer's protocol. The qRT-PCR amplifications were performed with a LightCycler® 480 system (Roche Biochemicals, Indianapolis, IN, USA) using TB Green® Premix Ex Taq™ II (Takara, Dalian, China) in a 10 μL reaction system. The thermal cycling parameters were 95°C for 30 s, followed by 40 cycles of 95°C for 5 s and 60°C for 30 s. Three biological replicates and three technical replicates were included in these experiments and the data were obtained using the $2^{-\Delta\Delta CT}$ method (31). The data were expressed as the mean ± SD (n = 3).

RESULTS

Survival Rates After First and Second Challenge With *V. harveyi*

To investigate the relationship between immune protection and initial dose of infection, two consecutive *V. harveyi* infection experiments were performed. In this study, five different concentrations of *V. harveyi* diluents were used. After the first immune stimulation, the survival rate decreased with increased infection concentration (**Figure 2A**). Among them, the survival rate in the V_6 group was 48.9%. Thus, a bacterial concentration

TABLE 1 | Summary of the transcriptome assembly.

Sample	Raw reads (×10^6)	Raw bases (×10^8)	Clean reads (×10^6)	Clean bases (×10^8)	Q20 (%)	Q30 (%)	GC content (%)	Mapped reads (×10^6)	Mapped ratio (%)
C12_1	44.55	67.26	44.08	65.43	98.82	95.98	45.64	25.86	58.67
C12_2	51.53	77.81	51.04	75.54	98.88	96.15	46.09	29.82	58.42
C12_3	53.52	80.82	53.07	78.82	98.95	96.35	46.60	31.67	59.68
L12_1	46.74	70.58	46.31	68.90	98.86	96.13	46.30	26.09	56.34
L12_2	50.08	75.62	49.72	73.88	98.99	96.45	45.30	29.00	58.33
L12_3	52.12	78.71	51.76	76.99	98.93	96.28	45.76	29.86	57.69
LL12_1	55.36	83.59	54.93	81.53	98.93	96.27	45.85	32.55	59.26
LL12_2	56.45	85.24	56.03	83.13	98.98	96.44	46.13	32.18	57.43
LL12_3	53.34	80.55	52.91	78.53	98.96	96.41	46.30	30.12	56.93

TABLE 2 | Sequences of the primers used in this study.

Primer	Primer sequence (5'-3')
β-actin-F	CCGTGACCTTACAGACTACCT
β-actin-R	TACCAGCGGATTCCATAC
TLR-F	CCTCAAAGAACGGTCCCA
TLR-R	CGTCAGGCAGAGCGAAA
TLR8-F	CCACCAGCGAGACTTTGC
TLR8-R	CTGTGCGGAACTCCATCA
SR-BI-F	CTATTCTTACAGGGAGCATCG
SR-BI-R	CGCTGAAACTCAAACCACC
TLR2-F	ACACAAAGCAAGGGTCAA
TLR2-R	TCAACAGCGTGGAGGAT
XBP-F	AGAGGGGCGTATTCAGA
XBP-R	GCCATTGGTCGGGTGTA
CatB-F	GTGGAAGGCTGGTAGAAACG
CatB-R	CATTGATGTCCTTTACACCCA
TNFSF6-F	CCAGACACCGCTGAGAATG
TNFSF6-R	GGACAATCAATACCGCAAATA
Lgmn-F	ATGGACAAGGTGCGAAAG
Lgmn-R	CCCTCCTGACAATCTCAAACT
ZIP10-F	GGCAAGCAAGAACCAAG
ZIP10-R	CCATTTCCCCTATGACCTG
PGRP-SC2-F	CCTCATTCCATCAGCCATCT
PGRP-SC2-R	CCTATCCTGTCCCAGCCAC
Px5-F	CCGAAAGAATACGACAAGG
Px5-R	GATGACCCAACGGTAGAAG
TNFSF6-X2-F	GGGCGGATTGACTTTGC
TNFSF6-X2-R	ATTCGGTTGTCTTGGATGTT

of 10^6 CFU mL^{-1} was selected for the second infection experiment. After the second infection, the log-rank test showed that the survival rates in all groups receiving the first immune stimulation were significantly higher than that in group V_{0+6} (**Figure 2B**), but there were no significant differences among groups V_{3+6}, V_{4+6}, V_{5+6}, V_{6+6} and V_{7+6} ($P < 0.05$). This implies that, the previous infection protected the abalone against a secondary infection. However, there was no positive correlation between immune protection and the initial dose of infection, as group V_{7+6} did not have the highest survival rate.

Analysis of Sequenced Data Quality

Nine cDNA libraries were constructed for Illumina sequencing and the data processing results are summarized in **Table 1**. After assembly, the length of these transcripts ranged from 201 to 16,691 bp with an average length of 885 bp, and the N50 length was 1,311 bp. The values of the Q30 were all > 95.9% and the GC percentage of the clean reads in the nine libraries ranged from 45.30% to 46.60%, suggesting a good assembled quality and sufficient for subsequent analysis. Raw sequencing data were archived under the accession ID SRR13931757-SRR13931765 in the NCBI Sequence Read Archive.

Cluster Analysis and Pairwise Comparisons

In order to comprehensively understand the distribution of different genes, a hierarchical cluster analysis was performed for all DEGs (**Supplementary File 1**). As shown in **Figure 3A**, the stimulus group sample, including L12 and LL12, formed one cluster, and were then grouped with C12. When compared with C12, 1092 DEGs were identified in L12 (289 up-regulated and 803 down-regulated genes) and 1,035 DEGs were identified in LL12 (415 up-regulated and 620 down-regulated genes). In addition, 304 DEGs were detected between L12 and LL12, including 226 up-regulated and 78 down-regulated genes (**Figure 3B**).

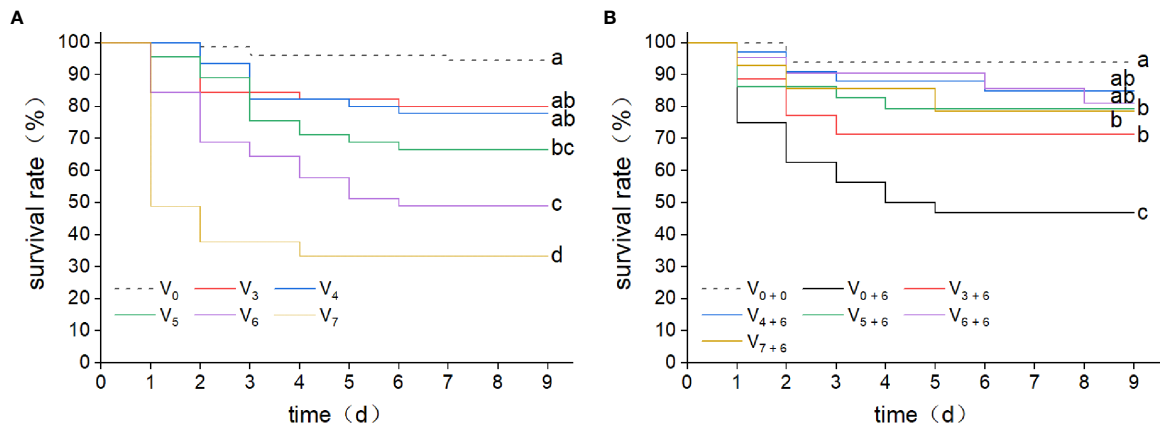

FIGURE 2 | Kaplan-Meier survival curves for abalone after two consecutive infections with *V. harveyi*. **(A)** Kaplan-Meier survival curves were generated from abalone following a first injection with *V. harveyi* at concentrations of either 1.42×10^3 CFU mL^{-1} (V_3), 1.42×10^4 CFU mL^{-1} (V_4), 1.42×10^5 CFU mL^{-1} (V_5), 1.42×10^6 CFU mL^{-1} (V_6) or 1.42×10^7 CFU mL^{-1} (V_7), or with SSW as control (V_0). A total of 360 abalone were used in each group (120 per tank). Mortalities were monitored for nine days after infection. Different letter labels next to the graph lines indicate statistically significant differences among treatments ($p < 0.05$, log-rank test, n = 360). **(B)** Kaplan-Meier survival curves were generated from abalone primed by injection with *V. harveyi* at five different concentrations, or with SSW, followed by a second injection with *V. harveyi* at 1.58×10^6 CFU mL^{-1} (V_{3+6}, V_{4+6}, V_{5+6}, V_{6+6} V_{7+6} and V_{0+6}) or with a second SSW injection as control (V_{0+0}). A total of 90 abalone were used in each group (30 per tank). Mortalities were monitored for nine days after infection. Different letter labels next to the graph lines indicate statistically significant differences among treatments ($p < 0.05$, log-rank test, n = 90).

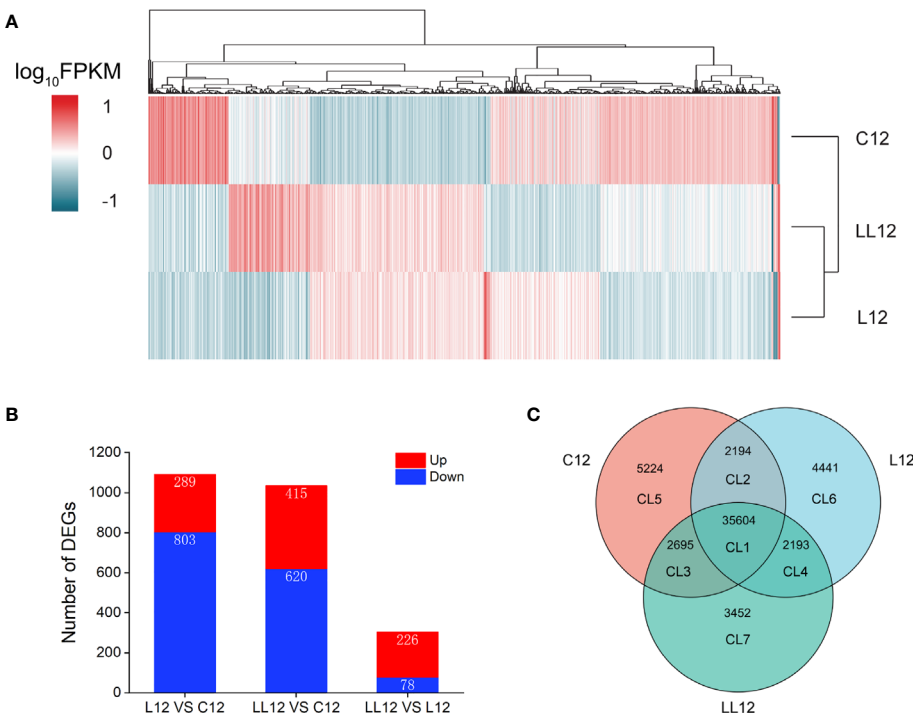

FIGURE 3 | Overview of the expression analysis for C12, L12 and LL12. **(A)** Hierarchical clustering heat map constructed based on DEGs. Each row represents a group, each column represents a DEG. The expression level of each DEG is shown as the $\log_{10}$(FPKM) value. Red and blue gradients indicate increased and decreased transcript abundance, respectively. **(B)** Number of DEGs in the different groups. **(C)** Venn diagram showing the number of commonly and uniquely expressed genes among different groups.

Venn Analysis of Expressed Genes Among Different Groups

In order to better study the DEGs, a Venn diagram was constructed base on unigenes of different groups, and 7 clusters (CLs) were generated (**Figure 3C**). CL1 showed co-expressed genes in all groups. CL2, CL3 and CL4 showed co-expressed genes between groups. CL5, CL6 and CL7 showed specific expressed genes in each group. DEGs were identified in CL1, CL2, CL3 and CL4. A total of 1174 DEGs were identified in CL1 and they were further studied (**Supplementary File 2**). In CL2, four nonimmune related DEGs were identified. Thirty DEGs were generated in CL3; however, only one was an immune-related gene; thus, no further analysis was performed. Finally, no DEGs were found in CL4.

Patterns of DEGs in CL1

The DEGs in CL1 from two consecutive *V. harveyi* infections were divided into 6 subclusters based on a K-means clustering algorithm. As shown in **Figure 4A**, similar patterns in gene expression were clustered together. In subcluster 1 and 4, genes were continuously down-regulated after the first and second infection. In subcluster 6, genes decreased after the first infection and increased after the second infection; however, the expression level was lower than that in the control group. Subcluster 2 and 5 represented a class of genes that were persistently highly expressed. In subcluster 3, genes were down-regulated after one infection; however, in the second infection, the expression level increased and exceeded the control group. In view of the expression pattern, the genes in subclasses 2, 3 and 5 appeared to be the most promising possible sources of immune priming, and they were analyzed in depth.

Immune Priming Related Genes in CL1

PRRs can bind to pathogen-associated molecular patterns (PAMPs) and are thought to be able to establish immunological memory. Eight PRRs were identified as up-regulated after the second immune challenge, including perlucin 4, C1q domain containing protein 2, scavenger receptor class B-like protein, deleted in malignant brain tumors 1 protein-like, TLR, TLR2, TLR3 and TLR8 (**Figure 4B**). Some immune-related pathways including the calcium signaling pathway and pathways associated with pathogen clearance (lysosome, phagosome, peroxisome, and Fc gamma R-mediated phagocytosis) were also activated when subjected to a continuous stimulus (**Figure 4C**). In addition, some immune effector factors including cytochrome P450 1B1-like, glutathione S-transferase 6, monomeric sarcosine oxidase, low affinity immunoglobulin epsilon Fc receptor, and lysozyme were also increased in the second infection (**Figure 4D**).

Pathway Analysis of CL6 and CL7

All genes collected in CL6 and CL7 were subjected to pathway analysis, respectively. As shown in **Figure 5**, six categories of the

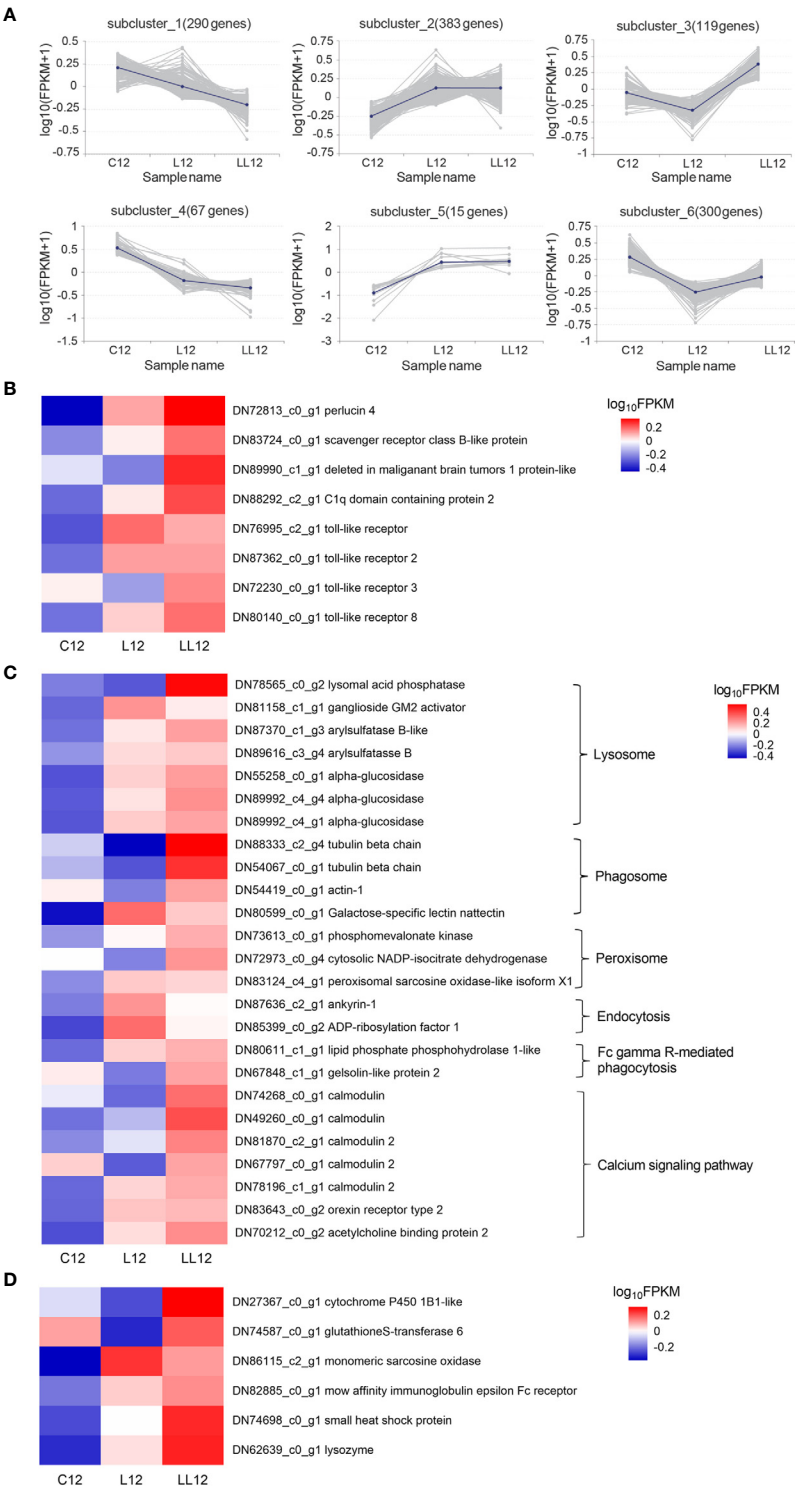

FIGURE 4 | Analysis of differentially expressed genes. **(A)** Patterns of DEGs in CL1 by K-means clustering analysis. The lines represent the expression tendency of DEGs. The number of genes represented by each pattern is shown above the graphs. **(B)** The DEGs involved in the PRRs; **(C)** The DEGs involved in the immune-related KEGG. **(D)** The DEGs involved in the immune effectors. The heatmap shows $\log_{10}$ (FPKM) values of DEGs among different groups.

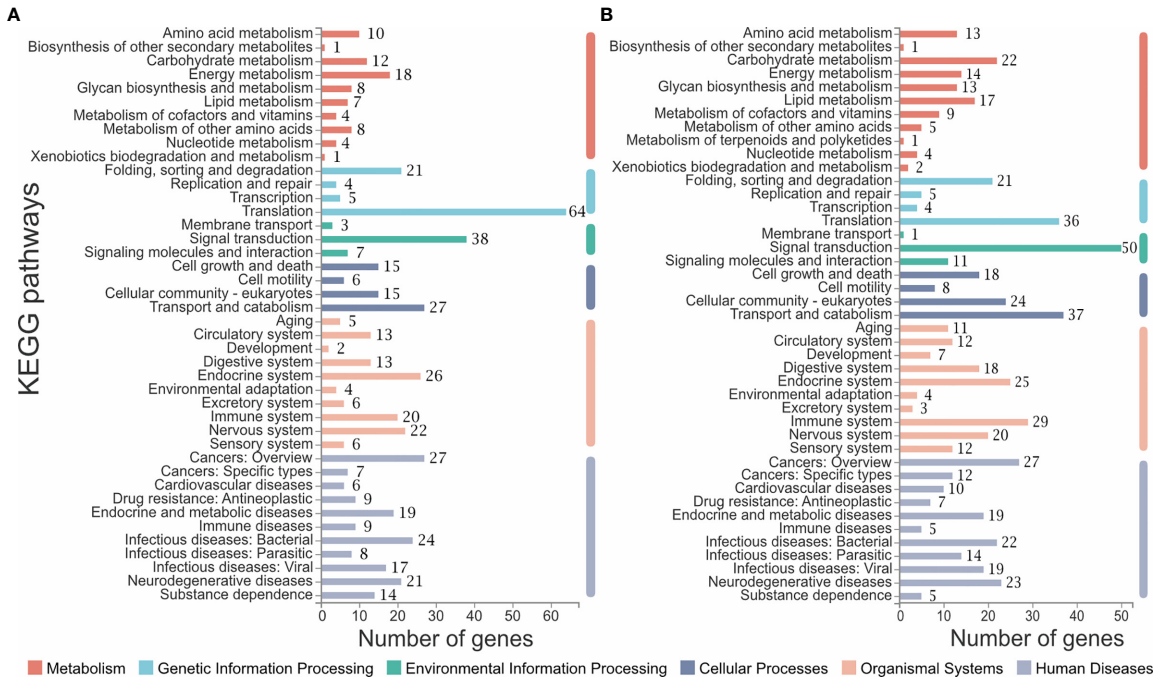

FIGURE 5 | Pathway analysis of CL6 and CL7. **(A)** Pathways constituted in CL6; **(B)** Pathways constituted in CL7. The number of genes belonging to each pathway are labeled on the right of the bar.

pathways were divided into metabolism, genetic information processing, environmental information processing, cellular processes, organismal systems and human diseases. There were different gene numbers within the same pathway in CL6 and CL7. Some pathways such as carbohydrate metabolism, lipid metabolism, signal transduction, digestive system and immune system had more gene members in CL7 than in CL6. Furthermore, immune-related pathways were analyzed in depth. As shown in **Table 3**, some pathways associated with pathogen clearance had more gene numbers in CL7 than in CL6, such as lysosome, phagosome, ubiquitin-mediated proteolysis, and autophagy-animal. Other signaling pathways such as the Ras signaling pathway, NOD-like receptor signaling pathway, MAPK signaling pathway, Toll-like receptor signaling pathway and Calcium signaling pathway also showed consistent results.

Validation of RNA-Seq Data by qPCR

In order to evaluate the accuracy of the RNA-seq results, 12 genes including TLR, TLR2, TLR8, SR-BI, XBP, CatB, TNFSF6, Lgmn, ZIP10, PGRP-SC2, Px5 and TNFSF6-x2 from DEG libraries were analyzed by qRT-PCR. Fold changes were compared with the DEG analysis results. As shown in **Figure 6**, the expression trends of selective genes by qRT-PCR were consistent with the DEG analysis results, and the Spearman's correlation was 0.875 (p value < 0.001), which indicated the reliability of the transcriptome data.

DISCUSSION

It was reported that immune priming was related to exposure dose and time post priming (2), only certain concentrations were able to induce a primed response, and low dose may lead to less obvious effects (23, 32). In the present study, the abalone were first injected with five different concentrations of *V. harveyi* diluents, which conferred the infected abalone with higher immune protection during subsequent re-exposure. We observed that different initial infection doses of *V. harveyi* provided different levels of protection; i.e., priming with the lowest initial infection dose provided the lowest immune protection, although the highest initial infection dose did not provide the highest immune protection (minimal immune protection was observed after priming with 1.42×10^3 CFU mL^{-1} of *V. harveyi*, but 1.42×10^7 CFU mL^{-1} did not offer maximum immune protection). Although enhanced immune protection has been found in many invertebrates, persistent immune protection time varied according to the invertebrate and pathogen examined (33–35). In mollusks, infection with *V. anguillarum* can offer *Chlamys farreri* immune protection for up to one week (17, 36). In *Biomphalaria glabrata*, immunological memory to *Schistosoma mansoni* was maintained for the rest of the animal's lifespan (37, 38). In poly(I:C) primed *Crassostrea gigas*, resistance to Ostreid herpesvirus 1 (OsHV-1) could last for more than 5 months (39); and this protection was even transmitted to offspring (40, 41). In the current study, the time interval between priming and re-exposure

TABLE 3 | Gene numbers in the immune-related pathways in CL6 and CL7.

pathway ID	Description	CL6 numbers	CL7 numbers
map04142	Lysosome	9	13
map04210	Apoptosis	7	11
map04510	Focal adhesion	7	10
map04145	Phagosome	10	10
map04014	Ras signaling pathway	4	9
map04621	NOD-like receptor signaling pathway	3	8
map04010	MAPK signaling pathway	3	7
map04120	Ubiquitin mediated proteolysis	6	7
map04620	Toll-like receptor signaling pathway	1	6
map04020	Calcium signaling pathway	2	6
map04140	Autophagy - animal	2	6
map04670	Leukocyte transendothelial migration	4	6
map04068	FoxO signaling pathway	0	5
map04750	Inflammatory mediator regulation of TRP channels	3	5
map04610	Complement and coagulation cascades	0	4
map04146	Peroxisome	1	4
map04150	mTOR signaling pathway	1	4
map04664	Fc epsilon RI signaling pathway	0	3
map04650	Natural killer cell mediated cytotoxicity	1	3
map04666	Fc gamma R-mediated phagocytosis	2	2
map04062	Chemokine signaling pathway	2	2
map04144	Endocytosis	9	5
map04151	PI3K-Akt signaling pathway	7	4
map04390	Hippo signaling pathway	6	5
map04024	cAMP signaling pathway	7	6

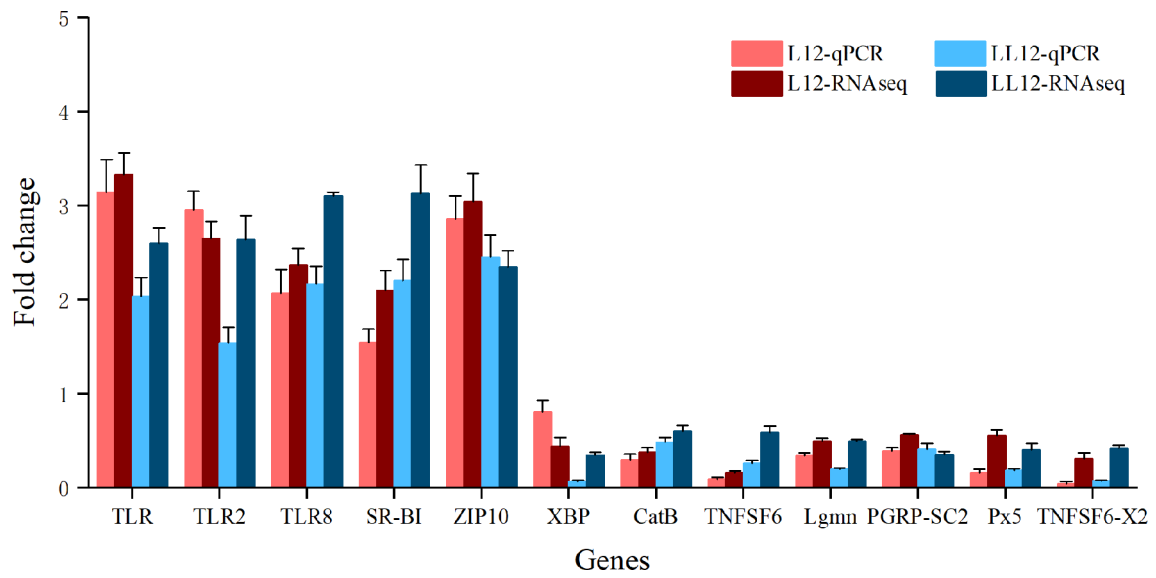

FIGURE 6 | Quantitative RT-PCR validation of 12 genes that are differentially expressed after two successive infections. The x-axis is the gene name and the y-axis represents the fold change in gene expression compared to the control. Data are represented as mean ± SD for three biological replicates.

was 15 days. Whether enhanced immune protection can last for longer time periods requires further research. However, in other species of abalone, it was reported that improved antibacterial response was induced within 25 days after injection of *V. fluvialis* in *H. discus hannai* (42). The appearance of a natural resistant population of the European abalone indicated that immune priming of abalone has strong plasticity, and functions within and across generations (26).

Previous studies have suggested that the formation of immune memory is related to the diversity of PRRs, the synergistic interactions between receptors and the expression level of receptors (43). In this study, PRRs in CL1 including perlucin 4,

C1q domain containing protein 2, scavenger receptor class B-like protein, deleted in malignant brain tumors 1 protein-like, and 4 TLRs showed increased expression after re-exposure to *V. harveyi*. C1q domain containing proteins can bind to LPS, PGN, polyI:C, beta-glucan, mannan, and yeast-glycan, giving them a broader bacterial agglutinating spectrum, and powerful function in the recognition strategy. In addition, they can act as opsonins to enhance phagocytic activity (44–46). Scavenger receptors (SRs) are major endocytic receptors that can bind Gram-negative and Gram-positive bacteria to promote hemocyte phagocytosis (47, 48). Perlucin is a typical C-type lectin, which can directly agglutinate bacterial pathogens to restrict their spread in plasma, and is involved in regulating the innate immunity by regulating phagocytosis and AMP expression (49). Toll and toll-like receptors are involved in pathogen recognition in plants, invertebrates and vertebrates (50). In Drosophila, the toll pathway was reported to regulate hemocyte proliferation (51), antimicrobial peptide expression (52), and initiate a systemic response in which hemocytes are mobilized and activated (53); more importantly, specific immune priming requires the toll pathway (19). In mollusks, a number of TLRs have been identified in various species, including hard clam (54), mussels (55, 56) and oysters (57, 58). TLRs were highly expressed in molluscan hemocytes and the TLR pathway was suggested to play a central role in initiating the cellular response to infection (59). It has been reported that TLR signaling is involved in enhanced immune protection of oysters against pathogen re-infection (60). In this study, the increased expression of PRRs suggested their contribution to improved immune protection during the re-exposure of abalone. Moreover, synergistic interactions may exist between different PRRs to enhance pathogen clearance.

In invertebrates, cellular immune responses are performed by hemocytes. Phagocytosis is the core defense mechanism for hemocytes to eliminate external invaders (14, 61). Many studies have shown that phagocytosis is necessary for the evaluation of immune memory in invertebrates. Studies have reported that specific primed immune responses of Drosophila (19) and silkworm (18, 62) were dependent on phagocytes. In mollusks, the total hemocyte count and phagocytic activity were increased after secondary infection in snails (63), scallop (36) and oysters (20, 64). In the present study, we demonstrated the importance of phagocytosis from a molecular perspective, as some genes in CL1 involved in lysosome, phagosome, endocytosis and Fc gamma R-mediated phagocytosis had higher expression levels in secondary infection. In addition, among the specifically expressed genes, CL7 contained more gene annotations to phagocytosis-related pathways than CL6. In oyster, sequencing results also showed that Fc gamma-mediated phagocytosis and ubiquitin-mediated proteolysis were significantly enriched, and phagocytosis was suggested to have a key role in second immune protection (60). In addition, the activation of immune-related pathways in CL4 also plays an important role in pathogen clearance (**Supplementary File 3**). With the exception of the classical immune-related pathway, some genes involved in the calcium signaling pathway were also significantly up-regulated in the present study. Calcium signaling is critical for diverse biological processes including fertilization, differentiation, proliferation and gene transcription (65). Calcium signaling also plays a vital role in immune function (66). Weavers et al. (67) demonstrated that calcium bursts mediate molecular memory generated by corpse engulfment by Drosophila macrophages. In addition, C1q domain containing proteins, scavenger receptors and perlucin functionally promote phagocytosis. Thus, it can be speculated that phagocytosis plays an important role in preventing re-infection of the same pathogen in abalone.

Effector factors are the most basic molecules, and are the main agents involved in the elimination of pathogens. Of these factors, antimicrobial peptides (AMPs) constitute the first line of host defense against pathogen infection, and are crucial components of the innate immune system in mollusks (68). To date, several types of AMPs have been identified and characterized from mollusks, including mytilins, myticins, mytimycins, mytimacins, defensins, big defensins, histones, lysozymes, abhisin and molluscidin (69–75). In marine mollusks, AMPs can bind the bacterial membrane directly and kill the invading bacterial pathogens by membrane disruption (76). In this study, only lysozyme in CL1 was found to be notably up-regulated in secondary infection. This may have been due to the sampling time points, as not all AMPs transcripts were increased 12 h after pathogen infection (77–79). However, AMPs are only effectors of the immune response and have a spectrum of antimicrobial characteristics, which can be induced indiscriminately, and the AMP transcripts quickly return to the baseline state after infection (19). Therefore, the AMPs are considered unable to establish a primed response (1, 18). We also found that a range of immune effectors associated with detoxification and antioxidant stress in CL1 were significantly increased during re-infection, including cytochrome P450 1B1-like, glutathione S-transferase 6 and small heat shock protein (80–82). Our sequencing results showed that the enhanced immune protection after secondary infection was not only due to the role of AMPs, but also involves the synergistic effect of multiple immune effectors.

In mammals, there is increasing evidence that trained immunity involves metabolic regulation such as glycolysis, oxidative phosphorylation, fatty acid and amino acid metabolism, which endows innate immune cells with the ability to respond more strongly to a second stimulus (83). Glycolysis, an alternative form of glucose metabolism, can produce ATP faster and it is thought to play a key role in immunity (84). Induction of glycolysis has recently been shown to be crucial for the initiation of trained immunity in human volunteers after BCG vaccination (85). Epigenetic modification also plays an important role in the establishment of innate immune memory. Several metabolites of glycolysis and the TCA cycle are also co-factors for epigenetic enzymes (86). Fatty acids can activate innate immune pathways, amino acids are the basic chemical building blocks during biogenesis, lipid metabolism and amino acid metabolism, and were proved to be necessary for the induction of innate immune memory (83, 87). In this study, we also found that many genes involved in glycolysis, fatty acid and amino acid metabolism were significantly up-regulated in CL1 (**Supplementary File 4**), and

more genes were found in CL7 than in CL6 (**Figure 5**; **Supplementary File 5**). This suggested that metabolic pathways also played a role in abalone immune priming. In addition, it was found that innate memory in macrophages could polarize other neighboring cells in ways that drive antibacterial, Th17 and M1 responses (88). This suggested that intercellular signal transduction played an important role in bacterial clearance in re-infections. The results in **Table 3** and **Figure 5** also demonstrated this, as more genes were annotated to signal transduction in CL7.

In summary, in the present study we demonstrated that an infection enhanced abalone immunity to secondary infection with the same pathogen, although this protection was not linearly correlated with the initial infection dose. Comparative transcriptome analysis has improved our understanding of the mechanism of enhanced immune protection in abalone. Increased immunity in abalone was due to the synergistic effect of the recognition of a variety of pattern recognition receptors, phagocytosis of hemocytes, detoxification and anti-oxidation of immune effectors, the enhancement of metabolism, and so on. The study on the mechanism of immune protection enhancement of abalone carried out in this study will enrich the content of invertebrate immunology, and contribute to a deeper understanding of the diversity of invertebrate immune priming mechanisms and the evolutionary process of the invertebrate immune system.

DATA AVAILABILITY STATEMENT

The datasets generated for this study can be found in the NCBI Short Read Archive database under the accession ID SRR13931757-SRR13931765.

ETHICS STATEMENT

The animal study was reviewed and approved by the Animal Care and Ethics Committee of South China Sea Fisheries Research Institute, Chinese Academy of Fishery Sciences.

AUTHOR CONTRIBUTIONS

TY and LY conceived, designed the experiment, and wrote the manuscript. TY and JL performed the experiments. CB and ZX analyzed the data. All authors contributed to the article and approved the submitted version.

FUNDING

This work was supported by grants from the National Key R&D Program of China (2019YFD0900105), the Science and Technology Planning Project of Guangzhou (202002030488), the China Agriculture Research System of MOF and MARA, the Central Public-interest Scientific Institution Basal Research Fund, CAFS (2020TD42 and 2021SD05), the Science and Technology Planning Project of Jieyang (2019029 and sxm029), the Professorial and Doctoral Scientific Research Foundation of Huizhou University (2020JB065), the Shellfish and Large Algae Industry Innovation Team Project of Guangdong Province (2020KJ146) and the Guangdong Rural Revitalization Strategy Special Funds (Fishery Industry Development) (YueCaiNong[2020]4).

SUPPLEMENTARY MATERIAL

The Supplementary Material for this article can be found online at: https://www.frontiersin.org/articles/10.3389/fimmu.2021.685896/full#supplementary-material

REFERENCES

1. Cooper D, Eleftherianos I. Memory and Specificity in the Insect Immune System: Current Perspectives and Future Challenges. *Front Immunol* (2017) 8:539. doi: 10.3389/fimmu.2017.00539
2. Milutinović B, Kurtz J. Immune Memory in Invertebrates. *Semin Immunol* (2016) 28:328–42. doi: 10.1016/j.smim.2016.05.004
3. Reimer-Michalski E-M, Conrath U. Innate Immune Memory in Plants. *Semin Immunol* (2016) 28:319–27. doi: 10.1016/j.smim.2016.05.006
4. Glass Z, Lee M, Li Y, Xu Q. Engineering the Delivery System for CRISPR-Based Genome Editing. *Trends Biotechnol* (2018) 36:173–85. doi: 10.1016/j.tibtech.2017.11.006
5. Barrangou R, Marraffini LA. CRISPR-Cas Systems: Prokaryotes Upgrade to Adaptive Immunity. *Mol Cell* (2014) 54:234–44. doi: 10.1016/j.molcel.2014.03.011
6. Levasseur A, Bekliz M, Chabrière E, Pontarotti P, La Scola B, Raoult D. MIMIVIRE Is a Defence System in Mimivirus That Confers Resistance to Virophage. *Nature* (2016) 531:249–52. doi: 10.1038/nature17146
7. Netea MG. Training Innate Immunity: The Changing Concept of Immunological Memory in Innate Host Defence. *Eur J Clin Invest* (2013) 43:881–4. doi: 10.1111/eci.12132
8. Netea MG, Quintin J, van der Meer JWM. Trained Immunity: A Memory for Innate Host Defense. *Cell Host Microbe* (2011) 9:355–61. doi: 10.1016/j.chom.2011.04.006
9. Netea MG, Schlitzer A, Placek K, Joosten LAB, Schultze JL. Innate and Adaptive Immune Memory: An Evolutionary Continuum in the Host's Response to Pathogens. *Cell Host Microbe* (2019) 25:13–26. doi: 10.1016/j.chom.2018.12.006
10. Kurtz J. Specific Memory Within Innate Immune Systems. *Trends Immunol* (2005) 26:186–92. doi: 10.1016/j.it.2005.02.001
11. Little TJ, Kraaijeveld AR. Ecological and Evolutionary Implications of Immunological Priming in Invertebrates. *Trends Ecol Evol* (2004) 19:58–60. doi: 10.1016/j.tree.2003.11.011
12. Kachroo A, Robin GP. Systemic Signaling During Plant Defense. *Curr Opin Plant Biol* (2013) 16:527–33. doi: 10.1016/j.pbi.2013.06.019
13. Jaskiewicz M, Conrath U, Peterhänsel C. Chromatin Modification Acts as a Memory for Systemic Acquired Resistance in the Plant Stress Response. *EMBO Rep* (2011) 12:50–5. doi: 10.1038/embor.2010.186
14. Syed Musthaq SK, Kwang J. Reprint of "Evolution of Specific Immunity in Shrimp – A Vaccination Perspective Against White Spot Syndrome Virus." *Dev Comp Immunol* (2015) 48:342–53. doi: 10.1016/j.dci.2014.07.016
15. Pinaud S, Portela J, Duval D, Nowacki FC, Olive M-A, Allienne J-F, et al. A Shift From Cellular to Humoral Responses Contributes to Innate Immune Memory in the Vector Snail *Biomphalaria glabrata*. *PLoS Pathog* (2016) 12: e1005361. doi: 10.1371/journal.ppat.1005361
16. Cong M, Song L, Qiu L, Li C, Wang B, Zhang H, et al. The Expression of Peptidoglycan Recognition Protein-S1 Gene in the Scallop *Chlamys farreri* Was Enhanced After a Second Challenge by *Listonella anguillarum*. *J Invertebr Pathol* (2009) 100:120–2. doi: 10.1016/j.jip.2008.10.004
17. Wang J, Wang L, Yang C, Jiang Q, Zhang H, Yue F, et al. The Response of mRNA Expression Upon Secondary Challenge With *Vibrio anguillarum* Suggests the Involvement of C-Lectins in the Immune Priming of Scallop *Chlamys farreri*. *Dev Comp Immunol* (2013) 40:142–7. doi: 10.1016/j.dci.2013.02.003

18. Wu G, Li M, Liu Y, Ding Y, Yi Y. The Specificity of Immune Priming in Silkworm, *Bombyx mori*, Is Mediated by the Phagocytic Ability of Granular Cells. *J Insect Physiol* (2015) 81:60–8. doi: 10.1016/j.jinsphys.2015.07.004
19. Pham LN, Dionne MS, Shirasu-Hiza M, Schneider DS. A Specific Primed Immune Response in Drosophila Is Dependent on Phagocytes. *PLoS Pathog* (2007) 3:e26. doi: 10.1371/journal.ppat.0030026
20. Li Y, Song X, Wang W, Wang L, Yi Q, Jiang S, et al. The Hematopoiesis in Gill and Its Role in the Immune Response of Pacific Oyster *Crassostrea gigas* Against Secondary Challenge With *Vibrio splendidus*. *Dev Comp Immunol* (2017) 71:59–69. doi: 10.1016/j.dci.2017.01.024
21. Cime-Castillo J, Arts RJW, Vargas-Ponce de León V, Moreno-Torres R, Hernández-Martínez S, Recio-Totoro B, et al. DNA Synthesis Is Activated in Mosquitoes and Human Monocytes During the Induction of Innate Immune Memory. *Front Immunol* (2018) 9:2834. doi: 10.3389/fimmu.2018.02834
22. Castro-Vargas C, Linares-López C, López-Torres A, Wrobel K, Torres-Guzmán JC, Hernández GAG, et al. Methylation on RNA: A Potential Mechanism Related to Immune Priming Within But Not Across Generations. *Front Microbiol* (2017) 8:473. doi: 10.3389/fmicb.2017.00473
23. Wu G, Yi Y, Lv Y, Li M, Wang J, Qiu L. The Lipopolysaccharide (LPS) of *Photorhabdus luminescens* TT01 Can Elicit Dose- and Time-Dependent Immune Priming in *Galleria mellonella larvae*. *J Invertebr Pathol* (2015) 127:63–72. doi: 10.1016/j.jip.2015.03.007
24. González-Tokman DM, González-Santoyo I, Lanz-Mendoza H, Córdoba Aguilar A. Territorial Damselflies Do Not Show Immunological Priming in the Wild. *Physiol Entomol* (2010) 35:364–72. doi: 10.1111/j.1365-3032.2010.00752.x
25. Reber A, Chapuisat M. No Evidence for Immune Priming in Ants Exposed to a Fungal Pathogen. *PLoS One* (2012) 7:e35372. doi: 10.1371/journal.pone.0035372
26. Dubief B, Nunes FLD, Basuyaux O, Paillard C. Immune Priming and Portal of Entry Effectors Improve Response to Vibrio Infection in a Resistant Population of the European Abalone. *Fish Shellfish Immunol* (2017) 60:255–64. doi: 10.1016/j.fsi.2016.11.017
27. Grabherr MG, Haas BJ, Yassour M, Levin JZ, Thompson DA, Amit I, et al. Full-Length Transcriptome Assembly From RNA-Seq Data Without a Reference Genome. *Nat Biotechnol* (2011) 29:644–52. doi: 10.1038/nbt.1883
28. Conesa A, Gotz S, Garcia-Gomez JM, Terol J, Talon M, Robles M. Blast2GO: A Universal Tool for Annotation, Visualization and Analysis in Functional Genomics Research. *Bioinformatics* (2005) 21:3674–6. doi: 10.1093/bioinformatics/bti610
29. Li B, Dewey CN. RSEM: Accurate Transcript Quantification From RNA-Seq Data With or Without a Reference Genome. *BMC Bioinf* (2011) 12:323. doi: 10.1186/1471-2105-12-323
30. Anders S, Huber W. Differential Expression Analysis for Sequence Count Data. *Genome Biol* (2010) 11:R106. doi: 10.1186/gb-2010-11-10-r106
31. Livak KJ, Schmittgen TD. Analysis of Relative Gene Expression Data Using Real-Time Quantitative PCR and the $2^{-\Delta\Delta ct}$ Method. *Methods* (2001) 25:402–8. doi: 10.1006/meth.2001.1262
32. Wu G, Zhao Z, Liu C, Qiu L. Priming *Galleria mellonella* (Lepidoptera: Pyralidae) Larvae With Heat-Killed Bacterial Cells Induced an Enhanced Immune Protection Against *Photorhabdus luminescens* TT01 and the Role of Innate Immunity in the Process. *J Econ Entomol* (2014) 107:559–69. doi: 10.1603/EC13455
33. Thomas AM, Rudolf VHW. Challenges of Metamorphosis in Invertebrate Hosts: Maintaining Parasite Resistance Across Life-History Stages. *Ecol Entomol* (2010) 35:200–5. doi: 10.1111/j.1365-2311.2009.01169.x
34. Haine ER, Moret Y, Siva-Jothy MT, Rolff J. Antimicrobial Defense and Persistent Infection in Insects. *Science* (2008) 322:1257–9. doi: 10.1126/science.1165265
35. Moret Y, Siva-Jothy MT. Adaptive Innate Immunity? Responsive-Mode Prophylaxis in the Mealworm Beetle, *Tenebrio molitor*. *Proc R Soc London Ser B Biol Sci* (2003) 270:2475–80. doi: 10.1098/rspb.2003.2511
36. Cong M, Song L, Wang L, Zhao J, Qiu L, Li L, et al. The Enhanced Immune Protection of Zhikong Scallop *Chlamys farreri* on the Secondary Encounter with *Listonella anguillarum*. *Comp Biochem Physiol Part B Biochem Mol Biol* (2008) 151:191–6. doi: 10.1016/j.cbpb.2008.06.014
37. Pinaud S, Portet A, Allienne JF, Belmudes L, Saint-Beat C, Arancibia N, et al. Molecular Characterisation of Immunological Memory Following Homologous or Heterologous Challenges in the Schistosomiasis Vector Snail, *Biomphalaria glabrata*. *Dev Comp Immunol* (2019) 92:238–52. doi: 10.1016/j.dci.2018.12.001
38. Portela J, Duval D, Rognon A, Galinier R, Boissier J, Coustau C, et al. Evidence for Specific Genotype-Dependent Immune Priming in the Lophotrochozoan *Biomphalaria glabrata* Snail. *J Innate Immun* (2013) 5:261–76. doi: 10.1159/000345909
39. Lafont M, Petton B, Vergnes A, Pauletto M, Segarra A, Gourbal B, et al. Long-Lasting Antiviral Innate Immune Priming in the Lophotrochozoan Pacific Oyster, *Crassostrea gigas*. *Sci Rep* (2017) 7:13143. doi: 10.1038/s41598-017-13564-0
40. Lafont M, Goncalves P, Guo X, Montagnani C, Raftos D, Green T. Transgenerational Plasticity and Antiviral Immunity in the Pacific Oyster (*Crassostrea Gigas*) Against Ostreid Herpesvirus 1 (OsHV-1). *Dev Comp Immunol* (2019) 91:17–25. doi: 10.1016/j.dci.2018.09.022
41. Green TJ, Helbig K, Speck P, Raftos DA. Primed for Success: Oyster Parents Treated With Poly(I:C) Produce Offspring With Enhanced Protection Against Ostreid Herpesvirus Type I Infection. *Mol Immunol* (2016) 78:113–20. doi: 10.1016/j.molimm.2016.09.002
42. Li T, Ding M, Xiang J, Liu R. Immunnological Studies on *Haliotis discus hannai* With *Vibrio Fluvialis-II*. *Oceanol Limnol Sin* (1997) 28:27–32. doi: CNKI:SUN:HYFZ.0.1997-01-004
43. Schulenburg H, Boehnisch C, Michiels NK. How do Invertebrates Generate a Highly Specific Innate Immune Response? *Mol Immunol* (2007) 44:3338–44. doi: 10.1016/j.molimm.2007.02.019
44. Wang L, Wang L, Kong P, Yang J, Zhang H, Wang M, et al. A Novel C1qDC Protein Acting as Pattern Recognition Receptor in Scallop *Argopecten irradians*. *Fish Shellfish Immunol* (2012) 33:427–35. doi: 10.1016/j.fsi.2012.05.032
45. Kong P, Zhang H, Wang L, Zhou Z, Yang J, Zhang Y, et al. AiC1qDC-1, A Novel Gc1q-Domain-Containing Protein From Bay Scallop *Argopecten irradians* With Fungi Agglutinating Activity. *Dev Comp Immunol* (2010) 34:837–46. doi: 10.1016/j.dci.2010.03.006
46. Kishore U, Ghai R, Greenhough TJ, Shrive AK, Bonifati DM, Gadjeva MG, et al. Structural and Functional Anatomy of the Globular Domain of Complement Protein C1q. *Immunol Lett* (2004) 95:113–28. doi: 10.1016/j.imlet.2004.06.015
47. Tang M, Li X, Yang L, Wang Q, Li W. A Class B Scavenger Receptor Mediates Antimicrobial Peptide Secretion and Phagocytosis in Chinese Mitten Crab (*Eriocheir Sinensis*). *Dev Comp Immunol* (2020) 103:103496. doi: 10.1016/j.dci.2019.103496
48. Wu YM, Yang L, Li XJ, Li L, Wang Q, Li WW. A Class B Scavenger Receptor From *Eriocheir sinensis* (EsSR-B1) Restricts Bacteria Proliferation by Promoting Phagocytosis. *Fish Shellfish Immunol* (2017) 70:426–36. doi: 10.1016/j.fsi.2017.09.034
49. Bi J, Ning M, Xie X, Fan W, Huang Y, Gu W, et al. A Typical C-Type Lectin, Perlucin-Like Protein, Is Involved in the Innate Immune Defense of Whiteleg Shrimp *Litopenaeus vannamei*. *Fish Shellfish Immunol* (2020) 103:293–301. doi: 10.1016/j.fsi.2020.05.046
50. Bell JK, Mullen GED, Leifer CA, Mazzoni A, Davies DR, Segal DM. Leucine-Rich Repeats and Pathogen Recognition in Toll-Like Receptors. *Trends Immunol* (2003) 24:528–33. doi: 10.1016/S1471-4906(03)00242-4
51. Qiu P, Pan PC, Govind S. A Role for the Drosophila Toll/Cactus Pathway in Larval Hematopoiesis. *Development* (1998) 125:1909–20. doi: 10.1007/s004290050153
52. Tzou P, Reichhart J-M, Lemaitre B. Constitutive Expression of a Single Antimicrobial Peptide Can Restore Wild-Type Resistance to Infection in Immunodeficient *Drosophila* Mutants. *Proc Natl Acad Sci* (2002) 99:2152–7. doi: 10.1073/pnas.042411999
53. Yang H, Hultmark D. Tissue Communication in a Systemic Immune Response of Drosophila. *Fly (Austin)* (2016) 10:115–22. doi: 10.1080/19336934.2016.1182269
54. Perrigault M, Tanguy A, Allam B. Identification and Expression of Differentially Expressed Genes in the Hard Clam, *Mercenaria mercenaria*, in Response to Quahog Parasite Unknown (QPX). *BMC Genomics* (2009) 10:377. doi: 10.1186/1471-2164-10-377
55. Philipp EER, Kraemer L, Melzner F, Poustka AJ, Thieme S, Findeisen U, et al. Massively Parallel RNA Sequencing Identifies a Complex Immune Gene Repertoire in the Lophotrochozoan *Mytilus edulis*. *PLoS One* (2012) 7:e33091. doi: 10.1371/journal.pone.0033091
56. Toubiana M, Gerdol M, Rosani U, Pallavicini A, Venier P, Roch P. Toll-Like Receptors and MyD88 Adaptors in *Mytilus*: Complete Cds and Gene Expression Levels. *Dev Comp Immunol* (2013) 40:158–66. doi: 10.1016/j.dci.2013.02.006
57. Tanguy A, Guo X, Ford SE. Discovery of Genes Expressed in Response to *Perkinsus marinus* Challenge in Eastern (*Crassostrea virginica*) and Pacific (*C. gigas*) Oysters. *Gene* (2004) 338:121–31. doi: 10.1016/j.gene.2004.05.019

58. Wang L, Zhang H, Wang M, Zhou Z, Wang W, Liu R, et al. The Transcriptomic Expression of Pattern Recognition Receptors: Insight Into Molecular Recognition of Various Invading Pathogens in Oyster *Crassostrea gigas*. *Dev Comp Immunol* (2019) 91:1–7. doi: 10.1016/j.dci.2018.09.021
59. Allam B, Raftos D. Immune Responses to Infectious Diseases in Bivalves. *J Invertebr Pathol* (2015) 131:121–36. doi: 10.1016/j.jip.2015.05.005
60. Wang W, Wang L, Liu Z, Song X, Yi Q, Yang C, et al. The Involvement of TLR Signaling and Anti-Bacterial Effectors in Enhanced Immune Protection of Oysters After *Vibrio splendidus* Pre-Exposure. *Dev Comp Immunol* (2020) 103:103498. doi: 10.1016/j.dci.2019.103498
61. Melillo D, Marino R, Italiani P, Boraschi D. Innate Immune Memory in Invertebrate Metazoans: A Critical Appraisal. *Front Immunol* (2018) 9:1915. doi: 10.3389/fimmu.2018.01915
62. Yi Y, Xu H, Li M, Wu G. RNA-Seq Profiles of Putative Genes Involved in Specific Immune Priming in *Bombyx mori* Haemocytes. *Infect Genet Evol* (2019) 74:103921. doi: 10.1016/j.meegid.2019.103921
63. de Melo ES, Brayner FA, Junior NCP, França IRS, Alves LC. Investigation of Defense Response and Immune Priming in *Biomphalaria glabrata* and *Biomphalaria straminea*, Two Species With Different Susceptibility to *Schistosoma mansoni*. *Parasitol Res* (2020) 119:189–201. doi: 10.1007/s00436-019-06495-4
64. Zhang T, Qiu L, Sun Z, Wang L, Zhou Z, Liu R, et al. The Specifically Enhanced Cellular Immune Responses in Pacific Oyster (*Crassostrea Gigas*) Against Secondary Challenge With *Vibrio splendidus*. *Dev Comp Immunol* (2014) 45:141–50. doi: 10.1016/j.dci.2014.02.015
65. Berridge MJ, Lipp P, Bootman MD. The Versatility and Universality of Calcium Signalling. *Nat Rev Mol Cell Biol* (2000) 1:11–21. doi: 10.1038/35036035
66. Rao A, Hogan PG. Calcium Signaling in Cells of the Immune and Hematopoietic Systems. *Immunol Rev* (2009) 231:5–9. doi: 10.1111/j.1600-065X.2009.00823.x
67. Weavers H, Evans IR, Martin P, Wood W. Corpse Engulfment Generates a Molecular Memory That Primes the Macrophage Inflammatory Response. *Cell* (2016) 165:1658–71. doi: 10.1016/j.cell.2016.04.049
68. Liao Z, Wang X, Liu H, Fan M, Sun J, Shen W. Molecular Characterization of a Novel Antimicrobial Peptide From *Mytilus coruscus*. *Fish Shellfish Immunol* (2013) 34:610–6. doi: 10.1016/j.fsi.2012.11.030
69. De Zoysa M, Nikapitiya C, Whang I, Lee JS, Lee J. Abhisin: A Potential Antimicrobial Peptide Derived From Histone H2A of Disk Abalone (*Haliotis Discus Discus*). *Fish Shellfish Immunol* (2009) 27:639–46. doi: 10.1016/j.fsi.2009.08.007
70. Li H, Parisi M-G, Toubiana M, Cammarata M, Roch P. Lysozyme Gene Expression and Hemocyte Behaviour in the Mediterranean Mussel, *Mytilus galloprovincialis*, After Injection of Various Bacteria or Temperature Stresses. *Fish Shellfish Immunol* (2008) 25:143–52. doi: 10.1016/j.fsi.2008.04.001
71. Seo JK, Lee MJ, Nam BH, Park NG. Cgmolluscidin, a Novel Dibasic Residue Repeat Rich Antimicrobial Peptide, Purified From the Gill of the Pacific Oyster, *Crassostrea gigas*. *Fish Shellfish Immunol* (2013) 35:480–8. doi: 10.1016/j.fsi.2013.05.010
72. Dorrington T, Villamil L, Gómez-chiarri M. Upregulation in Response to Infection and Antibacterial Activity of Oyster Histone H4. *Fish Shellfish Immunol* (2011) 30:94–101. doi: 10.1016/j.fsi.2010.09.006
73. Venier P, Varotto L, Rosani U, Millino C, Celegato B, Bernante F, et al. Insights Into the Innate Immunity of the Mediterranean Mussel *Mytilus galloprovincialis*. *BMC Genomics* (2011) 12:69. doi: 10.1186/1471-2164-12-69
74. Yao T, Lu J, Ye L, Wang J. Molecular Characterization and Immune Analysis of a Defensin From Small Abalone, *Haliotis diversicolor*. *Comp Biochem Physiol Part B Biochem Mol Biol* (2019) 235:1–7. doi: 10.1016/j.cbpb.2019.05.004
75. Gerdol M, De Moro G, Manfrin C, Venier P, Pallavicini A. Big Defensins and Mytimacins, New AMP Families of the Mediterranean Mussel *Mytilus galloprovincialis*. *Dev Comp Immunol* (2012) 36:390–9. doi: 10.1016/j.dci.2011.08.003
76. Zhang L, Yang D, Wang Q, Yuan Z, Wu H, Pei D, et al. A Defensin From Clam *Venerupis philippinarum*: Molecular Characterization, Localization, Antibacterial Activity, and Mechanism of Action. *Dev Comp Immunol* (2015) 51:29–38. doi: 10.1016/j.dci.2015.02.009
77. Yang J, Luo J, Zheng H, Lu Y, Zhang H. Cloning of a Big Defensin Gene and Its Response to *Vibrio parahaemolyticus* Challenge in the Noble Scallop *Chlamys nobilis* (Bivalve: Pectinidae). *Fish Shellfish Immunol* (2016) 56:445–9. doi: 10.1016/j.fsi.2016.07.030
78. De Zoysa M, Whang I, Lee Y, Lee S, Lee J-S, Lee J. Defensin From Disk Abalone *Haliotis discus discus*: Molecular Cloning, Sequence Characterization and Immune Response Against Bacterial Infection. *Fish Shellfish Immunol* (2010) 28:261–6. doi: 10.1016/j.fsi.2009.11.005
79. Muñoz M, Vandenbulcke F, Saulnier D, Bachère E. Expression and Distribution of Penaeidin Antimicrobial Peptides Are Regulated by Haemocyte Reactions in Microbial Challenged Shrimp. *Eur J Biochem* (2002) 269:2678–89. doi: 10.1046/j.1432-1033.2002.02934.x
80. Kao C-H, Sun C-N. *In Vitro* Degradation of Some Organophosphorus Insecticides by Susceptible and Resistant Diamondback Moth. *Pestic Biochem Physiol* (1991) 41:132–41. doi: 10.1016/0048-3575(91)90067-V
81. Wagner MA, Khanna P, Jorns MS. Structure of the Flavocoenzyme of Two Homologous Amine Oxidases: Monomeric Sarcosine Oxidase and *N* -Methyltryptophan Oxidase †. *Biochemistry* (1999) 38:5588–95. doi: 10.1021/bi982955o
82. Song L, Wang L, Zhang H, Wang M. The Immune System and Its Modulation Mechanism in Scallop. *Fish Shellfish Immunol* (2015) 46:65–78. doi: 10.1016/j.fsi.2015.03.013
83. Domínguez-Andrés J, Joosten LA, Netea MG. Induction of Innate Immune Memory: The Role of Cellular Metabolism. *Curr Opin Immunol* (2019) 56:10–6. doi: 10.1016/j.coi.2018.09.001
84. Van den Bossche J, Baardman J, Otto NA, van der Velden S, Neele AE, van den Berg SM, et al. Mitochondrial Dysfunction Prevents Repolarization of Inflammatory Macrophages. *Cell Rep* (2016) 17:684–96. doi: 10.1016/j.celrep.2016.09.008
85. Arts RJW, Moorlag SJCFM, Novakovic B, Li Y, Wang S-Y, Oosting M, et al. BCG Vaccination Protects Against Experimental Viral Infection in Humans Through the Induction of Cytokines Associated With Trained Immunity. *Cell Host Microbe* (2018) 23:89–100.e5. doi: 10.1016/j.chom.2017.12.010
86. Etchegaray J-P, Mostoslavsky R. Interplay Between Metabolism and Epigenetics: A Nuclear Adaptation to Environmental Changes. *Mol Cell* (2016) 62:695–711. doi: 10.1016/j.molcel.2016.05.029
87. Pérez-Vázquez D, Contreras-Castillo E, Licona-Limón P. Innate Immune Memory, the Missing Piece of the Immunological Response. *TIP Rev Espec en Cienc Químico-Biológicas* (2018) 21:112–23. doi: 10.22201/fesz.23958723e.2018.0.151
88. Van Belleghem JD, Bollyky PL. Macrophages and Innate Immune Memory Against *Staphylococcus* Skin Infections. *Proc Natl Acad Sci* (2018) 115:11865–7. doi: 10.1073/pnas.1816935115

Conflict of Interest: The authors declare that the research was conducted in the absence of any commercial or financial relationships that could be construed as a potential conflict of interest.

frontiers in Immunology

ORIGINAL RESEARCH
published: 09 July 2021
doi: 10.3389/fimmu.2021.656885

Global Transcriptomics Uncovers Distinct Contributions From Splicing Regulatory Proteins to the Macrophage Innate Immune Response

Allison R. Wagner[1†], Haley M. Scott[1†], Kelsi O. West[1†], Krystal J. Vail[1,2], Timothy C. Fitzsimons[1], Aja K. Coleman[1], Kaitlyn E. Carter[1], Robert O. Watson[1] and Kristin L. Patrick[1]*

[1] Department of Microbial Pathogenesis and Immunology, College of Medicine, Texas A&M Health, Bryan, TX, United States, [2] Department of Veterinary Pathobiology, Texas A&M University, College Station, TX, United States

OPEN ACCESS

Edited by:
Osamu Takeuchi,
Kyoto University, Japan

Reviewed by:
Taro Kawai,
Nara Institute of Science and Technology (NAIST), Japan
Takuya Uehata,
Kyoto University, Japan

***Correspondence:**
Kristin L. Patrick
kpatrick03@tamu.edu

[†]These authors have contributed equally to this work

Specialty section:
This article was submitted to Molecular Innate Immunity, a section of the journal Frontiers in Immunology

Received: 21 January 2021
Accepted: 01 June 2021
Published: 09 July 2021

Citation:
Wagner AR, Scott HM, West KO, Vail KJ, Fitzsimons TC, Coleman AK, Carter KE, Watson RO and Patrick KL (2021) Global Transcriptomics Uncovers Distinct Contributions From Splicing Regulatory Proteins to the Macrophage Innate Immune Response. Front. Immunol. 12:656885. doi: 10.3389/fimmu.2021.656885

Pathogen sensing *via* pattern recognition receptors triggers massive reprogramming of macrophage gene expression. While the signaling cascades and transcription factors that activate these responses are well-known, the role of post-transcriptional RNA processing in modulating innate immune gene expression remains understudied. Given their crucial role in regulating pre-mRNA splicing and other RNA processing steps, we hypothesized that members of the SR/hnRNP protein families regulate innate immune gene expression in distinct ways. We analyzed steady state gene expression and alternatively spliced isoform production in ten SR/hnRNP knockdown RAW 264.7 macrophage-like cell lines following infection with the bacterial pathogen *Salmonella enterica* serovar Typhimurium (*Salmonella*). We identified thousands of transcripts whose abundance is increased or decreased by SR/hnRNP knockdown in macrophages. Notably, we observed that SR and hnRNP proteins influence expression of different genes in uninfected versus *Salmonella*-infected macrophages, suggesting functionalization of these proteins upon pathogen sensing. Likewise, we found that knockdown of SR/hnRNPs promoted differential isoform usage (DIU) for thousands of macrophage transcripts and that these alternative splicing changes were distinct in uninfected and *Salmonella*-infected macrophages. Finally, having observed a surprising degree of similarity between the differentially expressed genes (DEGs) and DIUs in hnRNP K and U knockdown macrophages, we found that hnRNP K and U knockdown macrophages are both more restrictive to Vesicular Stomatitis Virus (VSV), while hnRNP K knockdown macrophages are more permissive to *Salmonella* Typhimurium. Based on these findings, we conclude

that many innate immune genes evolved to rely on one or more SR/hnRNPs to ensure the proper magnitude of their induction, supporting a model wherein pre-mRNA splicing is critical for regulating innate immune gene expression and controlling infection outcomes in macrophages *ex vivo*.

Keywords: pre-mRNA splicing, RNA binding protein, inflammation, hnRNP, SR protein, *Salmonella* Typhimurium

INTRODUCTION

When innate immune cells like macrophages sense pathogens, they undergo dramatic gene expression reprogramming and upregulate thousands of genes. Proper regulation of the timing and magnitude of innate immune gene induction is critical to ensure that the immune system is adequately stimulated to fend off microbial invaders without risking deleterious outcomes associated with hyperinflammation (1–3). While there has been great interest in the mechanisms of pathogen sensing and signaling events that activate transcription following an inflammatory signal, much less is known about how RNA processing steps downstream of transcription influence innate immune gene expression outcomes.

Consistent with the current "transcription-focused" paradigm of innate immune gene expression, research has categorized innate immune genes into primary and secondary response genes (4, 5). Primary, or early response genes, are readily induced upon activation of pathogen sensing cascades. Many of these transcripts reach maximal abundance as soon as 30 minutes post-pathogen sensing (6, 7). Secondary response genes require the activation of a transcription factor or expression of a cytokine before they can be maximally induced. The timing and induction of primary and secondary response genes relies on a number of tightly regulated mechanisms, including but not limited to, cooperative binding of transcription factors (8, 9), nucleosome occupancy and histone modification at promoters (10, 11), signal-dependent interactions between transcription factor subunits (12, 13), and selective interaction with the transcriptional elongation machinery (14).

Following this carefully orchestrated transcriptional activation, innate immune transcripts, like most eukaryotic transcripts, are subject to post-transcriptional regulation at the level of pre-mRNA splicing, cleavage and polyadenylation, mRNA export, and nonsense mediated decay. Pre-mRNA splicing is increasingly appreciated as an important regulatory node in cells undergoing stress or responding to extracellular triggers, including exposure to vitamins and metal ions (15), heat shock (16–18), and UV damage (19, 20). Specifically, there is growing interest in how RNA processing modulates innate immune gene expression and infection outcomes. Both *Salmonella enterica* and *Listeria monocytogenes* infection promote widespread 3'UTR shortening and exon inclusion in primary human macrophages (21) and alternative splicing and nonsense mediated decay play important roles in balancing isoform abundance of key antiviral innate immune molecules like *Oas1g* (22). Important kinetic studies of gene expression in Lipid A (a component of lipopolysaccharide)-treated primary murine macrophages showed that intron removal and release of processed innate immune transcripts from chromatin can be significantly delayed relative to onset of a gene's transcription (6, 7). While these findings argue that post-transcriptional regulatory mechanisms play a key role in controlling the timing and abundance of translation-competent immune mRNAs, we still know very little about the mechanisms that drive this regulation and the specific macrophage factors involved.

Extracellular signal transduction provides one potential mechanism through which splicing factors may be regulated during the innate immune response. Several studies have demonstrated that differential phosphorylation of SR family members triggers distinct splicing changes in cells responding to heat-shock (16–18). SR (serine-arginine rich) proteins direct the spliceosome to particular regions of a pre-mRNA by binding conserved sequences called exonic splicing enhancers or silencers. SR proteins are considered "activators" of gene expression and generally promote exon inclusion. Conversely, heterogenous nuclear ribonucleoproteins (hnRNPs) typically work to repress splicing by binding conserved sequences within introns. SR and hnRNP proteins often work cooperatively and antagonistically to control pre-mRNA splicing decisions. Recent global phosphoproteomics studies revealed that proteins involved in mRNA processing, including a number of SR and hnRNPs, are among the most differentially phosphorylated proteins in macrophages following infection with a bacterial (23, 24) or fungal pathogen (25). These findings motivated our interest to identify gene expression and alternative splicing changes dictated by SR and hnRNP family members in macrophages and to compare how these events change following infection with a bacterial pathogen.

To begin investigating how splicing regulatory proteins dictate gene expression and alternative splicing changes during the macrophage innate immune response, we took an unbiased approach and knocked down expression of ten members of the SR/hnRNP families of splicing regulatory factors. We infected these knockdown cell lines with *Salmonella enterica* serovar Typhimurium (*Salmonella*) and measured differentially expressed genes (DEGs) and differential isoform usage (DIU) in steady state RNA at a key early innate immune time point (4h post-infection). Our analysis found that these SR/hnRNPs regulate the abundance or splicing of many different cohorts of genes. Curiously, genes whose abundance changed in SR/hnRNP knockdowns (DEGs) were not also subject to differential isoform usage. While the reliance of innate immune transcripts on SR/hnRNPs did not correlate with induction level, gene length, or exon/intron number, we did observe that many primary response genes are hyperinduced in *Salmonella*-infected SR/

hnRNP knockdown macrophages, suggesting a role for splicing regulatory proteins in repressing the early innate immune response. Together, our data implicate splicing proteins in fine-tuning the magnitude of innate immune gene induction and highlight an underappreciated role for RNA binding proteins in controlling intracellular infection outcomes.

MATERIALS AND METHODS

Cell Lines and Bacterial Strains

RAW 264.7 macrophages (ATCC) (originally isolated from male BALB/c mice) were cultured at 37°C with a humidified atmosphere of 5% CO_2 in DMEM (Thermo Fisher) with 10% FBS (Sigma Aldrich) 0.5% HEPES (Thermo Fisher). For knockdown cell lines, RAW 264.7 macrophages were transduced with a pSICO-shRNA construct designed to target an exon or 3'UTR of an SR or hnRNP gene of interest. Knockdown macrophages were drug selected (hygromycin; Invitrogen) alongside a scramble (SCR) untargeted control. Each SR knockdown cell line was derived at the same time, as were the hnRNP cell lines. Knockdown efficiency of each factor was validated by RT-qPCR using exonic primer sets and the most efficient knockdown cell line (from 6 different knockdown constructs) was used for RNA-seq. The two most efficient knockdown cell lines were used for validation in **Figures 3** and **4**.

S. Typhimurium Infections

Infections with *Salmonella enterica* serovar Typhimurium were conducted by plating RAW 264.7 macrophages on tissue-cultured treated 12-well dishes at 7.5 $x10^5$ and incubated overnight. Overnight cultures of *S.* Typhimurium were diluted 1:20 in LB broth containing 0.3M NaCl and grown until they reached an OD600 of 0.9. Unless specified, cell lines at a confluency of 80% were infected with the *S.* Typhimurium strains at an MOI (multiplicity of infection) of 10 for 30 minutes in Hank's buffered salt solution (HBSS). Infected monolayers were spun for 10 minutes at 1,000rpm, washed twice in HBSS containing 100μg/ml of gentamycin, and refreshed with media plus gentamicin (10 μg/ml). After removal of supernatant, cells were lysed in Trizol (Thermo Fisher) for RNA collection and cDNA was analyzed using RT-qPCR. For colony forming units (CFUs), RAW 264.7 macrophages were plated on tissue-cultured treated 24-well dishes at 5 $x10^5$. Overnight cultures of *S.* Typhimurium were diluted to OD600 of 1.0 and cell lines at a confluency of 80% were infected at an MOI of 10 (as above). After removal of supernatant, cells were washed 2X in Phosphate-Buffered Saline (PBS). Cell were lysed in 1ml of PBS+1%TritonX100 + 0.01% SDS. Serial dilutions of the lysed cells were made in PBS and plated in duplicate on LB plates and incubated at 37°C overnight.

RNA-Seq

The RNA-Seq experiment was made up of 60 samples: biological triplicate of SCR uninfected, SCR *Salmonella*-infected, each knockdown uninfected, and each *Salmonella*-infected knockdown. RNA-Seq and library preparation was performed by Texas A&M AgriLife Genomics and Bioinformatics Service. Samples were sequenced on Illumina 4000 using 2 × 150-bp paired-end reads. Raw reads were filtered and trimmed and Fastq data was mapped to the Mus musculus Reference genome (RefSeq) using CLC Genomics Workbench 8.0.1. Differential expression analyses were performed using CLC Genomics Workbench. Relative transcript expression was calculated by counting Reads Per Kilobase of exon model per Million mapped reads (RPKM). statistical significance was determined by the EDGE test *via* CLC Genomics Workbench. Differentially expressed genes (DEGs) were selected as those with p value threshold < 0.05.

Gene Ontology (GO) Ingenuity Pathway Analysis and Hierarchical Clustering

To determine the most affected pathways in control versus knockdown RAW 264.7 macrophages, canonical pathway analysis was conducted using Ingenuity Pathway Analysis software from QIAGEN Bioinformatics. Genes that were differentially expressed with a p value < 0.05 from our RNA-SEQ analysis were used as input from uninfected and *Salmonella* Typhimurium infected cells. Hierarchical clustering was done in Cluster3 (3.0) with complete linkage, absolute correlation (centered) parameters and visualized using Java TreeView.

Scatter Plots and Correlation Analysis

For ($p<0.05$) differentially expressed genes, fold change was plotted to compare to coding sequence length which is identified by CLC Genomics Workbench to be equal to the total length of all exons (not all transcripts). Exon number and intron number were identified by CLC Genomics Workbench to be the number of exons/introns based on the mRNA annotations of the reference genome. Total gene length was calculated using "chromosome region start" and "chromosome region end" which are determined by CLC Genomics Workbench and the reference sequence to be the start position and end position of the annotated gene. Pearson Correlation was calculated using the values described above.

RNA Isolation and RT-qPCR Analysis

For transcript analysis, cells were harvested in Trizol and RNA was isolated using Direct-zol RNA Miniprep kits (Zymo Research) with 1 hr DNase treatment. cDNA was synthesized with iScript cDNA Synthesis Kit (Bio-Rad). RT-qPCR was performed using Power-Up SYBR Green Master Mix (Thermo Fisher) using a Quant Studio Flex 6 (Applied Biosystems). Averages of the raw values were normalized to average values for the same sample with the control gene, *Actb*. To analyze fold induction, the average of the treated sample was divided by the untreated SCR control sample, which was set at 1.

Alternative Splicing Analysis

Alternative splicing events were analyzed using Modeling Alternative Junction Inclusion Quantification (MAJIQ) and VOILA (a visualization package) with the default parameters (26). Briefly, uniquely mapped, junction-spanning reads were

used by MAJIQ to construct splice graphs for transcripts by using the RefSeq annotation supplemented with de-novo detected junctions. Here, de-novo refers to junctions that were not in the RefSeq transcriptome database but had sufficient evidence in the RNA-Seq data. The resulting gene splice graphs were analyzed for all identified local splice variations (LSVs). For every junction in each LSV, MAJIQ then quantified expected percent spliced in (PSI) value in control and knockdown samples and expected change in PSI (dPSI) between control and knockdown samples. Results from VOILA were then filtered for high confidence changing LSVs (whereby one or more junctions had at least a 95% probability of expected dPSI of at least an absolute value of 10 PSI units between control and knockdown) and candidate changing LSVs (95% probability, 10% dPSI). For these high confidence results (ΔPSI 10%), the events were further categorized as single exon cassette, multi-exon cassette, alternative 5′ and/or 3′ splice site, or intron-retention.

RBP Finder

For each gene, the canonical (longest) isoform of the gene (5' and 3' UTRs, plus CDS) as annotated by Ensembl [Mouse (GRCm38.p6)] was queried for SR/hnRNP motifs as defined by RBPmap. Stringency level was set on "High" and the Conservation Filter was applied. In cases where multiple motifs were listed, only a single "consensus" motif was chosen (27).

VSV Infection

$7x10^5$ RAW cells were seeded in 12-well plates 16h before infection. Cells were infected with VSV-GFP virus at multiplicity of infection (MOI) of 1 in serum-free DMEM (HyClone SH30022.01). After 1h of incubation with media containing virus, supernatant was removed, and fresh DMEM plus 10% FBS was added to each well. At indicated times post infection, cells were harvested with Trizol and prepared for RNA isolation.

Quantitation and Statistical Analysis

Statistical analysis of data was performed using GraphPad Prism software. Two-tailed unpaired Student's t tests were used for statistical analyses, and unless otherwise noted, all results are representative of at least three biological experiments [mean ± STDEV (n = 3 per group)].

RESULTS

SR and hnRNPs Regulate the Abundance of Distinct Sets of Transcripts in Uninfected and *Salmonella*-Infected Macrophages

To understand how splicing regulatory proteins shape global innate immune gene expression, we prioritized factors most likely to play a privileged role in the macrophage innate immune response. Two recent publications identified a number of splicing factors that were differentially phosphorylated during infection with the intracellular bacterial pathogen *Mycobacterium tuberculosis* in a murine macrophage-like cell line (RAW 264.7) (24) or in primary mouse macrophages (23). Based on these proteomics data (**Figure S1A**), we selected SRSF1, SRSF2, SRSF6, SRSF7, SRSF9, hnRNP C, hnRNP F, hnRNP K, hnRNP M, and hnRNP U for transcriptomics analysis. To begin, we generated RAW 264.7 cell lines in which each factor was stably knocked down *via* expression of an shRNA construct targeting an exon or the 3'UTR for each factor, with regions chosen to ensure that all protein coding isoforms of each factor would be targeted by the shRNA. Overall, six shRNA hairpins were tested for each SR/hnRNP and the two cell lines with the best knockdown efficiency were chosen for subsequent analysis. Interestingly, overall knockdown efficiency varied between factors, with only about 50% knockdown efficiency achieved for hnRNP C, hnRNP K, hnRNP U, SRSF1 and SRSF7 and 70-90% knockdown achieved for SRSF2, SRSF6, SRSF9, hnRNP F and hnRNP M (**Figure 1A**). We predict that variation in knockdown efficiency reflects the macrophage's ability to tolerate loss of each of these factors and likely correlates with the cell's reliance on each for maturation of essential housekeeping genes. The major risk of incomplete knockdown is missing phenotypes (false negatives), as opposed to reporting a false positive phenotype. Therefore, we concluded that these knockdown cell lines were sufficient to identify SR/hnRNP-sensitive innate immune genes and carried out our analysis with the caveat of differential knockdown efficiency in mind.

To induce macrophage innate immune gene expression, we infected each of the RAW 264.7 knockdown cell lines alongside two scramble shRNA hairpin-expressing (SCR) control cell lines with *Salmonella enterica* serovar Typhimurium at an MOI of 10. *Salmonella* is a gram-negative bacterium that triggers TLR4 sensing of *Salmonella* lipopolysaccharide (LPS). TLR4 signaling is unique amongst TLRs in that it activates two major innate immune transcription factor regulons: NFκB downstream of the MyD88 adapter protein, which activates expression of many pro-inflammatory cytokines and chemokines, and IRF3 downstream of the adapter TRIF (28), which turns on a type I interferon response characterized by *Ifnb* and interferon stimulated gene (ISG) expression (**Figure 1B**). We predicted that *Salmonella* infection, which triggers a physiologically-relevant macrophage response, would enable appreciation of even subtle contributions of SR/hnRNPs, while still allowing comparison between our findings and previous studies that focused on the dynamics of NFκB/IRF3 gene expression following direct delivery of LPS (6, 29). We collected total RNA from uninfected and *Salmonella*-infected macrophages at 4h post-infection and performed bulk RNA sequencing *via* an Illumina HiSeq 4000 sequencer (150bp; paired-end reads). An average of ~60.2 million raw sequencing reads were generated from three biological replicates (20 million reads per sample) of each knockdown (both in uninfected and *Salmonella*-infected conditions).

To determine if knockdown of SR and hnRNP proteins affected expression of different transcripts in uninfected vs. *Salmonella*-infected macrophages, we first identified transcripts whose expression was significantly altered ($p<0.05$; up- or down-regulated) in knockdown cell lines relative to controls. We deemed these "Differentially Expressed Genes" or DEGs. Venn diagrams were generated to visualize differences and overlap

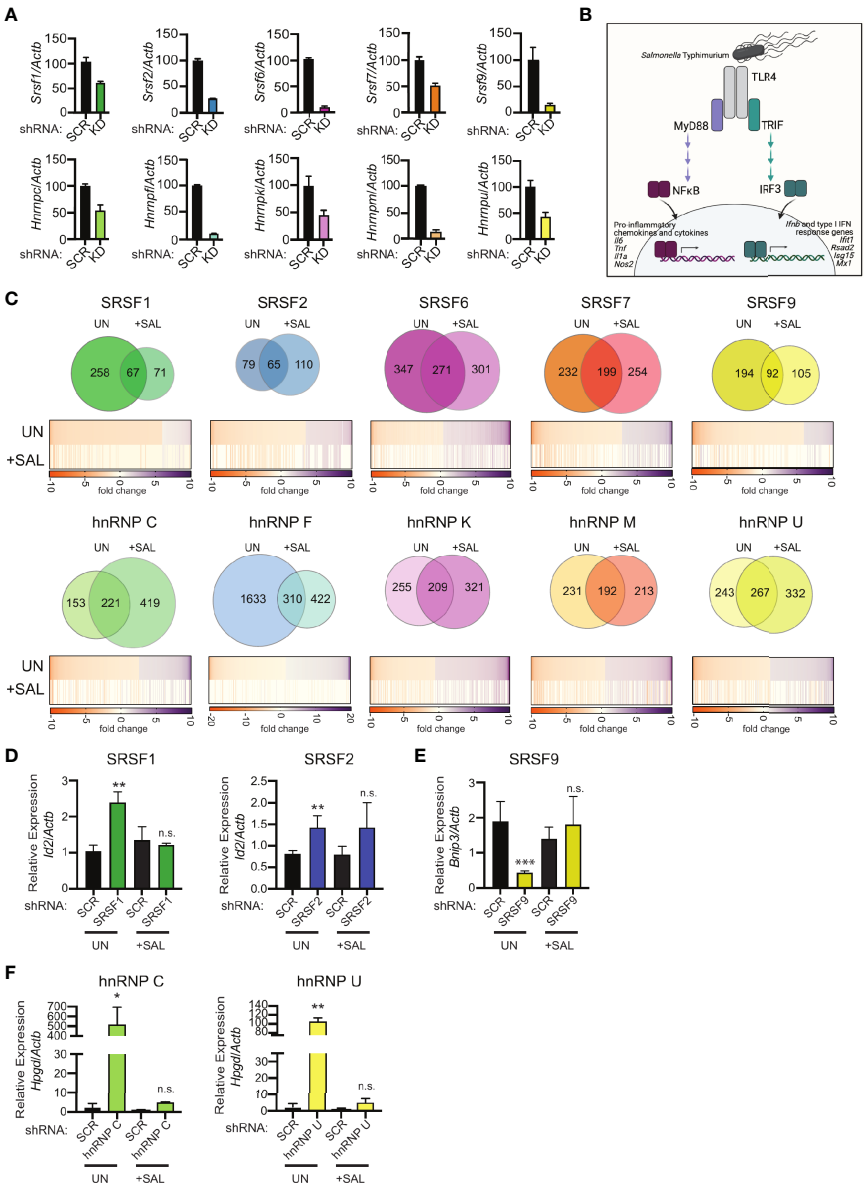

FIGURE 1 | RNA-Seq reveals distinct hnRNP- and SRSF-dependent regulons in uninfected and *Salmonella*-infected RAW 264.7 macrophages. **(A)** Knockdown efficiency for each SR and hnRNP factor as measured by RT-qPCR. Data is shown as hnRNP/SRSF expression, relative to *Actb*, compared to SCR control cells. Ratios are the mean of 3 biological replicates and error bars show standard deviation. **(B)** Schematic representation of transcription factor activation downstream of *Salmonella* Typhimurium sensing by TLR4. **(C)** (Top) Overlap of differentially expressed genes (DEGs) between uninfected and *Salmonella*-infected RAW 264.7 macrophages (4h post-infection; MOI = 10) *via* Venn Diagram. (Bottom) Heatmaps of up and down-regulated DEGs from uninfected macrophages (UN). The values of the same genes in *Salmonella*-infected macrophages are shown below, with "blank spots" indicating DEGs that are not significantly changed in *Salmonella*-infected SR/hnRNP knockdown cell lines (+SAL). Orange represents genes downregulated in knockdown vs. SCR; purple represents genes upregulated in knockdown vs. SCR (colorbar shown below). DEGs were defined as having a statistically significant fold-change relative to SCR; $p<0.05$. **(D)** Relative gene expression of *Id2* over *Actb* in uninfected (UN) and *Salmonella*-infected (+SAL) SRSF1 and SRSF2 knockdown macrophage cell lines. **(E)** As in **(D)** but for *Bnip3* expression in SRSF9 knockdown macrophages. **(F)** As in **(D)** but for *Hpgd* in hnRNP C and hnRNP U knockdown macrophages. For D-F RT-qPCRs, values are the mean of 3 biological replicates and error bars indicate standard deviation. *$p < 0.05$; **$p < 0.01$; ***$p < 0.001$; n.s, not statistically significant ($p > 0.05$). **(B)** was created using Biorender.

between affected genes in uninfected (UN) and Salmonella-infected (+SAL) macrophages (**Figure 1C** and **Supplementary Table 1**). About 1/3 of DEGs had altered expression in both uninfected and *Salmonella*-infected splicing factor knockdown cell lines (compared to SCR controls). This means that in the absence of any single splicing factor queried, about two-thirds of DEGs are unique to either condition (UN or +SAL) (**Figure 1C**, Venn diagrams). On average, expression of between 200-400 genes was altered in an SR or hnRNP knockdown cell line in either condition at this 4h time point. One notable exception, hnRNP F knockdown, altered the

abundance of 1943 genes in uninfected macrophages and 732 genes in *Salmonella*-infected macrophages (**Supplementary Table 1** contains all gene expression changes p<0.05). It is possible that the strength of this phenotype could be due in part to the high knockdown efficiency of hnRNP F (**Figure 1A**).

As expected, many of the DEGs in *Salmonella*-infected cells were not represented amongst the uninfected DEGs (**Figure 1C**, Venn Diagrams). Most innate immune genes including cytokines, chemokines, and antimicrobial mediators are dramatically upregulated upon pathogen sensing and these genes are either expressed at very low levels or not at all in uninfected macrophages. However, we were surprised to find that many genes involved in basic cellular homeostasis and metabolism whose expression was impacted by loss of SR/hnRNPs in uninfected (UN) macrophages were not as impacted in the context of *Salmonella* infection (+SAL) (**Figure 1C**, heatmap comparisons).

To begin to understand why many housekeeping genes are sensitive to loss of SR/hnRNPs in uninfected but not *Salmonella*-infected macrophages, we cross-referenced uninfected SR/hnRNP-sensitive genes against all downregulated genes in SCR control macrophages at 4h-post *Salmonella*-infection (**Supplementary Table 1**). We found that 365 genes were downregulated 2-fold or more (p<0.05) in SCR control macrophages at 4h post-*Salmonella* infection (**Supplementary Table 1**). Many of these genes (e.g. *Lhfpl2*, *Bhlhe41*, *Hyal1*, and *Tbc1d2*) have previously been reported as differentially expressed in M1 vs. M2 macrophages and their downregulation likely represents M1 polarization that occurs following *Salmonella* infection (30). Surprisingly, only a handful of these downregulated genes were among the SR/hnRNP-sensitive genes in uninfected macrophages (**Figure S1B**). To directly test whether SR/hnRNP-sensitive genes in uninfected macrophages are less abundant in *Salmonella*-infected cells, we performed RT-qPCR on a set of genes (*Bnip3*, *Id2*, *Hpgd*), which encode proteins involved in regulating cell death, transcription, and prostaglandin metabolism. Consistent with our RNA-seq data, we observed SR/hnRNP-dependent changes in *Bnip3*, *Id2*, and *Hpgd* abundance only in uninfected macrophages (**Figures 1D–F**, UN). We measured no detectable change in the abundance of these transcripts in uninfected vs. infected SCR control macrophages. Overall, we observed that no more than 6.3% of uninfected DEGs were downregulated upon *Salmonella* infection (**Figure S1B**), supporting our initial hypothesis that SR proteins and hnRNPs are functionalized such that they influence expression of distinct genes in uninfected and *Salmonella*-infected macrophages, and this includes genes that are constitutively expressed in both conditions.

SR and hnRNPs Contribute to Activation and Repression of Genes in Innate Immune-Related Pathways in *Salmonella*-Infected Macrophages

As another measure of how SR/hnRNPs differentially influence gene expression in uninfected vs. *Salmonella*-infected macrophages, we performed Ingenuity Pathway Analysis (IPA) (Qiagen) to identify pathways enriched for SR/hnRNP-sensitive DEGs. In uninfected macrophages, we observed significant enrichment for DEGs in pathways related to translation initiation, mTOR signaling, and phagosomal maturation (**Figure 2A**, uninfected and **Supplementary Table 1** for full list). This finding is consistent with our previous analysis of hnRNP M-sensitive genes in uninfected macrophages (31) and the well-characterized role for splicing in controlling translation outcomes *via* ribosomal protein gene processing (32–34). We also performed IPA for the aforementioned 365 genes that are downregulated (>2-fold down) upon *Salmonella* infection in control macrophages described above and saw no overlap between these pathways and those enriched for SR/hnRNP-sensitive DEGs (**Figure S2A**). This too supports our conclusion that SR/hnRNP regulated genes are not globally downregulated upon infection.

Major pathways enriched for SR/hnRNP DEGs in *Salmonella*-infected macrophages are generally related to innate immune responses and macrophage activation, including "Role of Pattern Recognition Receptors (PRRs) in Recognition of Bacteria and Viruses," "Communication between Innate and Adaptive Immune Cells", and "Granulocyte Adhesion and Diapedesis" (**Figure 2A**, +*Salmonella*). Consistent with our observation that many DEGs identified in uninfected macrophages "lose reliance" on SR/hnRNPs upon *Salmonella*-infection, the only pathway that was significantly enriched for DEGs in both conditions was the translation/mTOR related pathway "Regulation of eIF4 p70S6K," which remained significantly enriched for DEGs in SRSF6, SRSF9, and hnRNP F in *Salmonella*-infected macrophages (**Figure 2B**). We observed that while many transcripts had altered abundance in both SR and hnRNP knockdown macrophages, loss of SRs generally led to lower abundance (orange lines) while loss of hnRNPs led to higher abundance (purple lines). This same trend was evident for genes in innate immune pathways (**Figures 2C, D**). Interestingly, this gene-level analysis highlighted hnRNP-specific regulation of a diverse set of critical immune genes, including the potent anti-inflammatory mediator IL-10, members of the TNF superfamily (*Tnfsf12*, *Tnfsf10*, *Tnfsf9*), factors involved in the type I interferon response (*Ddx58* (RIG-I), *Ifih1*, *Oas1b*, *Oas2*, *Ifnb1*, *Oas3*, *Irf3*), as well as components of the complement cascade (*C3*, *C3ar1*) and the inflammasome (*Casp1*, *Nlrp3*) (**Figure 2C**). Together, these analyses suggest that proper gene expression levels in macrophages are maintained by balancing the activities of activating SR proteins and repressive hnRNPs.

To take a closer look at how SR/hnRNP knockdown impacts the macrophage transcriptome during *Salmonella* infection, we quantified the number of transcripts whose abundance was increased or decreased in the absence of each SR or hnRNP, compared to a SCR control (p<0.05). As visualized in **Figures 3A–E** (SRs) and **4A–E** (hnRNPs), we found that each SR and hnRNP queried can act as either a positive or negative regulator of gene expression To identify the most impacted DEGs, we generated heatmaps that show the top 10 most up and down DEGs (p<0.05) in each *Salmonella*-infected SR/hnRNP knockdown macrophage cell line compared to SCR (**Figures 3A–E** and **4A–E**). We then annotated innate immune-responsive genes by virtue of their being up- or

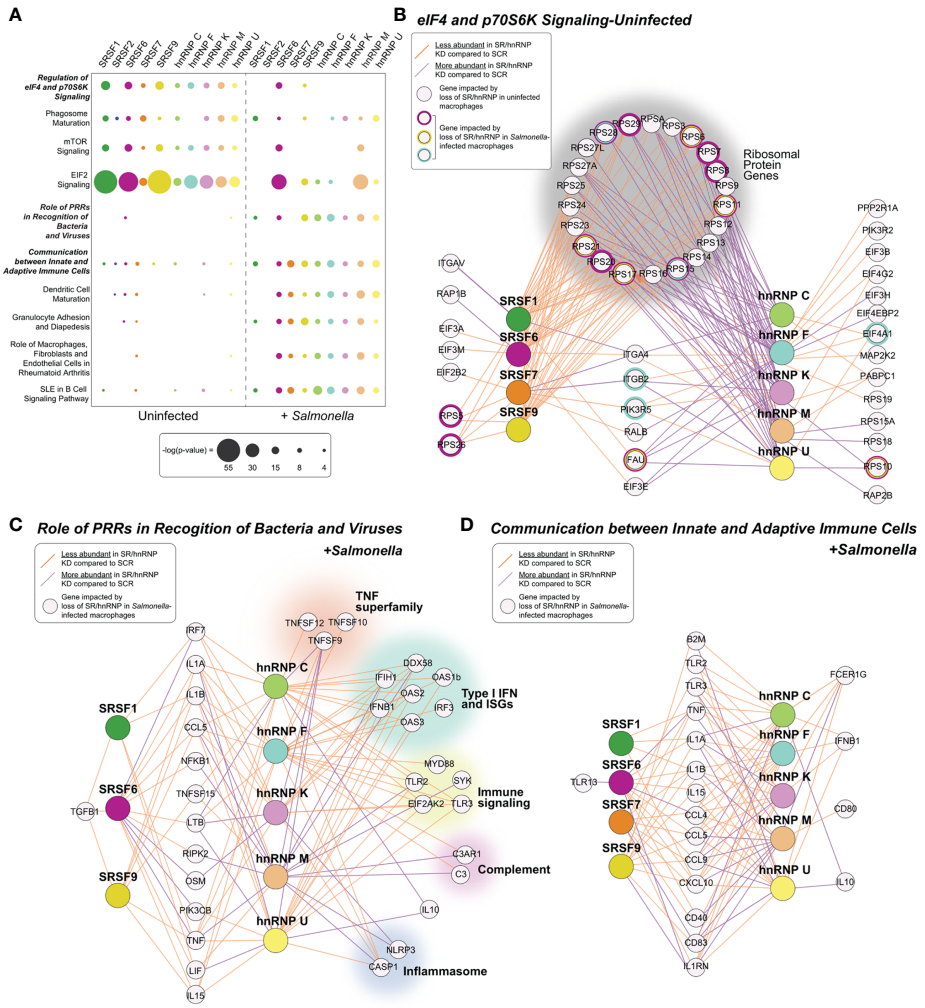

FIGURE 2 | Pathways enriched for SR/hnRNP-dependent DEGs differ between uninfected and *Salmonella*-infected macrophages. **(A)** Canonical Ingenuity pathway analysis (IPA) of functional cellular pathways enriched for differentially expressed genes (DEGs) in uninfected (UN) and *Salmonella*-infected (+SAL) SR and hnRNP knockdown RAW 264.7 macrophages. Pathways enriched in eight or more knockdown cell lines in at least one condition are shown. Statistical enrichment is expressed as [-log (p-value)]. **(B)** Network diagrams showing DEGs from the IPA category "eIF4 and p70S6K Signaling" from each SR/hnRNP knockdown cell line in uninfected and *Salmonella* infected RAW 264.7 macrophages. Only SR/hnRNPs that showed DEG enrichment for the eIF4 pathway are shown. **(C)** As in **(B)** but for DEGs in *Salmonella*-infected SR/hnRNP knockdown cell lines in the IPA category "Role of Pattern Recognition Receptors in Recognition of Bacteria and Viruses." **(D)** As in **(B)** but for the IPA category "Communication between Innate and Adaptive Immune Cells." Purple lines connect SR or hnRNPs with target genes whose expression is upregulated in knockdown vs. SCR control macrophages. Orange lines connect SR or hnRNPs with target genes whose expression is downregulated in knockdown vs. SCR control macrophages. Cut-off for inclusion in the IPA was $p < 0.05$ for differential expression between knockdown and SCR cells.

down-regulated in control macrophages in response to *Salmonella* infection (+/- 2.0 fold in SCR SAL vs. SCR UN; bolded genes in heatmaps). These heatmaps show clear hyper- or hypo-induction of many critical innate immune genes in SR/hnRNP knockdown macrophages (**Figures 3A–E** and **4A–E**). We validated the expression of a representative "top 10" DEG by RT-qPCR (**Figures 3A–E** and **4A–E**) using two different knockdown cell lines for each SR/hnRNP (efficiency of each knockdown at the RNA level, and protein level (when antibodies were readily accessible) is shown in **Figures S3A–E** and **S4A–E**).

Several interesting trends emerge from these data. First, we found that knockdown of SR and hnRNPs impacts expression of innate immune genes from distinct transcriptional regulons: NFκB (e.g. *Plau*, *Olr1*, *Csf2*, *Csf3*) and IRF3 (e.g. *Ifit1*, *Ifit3*, *Apol9a/b*, *Mx1*). Second, by creating Venn diagrams to identify common DEGs, we found that the hnRNPs queried share more DEGs than do the SRs (**Figures 3F** and **4F**; 104 vs. 11). This result echoes previous global analyses of hnRNP A1, A2/B1, F, H1, M, and U targets in human 293T cells, which described considerable cooperation between hnRNP family members (35). Third, we

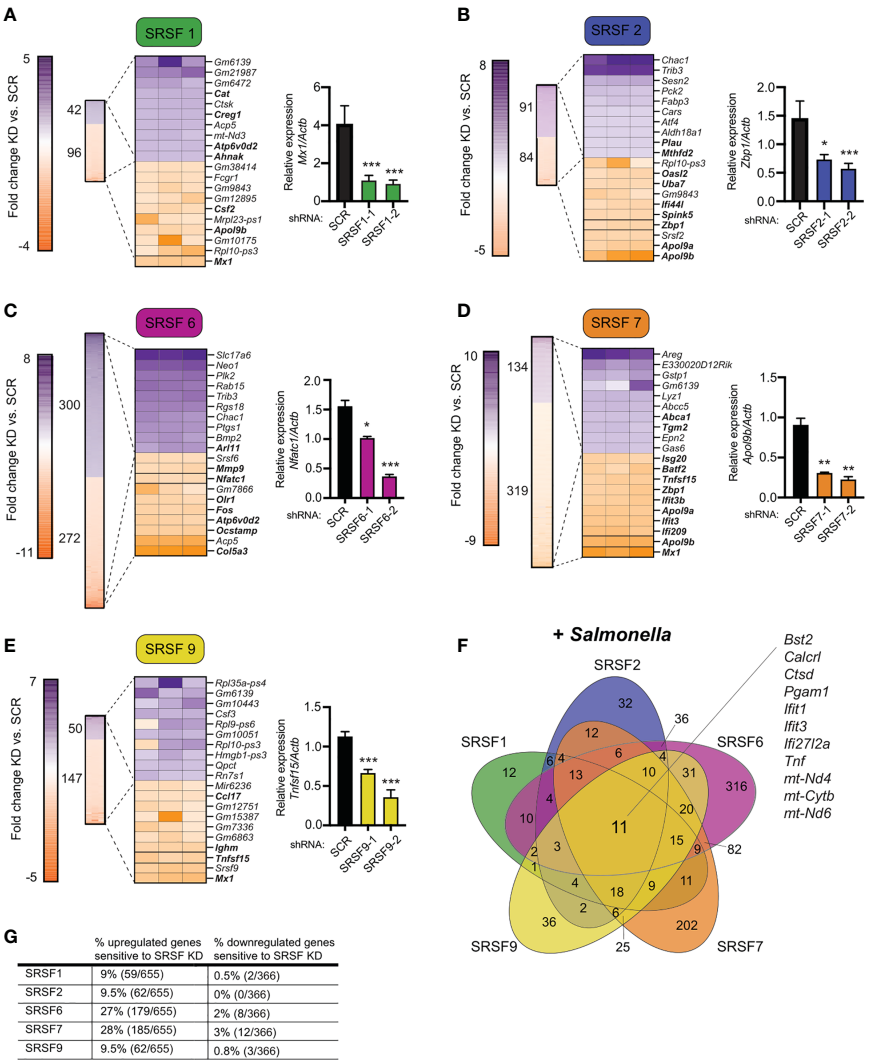

G

	% upregulated genes sensitive to SRSF KD	% downregulated genes sensitive to SRSF KD
SRSF1	9% (59/655)	0.5% (2/366)
SRSF2	9.5% (62/655)	0% (0/366)
SRSF6	27% (179/655)	2% (8/366)
SRSF7	28% (185/655)	3% (12/366)
SRSF9	9.5% (62/655)	0.8% (3/366)

FIGURE 3 | Knockdown of SR family members causes both up- and down-regulation of gene expression in *Salmonella*-infected macrophages. **(A)** On left, heatmap represents all up- and down-regulated genes in SRSF1 knockdown RAW 264.7 macrophages relative to SCR control at 4h post-*Salmonella* infection ($p<0.05$). Numbers next to heatmap indicate the total number of up- (purple) or down- (orange) regulated genes in SRSF1 knockdown cell lines vs. SCR. Zoom in represents the top 10 up- and down-regulated genes. Genes whose expression is up- or down-regulated by virtue of *Salmonella*-infection itself (i.e. innate immune regulated genes) according to analysis of *Salmonella*-infected SCR vs. uninfected SCR cells are bolded. Box indicates gene chosen for RT-qPCR validation. On right, RT-qPCR validation of a representative DEG (*Mx1*) in two SRSF1 knockdown cell lines vs. SCR control cells (data shown relative to *Actb*). **(B)** As in **(A)** but for SRSF2; RT-qPCR of *Zbp1*. **(C)** As in (A) but for SRSF6; RT-qPCR of *Nfatc1*; **(D)** As in **(A)** but for SRSF7; RT-qPCR of *Apol9b;* **(E)** As in **(A)** but for SRSF9; RT-qPCR of *Tnfsf15*. **(F)** Venn diagram of DEGs common to one or more SR knockdown cell line ($p<0.05$). The 11 genes whose expression is impacted by loss of all five SRSF proteins are highlighted. **(G)** Percentage of all genes induced at 4h post-*Salmonella* infection (>2.0-fold) that are differentially expressed in each SRSF knockdown macrophage cell line ($p<0.05$). For all RT-qPCRs, values are the mean of 2 or 3 biological replicates and error bars indicate standard deviation. *$p < 0.05$; **$p < 0.01$; ***$p < 0.001$.

discovered that certain genes, particularly those categorized as ISGs (36–38), including the viral restriction factors *Mx1*, *Ifit1*, *Ifit3*, and *Oasl2*, and the cytosolic DNA sensor *Zbp1*, show altered abundance in multiple SR/hnRNP knockdown cell lines. Lastly, we found that loss of either SR proteins (**Figure 3G**) or hnRNPs (**Figure 4G**) is more likely to impact steady state levels of genes that are upregulated (>2-fold) at 4h post-*Salmonella* infection than those that are downregulated (>2-fold).

SR/hnRNP-Mediated Alternative Splicing Events Are Not Common in DEGs

Data presented so far generally argue against a global up- or down-regulation of pre-mRNA splicing in *Salmonella*-infected macrophages and instead support a model whereby individual SRs and hnRNPs dictate RNA processing decisions for particular transcripts. While SR and hnRNP proteins have been implicated in many steps of gene expression and RNA processing, from

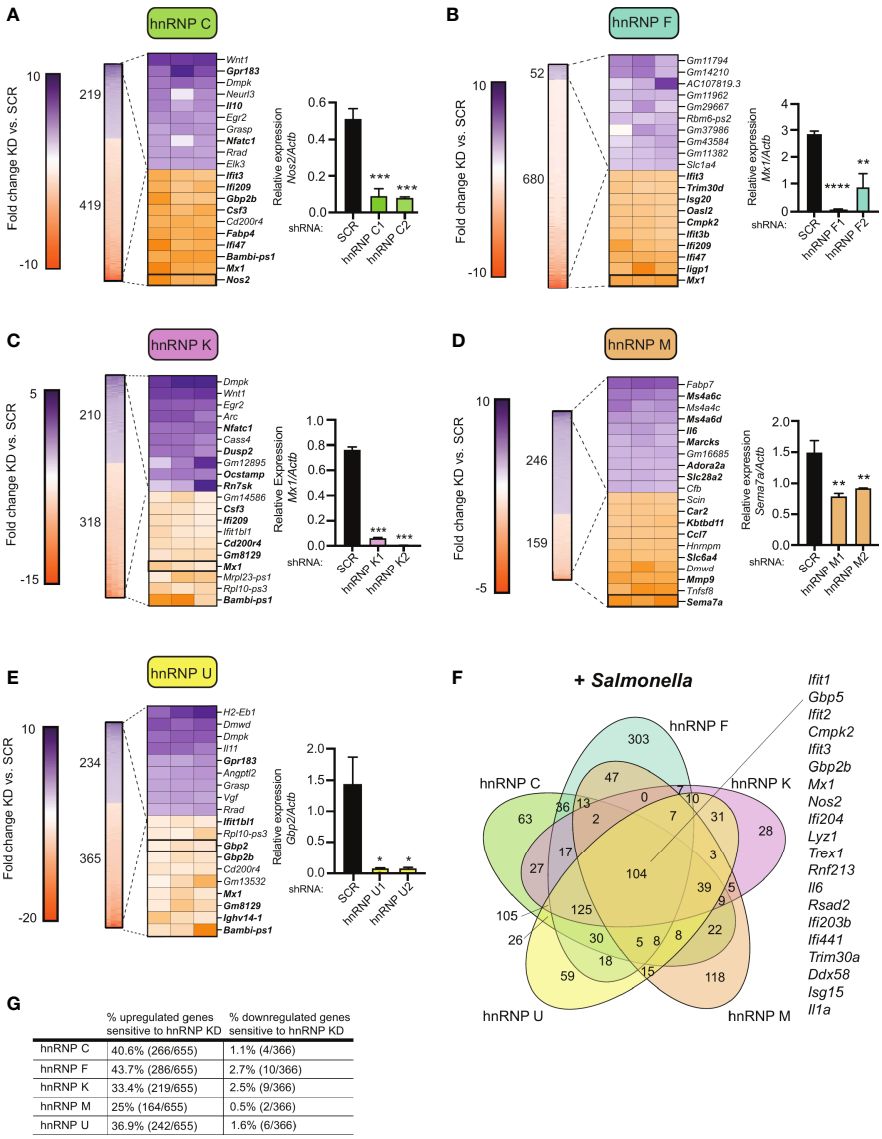

	% upregulated genes sensitive to hnRNP KD	% downregulated genes sensitive to hnRNP KD
hnRNP C	40.6% (266/655)	1.1% (4/366)
hnRNP F	43.7% (286/655)	2.7% (10/366)
hnRNP K	33.4% (219/655)	2.5% (9/366)
hnRNP M	25% (164/655)	0.5% (2/366)
hnRNP U	36.9% (242/655)	1.6% (6/366)

FIGURE 4 | Knockdown of hnRNP family members causes up- and down-regulation of gene expression in *Salmonella*-infected macrophages. **(A)** On left, heatmap represents all up- and down-regulated genes in hnRNP C knockdown macrophages relative to SCR control at 4h post-*Salmonella* infection ($p<0.05$). Numbers next to heatmap indicate the total number of up- (purple) or down- (orange) regulated genes in hnRNP C knockdown cell lines vs. SCR. Zoom in represents the top 10 up- and down-regulated genes. Genes whose expression is up- or down-regulated by virtue of *Salmonella*-infection itself (i.e. innate immune regulated genes) according to analysis of *Salmonella*-infected SCR vs. uninfected SCR cells are bolded. Box indicates gene chosen for RT-qPCR validation. On right, RT-qPCR validation of a representative DEG (*Nos2*) in two knockdown cell lines vs. a SCR control (data shown relative to *Actb*). **(B)** As in **(A)** but for hnRNP F; RT-qPCR of *Mx1*. **(C)** As in **(A)** but for hnRNP K; RT-qPCR of *Mx1*. **(D)** As in **(A)** but for hnRNP M; RT-qPCR of *Sema7*; **(E)** As in **(A)** but for hnRNP U; RT-qPCR of *Gbp2*; **(F)** Venn diagram of DEGs common to one or more hnRNP knockdown cell line ($p<0.05$). A subset of the 104 genes whose expression was impacted by loss of all five hnRNP proteins are highlighted. **(G)** Percentage of all genes induced at 4h post-*Salmonella* infection (>2.0-fold) that are differentially expressed in each hnRNP knockdown macrophage cell line ($p<0.05$). For all RT-qPCRs values are the mean of 2 or 3 biological replicates and error bars indicate standard deviation.
*$p < 0.05$; **$p < 0.01$; ***$p < 0.001$; ****$p < 0.0001$.

chromatin remodeling and transcription to mRNA export and stability (39–42), the main way that SR and hnRNPs shape the steady state transcriptome is by influencing pre-mRNA splicing decisions. To begin to appreciate how SR and hnRNPs mediate specific alternative splicing events in murine macrophages and determine whether these events are changed during *Salmonella* infection, we employed an algorithm to identify and quantify local splicing variations (LSV) called Modeling Alternative Junction Inclusion Quantification (MAJIQ) (26). MAJIQ allows identification, quantification, and visualization of diverse LSVs, including alternative 5′ or 3′ splice site usage, exon skipping, and intron retention across different experimental conditions.

Using MAJIQ, we quantified LSVs that were significantly changed in SR/hnRNP knockdown cells in both uninfected and

Salmonella-infected conditions (4h post-infection), generating a large dataset of SR/hnRNP-dependent alternative splicing changes (probability [|delta PSI|, ≥10%] >95%) (**Supplementary Table 1**). We observed all types of alternative splicing changes, with the majority of changes categorized as exon skipping events (>7000 total exon skipping events in UN or +SAL vs. >1600 intron retention, alternative 5' and 3'SS events in UN or +SAL), consistent with the canonical roles of SR and hnRNPs in enhancing or repressing exon inclusion (**Figure 5A**) (43–45). There were no dramatic differences between the overall number of LSVs between different SR/hnRNPs nor major differences in the number of LSVs in uninfected compared to *Salmonella*-infected macrophages (**Figure 5A**). HnRNP F knockdown macrophages stood out as a notable exception, whereby there were about one-quarter as many LSVs identified in *Salmonella*-infected macrophages vs. uninfected (**Figure 5A**).

Recent work from the Baltimore lab showed that innate immune transcripts are frequently regulated by alternative splicing events whereby poison exons introduce premature stop codons that target transcripts to nonsense mediated decay (22). To determine whether alternative splicing events could be contributing to differential gene expression in SR/hnRNP knockdown macrophages, we compared our lists of DEGs and genes with DIU in both conditions and visualized the overlap by generating Venn diagrams. Surprisingly, we observed that only a small fraction of SR/hnRNP-dependent DEGs were also subject to DIU (i.e. few transcripts were impacted at levels of both steady state abundance and alternative splicing) (**Figure S5A**). These trends were the same in uninfected and *Salmonella*-infected SR/hnRNP knockdown macrophages (**Figures S5A, B**). In line with this finding, we observed little to no enrichment for SR/hnRNP-dependent alternative splicing events in genes related to innate immune pathways *via* IPA. In fact, no pathway was enriched for genes with DIU more than -log(p-value) = 5 (**Supplementary Table 1**), suggesting that SR/hnRNP-dependent alternative splicing changes in macrophages do not generally occur in functionally related genes from any particular pathway. Other studies have also found a lack of overlap between steady state transcript level changes and alternative splicing events in *Salmonella*-infected human monocytes (21) as well as in influenza-infected A549 cells (46).

To gain additional insight into how SRs and hnRNPs influence macrophage biology during infection, we next looked at the most significant DIUs in each *Salmonella*-infected knockdown cell line using a more stringent isoform expression cut-off (probability [|delta PSI|, ≥20%] >95%). As supported by our pathway analysis, these genes fall into a variety of functional categories, including protein modification, intracellular trafficking, chromatin remodeling and transcription, and chromosome biology (**Figure S5D**). Notably, there are no obvious candidates for genes likely to globally alter the innate immune transcriptome, save for *Ikbke* (inhibitor of nuclear factor kappa-B kinase subunit epsilon), which is subject to intron retention in hnRNP F knockdown cells. A representative DIU in an innate immune-related gene (>20% delta PSI) is shown for each SR/hnRNP knockdown cell line (**Figures 5B–K**). Several of these splicing variations influence the protein coding capacity of their targets, with changes to the balance of exon skipping events in SRSF knockdowns (*Senp7* in SRSF1, **Figure 5B**; *Nrb1* in SRSF2, **Figure 5C**; *Cd37* in SRSF6, **Figure 5D**; and *Wnk1* in SRSF7, **Figure 5E**) and hnRNP knockdowns (*Emsy* in hnRNP C, **Figure 5G**; *Il2rg* in hnRNP F, **Figure 5H**; and *Ubqln1* in hnRNP M, **Figure 5J**). Interestingly, while most DIUs were detected in both uninfected and *Salmonella*-infected SR/hnRNP knockdown macrophages, changes in SRSF2 dependent-changes to *Nrb1*, SRSF9-dependent changes to *E2f1*, hnRNP C-dependent changes to *Emsy*, hnRNP K-dependent changes to *E2f1* hnRNP K, and hnRNP U-dependent changes to *Trim3* were only found in +SAL samples (**Figures 5C, F, G, I, K**) (**Supplementary Table 1**). Together, these data suggest that while SR/hnRNPs do not control macrophage transcript abundance *via* changes to alternative splicing, these factors can mediate distinct alternative splicing events in uninfected vs. *Salmonella*-infected macrophages.

A Gene's Induction Level, Length, and Number of Exons/Introns Do Not Correlate With a Transcript's Reliance on SR/hnRNPs for Proper Induction During *Salmonella* Infection

Having observed a lack of correlation between DEGs and DIU in each splicing factor knockdown cell line, we wanted to see if we could identify anything common to SR/hnRNP-sensitive innate immune genes. We hypothesized that genes whose expression is the most upregulated in response to *Salmonella* infection could be more sensitive to loss of SR/hnRNPs, perhaps *via* a need to sequester rate-limiting spliceosome components. To address this possibility, we first ranked all genes induced in SCR control macrophages at 4h post-*Salmonella* infection (**Figure 6A**). We observed dramatic upregulation of hundreds of macrophage genes at this early time point, with some inflammatory mediators like *Il1a* and *Il1b* upregulated approximately 1500-fold. We then generated another heatmap to visualize how the expression of each of these top 100 *Salmonella*-induced genes was impacted by SR/hnRNP knockdown. We observed no clear correlation between level of induction/expression level and whether or not a transcript was differentially regulated by loss of an SR/hnRNP. This is clearly evidenced by the heatmap itself, whereby DEGs induced 1000-fold and DEGs induced 5-fold in control cells were similarly impacted, both in terms of the number of SR/hnRNPs they were affected by and the magnitude of their expression change (**Figure 6B**; top vs. bottom genes). We can also see this outcome in RT-qPCR experiments, in which we measured how loss of SR/hnRNPs impacted expression of *Il1a* (500-1000 average fold-change in SCR controls; **Figure 6C**), *Nos2* (Nitric oxide synthase) (20-60 average fold-change; **Figure 6D**), and *Mx1* (MX Dynamin Like GTPase 1) (10-15 average fold-change; **Figure 6E**). Each of these representative innate immune genes responds to loss of particular SRs and hnRNPs in completely different ways. For example, loss of hnRNP M causes hyper-induction of *Mx1*, but does not affect *Il1a* levels. Loss of hnRNP C causes hyper-induction of *Il1a* but does not impact *Nos2* or *Mx1* abundance.

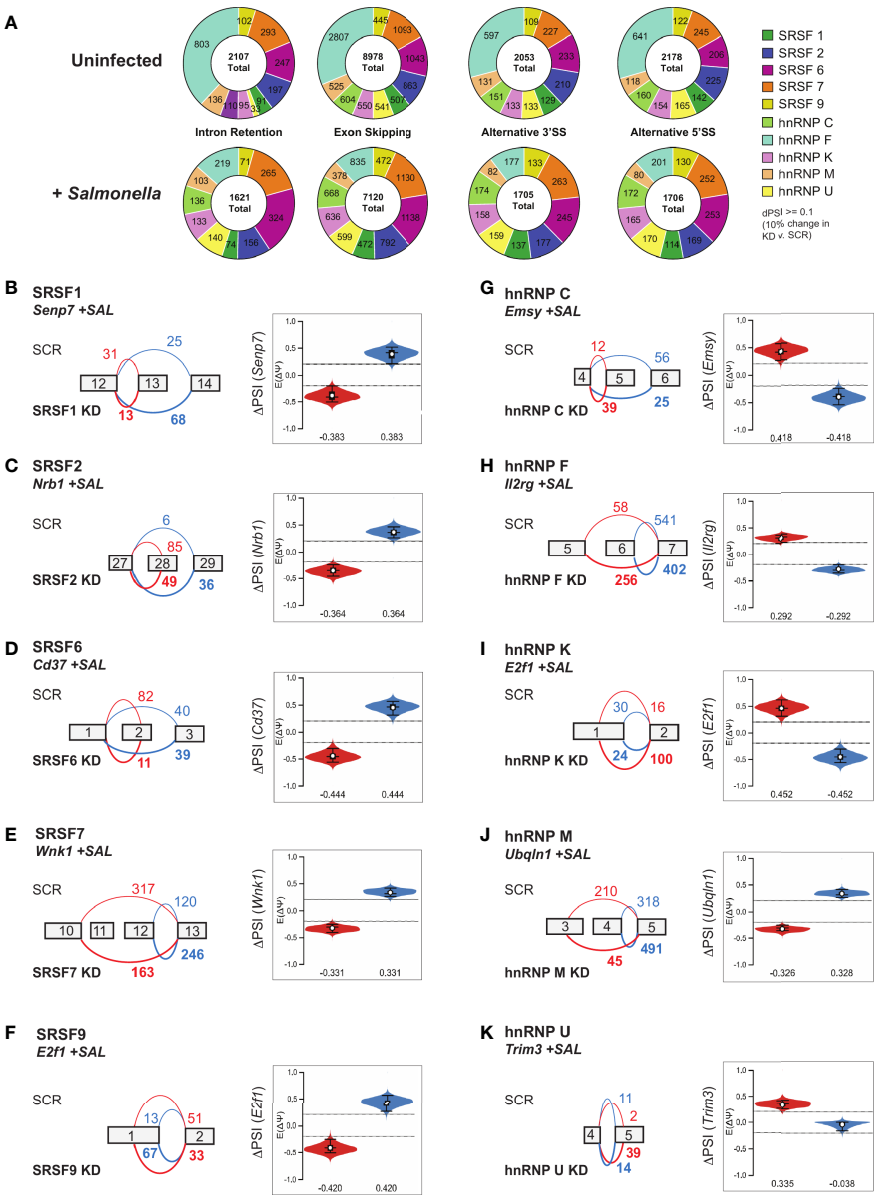

FIGURE 5 | Local splicing variations are abundant in SR/hnRNP knockdown macrophages, but they do not preferentially occur in SR/hnRNP-dependent differentially expressed genes. **(A)** Quantitation of intron retention, exon skipping, alternative 3' and 5' splice site events in uninfected and *Salmonella*-infected SR and hnRNP knockdown macrophages (probability [|delta PSI|, ≥10%], >95%). PSI is defined as "Percent Spliced In" and indicates the abundance of a particular alternatively spliced isoform. ΔPSI indicates the abundance of an isoform in knockdown vs. SCR macrophage cell lines. **(B)** (left) VOILA output, based on RNA-seq reads, of affected exons in a representative gene (Senp7) in SRSF1 knockdown or SCR RAW 264.7 cells infected with *Salmonella*. (right) Violin plots depicting the ΔPSI of the SRSF1-dependent local splicing variations of *Senp7*. Violin plot colors correspond to the events depicted in the gene schematic on the left. **(C)** As in **(B)** but for SRSF2 and *Nrb1*. **(D)** As in **(B)** but for SRSF6 and *CD37*. **(E)** As in **(B)** but for SRSF7 and *Wnk1*. **(F)** As in **(B)** but for SRSF9 and *E2f1*. **(G)** As in **(B)** but for hnRNP C and *Emsy*. **(H)** As in **(B)** but for hnRNP F and *Il2rg*. **(I)** As in **(B)** but for hnRNP K and *E2f1*. **(J)** As in **(B)** but for hnRNP M and *Unqln1*. **(K)** As in **(B)** but for hnRNP U and *Trim3*.

Using the computational prediction software RBPmap (27), we successfully identified one or more binding sites for each of the SR/hnRNPs that impacted *Il1a*, *Nos2*, and/or *Mx1* expression (**Figures S6A–C**). While this analysis is merely correlative, it does begin to support a model whereby exonic and intronic splicing enhancers/silencers are enriched in innate immune transcripts that rely on particular SR/hnRNPs for proper expression levels.

To examine if other attributes of a gene influenced whether its expression was altered by loss of an SR/hnRNP, we conducted Pearson's correlation tests to determine the relationship between differential expression ($p<0.05$) and gene length (**Figure 6F**),

exon length (total exonic sequence, or sum of all exon nucleotides) (**Figure 6G**), intron length (total intronic sequence, or sum of all intron nucleotides) (**Figure 6H**), and number of exons (**Figure 6I** and **Supplementary Table 1**). We observed little to no correlation between any of these gene attributes and the degree to which a gene's expression was altered in the hnRNP and SR knockdown cell lines, with all tests generating Pearson correlation coefficients close to zero. Thus, it is likely that additional features, for example the presence or absence of specific binding sites/consensus

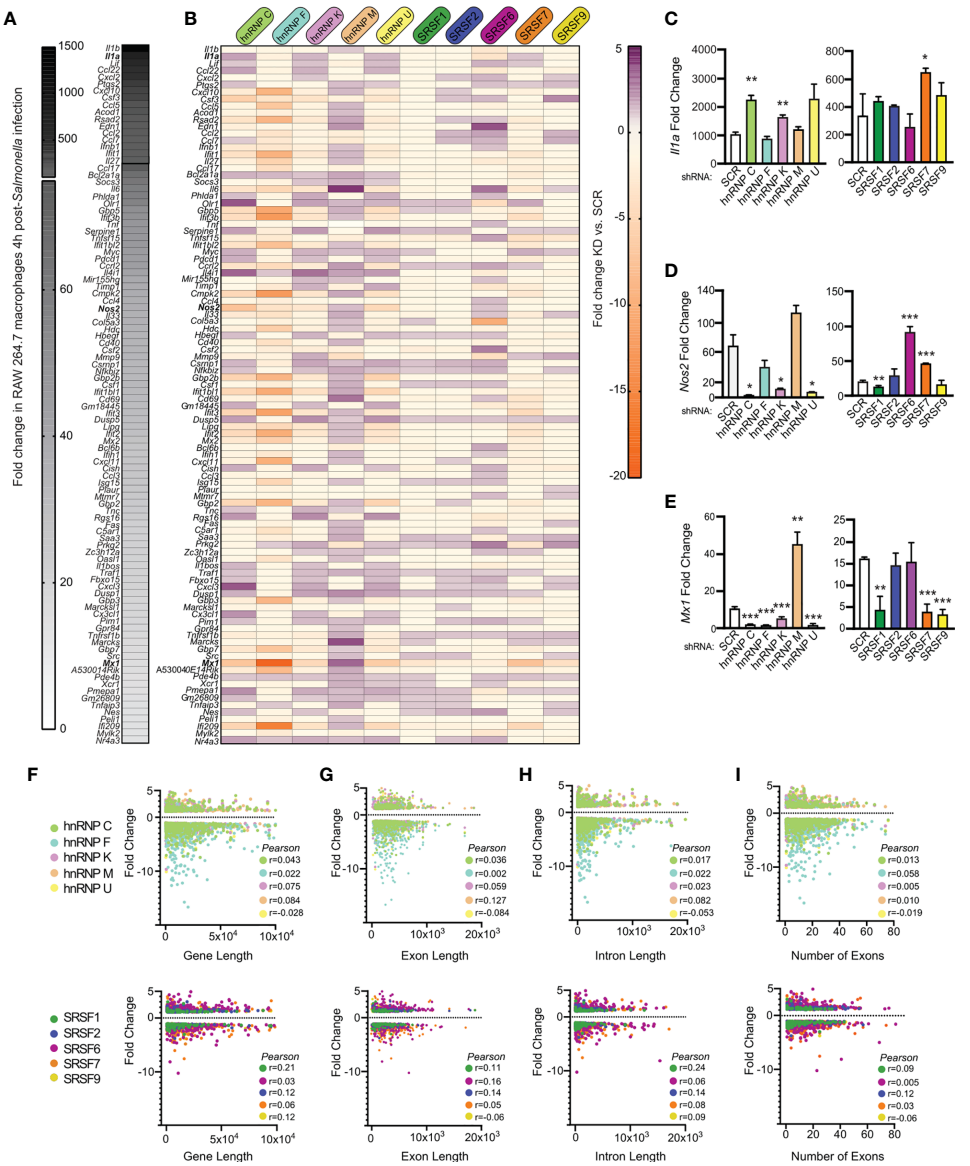

FIGURE 6 | Level of induction upon *Salmonella* infection, gene length, and number of introns/exons do not positively correlate with a gene's reliance on SR/hnRNPs to maintain proper expression levels. **(A)** Heatmap of the top 100 genes induced at 4h post-*Salmonella* infection in SCR control RAW 264.7 macrophages. Data shown as fold change in SCR cells + *Salmonella* vs. SCR cells uninfected. **(B)** Heatmap of up- or down-regulation (fold change) of each induced gene conferred by hnRNP or SRSF knockdown. Purple genes are upregulated in SR/hnRNP knockdowns relative to SCR; Orange genes are downregulated in SR/hnRNP knockdowns. **(C)** RT-qPCR of *Il1a* abundance relative to *Actb* in *Salmonella*-infected SRSF and hnRNP knockdown macrophages (shown as fold change relative to uninfected for each cell line). **(D)** As in **(C)** but for *Nos2*. **(E)** As in **(C)** but for *Mx1*. **(F)** Scatter plot depicting correlation of the fold change of each DEG vs. coding sequence (CDS) length in *Salmonella*-infected hnRNP (top) and SRSF (bottom) knockdown macrophages. **(G)** as in **(F)** but comparison of DEG fold change vs. exon length. **(H)** As in **(F)** but comparison of DEG fold change vs. intron length. **(I)** As in **(F)** but comparison of DEG fold change vs. number of exons in a DEG. Genes included in analysis were differentially expressed ($p < 0.05$) in each knockdown compared to SCR controls. Y-axes were made all the same to facilitate comparison between multiple knockdown cell lines. For all RT-qPCRs values are the mean of 2 or 3 biological replicates and error bars indicate standard deviation. *$p < 0.05$; **$p < 0.01$; ***$p < 0.001$.

sequences or misregulation of an upstream transcription or chromatin factor, dictate whether an innate immune transcript is sensitive to loss of a particular SR/hnRNP.

SR/hnRNP Knockdown Leads to Hyper-Induction of Early-Induced Innate Immune Genes

With no apparent correlation between various gene architecture attributes and SR/hnRNP reliance, we looked to see if we could correlate an innate immune gene's reliance on SR/hnRNPs for proper induction with the dynamics of its transcriptional activation as previously described by other studies (6, 7, 10). One commonly used categorization of innate immune genes is into primary and secondary response genes. Of the 53 LPS-driven primary response genes annotated by (10), 35 of them were more abundant in one or more SR/hnRNP knockdown cell line (**Figure 7A**, top heatmap; **Supplementary Table 1**). This suggests a role for factors like hnRNP C, K, M, U and SR6 in repressing the expression of primary response genes at the 4h time point we interrogated. A repressive role for these same factors was less evident for secondary response genes, which were mostly downregulated in the absence of the SR/hnRNPs (save for hnRNP M and SRSF6) (**Figure 7A**, bottom heatmap; **Supplementary Table 1**). This analysis begins to suggest that primary response genes may be particularly reliant on pre-mRNA splicing to control the proper magnitude of their induction than are secondary response genes, which rely on multiple additional layers of regulation.

We next looked at our data in a different way, leveraging macrophage gene categories as defined by (6). This study divided RefSeq genes exceeding 400bp in length into 12 clusters based on their pattern of transcript levels in three cellular compartments (chromatin, nucleoplasm, cytoplasm) in primary macrophages over a time-course of Lipid A treatment (**Figure S7A** and **Supplementary Table 1**). Resorting our own data into these groups, we found that the vast majority of genes we identified as SR/hnRNP-sensitive in *Salmonella*-infected RAW 264.7 macrophages fell into Groups 1-3 (**Figure S7A** and **Supplementary Table 1**), which are composed mainly of Lipid A-induced genes. This supports our hypothesis that SR/hnRNPs play a specific role in controlling macrophage genes that are activated upon pathogen sensing.

To gain additional insight into how different categories of induced genes respond to SR/hnRNP knockdown, we re-sorted our data again, this time using a more detailed grouping of macrophage induced genes from Bhatt et al. These groups of genes (A1-F; **Figure 7B** and **Supplementary Table 1**) were defined on basis of when chromatin-associated RNA-seq reads for each gene reach peak levels following Lipid A treatment: Group A1 peaks at 15 min, A2 at 30 min, B at 60 min, C and D levels peaked around 30 min and then were sustained through 2h, and Groups E and F steadily increased over the 2h time-course (represented schematically in **Figure 7B**). One interesting trend that emerged from this data is that the majority of SR/hnRNP-sensitive genes in Groups A1-C were hyper-induced (68.8% of Group A1 genes were upregulated in one or more knockdown macrophage cell line vs. SCR; 41.3% in Group A2 and 54.1% in Group C). This suggests that LPS-activated genes expressed *via* a transcriptional "burst" are uniquely sensitive to repression from SR/hnRNPs, in particular hnRNP C, hnRNP K, hnRNP M, hnRNP U, SRSF2, 6, and 7. We also found that genes in Group C were disproportionately impacted by loss of hnRNP M, with nearly half of all genes in the category (40/98) upregulated in hnRNP M knockdown macrophages at 4h post-*Salmonella* infection, including the chemokine receptor *Ccrl2*, the regulator of NFκB *Nfkbiz*, and the repressor of JAK/STAT signaling *Socs3*.

hnRNP U and hnRNP K Play a Role in the Control of Intracellular Viral and Bacterial Replication

Lastly, we wanted to test whether we could use DEG and/or DIU profiles of SR/hnRNP knockdown macrophages to predict if a particular knockdown cell line would be better or worse at restricting pathogen replication. We began by applying a simple hierarchical clustering algorithm to calculate similarities in DEG profiles between knockdowns (Cluster 3.0). We found significant similarity between genes affected by loss of hnRNP K and hnRNP U (and to a lesser extent, hnRNP C) in uninfected cells (correlation between K/U: 0.78; correlation between C/K/U: 0.69). Previous studies have shown that hnRNP K binds strongly to poly C stretches of RNA (47, 48) and hnRNP U preferentially binds CUGUGGAU and UGUAUUG motifs (35). At the amino acid level, hnRNP K and U proteins are only 31% similar in mice (EMBOSS Stretcher Pairwise Sequence Alignment). While their consensus binding motifs argue against their recognizing overlapping sequences, there is evidence from high-throughput studies in humans and mice that hnRNP K and U proteins immunopurify (49) and cofractionate (50, 51) together.

To determine if hnRNP K and U knockdown RAW 264.7 cell lines may be phenotypically similar, we identified several clusters of up- and down-regulated genes common to both cell lines. Two clusters of upregulated genes are highlighted in **Figure 8A**. Interestingly, Cluster 1 contains mostly ISGs (*Ifi202b*, *Bst2*, *Irf7*, *Ifitm3*, *Isg15*, *Ifi44l*, *Oasl1*) while Cluster 2 is enriched for a diverse group of kinases (*Dmpk*, *Ripk3*), regulators of GTPase activity (*Gng10*, *Rgs16*, *Fgd2*), and mitochondrial related factors (*Pmaip1, Ucp2*). Differential expression of ISGs in uninfected hnRNP K and U knockdown cell lines is notable because it suggests that loss of these factors somehow activates macrophages to upregulate type I interferon stimulated genes (see model in **Figure 1B**). This basal ISG phenotype can also be appreciated by looking at RNA-seq reads *via* the Integrated Genome Viewer (Broad), whereby *Isg15*, *Ifi44i*, and *Apol9a* are expressed at 2-3-fold higher than SCR controls in both hnRNP K and hnRNP U knockdown uninfected macrophages, but *Actb* showed no difference in expression (**Figure 8B**). We confirmed this high basal ISG phenotype *via* RT-qPCR in both hnRNP K and U knockdown cell lines for several representative ISGs: *Irf7* (**Figure 8C**), *Isg15* (**Figure 8D**), *Ifi44l* (**Figure 8E**), and *Trex1* (**Figure 8F**).

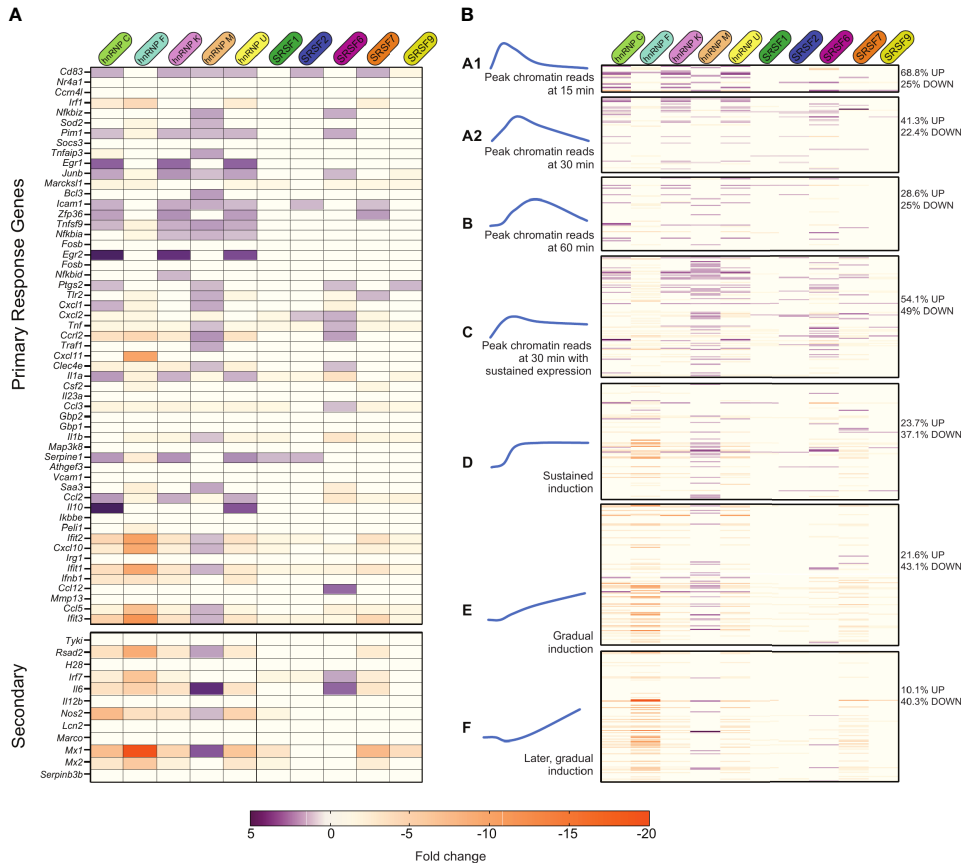

FIGURE 7 | Many primary response and early induced innate immune genes are repressed by SR/hnRNPs. **(A)** Fold change of SR/hnRNP DEGs in *Salmonella*-infected RAW 264.7 macrophages compared to SCR controls for genes categorized as primary (top) and secondary (bottom) response genes according to 10. 35/53 primary response genes are upregulated by loss of one or more SR/hnRNPs at 4h post-*Salmonella* infection. **(B)** Fold change of SR/hnRNP DEGs in *Salmonella*-infected RAW 264.7 macrophages compared to SCR controls with Lipid A-induced genes categorized on basis of induction kinetics as defined by 6. Percentages on right indicate the number of genes in each category that are differentially expressed (up- or down-regulated) by loss of one or more SR/hnRNP. (left) Blue curves are schematic representations of the induction kinetics of each Group (A1, A2, B, C, D, E, and F) over a 120-minute time course following Lipid A treatment. Adapted from 6.

While the profiles of SR/hnRNP-sensitive genes change dramatically upon *Salmonella* infection, we still observe significant correlation between genes impacted by loss of hnRNP K and hnRNP U (**Figure 8G**) (correlation between K/U: 0.79; correlation between C/K/U: 0.76). Interestingly, upon *Salmonella* infection, several of the Cluster 1 ISGs actually became less abundant relative to SCR controls (**Figure 8G**; *Oasl2*, *Ddx58*, *Isg15*, *Usp18*; +SAL Cluster 3), highlighting dysregulation of specific type I interferon genes in the absence of hnRNP K and U. Cluster 2 DEGs, on the other hand, were more abundant in both uninfected and *Salmonella*-infected hnRNP K and U knockdown macrophages (**Figure 8G**; +SAL Clusters 4 and 5). Overlap between hnRNP K and U DEGs and DIUs is illustrated by Venn diagrams that show that one-third of total DEGs are shared and three-fourths of DIUs (**Figure 8H**).

A major role for interferon stimulated genes is controlling viral replication through a variety of restriction mechanisms [e.g. limit viral entry, inhibit replication of the viral genome, interfere with host cell translation, etc. (36)]. Thus, we asked whether viral replication was impacted at early infection time points in hnRNP K and U knockdown cell lines compared to SCR controls. We infected SCR, hnRNP K and hnRNP U knockdown RAW 264.7 macrophages with vesicular stomatitis virus (VSV) at a MOI of 1 and measured viral replication over a 12h time course by quantifying expression of two viral genes, VSV-G and VSV-M by RT-qPCR. VSV is a single-stranded, enveloped RNA virus that can replicate and elicit robust gene expression changes in RAW 264.7 cells (52). Remarkably, we observed almost no replication of VSV in either hnRNP knockdown cell line at any time point (**Figures 8I, J**). A similar hyper-restriction phenotype was recently reported for hnRNP K knockdown A549 cell lines infected with influenza virus by (46). Thompson et al. attribute this phenotype to hnRNP K-dependent alternative splicing of a number of genes required for viral replication. Notably, we detect DIUs for several of the same genes (Setd5, Arhgap12, Gpbp1, and Eri2) (**Supplementary Table 1**), suggesting that hnRNP K's role in viral infection is conserved between mice and humans and may, in part, be mediated by the same alternative splicing events.

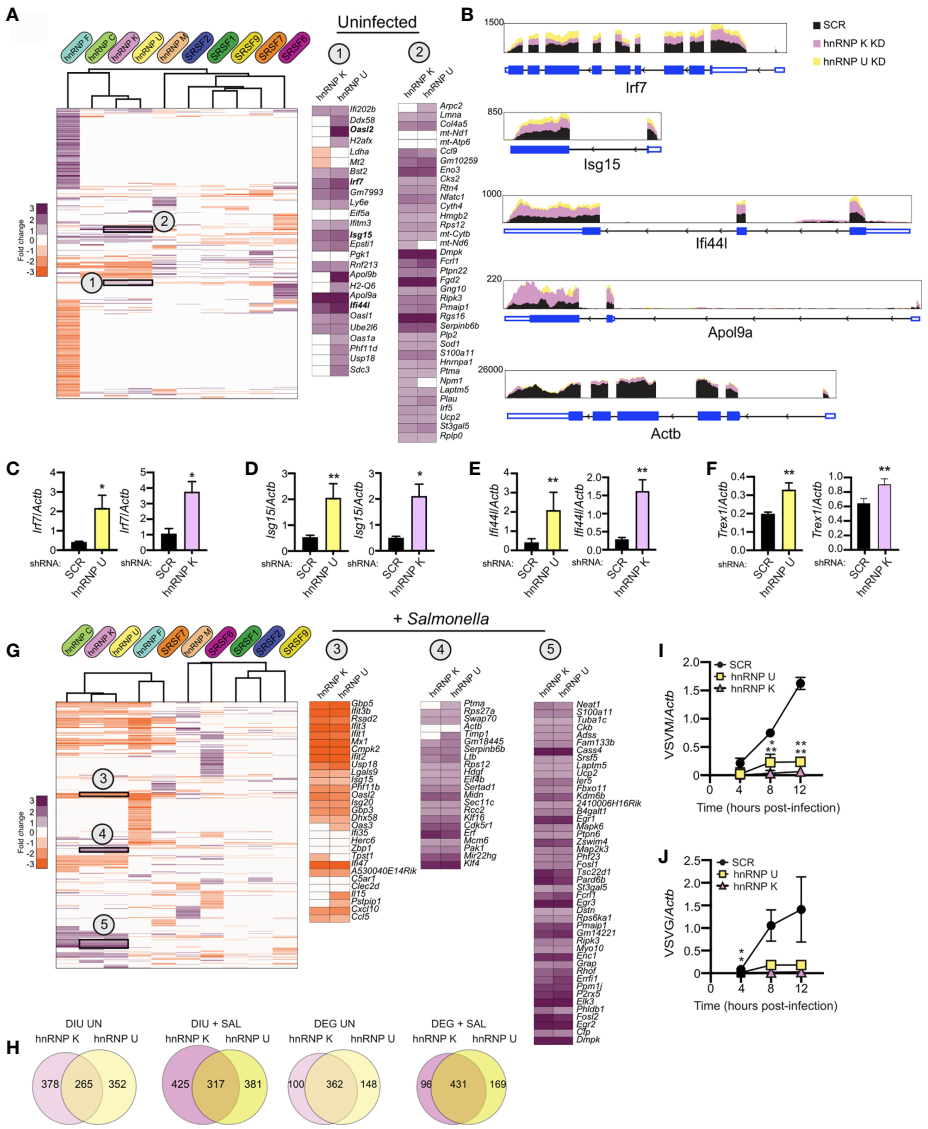

FIGURE 8 | Loss of hnRNP K and hnRNP U affects similar DEGs and DIU and impacts the ability of RAW 264.7 macrophages to control viral replication. **(A)** Hierarchical clustering of up- and down-regulated DEGs in uninfected macrophages (SR/hnRNP knockdown vs. SCR). Zoom-ins of clusters of interest (1 and 2) are shown to the right. Correlation of Cluster 1 is 0.84; Cluster 2 is 0.76. To allow for better visualization of DEGs, the scale is set at -3 to +3. **(B)** IGV tracks showing RNA-seq reads for *Irf7*, *Isg15, Ifi44l*, and *Apol9a* in hnRNP K and hnRNP U compared to SCR control reads. *Actb* is included as a representative unaffected control gene. **(C)** RT-qPCR validation of *Irf7* basal expression in hnRNP U and K knockdown cell lines vs. SCR controls. Data is displayed as *Irf7/Actb*. **(D)** As in **(C)** but for *Isg15*. **(E)** as in **(C)** but for *Ifi44l*. **(F)** as in **(C)** but for *Trex1*. **(G)** As in **(A)** but for *Salmonella*-infected macrophages. Correlation of Cluster 3 is 0.75; Cluster 4 is 0.78; Cluster 5 is 0.72. **(H)** Overlap of DIUs and DEGs in uninfected and *Salmonella*-infected hnRNP K and U knockdown macrophages. *(I)* Vesicular Stomatitis Virus (VSV) replication (as measured by RT-qPCR of the VSVM gene relative to *Actb*) in hnRNP K and hnRNP U knockdown macrophages compared to SCR controls (VSV MOI = 1) at 4, 8, and 12h post-infection. **(J)** as in **(I)** but for VSVG. For all RT-qPCRs, values are the mean of 3 biological replicates and error bars indicate standard deviation. *$p < 0.05$; **$p < 0.01$.

Lastly, we wanted to determine whether loss of hnRNP K or U impacted the outcome of *Salmonella* infection. We infected SCR, hnRNP K knockdown, and hnRNP U knockdown RAW 264.7 cell lines with an overnight culture of *Salmonella* (53) at an MOI of 10 and measured colony forming units (CFUs) at 2h (a measure of internalization) and 20h (a measure of intracellular replication) post-infection. We observed an almost two-fold increase in *Salmonella* replication in hnRNP K knockdown macrophages relative to SCR controls, but no apparent difference attributable to loss of hnRNP U (**Figure 9A**). Leveraging our transcriptomics and alternative splicing analysis, we looked to see if we could identify changes that were unique to hnRNP K. We observed that hnRNP K knockdown in RAW 264.7 macrophages preferentially impacted alternative splicing events of genes involved in RhoA and Cdc42 signaling (**Figure 9B**, top). These top enriched categories were very different from those in hnRNP U, which showed enrichment for

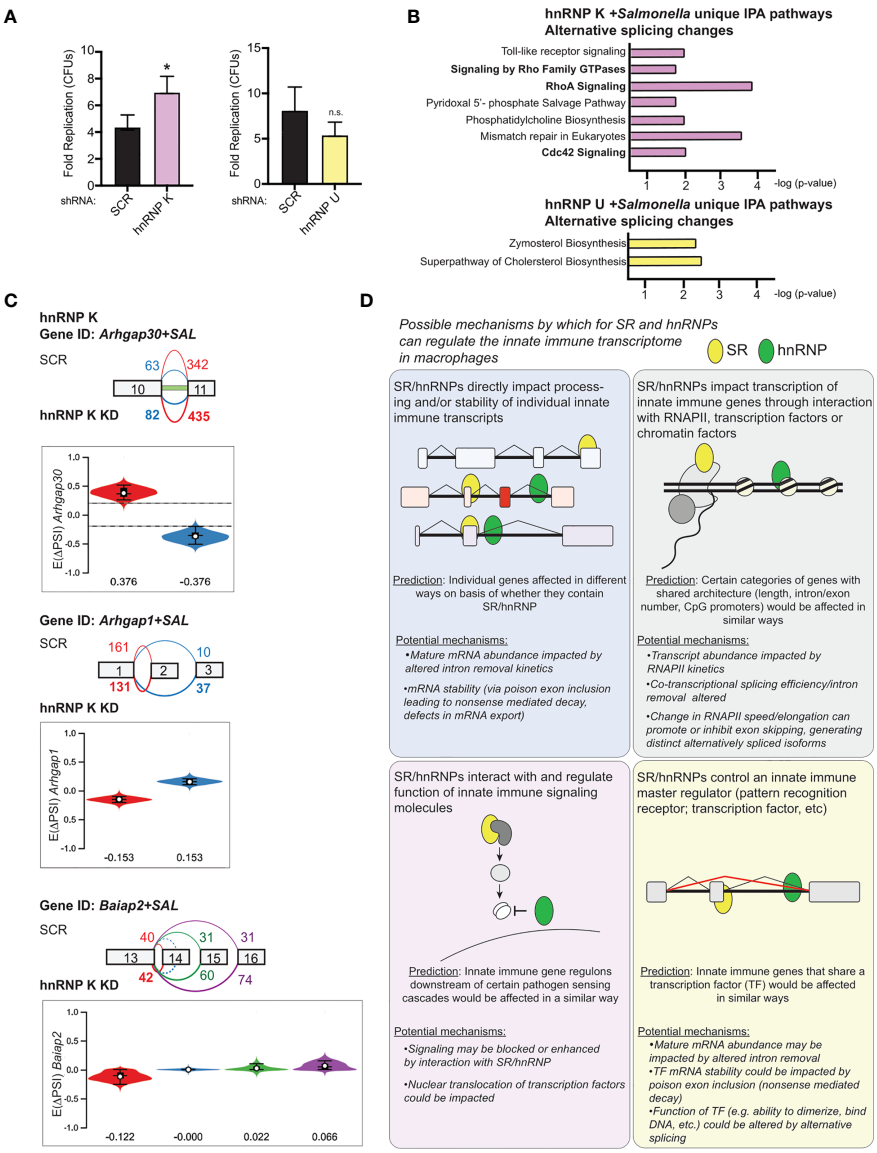

FIGURE 9 | hnRNP K regulates *Salmonella* replication and controls alternative splicing of genes involved in RhoA/Rac1-mediated reorganization of the actin cytoskeleton. **(A)** Colony forming units represented as fold replication (20h time point relative to 2h time point) in hnRNP K and hnRNP U knockdown RAW 264.7 macrophages infected with *Salmonella* Typhimurium (MOI = 10) **(B)** Ingenuity Pathway Analysis of hnRNP K (top) and hnRNP U (bottom) knockdown macrophages at 4h post-*Salmonella* infection. Pathways shown are unique to hnRNP K or hnRNP U cells and enrichment is shown as -log(p-value). **(C)** Local splicing variations identified in three genes related to Cdc42-mediated reorganization of the actin cytoskeleton: Arhgap30, Arhgap1, and Baiap2. Color of splicing events in the gene schematic corresponds to the colors in the violin plots (showing EΔPSI). **(D)** Model of the potential mechanisms through which SR and hnRNP family members could impact innate immune gene expression in macrophages. For all RT-qPCRs values are the mean of 2 or 3 biological replicates and error bars indicate standard deviation.*p < 0.05; n.s. is not statistically significant.

DIUs in genes involved in cholesterol biosynthesis (**Figure 9B**, bottom). RhoA and Cdc42 are Rho GTPases that co-ordinate cytoskeletal dynamics (54). We detected differential isoform usage for several transcripts involved in these pathways including *Arhgap30*, *Arhgap1*, and *Baiap2* (**Figure 9C**). In fact, the intron retention event in *Arhgap30* is the one of the most abundant DIUs in hnRNP K knockdown macrophages (E(ΔPSI) 0.376) (**Supplementary Table 1**). This DIU is predicted to decrease the relative abundance of protein coding-competent *Arhgap30* mRNA in the cell, while events in *Arhgap1* and *Baiap2* are predicted to change the amino acid sequence of the protein isoform. Our finding that *Salmonella* can replicate more efficiently in the presence of these alternative splicing changes is consistent with work showing that actin polymerization is critical for stabilization of the *Salmonella*-containing vacuole and replication of intravacuolar *Salmonella* in cells like macrophages (55, 56). These data suggest

that hnRNP K may impact actin dynamics through alternative splicing of *Arhgap30*, *Arhgap1*, and *Baiap2*. Furthermore, our results argue that individual splicing factors can contribute to innate immune and infection outcomes in unique ways and demonstrate that together, transcriptomics and alternative splicing analysis has the potential to identify host factors that regulate the host-pathogen interface.

DISCUSSION

Our study illustrates the diverse effects the SR/hnRNP family splicing factors have on the macrophage transcriptome both in uninfected macrophages and in cells infected with the gram-negative bacterial pathogen *Salmonella* Typhimurium. While implicating SR and hnRNPs in regulating gene expression is not remarkable, the degree to which each of the splicing factors queried impacts distinct gene regulons in each of these conditions is unexpected. Overall, we found that over 70% of the genes induced as part of the macrophage innate immune response (>2-fold at 4h post-infection) are hyper- or hypo-induced in the absence of one or more of the SR/hnRNPs we investigated. This work highlights a critical role for splicing regulatory proteins in controlling the magnitude of innate immune gene induction and calls for a rethinking of how the innate immune response is post-transcriptionally regulated.

One critical lingering question raised by these studies relates to the mechanism(s) through which genes are up or down regulated in SR/hnRNP knockdown RAW 264.7 macrophages. While our analysis did identify DIU in transcripts encoding several transcription factors in the IRF, STAT, and NFκB families (*Irf1*, *Irf5*, *Irf7*, *Irf9*, and *Stat1*), our data does not generally support a model whereby loss of a particular SR/hnRNP results in mis-splicing or functional alteration of a master regulator of a shared transcriptional regulon. Likewise, although individual cases likely exist, our data does not support a role for SR/hnRNPs in globally regulating innate immune transcript abundance *via* differential inclusion of poison exons (as DIU was not enriched in DEGs). Indeed, the most overlap between DIU and DEG we observed was for hnRNP F and even that was only 10% (**Figure S5**). Thus, the question remains: how do individual SR/hnRNPs activate and/or repress induction of innate immune genes? Several mechanisms are likely and are by no means mutually exclusive (**Figure 9D**). The first possible mechanism driving at least some of these changes is direct binding of SR/hnRNPs to target pre-mRNAs to promote or inhibit constitutive intron removal. Second, certain SRs and hnRNPs could contribute to transcriptional changes by interacting with RNA polymerase and/or other factors at the chromatin level. Indeed, to promote co-transcriptional splicing, some SR proteins interact with the CTD of RNA polymerase II (57–59) and some SR proteins have been shown to interact with histones (60). Third, SR/hnRNPs may alter innate immune gene expression by interacting with components of innate immune signaling cascades themselves, such as pathogen recognition receptors or downstream kinases/transcription factors. Such a mechanism was recently described for hnRNPA2B1, which controls initiation of the type I IFN response in part *via* interactions with the kinase TBK1 and its substrate IRF3 (61). Lastly, although our data does not provide strong support for such a model, it is possible that loss of SR/hnRNPs alters the abundance or function of innate immune transcription factors themselves at either the RNA or protein level. Implicating one or more of these mechanisms will require detailed follow-up analysis on individual SR/hnRNPs. Identifying the direct RNA and protein binding targets of these splicing factors in uninfected and *Salmonella*-infected macrophages will certainly help inform on these mechanisms, as will defining the subcellular localization of these RNA-binding proteins in the two conditions.

Previous work from our lab found hnRNP M knockdown leads to hyper-induction of a number of innate immune transcripts following inflammatory triggers, which suggests that slowing/inhibiting pre-mRNA maturation may be involved. Specifically, our earlier work found that overexpression of hnRNP M promotes accumulation of intron-containing *Il6* pre-mRNAs, while loss of hnRNP M increases removal of *Il6* intron 3 (31). From these findings we concluded that by repressing constitutive intron removal in *Il6*, hnRNP M slows early or spurious transcriptional activation of this pro-inflammatory cytokine. It is possible that other SR and hnRNPs work in the same way, by contributing to specific constitutive intron removal events that can fine-tune the kinetics of transcript maturation and influence steady state RNA levels. Such a model would predict increased levels of reads from particular introns in DEGs. Although we do not see evidence for this in our RNA-seq data, this is not particularly surprising given the low abundance of intron-containing pre-mRNAs relative to mRNAs. Indeed, an important caveat of these studies is that they were carried out at a single time point following *Salmonella* infection. While we chose this time point to maximize mRNA transcript accumulation, we may have inadvertently minimized our ability to detect transient accumulation of unprocessed transcript intermediates. Kinetic transcriptome analysis from the Black and Smale labs demonstrates that for most transcripts, pre-mRNA splicing of innate immune transcripts occurs co-transcriptionally but accumulation of nascent pre-mRNA at the chromatin level is generally not evident at time points following 15-30 minutes, except in select cases with especially long transcripts on which splicing catalysis is delayed (6, 7). Thus, it is possible that for many of our transcripts of interest, the most important contribution of SR/hnRNP proteins to constitutive and/or alternative splicing occurs during that early transcriptional burst, minutes after pathogen sensing. Thus, future attempts to elucidate the complexities of post-transcriptional control of inflammatory gene induction will want to broaden their scope to include additional early time points following macrophage activation.

At the onset of this study, we hypothesized that because SRSF1, 2, 6, 7, 9 and hnRNP C, F, K, M, and U have been shown to be differentially phosphorylated during bacterial and fungal infection of macrophages (23–25), they would impact distinct gene regulons in uninfected vs. S*almonella*-infected cell lines.

Several studies have linked environmental changes to post-translational modification (PTM) of splicing factors. For example, dephosphorylation of SRSF10 by the phosphatase PP1 represses splicing and limits gene expression in HeLa cells following heat shock (18, 20, 62). Additionally, arginine methylation of hnRNPA1/B2 triggers its export to the cytoplasm where it activates TBK1/IRF3 signaling following infection with a DNA virus (61). Recent work from the Lynch lab showed that hnRNP K is redistributed in the nucleus during influenza infection, becoming enriched in nuclear speckles (46). Indeed, subcellular redistribution is a common trait of SR/hnRNPs during infection (63, 64) and many viruses themselves require RNA binding proteins for the maintenance and processing of their genomes. Future studies designed to investigate how pathogen sensing influences post-translational modification of SR and hnRNPs will provide important insights into how splicing factors are functionalized during the macrophage innate immune response as well as in response to cellular stresses in general.

DATA AVAILABILITY STATEMENT

The datasets presented in this study can be found in online repositories. The name of the repository and accession number can be found below: National Center for Biotechnology Information (NCBI) Gene Expression Omnibus (GEO), https://www.ncbi.nlm.nih.gov/geo/, GSE171418.

AUTHOR CONTRIBUTIONS

KW and AW generated the knockdown cell lines, carried out *Salmonella* infections and performed RNA sequencing. KW performed bioinformatics analysis. AW, HS, AC, TF, and KC performed experimental validations. KV, KP, and RW contributed to data visualization. KP, RW, AW and HS prepared and edited the figures and manuscript. All authors contributed to the article and approved the submitted version.

FUNDING

This work was funded by the National Institutes of Health/NIGMS, R35GM133720 (KLP) and National Institutes of Health/NIAID R01AI125512 (ROW).

ACKNOWLEDGMENTS

We would like to thank members of the KP and RW labs for their critical reading of and feedback on this manuscript. We would also like to thank members of Phillip West's lab at TAMU COM for help with the VSV infections and Helene Andrews-Polymenis for sharing the SL1344 *Salmonella* Typhimurium strain. We would like to acknowledge Andrew Hillhouse and the Institute for Genome Sciences and Society at TAMU for performing our RNA-sequencing experiments.

SUPPLEMENTARY MATERIAL

The Supplementary Material for this article can be found online at: https://www.frontiersin.org/articles/10.3389/fimmu.2021.656885/full#supplementary-material

REFERENCES

1. Nathan C. Points of Control in Inflammation. *Nature* (2002) 420(6917):846–52. doi: 10.1038/nature01320
2. Foster SL, Medzhitov R. Gene-Specific Control of the TLR-induced Inflammatory Response. *Clin Immunol* (2009) 130(1):7–15. doi: 10.1016/j.clim.2008.08.015
3. Medzhitov R. Recognition of Microorganisms and Activation of the Immune Response. *Nature* (2007) 449(7164):819–26. doi: 10.1038/nature06246
4. Fowler T, Sen R, Roy AL. Regulation of Primary Response Genes. *Mol Cell* (2011) 44(3):348–60. doi: 10.1016/j.molcel.2011.09.014
5. Ahmed AU, Williams BR, Hannigan GE. Transcriptional Activation of Inflammatory Genes: Mechanistic Insight Into Selectivity and Diversity. *Biomolecules* (2015) 5(4):3087–111. doi: 10.3390/biom5043087
6. Bhatt DM, Pandya-Jones A, Tong AJ, Barozzi I, Lissner MM, Natoli G, et al. Transcript Dynamics of Proinflammatory Genes Revealed by Sequence Analysis of Subcellular Rna Fractions. *Cell* (2012) 150(2):279–90. doi: 10.1016/j.cell.2012.05.043
7. Pandya-Jones A, Bhatt DM, Lin CH, Tong AJ, Smale ST, Black DL. Splicing Kinetics and Transcript Release From the Chromatin Compartment Limit the Rate of Lipid a-Induced Gene Expression. *RNA* (2013) 19(6):811–27. doi: 10.1261/rna.039081.113
8. Thanos D, Maniatis T. Virus Induction of Human Ifn Beta Gene Expression Requires the Assembly of an Enhanceosome. *Cell* (1995) 83(7):1091–100. doi: 10.1016/0092-8674(95)90136-1
9. Agalioti T, Lomvardas S, Parekh B, Yie J, Maniatis T, Thanos D. Ordered Recruitment of Chromatin Modifying and General Transcription Factors to the IFN-beta Promoter. *Cell* (2000) 103(4):667–78. doi: 10.1016/S0092-8674(00)00169-0
10. Ramirez-Carrozzi VR, Braas D, Bhatt DM, Cheng CS, Hong C, Doty KR, et al. A Unifying Model for the Selective Regulation of Inducible Transcription by CpG Islands and Nucleosome Remodeling. *Cell* (2009) 138(1):114–28. doi: 10.1016/j.cell.2009.04.020
11. Ramirez-Carrozzi VR, Nazarian AA, Li CC, Gore SL, Sridharan R, Imbalzano AN, et al. Selective and Antagonistic Functions of SWI/SNF and Mi-2beta Nucleosome Remodeling Complexes During an Inflammatory Response. *Genes Dev* (2006) 20(3):282–96. doi: 10.1101/gad.1383206
12. Zhong H, May MJ, Jimi E, Ghosh S. The Phosphorylation Status of Nuclear Nf-Kappa B Determines its Association With CBP/p300 or HDAC-1. *Mol Cell* (2002) 9(3):625–36. doi: 10.1016/S1097-2765(02)00477-X
13. Dong J, Jimi E, Zhong H, Hayden MS, Ghosh S. Repression of Gene Expression by Unphosphorylated Nf-Kappab P65 Through Epigenetic Mechanisms. *Genes Dev* (2008) 22(9):1159–73. doi: 10.1101/gad.1657408
14. van Essen D, Engist B, Natoli G, Saccani S. Two Modes of Transcriptional Activation at Native Promoters by NF-kappaB P65. *PloS Biol* (2009) 7(3):e73. doi: 10.1371/journal.pbio.1000073
15. Richards AL, Watza D, Findley A, Alazizi A, Wen X, Pai AA, et al. Environmental Perturbations Lead to Extensive Directional Shifts in RNA Processing. *PloS Genet* (2017) 13(10):e1006995. doi: 10.1371/journal.pgen.1006995

16. Shin C, Feng Y, Manley JL. Dephosphorylated SRp38 Acts as a Splicing Repressor in Response to Heat Shock. *Nature* (2004) 427(6974):553–8. doi: 10.1038/nature02288
17. Zhong XY, Ding JH, Adams JA, Ghosh G, Fu XD. Regulation of SR Protein Phosphorylation and Alternative Splicing by Modulating Kinetic Interactions of SRPK1 With Molecular Chaperones. *Genes Dev* (2009) 23(4):482–95. doi: 10.1101/gad.1752109
18. Shi Y, Nishida K, Campigli Di Giammartino D, Manley JL. Heat Shock-Induced Srsf10 Dephosphorylation Displays Thermotolerance Mediated by Hsp27. *Mol Cell Biol* (2011) 31(3):458–65. doi: 10.1128/MCB.01123-10
19. Munoz MJ, Perez Santangelo MS, Paronetto MP, de la Mata M, Pelisch F, Boireau S, et al. Dna Damage Regulates Alternative Splicing Through Inhibition of RNA Polymerase II Elongation. *Cell* (2009) 137(4):708–20. doi: 10.1016/j.cell.2009.03.010
20. Shkreta L, Toutant J, Durand M, Manley JL, Chabot B. Srsf10 Connects Dna Damage to the Alternative Splicing of Transcripts Encoding Apoptosis, Cell-Cycle Control, and DNA Repair Factors. *Cell Rep* (2016) 17(8):1990–2003. doi: 10.1016/j.celrep.2016.10.071
21. Pai AA, Baharian G, Page Sabourin A, Brinkworth JF, Nedelec Y, Foley JW, et al. Widespread Shortening of 3' Untranslated Regions and Increased Exon Inclusion are Evolutionarily Conserved Features of Innate Immune Responses to Infection. *PloS Genet* (2016) 12(9):e1006338. doi: 10.1371/journal.pgen.1006338
22. Frankiw L, Mann M, Li G, Joglekar A, Baltimore D. Alternative Splicing Coupled With Transcript Degradation Modulates OAS1g Antiviral Activity. *RNA* (2020) 26(2):126–36. doi: 10.1261/rna.073825.119
23. Budzik JM, Swaney DL, Jimenez-Morales D, Johnson JR, Garelis NE, Repasy T, et al. Dynamic Post-Translational Modification Profiling of Mycobacterium Tuberculosis-Infected Primary Macrophages. *Elife* (2020) 9. doi: 10.7554/eLife.51461
24. Penn BH, Netter Z, Johnson JR, Von Dollen J, Jang GM, Johnson T, et al. An Mtb-Human Protein-Protein Interaction Map Identifies a Switch Between Host Antiviral and Antibacterial Responses. *Mol Cell* (2018) 71(4):637–48 e5. doi: 10.1016/j.molcel.2018.07.010
25. Pandey A, Ding SL, Qin QM, Gupta R, Gomez G, Lin F, et al. Global Reprogramming of Host Kinase Signaling in Response to Fungal Infection. *Cell Host Microbe* (2017) 21(5):637–49 e6. doi: 10.1016/j.chom.2017.04.008
26. Vaquero-Garcia J, Barrera A, Gazzara MR, Gonzalez-Vallinas J, Lahens NF, Hogenesch JB, et al. A New View of Transcriptome Complexity and Regulation Through the Lens of Local Splicing Variations. *Elife* (2016) 5: e11752. doi: 10.7554/eLife.11752
27. Paz I, Kosti I, Ares MJr., Cline M, Mandel-Gutfreund Y. Rbpmap: A Web Server for Mapping Binding Sites of RNA-binding Proteins. *Nucleic Acids Res* (2014) 42(Web Server issue):W361–7. doi: 10.1093/nar/gku406
28. Fitzgerald KA, Rowe DC, Barnes BJ, Caffrey DR, Visintin A, Latz E, et al. Lps-Tlr4 Signaling to IRF-3/7 and NF-kappaB Involves the Toll Adapters TRAM and TRIF. *J Exp Med* (2003) 198(7):1043–55. doi: 10.1084/jem.20031023
29. Tong AJ, Liu X, Thomas BJ, Lissner MM, Baker MR, Senagolage MD, et al. A Stringent Systems Approach Uncovers Gene-Specific Mechanisms Regulating Inflammation. *Cell* (2016) 165(1):165–79. doi: 10.1016/j.cell.2016.01.020
30. Orecchioni M, Ghosheh Y, Pramod AB, Ley K. Macrophage Polarization: Different Gene Signatures in M1(LPS+) vs. Classically and M2(LPS-) vs. Alternatively Activated Macrophages. *Front Immunol* (2019) 10:1084. doi: 10.3389/fimmu.2019.01084
31. West KO, Scott HM, Torres-Odio S, West AP, Patrick KL, Watson RO. The Splicing Factor Hnrnp M is a Critical Regulator of Innate Immune Gene Expression in Macrophages. *Cell Rep* (2019) 29(6):1594–1609 e5. doi: 10.1016/j.celrep.2019.09.078
32. Talkish J, Igel H, Perriman RJ, Shiue L, Katzman S, Munding EM, et al. Rapidly Evolving Protointrons in Saccharomyces Genomes Revealed by a Hungry Spliceosome. *PloS Genet* (2019) 15(8):e1008249. doi: 10.1371/journal.pgen.1008249
33. Pleiss JA, Whitworth GB, Bergkessel M, Guthrie C. Rapid, Transcript-Specific Changes in Splicing in Response to Environmental Stress. *Mol Cell* (2007) 27 (6):928–37. doi: 10.1016/j.molcel.2007.07.018
34. Munding EM, Shiue L, Katzman S, Donohue JP, Ares MJr. Competition Between pre-mRNAs for the Splicing Machinery Drives Global Regulation of Splicing. *Mol Cell* (2013) 51(3):338–48. doi: 10.1016/j.molcel.2013.06.012
35. Huelga SC, Vu AQ, Arnold JD, Liang TY, Liu PP, Yan BY, et al. Integrative Genome-Wide Analysis Reveals Cooperative Regulation of Alternative Splicing by hnRNP Proteins. *Cell Rep* (2012) 1(2):167–78. doi: 10.1016/j.celrep.2012.02.001
36. Schoggins JW. Interferon-Stimulated Genes: What Do They All do? *Annu Rev Virol* (2019) 6(1):567–84. doi: 10.1146/annurev-virology-092818-015756
37. Schoggins JW, Rice CM. Interferon-Stimulated Genes and Their Antiviral Effector Functions. *Curr Opin Virol* (2011) 1(6):519–25. doi: 10.1016/j.coviro.2011.10.008
38. Schoggins JW, Wilson SJ, Panis M, Murphy MY, Jones CT, Bieniasz P, et al. A Diverse Range of Gene Products are Effectors of the Type I Interferon Antiviral Response. *Nature* (2011) 472(7344):481–5. doi: 10.1038/nature09907
39. Krecic AM, Swanson MS. Hnrnp Complexes: Composition, Structure, and Function. *Curr Opin Cell Biol* (1999) 11(3):363–71. doi: 10.1016/S0955-0674(99)80051-9
40. Long JC, Caceres JF. The SR Protein Family of Splicing Factors: Master Regulators of Gene Expression. *Biochem J* (2009) 417p(1):15–27. doi: 10.1042/BJ20081501
41. Bradley T, Cook ME, Blanchette M. Sr Proteins Control a Complex Network of RNA-processing Events. *RNA* (2015) 21(1):75–92. doi: 10.1261/rna.043893.113
42. Geuens T, Bouhy D, Timmerman V. The Hnrnp Family: Insights Into Their Role in Health and Disease. *Hum Genet* (2016) 135(8):851–67. doi: 10.1007/s00439-016-1683-5
43. Han SP, Tang YH, Smith R. Functional Diversity of the Hnrnps: Past, Present and Perspectives. *Biochem J* (2010) 430(3):379–92. doi: 10.1042/BJ20100396
44. Busch A, Hertel KJ. Evolution of SR Protein and Hnrnp Splicing Regulatory Factors. *Wiley Interdiscip Rev RNA* (2012) 3(1):1–12. doi: 10.1002/wrna.100
45. Fu XD, Ares MJr. Context-Dependent Control of Alternative Splicing by RNA-binding Proteins. *Nat Rev Genet* (2014) 15(10):689–701. doi: 10.1038/nrg3778
46. Thompson MG, Dittmar M, Mallory MJ, Bhat P, Ferretti MB, Fontoura BM, et al. Viral-Induced Alternative Splicing of Host Genes Promotes Influenza Replication. *Elife* (2020) 9. doi: 10.7554/eLife.55500
47. Swanson MS, Dreyfuss G. Classification and Purification of Proteins of Heterogeneous Nuclear Ribonucleoprotein Particles by RNA-binding Specificities. *Mol Cell Biol* (1988) 8(5):2237–41. doi: 10.1128/MCB.8.5.2237
48. Matunis MJ, Michael WM, Dreyfuss G. Characterization and Primary Structure of the Poly(C)-Binding Heterogeneous Nuclear Ribonucleoprotein Complex K Protein. *Mol Cell Biol* (1992) 12(1):164–71. doi: 10.1128/MCB.12.1.164
49. Mikula M, Rubel T, Karczmarski J, Statkiewicz M, Bomsztyk K, Ostrowski J. Beads-Free Protein Immunoprecipitation for a Mass Spectrometry-Based Interactome and Posttranslational Modifications Analysis. *Proteome Sci* (2015) 13:23. doi: 10.1186/s12953-015-0079-0
50. Havugimana PC, Hart GT, Nepusz T, Yang H, Turinsky AL, Li Z, et al. A Census of Human Soluble Protein Complexes. *Cell* (2012) 150(5):1068–81. doi: 10.1016/j.cell.2012.08.011
51. Pourhaghighi R, Ash PEA, Phanse S, Goebels F, Hu LZM, Chen S, et al. Brainmap Elucidates the Macromolecular Connectivity Landscape of Mammalian Brain. *Cell Syst* (2020) 11(2):208. doi: 10.1016/j.cels.2020.08.006
52. Kandasamy RK, Vladimer GI, Snijder B, Muller AC, Rebsamen M, Bigenzahn JW, et al. A Time-Resolved Molecular Map of the Macrophage Response to VSV Infection. *NPJ Syst Biol Appl* (2016) 2:16027. doi: 10.1038/npjsba.2016.27
53. Drecktrah D, Knodler LA, Ireland R, Steele-Mortimer O. The Mechanism of Salmonella Entry Determines the Vacuolar Environment and Intracellular Gene Expression. *Traffic* (2006) 7(1):39–51. doi: 10.1111/j.1600-0854.2005.00360.x
54. Martin K, Reimann A, Fritz RD, Ryu H, Jeon NL, Pertz O. Spatio-Temporal Co-Ordination of RhoA, Rac1 and Cdc42 Activation During Prototypical Edge Protrusion and Retraction Dynamics. *Sci Rep* (2016) 6:21901. doi: 10.1038/srep21901
55. Meresse S, Unsworth KE, Habermann A, Griffiths G, Fang F, Martinez-Lorenzo MJ, et al. Remodelling of the Actin Cytoskeleton is Essential for Replication of Intravacuolar Salmonella. *Cell Microbiol* (2001) 3(8):567–77. doi: 10.1046/j.1462-5822.2001.00141.x

56. Yeung ATY, Choi YH, Lee AHY, Hale C, Ponstingl H, Pickard D, et al. A Genome-Wide Knockout Screen in Human Macrophages Identified Host Factors Modulating Salmonella Infection. *mBio* (2019) 10(5). doi: 10.1128/mBio.02169-19
57. Das R, Dufu K, Romney B, Feldt M, Elenko M, Reed R. Functional Coupling of RNAP Ii Transcription to Spliceosome Assembly. *Genes Dev* (2006) 20 (9):1100–9. doi: 10.1101/gad.1397406
58. de la Mata M, Munoz MJ, Allo M, Fededa JP, Schor IE, Kornblihtt AR. Rna Polymerase Ii Elongation at the Crossroads of Transcription and Alternative Splicing. *Genet Res Int* (2011) 2011:309865. doi: 10.4061/2011/309865
59. Sapra AK, Anko ML, Grishina I, Lorenz M, Pabis M, Poser I, et al. Sr Protein Family Members Display Diverse Activities in the Formation of Nascent and Mature Mrnps In Vivo. *Mol Cell* (2009) 34(2):179–90. doi: 10.1016/j.molcel.2009.02.031
60. Loomis RJ, Naoe Y, Parker JB, Savic V, Bozovsky MR, Macfarlan T, et al. Chromatin Binding of SRp20 and ASF/SF2 and Dissociation From Mitotic Chromosomes is Modulated by Histone H3 Serine 10 Phosphorylation. *Mol Cell* (2009) 33(4):450–61. doi: 10.1016/j.molcel.2009.02.003
61. Wang L, Wen M, Cao X. Nuclear Hnrnpa2b1 Initiates and Amplifies the Innate Immune Response to DNA Viruses. *Science* (2019) 365(6454). doi: 10.1126/science.aav0758
62. Zhou X, Wu W, Li H, Cheng Y, Wei N, Zong J, et al. Transcriptome Analysis of Alternative Splicing Events Regulated by SRSF10 Reveals Position-Dependent Splicing Modulation. *Nucleic Acids Res* (2014) 42(6):4019–30. doi: 10.1093/nar/gkt1387
63. Zhao W, Wang L, Zhang M, Wang P, Qi J, Zhang L, et al. Nuclear to Cytoplasmic Translocation of Heterogeneous Nuclear Ribonucleoprotein U Enhances TLR-induced Proinflammatory Cytokine Production by Stabilizing mRNAs in Macrophages. *J Immunol* (2012) 188(7):3179–87. doi: 10.4049/jimmunol.1101175
64. Cao P, Luo WW, Li C, Tong Z, Zheng ZQ, Zhou L, et al. The Heterogeneous Nuclear Ribonucleoprotein Hnrnpm Inhibits Rna Virus-Triggered Innate Immunity by Antagonizing Rna Sensing of RIG-I-like Receptors. *PloS Pathog* (2019) 15(8):e1007983. doi: 10.1371/journal.ppat.1007983

Conflict of Interest: The authors declare that the research was conducted in the absence of any commercial or financial relationships that could be construed as a potential conflict of interest.

frontiers in Immunology

MINI REVIEW
published: 19 July 2021
doi: 10.3389/fimmu.2021.715675

Regulation of Early Lymphocyte Development *via* mRNA Decay Catalyzed by the CCR4-NOT Complex

Taishin Akiyama[1,2*] *and Tadashi Yamamoto*[3]

[1] Laboratory for Immune Homeostasis, RIKEN Center for Integrative Medical Sciences, Yokohama, Japan, [2] Graduate School of Medical Life Science, Yokohama City University, Yokohama, Japan, [3] Cell Signal Unit, Okinawa Institute of Science and Technology Graduate University, Okinawa, Japan

Development of lymphocytes is precisely regulated by various mechanisms. In addition to transcriptional rates, post-transcriptional regulation of mRNA abundance contributes to differentiation of lymphocytes. mRNA decay is a post-transcriptional mechanism controlling mRNA abundance. The carbon catabolite repression 4 (CCR4)-negative on TATA-less (NOT) complex controls mRNA longevity by catalyzing mRNA deadenylation, which is the rate-limiting step in the mRNA decay pathway. mRNA decay, regulated by the CCR4-NOT complex, is required for differentiation of pro-B to pre-B cells and V(D)J recombination in pro-B cells. In this process, it is likely that the RNA-binding proteins, ZFP36 ring finger protein like 1 and 2, recruit the CCR4-NOT complex to specific target mRNAs, thereby inducing cell quiescence of pro-B cells. A recent study showed that the CCR4-NOT complex participates in positive selection of thymocytes. Mechanistically, the CCR4-NOT deadenylase complex inhibits abnormal apoptosis by reducing the expression level of mRNAs encoding pro-apoptotic proteins, which are otherwise up-regulated during positive selection. We discuss mechanisms regulating CCR4-NOT complex-dependent mRNA decay in lymphocyte development and selection.

Keywords: mRNA decay, CCR4-NOT complex, lymphocyte development, Apoptosis, VDJ recombination

OPEN ACCESS

Edited by:
Osamu Takeuchi,
Kyoto University, Japan

Reviewed by:
Xiaocui He,
La Jolla Institute for Immunology (LJI), United States
Ryuya Fukunaga,
Johns Hopkins University, United States

***Correspondence:**
Taishin Akiyama
taishin.akiyama@riken.jp

Specialty section:
This article was submitted to Molecular Innate Immunity, a section of the journal Frontiers in Immunology

Received: *27 May 2021*
Accepted: *05 July 2021*
Published: *19 July 2021*

Citation:
Akiyama T and Yamamoto T (2021) Regulation of Early Lymphocyte Development via mRNA Decay Catalyzed by the CCR4-NOT Complex. Front. Immunol. 12:715675. doi: 10.3389/fimmu.2021.715675

INTRODUCTION

Pleiotropic mechanisms control cytoplasmic mRNA abundance. Besides transcriptional regulation, post-transcriptional mechanisms are critical for controlling the level of cytoplasmic mRNA. mRNA decay is a post-transcriptional mechanism for reducing mRNA abundance. One major role of mRNA decay systems is to control homeostatic turnover and quality of mRNA. In addition, mRNA decay pathways actively regulate mRNA abundance, which is necessary to maintain and alter mRNA quantity in response to physiological signals. Many studies have suggested that active regulation of mRNA decay mechanisms must be critical for immune regulation and homeostasis (1–14). In this review, we focus on functions of the mRNA decay system regulated by the carbon catabolite repression 4 (CCR4)-negative on TATA-less (NOT) deadenylase complex in early lymphocyte development.

mRNA DECAY MECHANISMS

Functionally, mRNA decay comprises two classes. The first is the mRNA decay system required for RNA surveillance to prevent generation of potentially toxic proteins (15). Nonsense-mediated mRNA decay (NMD) is an mRNA quality control pathway that degrades aberrant mRNAs with premature termination codons (16–18). In addition, No-go decay and No-stop decay pathways lead to mRNA decay in cases of ribosome stalling due to accidental blockades of translation and failure of termination, respectively (19).

The second class is the mRNA decay system that actively regulates amounts of mRNA encoding functional proteins. Exonuclease and endonuclease mRNA decay pathways mainly contribute to this "active" mRNA decay (14, 16, 20). In addition, some recent studies have proposed involvement of the NMD mechanism in regulation of mRNAs encoding full-length proteins during embryonic development and tissue-specific cell differentiation (18, 21).

INITIATION OF THE mRNA DECAY PATHWAY BY DEADENYLATION

The exonuclease pathway of mRNA decay is initiated by removing polyA tails from mRNAs (16, 20). Following deadenylation of polyA tails, the 5' cap structure of deadenylated mRNAs is removed by recruiting the decapping complex (Dcp1/Dcp2). Then 5'-3' exoribonuclease 1 and 2 degrade decapped mRNAs from their 5′ ends.

Deadenylation of mRNA is the rate-limiting step for the exonuclease pathway. At present, three deadenylases have been reported: carbon catabolite repressor 4-negative on the TATA (CCR4-NOT) complex, polyA nuclease 2 (Pan2)-Pan3, and polyA-specific ribonuclease (PARN) (16, 20). A previous study suggested that cytoplasmic deadenylase activity of the CCR4-NOT complex predominated (22). In contrast, PAN2/3 trims relatively long tails of polyA (above 150 nt) and exerts minimal influence on the transcriptome.

In humans and mice, The CCR4-NOT complex is composed of eight protein subunits (23–25). CCR4-NOT transcription complex subunit 1 (CNOT1) serves as a scaffold to assemble the other subunits and recruits RNA-binding proteins (26–28). Two subunits, CNOT6/6L and CNOT7/8, have deadenylase activity (29–32). Other CNOT subunits (CNOT2, 3, 9,10, and 11) lack deadenylase activity and may regulate catalytic functions of the complex (6, 33, 34). Individual deletion of CNOT2, CNOT3 and CNOT10 destabilized the complex and caused degradation of other subunits (6, 33, 34). Thus, these CNOT subunits evidently also contribute to the integrity of the whole CCR4-NOT complex. In addition, CNOT2 and CNOT3 form a heterodimer that recruits RNA-binding proteins to the CCR4-NOT complex (35, 36). Moreover, *in vitro* reconstitution experiments showed that the CNOT2-CNOT3 heterodimer maximizes the deadenylase activity and poly (A) selectivity of the CCR4-NOT complex (37).

Ablation of genes encoding individual subunits of the CCR4-NOT complex revealed its roles in various physiological functions. For instance, CNOT3 is required for postnatal liver functions (38), pancreatic β cell function and identity (39), maintaining cardiac homeostasis (40), and bone resorption (41). CNOT7, a catalytic subunit, has non-redundant functions in spermatogenesis (42, 43). In addition, some studies showed a requirement of deadenylation induced by the CCR4-NOT complex in early lymphocyte development (3, 4, 6).

FUNCTIONS OF THE CCR4-NOT COMPLEX IN LYMPHOCYTE DEVELOPMENT

Early B cell differentiation has been widely studied (44, 45). Pro-B cells derived from common progenitor cells differentiate into pre-B cells and subsequently immature B cells. In the transition of pro-B cells to pre-B cells, generation of the immunoglobulin (Ig) μ heavy chain assembled from variable (V_H), diversity (D_H), and joining (J_H) gene segments in pro-B cells is essential. Together with surrogate light chains, Igμ heavy chains form a precursor B cell receptor (pre-BCR). Pre-BCR signaling terminates the V(D)J recombination and induces rapid proliferation. After quiescence is re-established by later signaling from pre-BCR, recombination of light chains occurs for further differentiation of pre-B cells into immature B cells.

In B cell development, CNOT3 protein is up-regulated during differentiation from pro-B cells to pre-B cells (3). Two studies reported a requirement for CNOT3 in B cell development (3, 4). Inoue et al. (3) showed that B cell-specific deletion of *Cnot3* in mice with *Mbl*1-Cre deleter resulted in a severe reduction of pre-B cell differentiation thereafter. Moreover, rearrangements resulting from joining of distal variable gene segments of the Ig heavy chain (*Igh*) gene (V_H) to its diversity and joining (D_H J_H) gene segments were impaired, although the proximal V_H to D_H J_H rearrangement and D_H to J_H rearrangement were not affected. Mechanistically, the CCR4-NOT complex mediates deadenylation of *Trp53* mRNA coding p53 protein, reducing its transcript level in pro-B cells. *Cnot3* deletion caused up-regulation of p53, thereby causing an increase in the expression level of pro-apoptotic genes regulated by p53. Interestingly, deletion of the *p53* gene partially rescued the defect of pro-B cell differentiation due to the CNOT3 deficiency, but it did not rescue the failure of the distal V_H to D_H J_H rearrangement. Thus, CCR4-NOT complex-mediated RNA decay ensures gene rearrangement in pro-B cells through p53-independent mechanisms and prevents abnormal apoptosis in both p53-dependent and independent mechanisms during the pro-B cell to pre-B cell transition (**Figure 1**).

Yang et al. also reported a defect in the transition from pro-B cells to pre-B cells due to deletion of the *Cnot3* gene (4). Because *Cnot3*-deletion throughout the body causes embryonic lethality, the tamoxifen-inducible Cre-driver mouse strain in addition to *Mbl1*-Cre mice was used. Even though both mouse lines showed pro-B cell arrest, the effect was more severe in the *Cnot3* deletion

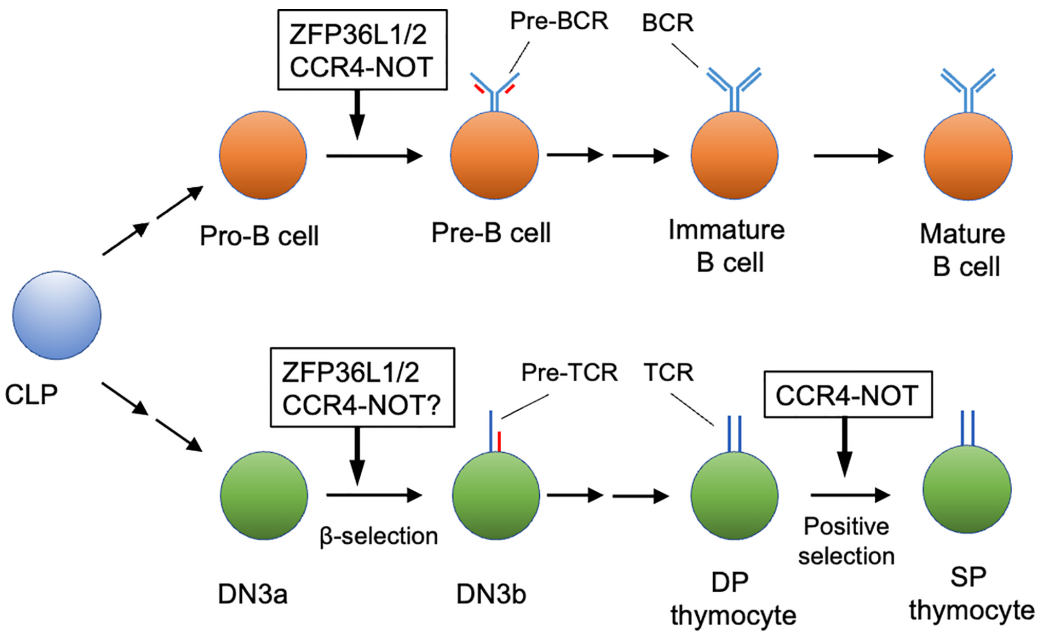

FIGURE 1 | Early lymphocyte development regulated by the CCR4-NOT complex. The CCR4-NOT complex is required for differentiation of pro-B cells to pre-B cells and positive selection of DP thymocytes. ZFP36L1 and ZFP36L2 (ZFP36L1/2) regulate the pro-B cell to pre-B cell transition and β-selection of the DN3 thymocyte stage. Involvement of the CCR4-NOT complex in β selection has not been verified yet. Some differentiation stages were omitted for simplicity. CLP, common lymphoid progenitor; DN, CD4 CD8 double negative thymocyte; DP, CD4 CD8 double positive thymocyte; SP, CD4 or CD8 single positive thymocytes.

in *Mbl1*-Cre. This difference seems to be due to genotoxic stress from excess nuclear accumulation of CRE protein, driven by the *Mbl1*-promoter. Notably, CNOT3 interacts with Early B-cell factor 1 (EBF1), which is critical for establishing B cell lineages. Mutation of a histidine residue in the DNA-binding domain (DBD) of EBF1 abolished its binding to CNOT3. Moreover, transduction of DBD mutant protein rescued the differentiation defect of EBF1-deficient B progenitors less efficiently *in vitro* compared to wild-type protein, suggesting that the interaction between CNOT3 and EBF1 is critical for B cell differentiation. Thus, the CCR4-NOT complex may function in both mRNA decay and transcription in pro-B cell differentiation. However, it is still not clear whether these two events are coupled and whether they influence each other.

Early development of conventional T cells occurs in the thymus (46). Briefly, T cell progenitors from bone marrow differentiate into $CD4^{-}CD8^{-}$ (DN) thymocytes. In the DN thymocyte stage, recombination of TCRβ chain genes and their selection occurs. DN thymocytes then differentiate into $CD4^{+}CD8^{+}$ (DP) thymocytes. After completing TCRα chain recombination, DP thymocytes undergo positive selection to test the quality and specificity of the TCR αβ complex. Positively selected DP thymocytes differentiate into CD4 or CD8 single-positive (SP) cells. In the process of positive selection, DP and SP thymocytes are further separated by expression levels of surface CD3 and CD69 (47). Before positive selection, DP thymocytes express low levels of CD69 and CD3. During positive selection, CD3 and CD69 expression are up-regulated by TCR signaling. After completion, the expression level of CD3 persists, but surface CD69 expression is down-regulated.

A recent study revealed the activity of the CCR4-NOT complex in positive selection (**Figure 1**). In thymic T cell development, some protein subunits of the CCR4-NOT complex (CNOT1, 2, 3 and 6) are up-regulated in the transition from DN thymocytes to DP thymocytes (6). T-cell-specific deletion of the murine *Cnot3* gene by the CD4-Cre deleter caused a severe developmental defect of CD4 and CD8SP thymocytes in the thymus. Specifically, the *Cnot3* deletion caused a severe reduction of $CD69^{hi}CD3^{hi}$ cells and $CD69^{lo}CD3^{hi}$ cells, but did not influence pre-selected $CD69^{lo}CD3^{int}$ thymocytes, suggesting that the CCR4-NOT complex is required during positive selection. mRNAs encoding pro-apoptotic molecules, DAB2-interacting protein (DAB2IP) (48) and BCL2-binding component 3 (BBC3) (49), were up-regulated and their polyA tails were elongated in *Cnot3*-deficient thymocytes during the course of positive selection. Moreover, transduction of anti-apoptotic Bcl-2 protein into *Cnot3*-deficient bone marrow progenitor cells rescued the developmental defect of thymocytes caused by *Cnot3*-deletion. Thus, by trimming their polyA tails, the CCR4-NOT complex promotes degradation of mRNAs encoding these pro-apoptotic proteins, which are up-regulated during positive selection. This regulation by the CCR4-NOT complex is necessary to prevent abnormal apoptosis during positive selection. Interestingly, up-regulation of *Dab2ip* resulting from *Cnot3* deletion occurred in the $CD69^{lo}CD3^{int}$

and CD69^{hi}CD3^{hi} stages, but not in the CD69^{lo}CD3^{hi} stage. In contrast, *Bbc3* was up-regulated from the CD69^{hi}CD3^{hi} stage in the absence of CNOT3. Thus, the CCR4-NOT complex may prevent thymocyte apoptosis during two distinct stages of positive selection *via* two different mechanisms.

UPSTREAM EVENTS LEADING TO CCR4-NOT-MEDIATED RNA DEGRADATION

Several mechanisms reportedly trigger RNA decay by recruiting the CCR4-NOT complex to target mRNAs (**Figure 2**). ZFP36 family proteins, including ZFP36, ZFP36 ring finger protein-like (ZFP36L) 1 and ZFP36L2, bind to specific sequences in 3' untranslated regions (UTRs) of mRNAs (50, 51). The CCR4-NOT complex is recruited by ZFP36L1 and ZFP36L2 (28), and initiates deadenlyation of mRNAs bound to ZFP36L1 and ZFP36L2, thereby promoting decay of targeted mRNAs. B cell-specific deletion of both *Zfp36l1* and *Zfp36l2* genes caused a severe reduction of cellularity from the pre-B cell stage onward (5). Furthermore, *Igμ* chain expression in pro-B and early pre-B cells was reduced in these mutant mice. Thus, ZFP36L1 or ZFP36L2 is required for differentiation of pro-B cells into pre-B cells and recombination of *Igh* in early B cells (**Figure 1**). Notably, phenotypes of these mutant mice were quite similar to those of B-cell-specific *Cnot3*-deficient mouse lines. Transcriptome analysis of late pre-B cells in *Zfp36l1* and *Zfp36l2* doubly-deficient mice showed an increase in the expression level of several cell-cycle related genes. Consistently, cell cycle analysis showed that pro-B cells in S phase were significantly increased and that those in G0 phase were severely reduced by depletion of ZFP36L1 and ZFP36L2. Progression of V(D)J recombination requires cellular quiescence because expression of RAG2 protein is restricted to G0 and G1 phase (52–55). Thus, ZFP36L1 and ZFP36L2 redundantly suppress cell cycle progression in early B cell stages *via* degradation of mRNAs encoding cell cycle-related genes, which may be required to promote V(D)J recombination. Putative target mRNAs of ZFP36L1 were upregulated in *Cnot3*-deficient pro-B cells (3). In addition, as described, CNOT3 deficiency resulted in failure of V(D)J recombination in pro-B cells in a p53-independent manner (3). Overall, these findings suggest that ZFP36L1 or ZFP36L2 recruits the CCR4-NOT complex and leads to degradation of mRNAs encoding cell cycle-promoting genes, thereby regulating cell cycle entry and exit to promote progression of V(D)J recombination. Because *Zfp36l1* and *Zfp36l2* genes are expressed throughout B cell development, there may be up-stream events activating ZFP36L1 and ZFP36L2, or promoting recruitment to their target mRNAs.

In addition to B cell development, ZFP36L1 and ZFP36L2 regulate early T cell differentiation. As in B cells, *Zfp36l1* and *Zfp36l2* genes are expressed throughout thymocyte development. Mice in which both ZFP36L1 and ZFP36L2 were depleted in early T cell progenitors developed T cell acute lymphoblastic leukemia (56). Importantly, V(D)J recombination of TCRβ gene was defective in DN thymocytes of these doubly-deficient mice. Thus, DN thymocytes in mutant mice by-pass the β-selection checkpoint without expression of TCRβ and are converted into T lymphoblasts. Mechanistically, the ZFP36L1- and ZFP36L2-

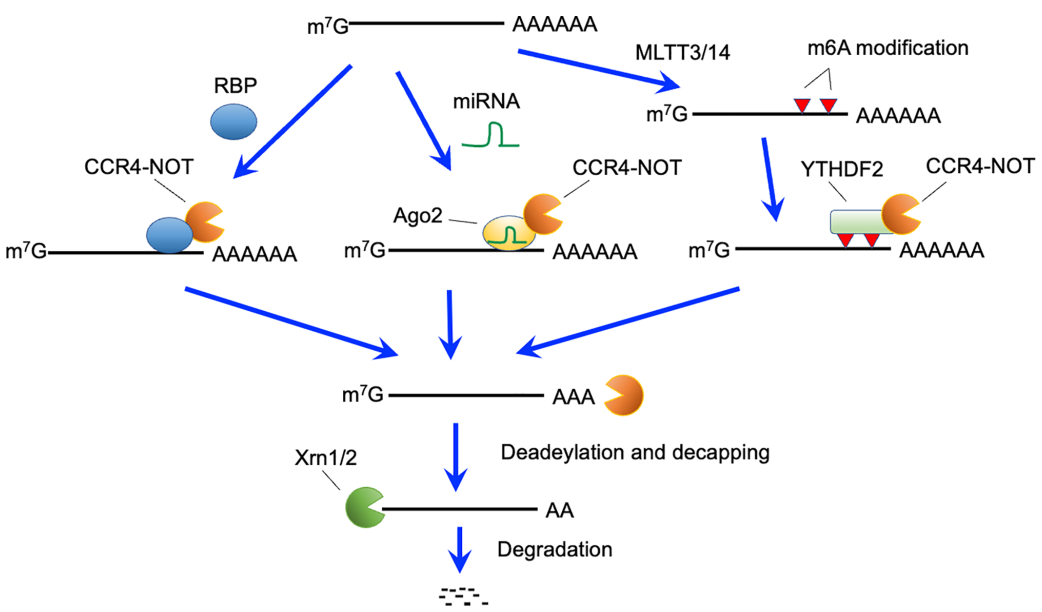

FIGURE 2 | Active RNA decay pathways mediated by the CCR4-NOT complex. The CCR4-NOT complex can be recruited by RNA binding proteins (RBP), miRNA-Ago2 complex, and YTHDF2 bound to N6-methyladeonsine, which is generated by the METTL3 and METTL14 methyltransferase complexes. The CCR4-NOT complex deadenylates polyA tails of recruited mRNAs. After deadenylation, 5'-decapping enzymes are recruited and eliminate the cap structure. Finally, 5'-exonucleases (Xrn1 and 2) causes degradation of target mRNAs.

dependent RNA decay pathway appeared to inhibit up-regulation of genes involved in DNA damage-response and cell proliferation (57). This suppression appeared crucial to induce cellular quiescence required for V(D)J recombination in DN thymocytes. Considering that V(D)J recombination occurs in both DN thymocytes and pro-B cell stages, functions of ZFP36L1 and ZFP36L2 may be similar in these two cell types (**Figure 1**). Although this may imply a requirement for CCR4-NOT complex-dependent RNA decay in the DN stages, involvement of the CCR4-NOT complex in V(D)J recombination of DN thymocytes has not been addressed yet.

Roquin family proteins, ROQUIN-1 and ROQUIN-2, can also recruit the CCR4-NOT complex in the 3'-UTRs of target mRNAs (58). T cell-specific deletion of both *Rc3h1* and *Rc3h2* (encoding ROQUIN-1 and ROQUIN-2, respectively) genes resulted in enhanced helper T cell activation and follicular helper T cell differentiation with spontaneous inflammation (10). Puzzlingly, these phenotypes have not been observed in T-cell-specific *Cnot3*-deficient mice. However, because T-cell-specific deletion of *Cnot3* severely impaired mature T cell development in the thymus, the phenotype that characterized the later T cell stage needs to be clarified. Alternatively, other mRNA decay systems may function downstream of these ROQUIN family proteins.

Among epigenetic modifications of mRNA, the N6-methyl adenosine (m6A) modification in RNA is intensively studied (59, 60). The m6A modification is recognized by the YT521-B homology domain-containing family 2 that recruits the CCR4-NOT complex (61) (**Figure 2**). Thus, m6A modification can lead to CCR4-NOT complex-mediated RNA decay. The N6-methylation of adenosine is catalyzed by methyl transferase (METTL) 3 and METTL14 complexes (62). CD4-Cre-mediated deletion of the *Mettl3* gene suppressed homeostatic proliferation of peripheral CD4-positive T cells under lymphopenic conditions (63). *Socs* mRNA degradation induced by interleukin 7-signaling, which is required for proliferation and differentiation of naïve T cells, was impaired in these mice. Notably, again, the link between m6A modification and CCR4-NOT complex-mediated mRNA decay is still obscure in T cells because of the severe reduction of mature naive T cells in T cell-specific *Cnot3*-deficient mice.

miRNAs form complexes with Argonaute family proteins on their target sequences (64, 65). The miRNA- Argonaute family complex recruits the CCR4-NOT complex or the PAN2-PAN3 complex, leading to degradation of target mRNAs (64, 65). Conditional depletion of Dicer, an enzyme critical for miRNA generation (66) in early B cells inhibited the transition of pro-B to pre-B cells, suggesting a requirement of miRNA for this differentiation stage (67). This phenotype is similar to that in mice deficient for CNOT3. However, the Dicer deficiency did not impair the V(D)J recombination reaction, whereas generation of an antibody repertoire was disturbed (67). Thus, the miRNA-CCR4-NOT complex axis in early B cells still needs to be clarified.

Although deletion of the *Dicer* gene in early thymocytes by the *Lck*-Cre deleter caused a severe reduction in cellularity of thymocytes, the percentage of each thymocyte fraction was not affected (68). Moreover, *Dicer* deletion by *CD4*-Cre showed normal thymocyte number and percentages of thymocyte subsets (69). Overall, miRNA-dependent mRNA decay through recruitment of the CCR4-NOT complex might not be essential for early thymocyte development and selection.

CONCLUDING REMARKS

Rapid, simultaneous and dynamic transcription of several mRNAs occurs during cell differentiation for generation of functional proteins. In addition, protein abundance must be precisely regulated to avoid deleterious cellular consequences. Regulation of mRNA levels should be an efficient way to control protein expression levels because one mRNA molecule generates about 3000 protein molecules on average in mammalian cells (70). However, once proteins are produced, RNA decay mechanisms should be less effective than direct protein degradation for regulating protein levels. Accordingly, it is likely that RNA decay-dependent regulation of protein concentrations by the CCR4-NOT complex is most effective when cells receive signals initiating production of large numbers of mRNA transcripts, such as during lymphocyte development.

It is likely that ZFP36L family proteins recruit the CCR4-NOT complex to suppress cell-cycle-related genes and DNA damage-responsive genes during early lymphocyte differentiation. In contrast, upstream events of CCR4-NOT complex-dependent regulation of thymic positive selection remain unknown. Moreover, possible upstream mechanisms of the CCR4-NOT complex, i.e., ROQUIN family, m6A modification, are necessary to regulate differentiation and functions of lymphocytes in later differentiation stages. Therefore, it is also important to address whether CCR4-NOT complex-induced RNA decay controls these lymphocyte differentiation and functions.

Finally, given that recent studies on human disease progression and onset by dysregulation of RNA decay systems (71–74), understanding RNA decay mechanisms would be beneficial for developing therapies and preventive measures against such diseases.

AUTHOR CONTRIBUTIONS

TA wrote the first draft of the manuscript and TY critically reviewed it. All authors contributed to the article and approved the submitted version.

ACKNOWLEDGMENTS

This work was supported by Grants-in-Aid for Scientific Research from the Japan Society for the Promotion of Science, Japan (20H03441) (TA), and CREST from Japan Science and Technology Agency (JPMJCR2011) (TA), and funding from the Okinawa Institute of Science and Technology Graduate University, Japan (TY).

REFERENCES

1. Matsushita K, Takeuchi O, Standley DM, Kumagai Y, Kawagoe T, Miyake T, et al. Zc3h12a Is an RNase Essential for Controlling Immune Responses by Regulating mRNA Decay. *Nature* (2009) 458(7242):1185–90. doi: 10.1038/nature07924
2. Yu D, Tan AH, Hu X, Athanasopoulos V, Simpson N, Silva DG, et al. Roquin Represses Autoimmunity by Limiting Inducible T-Cell Co-Stimulator Messenger RNA. *Nature* (2007) 450(7167):299–303. doi: 10.1038/nature06253
3. Inoue T, Morita M, Hijikata A, Fukuda-Yuzawa Y, Adachi S, Isono K, et al. CNOT3 Contributes to Early B Cell Development by Controlling Igh Rearrangement and p53 mRNA Stability. *J Exp Med* (2015) 212(9):1465–79. doi: 10.1084/jem.20150384
4. Yang CY, Ramamoorthy S, Boller S, Rosenbaum M, Rodriguez Gil A, Mittler G, et al. Interaction of CCR4-NOT With EBF1 Regulates Gene-Specific Transcription and mRNA Stability in B Lymphopoiesis. *Genes Dev* (2016) 30(20):2310–24. doi: 10.1101/gad.285452.116
5. Galloway A, Saveliev A, Lukasiak S, Hodson DJ, Bolland D, Balmanno K, et al. RNA-Binding Proteins ZFP36L1 and ZFP36L2 Promote Cell Quiescence. *Science* (2016) 352(6284):453–9. doi: 10.1126/science.aad5978
6. Ito-Kureha T, Miyao T, Nishijima S, Suzuki T, Koizumi SI, Villar-Briones A, et al. The CCR4-NOT Deadenylase Complex Safeguards Thymic Positive Selection by Down-Regulating Aberrant Pro-Apoptotic Gene Expression. *Nat Commun* (2020) 11(1):6169. doi: 10.1038/s41467-020-19975-4
7. Vinuesa CG, Cook MC, Angelucci C, Athanasopoulos V, Rui L, Hill KM, et al. A RING-type Ubiquitin Ligase Family Member Required to Repress Follicular Helper T Cells and Autoimmunity. *Nature* (2005) 435(7041):452–8. doi: 10.1038/nature03555
8. Lee SK, Silva DG, Martin JL, Pratama A, Hu X, Chang PP, et al. Interferon-Gamma Excess Leads to Pathogenic Accumulation of Follicular Helper T Cells and Germinal Centers. *Immunity* (2012) 37(5):880–92. doi: 10.1016/j.immuni.2012.10.010
9. Linterman MA, Rigby RJ, Wong RK, Yu D, Brink R, Cannons JL, et al. Follicular Helper T Cells Are Required for Systemic Autoimmunity. *J Exp Med* (2009) 206(3):561–76. doi: 10.1084/jem.20081886
10. Vogel KU, Edelmann SL, Jeltsch KM, Bertossi A, Heger K, Heinz GA, et al. Roquin Paralogs 1 and 2 Redundantly Repress the Icos and Ox40 Costimulator mRNAs and Control Follicular Helper T Cell Differentiation. *Immunity* (2013) 38(4):655–68. doi: 10.1016/j.immuni.2012.12.004
11. Essig K, Hu D, Guimaraes JC, Alterauge D, Edelmann S, Raj T, et al. Roquin Suppresses the PI3K-mTOR Signaling Pathway to Inhibit T Helper Cell Differentiation and Conversion of Treg to Tfr Cells. *Immunity* (2017) 47(6):1067–82 e12. doi: 10.1016/j.immuni.2017.11.008
12. Taylor GA, Carballo E, Lee DM, Lai WS, Thompson MJ, Patel DD, et al. A Pathogenetic Role for TNF Alpha in the Syndrome of Cachexia, Arthritis, and Autoimmunity Resulting From Tristetraprolin (TTP) Deficiency. *Immunity* (1996) 4(5):445–54. doi: 10.1016/S1074-7613(00)80411-2
13. Molle C, Zhang T, Ysebrant de Lendonck L, Gueydan C, Andrianne M, Sherer F, et al. Tristetraprolin Regulation of Interleukin 23 mRNA Stability Prevents a Spontaneous Inflammatory Disease. *J Exp Med* (2013) 210(9):1675–84. doi: 10.1084/jem.20120707
14. Akiyama T, Suzuki T, Yamamoto T. RNA Decay Machinery Safeguards Immune Cell Development and Immunological Responses. *Trends Immunol* (2021) 42(5):447–60. doi: 10.1016/j.it.2021.03.008
15. Wolin SL, Maquat LE. Cellular RNA Surveillance in Health and Disease. *Science* (2019) 366(6467):822–7. doi: 10.1126/science.aax2957
16. Labno A, Tomecki R, Dziembowski A. Cytoplasmic RNA Decay Pathways - Enzymes and Mechanisms. *Biochim Biophys Acta* (2016) 1863(12):3125–47. doi: 10.1016/j.bbamcr.2016.09.023
17. Yi Z, Sanjeev M, Singh G. The Branched Nature of the Nonsense-Mediated Mrna Decay Pathway. *Trends Genet* (2021) 37(2):143–59. doi: 10.1016/j.tig.2020.08.010
18. Nasif S, Contu L, Muhlemann O. Beyond Quality Control: The Role of Nonsense-Mediated mRNA Decay (NMD) in Regulating Gene Expression. *Semin Cell Dev Biol* (2018) 75:78–87. doi: 10.1016/j.semcdb.2017.08.053
19. Powers KT, Szeto JA, Schaffitzel C. New Insights Into No-Go, Non-Stop and Nonsense-Mediated mRNA Decay Complexes. *Curr Opin Struct Biol* (2020) 65:110–8. doi: 10.1016/j.sbi.2020.06.011
20. Schoenberg DR, Maquat LE. Regulation of Cytoplasmic mRNA Decay. *Nat Rev Genet* (2012) 13(4):246–59. doi: 10.1038/nrg3160
21. Mendell JT, Sharifi NA, Meyers JL, Martinez-Murillo F, Dietz HC. Nonsense Surveillance Regulates Expression of Diverse Classes of Mammalian Transcripts and Mutes Genomic Noise. *Nat Genet* (2004) 36(10):1073–8. doi: 10.1038/ng1429
22. Yi H, Park J, Ha M, Lim J, Chang H, Kim VN. Pabp Cooperates With the CCR4-NOT Complex to Promote Mrna Deadenylation and Block Precocious Decay. *Mol Cell* (2018) 70(6):1081–8.e5. doi: 10.1016/j.molcel.2018.05.009
23. Collart MA. The Ccr4-Not Complex Is a Key Regulator of Eukaryotic Gene Expression. *Wiley Interdiscip Rev RNA* (2016) 7(4):438–54. doi: 10.1002/wrna.1332
24. Inada T, Makino S. Novel Roles of the Multi-Functional CCR4-NOT Complex in Post-Transcriptional Regulation. *Front Genet* (2014) 5:135. doi: 10.3389/fgene.2014.00135
25. Shirai YT, Suzuki T, Morita M, Takahashi A, Yamamoto T. Multifunctional Roles of the Mammalian CCR4-NOT Complex in Physiological Phenomena. *Front Genet* (2014) 5:286. doi: 10.3389/fgene.2014.00286
26. Sandler H, Kreth J, Timmers HT, Stoecklin G. Not1 Mediates Recruitment of the Deadenylase Caf1 to mRNAs Targeted for Degradation by Tristetraprolin. *Nucleic Acids Res* (2011) 39(10):4373–86. doi: 10.1093/nar/gkr011
27. Petit AP, Wohlbold L, Bawankar P, Huntzinger E, Schmidt S, Izaurralde E, et al. The Structural Basis for the Interaction Between the CAF1 Nuclease and the NOT1 Scaffold of the Human CCR4-NOT Deadenylase Complex. *Nucleic Acids Res* (2012) 40(21):11058–72. doi: 10.1093/nar/gks883
28. Fabian MR, Frank F, Rouya C, Siddiqui N, Lai WS, Karetnikov A, et al. Structural Basis for the Recruitment of the Human CCR4-NOT Deadenylase Complex by Tristetraprolin. *Nat Struct Mol Biol* (2013) 20(6):735–+. doi: 10.1038/nsmb.2572
29. Chen J, Chiang YC, Denis CL. CCR4, a 3'-5' Poly(a) RNA and ssDNA Exonuclease, Is the Catalytic Component of the Cytoplasmic Deadenylase. *EMBO J* (2002) 21(6):1414–26. doi: 10.1093/emboj/21.6.1414
30. Viswanathan P, Ohn T, Chiang YC, Chen J, Denis CL. Mouse CAF1 can Function as a Processive Deadenylase/3'-5'-Exonuclease *In Vitro* But in Yeast the Deadenylase Function of CAF1 Is Not Required for mRNA Poly(a) Removal. *J Biol Chem* (2004) 279(23):23988–95. doi: 10.1074/jbc.M402803200
31. Bianchin C, Mauxion F, Sentis S, Seraphin B, Corbo L. Conservation of the Deadenylase Activity of Proteins of the Caf1 Family in Human. *RNA* (2005) 11(4):487–94. doi: 10.1261/rna.7135305
32. Yamashita A, Chang TC, Yamashita Y, Zhu W, Zhong Z, Chen CY, et al. Concerted Action of Poly(a) Nucleases and Decapping Enzyme in Mammalian mRNA Turnover. *Nat Struct Mol Biol* (2005) 12(12):1054–63. doi: 10.1038/nsmb1016
33. Ito K, Inoue T, Yokoyama K, Morita M, Suzuki T, Yamamoto T. CNOT2 Depletion Disrupts and Inhibits the CCR4-NOT Deadenylase Complex and Induces Apoptotic Cell Death. *Genes Cells* (2011) 16(4):368–79. doi: 10.1111/j.1365-2443.2011.01492.x
34. Farber V, Erben E, Sharma S, Stoecklin G, Clayton C. Trypanosome CNOT10 Is Essential for the Integrity of the NOT Deadenylase Complex and for Degradation of Many Mrnas. *Nucleic Acids Res* (2013) 41(2):1211–22. doi: 10.1093/nar/gks1133
35. Bhandari D, Raisch T, Weichenrieder O, Jonas S, Izaurralde E. Structural Basis for the Nanos-Mediated Recruitment of the CCR4-NOT Complex and Translational Repression. *Genes Dev* (2014) 28(8):888–901. doi: 10.1101/gad.237289.113
36. Raisch T, Bhandari D, Sabath K, Helms S, Valkov E, Weichenrieder O, et al. Distinct Modes of Recruitment of the CCR4-NOT Complex by Drosophila and Vertebrate Nanos. *EMBO J* (2016) 35(9):974–90. doi: 10.15252/embj.201593634
37. Raisch T, Chang CT, Levdansky Y, Muthukumar S, Raunser S, Valkov E. Reconstitution of Recombinant Human CCR4-NOT Reveals Molecular Insights Into Regulated Deadenylation. *Nat Commun* (2019) 10(1):3173. doi: 10.1038/s41467-019-11094-z
38. Suzuki T, Kikuguchi C, Nishijima S, Nagashima T, Takahashi A, Okada M, et al. Postnatal Liver Functional Maturation Requires Cnot Complex-Mediated Decay of mRNAs Encoding Cell Cycle and Immature Liver Genes. *Development* (2019) 146(4):dev168146. doi: 10.1242/dev.168146
39. Mostafa D, Yanagiya A, Georgiadou E, Wu Y, Stylianides T, Rutter GA, et al. Loss of Beta-Cell Identity and Diabetic Phenotype in Mice Caused by

Disruption of CNOT3-dependent mRNA Deadenylation. *Commun Biol* (2020) 3(1):476. doi: 10.1038/s42003-020-01201-y
40. Yamaguchi T, Suzuki T, Sato T, Takahashi A, Watanabe H, Kadowaki A, et al. The CCR4-NOT Deadenylase Complex Controls Atg7-dependent Cell Death and Heart Function. *Sci Signal* (2018) 11(516). doi: 10.1126/scisignal.aan3638
41. Watanabe C, Morita M, Hayata T, Nakamoto T, Kikuguchi C, Li X, et al. Stability of mRNA Influences Osteoporotic Bone Mass *Via* CNOT3. *Proc Natl Acad Sci USA* (2014) 111(7):2692–7. doi: 10.1073/pnas.1316932111
42. Nakamura T, Yao R, Ogawa T, Suzuki T, Ito C, Tsunekawa N, et al. Oligo-Astheno-Teratozoospermia in Mice Lacking Cnot7, a Regulator of Retinoid X Receptor Beta. *Nat Genet* (2004) 36(5):528–33. doi: 10.1038/ng1344
43. Berthet C, Morera AM, Asensio MJ, Chauvin MA, Morel AP, Dijoud F, et al. CCR4-Associated Factor CAF1 is an Essential Factor for Spermatogenesis. *Mol Cell Biol* (2004) 24(13):5808–20. doi: 10.1128/MCB.24.13.5808-5820.2004
44. Melchers F. Checkpoints That Control B Cell Development. *J Clin Invest* (2015) 125(6):2203–10. doi: 10.1172/JCI78083
45. Clark MR, Mandal M, Ochiai K, Singh H. Orchestrating B Cell Lymphopoiesis Through Interplay of IL-7 Receptor and Pre-B Cell Receptor Signalling. *Nat Rev Immunol* (2014) 14(2):69–80. doi: 10.1038/nri3570
46. Rothenberg EV. Programming for T-lymphocyte Fates: Modularity and Mechanisms. *Genes Dev* (2019) 33(17-18):1117–35. doi: 10.1101/gad.327163.119
47. Hare KJ, Jenkinson EJ, Anderson G. CD69 Expression Discriminates MHC-dependent and -Independent Stages of Thymocyte Positive Selection. *J Immunol* (1999) 162(7):3978–83.
48. Xie D, Gore C, Zhou J, Pong RC, Zhang H, Yu L, et al. DAB2IP Coordinates Both PI3K-Akt and ASK1 Pathways for Cell Survival and Apoptosis. *Proc Natl Acad Sci USA* (2009) 106(47):19878–83. doi: 10.1073/pnas.0908458106
49. Yu J, Zhang L. PUMA, a Potent Killer With or Without P53. *Oncogene* (2008) 27(Suppl 1):S71–83. doi: 10.1038/onc.2009.45
50. Adachi S, Homoto M, Tanaka R, Hioki Y, Murakami H, Suga H, et al. ZFP36L1 and ZFP36L2 Control LDLR mRNA Stability *Via* the ERK-RSK Pathway. *Nucleic Acids Res* (2014) 42(15):10037–49. doi: 10.1093/nar/gku652
51. Otsuka H, Fukao A, Tomohiro T, Adachi S, Suzuki T, Takahashi A, et al. ARE-Binding Protein ZFP36L1 Interacts With CNOT1 to Directly Repress Translation *Via* a Deadenylation-Independent Mechanism. *Biochimie* (2020) 174:49–56. doi: 10.1016/j.biochi.2020.04.010
52. Li Z, Dordai DI, Lee J, Desiderio S. A Conserved Degradation Signal Regulates RAG-2 Accumulation During Cell Division and Links V(D)J Recombination to the Cell Cycle. *Immunity* (1996) 5(6):575–89. doi: 10.1016/S1074-7613(00)80272-1
53. Zhang L, Reynolds TL, Shan X, Desiderio S. Coupling of V(D)J Recombination to the Cell Cycle Suppresses Genomic Instability and Lymphoid Tumorigenesis. *Immunity* (2011) 34(2):163–74. doi: 10.1016/j.immuni.2011.02.003
54. Johnson K, Chaumeil J, Micsinai M, Wang JM, Ramsey LB, Baracho GV, et al. IL-7 Functionally Segregates the Pro-B Cell Stage by Regulating Transcription of Recombination Mediators Across Cell Cycle. *J Immunol* (2012) 188 (12):6084–92. doi: 10.4049/jimmunol.1200368
55. Bendall SC, Davis KL, Amir el AD, Tadmor MD, Simonds EF, Chen TJ, et al. Single-Cell Trajectory Detection Uncovers Progression and Regulatory Coordination in Human B Cell Development. *Cell* (2014) 157(3):714–25. doi: 10.1016/j.cell.2014.04.005
56. Hodson DJ, Janas ML, Galloway A, Bell SE, Andrews S, Li CM, et al. Deletion of the RNA-binding Proteins ZFP36L1 and ZFP36L2 Leads to Perturbed Thymic Development and T Lymphoblastic Leukemia. *Nat Immunol* (2010) 11(8):717–24. doi: 10.1038/ni.1901
57. Vogel KU, Bell LS, Galloway A, Ahlfors H, Turner M. The RNA-Binding Proteins Zfp36l1 and Zfp36l2 Enforce the Thymic Beta-Selection Checkpoint by Limiting DNA Damage Response Signaling and Cell Cycle Progression. *J Immunol* (2016) 197(7):2673–85. doi: 10.4049/jimmunol.1600854
58. Leppek K, Schott J, Reitter S, Poetz F, Hammond MC, Stoecklin G. Roquin Promotes Constitutive mRNA Decay *Via* a Conserved Class of Stem-Loop Recognition Motifs. *Cell* (2013) 153(4):869–81. doi: 10.1016/j.cell.2013.04.016
59. Shulman Z, Stern-Ginossar N. The RNA Modification N(6)-methyladenosine as a Novel Regulator of the Immune System. *Nat Immunol* (2020) 21(5):501–12. doi: 10.1038/s41590-020-0650-4
60. Yang C, Hu Y, Zhou B, Bao Y, Li Z, Gong C, et al. The Role of M(6)a Modification in Physiology and Disease. *Cell Death Dis* (2020) 11(11):960. doi: 10.1038/s41419-020-03143-z
61. Du H, Zhao Y, He J, Zhang Y, Xi H, Liu M, et al. YTHDF2 Destabilizes M(6)a-Containing RNA Through Direct Recruitment of the CCR4-NOT Deadenylase Complex. *Nat Commun* (2016) 7:12626. doi: 10.1038/ncomms12626
62. Liu J, Yue Y, Han D, Wang X, Fu Y, Zhang L, et al. A METTL3-METTL14 Complex Mediates Mammalian Nuclear RNA N6-Adenosine Methylation. *Nat Chem Biol* (2014) 10(2):93–5. doi: 10.1038/nchembio.1432
63. Li HB, Tong J, Zhu S, Batista PJ, Duffy EE, Zhao J, et al. M(6)a mRNA Methylation Controls T Cell Homeostasis by Targeting the IL-7/STAT5/SOCS Pathways. *Nature* (2017) 548(7667):338–42. doi: 10.1038/nature23450
64. Iwakawa HO, Tomari Y. The Functions of MicroRNAs: mRNA Decay and Translational Repression. *Trends Cell Biol* (2015) 25(11):651–65. doi: 10.1016/j.tcb.2015.07.011
65. Jonas S, Izaurralde E. Towards a Molecular Understanding of microRNA-mediated Gene Silencing. *Nat Rev Genet* (2015) 16(7):421–33. doi: 10.1038/nrg3965
66. Ha M, Kim VN. Regulation of microRNA Biogenesis. *Nat Rev Mol Cell Biol* (2014) 15(8):509–24. doi: 10.1038/nrm3838
67. Koralov SB, Muljo SA, Galler GR, Krek A, Chakraborty T, Kanellopoulou C, et al. Dicer Ablation Affects Antibody Diversity and Cell Survival in the B Lymphocyte Lineage. *Cell* (2008) 132(5):860–74. doi: 10.1016/j.cell.2008.02.020
68. Cobb BS, Nesterova TB, Thompson E, Hertweck A, O'Connor E, Godwin J, et al. T Cell Lineage Choice and Differentiation in the Absence of the RNase III Enzyme Dicer. *J Exp Med* (2005) 201(9):1367–73. doi: 10.1084/jem.20050572
69. Muljo SA, Ansel KM, Kanellopoulou C, Livingston DM, Rao A, Rajewsky K. Aberrant T Cell Differentiation in the Absence of Dicer. *J Exp Med* (2005) 202 (2):261–9. doi: 10.1084/jem.20050678
70. Schwanhausser B, Busse D, Li N, Dittmar G, Schuchhardt J, Wolf J, et al. Global Quantification of Mammalian Gene Expression Control. *Nature* (2011) 473(7347):337–42. doi: 10.1038/nature10098
71. De Keersmaecker K, Atak ZK, Li N, Vicente C, Patchett S, Girardi T, et al. Exome Sequencing Identifies Mutation in CNOT3 and Ribosomal Genes RPL5 and RPL10 in T-Cell Acute Lymphoblastic Leukemia. *Nat Genet* (2013) 45(2):186–90. doi: 10.1038/ng.2508
72. Tavernier SJ, Athanasopoulos V, Verloo P, Behrens G, Staal J, Bogaert DJ, et al. A Human Immune Dysregulation Syndrome Characterized by Severe Hyperinflammation With a Homozygous Nonsense Roquin-1 Mutation. *Nat Commun* (2019) 10(1):4779. doi: 10.1038/s41467-019-12704-6
73. Kakiuchi N, Yoshida K, Uchino M, Kihara T, Akaki K, Inoue Y, et al. Frequent Mutations That Converge on the NFKBIZ Pathway in Ulcerative Colitis. *Nature* (2020) 577(7789):260–5. doi: 10.1038/s41586-019-1856-1
74. Nanki K, Fujii M, Shimokawa M, Matano M, Nishikori S, Date S, et al. Somatic Inflammatory Gene Mutations in Human Ulcerative Colitis Epithelium. *Nature* (2020) 577(7789):254–9. doi: 10.1038/s41586-019-1844-5

Conflict of Interest: The authors declare that the research was conducted in the absence of any commercial or financial relationships that could be construed as a potential conflict of interest.

frontiers in Immunology

REVIEW
published: 17 September 2021
doi: 10.3389/fimmu.2021.751313

Conceptual Advances in Control of Inflammation by the RNA-Binding Protein Tristetraprolin

*Pavel Kovarik**, *Annika Bestehorn and Jeanne Fesselet*

Max Perutz Labs, University of Vienna, Vienna Biocenter (VBC), Vienna, Austria

Regulated changes in mRNA stability are critical drivers of gene expression adaptations to immunological cues. mRNA stability is controlled mainly by RNA-binding proteins (RBPs) which can directly cleave mRNA but more often act as adaptors for the recruitment of the RNA-degradation machinery. One of the most prominent RBPs with regulatory roles in the immune system is tristetraprolin (TTP). TTP targets mainly inflammation-associated mRNAs for degradation and is indispensable for the resolution of inflammation as well as the maintenance of immune homeostasis. Recent advances in the transcriptome-wide knowledge of mRNA expression and decay rates together with TTP binding sites in the target mRNAs revealed important limitations in our understanding of molecular mechanisms of TTP action. Such orthogonal analyses lead to the discovery that TTP binding destabilizes some bound mRNAs but not others in the same cell. Moreover, comparisons of various immune cells indicated that an mRNA can be destabilized by TTP in one cell type while it remains stable in a different cell linage despite the presence of TTP. The action of TTP extends from mRNA destabilization to inhibition of translation in a subset of targets. This article will discuss these unexpected context-dependent functions and their implications for the regulation of immune responses. Attention will be also payed to new insights into the role of TTP in physiology and tissue homeostasis.

Keywords: tristetraprolin (TTP), zinc finger protein 36 (Zfp36), RNA binding protein, mRNA stability/decay, inflammation, immune system, immune homeostasis

OPEN ACCESS

Edited by:
Manuel Daniel Díaz-Muñoz, U1043 Centre de Physiopathologie de Toulouse Purpan (INSERM), France

Reviewed by:
Matthias Gaestel, Hannover Medical School, Germany
Heiko Mühl, Goethe University Frankfurt, Germany

****Correspondence:***
Pavel Kovarik
pavel.kovarik@univie.ac.at

Specialty section:
This article was submitted to Molecular Innate Immunity, a section of the journal Frontiers in Immunology

Received: *31 July 2021*
Accepted: *01 September 2021*
Published: *17 September 2021*

Citation:
Kovarik P, Bestehorn A and Fesselet J (2021) Conceptual Advances in Control of Inflammation by the RNA-Binding Protein Tristetraprolin. Front. Immunol. 12:751313. doi: 10.3389/fimmu.2021.751313

INTRODUCTION

It is now well accepted that regulation of mRNA stability by RNA-binding proteins (RBPs) is indispensable for healthy immune responses. RBPs orchestrate the immune system by modulating gene expression through mRNA destabilization or stabilization, or by controlling translation (1–3). Although this basic knowledge is established, many important questions remain unresolved.

These include mechanistic explanations of the phenotype caused by an RBP deletion in mice and the selective functions of RBPs in specific cell types despite ubiquitous expression. Improved models of the molecular mechanisms of RBP action are needed to answer the open questions. These models will likely abandon the linear schemes in which RBP binding to a target mRNA inevitably results in a canonical consequence, e.g. mRNA decay. The aim of this review is to provide a framework for updated models of RBP action in immune responses.

The history of mRNA decay research, both at the level of mechanisms and functions, is tightly connected to the immune system. The first evidence that selective mRNA degradation is driven by a cis-acting element was reported for the mRNA encoding the granulocyte/monocyte growth factor GM-CSF (4). This study established that an adenylate-uridylate-rich element (AU-rich element; ARE) in the 3' untranslated region (3' UTR) of the GM-CSF mRNA (encoded by the *CSF2* gene) confers mRNA instability if introduced into the 3' UTR of a stable mRNA. The autonomous effect of AREs on mRNA stability has been subsequently documented for many other mRNAs. The key role of ARE-dependent mRNA decay *in vivo* was revealed by the deletion of the ARE in the mouse *Tnf* gene which resulted in a spontaneous development of gut and joint inflammation (5). However, genome sequencing and transcriptome-wide mRNA stability assays indicated that the initial model of an autonomous function of 3' UTR-located AREs in mRNA destabilization was too simple. Approximately 20% of human genes contain AREs in their 3' UTRs, yet most of the corresponding mRNAs are stable (6, 7). The medium half-life of mRNA in human HepG3 cells is approximately 10 h with mRNAs of metabolic genes having on average the highest half-lives (6). In comparison, inflammation-associated mRNAs belong to those with the shortest average half-lives. For illustration, the decay rate of *TNF* mRNA is in the range of 20 – 40 min, depending on the cell type and stimulus (8, 9). Although inflammation-induced mRNAs are enriched in AREs, it is now accepted that the presence of an ARE is not sufficient to destabilize the mRNA. Hence, new and more comprehensive models of regulation of mRNA decay by cis-acting elements are needed.

MECHANISMS OF RBP-DRIVEN CHANGES IN mRNA STABILITY

mRNA-destabilizing RBPs bind and facilitate the target mRNA degradation in two ways, depending on the properties of the particular RBP (1, 2, 10, 11). One class of RBPs possesses an endonuclease activity which allows the RBP to cleave the target mRNA and generate ends devoid of the 5' m^7G cap and the 3' poly(A) tail. These unprotected ends serve as substrates for exonucleases which process the mRNA in 3' – 5' direction *via* the exosome and 5' - 3' direction *via* XRN1 (12, 13). The best characterized endonucleolytic RBP relevant for the immune system is Regnase-1 (gene name Zc3h12a) which destabilizes mRNAs of transcription factors and cytokines such as Icos, Ox40, c-Rel, IL-2 and IL-6 (14). Regnase-1-deficient mice show severe systemic inflammation associated with T and B cell activation. The phenotype is largely recapitulated by a T cell-specific deletion (14). The second class of RBPs destabilize the target mRNA by promoting the recruitment of the CCR4-NOT deadenylase and the DCP1/DCP2-containing decapping complexes (15, 16). A number of RBPs in this class are known to regulate the immune system. Tristetraprolin (TTP), as one of the most prominent members, will be described in detail below. Other well characterized members are Roquin-1 (gene name *Rc3h1*), Roquin-2 (*Rc3h2*), Zfp36l1, Zfp36l2 and Auf1. The Roquin proteins redundantly target the mRNAs of Icos and Ox40 to control T cell activation. Deletion of both Roquin-1 and Roquin-2 genes specifically in CD4 T cells results in an autoimmune phenotype resembling systemic lupus erythematosus while deletion of the single genes remains without severe consequences (17). The proteins Zfp36l1 and Zfp36l2 are members of the TTP family but, in contrast to TTP, have more pleotropic functions as demonstrated by embryonic or postnatal lethality of the respective knockouts in mice (18, 19). Zfp36l1 and Zfp36l2 are involved in the regulation of immune system in multiple ways. They control the expression of proliferative cell cycle regulators during B and T cell development: double deletion of Zfp36l1 and Zfp36l2 in T cells results in lymphopenia and malignant transformation of immature CD8 T cells while similar deletion in pro-B cells causes a block in B cell development owing to a failure in entering quiescence hence genome safeguarding prior to VDJ recombination (20, 21). The protein Auf1 exhibits anti-inflammatory functions by promoting the degradation of cytokine mRNAs as revealed by the hypersensitivity of Auf1-deficient mice to endotoxic shock (22). Auf1 has been subsequently found to regulate many other processes in addition to immune responses including telomere maintenance and muscle regeneration (23, 24).

mRNA-stabilizing RBPs are less well understood and their functions are more pleiotropic as compared to the destabilizing RBPs such as TTP. The general opinion is that mRNA-stabilizing RBPs act by preventing the destabilizing proteins from binding to the target. As a consequence, the target mRNAs are more stable and/or more efficiently translated. mRNA-stabilizing RBPs regulating immune responses include HuR (gene name *Elavl1*) and Arid5a. Deletion of HuR or Arid5a in mice resulted in increased resistance to experimental autoimmune encephalomyelitis (25, 26). Furthermore, HuR is required for antibody production by B cells (27). HuR is involved in regulation of other processes including liver metabolism, cell proliferation and cancer (28–30).

RNA BINDING OF RBPs CONTROLLING mRNA STABILITY

RBPs bind to RNA through interactions of their RNA-binding domains with specific sequences or defined structural elements in the target mRNA. The most frequent RNA-binding domain in the

immunoregulatory RBPs is the C3H1 (Cys-Cys-Cys-His) zinc finger domain present for example in TTP, Zfp36l1 and Zfp36l2 (2, 31). Regnase and Roquin contain a C3H1 zinc finger and an additional RNA-binding domain: a PIN domain and a ROQ domain, respectively (32, 33). Auf1 and HuR bind to RNA through the RNA recognition motif (RRM) domains which occur in 2 or 3 repeats in these proteins (34, 35). Arid5a interacts with RNA *via* an ARID domain which is known to recognize DNA in other ARID domain-containing proteins (26, 36).

The target site in the RNA is defined by the RNA-binding domain. The C3H1 zinc finger present in TTP, Zfp36l1 and Zfp36l2 binds preferentially to AREs with the core sequence UAUUUAU although divergent target sites have been identified as well (9, 21, 37). A preference for AU-rich sequences shows also the ARID domain of Arid5a (26). The RRM domain of Auf1 recognizes U- and GU-rich stretches and, albeit less frequently, AREs (38). The RRM motif of HuR prefers U-rich sequences (9, 39, 40). The preference of these binding domains for AREs or U-rich sequences reflects the unstructured nature of such sequences: AREs and U-rich sequences in general do not adopt a secondary structure. In contrast, Regnase and Roquin bind to RNAs exhibiting stem-loop folds with the loop part formed by three bases with a pyrimidine–purine–pyrimidine sequence while the stem is more variable both in length (5 – 8 bases in each half of the stem) and sequence (41, 42).

Transcriptome-wide binding assays revealed that most of these RBPs bind frequently to 3' UTR and, unexpectedly, introns (9, 21, 38–40). Binding to introns regulates splicing in case of HuR (40, 43). However, it appears that functional interactions are largely confined to elements located in the 3' UTRs as intronic binding in general does not result in changes in stability or splicing of the transcript.

THE TTP PROTEIN FAMILY: EVOLUTIONARY CONSERVED RBPs WITH DIVERSE FUNCTIONS FROM YEAST TO MAMMALS

TTP contains an RNA-binding domain formed by a characteristic tandem C3H1 zinc finger in the middle part and protein-protein interaction domains at the N- and C-termini (31). The tandem zinc finger and the overall domain structure are conserved in similar RBPs from yeast to plants and mammals hence these RBPs constitute the TTP protein family (44). Interestingly, no TTP protein members are found in birds despite their presence in reptiles (44). Although all these proteins facilitate mRNA degradation their functions in cells and/or organisms are diverse. For example, the yeast TTP family member Cth2 regulates mRNA stability upon iron deficiency while the Xenopus TTP proteins act during embryonic development and the *C. elegans* homologues are required for meiosis and oocyte production (45–47). Humans contain three TTP family members (Zfp36, Zfp36l1 and Zfp36l2) and mice express the Zfp36l3 member in addition. Much of what we now know about the functions of the TTP protein family has been learned from knockouts in mice carried out by the Blackshear laboratory. Deletion of Zfp36l1 (also known as BRF1 and TIS11b) is embryonic lethal because of failure in umbilical circulation resulting from absent fusion of the allantois with the chorion (18). Mice lacking Zfp36l2 (also known as BRF2 and TIS11D) die within a few weeks after birth due to a marked deficiency in hematopoiesis (19). Zfp36l3 is a paternally imprinted X chromosome gene which is likely involved in regulation of iron metabolism in the placenta; Zfp36l3 deletion results in decreased neonatal survival rates without obvious morphological aberrances in surviving offspring (48).

TTP: A TTP FAMILY MEMBER WITH UNIQUE SELECTIVITY FOR THE REGULATION OF IMMUNE RESPONSES

TTP (Zfp36) is an outstanding member of the TTP family as its function is remarkably specific and related to the regulation of immune responses. TTP knockout in mice results in systemic inflammation characterized by arthritis, dermatitis, conjunctivitis and cachexia (49). This so called TTP deficiency syndrome develops within approximately 8 weeks of birth and progressively worsens leading to death of most animals at around 6-8 months of age. TTP-deficient mice do not show any developmental abnormalities or health defects at birth; the mice are not fertile presumably owing to their poor health (49). The TTP deficiency syndrome was shown to be dependent on TNF signaling and mechanistically explained by increased stability of *Tnf* mRNA (49, 50). Subsequent studies established that the inflammatory disease of TTP-deficient mice is caused, albeit to variable extent, by increased stability of other cytokine and chemokine mRNAs as well, notably *Il23*, *Ccl3*, *Il1a* and *Il1b* mRNAs (51–53).

Given this multiple evidence for its indispensable role in the immune system, it comes with no surprise that TTP has become one of the best studied RBPs. However, many important questions remain open. For example, it is not well understood which cell types drive the inflammatory disease in TTP-deficient mice. Mice bearing LysM-Cre-mediated TTP deletion in the myeloid compartment are healthy which is unexpected given that myeloid cells are cells with arguably the highest TTP expression (54, 55). Although these mice exhibit lethal hypersensitivity to endotoxic shock, the absence of a spontaneous inflammation suggests that deletion of TTP in myeloid cells alone is not sufficient to cause the TTP deficiency syndrome. Similarly, mice with CD11c-Cre-driven deletion of TTP in dendritic cells remain without a spontaneous phenotype (56). Surprisingly, systemic inflammation arises upon deletion of TTP in keratinocytes (56). The inflammatory disease in these mice develops from psoriasis-like focal skin lesions containing neutrophilic infiltrates, indicating that persistent local inflammation can become systemic with time. The model of keratinocyte-specific TTP deletion suggests that TTP expression is particularly critical in barrier tissues, i.e. tissues constantly exposed to environmental cues. However, it is remarkable that the full-body TTP knockout mice remain without pathology in the intestinal or lung epithelium, i.e. the most prominent mucosal barriers. The absence of mucosal

inflammation in TTP-deficient mice suggests that TTP has more complex roles in these tissues. Such functional complexity is supported by findings showing that the lack of intestinal pathology in TTP knockout mice is associated with a local expansion of regulatory T cells (57). Moreover, Villin-Cre-driven TTP deletion in intestinal epithelial cells increases the resistance against dextran sulfate-induced colitis suggesting, that the lack of TTP might enhance the robustness of the intestinal barrier (58). Although the mechanism is yet to be determined, the improved mucosal barrier might be caused by accelerated tissue regeneration since these mice exhibit higher numbers of Goblet cells. These findings suggest that the absence of TTP augments proliferation signals that are commonly associated with inflammatory conditions. In agreement, skin inflammation caused by TTP deficiency in keratinocytes promotes tumorigenesis that appears to be causally associated with overproduction of the growth factor amphiregulin (59). Consistently, amphiregulin mRNA is a TTP target. However, TTP deficiency can cause increased cell numbers also by means of decreased apoptosis as shown for TTP-deficient neutrophils: neutrophils devoid of TTP express higher levels of the TTP target *Mcl1* mRNA which codes for an anti-apoptotic factor particularly relevant for neutrophils (60). Interestingly, this effect pertains only to immunostimulated (e.g. pathogen-engaged) neutrophils, not to the circulating dormant neutrophil pool.

Cumulatively, the available animal models of TTP deficiency clearly indicate that the major function of TTP is to control the immune response. Although TTP restricts cell numbers in some cases, this function is also largely related to control of inflammation: (i) by ameliorating inflammation TTP prevents the expression of inflammation-associated growth factors or anti-apoptotic proteins, (ii) TTP directly targets the mRNAs of several inflammation-associated growth or anti-apoptotic factors. More studies directly investigating cells from tissues are needed to complete our understanding of TTP effects *in vivo*.

mRNA DESTABILIZATION BY TTP

TTP promotes mRNA decay through the recruitment of the CCR4-NOT deadenylase and the DCP1/DCP2 decapping complexes to the bound target. The N- and C-termini of TTP represent the protein-protein interaction domains in this process. The CCR4-NOT deadenylase complex interacts with the N- and C-terminal domains with the CNOT1 subunit being directly involved in binding to TTP (61–64). The DCP1 and DCP2 decapping protein complexes interact with the N-terminal TTP domain (62). Following decapping and deadenylation, the target mRNA is degraded through the 5′-3′ exonuclease Xrn1 and the 3′-5′ exonuclease of the exosome, respectively. The identification of these interactions suggested that TTP-mediated mRNA degradation is governed by a protein recruitment cascade. However, this model does not explain why many TTP-bound RNAs (including mRNAs and introns) are stable as shown by more recent studies (9, 65–67). The surprising findings of these studies delineate that the process of mRNA destabilization by TTP is more complex and dependent on yet unidentified regulatory mechanisms.

TTP BINDING TO RNA

Both zinc finger domains are required for interaction of TTP with RNA as mutation of either of them abrogates RNA binding (68). Moreover, mutation of the first zinc finger in the TTP locus in mice phenocopied the complete TTP deletion (69). This was a significant finding as it definitively proved that the function of TTP is entirely dependent on its RNA binding activity. Initial characterization of the motif recognized by TTP focused on the TNF mRNA, the first known TTP target: the motif is a 9-mer with the sequence UUAUUUAUU which is repeated several times in the TNF 3' UTR (37, 70). Subsequent analysis of RNAs enriched in RNA immunoprecipitation assays suggested that TTP binds to AREs also in other target mRNAs (71). A precise genome-wide mapping of target sequences was generated by several CLIP-Seq (cross-linking immunoprecipitation-high-throughput sequencing) studies employing immune cells. Although these nucleotide resolution analyses confirmed the preference of TTP for the UAUUUAU sequence, they also provided several unexpected findings (9, 65–67). The studies showed that TTP binds also to sites that were divergent from the canonical TTP binding sequence as visualized in the searchable TTP Atlas (https://ttp-atlas.univie.ac.at) (9). Moreover, TTP binding was not limited to 3' UTRs but was detected at sites located in 5' UTRs, coding sequences and introns as well (**Figure 1**). Particularly striking was the high incidence of TTP binding to introns. Although the number of identified intronic binding sites was dependent on the CLIP-Seq method, the peak finding algorithm and experimental cell system, the studies convincingly established that TTP interacts with pre-mRNA in addition to mRNA. This finding implies that TTP can engage RNA interactions in the nucleus. The biological significance of the intronic binding remains to be determined as no effects on splicing or stability of the intron-bound RNA has so far been observed (9). Given the high frequency of TTP binding to introns it is possible that introns act as sponge to titrate away TTP molecules. This mechanism was reported for circular RNAs that function as sponge molecules for micro RNAs (72, 73). Similar to intronic binding, it is currently unclear whether interactions of TTP with 5' UTRs or coding sequences entail changes in RNA processing.

The CLIP-Seq data show that functional TTP bindings sites are located in 3' UTR. Remarkably, binding of TTP to 3' UTR does not always cause destabilization of the target mRNA, as revealed in recent studies. This enigmatic and probably significant property of TTP is discussed further below.

REGULATION OF TTP

TTP function is regulated in multiple ways with many of them remaining poorly understood. Moreover, it is likely that some key

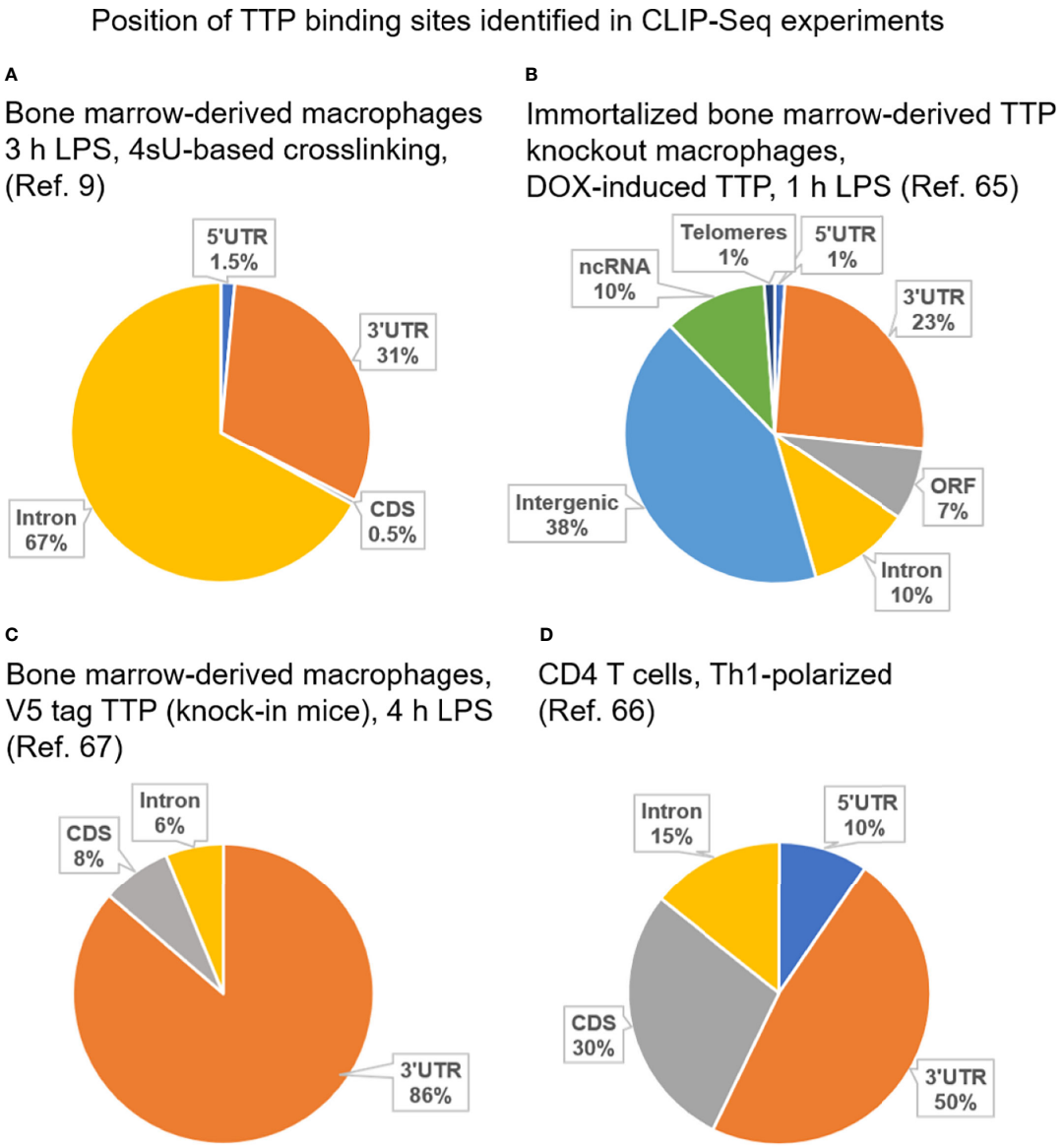

FIGURE 1 | Position of TTP binding sites identified in reported CLIP-Seq experiments employing immune cells. **(A)** CLIP-Seq experiment carried out using bone marrow-derived macrophages isolated from wild type mice (i.e. expressing solely endogenous TTP). Cells were stimulated for 3 h with LPS prior to CLIP-Seq which was based on thiouridine (4sU)-mediated crosslinking allowing crosslinking with 365 nm UV, i.e. mild conditions [Reference (9)]. **(B)** CLIP-Seq experiment performed using immortalized bone marrow-derived macrophages isolated from TTP knockout mice and engineered to express doxycycline-inducible TTP. Cells were treated with doxycycline and stimulated for 1 h with LPS prior to CLIP-Seq [Reference (65)]. **(C)** CLIP-Seq experiment carried out using bone marrow-derived macrophages isolated from mice expressing V5-tagged TTP from the endogenous locus (knock-in mice). Cells were stimulated for 4 h with LPS prior to CLIP-Seq [Reference (67)]. **(D)** CLIP-Seq experiment carried out using CD4+ T cells from wild type mice [(i.e. expressing solely endogenous TTP)]. CD4+ T cells were polarized under Th1 conditions prior to CLIP-Seq [Reference (66)]. 3' UTR, 3' untranslated region; 5' UTR, 5' untranslated region; CDS, coding sequence; ORF, open reading frame; ncRNA, non-coding RNA; DOX, doxycycline.

regulatory events are still not known. Comprehensive knowledge about the regulation of TTP is critical for our understanding of the remarkably selective function of TTP in the immune system and for the control of inflammation in general. TTP is regulated at the level of transcription, mRNA stability, protein stability and by posttranslational modifications (31, 74–76). As far as we can say, all these mechanisms are critical for the appropriate extent, timing and selectivity of TTP-driven mRNA degradation. They act in concert to allow the immune system launching an efficient but not exaggerated inflammatory response.

TTP mRNA levels are low under steady state conditions but dramatically induced in response to inflammatory stimuli which are mostly associated with stress signaling. The increase in TTP mRNA levels is achieved mostly by transcriptional induction and

to some extent also through mRNA stabilization. As an immediate early gene, TTP is transcriptionally activated rapidly after stimulation. The activation signals include growth factors, cytokines such as TNF, IL-4, IL-10, or IFN-γ, and bacterial products e.g. LPS (50, 77–80). The transcription factors involved in the transcriptional upregulation were characterized in few instances: IFNs, IL-10 and IL-4 drive TTP expression through STAT1, STAT3 and STAT6, respectively (78–80). STAT1 employs a GAS (Gamma interferon activation site) element which is conserved in the TTP promoter in mice and humans (78). This GAS element is likely involved also in response to IL-4 and IL-10. The activating signals often synergize to achieve maximal induction of TTP (78, 79).

Stabilization of TTP mRNA by p38 MAPK signaling contributes to induction of TTP expression (81). TTP mRNA contains AREs which interact with TTP protein suggesting that autoregulation is the mechanism underlying the low TTP mRNA stability. TTP mRNA is indeed moderately more stable in TTP knock-in mice expressing the zinc finger-inactivated mutant (69).

A central aspect of the regulation of TTP levels in cells is the control of TTP protein stability. TTP is continuously degraded in a proteasome-dependent way which appears to proceed without ubiquitination and is likely to involve the intrinsically unfolded N- and/or C-terminal domains (82, 83). The mechanism of this important process is not resolved and its elucidation would significantly advance our understanding of protein degradation in general. TTP protein stability increases by orders of magnitude upon phosphorylation of S52 and S178 (in mouse coordinates) (82, 84). Phosphorylation of these two residues is brought about by MK2, a kinase that is activated by p38 MAPK. Although the p38 MAPK/MK2-driven phosphorylation of S52 and S178 increases TTP protein stability and thereby positively regulates TTP levels, it inhibits the mRNA-destabilization activity of TTP. This phosphorylation-dependent TTP inhibition probably results from a combination of several processes: (i) S52 and S178 phosphorylation causes association of TTP with 14-3-3 proteins thereby preventing relocation of TTP to stress granules and processing bodies, (ii) 14-3-3 protein binding promotes export of TTP from the nucleus, (iii) S52 and S178 phosphorylation decreases association of TTP with the CCR4-NOT deadenylase, and (iv) MK2-dependent TTP phosphorylation diminishes TTP binding to RNA (85–88). Although the mechanistic details of the function of S52 and S178 phosphorylation are not fully understood, the biological consequences have been convincingly revealed by generation of double knock-in mice bearing S52A and S178A mutations in the TTP locus (89). These mice are unable to express high TTP protein levels, consistent with a rapid TTP protein degradation. Nevertheless, the mice are protected against LPS-induced systemic inflammation indicating that the S52A/S178A mutant acts as hyperactive TTP *in vivo*. The double knock-in mouse confirmed the previously proposed model of TTP function according to which p38 MAPK leads to accumulation of inactive (i.e. phosphorylated) TTP in the initial phase of inflammation. Later, i.e. in the resolution phase of inflammation, the gradual decrease of p38 MAPK activity releases TTP from its inhibited state thereby facilitating degradation of TTP target mRNAs (9, 55). In parallel, the diminishing phosphorylation accelerates proteasomal degradation of TTP rendering the cells responsive to a new inflammatory stimulus.

TTP contains more than 30 phosphorylation sites out of which only S52 and S178 have been functionally annotated in cells and animals (90). A recent quest for a better understanding of TTP phosphorylation has revealed MK2-dependent phosphorylation of T84, S85, T250, and S316 out of which the phosphorylation of S316 is the most robust one (91). Notably, S316 phosphorylation in not involved in regulation of TTP protein stability; instead, it appears to regulate interactions of TTP with the translation inhibition proteins (91). It will be exciting to see the progress in functional characterization of other phosphorylation sites as they likely impinge on TTP in unexpected ways.

TO DEGRADE OR NOT TO DEGRADE THE BOUND mRNA?

Transcriptome-wide mRNA stability studies coupled to CLIP-Seq analyses revealed that, surprisingly, TTP does not always cause degradation of the bound target. This has been convincingly demonstrated by employing bone marrow-derived macrophages expressing solely endogenous TTP (9). The study showed that 71% of mRNAs bound by TTP in their 3' UTR are stable. A similar conclusion was drawn from CLIP-Seq and mRNA stability assays in HEK293 cells overexpressing TTP (92). These observations were supported by other CLIP-Seq studies employing primary cells (i.e. cells not overexpressing TTP) although the evidence was indirect as it was based on differential expression analysis (RNA-Seq) but not on transcriptome-wide mRNA stability assessments (66, 67). These unexpected results indicate that a more complex model of TTP action needs to be developed. The model will probably involve proteins acting in cis with TTP which prevent recruitment of the RNA degradation machinery to stable transcripts or facilitate such recruitment to unstable transcripts (**Figure 2**). This new concept could also involve yet uncharacterized TTP phosphorylation events; in this scenario a particular phosphorylation (activating or inactivating) would occur only on certain target mRNAs and/or subcellular locations. The advanced concept of TTP function might also consider a recently reported hypothesis that TTP stabilizes mRNA under certain circumstances: The dramatic induction of TTP following an inflammatory stimulus was proposed to generate a pool of free TTP that sequesters the RNA degradation machinery thereby preventing mRNA decay, but a direct evidence for this hypothesis was not provided (93).

Related to the question of whether TTP destabilizes or not a specific subset of bound mRNAs are ribosome profiling data showing that TTP can affect mRNA stability but also inhibit translation (65–67). Particularly conclusive were studies

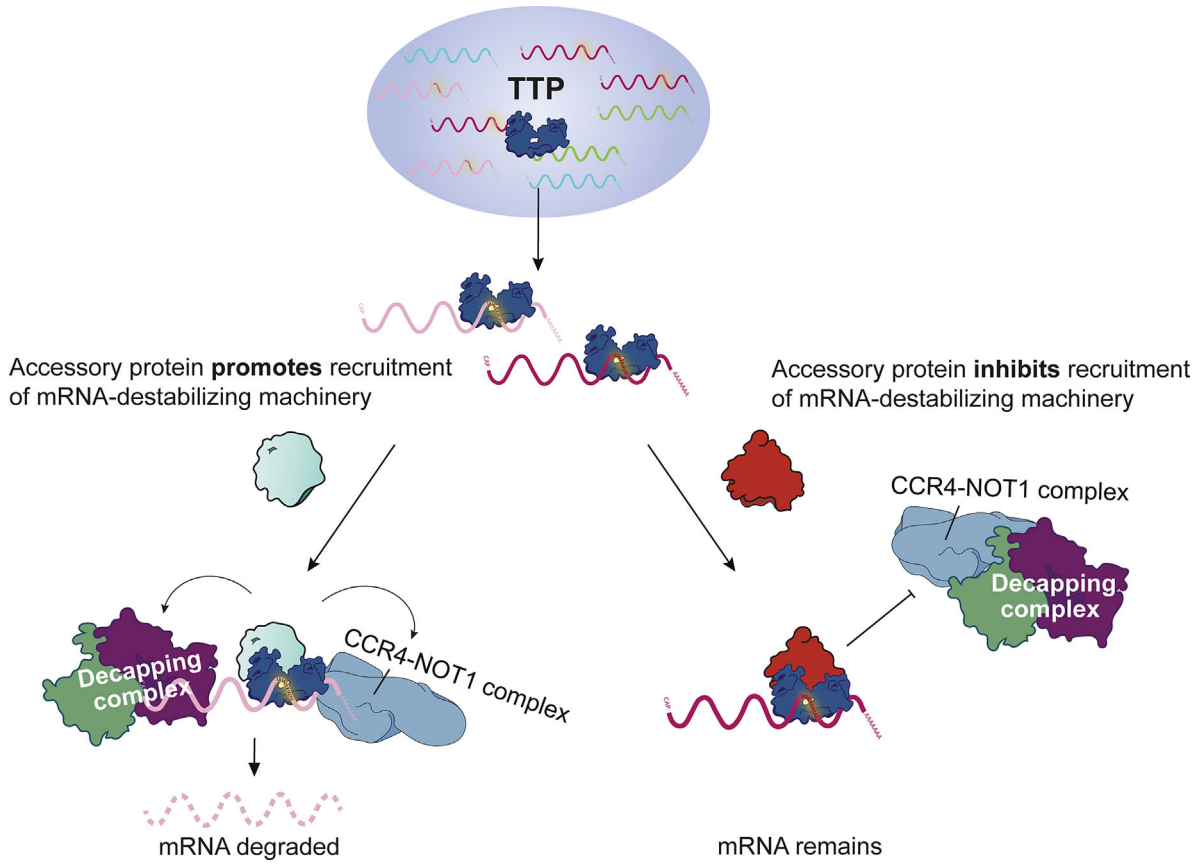

FIGURE 2 | Model of functional and silent binding of TTP to mRNA. Model of possible mechanisms explaining how mRNA-bound TTP destabilizes some mRNAs but not others.

employing primary macrophages and T cells, i.e. experimental systems expressing solely endogenous and naturally regulated TTP (66, 67). All these studies revealed transcript-selective effects of TTP on translation: some TTP target mRNAs were less abundant at polysomes while others were not depleted from polysomes. Negative regulation of translation has been also implicated in control of inflammatory gene expression in tumor-associated macrophages (94). All these data are consistent with an updated model of TTP function in which cis-acting and transcript-specific RBPs determine the final consequence of TTP binding to the target mRNA (**Figure 2**). This updated model is supported by the finding that TTP binds to the cytoplasmic poly(A)-binding protein and that such interactions are required for inhibition of translation by TTP in primary macrophages (67). The model will become more complex once data on tissue/cell type-specific functions of TTP are included. First data on biologically relevant cell type-specific effects of TTP have only recently become available: The mRNA coding for the IL-1β cytokine (*Il1b* mRNA) is destabilized by TTP in bone marrow-derived dendritic cells but not in bone marrow-derived macrophages despite strong binding to TTP (53). The regulation of *Il1b* expression by TTP is important *in vivo* as TTP-deficient mice show higher *Il1b* mRNA levels in several tissues. Moreover, genetic inactivation of IL-1 signaling in TTP-deficient animals ameliorates the TTP deficiency syndrome (53).

The extent of cell type-specific regulation of TTP activity can be indirectly estimated from a number of RNA-seq studies comparing mRNA levels in wild-type *versus* TTP knockout cells. For example, the levels of *Tnf* mRNA, the bona fide TTP target, are comparable in wild-type and TTP-deficient T cells, suggesting that TTP does not target Tnf mRNA for degradation in T cells in contrast to most other cell types (66). Similarly, *Il6* mRNA, which is known to be bound and destabilized by TTP in bone marrow-derived macrophages (BMDMs) (55), is more highly expressed also in TTP-deficient dendritic cells (upon 3 h or 6 h LPS stimulation) and T cells (upon 4 h activation) but not in peritoneal neutrophils (53, 60). Reported RNA-seq expression data for selected TTP targets in primary immune cells (BMDMs, BMDCs, peritoneal neutrophils and T cells) from wild-type and TTP-deficient mice are summarized in **Table 1**. These data convincingly visualize that a comparison of mRNA levels does not provide a definitive information about the destabilization of a particular mRNA by TTP since indirect

TABLE 1 | Expression data (FPKMs or counts) of selected TTP targets in different immune cell types from wild type and TTP-KO mice.

Gene_ID	Gene_name	BMDM, 3 h LPS, FPKM		BMDM, 6 h LPS, FPKM		BMDC, 3 h LPS, FPKM		BMDC, 6 h LPS, FPKM		Peritoneal neutrophils, 4 h LPS, FPKM		T cells, 4 h activation, counts		T cells, 3 day activation, counts	
		Wild-type	TTP-KO	Wild-type	TTP-KO	Wild-type	TTP-KO	Wild-type	TTP-KO	Wild-type	TTP-KO	Wild-type	TTP-KO	Wild-type	TTP-KO
ENSMUSG00000029378	Areg	ND	ND	ND	ND	3.93	8.12	0.17	0.88	12.05	9.68	89.50	51.75	217.00	87.00
ENSMUSG00000000982	Ccl3	6937.76	9117.56	4183.66	16518.37	1260.15	4309.57	814.67	4136.92	8134.45	9617.97	22.50	22.00	56187.67	21074.00
ENSMUSG00000018930	Ccl4	9008.07	10206.05	4422.39	6764.60	652.02	1358.16	234.16	971.93	4055.42	3860.08	201.25	210.00	134778.33	80107.67
ENSMUSG00000029380	Cxcl1	629.10	1589.36	24.27	443.73	309.38	692.45	127.86	374.72	1900.60	2273.85	1.00	3.50	0.00	0.00
ENSMUSG00000034855	Cxcl10	11244.27	10914.54	10272.14	9763.24	494.36	1296.76	435.80	1888.26	57.05	51.66	486.00	475.50	12.00	10.67
ENSMUSG00000058427	Cxcl2	1563.82	5658.09	179.03	3428.48	862.66	3066.80	325.44	2415.03	27007.28	45947.78	8.50	14.25	260.33	60.33
ENSMUSG00000029379	Cxcl3	384.68	351.67	35.31	230.81	948.92	1404.63	536.80	1536.96	3174.43	3472.62	13.50	26.50	808.67	422.67
ENSMUSG00000003541	Ier3	173.04	335.38	215.25	358.83	27.72	69.97	31.33	77.18	999.89	1081.84	106.00	190.25	3273.00	12006.67
ENSMUSG00000016529	Il10	71.76	171.35	129.47	680.55	0.67	5.57	0.22	2.99	347.01	719.35	3.75	6.25	105982.33	149397.33
ENSMUSG00000027399	Il1a	32.43	60.61	13.80	28.18	286.92	737.09	173.03	547.67	3642.63	4825.90	17.75	29.25	95.00	18.33
ENSMUSG00000027398	Il1b	138.34	150.00	70.07	82.29	412.66	1241.13	259.85	940.15	9785.50	14043.60	56.50	96.50	0.00	0.00
ENSMUSG00000025746	Il6	72.51	62.09	35.80	76.62	293.93	629.44	317.59	684.42	324.30	201.17	50.00	76.25	57.00	42.33
ENSMUSG00000032487	Ptgs2 (or Cox2)	206.85	155.98	1396.01	1288.74	1.09	3.96	3.14	12.91	6719.78	6566.11	5.25	9.50	26.00	49.67
ENSMUSG00000020826	Nos2	309.54	357.49	469.47	849.94	79.64	165.24	44.39	130.91	47.01	129.30	2.50	11.00	10609.00	5992.00
ENSMUSG00000038037	Socs1	487.62	538.13	159.49	206.37	60.32	124.91	55.28	208.53	24.88	11.66	1784.75	2112.00	2596.67	3844.00
ENSMUSG00000053113	Socs3	484.52	458.44	417.63	455.86	67.84	87.22	39.03	67.06	534.58	788.26	1327.50	1021.50	3515.00	11969.67
ENSMUSG00000024401	Tnf	3321.70	4880.01	939.77	2661.18	522.03	1837.24	163.15	1196.23	12713.94	16190.19	4658.50	4404.25	41631.00	38744.00

Data are extracted from reported RNA-seq experiments; BMDM, reference (9); BMDC, reference (53); peritoneal neutrophils, (60); reference, T cells; reference (66).
BMDM, bone marrow-derived macrophages.
BMDM, bone marrow-derived dendritic cells.
ND, not determined (too low expression).

(possibly cell type-specific) effects of transcription can mask differences in mRNA stability. A good example is *Il6* mRNA in T cells: while a short (4 h) activation results in 50% higher *Il6* mRNA levels in TTP-deficient T cells as compared to controls, consistent with *Il6* mRNA being destabilized by TTP, a 3-day activation causes TTP-deficient T cells to express 15% less *Il6* mRNA than the control cells [**Table 1** and (66)]. Thus, mRNA stability assays combined, whenever possible, with TTP binding analyses are required when defining a TTP target in a given cell type. A combination of transcriptome-wide mRNA stability and TTP binding assays has been so far reported only for BMDMs so that a comprehensive TTP target collection (searchable at https://ttp-atlas.univie.ac.at/) is available only for this cell type (9). Future studies should include transcriptome-wide mRNA stability analyses in other cell types.

In summary, these findings implicate that cell type-specific RBPs act together with TTP to stabilize or destabilize select TTP targets. Comprehensive biochemical studies including reconstitution assays are needed to precisely determine the underlying mechanisms. The results of these studies will be relevant for the entire TTP family, as the functional *versus* silent binding to target mRNA is important also for Zfp36l1 and Zfp36l2 (21, 95).

OUTLOOK

Despite more than 25 years of research, TTP continues to represent an important and fruitful model for studies on RBPs in general and on the regulation of immune responses by RBPs in particular. Technological progress in recent years and advanced animal models were instrumental for the identification of novel regulatory facets and functional consequences of TTP which fundamentally improved our understating of physiological and pathological inflammation. Most of these new findings remain mechanistically poorly defined and represent challenging topics for future research. This will include analyses of TTP-containing protein complexes and yet uncharacterized phosphorylation sites which will help addressing the mechanism of functional *versus* silent binding of TTP to RNA. An underexplored area are tissue- and cell type-specific functions of TTP *in vivo* to answer the still incompletely understood phenotype of TTP-deficient mice. Finally, an attractive avenue is the exploitation of TTP and mRNA decay in therapy of inflammatory diseases and cancer.

AUTHOR CONTRIBUTIONS

PK designed the concept and wrote the manuscript. AB wrote the manuscript and prepared figures. JF prepared figures. All authors contributed to the article and approved the submitted version.

FUNDING

This work was supported by the Austrian Science Fund (FWF) grants P33000-B, P31848-B and W1261 to PK.

REFERENCES

1. Turner M, Diaz-Munoz MD. RNA-Binding Proteins Control Gene Expression and Cell Fate in the Immune System. *Nat Immunol* (2018) 19:120–9. doi: 10.1038/s41590-017-0028-4
2. Akira S, Maeda K. Control of RNA Stability in Immunity. *Annu Rev Immunol* (2021) 39:481–509. doi: 10.1146/annurev-immunol-101819-075147
3. Carpenter S, Ricci EP, Mercier BC, Moore MJ, Fitzgerald KA. Post-Transcriptional Regulation of Gene Expression in Innate Immunity. *Nat Rev* (2014) 14:361–76. doi: 10.1038/nri3682
4. Shaw G, Kamen R. A Conserved AU Sequence From the 3' Untranslated Region of GM-CSF mRNA Mediates Selective mRNA Degradation. *Cell* (1986) 46:659–67. doi: 10.1016/0092-8674(86)90341-7
5. Kontoyiannis D, Pasparakis M, Pizarro TT, Cominelli F, Kollias G. Impaired on/Off Regulation of TNF Biosynthesis in Mice Lacking TNF AU-Rich Elements: Implications for Joint and Gut-Associated Immunopathologies. *Immunity* (1999) 10:387–98. doi: 10.1016/S1074-7613(00)80038-2
6. Yang E, van Nimwegen E, Zavolan M, Rajewsky N, Schroeder M, Magnasco M, et al. Decay Rates of Human mRNAs: Correlation With Functional Characteristics and Sequence Attributes. *Genome Res* (2003) 13:1863–72. doi: 10.1101/gr.1272403
7. Bakheet T, Hitti E, Al-Saif M, Moghrabi WN, Khabar KSA. The AU-Rich Element Landscape Across Human Transcriptome Reveals a Large Proportion in Introns and Regulation by ELAVL1/HuR. *Biochim Biophys Acta Gene Regul Mech* (2018) 1861:167–77. doi: 10.1016/j.bbagrm.2017.12.006
8. Hao S, Baltimore D. The Stability of mRNA Influences the Temporal Order of the Induction of Genes Encoding Inflammatory Molecules. *Nat Immunol* (2009) 10:281–8. doi: 10.1038/ni.1699
9. Sedlyarov V, Fallmann J, Ebner F, Huemer J, Sneezum L, Ivin M, et al. Tristetraprolin Binding Site Atlas in the Macrophage Transcriptome Reveals a Switch for Inflammation Resolution. *Mol Syst Biol* (2016) 12:868. doi: 10.15252/msb.20156628
10. Diaz-Munoz MD, Turner M. Uncovering the Role of RNA-Binding Proteins in Gene Expression in the Immune System. *Front Immunol* (2018) 9:1094. doi: 10.3389/fimmu.2018.01094
11. Yoshinaga M, Takeuchi O. RNA Binding Proteins in the Control of Autoimmune Diseases. *Immunol Med* (2019) 42:53–64. doi: 10.1080/25785826.2019.1655192
12. Labno A, Tomecki R, Dziembowski A. Cytoplasmic RNA Decay Pathways - Enzymes and Mechanisms. *Biochim Biophys Acta* (2016) 1863:3125–47. doi: 10.1016/j.bbamcr.2016.09.023
13. Zinder JC, Lima CD. Targeting RNA for Processing or Destruction by the Eukaryotic RNA Exosome and its Cofactors. *Genes Dev* (2017) 31:88–100. doi: 10.1101/gad.294769.116
14. Uehata T, Iwasaki H, Vandenbon A, Matsushita K, Hernandez-Cuellar E, Kuniyoshi K, et al. Malt1-Induced Cleavage of Regnase-1 in CD4(+) Helper T Cells Regulates Immune Activation. *Cell* (2013) 153:1036–49. doi: 10.1016/j.cell.2013.04.034
15. Collart MA. The Ccr4-Not Complex is a Key Regulator of Eukaryotic Gene Expression. *Wiley Interdiscip Rev RNA* (2016) 7:438–54. doi: 10.1002/wrna.1332
16. Grudzien-Nogalska E, Kiledjian M. New Insights Into Decapping Enzymes and Selective mRNA Decay. *Wiley Interdiscip Rev RNA* (2017) 8:e1379. doi: 10.1002/wrna.1379
17. Vogel KU, Edelmann SL, Jeltsch KM, Bertossi A, Heger K, Heinz GA, et al. Roquin Paralogs 1 and 2 Redundantly Repress the Icos and Ox40 Costimulator mRNAs and Control Follicular Helper T Cell Differentiation. *Immunity* (2013) 38:655–68. doi: 10.1016/j.immuni.2012.12.004
18. Stumpo DJ, Byrd NA, Phillips RS, Ghosh S, Maronpot RR, Castranio T, et al. Chorioallantoic Fusion Defects and Embryonic Lethality Resulting From Disruption of Zfp36L1, a Gene Encoding a CCCH Tandem Zinc Finger Protein of the Tristetraprolin Family. *Mol Cell Biol* (2004) 24:6445–55. doi: 10.1128/MCB.24.14.6445-6455.2004
19. Stumpo DJ, Broxmeyer HE, Ward T, Cooper S, Hangoc G, Chung YJ, et al. Targeted Disruption of Zfp36l2, Encoding a CCCH Tandem Zinc Finger RNA-Binding Protein, Results in Defective Hematopoiesis. *Blood* (2009) 114:2401–10. doi: 10.1182/blood-2009-04-214619
20. Hodson DJ, Janas ML, Galloway A, Bell SE, Andrews S, Li CM, et al. Deletion of the RNA-Binding Proteins ZFP36L1 and ZFP36L2 Leads to Perturbed Thymic Development and T Lymphoblastic Leukemia. *Nat Immunol* (2010) 11:717–24. doi: 10.1038/ni.1901
21. Galloway A, Saveliev A, Lukasiak S, Hodson DJ, Bolland D, Balmanno K, et al. RNA-Binding Proteins ZFP36L1 and ZFP36L2 Promote Cell Quiescence. *Science* (2016) 352:453–9. doi: 10.1126/science.aad5978
22. Lu JY, Sadri N, Schneider RJ. Endotoxic Shock in AUF1 Knockout Mice Mediated by Failure to Degrade Proinflammatory Cytokine mRNAs. *Genes Dev* (2006) 20:3174–84. doi: 10.1101/gad.1467606
23. Abbadi D, Yang M, Chenette DM, Andrews JJ, Schneider RJ. Muscle Development and Regeneration Controlled by AUF1-Mediated Stage-Specific Degradation of Fate-Determining Checkpoint mRNAs. *Proc Natl Acad Sci USA* (2019) 116:11285–90. doi: 10.1073/pnas.1901165116
24. Pont AR, Sadri N, Hsiao SJ, Smith S, Schneider RJ. mRNA Decay Factor AUF1 Maintains Normal Aging, Telomere Maintenance, and Suppression of Senescence by Activation of Telomerase Transcription. *Mol Cell* (2012) 47:5–15. doi: 10.1016/j.molcel.2012.04.019
25. Chen J, Cascio J, Magee JD, Techasintana P, Gubin MM, Dahm GM, et al. Posttranscriptional Gene Regulation of IL-17 by the RNA-Binding Protein HuR Is Required for Initiation of Experimental Autoimmune Encephalomyelitis. *J Immunol* (2013) 191:5441–50. doi: 10.4049/jimmunol.1301188
26. Masuda K, Ripley B, Nishimura R, Mino T, Takeuchi O, Shioi G, et al. Arid5a Controls IL-6 mRNA Stability, Which Contributes to Elevation of IL-6 Level *In Vivo*. *Proc Natl Acad Sci U.S.A.* (2013) 110:9409–14. doi: 10.1073/pnas.1307419110
27. Diaz-Munoz MD, Bell SE, Fairfax K, Monzon-Casanova E, Cunningham AF, Gonzalez-Porta M, et al. The RNA-Binding Protein HuR Is Essential for the B Cell Antibody Response. *Nat Immunol* (2015) 16:415–25. doi: 10.1038/ni.3115
28. Zhang Z, Zong C, Jiang M, Hu H, Cheng X, Ni J, et al. Hepatic HuR Modulates Lipid Homeostasis in Response to High-Fat Diet. *Nat Commun* (2020) 11:3067. doi: 10.1038/s41467-020-16918-x
29. Katsanou V, Milatos S, Yiakouvaki A, Sgantzis N, Kotsoni A, Alexiou M, et al. The RNA-Binding Protein Elavl1/HuR is Essential for Placental Branching Morphogenesis and Embryonic Development. *Mol Cell Biol* (2009) 29:2762–76. doi: 10.1128/MCB.01393-08
30. Lang M, Berry D, Passecker K, Mesteri I, Bhuju S, Ebner F, et al. HuR Small-Molecule Inhibitor Elicits Differential Effects in Adenomatosis Polyposis and Colorectal Carcinogenesis. *Cancer Res* (2017) 77:2424–38. doi: 10.1158/0008-5472.CAN-15-1726
31. Wells ML, Perera L, Blackshear PJ. An Ancient Family of RNA-Binding Proteins: Still Important! *Trends Biochem Sci* (2017) 42(4):285–96. doi: 10.1016/j.tibs.2016.12.003
32. Tan D, Zhou M, Kiledjian M, Tong L. The ROQ Domain of Roquin Recognizes mRNA Constitutive-Decay Element and Double-Stranded RNA. *Nat Struct Mol Biol* (2014) 21:679–85. doi: 10.1038/nsmb.2857
33. Yokogawa M, Tsushima T, Noda NN, Kumeta H, Enokizono Y, Yamashita K, et al. Structural Basis for the Regulation of Enzymatic Activity of Regnase-1 by Domain-Domain Interactions. *Sci Rep* (2016) 6:22324. doi: 10.1038/srep22324
34. Wagner BJ, DeMaria CT, Sun Y, Wilson GM, Brewer G. Structure and Genomic Organization of the Human AUF1 Gene: Alternative pre-mRNA Splicing Generates Four Protein Isoforms. *Genomics* (1998) 48:195–202. doi: 10.1006/geno.1997.5142
35. Pabis M, Popowicz GM, Stehle R, Fernandez-Ramos D, Asami S, Warner L, et al. HuR Biological Function Involves RRM3-Mediated Dimerization and RNA Binding by All Three RRMs. *Nucleic Acids Res* (2019) 47:1011–29. doi: 10.1093/nar/gky1138
36. Iwahara J, Clubb RT. Solution Structure of the DNA Binding Domain From Dead Ringer, a Sequence-Specific AT-Rich Interaction Domain (ARID). *EMBO J* (1999) 18:6084–94. doi: 10.1093/emboj/18.21.6084
37. Lai WS, Carballo E, Strum JR, Kennington EA, Phillips RS, Blackshear PJ. Evidence That Tristetraprolin Binds to AU-Rich Elements and Promotes the Deadenylation and Destabilization of Tumor Necrosis Factor Alpha mRNA. *Mol Cell Biol* (1999) 19:4311–23. doi: 10.1128/MCB.19.6.4311
38. Yoon JH, De S, Srikantan S, Abdelmohsen K, Grammatikakis I, Kim J, et al. PAR-CLIP Analysis Uncovers AUF1 Impact on Target RNA Fate and Genome Integrity. *Nat Commun* (2014) 5:5248. doi: 10.1038/ncomms6248
39. Lebedeva S, Jens M, Theil K, Schwanhausser B, Selbach M, Landthaler M, et al. Transcriptome-Wide Analysis of Regulatory Interactions of the RNA-Binding Protein HuR. *Mol Cell* (2011) 43:340–52. doi: 10.1016/j.molcel.2011.06.008

40. Mukherjee N, Corcoran DL, Nusbaum JD, Reid DW, Georgiev S, Hafner M, et al. Integrative Regulatory Mapping Indicates That the RNA-Binding Protein HuR Couples pre-mRNA Processing and mRNA Stability. *Mol Cell* (2011) 43:327–39. doi: 10.1016/j.molcel.2011.06.007
41. Leppek K, Schott J, Reitter S, Poetz F, Hammond MC, Stoecklin G. Roquin Promotes Constitutive mRNA Decay *via* a Conserved Class of Stem-Loop Recognition Motifs. *Cell* (2013) 153:869–81. doi: 10.1016/j.cell.2013.04.016
42. Mino T, Murakawa Y, Fukao A, Vandenbon A, Wessels HH, Ori D, et al. Regnase-1 and Roquin Regulate a Common Element in Inflammatory mRNAs by Spatiotemporally Distinct Mechanisms. *Cell* (2015) 161:1058–73. doi: 10.1016/j.cell.2015.04.029
43. Chang SH, Elemento O, Zhang J, Zhuang ZW, Simons M, Hla T. ELAVL1 Regulates Alternative Splicing of Eif4e Transporter to Promote Postnatal Angiogenesis. *Proc Natl Acad Sci USA* (2014) 111:18309–14. doi: 10.1073/pnas.1412172111
44. Blackshear PJ, Perera L. Phylogenetic Distribution and Evolution of the Linked RNA-Binding and NOT1-Binding Domains in the Tristetraprolin Family of Tandem CCCH Zinc Finger Proteins. *J Interferon Cytokine Res* (2014) 34:297–306. doi: 10.1089/jir.2013.0150
45. Puig S, Askeland E, Thiele DJ. Coordinated Remodeling of Cellular Metabolism During Iron Deficiency Through Targeted mRNA Degradation. *Cell* (2005) 120:99–110. doi: 10.1016/j.cell.2004.11.032
46. Treguer K, Faucheux C, Veschambre P, Fedou S, Theze N, Thiebaud P. Comparative Functional Analysis of ZFP36 Genes During Xenopus Development. *PloS One* (2013) 8:e54550. doi: 10.1371/journal.pone.0054550
47. Kaymak E, Ryder SP. RNA Recognition by the Caenorhabditis Elegans Oocyte Maturation Determinant OMA-1. *J Biol Chem* (2013) 288:30463–72. doi: 10.1074/jbc.M113.496547
48. Stumpo DJ, Trempus CS, Tucker CJ, Huang W, Li L, Kluckman K, et al. Deficiency of the Placenta- and Yolk Sac-Specific Tristetraprolin Family Member ZFP36L3 Identifies Likely mRNA Targets and an Unexpected Link to Placental Iron Metabolism. *Development* (2016) 143:1424–33. doi: 10.1242/dev.130369
49. Taylor GA, Carballo E, Lee DM, Lai WS, Thompson MJ, Patel DD, et al. A Pathogenetic Role for TNF Alpha in the Syndrome of Cachexia, Arthritis, and Autoimmunity Resulting From Tristetraprolin (TTP) Deficiency. *Immunity* (1996) 4:445–54. doi: 10.1016/S1074-7613(00)80411-2
50. Carballo E, Lai WS, Blackshear PJ. Feedback Inhibition of Macrophage Tumor Necrosis Factor-Alpha Production by Tristetraprolin. *Science* (1998) 281:1001–5. doi: 10.1126/science.281.5379.1001
51. Molle C, Zhang T, Ysebrant de Lendonck L, Gueydan C, Andrianne M, Sherer F, et al. Tristetraprolin Regulation of Interleukin 23 mRNA Stability Prevents a Spontaneous Inflammatory Disease. *J Exp Med* (2013) 210:1675–84. doi: 10.1084/jem.20120707
52. Kang JG, Amar MJ, Remaley AT, Kwon J, Blackshear PJ, Wang PY, et al. Zinc Finger Protein Tristetraprolin Interacts With CCL3 mRNA and Regulates Tissue Inflammation. *J Immunol* (2011) 187:2696–701. doi: 10.4049/jimmunol.1101149
53. Sneezum L, Eislmayr K, Dworak H, Sedlyarov V, Le Heron A, Ebner F, et al. Context-Dependent IL-1 mRNA-Destabilization by TTP Prevents Dysregulation of Immune Homeostasis Under Steady State Conditions. *Front Immunol* (2020) 11:1398. doi: 10.3389/fimmu.2020.01398
54. Qiu LQ, Stumpo DJ, Blackshear PJ. Myeloid-Specific Tristetraprolin Deficiency in Mice Results in Extreme Lipopolysaccharide Sensitivity in an Otherwise Minimal Phenotype. *J Immunol* (2012) 188:5150–9. doi: 10.4049/jimmunol.1103700
55. Kratochvill F, Machacek C, Vogl C, Ebner F, Sedlyarov V, Gruber AR, et al. Tristetraprolin-Driven Regulatory Circuit Controls Quality and Timing of mRNA Decay in Inflammation. *Mol Syst Biol* (2011) 7:560. doi: 10.1038/msb.2011.93
56. Andrianne M, Assabban A, La C, Mogilenko D, Salle DS, Fleury S, et al. Tristetraprolin Expression by Keratinocytes Controls Local and Systemic Inflammation. *JCI Insight* (2017) 2(11):e92979. doi: 10.1172/jci.insight.92979
57. La C, de Toeuf B, Bindels LB, Van Maele L, Assabban A, Melchior M, et al. The RNA-Binding Protein Tristetraprolin Regulates RALDH2 Expression by Intestinal Dendritic Cells and Controls Local Treg Homeostasis. *Mucosal Immunol* (2021) 14(1):80–91. doi: 10.1038/s41385-020-0302-x
58. Eshelman MA, Matthews SM, Schleicher EM, Fleeman RM, Kawasawa YI, Stumpo DJ, et al. Tristetraprolin Targets Nos2 Expression in the Colonic Epithelium. *Sci Rep* (2019) 9:14413. doi: 10.1038/s41598-019-50957-9
59. Assabban A, Dubois-Vedrenne I, Van Maele L, Salcedo R, Snyder BL, Zhou L, et al. Tristetraprolin Expression by Keratinocytes Protects Against Skin Carcinogenesis. *JCI Insight* (2021) 6. doi: 10.1172/jci.insight.140669
60. Ebner F, Sedlyarov V, Tasciyan S, Ivin M, Kratochvill F, Gratz N, et al. The RNA-Binding Protein Tristetraprolin Schedules Apoptosis of Pathogen-Engaged Neutrophils During Bacterial Infection. *J Clin Invest* (2017) 127:2051–65. doi: 10.1172/JCI80631
61. Lai WS, Kennington EA, Blackshear PJ. Tristetraprolin and its Family Members can Promote the Cell-Free Deadenylation of AU-Rich Element-Containing mRNAs by Poly(A) Ribonuclease. *Mol Cell Biol* (2003) 23:3798–812. doi: 10.1128/MCB.23.11.3798-3812.2003
62. Lykke-Andersen J, Wagner E. Recruitment and Activation of mRNA Decay Enzymes by Two ARE-Mediated Decay Activation Domains in the Proteins TTP and BRF-1. *Genes Dev* (2005) 19:351–61. doi: 10.1101/gad.1282305
63. Sandler H, Kreth J, Timmers HT, Stoecklin G. Not1 Mediates Recruitment of the Deadenylase Caf1 to mRNAs Targeted for Degradation by Tristetraprolin. *Nucleic Acids Res* (2011) 39:4373–86. doi: 10.1093/nar/gkr011
64. Fabian MR, Frank F, Rouya C, Siddiqui N, Lai WS, Karetnikov A, et al. Structural Basis for the Recruitment of the Human CCR4-NOT Deadenylase Complex by Tristetraprolin. *Nat Struct Mol Biol* (2013) 20:735–9. doi: 10.1038/nsmb.2572
65. Tiedje C, Diaz-Munoz MD, Trulley P, Ahlfors H, Laass K, Blackshear PJ, et al. The RNA-Binding Protein TTP is a Global Post-Transcriptional Regulator of Feedback Control in Inflammation. *Nucleic Acids Res* (2016) 44:7418–40. doi: 10.1093/nar/gkw474
66. Moore MJ, Blachere NE, Fak JJ, Park CY, Sawicka K, Parveen S, et al. ZFP36 RNA-Binding Proteins Restrain T Cell Activation and Anti-Viral Immunity. *eLife* (2018) 7. doi: 10.7554/eLife.33057
67. Zhang X, Chen X, Liu Q, Zhang S, Hu W. Translation Repression *via* Modulation of the Cytoplasmic Poly(A)-Binding Protein in the Inflammatory Response. *eLife* (2017) 6. doi: 10.7554/eLife.27786
68. Lai WS, Kennington EA, Blackshear PJ. Interactions of CCCH Zinc Finger Proteins With mRNA: non-Binding Tristetraprolin Mutants Exert an Inhibitory Effect on Degradation of AU-Rich Element-Containing mRNAs. *J Biol Chem* (2002) 277:9606–13. doi: 10.1074/jbc.M110395200
69. Lai WS, Stumpo DJ, Qiu L, Faccio R, Blackshear PJ. A Knock-In Tristetraprolin (TTP) Zinc Finger Point Mutation in Mice: Comparison With Complete TTP Deficiency. *Mol Cell Biol* (2018) 38(4):e00488–17. doi: 10.1128/MCB.00488-17
70. Brewer BY, Malicka J, Blackshear PJ, Wilson GM. RNA Sequence Elements Required for High Affinity Binding by the Zinc Finger Domain of Tristetraprolin: Conformational Changes Coupled to the Bipartite Nature of Au-Rich MRNA-Destabilizing Motifs. *J Biol Chem* (2004) 279:27870–7. doi: 10.1074/jbc.M402551200
71. Stoecklin G, Tenenbaum SA, Mayo T, Chittur SV, George AD, Baroni TE, et al. Genome-Wide Analysis Identifies Interleukin-10 mRNA as Target of Tristetraprolin. *J Biol Chem* (2008) 283:11689–99. doi: 10.1074/jbc.M709657200
72. Memczak S, Jens M, Elefsinioti A, Torti F, Krueger J, Rybak A, et al. Circular RNAs Are a Large Class of Animal RNAs With Regulatory Potency. *Nature* (2013) 495(7441):333–8. doi: 10.1038/nature11928
73. Hansen TB, Jensen TI, Clausen BH, Bramsen JB, Finsen B, Damgaard CK, et al. Natural RNA Circles Function as Efficient microRNA Sponges. *Nature* (2013) 495(7441):384–8. doi: 10.1038/nature11993
74. Sandler H, Stoecklin G. Control of mRNA Decay by Phosphorylation of Tristetraprolin. *Biochem Soc Trans* (2008) 36:491–6. doi: 10.1042/BST0360491
75. Kovarik P, Ebner F, Sedlyarov V. Posttranscriptional Regulation of Cytokine Expression. *Cytokine* (2017) 89:21–6. doi: 10.1016/j.cyto.2015.11.007
76. O'Neil JD, Ammit AJ, Clark AR. MAPK P38 Regulates Inflammatory Gene Expression *via* Tristetraprolin: Doing Good by Stealth. *Int J Biochem Cell Biol* (2018) 94:6–9. doi: 10.1016/j.biocel.2017.11.003
77. Lai WS, Thompson MJ, Taylor GA, Liu Y, Blackshear PJ. Promoter Analysis of Zfp-36, the Mitogen-Inducible Gene Encoding the Zinc Finger Protein Tristetraprolin. *J Biol Chem* (1995) 270:25266–72. doi: 10.1074/jbc.270.42.25266
78. Sauer I, Schaljo B, Vogl C, Gattermeier I, Kolbe T, Muller M, et al. Interferons Limit Inflammatory Responses by Induction of Tristetraprolin. *Blood* (2006) 107:4790–7. doi: 10.1182/blood-2005-07-3058

79. Schaljo B, Kratochvill F, Gratz N, Sadzak I, Sauer I, Hammer M, et al. Tristetraprolin is Required for Full Anti-Inflammatory Response of Murine Macrophages to IL-10. *J Immunol* (2009) 183:1197–206. doi: 10.4049/jimmunol.0803883
80. Suzuki K, Nakajima H, Ikeda K, Maezawa Y, Suto A, Takatori H, et al. IL-4-Stat6 Signaling Induces Tristetraprolin Expression and Inhibits TNF-Alpha Production in Mast Cells. *J Exp Med* (2003) 198:1717–27. doi: 10.1084/jem.20031701
81. Tchen CR, Brook M, Saklatvala J, Clark AR. The Stability of Tristetraprolin mRNA is Regulated by Mitogen-Activated Protein Kinase P38 and by Tristetraprolin Itself. *J Biol Chem* (2004) 279:32393–400. doi: 10.1074/jbc.M402059200
82. Brook M, Tchen CR, Santalucia T, McIlrath J, Arthur JS, Saklatvala J, et al. Posttranslational Regulation of Tristetraprolin Subcellular Localization and Protein Stability by P38 Mitogen-Activated Protein Kinase and Extracellular Signal-Regulated Kinase Pathways. *Mol Cell Biol* (2006) 26:2408–18. doi: 10.1128/MCB.26.6.2408-2418.2006
83. Ngoc LV, Wauquier C, Soin R, Bousbata S, Twyffels L, Kruys V, et al. Rapid Proteasomal Degradation of Posttranscriptional Regulators of the TIS11/tristetraprolin Family is Induced by an Intrinsically Unstructured Region Independently of Ubiquitination. *Mol Cell Biol* (2014) 34:4315–28. doi: 10.1128/MCB.00643-14
84. Hitti E, Iakovleva T, Brook M, Deppenmeier S, Gruber AD, Radzioch D, et al. Mitogen-Activated Protein Kinase-Activated Protein Kinase 2 Regulates Tumor Necrosis Factor mRNA Stability and Translation Mainly by Altering Tristetraprolin Expression, Stability, and Binding to Adenine/Uridine-Rich Element. *Mol Cell Biol* (2006) 26:2399–407. doi: 10.1128/MCB.26.6.2399-2407.2006
85. Clement SL, Scheckel C, Stoecklin G, Lykke-Andersen J. Phosphorylation of Tristetraprolin by MK2 Impairs AU-Rich Element mRNA Decay by Preventing Deadenylase Recruitment. *Mol Cell Biol* (2011) 31:256–66. doi: 10.1128/MCB.00717-10
86. Stoecklin G, Stubbs T, Kedersha N, Wax S, Rigby WF, Blackwell TK, et al. MK2-Induced Tristetraprolin:14-3-3 Complexes Prevent Stress Granule Association and ARE-mRNA Decay. *EMBO J* (2004) 23:1313–24. doi: 10.1038/sj.emboj.7600163
87. Johnson BA, Blackwell TK. Multiple Tristetraprolin Sequence Domains Required to Induce Apoptosis and Modulate Responses to TNFalpha Through Distinct Pathways. *Oncogene* (2002) 21:4237–46. doi: 10.1038/sj.onc.1205526
88. Tiedje C, Ronkina N, Tehrani M, Dhamija S, Laass K, Holtmann H, et al. The P38/MK2-Driven Exchange Between Tristetraprolin and HuR Regulates AU-Rich Element-Dependent Translation. *PloS Genet* (2012) 8:e1002977. doi: 10.1371/journal.pgen.1002977
89. Ross EA, Smallie T, Ding Q, O'Neil JD, Cunliffe HE, Tang T, et al. Dominant Suppression of Inflammation *via* Targeted Mutation of the mRNA Destabilizing Protein Tristetraprolin. *J Immunol* (2015) 195:265–76. doi: 10.4049/jimmunol.1402826
90. Clark AR, Dean JL. The Control of Inflammation *via* the Phosphorylation and Dephosphorylation of Tristetraprolin: A Tale of Two Phosphatases. *Biochem Soc Trans* (2016) 44:1321–37. doi: 10.1042/BST20160166
91. Ronkina N, Shushakova N, Tiedje C, Yakovleva T, Tollenaere MAX, Scott A, et al. The Role of TTP Phosphorylation in the Regulation of Inflammatory Cytokine Production by MK2/3. *J Immunol* (2019) 203:2291–300. doi: 10.4049/jimmunol.1801221
92. Mukherjee N, Jacobs NC, Hafner M, Kennington EA, Nusbaum JD, Tuschl T, et al. Global Target mRNA Specification and Regulation by the RNA-Binding Protein ZFP36. *Genome Biol* (2014) 15:R12. doi: 10.1186/gb-2014-15-1-r12
93. Mahmoud L, Moghrabi W, Khabar KSA, Hitti EG. Bi-Phased Regulation of the Post-Transcriptional Inflammatory Response by Tristetraprolin Levels. *RNA Biol* (2019) 16:309–19. doi: 10.1080/15476286.2019.1572437
94. Kratochvill F, Gratz N, Qualls JE, Van De Velde LA, Chi H, Kovarik P, et al. Tristetraprolin Limits Inflammatory Cytokine Production in Tumor-Associated Macrophages in an mRNA Decay-Independent Manner. *Cancer Res* (2015) 75:3054–64. doi: 10.1158/0008-5472.CAN-15-0205
95. Salerno F, Engels S, van den Biggelaar M, van Alphen FPJ, Guislain A, Zhao W, et al. Translational Repression of Pre-Formed Cytokine-Encoding mRNA Prevents Chronic Activation of Memory T Cells. *Nat Immunol* (2018) 19 (8):828–37. doi: 10.1038/s41590-018-0155-6

Conflict of Interest: The authors declare that the research was conducted in the absence of any commercial or financial relationships that could be construed as a potential conflict of interest.

frontiers in Immunology

ORIGINAL RESEARCH
published: 17 November 2021
doi: 10.3389/fimmu.2021.717324

RNA-Binding Protein Expression Alters Upon Differentiation of Human B Cells and T Cells

Nordin D. Zandhuis[1,2], *Benoit P. Nicolet*[1,2] *and Monika C. Wolkers*[1,2*]

[1] Department of Hematopoiesis, Sanquin Research and Landsteiner Laboratory, Amsterdam University Medical Center (UMC), University of Amsterdam, Amsterdam, Netherlands, [2] Oncode Institute, Utrecht, Netherlands

B cells and T cells are key players in the defence against infections and malignancies. To exert their function, B cells and T cells differentiate into effector and memory cells. Tight regulation of these differentiation processes is key to prevent their malfunction, which can result in life-threatening disease. Lymphocyte differentiation relies on the appropriate timing and dosage of regulatory molecules, and post-transcriptional gene regulation (PTR) is a key player herein. PTR includes the regulation through RNA-binding proteins (RBPs), which control the fate of RNA and its translation into proteins. To date, a comprehensive overview of the RBP expression throughout lymphocyte differentiation is lacking. Using transcriptome and proteome analyses, we here catalogued the RBP expression for human B cells and T cells. We observed that even though the overall RBP expression is conserved, the relative RBP expression is distinct between B cells and T cells. Differentiation into effector and memory cells alters the RBP expression, resulting into preferential expression of different classes of RBPs. For instance, whereas naive T cells express high levels of translation-regulating RBPs, effector T cells preferentially express RBPs that modulate mRNA stability. Lastly, we found that cytotoxic $CD8^+$ and $CD4^+$ T cells express a common RBP repertoire. Combined, our study reveals a cell type-specific and differentiation-dependent RBP expression landscape in human lymphocytes, which will help unravel the role of RBPs in lymphocyte function.

Keywords: RNA binding protein, T cells, B cells, B and T cell differentiation, T cell cytotoxicity, post transcriptional regulation (PTR)

OPEN ACCESS

Edited by:
Manuel Daniel Díaz-Muñoz, INSERM U1043 Centre de Physiopathologie de Toulouse Purpan (INSERM), France

Reviewed by:
Rami Bechara, University of Pittsburgh, United States
Laurent Delpy, UMR7276 Contrôle des réponses immunes B et des lymphoprolifération (CRIBL), France

***Correspondence:**
Monika C. Wolkers
m.wolkers@sanquin.nl

Specialty section:
This article was submitted to Molecular Innate Immunity, a section of the journal Frontiers in Immunology

Received: *30 May 2021*
Accepted: *27 October 2021*
Published: *17 November 2021*

Citation:
Zandhuis ND, Nicolet BP and Wolkers MC (2021) RNA-Binding Protein Expression Alters Upon Differentiation of Human B Cells and T Cells. Front. Immunol. 12:717324. doi: 10.3389/fimmu.2021.717324

INTRODUCTION

B cells and T cells are essential to eradicate microbial infections and malignant cells. Upon antigen recognition through their receptors, B cells produce antibodies and T cells produce cytokines and chemokines, respectively. Cytotoxic T cells also acquire the capacity to kill target cells. The critical contribution of these lymphocyte subsets to anti-microbial and anti-tumor responses was evidenced by the discovery of genetic mutations in humans that result in immune dysfunction in response to infections (1). Similarly, effective T cell responses are key for tumor immunosurveillance (2).

Importantly, tight regulation of B cell and T cell effector function is key for effective clearance of infections. The aberrant production of antibodies by B cells, and the overproduction of effector molecules by T cells has been correlated with several autoimmune disorders, including systemic

lupus erythematosus, rheumatoid arthritis and multiple sclerosis (3–6). Likewise, patients suffering from severe disease upon COVID-19 infection developed auto-antibodies against type-I interferons (7), and an excess cytokine production in COVID-19 patients can result in organ dysfunction (8). Conversely, in chronic HIV infections or in tumors, T cells gradually lose their capacity to produce effector cytokines and to kill target cells (9, 10). These findings combined highlight the necessity to fine-tune the effector function of B cells and T cells.

To perform their effector function, B cells and T cells need to undergo an intricate process of differentiation. B cells differentiate into antibody-producing plasmablasts in germinal centers (GC), and upon pathogen clearance into long-lived memory B cells. Likewise, upon T cell priming, T cells differentiate into effector T cells, and upon pathogen clearance are maintained as memory T cells to ensure long-term production from recurring infections. In the past decennia, important insights have been obtained how B cells and T cell differentiate. In particular, the role of transcription factors and of metabolic regulators was extensively studied (11–14).

For appropriate lymphocyte differentiation, the regulators of differentiation processes must be produced at the right time and the right amount. In fact, gene dosage of transcription factors was shown to be key for B cell and T cell differentiation (15–18). This fine-tuning of gene expression is - at least in part - regulated by post-transcriptional events governed by RNA-binding proteins (RBPs) and non-coding RNAs (19, 20). RBPs control a plethora of processes. They orchestrate RNA splicing, RNA polyadenylation and the subsequent export from the nucleus to the cytoplasm (21, 22). RBPs can also modify the RNA (23). Furthermore, RBPs control mRNA localization, translation and stability. For instance, the RBPs ZFP36L1 and ZFP36L2 induce quiescence in developing B cells to allow for efficient B cell receptor rearrangement (24). ZFP36L1 is also required for the maintenance of the marginal-zone B cell compartment (25). For germinal center B cells that undergo cell cycle progression and affinity maturation, the expression of the RBP PTBP1 is key (26). In thymocytes, ZFP36L1 and ZFP36L2 dampen the DNA-damage response, which promotes their differentiation into mature T cells (27). In the periphery, Roquin suppresses T helper cell differentiation (28, 29). Also m^6A modifications are important for T helper cell differentiation, as evidenced in mice lacking the methyltransferase METTL3 in T cells (30).

Not only T cell differentiation, but also T cell effector function is tightly regulated by RBPs. Genetic ablation of the RBP Regnase-1 reprogrammed $CD8^+$ T cells into long-lived effector $CD8^+$ T cells, resulting in increased tumour control (31). In a patient, a nonsense-mutation in *ROQUIN-1* resulted in hyperinflammation, including hypercytokinemia in T cells and monocytes (32). Another example is ZFP36L2, which blocks the cytokine production in memory $CD8^+$ T cells from pre-formed mRNA in the absence of activation signals, thereby preventing aberrant production of effector molecules (33).

Even though these examples clearly highlight the importance of RBPs in regulating gene expression in lymphocytes, studies have thus far only addressed the contribution of individual RBPs. The overall expression profile of RBPs in primary human B cells and T cells is not well-documented yet critical for our understanding of regulation of gene expression in lymphocytes.

In this study, we combined lists of previously experimentally defined and computationally predicted RBPs to generate a list of putative RBPs. As a proxy for RBP expression, we catalogued the mRNA and protein expression of these putative RBPs in primary human B cells and T cells. We observed clear differences of RBP expression levels between lymphocyte subsets. Furthermore, upon differentiation, the RBP expression profile significantly altered, which resulted in a shift of functional annotations of RBPs. Lastly, we identified an RBP signature that is specific for $CD4^+$ T cells and $CD8^+$ T cells with a high cytotoxic potential. In conclusion, RBP expression is lymphocyte-type specific and the RBP expression shows dynamic changes upon differentiation.

RESULTS

RNA-Binding Proteins Are Abundantly Expressed in Human B and T Lymphocytes

To investigate the overall mRNA and protein expression of RBPs in human lymphocytes, we first generated a comprehensive list of putative RBPs. We included RBPs that were identified by RNA-interactome capture on multiple cell lines including, HEK293, HeLa-S3, MCF7, MCF10A, U2OS and Jurkat cells (34–36). This list was supplemented with computationally predicted RBPs based on the presence of a defined list of RNA-binding domains (RBDs) (36, 37). This compiled list resulted in 3233 unique putative RBPs (from here on defined as 'RBPs') (**Figure 1A** and **Supplementary Table 1**).

To define the global RBP gene expression in human B and T lymphocytes, we compiled previously published RNA-sequencing (RNA-seq) data on human $CD19^+$ B cell, $CD4^+$ T cell and $CD8^+$ T cell subsets that were isolated from the blood of 3-4 healthy human donors (38). On average, $12.5x10^6$ reads per sample (range: $7.97x10^6$-$19.15x10^6$ reads) could be mapped onto the human transcriptome. A total of 12,830 gene products (>0.1 TPM) were detected in all lymphocyte subsets combined. 2983 of the 3233 RBPs (92.3% of our reference list) were detected at the RNA level in human B and T lymphocytes (>0.1 TPM, **Figure 1B** and **Supplementary Table 1**), of which 2189 were identified in RNA-interactome capture studies and 794 were computationally predicted RBPs. The number of RBP transcripts in human B and T lymphocytes was similar to that of the epithelial cell line HeLa-S3 and the myelogenous leukemia cell line K562 cells, and overlapped for 90.1% [HeLa-S3: 2843 RBPs, K562: 2826 RBPs, **Supplementary Figures 1A, B** (39)].

To calculate the number of RBPs expressed at the protein level in B and T lymphocytes, we used previously published mass spectrometry (MS) data of B cell and T cell subsets of 4 donors (40) that were similarly prepared and selected as the ones in the RNA-seq dataset we used (38). In total, 9436 proteins were identified in all B cell and T cell subsets combined, of which 96.8% (9136 proteins) were also expressed at the RNA level (**Supplementary Figure 1C**). Overall, 2617 RBPs (80.9% of our

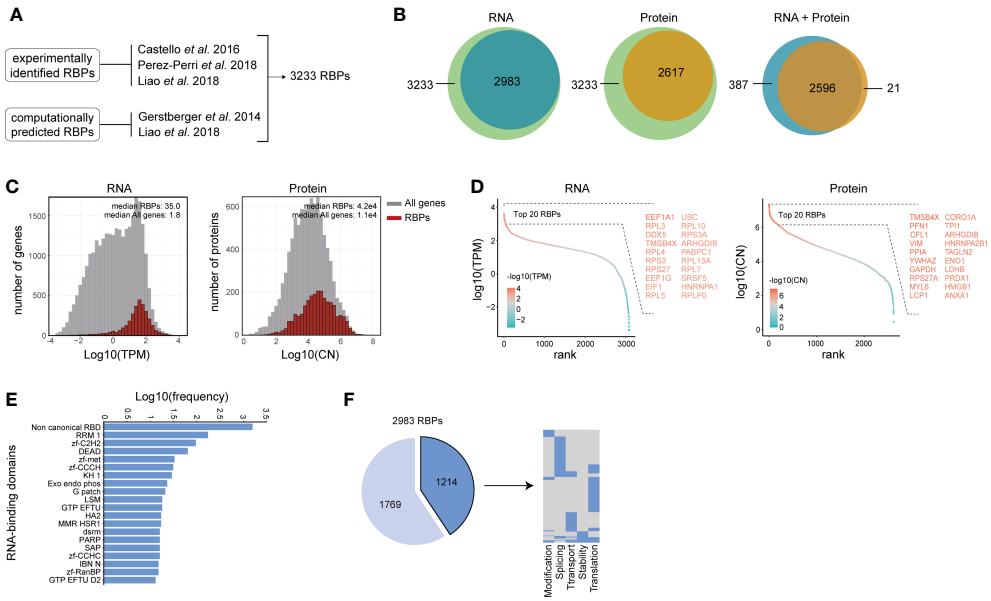

FIGURE 1 | Characterization of RNA-binding protein expression in human B and T lymphocytes. **(A)** Reference list of RNA binding proteins (RBPs) was generated by integrating experimentally validated RBPs (34–36) with computationally predicted RBPs based on the presence of a defined list of RNA-binding domains (36, 37). **(B)** RBPs that are detected in human lymphocytes at RNA level (left panel), at protein level (middle panel), and at both RNA and protein level (right panel). RNA: n=3-4 donors. Protein: 4 donors. (>0.1 TPM) **(C)** RNA abundance in transcript per kilobase per million (TPM) and protein abundance in protein copy number (CN) for all genes (gray) and RBPs (red) in human B cells and T cells. **(D)** Expression levels of RBPs detected at RNA level (left panel) and at protein level (right panel) was ranked according to expression levels. Names of the top 20 expressed RBPs are indicated. **(E)** Frequency of RNA-binding domains among the 2983 RBPs that were detected at RNA level. **(F)** Left panel: RBPs detected at RNA level in human B and T lymphocytes that are annotated for RNA splicing, stability, subcellular localization of RNA, RNA modification, and translation (dark blue), or for other processes (light blue). Right panel: Distribution of RBPs annotated for the five RNA-related processes as indicated. Each line depicts one RBP. TPM, Transcripts per kilobase per million; CN, Protein copy number.

reference list) were detected at the protein level (**Figure 1B**), and 2596 RBPs (80.2%) were detected at both RNA and protein level (**Figure 1B**). This high overlap corroborated with the overall high expression levels of RBPs (**Figure 1C**; p-value: 6.2e-12 for RNA and 2.1e-12 for protein). The top 20 expressed RBPs at RNA level included several ribosomal proteins (*RPL3, RPL4, RPS3, RPS27*), translation-related proteins (*EEF1A1*, *EEF1G*, *EIF1*) and splicing-related proteins *DDX5* (41), *SRSF5* (42), *HNRNPA1* (43); **Figure 1D**). At the protein level, the top 20 expressed RBPs included the RNA stability-related protein [VIM (44)], the splicing-related protein HNRNPA2B1 (45), the ribosomal protein RPS27A, and the moonlighting RBPs ENO1 and GAPDH [**Figure 1D** (46, 47)].

We next determined which RNA-binding domains (RBDs) are present in the RBPs detected at the RNA level. Using previously reported RBDs [**Supplementary Table 1** (36, 37)] and the protein families database [Pfam (48)], we detected a broad range of RBDs. (**Supplementary Table 1**). The top 20 RBDs included classical RBDs, such as the RNA-recognition motif (RRM; 5.8%, present in e.g. *CELF2*, *CNOT4*, *ELAVL2*, *HNRNPLL* and *PABPC1*) and the DEAD helicase motif (DEAD; 2.1%, present in e.g. *DDX1*, *DDX10*, *DHX16*). We also found a variety of zinc-finger protein domains, including the zinc-finger C2H2 (zf-C2H2; 3.2%, present in e.g. *ZNF638*, *ZMAT3*), zinc-finger metazoans (zf-met; 1.1%, present in e.g. *ZFR2*, *TUT1*), zinc-finger CCCH (zf-CCCH; 1.0%, present in e.g. *ZFP36L1*, *RBM27*, *ZC3H10*), zinc-finger CCHC (zf-CCHC; 0.5%, present in e.g. *ZCRB1*, *CPSF4*) and the zinc-finger Ran binding protein (zf-RanBP; 0.5%, present in e.g. *RBM5*, *RBM10*, **Figure 1E**). In addition, RBPs containing the top 20 RBDs were commonly identified using RNA-interactome capture studies (**Supplementary Figure 1D**). This included RBPs containing the zf-C2H2 domain, a known DNA-binding domain that has recently also been identified as a RNA binding domain (49, 50). 52.8% of the RBPs contained non-canonical RNA-binding domains (1574 RBPs; **Figure 1E**), which were by and large present in experimentally identified RBPs (**Supplementary Figure 1D**). These included ribosomal proteins (*RPL18* and *RPL5*), the RNA processing molecule *DUSP11*, RNA splicing-related RBPs (*AHNAK*, *PCF11*, *SNIP1*, *SCAF11, SNRNP40*) and the exoribonuclease *EXOSC3*. A similar distribution of the top 20 RBDs was present in RBPs detected in HeLa-S3 and K562 cells (**Supplementary Figure 1E**), indicating that the RBD distribution is not a specific feature of lymphocytes.

RBPs regulate many processes, which includes RNA splicing, stability, subcellular localization of RNA, RNA modification, and translation (51). Using protein annotations from the human protein atlas database (52), we found that 1178 RBPs (41.7%) were annotated as regulators of at least one of these five RNA-related processes (**Figure 1F**, left panel), of which 24% were

annotated for multiple RNA-related processes (**Figure 1F**, right panel). Combined, these data show that human lymphocytes express a wide variety of RBPs with a diverse set of RBDs.

Human B Cells and T Cells Have a Distinct RBP Signature

To determine whether and how RBP expression differed between B cells and T cells, we analyzed $CD19^+$ B cells, $CD4^+$ T cells, and $CD8^+$ T cells separately in the RNA-seq and MS datasets employed in **Figure 1**. Overall, 2923 RBPs (97.0%) and 2551 RBPs (97.5%) were detected in all three subsets at the RNA and protein level, respectively (**Supplementary Figures 2A, B** and **Supplementary Table 2**). Only a few RBPs were detected in one specific cell type (**Supplementary Figures 2A, B**). B cells exclusively expressed members of the ribonuclease A superfamily (*RNASE1, RNASE2 and RNASE3*) and the RBP *DAZL*. The RBPs *RBM24* and *PABPC3* were only detected in $CD4^+$ T cells, and *NCBPL2* and *A1CF* were specifically expressed in $CD8^+$ T cells (**Supplementary Table 2**). At the protein level, 6 RBPs were specifically detected in $CD19^+$ B cells, which included the ribonuclease *RNASE7*. The RBPs *CPEB2*, *PAIB2B* and *TRMT44* were exclusively detected in $CD4^+$ T cells, and the RBPs *AICDA* and *HENMT1* were specifically detected in $CD8^+$ T cells (**Supplementary Table 2**).

For the majority of RBPs detected in $CD19^+$ B cells (85.1%, 2550 RBPs), $CD4^+$ T cells (86.0%, 2571 RBPs) and $CD8^+$ T cells (85.6%, 2560 RBPs) transcript and protein expression was co-detected (**Supplementary Figure 2C**). Only 425 RBPs, 386 RBPs and 400 RBPs, were only detected at the RNA level, and 22 RBPs, 31 RBPs and 32 RBPs at the protein level in $CD19^+$ B cells, $CD4^+$ T cells and $CD8^+$ T cells, respectively (**Supplementary Figure 2C** and **Supplementary Table 2**). In line with the substantial overlap of RBPs co-detected at RNA and protein level, the correlation between the RNA and protein abundance for RBPs was high in $CD19^+$ B cells (Pearson's coefficient: 0.60), $CD4^+$ T cells (Pearson's coefficient: 0.60) and $CD8^+$ T cells (0.61) compared to non-RBP genes (Pearson's coefficients: 0.42-0.44, **Supplementary Figure 2D**).

We next questioned whether the global RBP expression differed between the three lymphocyte subsets. Principal Component Analysis (PCA) revealed that the RBP mRNA and protein expression alone separates B cells from T cells just as effectively as a PCA performed on all genes (**Figure 2A** and **Supplementary Figure 2E**). Differential expression (DE) analysis on all genes and protein, followed by filtering for RBPs, revealed clear differences between B cells and T cells. 695 and 644 DE RBPs (82.3% and 76.3% of the total DE RBPs) were found DE at the mRNA level between $CD19^+$ B cells and $CD4^+$ T cells, or $CD8^+$ T cells, respectively (**Figure 2B** and **Supplementary Table 2**; LFC > 0.5; p-adjusted<0.01). $CD4^+$ T cells and $CD8^+$ T cells were more closely related, with only 68 DE RBPs (8.1% of all DE RBPs, **Figure 2B** and **Supplementary Table 2**). Of note, to prevent a bias towards DE genes with relatively low transcript abundance we utilized the lfcShrink function, which shrinks log2 fold change (LFC) values of genes with low counts [(53), *see Methods*]. RBP protein expression showed similar trends, with 40 and 24 DE RBPs between $CD19^+$ B cells and $CD4^+$ T cells or $CD8^+$ T cells, respectively, and only 6 DE RBPs between $CD4^+$ T cells and $CD8^+$ T cells (**Supplementary Figure 2F** and **Supplementary Table 2**; LFC > 0.5; p-adjusted<0.05). 84.4% of the DE RBPs at protein level were also DE RBPs at RNA level (**Supplementary Figure 2G**). Indeed, unsupervised clustering of the DE RBPs clearly distinguished B cell- from T cell-associated RBP clusters (**Figures 2C, D**).

To investigate the functional annotation of the DE RBPs, we focused on RBPs that were significantly higher expressed by either B cell or T cell populations (**Figure 2E**). We studied RBPs that are annotated regulators of RNA splicing, stability, subcellular localization of RNA, RNA modification, and translation, as defined by protein annotation from the human protein atlas database. Of note, although we focus on individual RNA processes, every known RNA-related function of each individual RBP was included in this analysis. We examined 107 (32.5%) of the B cell-associated RBPs and 49 (28.0%) of the T cell-associated RBPs (**Figure 2F**, left panel). The majority of these RBPs (B cell RBPs: 82.2%, T cell RBPs: 83.7%) were annotated for one function, and 17.8% and 16.3% for multiple functions for B cells and T cells, respectively (**Figure 2F**, middle panel). Interestingly, the relative distribution of RBPs annotated for these five RNA processes differed between B cells and T cells. Whereas 52.3% of RBPs in B cells were annotated for translation, this was only the case for 30.6% in T cells (**Figure 2F**, right panel). Conversely, only 17.8% was annotated for RNA splicing in B cells, but reached 30.6% in T cells (**Figure 2F**, right panel). In conclusion, the overt differential RBP expression between human B cells and T cells shown here possibly reflects a distinct distribution between different classes of RBPs.

RBP Expression Changes Upon B Cell Differentiation

Several B cell subsets can be found in the peripheral blood including naive B cells, memory B cells and plasmablasts (**Figure 3A**). Whereas plasmablasts produce vast quantities of antibodies and are short-lived, memory B cells are long-lived and for the most part quiescent (54). We found that the phenotypical differences between these three B cell subsets is echoed in their RBP expression profile. We identified 1308 DE RBPs at RNA level, and 96 DE RBPs at protein level between naive B cells, memory B cells and plasmablasts (**Supplementary Figures 3A, B** and **Supplementary Table 3**). 69.1% of the DE RBPs at protein level are detected also at the RNA level (**Supplementary Figure 3C**). In particular, although only 151 DE RBPs were found between naive and memory B cells, plasmablasts showed a distinct RBP profile, with 1185 and 891 DE RBPs between naive or memory B cells and plasmablasts, respectively (**Supplementary Figure 3A** and **Supplementary Table 3**). The top 20 DE RBPs at both the RNA and protein level spanned a wide range of abundance, and included *RRM2*, *APOBEC3B*, *METTL5* and *LGALS3* (**Figures 3B, C** and **Supplementary Table 3**). Hierarchical clustering of DE RBPs at RNA level revealed three clusters between B cell subsets (**Figure 3D** and

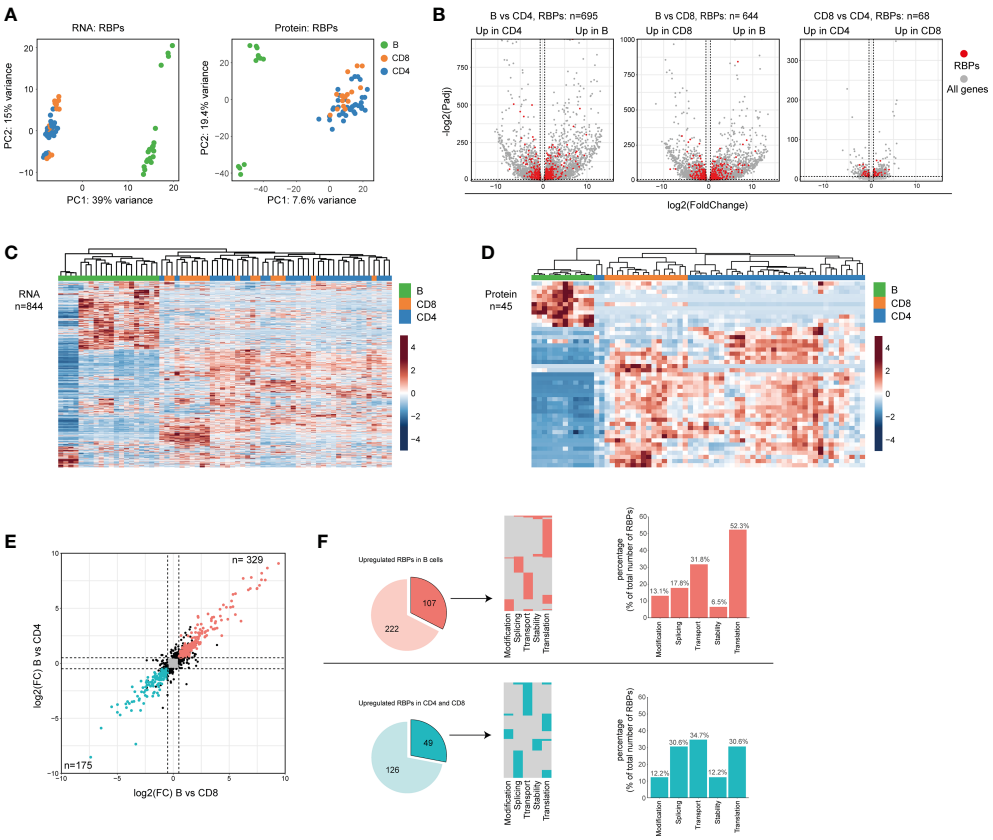

FIGURE 2 | Differential RBP expression between human B cells and T cells. **(A)** Principal component analysis (PCA) of RBP RNA (left panel) and protein (right panel) expression in CD19$^+$ B cells, CD4$^+$ T cells and CD8$^+$ T cells (n=4 donors). Each dot depicts one specific B cell or T cell subset from each donor. **(B)** Volcano plots of all differentially expressed genes (gray) and of differentially expressed RBPs (DE RBPs) (red) between CD19$^+$ B cells, CD4$^+$ T cells and CD8$^+$ T cells (LFC>0.5, P-adjusted<0.01). **(C, D)** Heatmap of unsupervised clustering of DE RBPs at RNA **(C)** or at protein level **(D)** in CD19$^+$ B cells, CD4$^+$ T cells and CD8$^+$ T cells. Each column corresponds to one T/B cell differentiation subset of a donor (n=4 donors). **(E)** Log2 Fold Change (LFC) of RBP mRNA expression between CD19$^+$ B cells and CD4$^+$ T cells (y-axis) and between CD19$^+$ B cells and CD8$^+$ T cells (x-axis). Red dots depict RBPs that are significantly upregulated in B cells, and blue dots indicate RBPs significantly upregulated in CD4$^+$ T cells and CD8$^+$ (significant in both comparisons, LFC>0.5, P-adjusted<0.01). **(F)** Left panels: RBPs annotated for RNA splicing, stability, subcellular localization of RNA, RNA modification, and translation (dark colors) or for other processes (light colors) that are upregulated in CD19$^+$ B cells (top row) or T cells (bottom row) as defined in **(E)** Middle panels: relative distribution between the 5 specific RBP classes. Right panels: Percentage of RBPs annotated for the indicated RNA-related biological processes.

Supplementary Table 3). 188 RBPs were highly expressed in plasmablasts (cluster 1), 541 RBPs were highly expressed in memory B cells (cluster 2) and cluster 3 with 579 RBPs were highly expressed in naive and memory B cells, respectively (cluster 3). Hierarchical clustering on protein levels revealed similar differential RBP expression patterns (**Figure 3E**). Within these three clusters of DE RBPs at the RNA level, we isolated RBPs annotated for RNA splicing, stability, subcellular localization of RNA, RNA modification, and translation. This included 67 (35.6%) RBPs in cluster 1, 204 (44.4%) RBPs in cluster 2, and 214 (37%) RBPs in cluster 3 (**Figure 3F**, left panel). Again, 75-78% of the RBPs was annotated for one function (**Figure 3F**, middle panel), and the prime annotation of RBPs was translation in all three clusters (**Figure 3F**, right panel). Interestingly, whereas RBPs annotated for RNA splicing were also abundant in naive and memory B cell subsets with 31.3% and 40.2%, respectively, plasmablasts (cluster 1) contained only 6.0% RBPs annotated for RNA splicing (**Figure 3F**, right panel). Instead, 44,8% of RBPs expressed in plasmablasts annotated for RNA transport (**Figure 3F**, right panel). STRING-analysis on splicing-related RBPS from cluster 3 (naive-memory B cells) revealed networks consisting of known splicing factors, such as the SR protein family members *SRSF1*, *SRSF4*, *SRSF3*, *SRSF6*, in addition to *NUDT21* and *HNRNPLL* (**Figure 3G**). For transport-annotated RBPs from cluster 1 (plasmablast), the interaction networks included the RBP *SLBP*, which regulates mRNA export (55), and the RBP *TST*, which regulates the transport of ribosomal RNA [**Figure 3H** (56)].

Gene Ontology (GO) analysis on the DE RBPs identified in cluster 2 and 3 showed a shared enrichment of GO-terms associated with various RNA-related processes, including RNA splicing, translation and RNA processing, while cluster 1 showed an enrichment of the GO-term associated with translation (**Supplementary Figure 3D** and **Supplementary Table 7**).

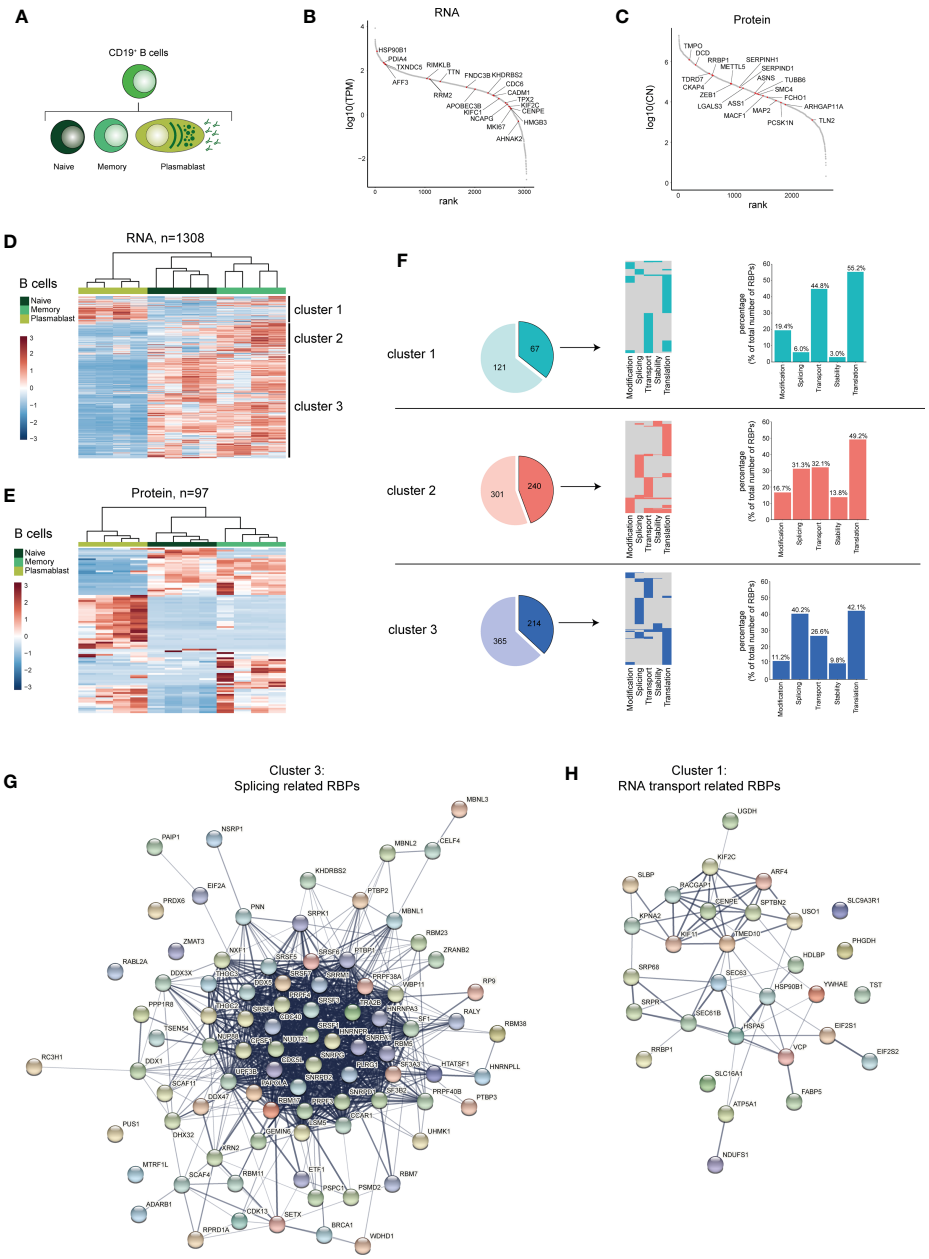

FIGURE 3 | RBP expression alters upon B cell differentiation. **(A)** Diagram depicting the analysed CD19$^+$ B cell subsets. **(B, C)** Expression levels of RBPs detected in B cells at RNA level **(B)** and at protein level **(C)**, ranked according to expression levels. Red dots indicate the top 20 most differentially expressed RBPs, ranked on Log2 Fold Change). **(D, E)** Heatmap of unsupervised clustering of DE RBPs at mRNA **(D)** and at protein level **(E)** between naive CD19$^+$ B cells, memory CD19$^+$ B cells and plasmablasts. n=4 donors. **(F)** Left panels: RBPs annotated for RNA splicing, stability, subcellular localization of RNA, RNA modification, and translation (dark colors) or for other processes (light colors) in the three clusters defined in **(D)**. Middle panels: relative distribution between the 5 specific RBP classes. Right panels: Percentage of RBPs annotated for the indicated RNA-related biological processes. **(G, H)** String analysis on splicing-related RBPs **(G)** identified in cluster 3 and on RNA transport-associated RBPs **(H)** identified in cluster 1. TPM, Transcripts per kilobase per million; CN, Protein copy number.

Cluster 3 displayed a moderate enrichment for GO-terms related to RNA stability (3'-UTR-mediated mRNA, mRNA destabilization) and regulation of RNA splicing (mRNA splice site selection, positive regulation of RNA splicing, negative regulation of RNA splicing; **Supplementary Figure 3D** and **Supplementary Table 7**). In conclusion, the RBP expression differs between B cell subsets, and involves different types of post-transcriptional regulatory functions.

RBP Expression Changes Upon CD4$^+$ T Cell Differentiation

Naive T cells (Tnaive) undergo differentiation into effector T cells, which are rarely found in the peripheral blood of healthy donors (57). Rather, central memory (Tcm) and effector memory (Tem) CD4$^+$ T cell subsets, which develop during the course of infections, are present in the blood and differentially contribute to recall responses upon recurring infections [**Figure 4A** (58)]. Similar to B cells, we find RBPs differentially expressed in the CD4$^+$ T cell subsets Tnaive, Tcm and Tem at RNA (n=774), and

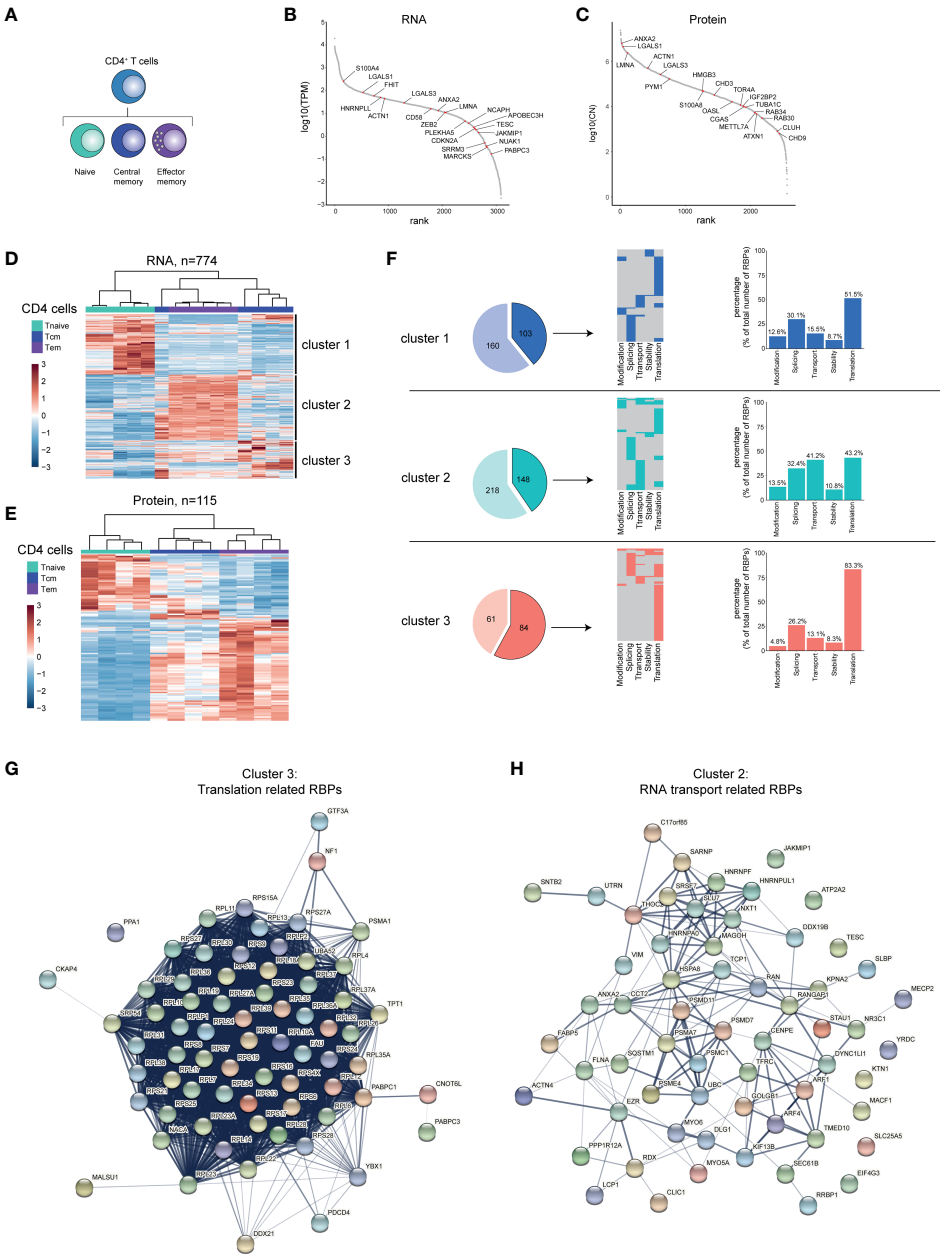

FIGURE 4 | RBP expression alters upon CD4$^+$ T cell differentiation. **(A)** Diagram depicting the analysed CD4$^+$ T cell subsets. **(B, C)** Expression levels of RBPs detected at RNA **(B)** or protein level **(C)** in human CD4$^+$ T cells ranked according to expression levels. Red dots indicate top 20 most differentially expressed RBPs based on Log2 Fold Change. **(D, E)** Unsupervised clustering of DE RBPs at RNA **(D)** or at protein level **(E)** between naive (Tnaive), central memory (Tcm) and effector memory (Tem) CD4$^+$ T cells depicted in a heatmap. RNA: n=5 donors, protein: n=4 donors. **(F)** Left panels: RBPs annotated for RNA splicing, stability, subcellular localization of RNA, RNA modification, and translation (dark colors) or for other processes (light colors) in the three clusters defined in **(D)**. Middle panels: relative distribution between the 5 indicated RBP classes. Right panels: Percentage of RBPs annotated for indicated RNA-related biological processes. **(G, H)** String analysis on translation-related RBPs **(G)** identified in cluster 3 and on RNA transport-associated RBPs **(H)** identified in cluster 2. TPM, Transcripts per kilobase per million; CN, Protein copy number.

at protein level (n=115; **Supplementary Figures 4A, B** and **Supplementary Table 4**). 48% of the DE RBPs at protein level are detected also at the RNA level (**Supplementary Figure 4C**). The top 20 DE RBPs included RBPs such as, *APOBEC3H* and *PAPBC3* (RNA level) and *OASL* and *ANXA2* (protein level, **Figures 4B, C** and **Supplementary Table 4**).

Hierarchical clustering of the DE RBPs revealed three clusters (**Figures 4D, E**), with cluster 1 (Tnaive) containing 145 RBPs, cluster 2 (Tem) containing 366 RBPs, and cluster 3 (Tcm) containing 263 RBPs (**Supplementary Table 4**). This differential expression of RBPs was also apparent at the protein level (**Figure 4E**, 115 DE RBPs, **Supplementary Table 4**). To gain more insights into the biological processes of the RBPs in the different clusters, we performed Gene Ontology (GO) analysis (**Supplementary Table 7**). Whereas metabolic processes were enriched in all three clusters, cluster 2 and 3 were enriched for GO-terms associated with translation (translation initiation, cytoplasmic translation) and with RNA transport (**Supplementary Figure 4D** and **Supplementary Table 7**). Cluster 2 also showed a moderate enrichment for RBPs associated with regulation of RNA stability (RNA destabilization, 3'-UTR-mediated mRNA destabilization; **Supplementary Figure 4D** and **Supplementary Table 7**).

When we specifically isolated RBPs annotated for RNA splicing, stability, subcellular localization of RNA, RNA modification, and translation, we found that 103 (39.2%) RBPs of the DE RBPs belong to these 5 RBP classes in cluster 1, 148 RBPs in cluster 2 (40.4%) and 84 RBPs in cluster 3 (57.9%) (**Figure 4F**, left panels). Only a fraction of RBPs is associated with more than one of these functions (cluster 1: 17.5%, cluster 2: 26.4%, cluster 3: 25%; **Figure 4F**, middle panel). When $CD4^+$ T cells differentiate, the relative distribution of functional RBP annotation alters. 83.3% of the RBPs associated with the 5 RBP classes were linked to translation in cluster 3 (Tcm), compared to 51.5% and 43.2% in cluster 1 (Tnaive) and cluster 2 (Tem), respectively (**Figure 4F**, right panels). Conversely, in cluster 2 (Tem), the percentage of RBPs annotated for RNA transport are with 41.2% primarily found in cluster 2 and much less so in cluster 2 and 3 with 15.5% and 13.1%, respectively (**Figure 4F**, right panels). STRING-analysis on the translation-related RBPs of cluster 3 revealed an enrichment of 53 ribosomal proteins and of other translation-associated RBPs, such as *PABPC1*, *YBX1* and *FAU* (**Figure 4G**). The RNA-transport-related RBPs of cluster 2 included the mRNA export-associated RBPs *DDX19B*, *SARNP*, *MAGOH* and *THOC2* (**Figure 4H**). Combined, our findings reveal that the RBP expression landscape changes throughout $CD4^+$ T cell differentiation, which results in a relative enrichment of specific RBP classes in different $CD4^+$ T cell subsets.

RBP Expression Changes Upon $CD8^+$ T Cell Differentiation

We then focused on the $CD8^+$ T cell differentiation subsets. Our dataset also included effector $CD8^+$ T cells (Teff), which was included in the analysis, in addition to Tnaive, Tcm and Tem $CD8^+$ T cell subsets (**Figure 5A**). 707 RBPs were differentially expressed at the RNA level between Tnaive, Tcm and Tem and Teff, and 115 RBPs at the protein level (**Supplementary Figures 5A, B** and **Supplementary Table 5**). 44.1% of DE RBPs at protein level were also detected at the RNA level (**Supplementary Figure 5C**). The top 20 DE RBPs included RBPs like *JAKMIP1* and *OASL* (RNA level) and EIF4EBP3 and FLNB (protein level, **Figures 5B, C** and **Supplementary Table 5**). Hierarchical clustering of RBP expression resulted 3 clusters (**Figure 5D**). Cluster 1 contained 297 RBPs highly expressed in Tem and Teff $CD8^+$ T cells (**Figure 5B** and **Supplementary Table 5**). Cluster 2 (176 RBPs) also included Tem an Teff $CD8^+$ cells, and to a lesser extent in Tcm cells. Cluster 3 (234 RBPs) included primarily Tnaive cells, but also Tcm cells (**Figure 5B** and **Supplementary Table 5**). Similar clusters were identified at RBP protein level (**Figure 5E**, 177 DE RBPs, **Supplementary Table 5**).

In $CD8^+$ T cell subsets, 67 RBPs in cluster 1 (38.1%), 84 RBPs in cluster 2 (35.9%), and 143 RBPs in cluster 3 (48.1%) were annotated as regulators of RNA splicing, stability, subcellular localization of RNA, RNA modification, or translation (**Figure 5F**, left panels), with a minority of RBPs (20-28%) linked to multiple functions (**Figure 5F**, middle panels). We found that cluster 3 was relatively enriched for translation-associated RBPs (71.3%), compared to cluster 1 and cluster 2 with 34.5% and 44.8%, respectively (**Figure 5F**, right panels). Conversely, cluster 1 and 2 were enriched for RBPs associated with RNA transport (cluster 1: 43.3%, cluster 2: 46.4%), and this RBP class was 12.6% only minor in cluster 3 (**Figure 5F**, right panels). STRING-analysis on translation-associated RBPs from cluster 3 revealed the interaction network between 56 ribosomal proteins and 10 eukaryotic translation initiation factors (**Figure 5G**). The RNA-transport associated RBPs in cluster 2 and 3 included RBPs involved in RNA export (*THOC5* (59) and *SARNP* (60), **Figure 5H**).

Gene Ontology (GO) analysis on the DE RBPs also showed in cluster 3 - in addition to catabolic processes - an enrichment of GO-terms associated with translation, i.e. cytoplasmic translation, translation initiation and positive regulation of translation (**Supplementary Figure 5D** and **Supplementary Table 7**). Cluster 1 displayed a moderate enrichment for GO-terms related to RNA stability (3'-UTR-mediated mRNA destabilization, regulation of mRNA stability, **Supplementary Figure 5D** and **Supplementary Table 7**). In conclusion, $CD8^+$ T cells change their RBP expression landscape throughout differentiation, with specific RBP classes enriched in different $CD8^+$ T cell subsets.

Specific RBP Expression Associates With T Cell Cytotoxicity

T cells can acquire cytotoxic function when they differentiate into effector cells. Importantly, whereas $CD8^+$ T cells are generally classified as cytotoxic, not all $CD8^+$ T cells display cytotoxic features (61–63). Conversely, a subset of human $CD4^+$ T cells also shows cytolytic features (64–66). We therefore sought to identify RBPs that were associated with a high cytotoxic capacity in human $CD8^+$ T cells and $CD4^+$ T cells. As source of T cells, we used previously published single-cell RNA-seq (scRNA-seq) data on blood-derived human $CD8^+$ and $CD4^+$ T cells (67–69).

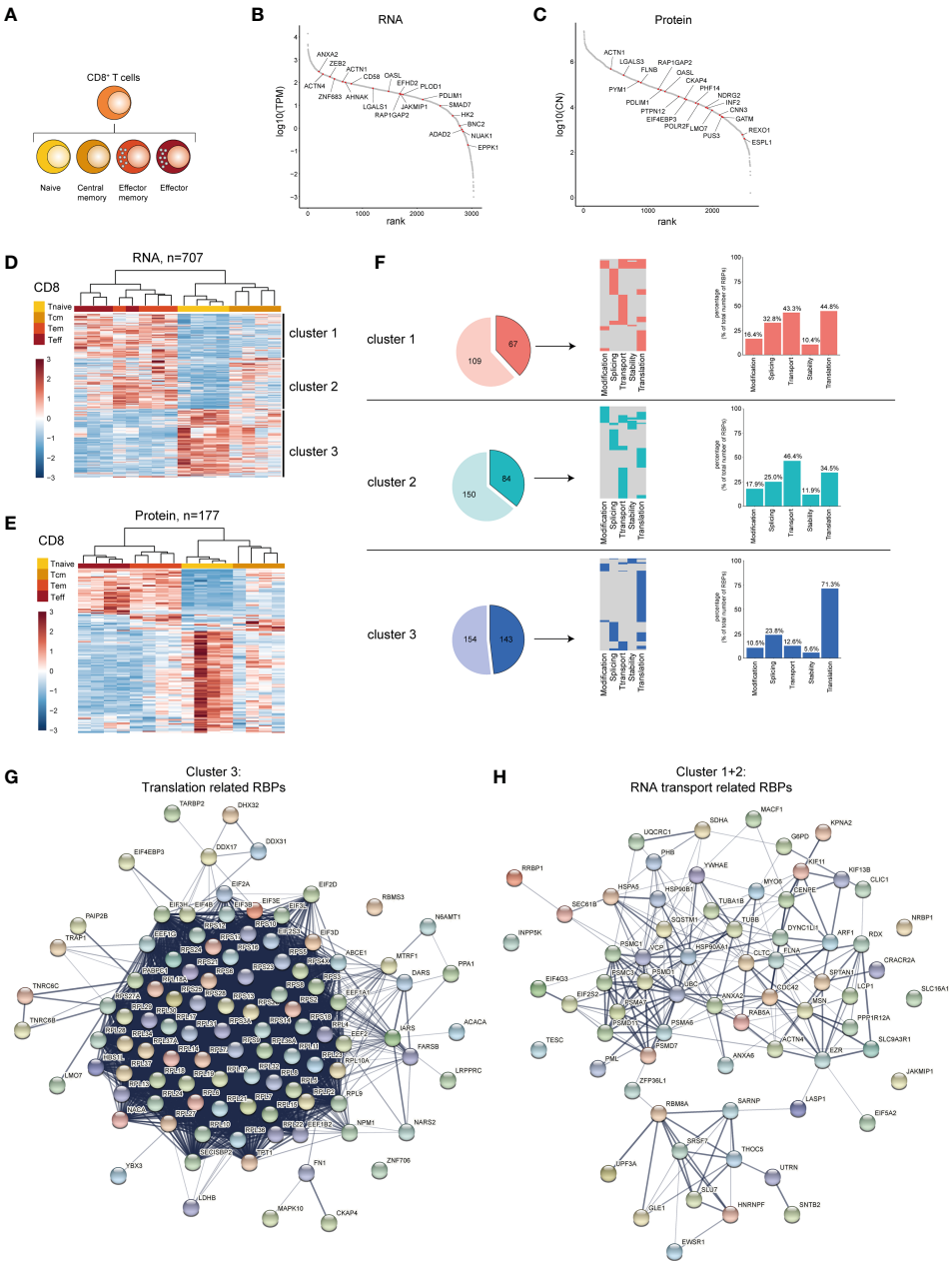

FIGURE 5 | RBP expression alters upon CD8$^+$ T cell differentiation. **(A)** Diagram depicting the analysed CD8$^+$ T cell subsets. **(B, C)** Expression levels of RBPs detected at RNA **(B)** and at protein level **(C)** in human CD8$^+$ T cells ranked according to expression levels. Red dots indicate top 20 most differentially expressed RBPs based on Log2 Fold Change. **(D, E)** Unsupervised clustering of DE RBPs at RNA **(D)** or protein level **(E)** between naive (Tnaive), central memory (Tcm), effector memory (Tem) and effector (Teff) CD8$^+$ T cells depicted in a heatmap. n=4 donors. **(F)** Left panels: RBPs annotated for RNA splicing, stability, subcellular localization of RNA, RNA modification, and translation (dark colors) or for other processes (light colors) in the three clusters defined in **(D)**. Middle panels: relative distribution between the 5 indicated RBP classes. Right panels: Percentage of RBPs annotated for indicated RNA-related biological processes. **(G, H)** String analysis on translation-related RBPs **(G)** identified in cluster 3 and on RNA transport-associated RBPs **(H)** identified in clusters 2 and 3. TPM, Transcripts per kilobase per million; CN, Protein copy number.

Because only memory and effector T cells can be cytotoxic, we excluded naive T cells from our analysis based on their high gene expression of *CCR7*, *LEF1* and *SELL* (**Supplementary Figures 6A–D**). We then identified and integrated the expression of 8 cytotoxic genes (9) i.e. *FGFBP2*, *GZMB*, *GZMH*, *PRF1*, *NKG7*, *CX3CR1*, *GNLY* and *ADGRG1* into a *cytotoxic score* (*see Methods*; **Figure 6A** and **Supplementary Figures 6E, F**). Dimensional reduction analysis revealed that CD8$^+$ and CD4$^+$ T cells with a low (bottom 10%) or high cytotoxic score (top 10%) form two distinct clusters

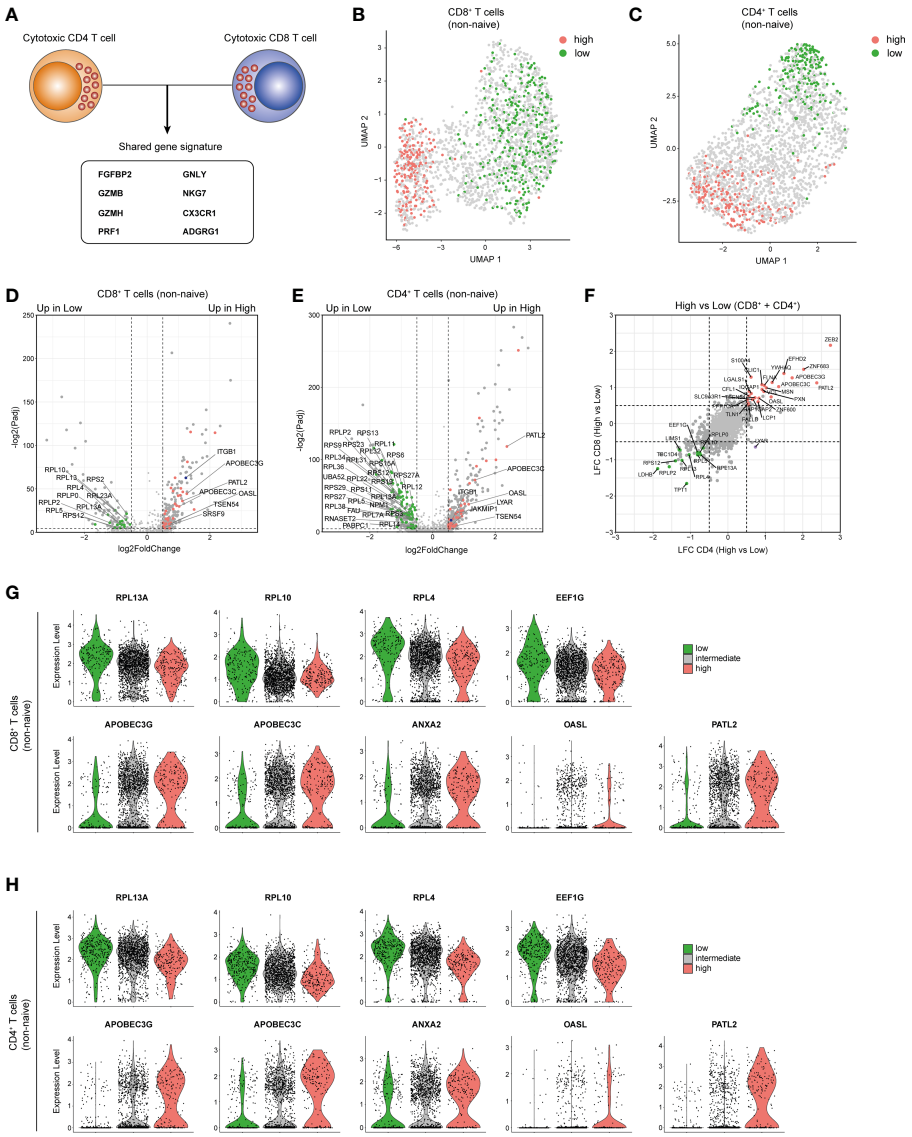

FIGURE 6 | Cytotoxic CD4$^+$ and CD8$^+$ T cells share an RBP expression profile. **(A)** Diagram indicating the cytotoxic gene signature shared by CD4$^+$ T cells and CD8$^+$ T cells as defined in **Supplementary Figures 6E, F**. **(B, C)** Uniform Manifold Approximation and Projection (UMAP) plot on non-naive CD8$^+$ T cells **(B)** and CD4$^+$ T cells **(C)** with a high (top 10%, red) or low (bottom 10%, green) cytotoxic score. **(D, E)** Volcano plot d DE RBPs (red) and other genes (gray) between non-naive CD8$^+$ T cells **(D)** and CD4$^+$ T cells **(E)**. Blue dot depicts *ITGB1*. **(F)** Log2 Fold Change values for RBPs with a high or low cytotoxic score of non-naive CD4$^+$ T cells (y-axis) and non-naive CD8$^+$ T cells (x-axis). Red and green dots indicate DE RBPs associated with a high and low cytotoxic score in both T cell types (LFC>0.5 P-adjusted<0.05). **(G, H)** Violin plots depicting expression levels and expression density of selected RBPs in CD8$^+$ T cells **(G)** or CD4$^+$ T cells **(H)** with a high (top 10%), intermediate (10-90%) or low (bottom 10%) cytotoxic score.

(**Figures 6B, C**). High expression of *ITGB1* in CD8$^+$ and CD4$^+$ T cells with a high cytotoxic score confirmed the selection for cytotoxic T cells [(61, 64), **Figures 6D, E**]. In addition, 16 RBPs were significantly upregulated in CD8$^+$ T cells with a low cytotoxic score, whereas 36 RBPs were preferentially expressed in CD8$^+$ T cells with a high cytotoxic score (**Figure 6D** and **Supplementary Table 6**; LFC>0.5; P-adjusted<0.01). Likewise, 87 RBPs and 41 RBPs were upregulated in CD4$^+$ T cells with a low and with a high cytotoxic score, respectively (**Figure 6E** and **Supplementary Table 6**).

Intriguingly, the differential RBP expression between CD8$^+$ and CD4$^+$ T cells with a low or high cytotoxic score was strikingly similar (**Figure 6F**). 13 RBPs were upregulated in CD8$^+$ and CD4$^+$ T cells with a low cytotoxic score (**Figure 6F**), which included 8 ribosomal proteins, e.g. *RPL13A*, *RPL10* and *RPL4* which are accessory to the translation regulation (70), and the translation initiation factor *EEF1G* (**Figures 6G, H**). 25 RBPs that were upregulated in both CD8$^+$ and CD4$^+$ T cells with a high cytotoxic score (**Figure 6F**) included cytidine deaminases APOBEC3G and APOBEC3C,

the poly(G) binding protein ANXA2 (71), the viral dsRNA binder OASL (72) and the translational repressor PATL2 [**Figures 6G, H** (73)]. In summary, $CD8^+$ and $CD4^+$ T cells with a high cytotoxic potential express a specific set of RBPs.

DISCUSSION

In this report, we catalogued the transcript and protein expression of putative RBPs in human B cells and T cells. We found that the overall expression pattern of RBPs is remarkably well conserved between lymphocytes and HeLa-S3 and K562 cells (>90% overlap), and >97% of the RBPs were co-detected in B cells, $CD4^+$ and $CD8^+$ T cells. Nonetheless, differential expression analysis of RBPs clearly distinguishes B cells from T cells. RBP expression also alters during differentiation. This finding suggests - similar to what is observed for transcription factors (15, 16) - that the relative abundance of RBPs defines the fate of RNA and of translation into proteins, and thus the differentiation status of lymphocyte subsets.

Intriguingly, the differential expression of RBPs upon lymphocyte differentiation resulted in a shift of functional annotations of the expressed RBPs. For instance, plasmablasts are enriched for RBPs annotated for RNA transport, a feature that may support their antibody producing function. Effector and effector memory type $CD4^+$ and $CD8^+$ T cells also showed a preference of RBPs annotated for RNA transport, albeit to a lesser extent. Conversely, central memory $CD4^+$ T cells, and naive and central memory $CD8^+$ T cells preferentially express RBPs that are annotated for translation regulation. Even though this finding may be counter-intuitive, it is important to note that quiescent naive or memory T cells continuously receive signals that drive their survival and their state of alertness for activation (74). Indeed, recent studies indicated a tight gene-specific regulation of translation in naive T cells (75–78), and the concept of translational preparedness of naive and memory T cells (75). It is therefore tempting to speculate that the enrichment for RBPs involved in translation regulation we find here contributes to the translation control in naive and memory T cells. Tem cells were also enriched for RBPs involved in RNA stability. This finding correlates with our previous observations that RNA stability is a key driver in defining the magnitude and duration of cytokine production in T cells and that the strength and type of signal a T cell receives defines the level of RNA stability (79–81). We therefore hypothesize that RBPs defining RNA stability are critical to modulate the T cell effector function and are therefore enriched in Tem cells.

Although significant differences in RBP mRNA expression were observed upon lymphocyte differentiation, these differences were not reflected to the same extent at the protein level. This discrepancy can be partially attributed to post-transcriptional regulation of RBPs as previously described (82). Secondly, quantitative proteomics analysis is less sensitive and may thus have a decreased ability to detect low abundance proteins (83). More in depth studies of specific DE RBPs will thus be required to determine whether the difference in RNA abundance is also echoed at the protein level.

Also, cytotoxic T cells display a unique RBP expression profile. Compared to non-cytotoxic T cells, cytotoxic T cells express lower mRNA levels of several ribosomal proteins. Whether the differences at the mRNA level for ribosomal proteins is also reflected at the protein level is still unknown. In addition, whether some of these ribosomal proteins display any transcript specificity, as was shown for RPL10A and RPS25 (70), remains to be defined. Interestingly, a T-cell specific loss of Rps26 did not affect overall translation rates, but rather increased p53 signalling, and thus resulted in cell death (84). A significant increase of p53 expression was also observed in HeLa cells upon knock down of 24 out of 80 ribosomal proteins and has been attributed to the accumulation of free ribosomal proteins in the nucleus (85, 86). This decreased viability will thus impede the study of at least a subset of ribosomal proteins in T cells.

Cytotoxic T cells also exhibited an increased expression of the mRNA cytidine deaminases APOBEC3C and APOBEC3G. Previous studies reported that APOBEC expression increases upon T cell activation (87), which was primarily associated with viral restriction (88). It is also conceivable that increased APOBEC expression is involved in regulating the fate of endogenous mRNAs in cytotoxic T cells. Interestingly, the specific RBP profile linked to cytotoxicity is shared by $CD4^+$ T cells and $CD8^+$ T cells, a feature which may point to a similar differentiation program towards cytotoxicity.

RNA-binding proteins are critical mediators in shaping lymphocyte differentiation and effector function (24–28, 30–33). The RBP expression catalogue we provide here should help to further dissect the role of RBPs in B cell and T cell differentiation and function. It is important to note that this RBP catalogue primarily serves as a resource, and thus as a starting point for uncovering the RBP-mediated regulation in lymphocyte differentiation. Indeed, whether alterations in the RBP signature during lymphocyte differentiation are the cause or consequence of differentiation is yet to be determined. Furthermore, RBP expression by itself cannot be interpreted as direct interaction of RBPs with RNA. In fact, RNA interactome capture in cell-cycle arrested U2OS cells revealed that increases in protein abundance of some RBPs did not result in increased RNA binding (89). In addition, the regulation of RBPs is highly context-dependent and is most likely variable between cell types (90). The recent development of novel RNA interactome capture methodologies will be instrumental in identifying the RBPs that truly interact with RNA in human lymphocytes (89, 91, 92).

RBP interactions with RNAs can be highly versatile and are subject to rapid changes upon extrinsic signals. For instance, the RBP ZFP36L2 is expressed to a similar extent in memory T cells and re-activated T cells, yet only blocks translation in resting memory T cells (33). Similarly, a large fraction of ribosomal proteins does not interact with ribosomal RNA. The mode of action of these non-ribosomal RNA binding ribosomal proteins (RPs) is to date enigmatic and requires further investigation. Lastly, in addition to classical RBPs, recent studies have revealed the presence of enigmatic RBPs, which are primarily annotated

for other cellular, non-RNA binding related functions. This is exemplified by metabolic enzymes from the tricarboxylic acid (TCA) cycle (93–95). Their relative contribution to RNA regulation during lymphocyte differentiation and effector function is yet to be experimentally confirmed. Nonetheless, the role of RBPs in genetic diseases is becoming appreciated (96), and defining the RBP expression presented in the study presented here may contribute to deciphering dysregulated RBP expression and function also in immune-related diseases.

MATERIAL AND METHODS

Data Sets

Raw RNA-sequencing (RNA-seq) data were retrieved from the gene expression omnibus repository (GEO, NCBI) or from the European Nucleotide Archive (ENA). Data from $CD19^+$ B cells and from B cell differentiation subsets (n=4 donors with 4 B cell populations each), from $CD4^+$ T cells (n=3-4 donors with 7-8 $CD4^+$ T cell populations each) and $CD8^+$ T cells and respective differentiation subsets (n=4 donors with 4 $CD8^+$ T cell populations each) were retrieved from Monaco et al. [(38); accession number: GSE107011)]. RNA-sequencing libraries from Monaco et al. (38) were composed of poly(A) enriched RNA. RNA seq data of $CD4^+$ T cell subsets (n=5 donors with 3 $CD4^+$ T cell populations each) were retrieved from Ranzani et al. [(97); PRJEB5468]. RNA-sequencing libraries from Ranzani et al. (97) consisted of poly(A) enriched RNA. RNA-seq data of HeLa-S3 cells and K562 cells were obtained from Martinez et al. [(39); GSE125218] and were comprised of RNA-sequencing libraries composed of poly(A) enriched RNA. Quantitative mass spectrometry (MS) data, consisting of imputed label-free quantification (LFQ) and protein copy numbers (CN), were retrieved from Rieckmann et al. (40) and encompassed $CD19^+$ B cells, $CD4^+$ and $CD8^+$ T cells and their respective differentiation subsets (n=4 donors). Data sets were selected based on using near identical markers for selecting lymphocyte subsets: Lymphocyte subsets in the RNA-seq and MS data sets were prepared as follows: $CD19^+$ B cells: naive (RNA-seq: $CD27^-$ IgD^+, MS: $CD27^-$ $Mitotracker^-$), memory (RNA-seq: $CD27^+$ $CD38^-$ IgD^-, MS: $CD27^+$ $CD38^-$ $Mitotracker^-$) and plasmablasts (RNA-seq: $CD27^+$ $CD38^+$ IgD^-, MS: $CD27^+$ $CD38^+$ $Mitotracker^-$); $CD4^+$ T cells: naive (RNA-seq: $CCR7^+$ $CD45RA^+$ $CD45RO^-$, MS: $CCR7^+$ $CD45RA^+$), memory (RNA-seq: $CCR7^+$ $CD45RA^-$ $CD45RO^+$, MS: $CCR7^+$ $CD45RA^-$), and effector memory (RNA-seq: $CCR7^-$ $CD45RA^-$ $CD45RO^+$, MS: $CCR7^+$ $CD45RA^-$); $CD8^+$ T cells: naive ($CCR7^+$ $CD45RA^+$), memory ($CCR7^+$ $CD45RA^-$), effector memory ($CCR7^-$ $CD45RA^-$) and effector $CD8^+$ T cells ($CCR7^-$ $CD45RA^+$).

Single-cell RNA-sequencing (scRNA-seq) data of blood-derived $CD4^+$ and $CD8^+$ T cells were retrieved from the GEO repository: Zheng et al. (69); GSE98638, Guo et al. (67); GSE99254, Zhang et al. (68); GSE108989.

RBP Reference List

The list of annotated human RNA-binding proteins (RBPs) was created by aggregating published data of RNA interaction capture assays that were performed on HEK293, HeLa, MCF7, MCF10A, U2OS and Jurkat cells (34–36), which resulted in a list of 2356 RBPs. This list was supplemented with 977 computationally identified RBPs from Gerstberger et al. (37), and the EuRBP-DB (36), http://eurbpdb.syshospital.org/, accessed on 19-11-2019. This RBP list with 3333 proteins was manually curated to exclude histones (18 histones), possible contaminants (ITGA1 and ITGB1), and mitochondrial RBPs (80 RBPs), resulting in a list of 3233 RBPs.

RNA-Sequencing Analysis

RNA-sequencing reads were quasi-mapped using Salmon [version 1.0 (98)] onto the human coding transcriptome GRCh38 from Gencode (v36, May 2020). Of the $CD4^+$ T cell, $CD8^+$ T cell and $CD19^+$ B cell samples retrieved from Monaco et al. (38), an average of 12.5×10^6 reads was quasi-mapped onto the human coding transcriptome. For the $CD4^+$ T cell differentiation samples, retrieved from Ranzani et al. (97), an average of 11.4×10^6 reads was quasi-mapped onto the human coding transcriptome. Transcript-level estimates were imported and summarized to the gene-level by using the tximport function [tximport package, version 1.16.1 (99)]. To define the overall expression of RBPs subsets were grouped together as indicated. Differential gene expression analysis was performed on all detected genes using DESeq2 [version 1.28.1 (53)]. *P*-value was adjusted using the Bejamini-Hochberg procedure. Log2 fold change values were adjusted using the lfcShrink function, which is part of the DESeq2 package. Genes were considered differentially expressed with an absolute log2 fold change (LFC) >0.5 and a *p*-adjusted <0.01. RBPs that were differentially expressed were filtered from the list of differentially expressed genes. For differential gene expression analysis of total B cells, $CD4^+$, and $CD8^+$ T cells populations, we averaged the RNA-seq counts of differentiation subsets per donor. TPM (transcript per kilobase per million) counts were calculated by Salmon and used for plotting. Of note, TPM counts are corrected for library depth, library size, and transcript length, and thereby allow a fair comparison between populations. The number of detected RBPs per cell type, and the RBP expression rank were based on averaged TPM per cell type. Top 20 differentially expressed proteins were identified based on the log2 fold change values.

Single Cell RNA-Seq Data Analysis

ScRNA-seq datasets were analysed using Seurat [version 4.0.1 (100)]. Count matrices of (67–69) were filtered for "PTC", corresponding to peripheral blood-derived $CD8^+$ T cells ($CD3^+CD8^+$). To identify conventional blood-derived $CD4^+$ T cells, count matrices of references (67–69) were filtered for "PTH" ($CD3^+CD4^+CD25^-$) and "PTY" ($CD3^+CD4^+CD25^{int}$). To correct for dataset specific effects from the three individual scRNA-seq datasets, we employed a published scRNA-seq data integration method (101). The inter-individual donor batch-effect was corrected using the *vars.to.regress* argument in SCTransform (Seurat v4). Unsupervised clustering was performed on Uniform Manifold Approximation and Project (UMAP) dimensional reduction using the top 30 principal components (PCs). Cells expressing high levels of naive T cell associated genes like *CCR7*, *LEF1* and *SELL* (102, 103) were

excluded from downstream analysis. Differential gene expression analysis was performed using the Model-based Analysis of Single-cell Transcriptomics (MAST) test (104). Genes were considered differentially expressed based on a *p*-adjusted < 0.05 and an absolute log2 fold change > 0.5.

Cytotoxic Score Calculation

The cytotoxic score of $CD4^+$ T cells and $CD8^+$ T cells was obtained from the scRNA-seq data by selecting for the top 7 most correlated (Pearson's correlation) genes with *FGFBP2* expression (9). (**Supplementary Figures 6A, B**). To obtain the cytotoxic score for each cell, a Z-score of expression for each of the 8 cytotoxic genes (*FGFBP2*, *GZMB*, *GZMH*, *PRF1*, *NKG7*, *CX3CR1*, *GNLY* and *ADGRG1)* was calculated for the whole dataset. Z-scores from all 8 genes were averaged per cell and served as the cytotoxic score. Cells with high (top 10%), intermediate (10-90%) or low (bottom 10%) cytotoxic score were selected and used for analysis.

Mass Spectrometry Analysis

Differential protein expression analysis was performed with Differential Enrichment analysis of Proteomics data (DEP) [version 1.12.0 (105)] using the imputed LFQ values. LFQ values of all detected proteins were used for differential protein expression analysis. Proteins were considered differentially expressed with a *p*-adjusted value < 0.05 and an absolute log2 fold change > 0.5. RBPs that were differentially expressed were filtered from the list of differentially expressed proteins. Protein abundance was presented in CN values and were filtered for expression levels (CN > 1). The number of RBPs detected among the different cell types was based on averaged CN values across cell types obtained from 4 donors. RBP rankings according to protein abundance was performed by using averaged CN values per cell type. The top 20 differentially expressed proteins were identified based on the log2 fold change values.

RBD Annotation

RNA-binding domain names were obtained from Gerstberger et al. (2014) and Liao et al. (2020). The existence of each RNA-binding domain was verified and updated based on information present in the protein families database [Pfam (48)] (**Supplementary Table 1**). Proteins containing RNA-binding domains were obtained from the PFAM database. When RBPs contained more than one RBD, each RBD was counted and included in the analysis. Human Protein Atlas annotations [HPA, https://www.proteinatlas.org on 28-03-2021 (52)] were used to classify proteins associated with RNA modification (keywords: "RNA AND Modification"), RNA splicing (keywords: "Spliceosome"), RNA stability (keywords: "RNA AND Stability"), RNA transport (keywords: "RNA AND Transport"), and Translation (keywords: "Translation"). Protein-protein association networks were generated using the STRING database [https://string-db.org/ (106)]. Gene ontology analysis was performed with the Panther database [version 16.0 (107)] on differentially expressed RBPs. A statistical overrepresentation test (Fisher's exact with FDR multiple test correction) was performed with a reference list composed of all Homo Sapiens genes in the database. Overrepresented GO terms (FDR<0.05) were filtered for RNA-related functions. Full lists of overrepresented GO terms are provided in **Supplementary Table 7**.

Plots and Graphs

Plots and graphs were generated using ggplot2 [version 3.3 (108)]. Principal components analysis was performed using the plotPCA function from DESeq2 (53). Heatmaps were generated using the Pheatmap package [version 1.0.12 (109)] in R (version 4.0.3). Venn diagrams were generated using the Venn diagram tool from the University of Gent (accessed at http://bioinformatics.psb.ugent.be/webtools/Venn/).

DATA AVAILABILITY STATEMENT

Publicly available datasets were analyzed in this study. This data can be found here: https://www.ncbi.nlm.nih.gov/geo/query/acc.cgi?acc=GSE107011 Gene Expression Omnibus GSE107011

https://www.ebi.ac.uk/ena/browser/view/PRJEB5468 European Nucleotide Archive PRJEB5468

https://www.ncbi.nlm.nih.gov/geo/query/acc.cgi?acc=GSE125218 Gene Expression Omnibus GSE125218

https://www.nature.com/articles/ni.3693 https://www.ncbi.nlm.nih.gov/geo/query/acc.cgi?acc=GSE98638 Gene Expression Omnibus GSE98638

https://www.ncbi.nlm.nih.gov/geo/query/acc.cgi?acc=GSE99254 Gene Expression Omnibus GSE99254

https://www.ncbi.nlm.nih.gov/geo/query/acc.cgi?acc=GSE108989 Gene Expression Omnibus GSE108989.

AUTHOR CONTRIBUTIONS

NZ analyzed the data. BN provided technical and intellectual input on the data analysis. MW directed the study. NZ, BN, and MW wrote the manuscript. BN and MW conceptualized the study. All authors contributed to the article and approved the submitted version.

FUNDING

This study was supported by the ERC consolidator grant PRINTERS (817533) and the Oncode Institute.

ACKNOWLEDGMENTS

The authors would like to thank Drs. B. Popovic and I. Foskolou for critical reading of the manuscript.

SUPPLEMENTARY MATERIAL

The Supplementary Material for this article can be found online at: https://www.frontiersin.org/articles/10.3389/fimmu.2021.717324/full#supplementary-material

REFERENCES

1. Casanova JL, Abel L. Lethal Infectious Diseases as Inborn Errors of Immunity: Toward a Synthesis of the Germ and Genetic Theories. *Annu Rev Pathol Mech Dis* (2021) 16:23–50. doi: 10.1146/annurev-pathol-031920-101429
2. Dunn GP, Old LJ, Schreiber RD. The Immunobiology of Cancer Immunosurveillance and Immunoediting. *Immunity* (2004) 21:137–48. doi: 10.1016/j.immuni.2004.07.017
3. Chemin K, Gerstner C, Malmström V. Effector Functions of CD4+ T Cells at the Site of Local Autoimmune Inflammation-Lessons From Rheumatoid Arthritis. *Front Immunol* (2019) 10:353. doi: 10.3389/fimmu.2019.00353
4. Das D, Akhtar S, Kurra S, Gupta S, Sharma A. Emerging Role of Immune Cell Network in Autoimmune Skin Disorders: An Update on Pemphigus, Vitiligo and Psoriasis. *Cytokine Growth Factor Rev* (2019) 45:35–44. doi: 10.1016/j.cytogfr.2019.01.001
5. Killestein J, Eikelenboom MJ, Izeboud T, Kalkers NF, Adèr HJ, Barkhof F, et al. Cytokine Producing CD8+ T Cells Are Correlated to MRI Features of Tissue Destruction in MS. *J Neuroimmunol* (2003) 142:141–8. doi: 10.1016/S0165-5728(03)00265-0
6. Arbuckle MR, McLain MT, Rubertone MV, Scofield RH, Dennis GJ, James JA. Development of Auto-Antibodies Before the Clinical Onset of Systemic Lupus Erythematosus. *Rev Med Interne* (2004) 25:175–6. doi: 10.1016/j.revmed.2003.10.007
7. Bastard P, Rosen LB, Zhang Q, Michailidis E, Hoffmann HH, Zhang Y, et al. Autoantibodies Against Type I IFNs in Patients With Life-Threatening COVID-19. *Sci (80)* (2020) 370. doi: 10.1126/science.abd4585
8. Leisman DE, Ronner L, Pinotti R, Taylor MD, Sinha P, Calfee CS, et al. Cytokine Elevation in Severe and Critical COVID-19: A Rapid Systematic Review, Meta-Analysis, and Comparison With Other Inflammatory Syndromes. *Lancet Respir Med* (2020) 8:1233–44. doi: 10.1016/S2213-2600(20)30404-5
9. Li H, van der Leun AM, Yofe I, Lubling Y, Gelbard-Solodkin D, van Akkooi ACJ, et al. Dysfunctional CD8 T Cells Form a Proliferative, Dynamically Regulated Compartment Within Human Melanoma. *Cell* (2019) 176:775–89.e18. doi: 10.1016/j.cell.2018.11.043
10. Fenwick C, Joo V, Jacquier P, Noto A, Banga R, Perreau M, et al. T-Cell Exhaustion in HIV Infection. *Immunol Rev* (2019) 292:149–63. doi: 10.1111/imr.12823
11. Kallies A, Xin A, Belz GT, Nutt SL. Blimp-1 Transcription Factor Is Required for the Differentiation of Effector CD8+ T Cells and Memory Responses. *Immunity* (2009) 31:283–95. doi: 10.1016/j.immuni.2009.06.021
12. Roychoudhuri R, Clever D, Li P, Wakabayashi Y, Quinn KM, Klebanoff CA, et al. BACH2 Regulates CD8 + T Cell Differentiation by Controlling Access of AP-1 Factors to Enhancers. *Nat Immunol* (2016) 17:851–60. doi: 10.1038/ni.3441
13. Maciver NJ, Michalek RD, Rathmell JC. Metabolic Regulation of T Lymphocytes. *Annu Rev Immunol* (2013) 31:259–83. doi: 10.1146/annurev-immunol-032712-095956
14. Boothby M, Rickert RC. Metabolic Regulation of the Immune Humoral Response. *Immunity* (2017) 46:743–55. doi: 10.1016/j.immuni.2017.04.009
15. Rivas MA, Meydan C, Chin CR, Challman MF, Kim D, Bhinder B, et al. Smc3 Dosage Regulates B Cell Transit Through Germinal Centers and Restricts Their Malignant Transformation. *Nat Immunol* (2021) 22:240–53. doi: 10.1038/s41590-020-00827-8
16. Shin H, Blackburn SD, Intlekofer AM, Kao C, Angelosanto JM, Reiner SL, et al. A Role for the Transcriptional Repressor Blimp-1 in CD8+ T Cell Exhaustion During Chronic Viral Infection. *Immunity* (2009) 31:309–20. doi: 10.1016/j.immuni.2009.06.019
17. Finkin S, Hartweger H, Oliveira TY, Kara EE, Nussenzweig MC. Protein Amounts of the MYC Transcription Factor Determine Germinal Center B Cell Division Capacity. *Immunity* (2019) 51:324–36.e5. doi: 10.1016/j.immuni.2019.06.013
18. Meffre E, Casellas R, Nussenzweig MC. Antibody Regulation of B Cell Development. *Nat Immunol* (2000) 1:379–85. doi: 10.1038/80816
19. Gagnon JD, Ansel KM. MicroRNA Regulation of CD8+ T Cell Responses. *Non-Coding RNA Investig* (2019) 3:24–4. doi: 10.21037/ncri.2019.07.02
20. Salerno F, Turner M, Wolkers MC. Dynamic Post-Transcriptional Events Govern T Cell Homeostasis and Effector Function. *Trends Immunol* 41 (3):240–54. doi: 10.1016/j.it.2020.01.001
21. Witten JT, Ule J. Understanding Splicing Regulation Through RNA Splicing Maps. *Trends Genet* (2011) 27:89–97. doi: 10.1016/j.tig.2010.12.001
22. Müller-Mcnicoll M, Neugebauer KM. How Cells Get the Message: Dynamic Assembly and Function of mRNA-Protein Complexes. *Nat Rev Genet* (2013) 14:275–87. doi: 10.1038/nrg3434
23. Song J, Yi C. Chemical Modifications to RNA: A New Layer of Gene Expression Regulation. *ACS Chem Biol* (2017) 12:316–25. doi: 10.1021/acschembio.6b00960
24. Galloway A, Saveliev A, Łukasiak S, Hodson DJ, Bolland D, Balmanno K, et al. RNA-Binding Proteins ZFP36L1 and ZFP36L2 Promote Cell Quiescence. *Sci (80)* (2016) 352:453–9. doi: 10.1126/science.aad5978
25. Newman R, Ahlfors H, Saveliev A, Galloway A, Hodson DJ, Williams R, et al. Maintenance of the Marginal-Zone B Cell Compartment Specifically Requires the RNA-Binding Protein ZFP36L1. *Nat Immunol* (2017) 18:683–93. doi: 10.1038/ni.3724
26. Monzón-Casanova E, Screen M, Díaz-Muñoz MD, Coulson RMR, Bell SE, Lamers G, et al. The RNA-Binding Protein PTBP1 is Necessary for B Cell Selection in Germinal Centers Article. *Nat Immunol* (2018) 19:267–78. doi: 10.1038/s41590-017-0035-5
27. Galloway A, Ahlfors H, Turner M, Bell LS, Vogel KU. The RNA-Binding Proteins Zfp36l1 and Zfp36l2 Enforce the Thymic β-Selection Checkpoint by Limiting DNA Damage Response Signaling and Cell Cycle Progression. *J Immunol* (2016) 197:2673–85. doi: 10.4049/jimmunol.1600854
28. Essig K, Hu D, Guimaraes JC, Alterauge D, Edelmann S, Raj T, et al. Roquin Suppresses the PI3K-mTOR Signaling Pathway to Inhibit T Helper Cell Differentiation and Conversion of Treg to Tfr Cells. *Immunity* (2017) 47:1067–82.e12. doi: 10.1016/j.immuni.2017.11.008
29. Cui X, Mino T, Yoshinaga M, Nakatsuka Y, Hia F, Yamasoba D, et al. Regnase-1 and Roquin Nonredundantly Regulate Th1 Differentiation Causing Cardiac Inflammation and Fibrosis. *J Immunol* (2017) 199:4066–77. doi: 10.4049/jimmunol.1701211
30. Li HB, Tong J, Zhu S, Batista PJ, Duffy EE, Zhao J, et al. M 6 A mRNA Methylation Controls T Cell Homeostasis by Targeting the IL-7/STAT5/SOCS Pathways. *Nature* (2017) 548:338–42. doi: 10.1038/nature23450
31. Wei J, Long L, Zheng W, Dhungana Y, Lim SA, Guy C, et al. Targeting REGNASE-1 Programs Long-Lived Effector T Cells for Cancer Therapy. *Nature* (2019) 576:471–6. doi: 10.1038/s41586-019-1821-z
32. Tavernier SJ, Athanasopoulos V, Verloo P, Behrens G, Staal J, Bogaert DJ, et al. A Human Immune Dysregulation Syndrome Characterized by Severe Hyperinflammation With a Homozygous Nonsense Roquin-1 Mutation. *Nat Commun* (2019) 10:4779. doi: 10.1038/s41467-019-12704-6
33. Salerno F, Engels S, van den Biggelaar M, van Alphen FPJ, Guislain A, Zhao W, et al. Translational Repression of Pre-Formed Cytokine-Encoding mRNA Prevents Chronic Activation of Memory T Cells. *Nat Immunol* (2018) 19:828–37. doi: 10.1038/s41590-018-0155-6
34. Castello A, Fischer B, Frese CK, Horos R, Alleaume AM, Foehr S, et al. Comprehensive Identification of RNA-Binding Domains in Human Cells. *Mol Cell* (2016) 63:696–710. doi: 10.1016/j.molcel.2016.06.029
35. Perez-Perri JI, Rogell B, Schwarzl T, Stein F, Zhou Y, Rettel M, et al. Discovery of RNA-Binding Proteins and Characterization of Their Dynamic Responses by Enhanced RNA Interactome Capture. *Nat Commun* (2018) 9:4408. doi: 10.1038/s41467-018-06557-8
36. Liao JY, Yang B, Zhang YC, Wang XJ, Ye Y, Peng JW, et al. EuRBPDB: A Comprehensive Resource for Annotation, Functional and Oncological Investigation of Eukaryotic RNA Binding Proteins (RBPs). *Nucleic Acids Res* (2020) 48:D307–13. doi: 10.1093/nar/gkz823
37. Gerstberger S, Hafner M, Tuschl T. A Census of Human RNA-Binding Proteins. *Nat Rev Genet* (2014) 15:829–45. doi: 10.1038/nrg3813
38. Monaco G, Lee B, Xu W, Mustafah S, Hwang YY, Carré C, et al. RNA-Seq Signatures Normalized by mRNA Abundance Allow Absolute Deconvolution of Human Immune Cell Types. *Cell Rep* (2019) 26:1627–40.e7. doi: 10.1016/j.celrep.2019.01.041
39. Martinez TF, Chu Q, Donaldson C, Tan D, Shokhirev MN, Saghatelian A. Accurate Annotation of Human Protein-Coding Small Open Reading Frames. *Nat Chem Biol* (2020) 16:458–68. doi: 10.1038/s41589-019-0425-0

40. Rieckmann JC, Geiger R, Hornburg D, Wolf T, Kveler K, Jarrossay D, et al. Social Network Architecture of Human Immune Cells Unveiled by Quantitative Proteomics. *Nat Immunol* (2017) 18:583–93. doi: 10.1038/ni.3693
41. Legrand JMD, Chan AL, La HM, Rossello FJ, Änkö ML, Fuller-Pace FV, et al. DDX5 Plays Essential Transcriptional and Post-Transcriptional Roles in the Maintenance and Function of Spermatogonia. *Nat Commun* (2019) 10:2278. doi: 10.1038/s41467-019-09972-7
42. Diamond RH, Du K, Lee VM, Mohn KL, Haber BA, Tewari DS, et al. Novel Delayed-Early and Highly Insulin-Induced Growth Response Genes. Identification of HRS, a Potential Regulator of Alternative pre-mRNA Splicing. *J Biol Chem* (1993) 268:15185–92. doi: 10.1016/s0021-9258(18)82454-1
43. Mayeda A, Krainer AR. Regulation of Alternative pre-mRNA Splicing by hnRNP A1 and Splicing Factor SF2. *Cell* (1992) 68:365–75. doi: 10.1016/0092-8674(92)90477-T
44. Challa AA, Stefanovic B. A Novel Role of Vimentin Filaments: Binding and Stabilization of Collagen mRNAs. *Mol Cell Biol* (2011) 31:3773–89. doi: 10.1128/mcb.05263-11
45. Alarcón CR, Goodarzi H, Lee H, Liu X, Tavazoie S, Tavazoie SF. HNRNPA2B1 Is a Mediator of M6a-Dependent Nuclear RNA Processing Events. *Cell* (2015) 162:1299–308. doi: 10.1016/j.cell.2015.08.011
46. Castello A, Hentze MW, Preiss T. Metabolic Enzymes Enjoying New Partnerships as RNA-Binding Proteins. *Trends Endocrinol Metab* (2015) 26:746–57. doi: 10.1016/j.tem.2015.09.012
47. Chang CH, Curtis JD, Maggi LB, Faubert B, Villarino AV, O'Sullivan D, et al. Posttranscriptional Control of T Cell Effector Function by Aerobic Glycolysis. *Cell* (2013) 153:1239. doi: 10.1016/j.cell.2013.05.016
48. Finn RD, Bateman A, Clements J, Coggill P, Eberhardt RY, Eddy SR, et al. Pfam: The Protein Families Database. *Nucleic Acids Res* (2014) 42:222–30. doi: 10.1093/nar/gkt1223
49. Lu D, Searles MA, Klug A. Crystal Structure of a Zinc-Finger-RNA Complex Reveals Two Modes of Molecular Recognition. *Nature* (2003) 426:96–100. doi: 10.1038/nature02088
50. Hall TMT. Multiple Modes of RNA Recognition by Zinc Finger Proteins. *Curr Opin Struct Biol* (2005) 15:367–73. doi: 10.1016/j.sbi.2005.04.004
51. Díaz-Muñoz MD, Turner M. Uncovering the Role of RNA-Binding Proteins in Gene Expression in the Immune System. *Front Immunol* (2018) 9:1094. doi: 10.3389/fimmu.2018.01094
52. Uhlén M, Fagerberg L, Hallström BM, Lindskog C, Oksvold P, Mardinoglu A, et al. Tissue-Based Map of the Human Proteome. *Sci (80)* (2015) 347:1260419. doi: 10.1126/science.1260419
53. Love MI, Huber W, Anders S. Moderated Estimation of Fold Change and Dispersion for RNA-Seq Data With Deseq2. *Genome Biol* (2014) 15:1–21. doi: 10.1186/s13059-014-0550-8
54. Nutt SL, Hodgkin PD, Tarlinton DM, Corcoran LM. The Generation of Antibody-Secreting Plasma Cells. *Nat Rev Immunol* (2015) 15:160–71. doi: 10.1038/nri3795
55. Battle DJ, Doudna JA. The Stem-Loop Binding Protein Forms a Highly Stable and Specific Complex With the 3′ Stem-Loop of Histone mRNAs. *Rna* (2001) 7:123–32. doi: 10.1017/S1355838201001820
56. Smirnov A, Comte C, Mager-Heckel AM, Addis V, Krasheninnikov IA, Martin RP, et al. Mitochondrial Enzyme Rhodanese is Essential for 5 S Ribosomal RNA Import Into Human Mitochondria. *J Biol Chem* (2010) 285:30792–803. doi: 10.1074/jbc.M110.151183
57. Ding Y, Zhou L, Xia Y, Wang W, Wang Y, Li L, et al. Reference Values for Peripheral Blood Lymphocyte Subsets of Healthy Children in China. *J Allergy Clin Immunol* (2018) 142:970–73.e8. doi: 10.1016/j.jaci.2018.04.022
58. Sallusto F, Lenig D, Förster R, Lipp M, Lanzavecchia A. Two Subsets of Memory T Lymphocytes With Distinct Homing Potentials and Effector Functions. *Nature* (1999) 401:708–12. doi: 10.1038/44385
59. Tran DDH, Koch A, Tamura T. THOC5, a Member of the mRNA Export Complex: A Novel Link Between mRNA Export Machinery and Signal Transduction Pathways in Cell Proliferation and Differentiation. *Cell Commun Signal* (2014) 12:1–9. doi: 10.1186/1478-811X-12-3
60. Dufu K, Livingstone MJ, Seebacher J, Gygi SP, Wilson SA, Reed R. ATP is Required for Interactions Between UAP56 and Two Conserved mRNA Export Proteins, Aly and CIP29, to Assemble the TREX Complex. *Genes Dev* (2010) 24:2043–53. doi: 10.1101/gad.1898610
61. Nicolet BP, Guislain A, van Alphen FPJ, Gomez-Eerland R, Schumacher TNM, van den Biggelaar M, et al. CD29 Identifies IFN-γ-Producing Human CD8+ T Cells With an Increased Cytotoxic Potential. *Proc Natl Acad Sci USA* (2020) 117:6686–96. doi: 10.1073/pnas.1913940117
62. St. Paul M, Ohashi PS. The Roles of CD8+ T Cell Subsets in Antitumor Immunity. *Trends Cell Biol* (2020) 30:695–704. doi: 10.1016/j.tcb.2020.06.003
63. Loyal L, Warth S, Jürchott K, Mölder F, Nikolaou C, Babel N, et al. SLAMF7 and IL-6R Define Distinct Cytotoxic Versus Helper Memory CD8+ T Cells. *Nat Commun* (2020) 11:6357. doi: 10.1038/s41467-020-19002-6
64. Nicolet BP, Guislain A, Wolkers MC. CD29 Enriches for Cytotoxic Human CD4 T Cells. *bioRxiv* (2021). doi: 10.1101/2021.02.10.430576
65. Oh DY, Kwek SS, Raju SS, Li T, McCarthy E, Chow E, et al. Intratumoral CD4+ T Cells Mediate Anti-Tumor Cytotoxicity in Human Bladder Cancer. *Cell* (2020) 181:1612–25.e13. doi: 10.1016/j.cell.2020.05.017
66. Cachot A, Bilous M, Liu Y-C, Li X, Rockinger A, Saillard M, et al. Tumor-Specific Cytolytic CD4 T Cells Mediate Protective Immunity Against Human Cancer. *J Immunother Cancer* (2020) 8:A581–1. doi: 10.1136/jitc-2020-sitc2020.0545
67. Guo X, Zhang Y, Zheng L, Zheng C, Song J, Zhang Q, et al. Global Characterization of T Cells in Non-Small-Cell Lung Cancer by Single-Cell Sequencing. *Nat Med* (2018) 24:978–85. doi: 10.1038/s41591-018-0045-3
68. Zhang Y, Zheng L, Zhang L, Hu X, Ren X, Zhang Z. Deep Single-Cell RNA Sequencing Data of Individual T Cells From Treatment-Naive Colorectal Cancer Patients. *Sci Data* (2019) 6:131. doi: 10.1038/s41597-019-0131-5
69. Zheng C, Zheng L, Yoo JK, Guo H, Zhang Y, Guo X, et al. Landscape of Infiltrating T Cells in Liver Cancer Revealed by Single-Cell Sequencing. *Cell* (2017) 169:1342–56.e16. doi: 10.1016/j.cell.2017.05.035
70. Shi Z, Fujii K, Kovary KM, Genuth NR, Röst HL, Teruel MN, et al. Heterogeneous Ribosomes Preferentially Translate Distinct Subpools of mRNAs Genome-Wide. *Mol Cell* (2017) 67:71–83.e7. doi: 10.1016/j.molcel.2017.05.021
71. Filipenko NR, MacLeod TJ, Yoon CS, Waisman DM. Annexin A2 Is a Novel RNA-Binding Protein. *J Biol Chem* (2004) 279:8723–31. doi: 10.1074/jbc.M311951200
72. Ishibashi M, Wakita T, Esumi M. 2′,5′-Oligoadenylate Synthetase-Like Gene Highly Induced by Hepatitis C Virus Infection in Human Liver is Inhibitory to Viral Replication *In Vitro*. *Biochem Biophys Res Commun* (2010) 392:397–402. doi: 10.1016/j.bbrc.2010.01.034
73. Marnef A, Maldonado M, Bugaut A, Balasubramanian S, Kress M, Weil D, et al. Distinct Functions of Maternal and Somatic Pat1 Protein Paralogs. *Rna* (2010) 16:2094–107. doi: 10.1261/rna.2295410
74. Jurgens AP, Popović B, Wolkers MC. T Cells at Work: How Post-Transcriptional Mechanisms Control T Cell Homeostasis and Activation. *Eur J Immunol* (2021) 51:2178–87. doi: 10.1002/eji.202049055
75. Wolf T, Jin W, Zoppi G, Vogel IA, Akhmedov M, Bleck CKE, et al. Dynamics in Protein Translation Sustaining T Cell Preparedness. *Nat Immunol* (2020) 21:927–37. doi: 10.1038/s41590-020-0714-5
76. Howden AJM, Hukelmann JL, Brenes A, Spinelli L, Sinclair LV, Lamond AI, et al. Quantitative Analysis of T Cell Proteomes and Environmental Sensors During T Cell Differentiation. *Nat Immunol* (2019) 20:1542–54. doi: 10.1038/s41590-019-0495-x
77. Myers DR, Norlin E, Vercoulen Y, Roose JP. Active Tonic Mtorc1 Signals Shape Baseline Translation in Naive T Cells. *Cell Rep* (2019) 27:1858–74.e6. doi: 10.1016/j.celrep.2019.04.037
78. Araki K, Morita M, Bederman AG, Konieczny BT, Kissick HT, Sonenberg N, et al. Translation is Actively Regulated During the Differentiation of CD8 + Effector T Cells. *Nat Immunol* (2017) 18:1046–57. doi: 10.1038/ni.3795
79. Salerno F, Freen-van Heeren JJ, Guislain A, Nicolet BP, Wolkers MC. Costimulation Through TLR2 Drives Polyfunctional CD8 + T Cell Responses. *J Immunol* (2019) 202:714–23. doi: 10.4049/jimmunol.1801026
80. Salerno F, Guislain A, Cansever D, Wolkers MC. TLR-Mediated Innate Production of IFN-γ by CD8 + T Cells Is Independent of Glycolysis. *J Immunol* (2016) 196:3695–705. doi: 10.4049/jimmunol.1501997
81. Salerno F, Paolini NA, Stark R, von Lindern M, Wolkers MC. Distinct PKC-Mediated Posttranscriptional Events Set Cytokine Production Kinetics in

CD8 $^{+}$ T Cells. *Proc Natl Acad Sci* (2017) 114:201704227. doi: 10.1073/pnas.1704227114
82. Buccitelli C, Selbach M. mRNAs, Proteins and the Emerging Principles of Gene Expression Control. *Nat Rev Genet* (2020) 21:630–44. doi: 10.1038/s41576-020-0258-4
83. Nguyen CDL, Malchow S, Reich S, Steltgens S, Shuvaev KV, Loroch S, et al. A Sensitive and Simple Targeted Proteomics Approach to Quantify Transcription Factor and Membrane Proteins of the Unfolded Protein Response Pathway in Glioblastoma Cells. *Sci Rep* (2019) 9:1–11. doi: 10.1038/s41598-019-45237-5
84. Chen C, Peng J, Ma S, Ding Y, Huang T, Zhao S, et al. Ribosomal Protein S26 Serves as a Checkpoint of T-Cell Survival and Homeostasis in a P53-Dependent Manner. *Cell Mol Immunol* (2021) 18:1844–6. doi: 10.1038/s41423-021-00699-4
85. Kang J, Brajanovski N, Chan KT, Xuan J, Pearson RB, Sanij E. Ribosomal Proteins and Human Diseases: Molecular Mechanisms and Targeted Therapy. *Signal Transduct Target Ther* (2021) 6:323. doi: 10.1038/s41392-021-00728-8
86. Nicolas E, Parisot P, Pinto-Monteiro C, De Walque R, De Vleeschouwer C, Lafontaine DLJ. Involvement of Human Ribosomal Proteins in Nucleolar Structure and P53-Dependent Nucleolar Stress. *Nat Commun* (2016) 7:11390. doi: 10.1038/ncomms11390
87. Refsland EW, Stenglein MD, Shindo K, Albin JS, Brown WL, Harris RS. Quantitative Profiling of the Full APOBEC3 mRNA Repertoire in Lymphocytes and Tissues: Implications for HIV-1 Restriction. *Nucleic Acids Res* (2010) 38:4274–84. doi: 10.1093/nar/gkq174
88. Gillick K, Pollpeter D, Phalora P, Kim E-Y, Wolinsky SM, Malim MH. Suppression of HIV-1 Infection by APOBEC3 Proteins in Primary Human CD4 + T Cells Is Associated With Inhibition of Processive Reverse Transcription as Well as Excessive Cytidine Deamination. *J Virol* (2013) 87:1508–17. doi: 10.1128/jvi.02587-12
89. Queiroz RML, Smith T, Villanueva E, Marti-Solano M, Monti M, Pizzinga M, et al. Comprehensive Identification of RNA–Protein Interactions in Any Organism Using Orthogonal Organic Phase Separation (OOPS). *Nat Biotechnol* (2019) 37:169–78. doi: 10.1038/s41587-018-0001-2
90. Fu XD, Ares M. Context-Dependent Control of Alternative Splicing by RNA-Binding Proteins. *Nat Rev Genet* (2014) 15:689–701. doi: 10.1038/nrg3778
91. Urdaneta EC, Vieira-Vieira CH, Hick T, Wessels HH, Figini D, Moschall R, et al. Purification of Cross-Linked RNA-Protein Complexes by Phenol-Toluol Extraction. *Nat Commun* (2019) 10:1–17. doi: 10.1038/s41467-019-08942-3
92. Trendel J, Schwarzl T, Horos R, Prakash A, Bateman A, Hentze MW, et al. The Human RNA-Binding Proteome and Its Dynamics During Translational Arrest. *Cell* (2019) 176:391–403.e19. doi: 10.1016/j.cell.2018.11.004
93. Beckmann BM, Horos R, Fischer B, Castello A, Eichelbaum K, Alleaume AM, et al. The RNA-Binding Proteomes From Yeast to Man Harbour Conserved enigmRBPs. *Nat Commun* (2015) 6:10127. doi: 10.1038/ncomms10127
94. Huppertz I, Perez-Perri JI, Mantas P, Sekaran T, Schwarzl T, Dimitrova-Paternoga L, et al. RNA Regulates Glycolysis and Embryonic Stem Cell Differentiation *via* Enolase 1. *bioRxiv* (2020) 2020.10.14.337444. doi: 10.1101/2020.10.14.337444
95. Guiducci G, Paone A, Tramonti A, Giardina G, Rinaldo S, Bouzidi A, et al. The Moonlighting RNA-Binding Activity of Cytosolic Serine Hydroxymethyltransferase Contributes to Control Compartmentalization of Serine Metabolism. *Nucleic Acids Res* (2019) 47:4240–54. doi: 10.1093/nar/gkz129
96. Gebauer F, Schwarzl T, Valcárcel J, Hentze MW. RNA-Binding Proteins in Human Genetic Disease. *Nat Rev Genet* (2021) 22:185–98. doi: 10.1038/s41576-020-00302-y
97. Ranzani V, Rossetti G, Panzeri I, Arrigoni A, Bonnal RJP, Curti S, et al. The Long Intergenic Noncoding RNA Landscape of Human Lymphocytes Highlights the Regulation of T Cell Differentiation by Linc-MAF-4. *Nat Immunol* (2015) 16:318–25. doi: 10.1038/ni.3093
98. Patro R, Duggal G, Love MI, Irizarry RA, Kingsford C. Salmon Provides Fast and Bias-Aware Quantification of Transcript Expression. *Nat Methods* (2017) 14:417–9. doi: 10.1038/nmeth.4197
99. Soneson C, Love MI, Robinson MD. Differential Analyses for RNA-Seq: Transcript-Level Estimates Improve Gene-Level Inferences [Version 2; Referees: 2 Approved]. *F1000Research* (2016) 4:1–23. doi: 10.12688/F1000RESEARCH.7563.2
100. Satija R, Farrell JA, Gennert D, Schier AF, Regev A. Spatial Reconstruction of Single-Cell Gene Expression Data. *Nat Biotechnol* (2015) 33:495–502. doi: 10.1038/nbt.3192
101. Stuart T, Butler A, Hoffman P, Hafemeister C, Papalexi E, Mauck WM, et al. Comprehensive Integration of Single-Cell Data. *Cell* (2019) 177:1888–902.e21. doi: 10.1016/j.cell.2019.05.031
102. Willinger T, Freeman T, Herbert M, Hasegawa H, McMichael AJ, Callan MFC. Human Naive CD8 T Cells Down-Regulate Expression of the WNT Pathway Transcription Factors Lymphoid Enhancer Binding Factor 1 and Transcription Factor 7 (T Cell Factor-1) Following Antigen Encounter *In Vitro* and *In Vivo*. *J Immunol* (2006) 176:1439–46. doi: 10.4049/jimmunol.176.3.1439
103. Yang C, Khanniche A, Dispirito JR, Ji P, Wang S, Wang Y, et al. Transcriptome Signatures Reveal Rapid Induction of Immune-Responsive Genes in Human Memory CD8+ T Cells. *Sci Rep* (2016) 6:1–8. doi: 10.1038/srep27005
104. Finak G, McDavid A, Yajima M, Deng J, Gersuk V, Shalek AK, et al. MAST: A Flexible Statistical Framework for Assessing Transcriptional Changes and Characterizing Heterogeneity in Single-Cell RNA Sequencing Data. *Genome Biol* (2015) 16:1–13. doi: 10.1186/s13059-015-0844-5
105. Zhang X, Smits AH, Van Tilburg GBA, Ovaa H, Huber W, Vermeulen M. Proteome-Wide Identification of Ubiquitin Interactions Using UbIA-MS. *Nat Protoc* (2018) 13:530–50. doi: 10.1038/nprot.2017.147
106. Szklarczyk D, Gable AL, Lyon D, Junge A, Wyder S, Huerta-Cepas J, et al. STRING V11: Protein-Protein Association Networks With Increased Coverage, Supporting Functional Discovery in Genome-Wide Experimental Datasets. *Nucleic Acids Res* (2019) 47:D607–13. doi: 10.1093/nar/gky1131
107. Mi H, Muruganujan A, Ebert D, Huang X, Thomas PD. PANTHER Version 14: More Genomes, a New PANTHER GO-Slim and Improvements in Enrichment Analysis Tools. *Nucleic Acids Res* (2019) 47:D419–26. doi: 10.1093/nar/gky1038
108. Wickham H. *Ggplot2: Elegant Graphics for Data Analysis*. Springer-Verlag (2009). p. 41–62.
109. Kolde R. *Pheatmap: Pretty Heatmaps* (2015). Available at: https://cran.r-project.org/web/packages/pheatmap/index.html.

Conflict of Interest: The authors declare that the research was conducted in the absence of any commercial or financial relationships that could be construed as a potential conflict of interest.

Publisher's Note: All claims expressed in this article are solely those of the authors and do not necessarily represent those of their affiliated organizations, or those of the publisher, the editors and the reviewers. Any product that may be evaluated in this article, or claim that may be made by its manufacturer, is not guaranteed or endorsed by the publisher.

frontiers in Immunology

ORIGINAL RESEARCH
published: 07 December 2021
doi: 10.3389/fimmu.2021.733730

miR-10c Facilitates White Spot Syndrome Virus Infection by Targeting Toll3 in *Litopenaeus vannemei*

Hongliang Zuo[1,2,3], *Xinxin Liu*[1], *Mengting Luo*[1], *Linwei Yang*[1,2,3], *Zhiming Zhu*[2], *Shaoping Weng*[1,2,3], *Jianguo He*[1,2,3*] *and Xiaopeng Xu*[1,2,3*]

[1] State Key Laboratory of Biocontrol, School of Life Sciences, Sun Yat-Sen University, Guangzhou, China, [2] Southern Marine Science and Engineering Guangdong Laboratory (Zhuhai), Zhuhai, China, [3] Institute of Aquatic Economic Animals and Guangdong Province Key Laboratory for Aquatic Economic Animals, Sun Yat-Sen University, Guangzhou, China

OPEN ACCESS

Edited by:
Osamu Takeuchi,
Kyoto University, Japan

Reviewed by:
Paramananda Saikia,
Cleveland Clinic, United States
Akira Goto,
Institut National de la Santé et de la Recherche Médicale (INSERM), France
Neda Barjesteh,
Université de Montréal, Canada
Hong Shi,
State Oceanic Administration, China
Alphis G. Ponniah,
Retired, Chennai, India

***Correspondence:**
Xiaopeng Xu
xuxpeng@mail.sysu.edu.cn
Jianguo He
lsshjg@mail.sysu.edu.cn

Specialty section:
This article was submitted to Molecular Innate Immunity, a section of the journal Frontiers in Immunology

Received: 30 June 2021
Accepted: 14 October 2021
Published: 07 December 2021

Citation:
Zuo H, Liu X, Luo M, Yang L, Zhu Z, Weng S, He J and Xu X (2021) miR-10c Facilitates White Spot Syndrome Virus Infection by Targeting Toll3 in Litopenaeus vannemei. Front. Immunol. 12:733730. doi: 10.3389/fimmu.2021.733730

Toll-like receptors (TLRs) are canonical cell membrane receptors functioning to recognize pathogens and transduce signals to activate immune responses. It has been known that Toll3 in Pacific white shrimp *Litopenaeus vannamei* (LvToll3) plays a critical role in antiviral immunity by inducing the transcription of interferon regulatory factor (IRF), which mediates a signaling axis that is similar to the interferon system of vertebrates. However, the regulatory mechanism of the Toll3-IRF signaling is still unclear. In this study, a novel microRNA (miRNA) of miR-10 family, temporarily named as miR-10c, was identified from *L. vannamei*. miR-10c may play a nonnegligible regulatory role in shrimp immune responses since it was constitutively expressed in all detected tissues and transcriptionally induced by immune stimulation. Functional analysis validated that miR-10c could target LvToll3 to inhibit its expression, through which miR-10c blocked the nuclear translocation of IRF and facilitated white spot syndrome virus (WSSV) infection. To our knowledge, the present study revealed the first report of a Toll targeted by miRNA in crustaceans and provided a solid evidence base for supporting the role of LvToll3 in antiviral defense by activating IRF signaling in *L. vannamei*. Identification of the miR-10c/Toll3/IRF regulatory axis in shrimp provides new insights into the participation of miRNA in the regulation of immune responses and contributes to in-depth understanding of the mechanisms of Toll-induced immune responses in *L. vannamei*.

Keywords: microRNA, Toll-like receptor, regulatory factor, antiviral immunity, *Litopenaeus vannemei*

INTRODUCTION

Tolls/Toll-like receptors (TLRs) are one of the most common pathogen sensors in metazoans, recognizing diverse pathogens such as Gram-positive and Gram-negative bacteria, RNA or DNA viruses, fungi, and other protozoans in the early stage of host immune response (1). After pathogen recognition, Tolls transduce signals into cells through various signal pathways to activate expression of a series of immune and inflammatory genes for the establishment of the immune activation state

in the host (2). To date, there are 10 and 12 TLRs identified in humans and mice, respectively, in which TLR1, TLR2, TLR5, TLR6, and TLR10 are responsible for microbial lipid, polysaccharide, and protein recognition, while TLR3, TLR7, TLR8, and TLR9 are responsible for viral nucleic acid recognition (3, 4). In invertebrates, the number of Tolls/TLRs varies among different organisms. For example, *Drosophila melanogaster* has nine TLRs, while *Caenorhabditis elegans* has only one and *Paracentrotus lividus* has up to 222 TLRs in their genomes (5–7). Stimulation of TLRs results in the activation of different intracellular signaling cascades, generally leading to the activation of NF-κB and activating protein-1 (AP-1) in MyD88-dependent pathways and type I interferons (IFNs) in TRIF-dependent antiviral pathways (8, 9).

Litopenaeus vannamei is the major aquaculture shrimp in the world, the culture of which was threatened by various pathogens, such as *Vibrio*, white spot syndrome virus (WSSV), and *Enterocytozoon hepatopenaei* (EHP), which have caused tremendous economic losses (9, 10). More and more research attentions have focused on the regulation of the innate immune system of *L. vannamei*, which is also centered on the Toll receptor-mediated signaling. Among the identified *L. vannamei* Tolls, the Toll3, highly homologous to *Drosophila* Toll6, has been known to be transcriptionally induced by double-stranded RNA (dsRNA) and can facilitate the expression of interferon regulatory factor (IRF) and the downstream Vago 4/5 (11, 12). It has been known that the IRF-Vago-JAK/STAT regulatory axis plays an essential role in antiviral immunity in shrimp (13). These indicated that LvToll3 may also play a role in virus infection, which still lacks solid evidence so far.

MicroRNAs (miRNAs) are a sort of evolutionary conserved, small (18–26 nt), endogenous noncoding RNAs which transcribed from genomic clusters and involved in multiple biological processes by suppressing the target gene on posttranscriptional level (14). MiRNAs are initially transcribed as primary miRNAs (pri-miRNAs) by RNA polymerase II or III, processed into precursor miRNAs (pre-miRNA) by Drosha/DGCR8 complex in the nucleus, exported to the cytoplasm, and finally cleaved to mature miRNA by Direr complex (15, 16). After incorporating into a RNA-induced silencer complex (RISC), the mature miRNAs combine with target mRNAs and induce their cleavage through the imperfect complementary binding sites located in the 3′-untranslated region (3′-UTR) or open reading frame (ORF) (17, 18). Accumulating evidence proves that miRNAs play nonnegligible regulatory roles in innate immunity by adjusting enzyme activities, regulating apoptosis or phagocytosis, and modulating signal transduction in mammals (19, 20). Recent studies have shown that the miRNA system also plays an important role in regulation of shrimp immunity. For instance, the *L. vannamei* miR-1959 mediates an intrapathway regulatory feedback loop to positively enhance the activation of the dorsal pathway by targeting cactus (21). The miR-1 mediated the inhibitory signaling from the JAK-STAT pathway to the NF-κB signaling by targeting MyD88, the vital signal transducer of dorsal activation (22). In the current study, we identified a novel miRNA from miR-10 family in *L. vannemei* and unveiled its regulatory role in shrimp antiviral immunity *via* targeting LvToll3 and further regulating IRF expression. This study may enrich the knowledge on Toll-mediated signaling in crustaceans and provide new insights into the regulatory effects of miRNAs on immunity in invertebrates (23).

MATERIALS AND METHODS

Shrimps

L. vannamei (~5 g) were obtained from an aquaculture farm in Zhuhai, China, acclimated at ~28°C in a recirculating water system filled with air-pumped seawater (5% salinity) and fed with 3% body weight artificial diet for two times each day. Five percent of reared shrimps were sampled randomly and detected by PCR to ensure free of WSSV and *Vibrio parahaemolyticus*.

Cloning of Mature miR-10c

miR-10c sequence was obtained from a small RNA transcriptome sequencing library and verified using stem-loop real-time RT-PCR following methods as previously reported (21). Briefly, total RNA was extracted from mixed tissues including gill, hepatopancreas, stomach, and muscle of *L. vannamei* using Trizol reagent (Ambion, Austin, TX, USA), and cDNA was then synthesized with stem-loop primer of miR-10c-RT (**Table 1**) using PrimeScript RT reagent kit (Takara, Japan). To verify the sequence of miR-10c, the mature miRNA sequence was cloned and sequenced with primers of miR-10c-IF and miR-10c-IR as previously described (24).

Quantitative Real-Time PCR

For expression analysis of miRNA, total RNA of different samples was extracted using Trizol reagent (Ambion), and cDNAs were synthesized using stem-loop primer of miR-10c-RT as mentioned above. Small nuclear RNA U6 was separately reversed using primers of U6-RT (**Table 1**) and set as internal control. For expression analysis of mRNA, total RNA of different samples were extracted using a RNeasy Plus Mini Kit (QIAGEN, Los Angeles, CA, USA), cDNAs were synthesized using a PrimeScript RRT Kit (Takara, Japan), and shrimp elongation factor 1-alpha (EF1α, GenBank Accession No. GU136229.1) gene was set as internal control. Quantitative real-time PCR (qRT-PCR) was performed on a LightCycler 480 System (Roche, Basel, Switzerland) using specific primers list in **Table 1**, and the qRT-PCR protocols and parameters were set as previously described (21). The expression levels of miRNA and mRNA were calculated using $2^{-\Delta\Delta Ct}$ method after normalization to U6 and EF1α, respectively (25).

Northern Blot

After pre-electrophoresis of a 12% denaturing polyacrylamide gel at 200 V for 1 h, total RNAs (10 μg) isolated from different samples were separated at 200 V for 1 h and transferred onto a positively charged nylon membrane (Roche, USA) using a Trans-Blot SD Semi-Dry Transfer Cell system (Bio-Rad, Hercules, CA, USA). Separated RNAs were crosslinked to the membrane by UV (254 nm) and prehybridized at 68°C for 30 min

TABLE 1 | Primers and probes used in this study.

Name	Sequence (5′–3′)
miRNA identification	
miR-10c-RT	GTCGTATCCAGTGCAGGGTCCGAGGTATTCGCACTGGATACGACACACAAG
miR-10c-IF	CTCCAGCTGACCTTGTAGAT
miR-10c-IR	ACCCTGCACTGGATACGAC
Northern blot and *in situ* hybridization	
miR-10c probe	/5DigN/ACACAAGTTCGGATCTACAAGGT/3Dig_N/
U6 probe	/5DigN/CACGAUUUUGCGUGUCAUCCUU/3Dig_N/
Scrambled miRNA probe	/5DigN/GUGUAACACGUCUAUACGCCCA/3Dig_N/
Dual-luciferase reporter assays	
Toll3-3′-AscIF	AATGGCGCGCCAGATCCTGCGGAACTCCCTG
Toll3-3′-FseIR	ATAGGCCGGCCAAACGACGTGACAATGGTTACAC
Toll3-3′-MutF	ACAGAGCGGAACATTTTGATGTCGGCACAAGCATAATCTCAGAGCTCTACCTAG
Toll3-3′-MutR	TTGTGCCGACATCAAAATGTTCCGCTCTGTGATGAAAGCTCCTGGCTGTG
dsRNA synthesis	
Toll3-dsT7F	GGATCCTAATACGACTCACTATAGGGCCTGTGATTGCGAGATGAC
Toll3-dsT7R	GGATCCTAATACGACTCACTATAGGAGGATAACCACGACGACGAAG
Toll3-dsF	GCCTGTGATTGCGAGATGAC
Toll3-dsR	AGGATAACCACGACGACGAAG
GFP-dsT7F	GGATCCTAATACGACTCACTATAGGATGGTGAGCAAGGGCGAGGAG
GFP-dsT7R	GGATCCTAATACGACTCACTATAGGTTACTTGTACAGCTCGTCCATGCC
GFP-dsF	ATGGTGAGCAAGGGCGAGGAG
GFP-dsR	TTACTTGTACAGCTCGTCCATGCC
qRT-PCR	
U6-RT	AAATGTGGAACGCTTCAC
U6-qRTF	GTACTTGCTTCGGCAGTACATATAC
U6-qRTR	TGGAACGCTTCACGATTTTGC
10c-qRTF	CTCCAGCTGACCTTGTAGATC
10c-qRTR	ACCCTGCACTGGATACGAC
Toll3-qRTF	TTCAGAACAGCCAGCGAGTG
Toll3-qRTR	GCATTGACGCTGGACTGTTG
IRF-qRTF	ATCCAACCTGTCTTCAGTGGAG
IRF-qRTR	GGACCACGCTGTGAACCTG
Vago4-qRTF	GAAGTGCTGGCTGCCCAAG
Vago4-qRTR	GACCGCATGTAGCATACTCGAC
Vago5-qRTF	CTCTCCAACATCTGATCGCAG
Vago5-qRTR	CAGTGTGCCCGTACACAGC
ALF2-qRTF	TAGCGTGACACCGAAATTCAAG
ALF2-qRTR	CGAAGTCTTGCGTAGTTCTGC
ALF3-qRTF	CGGTGACATTGACCTCGTTG
ALF3-qRTR	TGACGGACCCGATGAAGTAG
ALF5-qRTF	TGGTGAAGGCTTCCTACAAGAG
ALF5-qRTR	CATCAGCAGTAGCAGTGTCA
ie1-qRTF	GCCATGAAATGGATGGCTAGG
ie1-qRTR	ACCTTTGCACCAATTGCTAGTAG

using ULTRAhyb Ultrasensitive Hybridization Buffer (Ambion, USA), and hybridized overnight with miR-10c and U6 LNA probes (Exqion, Copenhagen, Denmark, **Table 1**) at a final concentration of 0.1 nM at 60°C, respectively. Membranes were blocked by DIG Wash and Block Buffer Set (Roche, USA) and incubated with 1:10,000 diluted Anti-Digoxigenin-AP, Fab fragments (Roche, USA). The signals were detected using CDP-Star (Roche, USA) chemiluminescent substrate and captured by Amersham Imager 600 (GE, Chicago, IL, USA).

In Situ Hybridization

The gill and hepatopancreas of healthy shrimps were fixed in 4% paraformaldehyde, dissolved by PBS (0.1 M, pH: 7.4) overnight and embedded in paraffin. The embedded tissues were cut into 5 μm thick paraffin slices and fixed onto silicified slides. *In situ* hybridization was performed using miRCURY LNA miRNA ISH optimization kit (Exqion, Denmark) according to the procedures mentioned previously (21). In brief, slides were deparaffinized in xylene and gradient-diluted ethanol solutions at room temperature (RT). The preprocessed slides were then incubated with proteinase-K (10 mg/ml) for 15 min at 37°C, washed with PBS, dehydrated in gradient-diluted ethanol solutions, and air dried for 15 min at RT. Dehydrated tissues were incubated with hybridization buffer containing 20 nM miR-10c probes, 5 nM U6 probes, or 20 nM scrambled miRNA probes (Exiqon, Denmark) for 1 h at 50°C in a humidifying chamber. Slides were then washed in SSC buffers at the hybridization temperature, blocked with a blocking solution for 15 min at RT, incubated with 1:500 diluted Anti-Digoxigenin-AP, Fab fragments (Roche, USA) for 1 h at RT, developed with NBT/BCIP (Roche, USA) substrate for

2 h at 30°C, counterstained with Nuclear Fast Red (Sigma, St. Louis, MO, USA) for 1 min at RT, and finally captured using a Leica DM4 light microscopy (Leica, Wetzlar, Germany).

Immune Challenge

After culturing to logarithmic phase, *V. parahaemolticus* was diluted to 10^5 colony forming unit (CFU) in 50 μl PBS. WSSV used in this study was prepared from moribund shrimps artificially infected with the preserved WSSV that was stored in −80°C in our lab. Virus stock was prepared freshly and quantified using absolute qRT-PCR and diluted to 10^6 copies in 50 μl PBS according to procedure as mentioned previously (26). Five micrograms of litopolysaccharide (LPS) or poly(I:C) was diluted in 50 μl PBS before use as the experimental inoculum.

Healthy shrimps were divided into several experimental groups and acclimated in independent recirculating water tank systems for 1 week before immune challenge. For expression pattern analysis of miR-10c after pathogen stimulation, shrimps were injected with 10^5 CFU of *V. parahaemolticus*, 10^6 copies of WSSV fresh extracted WSSV, 5 μg LPS, 5 μg poly(I:C), and PBS at the second abdominal segment. The gill and hepatopancreas were isolated from six randomly sampled shrimps in each group at 0, 4, 12, 24, 48, 72, and 96 h poststimulant injection. Total RNAs were then isolated, cDNAs were synthesized by stem loop primer, and expression of miR-10c was detected using qRT-PCR as described above.

Dual-Luciferase Reporter Assays

The wild-type 3′-UTR of LvToll3 was cloned using primers of Toll3-3′-AscIF/Toll3-3′-AscIR (**Table 1**) and inserted into pGLDr249, a dual-luciferase miRNA target expression vector constructed from pmirGLO vector (Promega, USA), after the ORF of luciferase to generate pGLDr249-Toll3 vector. Since both 5′ and 3′ end of miRNAs potentially dominant the target sites, the whole predicted target site of miR-10c in LvToll3 (5' ACACGGCUGUAGUUUUACAAGG 3′) was mutated to complement sequence (5′ UGUGCCGACAUCAAAAA UGUUCC 3′) using primers of Toll3-3′-MutF/Toll3-3′-MutR (**Table 1**) and constructed into pGLDr-249 to generate pGLDr249-Toll3-Mut.

To verify the posttranscriptional inhibiting effects of miR-10c *via* the target site in 3′-UTR of LvToll3, *Drosophilla* (S2) cells were plated on a 96-well plate with 80% confluent and acclimated overnight at 28°C in Schneider's insect medium (Sigma, USA) in the presence of 10% serum (Gibco, Waltham, MA, USA). For each well, 100 ng pGLDr249-Toll3 or pGLDr249-Toll3-Mut was cotransfected with 15 pmol miR-10c mimics or miR-NC (GenePharma, Shanghai, China) (final concentration of 100 nM) into S2 cells using FuGENE® HD Transfection Regent (Promega, USA). Cells were harvested and lysed at 48 h posttransfection, and the activity of luciferase was detected using Dual-Luciferase® Reporter Assay System (Promega, USA) according to the instruction of manufactures. Parallel with the luminescence detection, the protein levels of firefly and Renilla luciferases in the cell lysates were verified by Western blot using specific antibodies against firefly and Renilla luciferases (Abcam, USA), respectively.

miRNA Regulation and mRNA Knockdown *In Vivo*

To verify the posttranscriptional suppression of LvToll3 *in vivo*, *L. vannamei* were treated with chemosynthetic and cholesterol-modified miR-10c mimics (agomiR-10c) or miR-10c inhibitor (antagomiR-10c). Healthy shrimps were randomly divided into four groups (n = 40 in each group) and injected with agomiR-10c, agomiR-NC, antagomiR-10c, or antagomiR-NC at the second abdominal. Hemocytes and gills were pooled from 15 shrimps of each treatment at 48 h postinjection for the following transcriptional and proteomic analyses.

The expression of LvToll3 was inhibited by RNA interference *via* dsRNA injection *in vivo*. The dsRNAs targeting LvToll3 or green fluorescent protein (GFP, set as negative control) were synthesized *in vitro* using T7 RiboMAX™ Express RNAi system (Promega, USA). The template sequence of LvToll3 and GFP were cloned from the cDNA of *L. vannamei* and pAc5.1-GFP plasmid and incorporated with T7 RNA polymerase promoter at the 5′ end using primers of Toll3-dsF/Toll3-dsR and GFP-dsF/GFP-dsR (**Table 1**), respectively. The target-specific dsRNAs were annealed from two independently transcribed single-strand RNAs and then purified according to the manufacturer's instruction. Two groups (n = 40) of healthy shrimps were intramuscularly injected with 5 μg LvToll3 and GFP dsRNA, respectively. At 48 h post-dsRNA injection, hemocytes and gills were sampled from 15 shrimps in each group for the following mRNA and protein analyses as described above.

Nuclear Localization Analysis of IRF

At 48 h post-miRNA or dsRNA injection, shrimps were challenged with poly(I:C) as mentioned above and 24 h later, samples were pooled and subjected to Western blot analysis. In brief, total nuclear protein of hemocyte and gill, dispersed through 200 mesh screen, was isolated using Nuclear and Cytoplasmic Protein Extraction Kit (Beyotime, Haimen, China), and then quantified and diluted to equal concentration using BCA protein Assay kit (Beyotime, China). Protein samples were separated by SDS-PAGE and transferred onto a nitrocellulose membrane (GE, USA). After blocking, membrane was incubated with prepared rabbit anti-LvToll3 Ab (GL Biochem, Shanghai, China), and simultaneously, a parallel membrane was incubated with rabbit anti-HistoneH3 mAb (CST, Houston, TX, USA) as internal control. Another parallel membrane was incubated with rabbit anti-GAPDH antibody (Sigma, USA) to verify no contamination of cytoplasmic protein. The signals were detected using anti-rabbit IgG (H+L)-HRP Conjugate (Promega, USA), developed using SuperSignal West Femto (Thermo, USA) and captured by Amersham Imager 600 (GE, USA). The gray values of visualized Western blot signals were quantitated using Quantity one (Bio-Rad, USA) by Gauss model with different rolling disk sizes (5, 10, and 15).

Analysis of the Antiviral Function of miR-10c and LvToll3

To analyze the immune status of miR-10c, shrimps were injected with miRNA mimics and inhibitor as mentioned above. Gills were sampled from nine shrimps in each group at 48 h after injection. Total RNAs were isolated, cDNAs were synthesized, and then the transcription of immune-related genes, including Vagos, anti-lipopolysaccharide factors (ALF), and C-type lectins (CTL), were analyzed using qRT-PCR with specific primers (**Table 1**). The *L. vannamei* elongation factor 1-α (EF1-α) (GenBank Accession No.: GU136229) was set as internal control.

Shrimps ($n = 50$) were challenged with 10^6 copies of WSSV at 48 h after the injection of miR-10c mimics/inhibitor or LvToll3 dsRNA as mentioned above. The cumulative mortality was recorded days after WSSV challenge. Parallel experiments were performed to detect the WSSV copy number in muscle after the immune challenge. To verify the role of antiviral immunity of miR-10c, shrimps were coinjected with miRNA mimics and dsRNA and challenged with 10^6 copies of WSSV at 48 h postinjection. The cumulative mortality was recorded and parallel experiments were performed to detect the WSSV copy number in muscle. Total RNA of muscles was isolated and the WSSV copies were detected by relative qRT-PCR with the EF1-α as internal control.

Bioinformatics Analysis and Statistical Analysis

The target of miR-10c was predicted using RNAhybrid (https://bibiserv.cebitec.uni-bielefeld.de/rnahybrid/submission.html) based on the mRNA transcriptome of *L. vannamei* with the parameter of hits per target of 3, energy threshold of −25, No G:C in seed, helix constraint from 2 to 8, max bulge loop length of 3, mas internal loop length of 3, and approximate *p*-value of 3utr_fly (27). The multiple sequence alignment of miR-10 homologs was performed using ClustalX 2.1, and the phylogenetic tree was constructed using MEGA 5.0. All data were presented as mean ± SD. The significance of difference between groups of numerical data was calculated using Student's *t*-test. The cumulative mortalities were analyzed using GraphPad Prism 5.01 to generate the Kaplan-Meier plot (log rank χ^2 test).

RESULTS

miR-10c Identification

To investigate miRNA profiles of *L. vannemei* during the responses to virus, small RNAs were isolated from hemocytes at 4, 12, 24, and 48 h after the intramuscular injection of WSSV and the miRNA libraries were constructed and sequenced on the Illumina HiSeq 2000 sequencing platform. Two hundred eighty-eight differentially expressed miRNAs (DEmiRNAs) had been classified as a data set (**Supplementary File 1**). In this data set, the richness of a small RNA sequence (5′ ACCTTGTAGATCCGAACTTGTGT 3′), highly homologous to the miR-10a of *Xenopus laevis* and temporarily named Lva-miR-10c, was increased from 1,057 to 5,879 reads at 4 to 48 h post WSSV injection. The mature sequence of miR-10c was verified by the five identified base pairs using stem-loop RT-PCR. Generally, the cDNA of miR-10c was reverse transcribed by stem-loop primer of miR-10c-RT through the combination between its unpaired 7 nucleotides and the 3′ end of miR-10c (**Figure 1A**). After then, the stem-loop conjugated miR-10c was amplified by the identification primers of miR-10c-IF and miR-10-IR with partial complementation of the forward primer and complete complementation of the reverse primer. PCR products were purified through agarose gel electrophoresis (**Figure 1B**) and sequenced after cloning in *Escherichia coli* system. The accuracy of the cloning results was verified by the uncombined sequence in miR-10c (black box in **Figure 1A**). Northern blot further confirmed that miR-10c and its precursor were expressed in *L. vannemei* with the control of small nuclear RNA U6 (**Figure 1C**). Homology analysis demonstrated that miR-10c shared high homology with the miR-10/miR-10a family from vertebrates and invertebrates with 2 nt of difference at positions of 4 and 17 (**Figure 1D**), and it was named after Lva-miR-10b following the principles presented in Ambros's study (28). The phylogenetic tree also revealed that miR-10c was located at the distinct evolutionary branch from the analyzed miR-10, miR-10a, and miR-10b (**Figure 1E**). These results suggested that miR-10c could be a novel identified miRNA from the miR-10 family of *L. vannamei*.

The Distribution of miR-10c in *L. vannamei*

The expression level of miR-10c in 12 tissues of *L. vannamei* was detected by stem-loop qRT-PCR (**Figure 2A**). Results showed that miR-10c could be detected in all examined tissues, with the lowest expression level in hemocyte. The level of miR-10c in heart, pyloric cecum, gill, intestine, epithelium, stomach, hepatopancreas, and eyestalk was 2.75-, 4.71-, 5.98-, 8.77-, 10.13-, 14.94-, and 16.78-fold over that in hemocyte, respectively. MiR-10c was highly expressed in scape, muscle, and nerve, which was 22.63-, 39.95-, and 41.93-fold over that in hemocyte. The results were further verified by Northern blot (**Figure 2B**). Besides, results of *in situ* hybridization showed that the expression of miR-10c, mainly detected in cytoplasm, was visually higher in hepatopancreas than in gill (**Figure 2C**). As a positive control, the U6 RNA was mainly detected in the nucleus.

Expression Profiles of miR-10c After Immune Stimulation

The expression profiles of miR-10c in gill and hepatopancreas were detected after the injection of WSSV, *V. parahaemolticus*, LPS, and poly(I:C) (**Figures 3A, B**). The expression of miR-10c was slightly and irregularly changed in both gill and hepatopancreas after PBS injection. Upon WSSV stimulation, compared with the PBS control at the same time points, miR-10c was significantly upregulated to 1.43-, 2.51-, 2.09-, 1.49-, 2.28-, and 2.71-fold at 4, 12, 24, 48, 72, and 96 h postinjection (hpi) in gill, respectively, while it was periodical upregulated in hepatopancreas with the two peaks of 2.88- and 2.46-fold at 48 and 96 hpi, respectively. Similar to WSSV, the viral mimic poly(I:C) significantly upregulated the expression of miR-10c in gill during the later period of stimulation, which reached to the peak of 2.03-fold at 96 hpi, however, it showed no solid activatory effect on miR-10c expression in hepatopancreas except a peak of 2.98-fold at

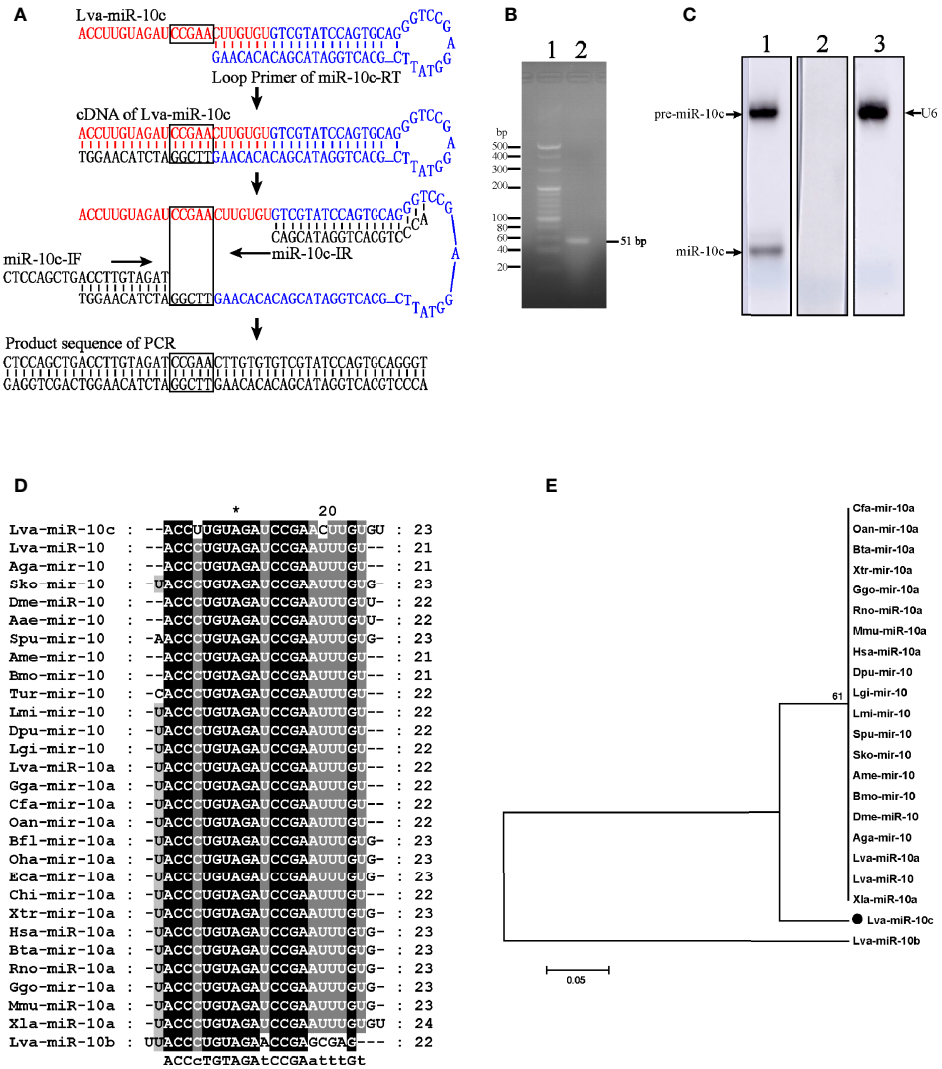

FIGURE 1 | Identification and homology analysis of Lva-miR-10c. **(A)** Schematic diagram of the verification of miR-10c by stem-loop RT-PCR. The mature miR-10c and stem-loop primer were marked in red and blue, respectively. The base pairs for identification were framed. **(B)** Electrophoresis of the stem-loop RT-PCR product. Lane 1, 20 bp DNA ladder; lane 2, the PCR product. **(C)** Northern blot analysis of miR-10c in total RNA of *L. vannamei*. Lane 1, miR-10c-specific probe; lane 2, scrambled probe; lane 3, U6-specific probe. **(D)** Multiple sequence alignment of miR-10 homologs. **(E)** Phylogenetic tree of miR-10 homologs. Sequences analyzed include *L. vannamei* miRNAs from GenBank: Lva-miR-10c (GenBank Accession No. MZ462071), Lva-miR-10a (MZ462069), and miR-10b (MZ462070) and other miRNAs from miRbase: Lva-miR-10, *L. vannamei* (miRbase Accession No. MIMAT0032193); Aga-miR-10, *Anopheles gambiae* (MIMAT0001497); Sko-mir-10, *Saccoglossus kowalevskii* (MIMAT0004419); Lgi-mir-10, *Lottia gigantea* (MIMAT0009563); Dpu-mir-10, *Daphnia pulex* (MIMAT0012636); Lmi-mir-10, *Locusta migratoria* (MIMAT0010144); Aga-mir-10, *Anopheles gambiae* (MIMAT0001497); Spu-mir-10 *Strongylocentrotus purpuratus* (MIMAT0009654); Bmo-mir-10, *Bombyx mori* (MIMAT0004195); Dme-miR-10, *Drosophila melanogaster* (MIMAT0000115); Oan-mir-10a, *Ornithorhynchus anatinus* (MIMAT0007122); Gga-mir-10a, *Gallus gallus* (MIMAT0007731); Cfa-mir-10a, *Canis familiaris* (MIMAT0006737); Hsa-miR-10a, *Homo sapiens* (MIMAT0000253); Xtr-mir-10a, *Xenopus tropicalis* (MIMAT0003557); Mmu-miR-10a, *Mus musculus* (MIMAT0000648); Bta-mir-10a, *Bos taurus* (MIMAT0003786); Rno-miR-10a, *Rattus norvegicus* (MIMAT0000782); Ggo-mir-10a, *Gorilla gorilla* (MIMAT0002486); and *Xla-miR-10a, Xenopus laevis* (MIMAT0046422).

48 hpi. In response to *V. parahaemolticus* (Vpa) infection, the expression of miR-10c in gill and hepatopancreas were generally upregulated and showed diverse expression patterns. It was activated at the late stage in gill and the early stage in hepatopancreas after infection. After the stimulation with LPS, the major pathogen-associated molecular pattern (PAMP) of bacterial pathogens, expression of miR-10c was oscillatorily activated in gill with two peaks of 2.84- and 2.28-fold at 4 and 96 hpi, respectively, which differed from the prolonged activation in hepatopancreas. Similar expression profiles of miR-10c in gill after immune stimulation were verified by Northern blot, which were generally consistent with the results of stem-loop qRT-PCR as mentioned above (**Figure 3C**).

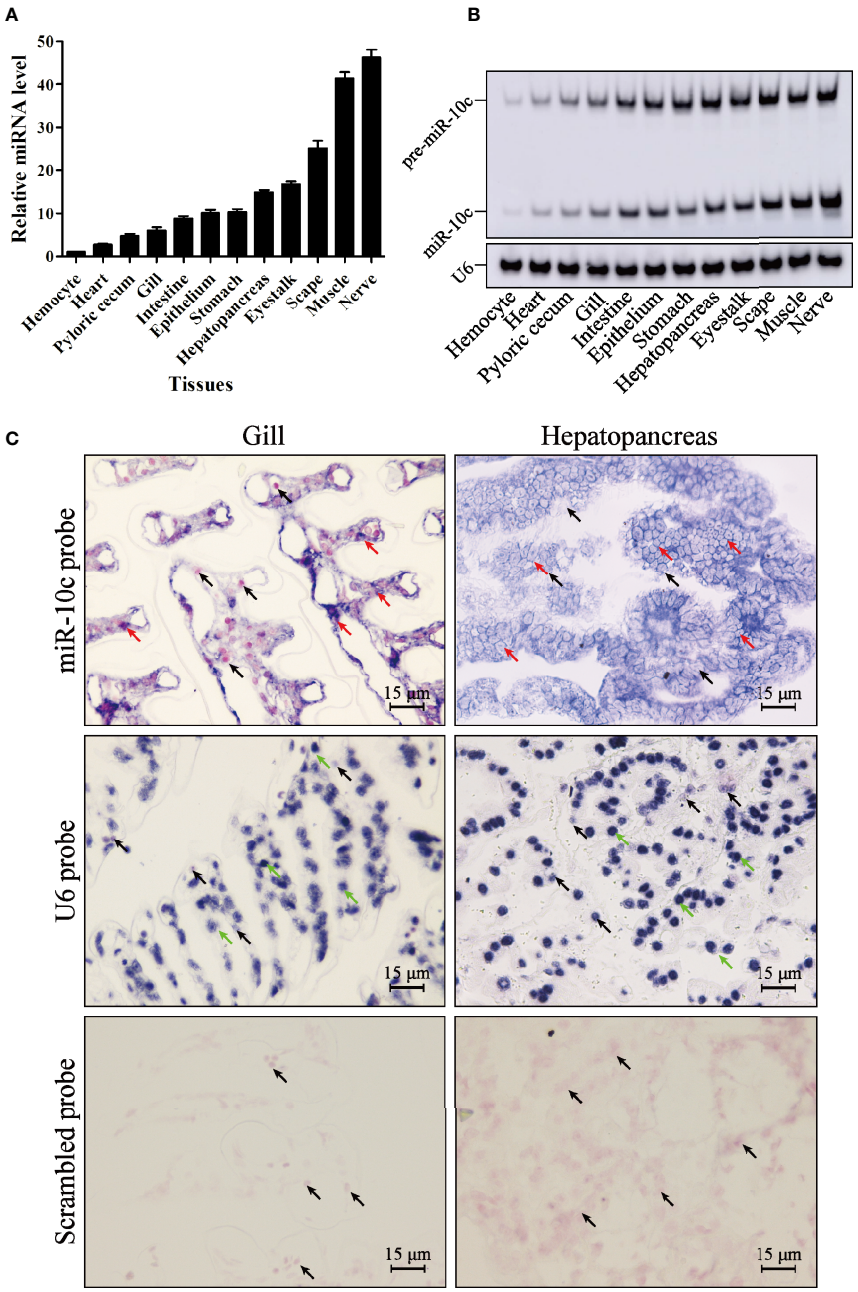

FIGURE 2 | MiR-10c distribution in *L. vannamei* tissues. **(A)** Expression of miR-10c in *L. vannamei* tissues detected by stem-loop qRT-PCR with U6 RNA as internal control. The expression level of miR-10c in hemocyte was set as baseline (1.0). **(B)** The tissue distribution of miR-10c analyzed by Northern blot. **(C)** *In situ* hybridization analysis of miR-10c in hepatopancreas and gill tissues. The signals of miR-10c (red arrows) and U6 RNA (green arrows) were colored dark blue and the nuclei were counterstained red by Nuclear Fast Red (black arrows).

Target Identification of miR-10c

To reveal the regulatory role of miR-10c in immunity, 3′-UTR sequence of many reported genes (**Supplementary File 2**) that play regulatory role in the antiviral immunity of *L. vannaemi* was gathered and formatted as a target database to screen the target site of miR-10c. Results demonstrated that miR-10c was incompletely complementary with the 3′-UTR of LvToll3 mRNA (**Figure 4A**). Dual-luciferase reporter assays proved that miR-10c suppressed the expression level of firefly luciferase, the ORF of which was suffixed with the wild-type 3′-UTR of LvToll3, by 44.8% (**Figure 4B**). Western blot also showed that the protein level of firefly luciferase in the dual-luciferase reporter assay was significantly decreased compared with the control (**Figure 4C**). In contrast, both miR-10c and

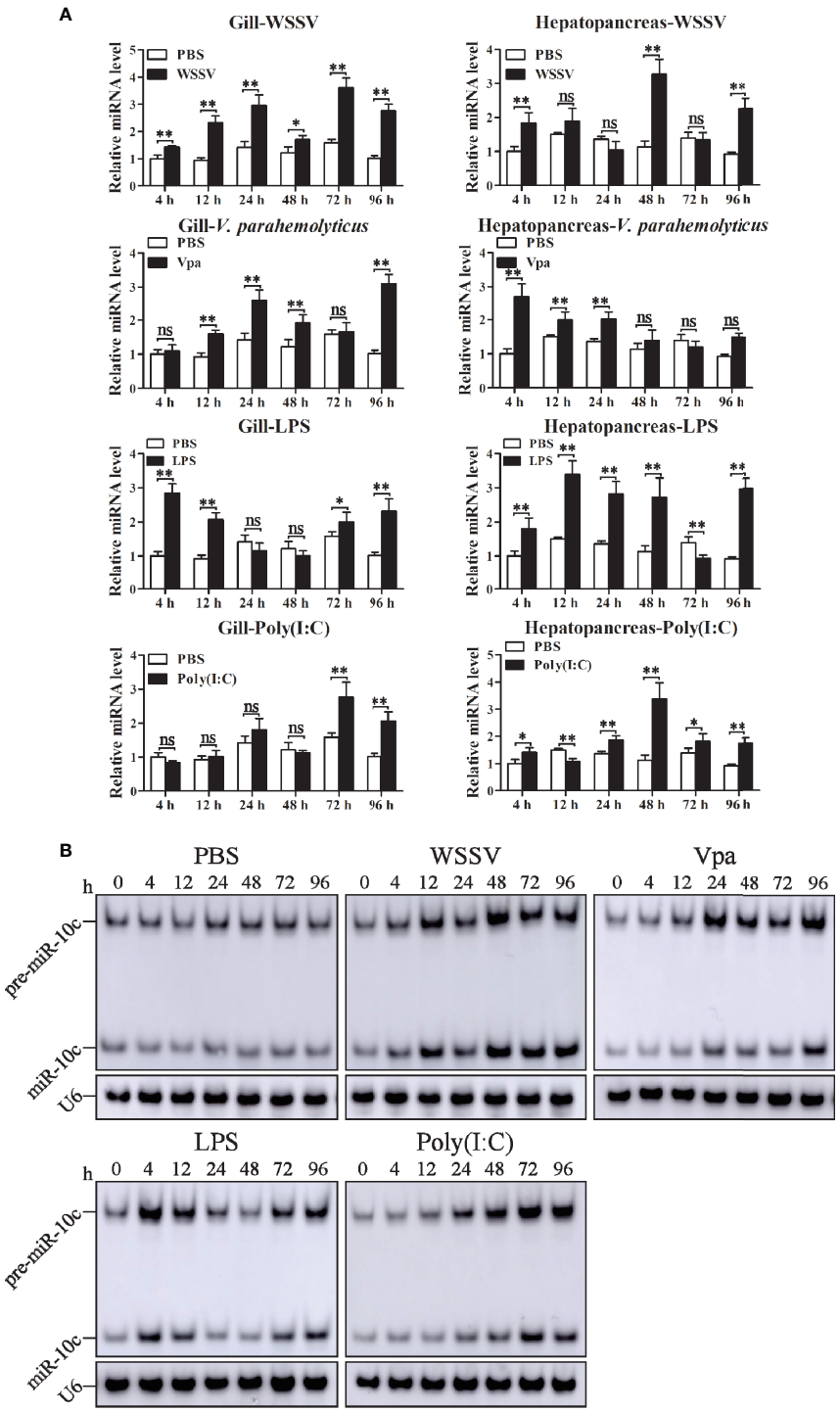

FIGURE 3 | The expression of miR-10c after immune stimulation. **(A)** Stem-loop qRT-PCR analysis of miR-10c expression in gill and hepatopancreas of PBS (negative control), WSSV, *V. parahaemolticus* (Vpa), LPS, and poly(I:C)-stimulated shrimp. The U6 RNA was used as internal control. Data are representative of three experiments and presented as means ± SD of four parallel detections. In each panel, the value at 0 h was set as the baseline (1.0). Each bar represents the mean ± SD (n = 4), $^{*}p < 0.05$, $^{**}p < 0.01$, and ns > 0.05 by one-way ANOVA with Dunnett's *post-hoc* test compared with 0 h. **(B)** Northern blot analysis of miR-10c expression after stimulations in gill. The expression level of miR-10c was detected at 0, 4, 12, 24, 48, 72, and 96 h postinjection of PBS, WSSV, *V. parahaemolticus* (Vpa), LPS, and poly(I:C).

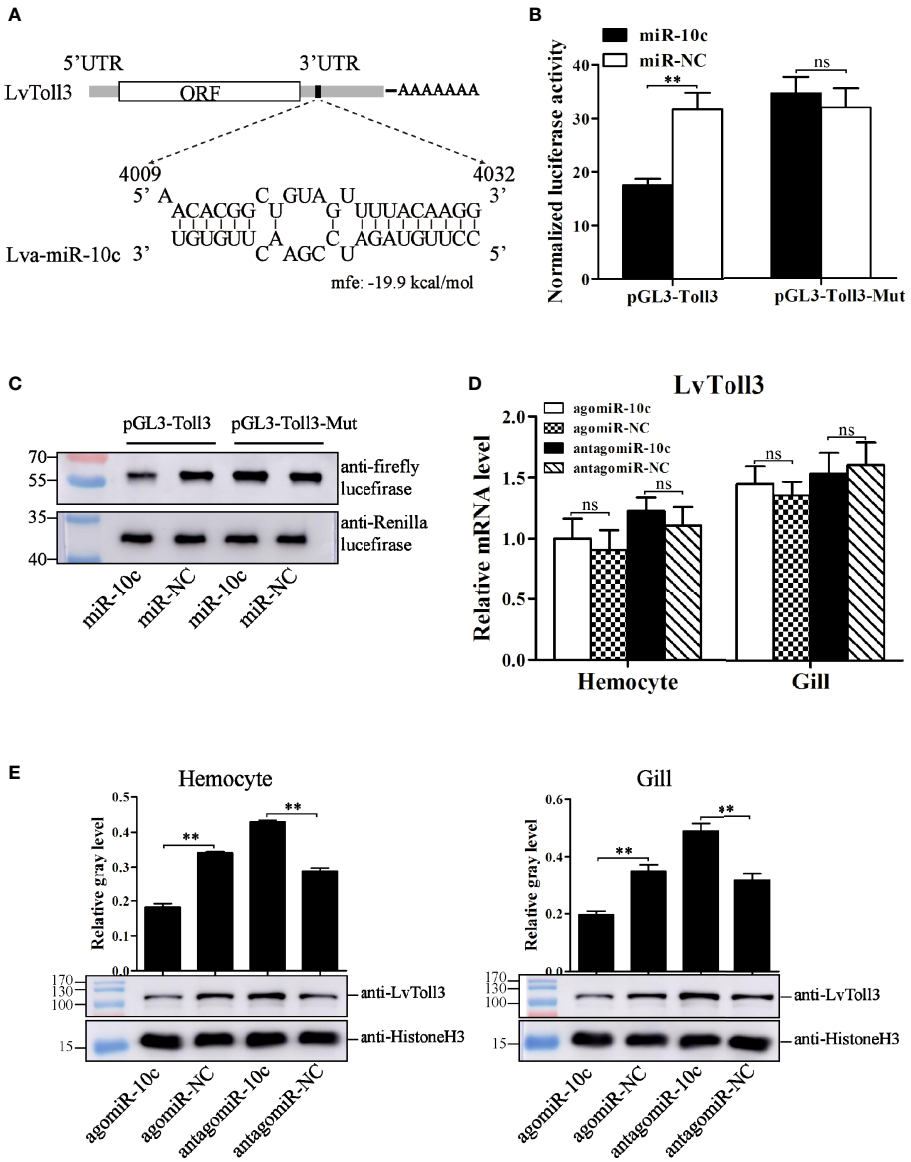

FIGURE 4 | Target identification of miR-10c. **(A)** Scheme of the predicted target site of miR-10c in the 3′-UTR of LvToll3. **(B)** Dual-luciferase reporter assay analysis of the inhibitory effect of miR-10c mimics and its control on the 3′-UTR of LvToll3 and miR-10c binding site-mutated 3′-UTR of LvToll3 (Toll3-Mut). Each bar represents the mean ± SD (n = 8), $^{**}p < 0.01$ and $^{*}p > 0.05$ by two-tailed unpaired Student's t-test. **(C)** Western blot analysis of the protein level of firefly and Rellina luciferases in the cell lysates of the dual-luciferase reporter assay. **(D)** qRT-PCR analysis of the effects of miR-10c mimics (agomiR-10c) and inhibitor (antagomiR-10c) on mRNA level of LvToll3 in hemocyte and gill. Each bar represents the mean ± SD (n = 4), ns > 0.05 by two-tailed unpaired Student's t-test. **(E)** Western blot analysis of the protein level of LvToll3 in hemocyte and gill after treatment with miR-10c mimics and inhibitor in shrimp. The protein level of LvToll3 protein bands were normalized to those of the internal control Histone H3. Each bar is mean ± SD of three independent quantification of the electrophoretic bands, $^{**}p < 0.01$ by two-tailed unpaired Student's t-test.

miR-NC mimics showed no effects on the expression of luciferase suffixed with the miR-10c target mutated 3′-UTR of LvToll3 (Toll3-Mut). To validate the suppression of LvToll3 by miR-10c, shrimp were treated with miR-10c mimics or inhibitor and the expression of LvToll3 was analyzed. As the results demonstrated (**Figures 4D, E**), although the mRNA level of LvToll3 showed no obvious change after treatment with miR-10c mimics/inhibitor both in hemocyte and gill, the protein level of LvToll3 was significantly decreased by 46.5% and 44.0% compared with the control mimics (agomiR-NC) in hemocyte, and increased by 48.9% and 54.7% compared with the control inhibitor (antagomiR-NC) in hemocyte and gill, respectively. These results confirmed that miR-10c could target the LvToll3 gene at posttranscriptional level. To further investigate the correlationship between miR-10c and LvToll3, the protein level of LvToll3 in gill was detected using Western blot after immune

stimulation (**Supplementary Figure S1**). Results showed that expression of LvToll3 was gradually decreased after the PBS injection, which was generally contrary the expression trend of miR-10c (**Figure 3**). However, the expression of LvToll3 was gradually increased after WSSV injection and showed a similar expression trend with that of miR-10c. The opposite expression trend of miR-10c and LvToll3 was only observed at 96 h after the injection of *V. parahaemolyticus*. These imply that the expression of LvToll3 may be regulated by diverse factors more than miR-10c.

Regulatory Effects of miR-10c on the Function of IRF

It had been corroborated that LvToll3 could facilitate the transcription of IRF, a transcription factor with a critical role in antiviral immunity of *L. vannamei* (11). In this study, the relationship between LvToll3 and IRF was further investigated *in vivo*. Shrimps were injected with dsRNA-GFP and dsRNA-Toll3, and 48 h later were further stimulated with poly(I:C). Compared with that in the control group, expression of LvToll3 was significantly downregulated by 61.9% and 73.1% in hemocyte and gill, respectively (**Figure 5A**). After knockdown of LvToll3 and stimulation of poly(I:C), total nuclear protein was isolated from hemocytes and gills and the protein level of IRF was analyzed by Western blot. Results demonstrated that the level of nuclear-translocated IRF, normalized to the nuclear internal control of Histone H3, was significantly decreased by 60.2% and 68.2% in hemocyte and gill compared with the control, respectively (**Figure 5B**). Consistently, the nuclear-translocated IRF was decreased by 44.0% and 80.0% after the treatment of miR-10c mimics in hemocyte and gill compared with the control, respectively (**Figure 5C**). By contrast, the nuclear-translocated IRF was increased by 18.5% and 189.7% after the inhibition of miR-10c in hemocyte and gill, respectively. These results elucidate that miR-10c may attenuate the transcriptional regulatory function of IRF by targeting LvToll3.

The NF-κB pathways are important signaling channels downstream of many Tolls/TLRs in animals. We further explored the regulatory relationship between miR-10c and dorsal, a NF-κB family member in shrimp (**Supplementary Figure S2**). After dorsal silencing in shrimp (**Supplementary Figure 2A**), expression of miR-10c did not change significantly (**Supplementary Figure 2B**). The miR-10c mimics and inhibitors could not affect expression of Dorsal *in vivo* as well (**Supplementary Figure 3C**). These were consistent with a previous study that Dorsal could not be a downstream transcription factor of LvToll3 in shrimp (12).

Roles of miR-10c and LvToll3 in Antiviral Immunity

The above results indicated a regulatory cascade of miR-10c/Toll3/IRF in shrimp. The role of miR-10c and LvToll3 in antiviral immunity was further investigated *in vivo*. The expression of IRF, vago 4/5, and a set of canonical immune effector genes in gill were detected by qRT-PCR. Results demonstrated that the expression of IRF, Vago4/5, ALF2, ALF3, ALF5, CTL2, and CTL5 was decreased by treatment with miR-10c mimics and increased by the inhibition of miR-10c (**Figure 6A**). Notably, it had been validated that the transcription of Vago4/5 can be activated by IRF in *L. vannamei* (13). The effects of miR-10c on the transcription of IRF and Vago4/5 may indicate that miR-10c could suppress the regulatory cascade mediated by IRF.

The role of miR-10c in antiviral immunity was further investigated (**Figures 6B, C**). Comparing with the control mimics, miR-10c mimics significantly increased the cumulative mortality of the WSSV-infected shrimp by 37.9% at 7 days postinfection (dpi) and elevated the virus loads in muscle by 148.4% and 698.6% at 3 and 5 dpi, respectively. On the contrary, comparing with the control inhibitor, miR-10c inhibitor alleviated the virulence of WSSV and decreased the cumulative mortality by 28.1% at 7 dpi and reduced the virus loads in muscle by 79.8% and 80.8% at 3 and 5 dpi, respectively. Consistent with these, after the knockdown of LvToll3, the cumulative mortality was significantly increased by 60% at 9 dpi and the virus loads in muscle were elevated by 339.2% and 914.4% at 3 and 5 dpi compared with GFP control, respectively(**Figures 7A, B**).

miR-10c Regulates the Antiviral Immunity of Shrimp Through Targeting LvToll3

To investigate whether the attenuation of shrimp antiviral immunity by LvmiR-10c is mediated by LvToll3 (**Figures 7C, D**), dsRNA and miRNA mimics were coinjected into shrimp, which were further challenged with WSSV. Results demonstrated that in the control GFP dsRNA-treated group, the cumulative mortality was increased by 54.5% after miR-10c mimic treatment compared with the mimic control. Accordingly, the virus load in muscle was increased by 119.2% and 242.8% at 3 and 5 dpi in the miR-10c mimic treatment group, respectively. In contrast, in the LvToll3-silenced group, there was no significant change of the cumulative mortality of shrimp after miR-10c mimic treatment compared with the mimic control. Although the virus load in the Toll3-dsRNA/miR-10c mimics together-treated shrimp was slightly increased by 18.5% and 10.2% at 3 and 5 dpi compared with the control, respectively, there was no statistically difference between the control and experimental groups. These suggested that LvToll3 is essential for the role of LvmiR-10c in antiviral immunity.

DISCUSSION

At present, more than 23,365 known miRNAs and 481 novel miRNA candidates have been reported in *L. vannamei* in total, several of which are known or predicted to be involved in virus infection, cold or heat adaption, ER stress, and hypoxia stimulation (29–31). Three miR-10 family members have been unveiled in *L. vannamei* (32). Based on the constructed *L. vannamei* miRNA libraries, the current study identified a novel sequence high homologous to miR-10 and miR-10a from other organisms. The two unconserved bases compared with other miR-10 homologs imply that miR-10c is a novel miRNA, which was further confirmed by stem-loop PCR, *in situ* hybridization, and in particular Northern

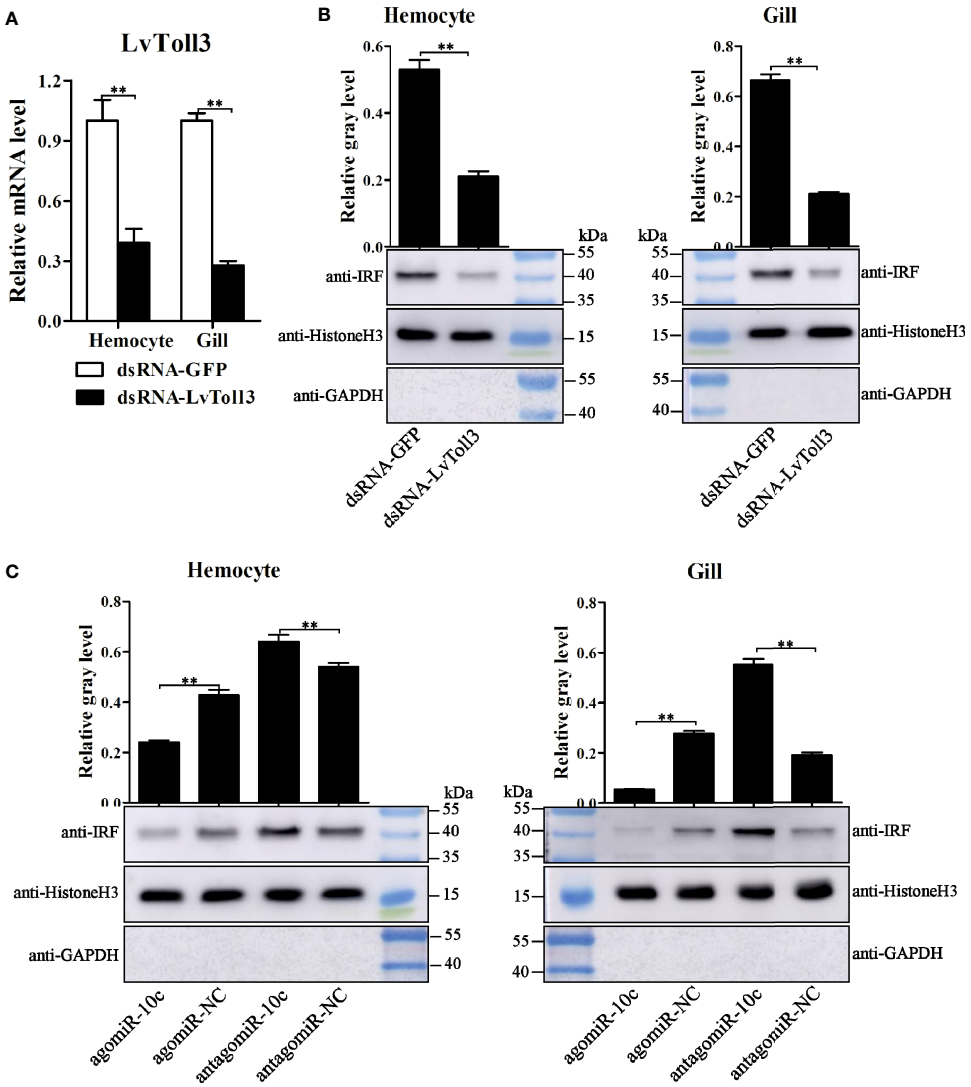

FIGURE 5 | IRF nuclear-translocation regulated by LvToll3 and miR-10c. **(A)** qRT-PCR analysis of the knockdown efficiency of LvToll3. Values in the dsRNA-GFP control group were set as the baseline (1.0). Each bar represents the mean ± SD (n = 4), $^{**}p < 0.01$ by two-tailed unpaired Student's t-test. **(B, C)** Western blot analysis of the nuclear translocation of IRF after treatment with miR-10c mimics/inhibitor *in vivo*. The gray values of IRF (41.0 kDa) bands were normalized to those of the nuclear internal control of Histone H3 (15.4 kDa). GAPDH (35.5 kDa) protein was detected to verify no contamination of cytoplasmic protein. Each bar is mean ± SD of three independent quantification of the electrophoretic bands, $^{**}p < 0.01$ by two-tailed unpaired Student's t-test.

blot, a gold standard for identification of miRNAs. Because the whole genome data of *L. vannamei* are incomplete currently (33), the genomic location of miR-10c has not been determined. In addition, it has been reported that the miRNAs in shrimp could undergo posttranscriptional edition (34). It is worthy of further study to investigate whether miR-10c is also a posttranscriptionally edited product of other miR-10 family members.

Toll/TLRs are a group of most important pattern recognition receptors (PRRs) that recognize invading pathogens to trigger innate immune response in both vertebrates and invertebrates (35, 36). So far, there are nine Toll receptors, named as Toll1–9 in chronological order of identification, found in *L. vannamei* genome. Toll4 had been extensively studied as an important recognition receptor to sense WSSV infection and transduce signals to activate nuclear translocation and phosphorylation of dorsal, ultimately activating the antiviral response in shrimp (37). It has also been reported that expression of Toll1 responded to the *V. alginolyticus* stimulation, and LvToll2 but not LvToll3 could significantly activate the promoters of NF-κB signaling pathway downstream AMP genes in S2 cells (12). The current study also demonstrated that there was no regulatory relationship between dorsal and miR-10c, suggesting that dorsal could not be a downstream transcription factor of the miR-10c-Toll3 signaling. A recent study showed that the *L. vannamei* Toll3 facilitated the transcription of IRF and its regulatory target genes Vago4/5 (11, 12). The IRF/Vago/JAK-STAT axis in shrimp is known to be similar to

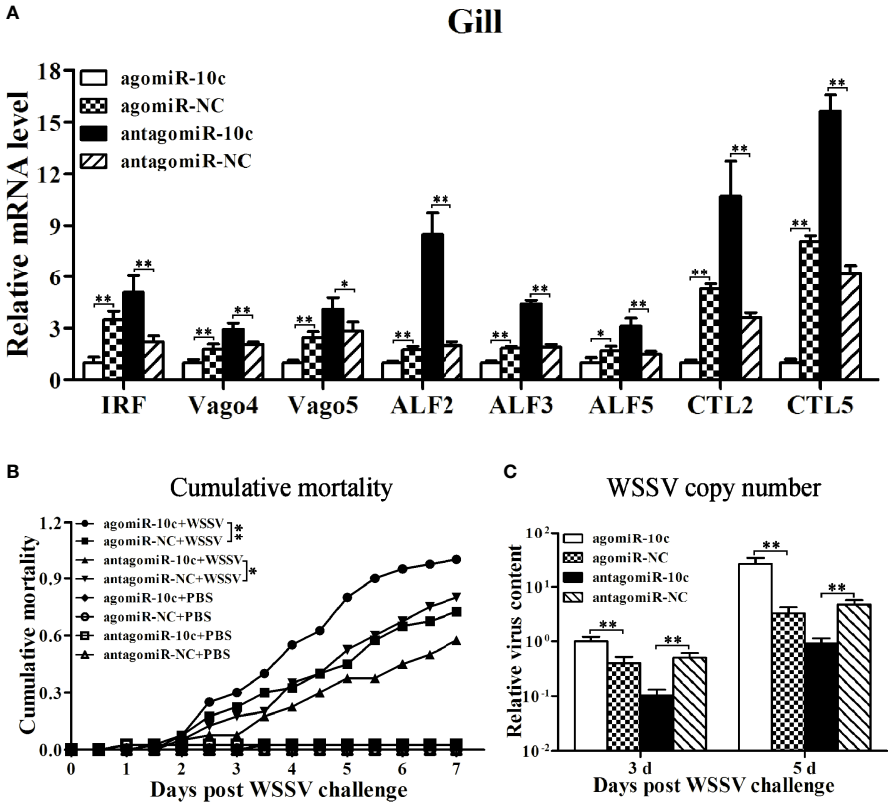

FIGURE 6 | The roles of miR-10c in antiviral immunity. **(A)** qRT-PCR analysis of effects on mRNA level of immune-related genes in gill regulated by miR-10c. Values in the agomiR-10c group were set as the baseline (1.0). Each bar represents the mean ± SD (n = 4), $^{**}p < 0.01$ and $^{*}p < 0.05$ by two-tailed unpaired Student's t-test. **(B)** Cumulative mortality of miR-10c mimics/inhibitor-treated shrimps after WSSV infection. Data were recorded every 4 h and $^{**}p < 0.01$ and $^{*}p < 0.05$ by Kaplan-Meier log-rank χ^2 tests. **(C)** Relative viral copy numbers in muscle analyzed by qRT-PCR with the DNA of *EF1-α* gene as the internal control. The value in agomiR-10c-treated group at 3 days was set as baseline (1.0). Each bar represents the mean ± SD (n = 4), $^{**}p < 0.01$ by two-tailed unpaired Student's t-test.

the interferon system of mammals and also play essential role in antiviral response (10). The connection of LvToll3 with IRF may indicate its involvement in regulation of this regulatory axis. However, the roles of LvToll3 in IRF pathway activation as well as in immune responses against WSSV infection are still unclear. This study further showed that silencing of LvToll3 *in vivo* significantly downregulated the protein level of IRF, confirming the regulatory effect of LvToll3 on the IRF pathway. Furthermore, the LvToll3-silenced shrimp were highly susceptible to WSSV infection compared with the control. These indicated that LvToll3 could enhance the antiviral immunity of shrimp *via* being involved in activation of the IRF/Vago/JAK-STAT axis.

In mammals, the miR-10 family consists of a series of well-studied miRNAs that have attracted more and more attentions because of their conservation and genomic position within the *Hox* clusters of developmental regulators (38, 39). The miR-10 family members are known to be implicated in development of various species, including mammals, fly, and worm, through targeting *Hox* genes (40). Some studies have found that miR-10 family members are de-regulated and play critical regulatory role in the progression of several types of cancers, which is generally related to Hox genes (30, 41). Although several shrimp Hox genes have been identified (**Supplementary File 3**), the localization of the Hox cluster in *L. vannamei* genome has not been determined because of the incomplement of the now available genomic data. The relationship between miR-10c functions and the shrimp Hox cluster is worthy of further investigation.

In contrast with that in other biological processes, the involvement of the miR-10 family in immunity was only concerned in few researches. In mice, the miR-10a targets Prdm1 gene to suppress the production of IL-10 in $CD4^+$ T cells, playing important roles in regulation of intestinal homeostasis and in pathogenesis of autoimmune diseases (42). The parasites *Taenia solium* and *T. crassiceps* produce an abundance of miR-10-5p, which is important for establishment of immunosuppressive mechanisms in the host by acting on host cells to regulate expression of proinflammatory cytokines in macrophages M(IFN-γ) and anti-inflammatory cytokines in macrophages M(IL-4) (43). As the novel identified miRNA, miR-10c has a base different from known miR-10 and miR-10a in the seed region, and its targeting genes may be different from those of miR-10. The current study identified LvToll3 as a target of miR-10c, suggesting its involvement in innate immune responses. We showed that miR-10c could directly downregulate the expression of LvToll3 and also

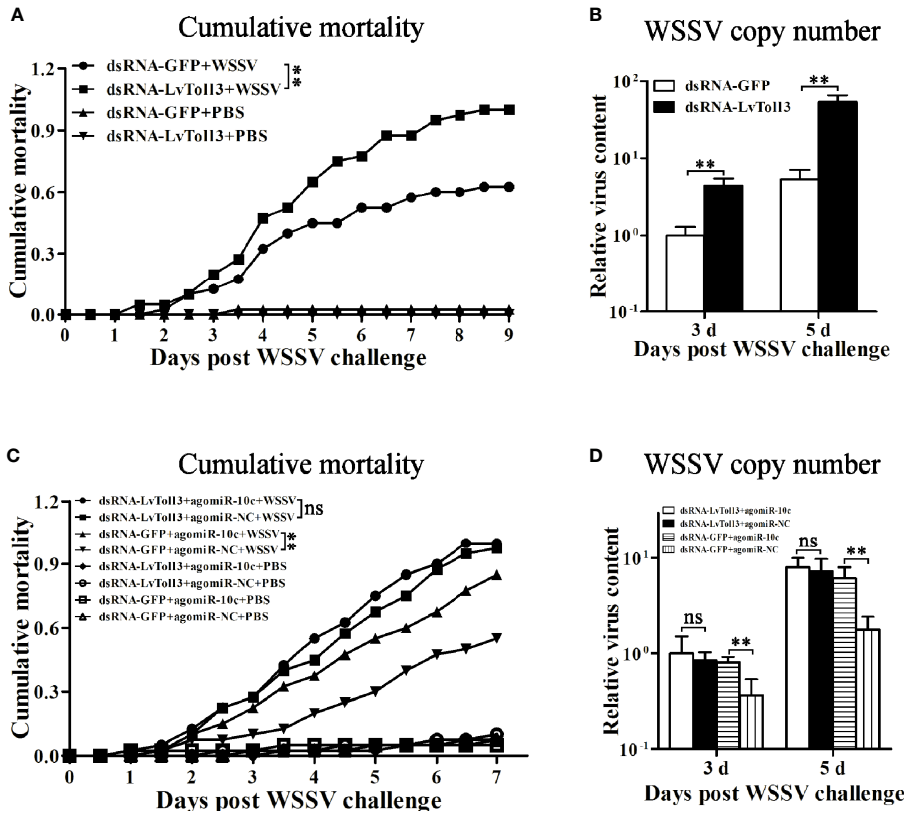

FIGURE 7 | Validation of LvToll3-mediated antiviral immunity regulated by miR-10c. **(A)** Cumulative mortality of LvToll3-knockdown shrimps after WSSV infection. Data were recorded every 4 h and $^{**}p < 0.01$ by Kaplan-Meier log-rank χ^2 tests. **(B)** Relative viral copy numbers in muscle were analyzed by qRT-PCR with the DNA of *EF1-α* gene as the internal control. The value in agomiR-10c treated group at 3 days was set as baseline (1.0). Each bar represents the mean ± SD ($n = 4$), $^{**}p < 0.01$ by two-tailed unpaired Student's *t*-test. **(C)** Cumulative mortality of dsRNA- and miRNA mimic-coinjected shrimps after WSSV infection. Data were recorded every 4 h and $^{**}p < 0.01$ and ns > 0.05 by Kaplan-Meier log-rank χ^2 tests. **(D)** Relative viral copy numbers in muscle analyzed by qRT-PCR with the DNA of *EF1-α* gene as the internal control. The value in LvToll3 dsRNA and miR-10c mimic-coinjected group at 3 days was set as baseline (1.0). Each bar represents the mean ± SD ($n = 4$), $^{**}p < 0.01$ by two-tailed unpaired Student's *t*-test.

significantly influence the nuclear translocation of IRF. These indicated that miR-10c was involved in the regulation of the IRF/Vago/JAK-STAT regulatory axis and may play a role in immune response against virus infection. The supporting evidence was from the qPCR results showing that miR-10c exerted regulatory effects on expression of immune effector genes, such as several AMPs and C-type lectins with antiviral activities. More importantly, miR-10c could also regulate the expression of IRF and Vago 4/5, the central components of the IRF/Vago/JAK-STAT axis (13, 23), confirming the important role of miR-10c in the LvToll3-IRF signaling cascade. Further analyses demonstrated that miR-10c could promote WSSV infection in shrimp, which was consistent with the result of LvToll3 silencing *in vivo*. However, compared with the control, the effects of miR-10c on WSSV infection were abolished by silencing of LvToll3. These confirmed that miR-10c could negatively regulate the antiviral response in shrimp by targeting LvToll3. To further explore the role of miR-10c in immunity, other target genes of miR-10c require to be identified. In addition, it has been reported that the *L. vannmei* miR-10a could be annexed by WSSV to directly target the 5′-UTRs of vp26, vp28, and wssv102 genes of WSSV to enhance the translocation of viral proteins (44). To further explore the role of miR-10c in WSSV infection, whether miR-10c could target WSSV genes is also worth in-depth investigations.

Taken together, the current study identified a novel miR-10 family member in *L. vannamei*, a target of which was determined as Toll3 receptor. Through modulating the Toll3-IRF signaling, miR-10c could play a role in maintenance of immune homeostasis to avoid overactivation of immune responses. However, miR-10c also attenuated the antiviral defense to promote WSSV infection, which could contribute to the pathogenesis of white spot syndrome, thus may serve as a potential target for preventing WSSV infection.

DATA AVAILABILITY STATEMENT

The datasets presented in this study can be found in online repositories. The names of the repository/repositories and

accession number(s) can be found below: https://www.ncbi.nlm.nih.gov/genbank/, MZ462071 https://www.ncbi.nlm.nih.gov/genbank/, MZ462069 https://www.ncbi.nlm.nih.gov/genbank/, MZ462070.

AUTHOR CONTRIBUTIONS

XX and JH supervised the overall project and designed the experiments. HZ wrote the manuscript, performed the experiments, and analyzed data with the help from XL, ML, LY, and SW. All authors contributed to the article and approved the submitted version.

FUNDING

This work was funded by the National Natural Science Foundation of China under grant Nos. 31972823, 31772881, and 32073004; Natural Science Foundation of Guangdong Province, China 2020A1515011152 and 2021A1515010539; National Key Research and Development Program of China 2018YFD0900505; China Agriculture Research System CARS48; and Key-Area Research and Development Program of Guangdong Province, China 2019B020217001, Science and Technology Planning Project of Guangdong Province of China, 2018A050506027.

SUPPLEMENTARY MATERIAL

The Supplementary Material for this article can be found online at: https://www.frontiersin.org/articles/10.3389/fimmu.2021.733730/full#supplementary-material

Supplementary File 1 | Differentially expressed miRNAs after WSSV infection in *L. vannamei*.

Supplementary File 2 | 3′-UTR sequences of screened genes for miR-10 targets.

Supplementary File 3 | Hox homologs identified in *L. vannamei*.

Supplementary Figure 1 | Western blot analysis of the protein level of LvToll3 after PBS, WSSV, and *V. parahaemolticus* injections, respectively. The protein levels of LvToll3 were normalized to those of the internal control Histone H3. Each bar is mean ± SD of three independent quantification of the electrophoretic bands, $^{**}p < 0.01$ and $^{*}p < 0.05$ by two-tailed unpaired Student's *t*-test.

Supplementary Figure 2 | Regulatory relationship between miR-10c and dorsal. **(A)** qRT-PCR analysis of the knockdown efficiency of dorsal. **(B)** Stem-loop qRT-PCR analysis of miR-10c expression in hemocyte and gill after the knockdown of dorsal. Values in the dsRNA-GFP control group were set as the baseline (1.0). Each bar represents the mean ± SD ($n = 4$), $^{**}p < 0.01$ by two-tailed unpaired Student's *t*-test. **(C)** Western blot analysis of dorsal expression in hemocyte and gill after treatment with miR-10c mimics and inhibitor in shrimp. The protein levels of dorsal protein were normalized to those of the internal control Histone H3. Each bar is mean ± SD of three independent quantifications of the bands, $^{**}p < 0.01$ and $^{*}p < 0.05$ by two-tailed unpaired Student's *t*-test.

REFERENCES

1. Kumar H, Kawai T, Akira S. Pathogen Recognition by the Innate Immune System. *Int Rev Immunol* (2011) 30:16–34. doi: 10.3109/08830185.2010.529976
2. Creagh EM, O'Neill LA. TLRs, NLRs and RLRs: A Trinity of Pathogen Sensors That Co-Operate in Innate Immunity. *Trends Immunol* (2006) 27:352–57. doi: 10.1016/j.it.2006.06.003
3. Areal H, Abrantes J, Esteves PJ. Signatures of Positive Selection in Toll-Like Receptor (TLR) Genes in Mammals. *BMC Evol Biol* (2011) 11:368. doi: 10.1186/1471-2148-11-368
4. Vidya MK, Kumar VG, Sejian V, Bagath M, Krishnan G, Bhatta R. Toll-Like Receptors: Significance, Ligands, Signaling Pathways, and Functions in Mammals. *Int Rev Immunol* (2018) 37:20–36. doi: 10.1080/08830185.2017.1380200
5. Couillault C, Pujol N, Reboul J, Sabatier L, Guichou JF, Kohara Y, et al. TLR-Independent Control of Innate Immunity in Caenorhabditis Elegans by the TIR Domain Adaptor Protein TIR-1, an Ortholog of Human SARM. *Nat Immunol* (2004) 5:488–94. doi: 10.1038/ni1060
6. Leclerc V, Reichhart JM. The Immune Response of Drosophila Melanogaster. *Immunol Rev* (2004) 198:59–71. doi: 10.1111/j.0105-2896.2004.0130.x
7. Russo R, Chiaramonte M, Matranga V, Arizza V. A Member of the Tlr Family Is Involved in dsRNA Innate Immune Response in Paracentrotus Lividus Sea Urchin. *Dev Comp Immunol* (2015) 51:271–77. doi: 10.1016/j.dci.2015.04.007
8. Kumar H, Kawai T, Akira S. Pathogen Recognition in the Innate Immune Response. *Biochem J* (2009) 420:1–16. doi: 10.1042/BJ20090272
9. Li C, Wang S, He J. The Two NF-KappaB Pathways Regulating Bacterial and WSSV Infection of Shrimp. *Front Immunol* (2019) 10:1785. doi: 10.3389/fimmu.2019.01785
10. Li C, Weng S, He J. WSSV-Host Interaction: Host Response and Immune Evasion. *Fish Shellfish Immunol* (2019) 84:558–71. doi: 10.1016/j.fsi.2018.10.043
11. Guanzon D, Maningas M. Functional Elucidation of LvToll 3 Receptor From P. Vannamei Through RNA Interference and Its Potential Role in the Shrimp Antiviral Response. *Dev Comp Immunol* (2018) 84:172–80. doi: 10.1016/j.dci.2018.01.020
12. Wang PH, Liang JP, Gu ZH, Wan DH, Weng SP, Yu XQ, et al. Molecular Cloning, Characterization and Expression Analysis of Two Novel Tolls (LvToll2 and LvToll3) and Three Putative Spatzle-Like Toll Ligands (LvSpz1-3) From Litopenaeus Vannamei. *Dev Comp Immunol* (2012) 36:359–71. doi: 10.1016/j.dci.2011.07.007
13. Li C, Li H, Chen Y, Chen Y, Wang S, Weng SP, et al. Activation of Vago by Interferon Regulatory Factor (IRF) Suggests an Interferon System-Like Antiviral Mechanism in Shrimp. *Sci Rep* (2015) 5:15078. doi: 10.1038/srep15078
14. McDaneld TG. MicroRNA: Mechanism of Gene Regulation and Application to Livestock. *J Anim Sci* (2009) 87:E21–8. doi: 10.2527/jas.2008-1303
15. Bushati N, Cohen SM. microRNA Functions. *Annu Rev Cell Dev Biol* (2007) 23:175–205. doi: 10.1146/annurev.cellbio.23.090506.123406
16. Feng Y, Zhang X, Graves P, Zeng Y. A Comprehensive Analysis of Precursor microRNA Cleavage by Human Dicer. *RNA* (2012) 18:2083–92. doi: 10.1261/rna.033688.112
17. Kim Y, Kim VN. MicroRNA Factory: RISC Assembly From Precursor microRNAs. *Mol Cell* (2012) 46:384–86. doi: 10.1016/j.molcel.2012.05.012
18. Wang HW, Noland C, Siridechadilok B, Taylor DW, Ma E, Felderer K, et al. Structural Insights Into RNA Processing by the Human RISC-Loading Complex. *Nat Struct Mol Biol* (2009) 16:1148–53. doi: 10.1038/nsmb.1673
19. Gantier MP. New Perspectives in MicroRNA Regulation of Innate Immunity. *J Interferon Cytokine Res* (2010) 30:283–89. doi: 10.1089/jir.2010.0037
20. Momen-Heravi F, Bala S. miRNA Regulation of Innate Immunity. *J Leukoc Biol* (2018) 103:1205–17. doi: 10.1002/JLB.3MIR1117-459R
21. Zuo H, Yuan J, Chen Y, Li S, Su Z, Wei E, et al. A MicroRNA-Mediated Positive Feedback Regulatory Loop of the NF-kappaB Pathway in Litopenaeus Vannamei. *J Immunol* (2016) 196:3842–53. doi: 10.4049/jimmunol.1502358
22. Zuo H, Weng K, Luo M, Yang L, Weng S, He J, et al. A MicroRNA-1-Mediated Inhibition of the NF-kappaB Pathway by the JAK-STAT Pathway in the Invertebrate Litopenaeus Vannamei. *J Immunol* (2020) 204:2918–30. doi: 10.4049/jimmunol.2000071

23. Yan M, Li C, Su Z, Liang Q, Li H, Liang S, et al. Identification of a JAK/STAT Pathway Receptor Domeless From Pacific White Shrimp Litopenaeus Vannamei. *Fish Shellfish Immunol* (2015) 44:26–32. doi: 10.1016/j.fsi.2015.01.023
24. Gao L, Zuo H, Liu K, Li H, Zhong G. A New Strategy for Identification of Highly Conserved microRNAs in Non-Model Insect, Spodoptera Litura. *Int J Mol Sci* (2012) 13:612–27. doi: 10.3390/ijms13010612
25. Livak KJ, Schmittgen TD. Analysis of Relative Gene Expression Data Using Real-Time Quantitative PCR and the 2(-Delta Delta C(T)) Method. *Methods* (2001) 25:402–08. doi: 10.1006/meth.2001.1262
26. Zuo H, Li H, Wei E, Su Z, Zheng J, Li C, et al. Identification and Functional Analysis of a Hemolin Like Protein From Litopenaeus Vannamei. *Fish Shellfish Immunol* (2015) 43:51–9. doi: 10.1016/j.fsi.2014.12.004
27. Rehmsmeier M, Steffen P, Hochsmann M, Giegerich R. Fast and Effective Prediction of microRNA/Target Duplexes. *RNA* (2004) 10:1507–17. doi: 10.1261/rna.5248604
28. Ambros V, Bartel B, Bartel DP, Burge CB, Carrington JC, Chen X, et al. A Uniform System for microRNA Annotation. *RNA* (2003) 9:277–79. doi: 10.1261/rna.2183803
29. He P, Wei P, Zhang B, Zhao Y, Li Q, Chen X, et al. Identification of microRNAs Involved in Cold Adaptation of Litopenaeus Vannamei by High-Throughput Sequencing. *Gene* (2018) 677:24–31. doi: 10.1016/j.gene.2018.07.042
30. Shekhar MS, Karthic K, Kumar KV, Kumar JA, Swathi A, Hauton C, et al. Comparative Analysis of Shrimp (Penaeus Vannamei) miRNAs Expression Profiles During WSSV Infection Under Experimental Conditions and in Pond Culture. *Fish Shellfish Immunol* (2019) 93:288–95. doi: 10.1016/j.fsi.2019.07.057
31. Wang W, Zhong P, Yi JQ, Xu AX, Lin WY, Guo ZC, et al. Potential Role for microRNA in Facilitating Physiological Adaptation to Hypoxia in the Pacific Whiteleg Shrimp Litopenaeus Vannamei. *Fish Shellfish Immunol* (2019) 84:361–69. doi: 10.1016/j.fsi.2018.09.079
32. Peterson KJ, Su YH, Arnone MI, Swalla B, King BL. MicroRNAs Support the Monophyly of Enteropneust Hemichordates. *J Exp Zool B Mol Dev Evol* (2013) 320:368–74. doi: 10.1002/jez.b.22510
33. Zhang X, Yuan J, Sun Y, Li S, Gao Y, Yu Y, et al. Penaeid Shrimp Genome Provides Insights Into Benthic Adaptation and Frequent Molting. *Nat Commun* (2019) 10:356. doi: 10.1038/s41467-018-08197-4
34. Cui Y, Huang T, Zhang X. RNA Editing of microRNA Prevents RNA-Induced Silencing Complex Recognition of Target mRNA. *Open Biol* (2015) 5:150126. doi: 10.1098/rsob.150126
35. Wang Y, Zhang S, Li H, Wang H, Zhang T, Hutchinson MR, et al. Small-Molecule Modulators of Toll-Like Receptors. *Acc Chem Res* (2020) 53:1046–55. doi: 10.1021/acs.accounts.9b00631
36. Fitzgerald KA, Kagan JC. Toll-Like Receptors and the Control of Immunity. *Cell* (2020) 180:1044–66. doi: 10.1016/j.cell.2020.02.041
37. Li H, Yin B, Wang S, Fu Q, Xiao B, Lu K, et al. RNAi Screening Identifies a New Toll From Shrimp Litopenaeus Vannamei That Restricts WSSV Infection Through Activating Dorsal to Induce Antimicrobial Peptides. *PloS Pathog* (2018) 14:e1007109. doi: 10.1371/journal.ppat.1007109
38. Enright AJ, John B, Gaul U, Tuschl T, Sander C, Marks DS. MicroRNA Targets in Drosophila. *Genome Biol* (2003) 5:R1. doi: 10.1186/gb-2003-5-1-r1
39. Tanzer A, Amemiya CT, Kim CB, Stadler PF. Evolution of microRNAs Located Within Hox Gene Clusters. *J Exp Zool B Mol Dev Evol* (2005) 304:75–85. doi: 10.1002/jez.b.21021
40. Orom UA, Nielsen FC, Lund AH. MicroRNA-10a Binds the 5'UTR of Ribosomal Protein mRNAs and Enhances Their Translation. *Mol Cell* (2008) 30:460–71. doi: 10.1016/j.molcel.2008.05.001
41. Ma L, Teruya-Feldstein J, Weinberg RA. Tumour Invasion and Metastasis Initiated by microRNA-10b in Breast Cancer. *Nature* (2007) 449:682–88. doi: 10.1038/nature06174
42. Yang W, Chen L, Xu L, Bilotta AJ, Yao S, Liu Z, et al. MicroRNA-10a Negatively Regulates CD4(+) T Cell IL-10 Production Through Suppression of Blimp1. *J Immunol* (2021) 207:985–95. doi: 10.4049/jimmunol.2100017
43. Landa A, Navarro L, Ochoa-Sanchez A, Jimenez L. Taenia Solium and Taenia Crassiceps: Mirnomes of the Larvae and Effects of miR-10-5p and Let-7-5p on Murine Peritoneal Macrophages. *Biosci Rep* (2019) 39:1–15. doi: 10.1042/BSR20190152
44. Huang JY, Kang ST, Chen IT, Chang LK, Lin SS, Kou GH, et al. Shrimp miR-10a Is Co-Opted by White Spot Syndrome Virus to Increase Viral Gene Expression and Viral Replication. *Front Immunol* (2017) 8:1084. doi: 10.3389/fimmu.2017.01084

Conflict of Interest: The authors declare that the research was conducted in the absence of any commercial or financial relationships that could be construed as a potential conflict of interest.

Publisher's Note: All claims expressed in this article are solely those of the authors and do not necessarily represent those of their affiliated organizations, or those of the publisher, the editors and the reviewers. Any product that may be evaluated in this article, or claim that may be made by its manufacturer, is not guaranteed or endorsed by the publisher.

frontiers in Immunology

REVIEW
published: 11 January 2022
doi: 10.3389/fimmu.2021.796012

Shaping the Innate Immune Response Through Post-Transcriptional Regulation of Gene Expression Mediated by RNA-Binding Proteins

Anissa Guillemin[1], *Anuj Kumar*[2], *Mélanie Wencker*[1,3] *and Emiliano P. Ricci*[1]*

[1] LBMC, Laboratoire de Biologie et Modelisation de la Cellule, Université de Lyon, ENS de Lyon, Universite Claude Bernard Lyon 1, CNRS, UMR 5239, INSERM, U1293, Lyon, France, [2] CRCL, Centre de Recherche en Cancérologie de Lyon, INSERM U1052, CNRS UMR 5286, Lyon, France, [3] CIRI, Centre International de Recherche en Infectiologie, Université de Lyon, ENS de Lyon, CNRS, UMR 5308, INSERM, Lyon, France

Innate immunity is the frontline of defense against infections and tissue damage. It is a fast and semi-specific response involving a myriad of processes essential for protecting the organism. These reactions promote the clearance of danger by activating, among others, an inflammatory response, the complement cascade and by recruiting the adaptive immunity. Any disequilibrium in this functional balance can lead to either inflammation-mediated tissue damage or defense inefficiency. A dynamic and coordinated gene expression program lies at the heart of the innate immune response. This expression program varies depending on the cell-type and the specific danger signal encountered by the cell and involves multiple layers of regulation. While these are achieved mainly *via* transcriptional control of gene expression, numerous post-transcriptional regulatory pathways involving RNA-binding proteins (RBPs) and other effectors play a critical role in its fine-tuning. Alternative splicing, translational control and mRNA stability have been shown to be tightly regulated during the innate immune response and participate in modulating gene expression in a global or gene specific manner. More recently, microRNAs assisting RBPs and post-transcriptional modification of RNA bases are also emerging as essential players of the innate immune process. In this review, we highlight the numerous roles played by specific RNA-binding effectors in mediating post-transcriptional control of gene expression to shape innate immunity.

Keywords: innate immunity, RNA-binding proteins, RNA, virus, immune cells, post-transcriptional regulation, inflammation, pathogen

OPEN ACCESS

Edited by:
Osamu Takeuchi,
Kyoto University, Japan

Reviewed by:
Yukio Kawahara,
Osaka University, Japan
Guanqun L. Liu,
Cleveland Clinic Florida, United States

***Correspondence:**
Emiliano P. Ricci
emiliano.ricci@ens-lyon.org

Specialty section:
This article was submitted to Molecular Innate Immunity, a section of the journal Frontiers in Immunology

Received: *15 October 2021*
Accepted: *13 December 2021*
Published: *11 January 2022*

Citation:
Guillemin A, Kumar A, Wencker M and Ricci EP (2022) Shaping the Innate Immune Response Through Post-Transcriptional Regulation of Gene Expression Mediated by RNA-Binding Proteins. Front. Immunol. 12:796012. doi: 10.3389/fimmu.2021.796012

1 INTRODUCTION

Host's defense mechanisms form a complex interplay between molecular and cellular actors and require a plethora of processes to detect and eliminate pathogens or damage, such as loss of tissue integrity, irritants, or cancer. While infection or damage generally occur at barrier sites (at the interface between internal and external milieu), local cells are prone to rapidly sense any tissue dysregulation and to send signals of danger that initiate the innate arm of immune responses. Local

cellular sensors include epithelial cells, stromal cells and fibroblasts, whose role will be essential when being the initial target of infection (in case of strictly intracellular pathogens) or injury (1–4). In addition, resident immune cells, such as macrophages and dendritic cells (DC), if not directly affected, will be able to detect microbial components within the environment, or capture damaged cellular material leading to their subsequent activation (5). Sensing of damage leads to a cascade of events that generate a local inflammation, thus allowing the recruitment of circulating innate cells (*e.g.* neutrophils or circulating monocytes/macrophages), phagocytosis of infected/damaged cells and antigen presentation to T- and B- lymphocytes, the adaptive arm of immune response. In that regard, innate immune responses are crucial for the generation of a robust, antigen-specific adaptive response, and the maintenance of memory (6, 7).

At the molecular level, innate responses thus start with the recognition of danger. This is allowed by the expression of a set of receptors, called Pattern Recognition Receptors (PRRs), each being specific for classes of molecules known as Pathogen Associated Molecular Patterns (PAMPs) or Damage Associated Molecular Pattern (DAMPs) (8). Essentially all cells express a set of PRRs, the most common families being Toll-like receptors (TLRs), RIG-I-like receptors (RLRs), NOD-like receptors (NLRs) or cGAS (9). PRRs can be discriminated according to their specificity (*e.g.* double-stranded (ds) or single-stranded (ss) RNA, dsDNA, peptides…), or their location (*e.g.* cytosol, mitochondria, extracellular domains). Upon ligand binding, each family of PRRs recruits a specific adaptor such as myeloid differentiation primary response 88 (MyD88), mitochondrial antiviral signaling protein (MAVS) or stimulator of interferon genes (STING) for TLRs, RLRs or cGAS, respectively (**Figure 1A**). This initiates a signaling cascade, mostly involving IRF3/7, MAPK and NFκB pathways, ultimately leading to the expression of type I and III IFN (10, 11) and/or the secretion of cytokines, that orchestrate the various events happening during the inflammation process (12, 13), or chemokines, that will attract immune cells to the affected tissue. Depending on many parameters such as the nature of the activating signals or the timing, cytokines produced are either pro-inflammatory (*e.g.* TNF-α, IL-6, IL-1β, *etc*…), or anti-inflammatory (*e.g.* IL-4, IL-10, IL-13, IFN-α, *etc*…) (14, 15), even though this dichotomy has been shown to be realistically less simple (16).

Altogether, innate immunity plays an essential role during immune responses: guardian of tissue integrity, local cells act as a communication platform to detect, alert and, at least partially, eliminate infection or damage. However, the complex underlying program of innate responses has to be tightly regulated to avoid any hazardous effect. Indeed, overexpression of inflammatory components can damage the host (*e.g.* intolerance, auto-immunity), whereas their under-expression leads to an inefficient defense strategy (17, 18). This highlights the necessity of a rapid and efficient innate response, balanced with appropriate transcriptional and post-transcriptional regulations that finely tune the underlying gene expression program. While transcriptional regulation clearly plays a major role during inflammation and has been widely studied as a model for cell stimulation (19, 20), post-transcriptional control more recently emerged as indispensable to properly tune the innate response (21–23).

RNA-Binding Proteins (RBPs) are key effectors of post-transcriptional regulatory processes (24–26) by targeting specific sequences, structures or post-transcriptional chemical modifications occurring on RNA bases, such as N^6-methyladenosine (m^6A). Altogether, RBPs act at all steps of the life of RNAs: pre-RNA processing (5' RNA capping, splicing, polyadenylation and base editing), mRNA transport, ribosome biogenesis, translation, and finally RNA decay (27–29). In line with this, recent system-wide analyses have revealed the importance of the RNA binding proteome (RBPome) during viral infections (30, 31) and activation of cells of the innate immune system (32). More recently, the global analysis of RNA–protein interactome has shown that a third of the RBPome is remodeled upon SARS-COV-2 infection in human cells, highlighting the importance of targeting RBPs for therapeutic strategies against COVID-19 (33, 34).

Here, we review the multiple roles played by RBPs in shaping the innate immune response, from pathogen and danger detection to the regulation of signal transduction and effector functions.

2 TECHNICAL APPROACHES TO STUDY RBPs

Advances in mass-spectrometry and high-throughput sequencing have substantially increased the list of cellular proteins which are known to interact with RNAs and allowed, for many of them, to identify their precise RNA binding sites. Depending on the biological questions to be addressed, RBP's studies can be performed *via* RNA-centric or protein-centric methods (35). One way to capture protein/RNA interactions is through cross-linking, which creates a covalent bond between the RNA molecule and its associated protein. Different RNA-Protein cross-linking methods exist, each with its own benefits and limitations. In order to identify proteins that interact directly with RNA, irradiation of cells with ultraviolet (UV) light (254nm) is the most commonly used approach, since it irreversibly cross-links amino acid residues to nucleic-acids, without inducing protein-protein covalent bonds. Additionally, the covalent bond created between the amino-acids and RNA bases can provide information related to precise binding site at single-nucleotide resolution (36). However, the efficiency of UV-crosslinking can differ depending on the nature of the amino acids involved in the interaction with RNA bases (37). Furthermore, RBPs that bind to dsRNA structures have been shown to cross-link poorly when exposed to UV radiation due to low accessibility of the RNA bases to the amino acids residues involved in RNA binding (38, 39). Finally, the overall efficiency of RNA/protein cross-linking induced by 254nm UV light is relatively low (5%) (40, 41) and UV light does not penetrate complex tissues or liquid cultures very efficiently, thus limiting its

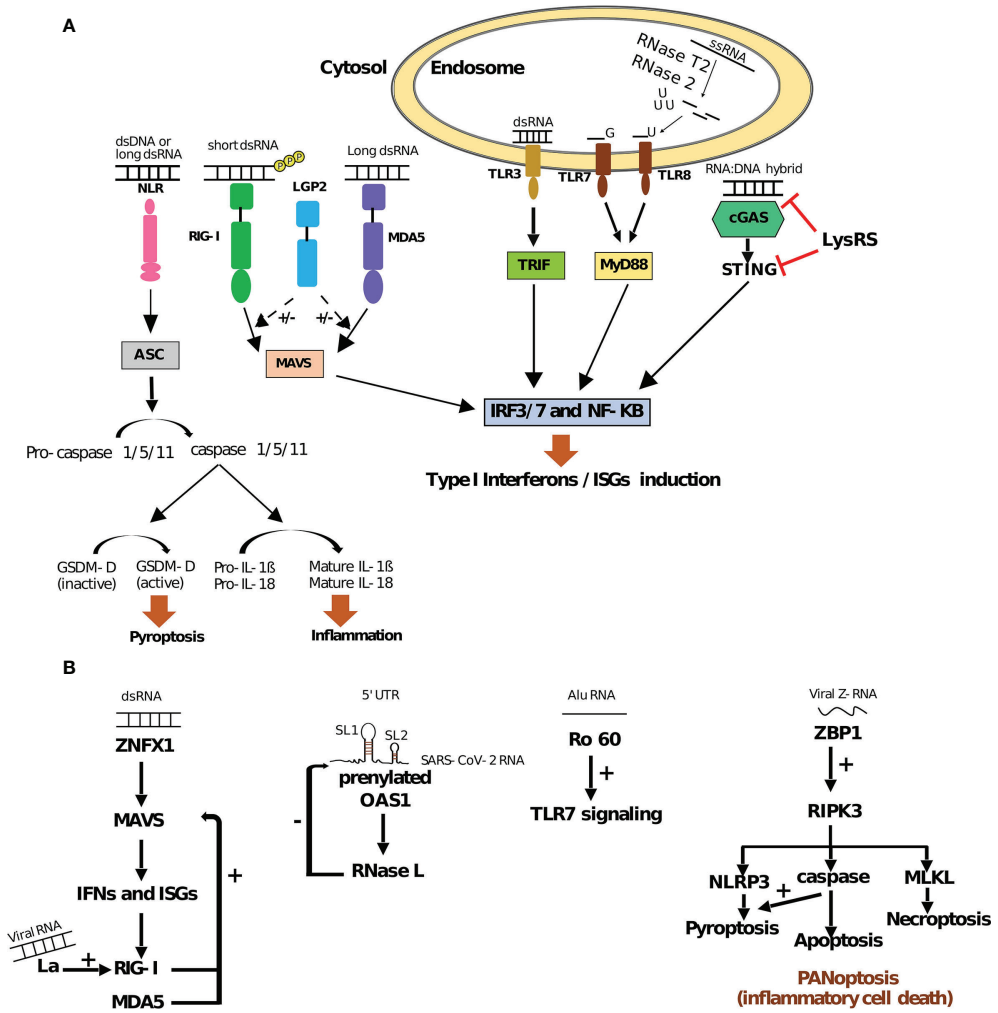

FIGURE 1 | RNA binding PRRs and their regulation **(A)** Innate immune signaling pathways triggered by RNA binding PRRs. Interaction of endosomal TLRs (TLR3, TLR7 and TLR8), cytosolic RLRs (RIG-I and MDA5) and cGAS with different RNA substrates activates IRF3/7 and NFκkB pathway in TRIF/MyD88, MAVS and STING dependent manner, respectively. This activation leads to an induction of ISGs (IFN stimulated genes) as a part of the type I IFN response. On the other hand, NLRs (*e.g.* NLPRP1/3) promote apoptosis speck-like protein (ASC)/caspase-mediated signaling. Caspase-dependent cleavage of Gasdermin-D (GSDM-D) and maturation of pro-IL-1β and pro-IL-18 lead to pyroptosis and inflammation, respectively. All these pathways contribute to developing cellular innate immunity and counteracting the effect of different pathogens. While LGP2 can positively (+) and negatively (–) regulate RIG-I and MDA5 pathways, LysRS inhibits the cGAS-STING pathway (9, 64, 75–77). **(B)** RNA sensing by non-PRR RBPs. Upon dsRNA binding, ZNFX1 driven type I IFN response *via* MAVS leads to the expression of ISGs: RIG-I and MDA5, which autoregulate their expression by a positive feedback loop. In addition, La, an autoantigen, could promote RIG-I induction upon viral RNA binding. Sensing of dsRNA structures containing stem-loops 1 and 2 (SL1 and SL2) within SARS-CoV-2 5'UTR by prenylated OAS1 promotes RNase L mediated degradation of the viral RNA and hence displays negative effect (–) on SARS-CoV-2. Ro60 interaction with Alu RNA elicits innate immunity by positively regulating TLR7 signaling. ZBP1 interaction with viral or host Z-RNA activates NLRP3 signaling by positively regulating RIPK3, which encourages the NLPRP3 pathway directly or *via* caspases. These pathways (along with MLKL mediated necroptosis) lead to PANoptosis or inflammatory cell death (78–85).

use to cell monolayers or requiring dissociation of the tissue prior to UV irradiation (42). Some of the drawbacks of classical 254nm UV cross-linking can be overcome by the use of photoreactive ribonucleoside analogs 4-thiouridine (4SU), or 6-thioguanosine (6-SG). These ribonucleoside analogs are fed to cultured cells, incorporate into nascent transcripts and allow more efficient cross-linking of RNA to proteins following irradiation with long-wavelength UV light (365nm) that also penetrates samples more efficiently than the commonly used short-wavelength UVs (28). Moreover, this method, known as Photoactivatable-Ribonucleoside-Enhanced Crosslinking (PAR-CL), is also able to score the transitions from thymidine (T) to cytidine (C) that occur at cross-linking sites upon reverse-transcription, which are used to identify precisely the RBP binding sites (43). Methylene blue can be an efficient alternative to UV irradiation when studying dsRBPs. It intercalates between RNA bases of a dsRNA structure and allow efficient dsRBP/RNA crosslinking through visible light, thus overcoming the poor cross-linking activity of UV (38, 44). Formaldehyde can also be used to cross-link single-strand and double-strand RBPs to their RNA targets

(39, 45–48). It also has the advantage to be reversible upon incubation of samples at high temperature, which can facilitate RNA recovery and downstream processing such as reverse-transcription. However, formaldehyde cross-linking is not restricted to RNA/proteins but also generates covalent bonds between proteins. As a consequence, ribonucleoprotein complexes can be cross-linked together, therefore making it impossible to discriminate between direct RBPs and non-RBPs that interact indirectly with RNA. Nevertheless, this drawback has been useful in determining the target sites of closely related RNP complexes such as different sub-types of the exon-junction complex (49).

Upon cross-linking, RNA-centric protocols rely on the purification of poly(A) mRNAs (corresponding to protein coding RNAs) (50), total RNA (that gives information on all RNAs including mRNAs and non-coding RNAs such as ribosomal RNA and microRNAs among other) (51), or specific RNA species (52). The RNA purification step is then followed by the identification and quantification of RBPs that were bound to the purified RNAs by mass spectrometry or western-blotting (53). Variations of these protocols combined with purification of poly(A) mRNAs with partial protease treatment have also enabled the characterization of the protein domains that are involved in RNA recognition (54). Altogether, these protocols have allowed the unbiased identification of RBPs in a wide-variety of organisms and biological contexts, but also of new types of RNA recognition domains within RBPs (55, 56). They have also been used to characterize the dynamics of RBP binding to RNA during a wide range of physiological and pathological processes (31, 32). For instance, comparison of the RBPome between resting and LPS-stimulated macrophages uncovered 91 RBPs not previously annotated to interact with RNA. Among identified RBPs, many displayed changes in their RNA-binding capacity upon LPS-stimulation (32). These include the HSP90 co-chaperone P23, which interacts with the mRNA coding for Kinesin 15 (KIF15) (32, 57). Upon macrophage activation, P23 binding to Kif15 mRNA decreases, leading to mRNA destabilization and down-regulation of KIF15 protein abundance, which stimulates macrophage migration (57).

In contrast to RNA-centric approaches, protein centric methods rely on the immuno-purification of a specific RNA-binding protein upon cross-linking (also known as cross-linking immuno-purification or CLIP) followed by RNA-sequencing in order to identify the RNA species bound to the RBP of interest. One can access to the precise RNA sequence where the RBP is binding by coupling immuno-purification with a RNase treatment and small-RNA sequencing (58). Several protocols exist, relying on UV or formaldehyde cross-linking, that allow either the characterization of the RNA-binding sites of isolated RBPs or protein complexes with RNA-binding capacity. Among these protocols, those relying on short and long wave UV crosslinking [such as iCLIP (59), eCLIP (60) and PAR-CLIP (43)] are largely the most frequently used in the literature thanks to their single-nucleotide resolution, availability of commercial kits for sample preparation and development of many data analysis pipelines [some with intuitive graphic user interfaces (61)] that facilitate processing of the sequencing results for non-experts. Furthermore, UV-based CLIP-seq protocols [specifically eCLIP (60)] concentrate most of the efforts made by the Encyclopedia of DNA Elements (ENCODE) project to provide large-scale characterization of the RNA binding sites of hundreds of RBPs in a robust and reproducible manner, providing the scientific community with homogeneous datasets that can be compared across different RBPs and cell types (62). More recently, a CLIP-seq protocol using short laser pulses of UV-light through different time lengths has been able to uncover the *in vitro* kinetics of binding and dissociation of the RBP DAZL to a thousands of RNA targets (e.g. Thbs1 transcript) in a transcriptome-wide manner (63). Once applied to other RBPs, such a protocol could greatly improve our understanding of the biological roles of RBPs and the regulation of their binding and functional activity on their target RNAs.

Altogether, RNA-centric and protein-centric protocols have greatly participated in our understanding of RBPs and their functional role in a myriad of different cellular processes including the innate immune response.

3 RNA SENSING BY CANONICAL PRRs AND OTHER RBPs

While RNAs are essential components of cellular functions, they can also generate protective immune responses as it has been largely described following infection with RNA viruses (*e.g.* Influenza, SARS, Hepatitis, Measles, *etc.*). Although sensing of foreign RNA leads to a substantial and rapid antiviral response, it must be tightly controlled in order to avoid hazardous effects [for extensive review, see (64)]. Similarly, inappropriate host RNA recognition can also occur during several processes such as apoptosis (65) or cancer progression (66), leading to uncontrolled immune responses and/or auto-immunity. The capacity to discriminate between host and foreign RNAs is therefore essential to avoid unsuitable immune responses. PRRs that are specific for RNA components are well-known actors of innate immunity, especially in response to viral infections. They represent, as such, prototypic RBPs. However, several non-canonical PRR RBPs have been recently shown to participate in the sensing and/or regulation of RNA sensing and to have a significant role in modulating innate immunity, as examined below.

3.1 RNA Sensing by Canonical PRRs

Foreign RNAs can display specific features that distinguish them from endogenous RNAs and allow them to trigger an immune response through sensing by PRRs. These features can be linked to their structure, nucleotide composition and chemical modifications, or their subcellular location.

TLR3 was the first PRR described to interact with foreign RNA (67). Among all TLRs, TLR3, TLR7 and TLR8 are able to

recognize RNA substrates under different forms: TLR3 can recognize long dsRNAs, as well as short dsRNAs and structured ssRNAs (>35bp) (68, 69), while TLR7 and TLR8 rely on leucine-rich repeats to detect GU-rich ssRNA species (70) but also by-products of ssRNA degradation including endogenous microRNAs and exogenous siRNAs (71–73). TLR3/7/8 are transmembrane proteins localized within endosomal compartments. RNA sensing through these TLRs therefore requires uptake and endocytosis of extracellular RNAs which generally occurs during viral infection or phagocytosis of necrotic/apoptotic cells (67, 74). This allows a spatial compartmentalization of RNA-binding to TLRs, to avoid any activation by host cell RNAs. Upon activation of TLRs, Toll/IL-1 receptor (TIR) domain-containing adaptor inducing interferon-β (TRIF)-dependent pathway is activated, leading to the phosphorylation of transcription factors such as IFN regulatory factor 3 (IRF3) and IRF7 and their subsequent nuclear translocation. IRF3/7 thus turn on the antiviral response in infected host cells, through specific transactivation of type I IFN genes (see **Figure 1A**). In addition, both TLR7 and TLR8 contain two binding sites that synergize to induce TLR dimerization and activation. One binding site is for small ligands (including guanosine for TLR7 and uridine for TLR8) and one for short oligonucleotides (73, 86). For TLR8, the generation of those specific ligands requires both the endolysosomal endonucleases RNase T2 and RNase 2, each cleaving ssRNA upstream and downstream of uridines, respectively, to generate free uridine and short RNA oligonucleotides (71, 87). For TLR7, the source of guanosine and short nucleotides required for its activation are less well-characterized. RNAse T2 is seemingly required for activation of TLR7 in macrophages (88) and crystallography studies suggest that successive U-containing ssRNA sequences are required for full binding to TLR7 (89). Studies in macrophages moreover suggested that accumulation of nucleosides in the lysosomal compartment upon inactivation of the lysosomal transmembrane protein SLC29A3 (a nucleoside transporter from lysosomes to the cytoplasm) leads to TLR7 activation following phagocytosis of necrotic cells (90). Interestingly, in monocytes, macrophages, and dendritic cells, the accumulation of nucleosides within lysosomes is responsible for inflammatory disorders like histiocytosis, further emphasizing the importance of a tight control of RNA mediated TLR activation (91).

Unlike TLRs, whose expression depends on TLR subtype and cellular subset, retinoic acid-inducible gene I (RIG-I)-like receptors (RLRs) are expressed in most cell types. Located in the cytosol, members of the RLR family include RIG-I, the melanoma differentiation-associated protein 5 (MDA5) and the laboratory of genetics and physiology 2 (LGP2) factors. All three RLRs share a central ATP-dependent helicase domain and a carboxy-terminal domain (CTD), both domains displaying RNA-binding activity. RIG-I and MDA5, but not LGP2, have two additional caspase activation and recruitment domains (CARDs) that are essential for downstream signal transduction through MAVS, upon RNA binding. RIG-I recognizes short dsRNA structures bearing a triphosphate or diphosphate group at their 5' end (5'-PPP or 5'-PP) (92–94) and lacking a methyl group at the 2'-O position of the 5' terminal nucleotide (95). These structural features, present in many viral RNAs, but generally absent in endogenous cytosolic RNAs, allow RIG-I to discriminate between self and non-self RNAs. MDA5 on the other hand preferentially binds long dsRNAs molecules (including the synthetic poly(I:C) molecule), as shown by several reports (96–98).

However as opposed to RIG-I, the molecular determinants of MDA5 binding to foreign RNAs are less well understood. The presence of higher order RNA structures (combination of single-stranded and double-stranded RNA structures) appears to be important (97), as well as AU-rich sequences, although not specifically under the form of RNA duplex structures (99). Upon recognition of its target RNA, MDA5 oligomerizes into filaments in a cooperative manner and the CARDs domains allow the nucleation of MAVS leading to its activation (100). Interestingly, the ATP hydrolysis activity of MDA5 is stimulated by dsRNA binding and favors the dissociation of MDA5 at a rate that is inversely proportional to the length of the dsRNA substrate. This could explain the length requirement for dsRNAs to trigger MDA5-dependent signaling (101). Finally, the third member of the RLR family, LGP2, displays RNA-binding activity but lacks the CARDs domains required for downstream signal transduction. LGP2 recently emerged as both a positive and a negative regulator of RIG-I and MDA5 activities [for a recent review, see (75)], as supported by the fact that LGP2 deficient mice display disparate susceptibility to infection with RNA viruses (see **Figure 1A**) (102).

Finally, inflammasome-forming nucleotide-binding domain leucine-rich repeat (NLR) proteins are a group of cytosolic PRRs that assemble inflammasome in response to PAMP and DAMPs. Briefly, inflammatory ligand recognition by NLR leads to the recruitment of the apoptosis speck-like protein (ASC) adaptor, allowing the activation of caspase-1. Caspase-1 dependent cleavage of both Gasdermin-D and pro-IL-1β or pro-IL-18, further induces cell death by pyroptosis or inflammation, respectively [**Figure 1A**, for a review, see (103)]. NLRs may rely on other PRRs and RBPs to trigger inflammasome activation and, for some of them, direct ligands remain to be characterized. For example, NLRP1 (nucleotide-binding domain leucine-rich repeat protein 1), was one of the first inflammasome-forming PRRs to be identified but its role in pathogen defense and its direct ligands were poorly understood. However, a recent report has shown that human NLRP1 can bind both dsDNA and dsRNA through its leucine-rich repeat domain, but only long dsRNAs [including poly(I:C)] are able to trigger NLRP1 activation (104). Interestingly, in several cell lines and primary cells tested (including primary human epidermal keratinocytes and immortalized human HBEC3-KT bronchial epithelial cells), the sensing of poly(I:C) or infection with Semliki Forest Virus (a positive-strand RNA virus) and its effect on cell viability are fully dependent on NLRP1 expression thus suggesting a non-redundant role of this NLR in sensing dsRNA and triggering activation of the inflammasome (104).

3.2 RNA Sensing and Regulation of PRR Activity by Non-PRR RBPs

PRRs are receptors of host defense mechanism that identify pathogens by sensing specific patterns (9). In addition to the layer that relies on canonical RNA-binding PRRs, numerous RBPs, that are not necessarily specific to immune cells, can interact with a large variety of RNAs in order to directly trigger an innate immune response or modulate the activity of canonical PRRs (see **Figure 1B**).

ZNFX1 (zinc finger NFX1-type containing 1) is a member of the helicase superfamily 1 (SF1) localized in the outer membrane of the mitochondria. Similar to RIG-I and MDA5, ZNFX1 can bind viral dsRNAs and interacts with MAVS, in order to promote IFN expression and IFN-stimulated genes (ISGs) (see **Figure 1B**) (78). However, ZNFX1 appears as an early sensor of dsRNA: as opposed to RIG-I and MDA5 whose expression and mitochondrial translocation is induced only following viral infection, ZNFX1 is constitutively localized within mitochondria and its expression, further increased by viral infection, reaches a peak much earlier than RIG-I and MDA5. ZNFX1 has further been shown to enhance the expression of RLRs, therefore priming the subsequent antiviral defense (78). As a consequence, mice deficient for ZNF1X show increased susceptibility to viral infection (78) and those results have been recently confirmed in human with biallelic ZNFX1 deficiencies (105). Thus, ZNFX1 is seen as an early sensor for viral RNAs able to trigger a rapid antiviral response in two different manners: directly through IFN signaling pathway and indirectly through RLRs activation. Interestingly, deficiencies in ZNFX1 are also associated with uncontrolled inflammation following viral infection, in both humans and mice. Although the underlying mechanisms will need further investigation, it highlights the importance of a timely tune innate response, allowing proper elimination of viral spread, while preventing over inflammation. Another recent study involving an ISGs expression screening, has revealed that OAS1 (2'-5'-Oligoadenylate Synthetase 1), a dsRNA sensor, is able to inhibit SARS-CoV-2 through the action of RNase L (see **Figure 1B**) (80). Indeed, by performing iCLIP against OAS1, infection by SARS-CoV-2 was shown to enhance the RNA-binding activity of OAS1, which interacts primarily with highly structured host RNAs (*e.g.* snoRNAs, lncRNAs, intronic regions of mRNAs) as well as with specific stem loops (SL1 and SL2) located withing the first 54 nucleotides of the 5'UTR of all positive-sense SARS-CoV-2 RNAs (80, 106). Importantly, the sensing of SARS-CoV-2 RNAs is dependent on the C-terminal prenylation of OAS1 (addition of hydrophobic molecules) (80), that leads at its translocation to membranous viral replicative organelles (107). The binding of SARS-CoV-2 dsRNAs by OAS1 activates RNase L, which in turn initiates the cleavage of viral and host RNAs harboring single-stranded UpU and UpA motifs (108).

In addition to dsRNA sensing in the cytoplasm, RBPs that are non-canonical PRRs can also act as sensors within the nucleus and potentiate robust immune responses. For instance, a nuclear matrix protein hnRNP U (also known as SAFA for scaffold attachment factor A) directly binds nuclear viral RNAs from DNA and RNA viruses (109). The infection of mouse Bone Marrow-Derived macrophages (BMDMs) by HSV-1, a DNA virus, or by Vesicular Stomatitis Virus (VSV), a ssRNA virus, induced their recognition by hnRNP U in the nucleus. This sensing triggers its oligomerization, inducing its interaction with chromatin remodelers such as the DNA topoisomerase 1 (TOP1) and SWI/SNF-related matrix-associated actin-dependent regulator of chromatin subfamily A member 5 (SMARCA5). This further activates distal and proximal enhancers of type I IFN and other host defense genes (*e.g.* Oasl1, IL-15, CXCL10, Irf1), therefore promoting robust antiviral responses (109). Thus, with its dual function as a viral RNA sensor and a transcriptional regulator, hnRNP U in the nucleus is an advantage against virus evasion strategy.

More recently, the role of the DEAD-box (Asp-Glu-Ala-Asp motif) or DEAH-box (Asp-Glu-Ala-His motif) helicase proteins during innate immune sensing has emerged in the literature [for a more detailed review, see (110)], with promising contribution in treatment of infectious diseases. They are categorized into two groups, based on their activity: (i) those which directly act as RNA sensors, independently of PRRs such as DDX1 or DHX9, and (ii) those which act as co-sensors of RLRs and NLRs, thus improving their activation such as DDX3 or DDX60. For instance, the first category involves proteins able to bind dsRNA. This is exemplified by DDX1, DHX9 and DHX33 that have been shown to directly interact with poly(I:C) or dsRNA from viruses such as Influenza A or reovirus, in myeloid DCs (111, 112). Thus, sensing by DDX1, DHX9 or DHX33 directly induces the production of IFN-α/β and/or pro-inflammatory cytokines responses, *via* MAVS (DHX9, DHX33) or TRIF (DDX1), independently of canonical PRRs. In addition, DHX9 (in murine intestinal cells) and DHX33 (in THP-1 macrophages cell line) are able to sense RNA and trigger NLRP9 and NLRP3 inflammasome, respectively (113, 114). The second category includes co-sensors such as DDX3 or DDX60. While DDX3 can directly associate with poly(I:C), it also form a complex with MAVS and RLRs to potentiate type I IFN responses, following stimulation (115). Similarly DDX60 interacts with RLRs to promote their downstream signaling (116).

Similarly, viral RNAs sensing are also modulated by several autoantigens such as La/SS-B (La). La has been recently shown to directly bind RIG-I once bound to a viral dsRNA (79), resulting in strengthened interaction between RIG-I and its RNA ligand and eventually empowered RIG-I-mediated type I and type III IFN production. In addition, La also promotes the activation of MAVS, a mitochondrial-associated adaptor downstream of RIG-I (79) (**Figure 1B**). Indeed, RNA recognition results in RIG-I exposing its activator CARD domains, which in turn binds the CARD domain of MAVS (117). The activation of MAVS leads to the formation of a complex with two other proteins (CARD9 and BCL-10) that eventually turn on the NFκB signaling pathway (118). Therefore, upon infection, La reinforces the activation of MAVS through RIG-I and empowers the immune response. By contrast, Ro60, another viral RNA binding autoantigen, is known to negatively regulate the inflammatory response by buffering the recognition of viral RNAs by RNA sensors. Ro60 is a component of a ribonucleoprotein complex that targets misfolded cellular

RNAs (potentially foreign RNAs) for destruction, thus slowing down their detection by immune RNA sensors and delaying the alarm signal (81).

In addition to directly sensing or potentiating detection of viral RNAs, RBPs also modulate immune responses through the direct recognition of endogenous RNAs (119–122). This is for example the case for Alu transposable elements (TEs), which account for over 10% of the human genome (123, 124). Alu elements belong to the Short interspersed nuclear element (SINE) family of transposable elements (125). They are primate specific repeat sequences of around 280bp long, that can be found in intergenic regions but also embedded within introns and exons of protein coding genes and expressed together with the gene in which they are integrated. Functional Alu elements can be transcribed from their own promoter by RNA polymerase III and depend on the reverse transcriptase activity of the ORFp2 protein from LINE-1 elements to reverse transcribe and integrate into new genomic loci (125). Transcribed Alu elements can bind several cellular RBPs such as Ro60, which negatively regulates their abundance (81). In Hela cells, infection with adenovirus type 5 and herpes simplex virus type 1 have been described to activate RNA polymerase III-dependent transcription of Alu TEs (122, 126). Alu TE are also strongly transcribed upon exposure to type I IFN and pro-inflammatory cytokines, both from their own promoter and as part of induced gene transcripts with embedded Alu elements (127). Interestingly, the high abundance of Alu transcripts induced upon IFN exposure has been shown to saturate Ro60 and allow their recognition by TLR7, to further amplify the IFN response through classical signaling pathways (MAPK, NFκB) (81, 128) (**Figure 1B**). In line with this, auto-antibodies bound to Ro60-Alu RNA/protein complexes have been detected in the blood of Sjögren's Syndrome patients and have been proposed to mediate TLR7-dependent signaling in B cells (upon endosomal uptake), leading to their aberrant activation and production of inflammatory cytokines (81). Ro60 can therefore play a dual role in restricting Alu abundance to limit their recognition by PRRs under physiological conditions, while also being responsible for inducing a pathological innate immune response in the context of an autoimmune disease.

In addition to Alu RNAs transcribed from their own promoter, Alu elements embedded within mRNAs can act as scaffolds for the recruitment of RBPs in the context of innate immunity. Many cellular transcripts harbor two or more embedded Alu copies in inverted orientation (Alu inverted repeat, AIR) mostly located in their 3'UTRs (129). AIRs can base-pair with each other and the closer the inverted Alu sequences are, the more frequently they tend to base-pair with each other (39). The resulting dsRNA structure has been shown to form Z-RNA (a left handed dsRNA helix with Z-conformation) (130) that is recognized by the Zα domain of ADAR1 (131) and Z-DNA binding protein 1 (ZBP1) (83) with different outcomes. ZBP1 is a sensor for viral as well as endogenous Z-RNAs, promoting NLRP3 inflammasome and pyroptosis *via* Receptor Interacting Protein Kinase 3 (RIPK3) (83–85). More recently, ZBP1 has also been shown to induce PANoptosis, a form of inflammatory cells death, through a large multi-protein complex named AIM2 PANoptosome (**Figure 1B**) (82). By contrast, ADAR1 appears more like a guardian of homeostasis, by limiting inflammation. Indeed, ADAR1 binding to Z-RNA mediates adenosine to inosine conversion (also known as A-to-I editing) within the dsRNA structure (132). A-to-I editing disrupts the continuity in the dsRNA structure avoiding its recognition by the dsRNA sensors MDA5 and PKR. Interestingly, gain of function mutations in MDA5 associated with human immune disorders such as Aicardi-Goutières syndrome, have been shown to render MDA5 more tolerant to the irregular AIRs dsRNA structures generated upon ADAR1 A-to-I editing and inducing an aberrant antiviral response (133). Similarly, a recent study has shown that ADAR1 could act as a negative regulator of ZBP1 mediated PANoptosis (134). Those results suggest that the specificity of MDA5 and ZBP1 in recognizing its RNA substrates is under strong selection to maintain a trade-off between efficient pathogen recognition and self-tolerance.

Another strategy to regulate immune responses through PRRs sensing is to physically mask host RNAs with RBPs. For instance, under physiological context, a host-derived RNA called 5S ribosomal RNA pseudogene 141 (RNA5SP141) is present in the nucleus. When RNA5SP141 translocates into the cytoplasm, it recruits different RBPs such as ribosomal protein L5 (RPL5) and mitochondrial ribosomal protein L18 (MRPL18), avoiding unwanted activation of the immune system by PRRs. Some DNA viruses [*e.g.* herpes simplex virus 1 (HSV-1), Epstein-Barr virus (EBV) and influenza A virus (IAV)] have been shown to disrupt the nucleus membrane and to induce a global downregulation of host proteins' synthesis. This leads to increased availability of RNA5SP141 in the cytoplasm and its unmasking from the RBPs (135). RIG-I thus recognizes the RBP-free RNA5SP141, inducing type I IFN stimulation and antiviral immunity. This study shows how RBPs protect host RNAs from PRR recognition and highlights a mechanism used by the host to induce PRR activation during infection by DNA viruses.

Finally, dsRNA or ssRNA are not the only molecules recognized by RBPs. RNAs can base-pair with DNA during different physiological processes (*e.g.* DNA transcription, DNA replication, dsDNA break repairs) or as intermediates of replication for certain viruses and endogenous retroelements (*e.g.* retroviruses, hepadnaviruses and LINE-1 retroelements). Viral RNA : DNA hybrids have been shown in mouse bone marrow-derived conventional DCs (cDCs) and human Peripheral Blood Mononuclear Cells (PBMCs), but not in BMDMs, to be recognized by TLR9, leading to the production of pro-inflammatory cytokines, such as IL-6 and IFN, in a Myd88-dependent manner (136). Similarly, the cyclic GMP-AMP synthase (cGAS), classically seen as a DNA sensor that activates inflammatory response *via* its adaptor STING (137) can also detect RNA : DNA hybrids and induce STING activation leading to IFN-β and ISG expression (138). However, this property appears highly regulated, probably to prevent over-inflammation following infection, or unwanted immune responses during biological processes involving RNA : DNA

hybrid intermediates. Indeed, the Lysyl tRNA synthetase (LysRS), a component of the cytosolic multi-tRNA synthetase complex (MSC) involved in mRNA translation (139–141), has recently been shown to directly interact with RNA : DNA hybrids and compete with cGAS to delay STING activation and downstream type I IFN response (142). In addition to competing with cGAS, binding of LysRS to RNA : DNA hybrids leads to LysRS-dependent production of diadenosine tetraphosphate (Ap4A), which is able to directly bind STING and prevent its interaction with 2'3'-cyclic GMP-AMP (cGAMP) and decreases downstream production of type I IFN (see **Figure 1A**) (142).

Altogether, RBPs are important players in the direct recognition and/or modulation of the recognition of foreign RNAs and in triggering a robust innate response against a wide-range of pathogens.

4 ROLE OF RBPs IN RNA PROCESSING DURING INNATE IMMUNITY

4.1 Mechanisms of Alternative Splicing

In eukaryotes, protein-coding genes contain sequences that are found in mature mRNAs (exons) and sequences that are removed during mRNA maturation (introns) through a process called splicing and catalyzed by the spliceosome (143–145). By skipping or retaining specific exonic sequences, pre-mRNA splicing can create various RNA isoforms from a single transcription unit in a process known as alternative splicing. The spliceosome is a megadalton machinery composed of small nuclear RNAs (snRNAs) and proteins that associate to form small nuclear ribonucleoprotein particles (snRNPs termed as U1, U2, U4, U5, and U6) (146). Each intron has specific conserved sequences, the splice donor site that defines the 5' exon/intron junction, the splice acceptor site that defines the 3' intron/exon junction and the branch site that is essential during the first step of the splicing reaction. These sequences are recognized by snRNPs that assemble in a chronological order to perform two transesterification reactions that lead to the cleavage and release of the intron, while performing phosphodiester bonds to ligate the exons (146). Selection of the splice donor and acceptor sites can be modulated by surrounding cis-acting sequences, such as exonic and intronic splicing enhancers or silencers, that recruit RBPs including serine/arginine-rich family of nuclear phosphoproteins (SR proteins) and heterogeneous nuclear ribonucleoproteins (hnRNPs) [for a short review, see (147)]. Differential recognition of splice donor and acceptor sites leads to the process of alternative splicing, creating multiple transcript isoforms with different coding sequences or alternative 5'UTRs. Alternative-splicing plays a critical role in numerous cellular processes such as the establishment of cell identity or sex selection (148, 149). In the context of immunity, alternative splicing has been shown to play an important role in the differentiation, homeostasis, and regulation of immune cells (150–153). Importantly, it appears as a major regulator of inflammation in innate immune cells. For instance, in mouse macrophages isolated from the lung at different time-point following intra-tracheal injection of LPS, global changes in alternative splicing were observed at the pic of the inflammatory response. In that context, genes involved in cellular metabolism and chemotactism were shown to be highly regulated by alternative splicing. Moreover, alternative splicing appears to regulate different set of pre-mRNA in recruited macrophages (mostly pro-inflammatory) as compared to resident macrophages, likely explaining their different metabolic requirement (154). Similarly, in monocyte derived macrophages obtained from human blood, bacterial infection is associated with global changes in mRNA isoform usage, with increased cassette exon inclusion (155). Finally, numerous important immune molecules transcripts downstream of PRR signaling (*e.g.* MyD88, IL-1 receptor-associated kinase (IRAK)), and even some TLR mRNA themselves also see their expression regulated by alternative splicing to give rise to protein isoforms with differential biological activities (156–158). However, although alternative splicing is mainly modulated by RBPs such as SR and hnRNP proteins, their role in the context of innate immunity is still poorly understood at the molecular level.

4.2 Alternative Splicing of PRRs and Their Downstream Signaling Factors

As the key contact between the noxious molecule and the host cells, PRRs and their downstream factors, represent a central hub of regulation. Alternative splicing has been shown to regulate activation and/or functions of those receptors, in order to control the intensity of immune responses and their shutdown upon clearance of infection or damage, as well as to prevent inappropriate inflammatory responses and autoimmunity.

While PRRs play an essential role during innate immunity by sensing specific patterns and alarming the immune system, their activity needs to be downregulated upon activation, to avoid over-inflammation. In line with this, alternative splicing appears as an important mechanism to limit PRR signaling. For example, LPS recognition by TLR4 requires TLR4 interaction with Myeloid Differentiation Factor 2 (MD-2) and the subsequent signaling cascade will lead to the expression of an MD-2 spliced isoform (MD-2s) that will inhibit TLR4 signaling (158). *In vivo*, delivery of MD-2s in the lung substantially decreases LPS-induced inflammation (159). Such a negative feedback loop has also been observed for TLR3, which recognizes dsRNA. In human astrocytes cell lines, TLR3 activation leads to type I IFN production that, in turn, induces the expression of an alternative spliced TLR3 isoform that acts as a negative regulator of TLR3 downstream signaling pathways (160).

In a different context, alternative splicing has been shown to regulate the relative production of membrane-bound and soluble forms of immune receptors, with opposite effect on inflammation. This is the case for Siglec-14, a glycan recognition protein that can elicit pro-inflammatory responses, in response to bacterial pathogens. Siglec-14 is classically paired with Siglec-5, that acts as an inhibitory receptor for bacterial pathogens, providing a

first level of regulation in pro-inflammatory processes (161). Thus, in LPS-stimulated neutrophils, Siglec-14 has been found to be up-regulated and Siglec-5 down-regulated, suggesting a positive feed-back loop that increases myeloid inflammatory responses (162). As an additional layer of regulation, it has been found that a soluble form of Siglec-14 (sSiglec14) is able to interfere with the interaction between TLR2 and the membrane-bound form of Siglec-14 (mSiglec-14), in myeloid cells (163). The soluble form of Siglec14 is due to the retention of intron 5 during pre-mRNA splicing, which contains a C-terminal hexapeptide before the translation termination codon (164). While sSiglec14 is involved in the suppression of pro-inflammatory cytokines production (164), these results suggest a negative feedback mechanism regulating the myeloid pro-inflammatory responses elicited by the engagement of mSiglec-14. Thus, the switching between sSiglec-14 and mSiglec-14 might be used by the innate system to control a potential unwanted inflammatory response that could damage the host tissues.

In addition to PRRs, the activity of immune receptor's adaptors such as MyD88 or TRIF has been shown to be dynamically modulated through alternative splicing (165). The cytoplasmic portion of most of the TLRs shows high similarities with the interleukin-1 (IL-1) receptors family and is thus called the TIR domain, for Toll/IL-1 receptor (165). TIR domain thus serves as a platform to recruit TIR domain-containing adapter, such as MyD88 (166). Upon stimulation, MyD88 recruits IL-1 receptor-associated kinase (IRAK), a serine/threonine kinase, also containing a TIR domain. IRAK is then activated by phosphorylation and interacts with TRAF6. Altogether, this signaling cascade leads to the activation of MAPK and NFκB signaling pathways that are crucial for completion of innate immune response (165). Thus, the regulation of TLR's adaptors are critical for the control of immune defense. Interestingly, a MyD88 splice variant (MyD88s) induced upon LPS activation in monocytes codes for a protein isoform that lacks the IRAK-interacting domain, thus acting as a dominant negative by preventing IRAK phosphorylation and downstream NFκB activation to inhibit the LPS induced signaling pathway (167, 168). In resting cells, MyD88s alternative splicing is regulated by SF3A, SF3B and EFTUD2 that specifically inhibits the generation of the MyD88s isoform (lacking the IRAK-interacting domain), thus ensuring a robust initial innate response (see **Figure 2A**) (169, 173). Interestingly, in macrophages, SF3A knockdown preferentially affects splicing events related to innate immunity, such as the TLR signaling pathway, highly suggesting a more global role of this splicing factor in controlling the intensity of inflammation (170).

4.3 ISG Control by RBP-Mediated Alternative Splicing

In the case of a viral infection, the innate immune system reacts by disrupting the functions and pathways vital for the pathogen's life cycle. Once PRRs are activated by viral components, antiviral cytokines are produced. Among the earliest cytokines to be produced are type I IFNs (*e.g.*, IFN-β, IFN-α, *etc.*) that trigger the JAK/STAT signaling pathway in order to induce expression of ISGs (174). These ISGs (*e.g.*, IFIT1-3) generally act as antiviral effectors that control viral replication and spread (175, 176). Modulating ISG expression is critical to manage an efficient defense against pathogens while preventing detrimental adverse immune effects. RNA splicing is one way among others to ensure the proper timing and intensity of ISG expression. Splicing regulation involves one or more splicing factors acting like a regulatory node, as illustrated by heterogeneous nuclear RiboNucleoProteins (hnRNPs) (177). hnRNPs are complexes comprising typical RNA-binding and modular proteins mostly present in the nucleus (178). Using UV cross-linking followed by oligo(dT) purification of RNAs, about 20 species of hnRNPs have been identified (hnRNP A-U) (179). These 'RNA scaffolds' play various roles associated with the fate of the RNA such as the regulation of splicing or the transcriptional responses to DNA damage (180–183). It has been recently shown that a loss of hnRNP M results in overproduction of several innate immune transcripts such as antimicrobial factors as well as ISGs (171). In early stages of macrophage activation, the splicing factor hnRNP M associates with nascent IL-6 mRNA and slows down its initial ramping, acting probably as a safeguard of the inflammatory response. Once the macrophage is fully activated, hnRNP M is phosphorylated (downstream of the TLR pathway) and is then released from mRNA transcripts, promoting their splicing and full maturation (see **Figure 2B**) (171). Zinc finger RNA-binding protein, ZFR, is another example of alternative splicing regulation that has been shown to suppress the IFN response by regulating ISGs splicing (172). ZFR contains double-stranded RNA binding motifs as well as several Cys-Cys-His-His (CCHH) zinc finger domains (184). This zinc finger protein has been shown to prevent aberrant splicing of the histone variant macroH2A1 (mH2A1), which in turn binds and represses IFN-β activation and ISG expression (see **Figure 2C**) (172). Although the precise mechanisms of both ZFR impact on mH2A1 splicing and mH2A1 negative effect on type I IFN responses still remain to be determined, it again highlights the high level of regulation underlying type I IFN-responses.

4.4 Specialized Splicing in Non-Canonical Nuclear Bodies During Inflammation

The nucleus is highly organized into membrane-less structures called nuclear bodies. Different nuclear bodies have been described, endowed with specific proteins and RNA composition, and functional specificity. One example of such sub-nuclear compartments are Cajal Bodies (CB), that act as an organizer of spliceosomal small nuclear ribonucleoproteins (snRNP) biogenesis (185). On a mechanistic point of view, Coilin, a multivalent scaffold protein, has been shown to interact with small nuclear RNAs (snRNAs), targeting them to CB to achieve snRNP assembly (186, 187). Coilin interacts with U snRNPs and with a CB component called survival of motoneurons (SMN) in order to participate in the formation and integrity of CB themselves (188). In an inflammation context such as LPS-activated macrophages, Coilin interacts with higher affinity to SMN, leading to snRNA release and CB destabilization (**Figure 3**). Simultaneously, Tat-activating regulatory DNA-

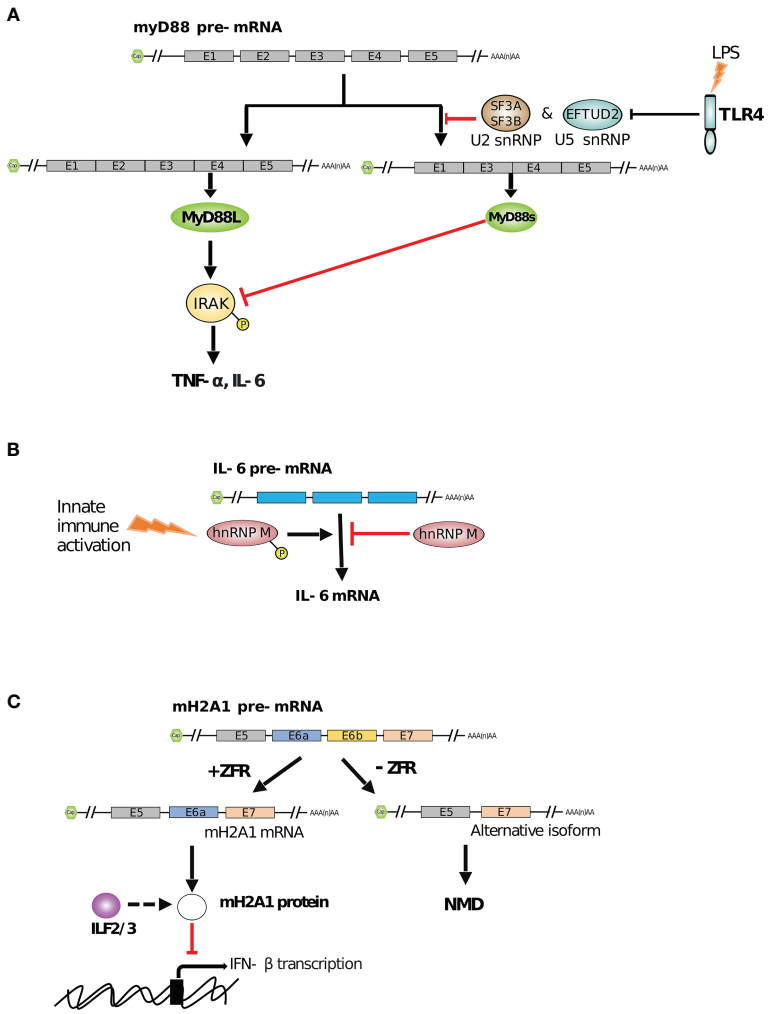

FIGURE 2 | RBP mediated regulation of innate immune functions by alternative splicing. **(A)** The smaller isoform (myD88s) of TLR4 signaling adaptor myD88 inhibits the production of cytokines (such as TNF-α and IL-6) by inhibiting myD88L mediated phosphorylation of IRAK. However, SF3A/3B and EFTUD2, in complexes with other snRNPs, reduce the production of myD88s to maintain cytokine expression (169, 170). **(B)** hnRNP M represses the splicing of IL-6 mRNA. However, innate immune activation in infected macrophages leads to phosphorylation of hnRNP M and relieves this splicing suppression (171). **(C)** ZFR facilitates correct splicing of mH2A1 transcript by exon inclusion which prevents the formation of an aberrantly spliced isoform. mH2A1 protein, which ILF2/3 possibly regulates, further promotes IFN-β mRNA expression to enhance type I IFN response (172).

binding protein-43 (TDP-43), a highly conserved hnRNP involved in RNA processing (*e.g.* splicing, trafficking, *etc*…), becomes ubiquitinylated, decreases its binding to SMN and competitively recruits snRNAs and other components from spliceosomal snRNPs creating a novel sub-nuclear body different from CBs (189). TDP-43 also binds cytokine IL-6 and IL-10 pre-mRNAs in a sequence-specific manner (through short GC-rich palindromic repeats separated by a short spacer with a conserved 'ACU' sequence located in intron 2 of IL-6 and intron 1 of IL-10), thereby favoring their splicing within the sub-nuclear body dubbed InSAC (which stands for Interleukin-6 and -10 Splicing Activating Compartment) (see in **Figure 3**) (189). By hijacking components from CBs and controlling the distribution of subnuclear compartments, TDP-43 functions as a scaffold protein within InSACs, which become a specific cytokine pre-mRNA splicing compartment and an important effector of the immune response during inflammation (190).

4.5 Polyadenylation

Most mRNAs, with the exception of those coding for canonical histones, bear a 3' poly(A) tail added during the maturation of mRNA, in a process called polyadenylation. Polyadenylation is a co-transcriptional process involving the recognition of a cleavage/polyadenylation site (typically "AAUAAA" in a GU or U-rich context) in the nascent pre-mRNA, followed by endonucleolytic cleavage of the pre-mRNA (35 nt downstream of the cleavage/polyadenylation signal) and addition of a poly(A) sequence (50-250 nt long) at the 3' end of the cleavage site (191).

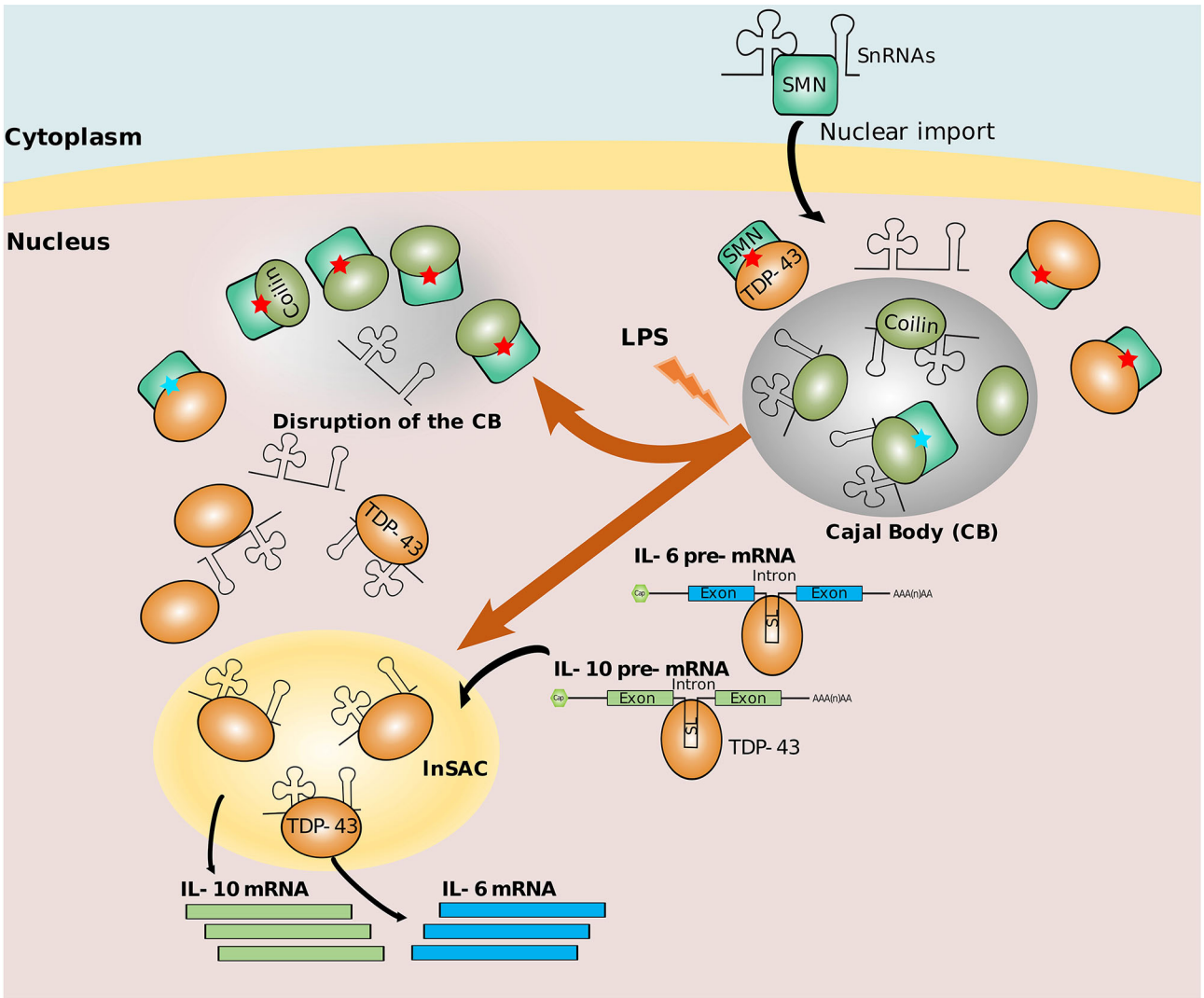

FIGURE 3 | Nuclear bodies for splicing. In a physiological context, Cajal Body (CB) recruits snRNAs and snRNPs for maturation. Coilin interacts with SMN with low affinity (represented by blue stars). In infection context, Coilin strongly interacts with SMN (represented by red stars), and TDP-43 hijacks snRNAs and stabilizes InSAC (a sub-nuclear body favoring the splicing of IL-6 and IL-10). Simultaneously, TDP-43 recruits cytokine transcripts through their putative stem loop (SL) into InSAC and promotes their splicing (189, 190).

An estimated 80% of mammalian genes contain multiple cleavage/polyadenylation sites generally leading to transcript isoforms with alternative 3' untranslated regions (3'UTRs) (192). Use of alternative polyadenylation (APA) sites is a dynamic process regulated by the abundance of the RNA-binding proteins involved in the polyadenylation process itself or by other RBPs, such as HuR, that can bind close to the cleavage/polyadenylation site and block its recognition (193). Ultimately, 3'UTR is the target of several RBP and/or antisense RNAs that regulate mRNA destiny. Modifications of mRNA 3'UTRs have thus important consequences on mRNA sub-cellular localization, translation efficiency or stability (194).

APA has been shown to also play an important role in innate immunity. For example, the sequencing of the human genome in 2001 helped to reveal that most TLRs have between two and four predicted APA sites (195). In line with this, several subsequent studies could underline that infected or inflamed macrophages display rapid and extensive changes in APA leading to a global shortening of 3'UTRs (155, 196). In LPS stimulated macrophages (BMDM and RAW 264.7 mouse cell line), this has been explained by the expression of Cstf-64, a 64kDa Cleavage stimulatory factor, that likely contributes to alternative polyadenylation of numerous genes associated with a global change in their expression (197). Similarly, macrophages derived from human blood monocytes infected by *Salmonella typhimurium* or *Listeria monocytogenes* show a near universal shift toward usage of more upstream polyadenylation sites, leading to shorter 3'UTR in genes where longer 3'UTR are targeted by miRNA negative regulation (155).

Altogether, those observations argue for a role of 3'UTR shortening in the escape from immune repression, allowing a rapid establishment of innate immune responses. Consistent with this, infection of primary human monocyte derived macrophages and mouse peritoneal macrophages with VSV leads to a gradual shortening of 3'UTRs through the use of proximal cleavage/polyadenylation sites. From 2 to 16 hours post infection, mRNA displaying altered APA are enriched in immune-related Gene Ontology categories and this is accompanied by increased levels of several innate-related proteins such as RIG-1, RIPK1 (a kinase involved in host defense) (198) or DDX3Y (a RNA helicase involved in type I IFN production) (199). In line with this, down-regulation of different RBPs involved in 3' mRNA processing prior to infection with VSV, promoted virus replication. Although it remains to be determined whether certain RBPs involved in 3'UTR processing are themselves regulated by APA and how viral infection modifies their expression/activity, this further validates the hypothesis about the important role of APA in regulating innate immunity (196). By contrast, Jia et al. study interestingly highlights a picture that is likely more sophisticated, where the impact of 3' UTR shortening does not necessarily correlate with increased protein output. Indeed, while APA usage leads to stabilization and increased translation of several mRNAs, other immune-related mRNAs were negatively impacted by the viral induction of 3'UTR shortening, including Fos, SOS1 [a negative regulator of TLR signaling (200)], TNFRSF10D [a TRAIL-receptor with a truncated death domain (201)], CASP6, PPSB1, N4BP1 [a suppressor of cytokine response (202)], (196). Although more extensive analysis should be performed in relevant models, the impact of APA and 3'UTR shortening in the context of infection overall appears as an additional regulator of protein output with a putative role in the interplay between positive and negative regulators of innate responses.

5 TRANSLATIONAL CONTROL DURING INNATE IMMUNITY

5.1 mRNA Translation Process

Once matured, mRNAs are transported from the nucleus to the cytoplasm, where they can recruit specific initiation factors and ribosomes to undergo translation. The control of this step plays a critical role in most cellular processes as it provides a rapid response to endogenous and exogenous cues without requiring *de novo* transcription. Furthermore, translational control is versatile as it can be exerted on a global scale or restricted to specific mRNA species. The translation process itself can be split into four phases: initiation, elongation, termination and ribosome recycling. Translation initiation is commonly assumed to be the rate limiting and the most regulated step of the process. However, the advent of high-throughput sequencing and protocols such as ribosome profiling (203), which allows to map the position of individual ribosomes across all expressed transcripts at a single-nucleotide resolution, has uncovered many additional layers of regulation taking place during elongation and termination of translation. Altogether, mRNA translation can thus be regulated by RBPs through multiple mechanisms involving binding to either specific RNA sequences or structures found in the 5'UTR, coding sequence, 3'UTR or poly(A) tail of cellular and viral RNAs, or as a consequence of the detection of non-self RNAs.

5.2 Individual RBP-Mediated Translation Silencing

The nucleolysin TIA-1 (TIA1 Cytotoxic Granule Associated RNA Binding Protein) and its closely related homologue TIAR are both RBPs containing three RNA Recognition Motif (RRM) domains in their N-terminal (204–206). In response to stress-induced phosphorylation of the translation initiation factor eIF2α, these proteins participate in the assembly of membrane-less cytosolic structures called stress granules (SGs). In cooperation with other RBPs, TIA-1 binds and sequesters untranslated mRNAs into the SGs, away from ribosomes (207). This occurs in five steps: (i) phosphorylation of eIF2α results in abortive initiation complexes preventing ribosome elongation and resulting in the formation of 48S messenger RiboNucleoParticle (mRNPs); (ii) free 48S mRNP are aggregated by factors such as TIAR or TIA-1, initiating SG nucleation; (iii) secondary aggregation where mRNA transcripts bind to multiple proteins forming microscopically visible SGs; (iv) integration and signaling in which proteins that lack RNA-binding domains (RBDs), such as TIA-1 binding proteins (*e.g.* SRC3, FAST or PMR1), bind in a 'piggyback' manner proteins involved in SGs assembly; (v) mRNA triage: SGs are organized into compartments. In each compartment, transcripts are specifically selected for decay or stabilized for further export and integration into polysomes, or stored (208). In LPS-activated macrophages, it has been shown that TIA-1 and TIAR bind U-rich motifs of mRNAs and selectively induce the silencing of TNF-α translation, while other cytokines such as IL-1β or IL-6, are largely unaffected (209, 210). Similarly, activated macrophages from TIA-1–/– mice were shown to produce significantly more TNF-α as compared to macrophages from wild type mice (210). Although the direct link between TIA-dependent silencing of TNF-α and stress granules has not been formally shown in that cellular context, several lines of evidence suggest that TNF-α silencing is linked to a stress response. By contrast, stimulation of the integrated stress pathway, a cytoprotective response that regulates cellular homeostasis, can prevent the production of IL-1β in LPS-activated macrophages. Indeed, incubation of murine macrophages with Arsenic, a known inducer of eIF2α phosphorylation and stress granule formation, after LPS activation or bacterial infection, results in a decreased production of IL-1β. Mechanistically, this decrease is explained by the formation of stress granules, through the interaction of IL-1β mRNA with TIA-1/TIAR, that eventually leads to IL-1β mRNA degradation (211).

Altogether, these studies suggest that TIA-1 and TIAR constitute specific translational silencers regulating the cellular response to environmental stress. The fact that, depending on the environmental context, such a stress-response targets specific cytokine-encoding mRNAs, further suggests the existence of additional elements of specificity, as exampled in non-immune cellular context (212).

5.3 GAIT Complex-Mediated Translational Regulation

RBP-containing protein complexes such as the IFN-γ-activated inhibitor of translation (GAIT) complex play an important role

in regulating transcript-specific translation during innate immunity (213).

GAIT is a heterotetrameric complex formed by the glutamyl-prolyl tRNA synthetase (known as EPRS), heterogeneous nuclear ribonucleoprotein Q (known as hnRNP Q or NSAP1), glyceraldehyde-3-phosphate dehydrogenase (GAPDH) and the ribosomal protein L13a [also known as uL13 in the new ribosomal protein naming system (214)]. Assembly of the GAIT complex in response to IFN-γ exposure occurs in two distinct stages that are temporally regulated (see **Figure 4**). The first stage, which occurs within 8 hours from IFN-γ exposure, is triggered by the phosphorylation of EPRS mediated by several kinases (*e.g.* CDK5, p35, mTORC1) (217, 218). This induces its release from the tRNA synthetase complex (MSC) and its interaction with hnRNP Q to form a 'pre-GAIT complex' that is not functional. The second stage occurs after 12-24h of IFN-γ exposure, when ribosomal protein uL13 is phosphorylated, and triggers its release from the 60S ribosomal subunit. uL13 then binds GAPDH and the 'pre-GAIT complex' formed by EPRS and hnRNP Q to generate a functional heterotetrameric GAIT complex (215, 219). Once functional, the GAIT complex becomes competent for binding transcripts containing specific RNA stem-loops in their 3'UTRs sequence (*i.e.* GAIT elements), that are present in numerous pro-inflammatory mRNAs. GAIT complex likewise represses their translation through a direct interaction between uL13 from the GAIT complex and the translation initiation factor eIF4G, which inhibits the association of eIF4G and eIF3 (217, 220). uL13 deficiency, however, does not impair ribosome assembly in general or its global translation capacity, highlighting a non-essential role for uL13 as a regulator of specific mRNA translation (221).

Macrophage specific knockout of uL13 in mice has shown that translational control driven by the GAIT complex is an important player in the resolution of inflammation (219, 222, 223). Indeed, many cellular transcripts involved in the inflammatory response contain GAIT elements in their 3'UTR and are translationally regulated by the GAIT complex following stimulation with IFN-γ. These include transcripts coding for chemokines, chemokine receptors (219) and cytokines (222).

Similarly, treatment of human monocytic U937 cell line with IFN-γ induces strong expression of vascular endothelial growth factor A (VEGF-A that promotes angiogenesis during inflammation) mRNA after 8 and 24 hours. However, while VEGF-A protein levels are increased 8 hours post IFN-γ treatment, its level returns to baseline at 24 hours. Indeed, VEGF-A translation is repressed by the GAIT complex *via* the binding of GAIT to its GAIT element (224). Conversely, VEGF-A mRNA is positively regulated by the HILDA ribonucleoprotein complex composed of the RBPs, hnRNP L, DRBP76 (or ILF3, a dsRBP), and hnRNP A2/B1 that promotes angiogenesis under hypoxia conditions (216, 225). Interestingly, the GAIT element located in the 3'UTR of VEGF-A is in vicinity of an RNA binding site for HILDA complex (**Figure 4**). Binding of the GAIT or HILDA complex is mutually exclusive and results in a conformational switch of the RNA that impedes binding of the

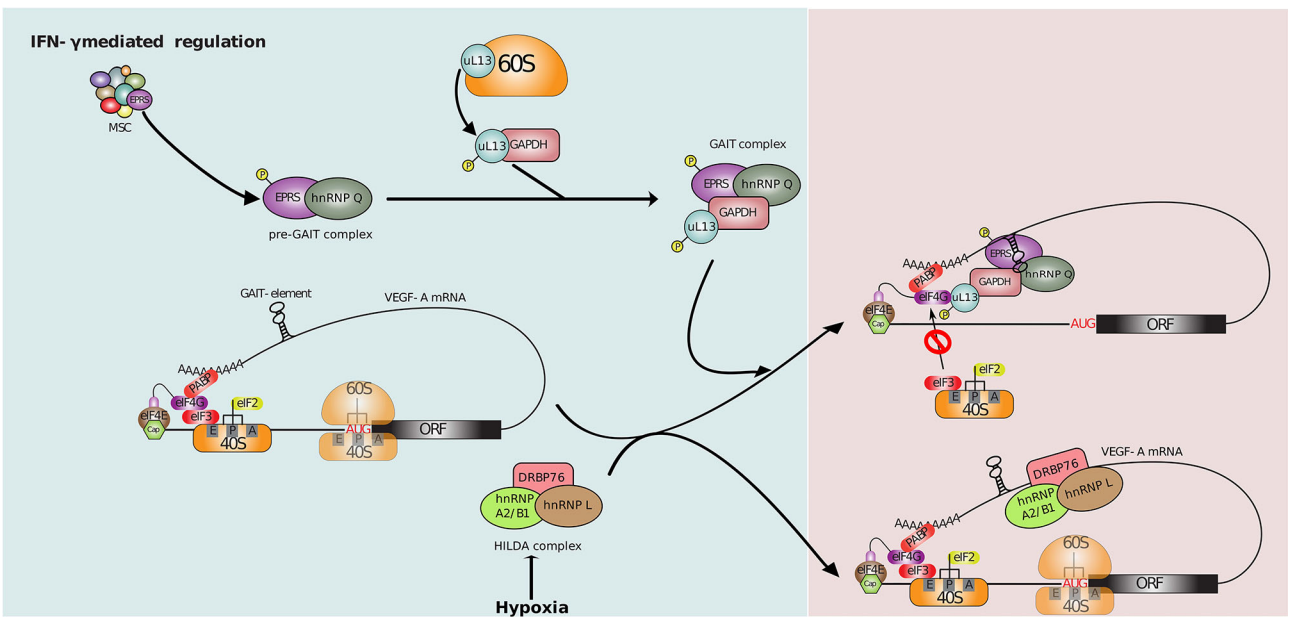

FIGURE 4 | Translational control of VEGF-A mRNA. 1-8 hr post-IFN-γ induction, phosphorylation mediated release of EPRS from MSC followed by its association with hnRNP Q forms an inactive pre-GAIT (IFN-γ activated inhibitor of translation) complex. This complex joins uL13, released from the 60S ribosomal subunit, and GAPDH to form the heterotetrameric GAIT complex at 12-24hr. This functional GAIT complex suppresses the translation of many cellular transcripts including VEGF-A mRNA by blocking the interaction between eIF4G and eIF3 upon binding to a stem-loop RNA structure at 3'UTR called as GAIT element (213, 215). The hypoxic stimulus-based regulation: the binding of the HILDA (hypoxia-induced hnRNP L - DRBP76 - hnRNP A2/B1) complex adjacent to the GAIT element under hypoxia prevents the binding of the GAIT complex and restores VEGF-A translation (213, 215, 216).

other complex (216, 225). This conformational switch, dependent on normoxic or hypoxia cell condition, enables efficient VEGF-A regulation and tissue oxygenation following inflammation, through translational control. Altogether, this process highlight a translation-dependent mechanism by which monocytes/macrophages can handle conflicted clues in complex environment such as inflammation (216).

5.4 Viral RNA Translation Control

Many ISGs with RNA-binding capacity (*i.e.* ISG-RBPs) boost immune response by restricting viral replication through the regulation of mRNA translation (either self or foreign mRNA), some acting on bulk translation while other targeting specific transcripts (226, 227). Among these, the best characterized is the dsRNA-activated protein kinase (PKR). PKR contains two dsRBDs that recognizes dsRNA structures longer than 30 nucleotides through its N-terminal end, which are an abundant replication intermediate for RNA viruses (228). Binding of dsRNA by PKR induces homodimerization and autophosphorylation of PKR C-terminal kinase domain, leading to its activation. One major target of PKR is the translation initiation factor eIF2α, which becomes phosphorylated upon PKR activation. Phosphorylated eIF2α cannot be recycled and is no longer able to form a ternary complex with the initiating Met-tRNA and a molecule of GTP. This results in a global inhibition of translation initiation affecting both cap-dependent and most forms of IRES-dependent translation (IRES for internal ribosome entry site, an RNA element often located in 5' UTR that allows translation initiation in a cap-independent manner). However, certain cellular mRNAs are selectively translated in the presence of high levels of phosphorylated eIF2α and many viruses are able to overcome this arrest (229). Additionally, PKR is also present in stress granules containing stalled 48S ribosomes (**Figure 5A**). The activation of the stress granule localized PKR contributes to amplifying the innate immunity without the need for viral dsRNA pattern recognition (231) highlighting another antiviral mechanism of PKR. In line with this, PARP12, an ISG-RBP phosphorylated by PKR, has been shown to localize into SGs and p62/SQSTM1 containing structures (an adaptor protein involved in innate signaling and autophagy). Regulated by type I IFN during LPS stimulation, PARP12 contributes to the cellular antiviral response by increasing the SG-mediated translational silencing of viral and cellular RNAs. PARP12 contains five Cys-Cys-Cys-His (CCCH) zinc finger domains, the N-terminal one being essential for its subcellular location and function (235, 236). ISG20, another ISG-RBP, contains an RNase I domain and displays antiviral activities (237). ISG20 is upregulated by the three types of IFN and appears to perturb both viral mRNA translation and stability either directly, or *via* host factors (238). At the opposite of PARP12, ISG20 has been shown to specifically inhibit translation of a large number of non-self RNAs but not that of host mRNAs, participating in the discrimination between self and non-self substrates, however its mechanism of action still remains elusive (239). This is also the case for ZAP, a zinc-finger antiviral protein, also known as ZC3HAV1 that promotes translational repression of spliced viral mRNAs, by binding specific ZAP responsive element present in target viral RNAs. Once bound to viral RNAs, ZAP disrupts the interaction between the translational initiation factors (eIF4G, eIF4A) and the viral mRNAs, leading to their translational silencing (240, 241). ZAP also participates in maintaining the integrity of stress granules which could potentially be linked to its ability to restrict virus infection (230). More recently, the long isoform of ZAP has been shown to be essential for limiting translation of viral RNAs (242). At the opposite of the short isoform, the long isoform of ZAP contains a PARP domain and a CaaX motif (amino acids "CVIS") at its C-terminus. Because ZAP is known to lead to degradation or translational inhibition by binding CpG dinucleotides in viral RNAs (243), CpG-enriched viruses have been used to highlight the antiviral activity of ZAP RBP. First, it has been shown that not only the N-terminal RBD, but also the C-terminal PARP domain both contribute to the restriction of CpG-enriched HIV-1. Second, the presence of the well-conserved CVIS sequence of the CaaX box mediates S-farnesylation (addition of a hydrophobic group). This post-transcriptional modification combined with the presence of the PARP domain are required for a full antiviral activity, through the recruitment of important co-factors such as TRIM25 and KHNYN proteins and the localization of ZAP into intracellular membranes. The subcellular distribution of this RBP has been shown to be critical for the antiviral restriction of both CpG-enriched HIV-1 and SARS-CoV-2 viruses (242).

RBPs can also recognize specific RNA patterns carried by some viruses in order to restrict their translation. For example, IFIT1 (interferon-induced protein with tetratricopeptide repeats 1), induced by IFN-α/β upon viral infection, binds a triphosphate group on the 5' terminal of viral RNAs (PPP-RNA) (244) in a sequence-independent manner and form a complex with IFIT2 and IFIT3 (and other proteins from IFIT family) to physically sequester the viral RNA and limit the assembly of viral particles (see **Figure 5A**) (245, 246). IFIT1 also interacts with eIF3 thereby blocking its association with the ternary complex (eIF2-GTP-Met-itRNA) to further inhibit translation of viral RNAs (247). In addition, the lack of 2'-O methylation of viral RNAs increases the interaction with IFIT1 and therefore raises the translational silencing (248). However, host mRNAs lacking 2'-O-methylation can also be targeted by IFIT1-mediated silencing. Interestingly, one way to circumvent this issue is mediated by CMTR1, another ISG also known as ISG95. CMTR1 is responsible for the catalysis of 2'O-methylation, which prevents IFIT1-mediated repression, especially for some ISG transcripts (see **Figure 5B**) (233). By doing so, CMTR1 promotes ISG protein expression in response to type I IFN. This example underlines the complex relation between (viral and host) RNA and RBPs and the requirement of several layers of regulation to optimize the antiviral response induced by the infection.

Altogether, a broad panel of RBPs exists, that regulate RNA dynamics through the modulation of translation. Their molecular and functional structure are divergent but they all converge into shaping the intensity and the efficiency of the innate immune response in time and space.

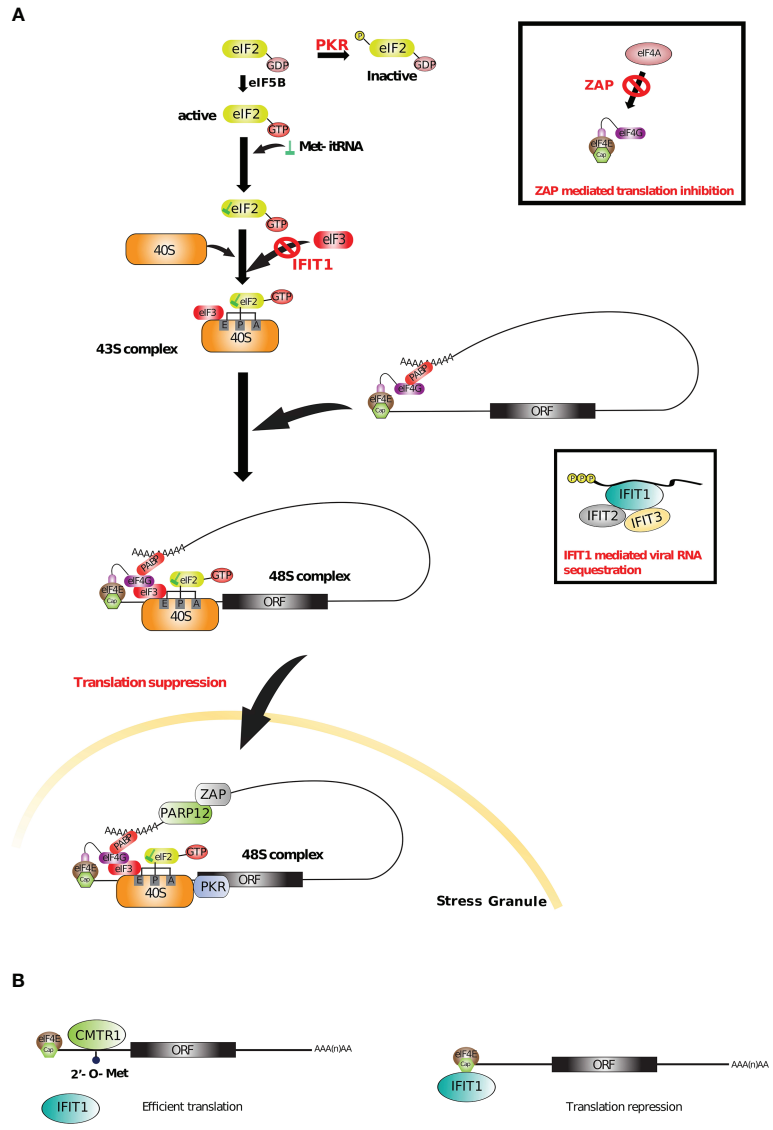

FIGURE 5 | Translational control by ISG-RBPs. **(A)** Upon viral infection, several ISGs (such as PKR, ZAP and IFIT1) suppress viral and/or cellular translation by recognizing different RNA sequences or structures and targeting important initiation and elongation factors. With PARP12, PKR and ZAP also participate in stress granule mediated antiviral response (227, 230–232). **(B)** 2'O methylation of cellular mRNAs recruits CMTR1 that inhibits IFIT1 mediated translation repression (233, 234).

6 mRNA STABILITY

6.1 mRNA Decay Process

The number of proteins synthesized from any given mRNA molecule is defined by its translation and degradation rates (249, 250). In eukaryotes, for most cellular transcripts, decay involves deadenylation and/or decapping. Deadenylation of the mRNA 3' end is mainly dependent on the CCR4-NOT complex among other deadenylases (251, 252), while decapping at the 5' end is performed by the mRNA decapping complex Dcp2-Dcp1 (253, 254). Each of these events is followed by exonucleolytic degradation from one or the other transcript extremity: from 5' to 3' by the exonuclease Xrn1 (255) and from 3' to 5' by the RNA exosome complex (256). Degradation of mRNAs by decapping complexes is thought to occur in cytoplasmic processing bodies (P-bodies) that are cytosolic membraneless structures composed of aggregates of proteins involved in RNA metabolism (including the decapping complex and Xrn1 among many others) and untranslated mRNAs (257). However, this model has been challenged in the past few years by studies indicating that P-bodies can be sites of mRNA storage and "triage" before resuming translation or being degraded (258, 259). Furthermore, growing evidence points to a close link between mRNA translation and degradation, which can occur simultaneously, outside of P-bodies (249, 260–263). Finally, endonuclease-associated mRNA decay can also occur, initiated by internal cleavage and followed by bidirectional exonuclease degradation (264). However this mechanism is not involved in

bulk mRNA degradation and is usually restricted to a subset of mRNAs with specific features.

RNA-seq technology combined with metabolic labeling of nascent mRNA transcripts allows to measure transcriptome-wide mRNA degradation rates in different conditions (*e.g.* LPS, TNF-α in myeloid cells or fibroblast) (265–267). Even in the absence of metabolic labeling, recent mathematical models are able to estimate with accuracy mRNA degradation rates from total RNA-seq datasets (268, 269). These analyses showed that in cells stimulated with LPS or TNF-α, the raise of mRNA levels induced by pro-inflammatory stimuli is mainly due to a global increase at the transcriptional level, with a globally constant mRNA degradation rate (265, 266). However, following LPS stimulation of DCs, a small set of mRNA show a rapid increase in their degradation rate, following an initial increase in their translation, thus affecting their cellular level within the first 3 hours after stimulation. Interestingly, most of the concerned mRNA were immediate-early genes (e.g. Fos, Jun, Egr1, Tristetraprolin) suggesting that, in the context of a rapid and transient response, the rate of the mRNA decay is an important parameter controlling mRNA output (266).

Rapid mRNA degradation mechanisms are essential for shaping the innate immune responses and the binding by RBPs to transcripts happens in a sequence or structure dependent manner. The most widely targeted cis-elements are AU-rich elements (AREs), with RBPs stimulating the deadenylation of mRNA (270).

6.2 ARE-Mediated Regulation

ARE usually consists in several clusters of the AUUUA pentamer or UUAUUUA(U/A)(U/A) nonamer sequence located in the 3'UTR of protein-coding transcripts (271). Their sequence is specifically recognized by ARE-binding proteins that can compete against each-other for ARE binding and thus, depending on the relative expression of ARE-binding proteins as well as the nucleotide context in proximity of a given ARE, these elements can either lead to transcript destabilization (272), translational control (273) or stabilization (274) [for a review, see (275)]. Historically, AU-rich elements were discovered as cis-acting elements responsible for inducing mRNA degradation of transcripts coding for inflammatory mediators (276). Indeed, it has been shown that early and transient mRNA transcripts induced after LPS or TNF-α stimulation in macrophages are enriched in AREs in their 3'UTRs, which is in line with the essential control of the immune response duration by rapid mRNA decay (277, 278). Consequently, ARE-mediated regulation affects many pro- or anti-inflammatory cytokines such as IL−2, TNF-α, IL−1β or Granulocyte Macrophages Colony Stimulating Factor (GM−CSF) (279). Their AU-rich sequence are recognized by over 20 different ARE-binding proteins with different roles in regulating mRNA metabolism (24, 279).

One of the most well-known examples of ARE binding proteins involved in inflammatory process is Tristetraprolin (TTP, a Cys-Cys-Cys-His (CCCH) zinc finger protein). It has been identified in various organisms from human to yeast (280–282) and has been shown to bind to the ARE contained within the 3'UTR of targeted mRNAs *via* its zinc finger domain. Well known targets are mRNAs displaying high turnover rates such as cytokines and growth factors (283–285). Mechanistically, TTP recruits the CNOT1 subunit of the CCR4-NOT complex (286), leading to deadenylation which accelerates degradation of the target mRNA. In addition to inducing deadenylation, TTP has also been described to stimulate mRNA-decay by decapping through the involvement of decapping proteins (Dcp1/2) (see **Figure 6A**) (292). TTP is therefore highly controlled to maintain a proper innate response intensity and duration. In mouse BMDMs (Bone Marrow-Derived macrophages), TTP expression is ubiquitous and low in resting conditions but, during the first hours of inflammation, TTP is phosphorylated by MK2 and further sequestered by 14-3-3 proteins (293, 294), therefore leading to pro-inflammatory cytokines mRNAs stabilization and accumulation (see **Figure 6A**) (295). Following this, TTP expression is empowered both transcriptionally and post-transcriptionally by inflammatory stimuli [as described upon activation of TLR4 (296, 297)] leading to the destabilization of several inflammation-associated mRNAs, such as TNF-α (283, 298, 299). By alternating between sequestration and release, TTP is able to regulate the stability of important inflammation-related mRNAs in a temporal manner.

6.3 Non ARE-Mediated Regulation

Non ARE-mediated regulation refers to mRNA regulation (decay or stabilization) by RBPs, through the recognition of specific sequences and RNA structures in the 3'UTR of targeted mRNAs, that are not ARE. For example, Constitutive Decay Element (CDE) relates to a decay through deadenylation, that is mediated by a 3'UTR conserved sequence with a stem-loop structure specifically recognized by Roquin and Roquin2 (300–302).

Non ARE-mediated regulation thus further regulates RNA stability of pro- and anti-inflammatory elements. For example, in addition to an ARE element in its 3'UTR, TNF-α encoding mRNA contains a non-ARE CDE that tightly regulate its expression, and overall prevent excessive TNF-α production in inflamed macrophages (300). Following macrophages (mouse RAW 264.7 cell line and BMDMs) stimulation by LPS, the CDE (which corresponds to a conserved 37 nucleotide long RNA stem-loop structure) is recognized by Roquin and Roquin2 (see **Figure 6B**). Roquin proteins actively recruit the CCR4-Caf1-Not deadenylase complex (a major multi-subunit complex responsible for the deadenylation of a large number of eukaryotic transcripts) through their C-terminal domain, which mediates deadenylation of the TNF-α mRNA and its accelerated clearance (301). Within this complex, Caf1a was identified as the factor directly responsible for deadenylation, since expression of a dominant-negative mutant of Caf1a, completely abolished Roquin mediated mRNA decay of CDE-containing mRNAs (301). The binding of a decapping enzyme Edc 4 (enhancer of mRNA decapping protein 4) and the RNA helicase Rckat 5'end also contributes to this mRNA degradation process. In addition to TNF-α transcripts, conserved CDEs were

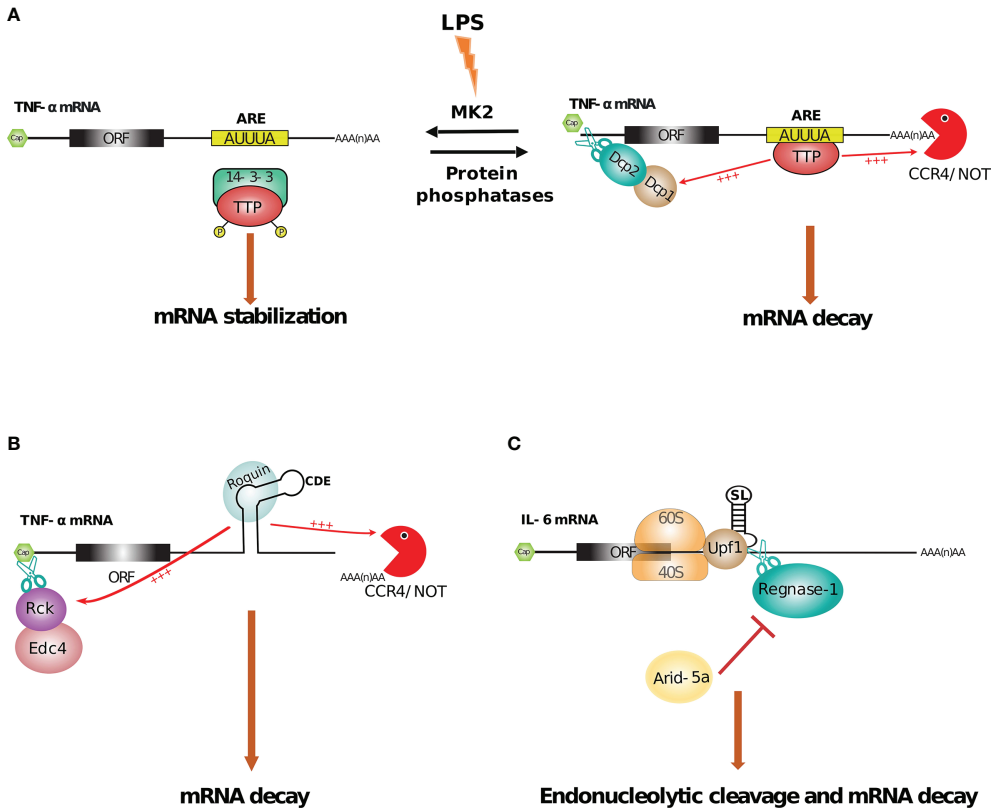

FIGURE 6 | RBPs mediated regulation of mRNA stability. **(A)** TTP facilitates TNF-α mRNA decay by binding to an AU-rich element (ARE) followed by recruitment of decapping enzymes DCP1/2 and CCR4-NOT deadenylating complex at 5' and 3'end respectively. Conversely, in mice BMDM, LPS mediated activation of MK2 kinase suppresses this process by phosphorylating TTP followed by its sequestration by 14-3-3 protein, which results in TNF-α mRNA stabilization (287–289). **(B, C)** Roquin and Regnase-1 promote decay of several inflammatory mRNAs by binding to stem-loop structures present near the 3'end. For example, Roquin facilitates deadenylation *via* CCR4-NOT complex and decapping *via* Rck/Edc4 by binding to a constitutive decay element (CDE) located in the 3'UTR of TNF-α mRNA. Whereas, Regnase-1, in cooperation with Upf1, leads to endonucleolytic cleavage of IL-6 mRNA by recognizing a specific stem-loop (SL). This process is inhibited by Arid-5a protein (64, 290, 291).

identified in more than 50 other cellular transcripts, enriched in T cell differentiation, nucleic acids metabolism and transcription factor functions, suggesting a wider role of Roquin proteins and their CDE target elements in modulating immune responses (301). In addition to AREs and CDEs, embryo deadenylation element (EDEN)-like sequences (rich in uridine–purine dinucleotides) present in immune related transcripts such as TNF-α and c-fos where they are scattered throughout the mRNA, are recognized by CUG-BP1 (CUG triplet repeat RNA-binding protein 1, also known as CELF1). In this case, CUG-BP1 is able to directly recruit the PARN deadenylase to induce target mRNA decay (303). Multiple mRNA decay pathways implicating different cis-acting RNA elements, specific adaptor proteins and leading to the recruitment of different effector proteins or complexes are responsible for modulating the stability of hundreds of transcripts during the inflammatory response. Some transcripts, such as those coding for TNF-α contain multiple different cis-acting RNA elements responsible for inducing mRNA destabilisation, allowing for complex regulatory networks responding to multiple inputs.

6.4 Translation-Dependent mRNA Decay

mRNA degradation can be strongly interconnected to other processes such as translation. For example, mRNA quality control pathways, such as nonsense-mediated decay (NMD), no-go decay (NGD) and non-stop decay (NSD) also rely on translation to induce degradation of aberrant mRNAs [for a review see (263)]. However, accumulating evidence indicates that functional mRNAs can be degraded co-translationally, and therefore the rate of translation can influence their degradation rate (262). Other mRNA degradation pathways such as the one mediated by microRNAs have been shown to occur co-translationally and in some cases to depend on target mRNA translation to trigger degradation (304–306). Finally, some target-specific mRNA degradation pathways driven by RBPs have been shown to require mRNA translation in order to license for degradation.

This is illustrated by Regnase-1 (also known as MCPIP1 or ZC3H12A), a RBP recognizing specific stem loop in 3'UTR and harboring an endoribonucleolytic activity thought to act as a negative regulator of pro-inflammatory processes (**Figure 6C**).

Regnase-1-deficient mice develop severe immune disorder and mostly die around 12 weeks old (307) [for an extensive review, see (308)]. In peritoneal macrophages from mice deficient for Regnase-1, TLR-stimulation induces increased levels of IL-6 and IL-12p40 secretion, while TNF-α remains unaffected (307). In line with this, stimulation of human monocytes derived macrophages with IL-1β induces Regnase-1 expression that will, in turn, shorten IL-1β mRNA half life (309). In both studies, the function of Regnase-1 has been linked to its ability to bind RNA stem-loops in the 3'UTR of target mRNAs and induce their rapid degradation through a putative amino-terminal nuclease domain (290). Interestingly, Regnase-1 not only plays its role of anti-inflammatory regulator in myeloid cells, but also in epithelial cells by exerting RNase activity towards the IL-8 mRNA, that stimulates immune cell migration and phagocytosis (310). More recently, Mino et al. could show that Regnase-1 mediated decay occurred in a translation-dependent manner. In this process, the stem-loop RNA structure is first recognized by Regnase-1 prior to the pioneer round of translation. However, this interaction alone is not sufficient for Regnase-1 to induce mRNA cleavage and decay. Instead, during the first round of mRNA translation, translation termination recruits the RNA helicase Upf1 to Regnase-1 which stimulates its RNA-helicase activity leading to unwinding of the stem-loop structure bound by Regnase-1 and allowing target mRNA cleavage (311). Remarkably, Regnase-1 and Roquin share multiple target sites in several transcripts, although not all [as shown for TNF-α whose decay depend on Roquin but not Regnase-1 (301, 307)]. This observation led to the conclusion that Regnase-1 and Roquin could, to some extent, act in concert for a spatio-temporal regulation of common immune-related genes. Indeed, Regnase-1 mediated mRNA decay occurs in the ribosome/endoplasmic reticulum and is translation-dependent, likely playing a role during the early acute phase of immune response. By contrast, Roquin is mainly localized within stress granule, targeting translationally inactive mRNA, in line with a role during the late phase of immune response (290).

MicroRNAs (miRNAs or miR) are other important modulators of mRNA decay and translation by interacting with the 3'UTR of the target transcripts. miRNAs are short (22 to 25 nt long) noncoding RNAs that regulate gene expression in numerous cellular processes. By targeting the 3'UTR of protein coding transcripts, they might directly regulate expression of about 60% of all mammalian genes (312, 313). miRNAs act by guiding the RNA-induced silencing complex (RISC) to interact with mRNAs, inducing translational repression followed by mRNA decay (314). miRNAs have been shown to be critical regulators of immune responses (315, 316). For instance, in hepatocytes, miR-122 is able to repress expression of several kinases involved in STAT3 phosphorylation and promote antiviral immunity by repressing STAT3 signaling pathway (317). Similarly, miR-155 is an important regulator of the innate and adaptive immune response. Its expression is induced in response to pathogen infection and several inflammatory stimuli, and repressed in response to anti-inflammatory cytokines (316, 318). Finally, it has been shown that ISGs have more conserved miRNA target sites in their 3'UTRs than all other cellular mRNAs and are therefore more prone to regulation by the RISC complex (319). Interestingly, infection with viruses or synthetic ligands that activate an antiviral response result in a global inhibition of RISC that removes the negative effect of miRNAs on ISG transcripts to improve their expression and potentiate the antiviral response (319). Furthermore, in some contexts such as during Poxvirus infection, the host miRNA activity is ablated by the viral machinery to avoid direct translation silencing of its own transcripts (320). This action probably outweighs the costs of any possible increase of ISG toxicity. In addition to a direct role of miRNAs in the cell in which they were produced, horizontal transfer of miRNAs through specific vesicles such as exosomes might be a key factor in inflammatory response (321). For example, after binge or chronic alcohol consumption, the number of exosomes containing miR-122 drastically increases in circulation. They are transferred from hepatocytes to monocytes, sensitizing them to the inflammatory response (322). Similarly, alcohol-exposed monocytes communicate with naive monocytes *via* the release of extracellular vesicles containing high levels of miR-27a. These miR-27a cargos lead naive monocytes to differentiate into M2 macrophages (an alternative group of macrophages) (323). Furthermore, macrophages are not the only cell-type sensitive to horizontal transfer of miRNAs during innate responses. This process can also occurs between DCs (324) or between T cells and DCs (325). miRNAs, by binding RNAs, regulating their expression, and being the communication support between immune cells, participate in modulating immune response in quantitative and qualitative ways.

6.5 Stabilization of RNA

Some RBPs, instead of promoting mRNA degradation, increase the stability of both cellular and viral mRNA, either by direct competition for mRNA binding with RBPs involved in mRNA degradation, or indirectly through the regulation of factors involved in mRNA decay. For example, the RBP Arid-5a is exported from the nucleus to the cytoplasm during LPS-mediated macrophage activation. Cytoplasmic Arid-5a thus promotes mRNA stabilization of cytokines such as IL-6, by suppressing the function of Upf1, which is essential for Regnase-1-mediated mRNA decay function (see **Figure 6C**) (326). Notably, these cytokines (*e.g.* IL-6 mRNA) can also be stabilized through the inactivation of miRNAs. Indeed, IL-6 mRNA can be targeted by miR-26 family members for degradation. However, miR-26 family members can be inactivated by TUT4 (Terminal uridylyltransferase 4, also called zcchc11), a ribonucleotidyltransferase (327) which adds uridine residues to the 3' ends of miRNAs, thereby inactivating them. Inactivation of miR-26, that act as inhibitors of IL-6 translation and, thus indirectly promoting IL-6 mRNA stability (328).

Another example of RBP-mediated stability relates to HuR, an ubiquitously expressed RNA binding protein, (also known as ELAV-like protein 1), which is known as one of the most

important AU-rich element (ARE)-containing mRNA stabilizing proteins (329). This RBP contains three RNA recognition motifs (RRMs) called RRM1-to-3. RRM1 & RRM2 domains bind to U/AU-rich RNA (330), whereas the RRM3 domain is able to interact with poly(A) tails of HuR's mRNA targets (331). HuR positively regulates antiviral responses by stabilizing diverse mRNAs in response to RLR or cGAS stimulation, including IFN-β (332), ISGs and regulators of host defense mechanism (332, 333). For example, following RLR stimulation, Polo-like kinase 2 (PLK2), regulates the nuclear translocation of IRF3. HuR has been found to stabilize the mRNA coding for PLK2 (334), increasing PLK2 levels and therefore assisting IRF3 transit into the nucleus in order to activate the transcription of IFNs and ISGs [for extensive review about IRF, see (335)]. Interestingly, HuR mode of action appears to be closely linked to its subcellular localization, that itself depends on the cell type, and the cellular context (*e.g.* naive versus activated cells). Initial studies performed in HEK293 cells, by combining data from different experimental systems such as PAR-CLIP, and whole-transcript expression profiling, have shown that HuR is involved in coupling pre-mRNA processing and mRNA stability, highlighting an important role of HuR within the nucleus through its binding at intronic sequences (336). However, further analysis using THP-1 cells (that, in their naive state, shared HuR properties observed in HEK293 cells) revealed that HuR dramatically modifies its binding properties upon activation. Indeed, cGAMP stimulation was associated with an accumulation of HuR in the cytoplasm, and a concomitant enrichment in cellular transcript 3'UTR binding (333). Those results underline a dynamic network in which RBP tightly regulate the complex changes that occur during immune activation.

RBP-mediated RNA stabilization is also important in the mechanism of action of specific therapeutic regiments or, by contrast, during viral immune escape. For example, under DNA-methyltransferase inhibitors (DNMTis) cancer therapy, myelodysplastic syndrome (MDS) or acute myeloid leukemia (AML) patients are treated with decitabine or azacitidine. This induces the expression of dsRNAs from endogenous retroviruses (ERVs), that are normally silenced by epigenetic regulation. ERVs are in turn recognized by a specific PRR, MDA5, that stimulates an immune response, leading to the death of the cancer cell. Concomitantly, STAU1, which contains multiple dsRBDs, has been shown to cooperate with a long non coding RNA, TINCR, to binds ERV transcripts. The STAU1-TINCR-ERV complex stabilizes ERV transcripts and is required to promote the expected immune response and cell death (337). Therefore, by mediating the efficiency of the DNMTis treatments, levels of STAU1 and TINCR are important indicators of patient receiving DNMTis treatment. Following the same principle, STAU1 has been found to bind and stabilize infectious bursal disease virus (IBDV) dsRNAs, although with a different outcome. Indeed, as opposed to the previous example, binding of STAU1 allows IBDV to escape its recognition by MDA5 and favoring IBDV replication and escape from host antiviral response (*i.e.* IFN response) (338).

In combination, all these RBPs participate in a regulatory network that finely tune inflammation by controlling the fate of diverse mRNAs. RBPs deploy mRNA decay and/or stability mechanisms to maintain immune homeostasis. This is allowed through a timely regulation of RBP activity during immune responses. Indeed, RBPs participate in the positive regulation of rapid pro-inflammatory processes at the onset of immune response and, conversely, appear to play an even more important role in shutting down or reducing inflammation at later time points, thus preventing detrimental tissue damage. Interestingly, this tight regulation appears often regulated by the subcellular localization of RBPs, with RBP harboring different function depending on their local interacting environment. As the mechanisms behind these interactions are still not fully characterized, it will be important to further investigate the different roles and molecular mechanisms by which RBPs regulate mRNA stability during the course of innate immune responses.

7 EPITRANSCRIPTOMICS

In analogy to the epigenetics field, epitranscriptomics involves a biochemical modification of the ribonucleotide sequence. This field of RNA modification has been recently recognized as an important layer in post-transcriptional regulation of gene expression. The source of this emergence comes from the technical advances in the detection and mapping of chemically modified bases (339, 340). Transfer RNA (tRNAs) are the most modified RNA species, with up to 25% of their bases being post-transcriptionally modified (341, 342). tRNAs but also rRNA, snRNA, lncRNA, miRNA or mRNA, among others, can bear such modifications (341–343). These modifications can be simple methylations but also complex multistep transformation with incorporation of low-molecular-weight metabolites (341). A large number of modifications have thus been identified in coding and non-coding RNAs. While m^6A is the most common mRNA reversible post-transcriptional modification (344), alternative reversible methylation can also occur on the carbon of the fifth position on cytosine (5-methylcytidine or m^5C) or on the nitrogen of the first position on adenine (N^1-methyladenosine or m^1A). Other types of RNA modifications such as Cytidine-to-Uracil or Adenine-to-Inosine RNA editing (C-to-U or A-to-I, respectively) can lead to changes in the secondary structure of the edited RNA (345) and in the protein sequence encoded by the mRNAs in case of editing events taking place within the coding sequence (346). Pseudouridine, a C5-glycoside isomer of uridine, is necessary to support proper secondary and tertiary structures of rRNAs and tRNAs, thus affecting mRNA translation (347). Mechanistically, most of these RNA modifications involve writer and reader proteins. Others, such as m^6A and m^1A, can involve additional eraser proteins allowing reversible and dynamic modifications (348). The writers are the RNA-modifying enzymes able to catalyze the transfer of the chemical group on the ribonucleotide targets (*e.g.*

methyltransferase), while the eraser proteins can reverse the modifications by specifically removing the chemical groups from the RNA targets. Finally, the readers are the RNA-binding proteins able to specifically bind the RNA bases bearing the chemical modification (see **Figure 7A**) (342, 358).

It is now well recognized that epitranscriptomics affects several molecular processes. In the immune system, while epitranscriptomics appears important during hematopoietic stem cell differentiation (359), it is currently viewed as a major mechanism that allows self- and non-self dsRNAs discrimination during innate responses (348, 360). Indeed, while dsRNA is a feature found in numerous viruses, endogenous dsRNAs are also found in healthy cells, originating from transcription of endogenous retroviruses, mitochondrial transcripts, or inverted-Alu repeat sequences (353, 361). This raises an important challenge for innate receptors (*e.g.* RIG-I or MDA5), since they need to discriminate between self and non-self dsRNA molecules. While evolutionary elimination of dsRNA sequences within cellular mRNAs has been observed, which should limit innate immune activation against host RNAs, dsRNAs remain frequent in pre-mRNAs (362). One way to circumvent this issue is through modification of dsRNAs in order to prevent their recognition by PRRs and downstream type I IFN responses. Such a mechanism is well illustrated by the Aicardi Goutieres Syndrom, an inflammatory disorder affecting mainly the brain and the skin and associated with aberrant type I IFN production. Aicardi Goutieres Syndrom is associated with mutations in ADAR1, a dsRNA specific adenosine deaminase responsible for the most common cellular RNA editing through hydrolytic deanylation of Adenosine to Inosine (A-I editing) (363, 364). In line with this, ADAR1 deficient human monocytes derived macrophages leads to increased RLR signaling and pro-inflammatory cytokines (*e.g.* IFNs, IL-1, IL-6) production.

Through A-I editing, ADAR1 appears to modify host dsRNAs, preventing their recognition by dsRNA innate sensors. Accordingly, mutant mice carrying an ADAR1 protein that is editing deficient ($ADAR1^{E861A/E861A}$) are embryonically lethal, and present over-activation of IFNs and dsRNA-sensing pathways. This deregulated innate responses are due to a lack of A-I editing in ADAR1 $ADAR1^{E861A/E861A}$ embryos, as further shown by a decrease in A-I editing in a vast majority of RNA targets. Moreover, the phenotype of ADAR1 $ADAR1^{E861A/E861A}$ can be rescued by a concurrent deletion of MDA5 (352). Similarly ADAR1-/- mice are embryonically lethal and this phenotype can be rescued by crossing ADAR1-/- to MAVS-/- mice (348). In those double knock-out mice, the aberrant type I IFN response induced by ADAR deficiency is prevented by inhibiting the RLR pathway (348, 352). Likewise, ADAR1 deficiency confers A549 human lung epithelial cell lines with a lethal phenotype and MAVS ablation partially restores ADAR1-/- cells' survival. However, in this cell type, full rescue of ADAR1-/- lethality is obtained by an additional ablation of RNase L, an ISG induced upon dsRNA sensing that leads to translation arrest by cleaving rRNAs and mRNAs (see section *RNA Sensing and Regulation of PRR Activity by Non-PRR RBPs*). ADAR1 appears as an essential protein in protecting host dsRNA from innate recognition, thus preventing aberrant innate responses against self (see **Figure 7B**) (348).

Altogether, these results led to the elegant hypothesis that editing of host RNAs by ADAR1 could prevent their recognition by innate sensors (*e.g.* RLR, RNase L) while viral RNAs, which are not edited, would trigger robust innate responses (348). However, in some contexts of infection, several studies have described ADAR1 as a proviral factor. This is notably the case following infection with Vesicular Stomatitis Virus (VSV) (365), Zika virus (366), HIV (367), HCV (364) or Measles Virus (368). One major mechanism by which ADAR1 promotes viral replication is through inhibition of PKR. As mentioned earlier (section *Viral RNA Translation Control*), PKR is an IFN-inducible protein that, following dsRNA recognition, phosphorylates eIF2α, favors the formation of stress granules, and acts as a major inhibitor of global translation (for both cellular and viral mRNAs). ADAR1 mediated inhibition of PKR occurs in a editing-dependent or -independent way, and mostly requires direct interactions between ADAR1 and PKR (353, 369). ADAR1 is thus seen as an important inhibitor of self-recognition in homeostatic conditions, to prevent auto-immune disorder, but paradoxically might, in some context, favor viral replication following infection. Finally, two distinct isoforms have recently been described for ADAR1, a cytoplasmic isoform (p150) and a nuclear one (p110), endowed with pro- and anti-viral properties, respectively (370). This suggest additional levels for ADAR1 regulation, and further studies will be required to fully comprehend the overall impact of ADAR1 activity in homeostatic condition or following infection.

Other RNA modification mechanisms have been described, that allow induction of innate responses specifically towards viral RNAs, while protecting host RNA recognition by innate sensors. For example, PKR is able to recognize short stem loops in a 5' triphosphate dependent manner, knowing that 5' triphosphate are mostly present in viral or bacterial transcript (369). Likewise in DCs, RNA from bacteria that is devoid of nucleoside modifications, induces strong activation of TLR3, TLR7 and TLR8, while host RNAs carrying modified nucleosides (m^5c, m^6A, m^5U, s^2U or pseudo-uridine) induce little or no stimulation (371). Similarly, the presence of m^6A modifications in host circular RNAs inhibits their recognition by PRR while unmodified circular RNAs, present mostly in viral genomes, are known to activate RIG-I leading to downstream stimulation of IFN gene expression (372). The latter example also emphasize the importance of nucleoside modification readers. Indeed, YTHDF2 reader allows the discrimination between host *versus* foreign circular RNAs through the binding and the sequestration of m^6A containing host circular RNAs (372). m^6A modification can have additional impact during innate immune responses, favoring the expression of important immune players. Thus, it has been shown in DCs that methyltransferase-like 3 (METTL3), a well know writer of m^6A modification (373), catalyzes the m^6A modification of membrane co-stimulatory molecules, CD40, CD80 and a TLR signaling adaptor Tirap, during DC maturation. These modifications are read by YTHDF1, which promotes their translation by associating with translation

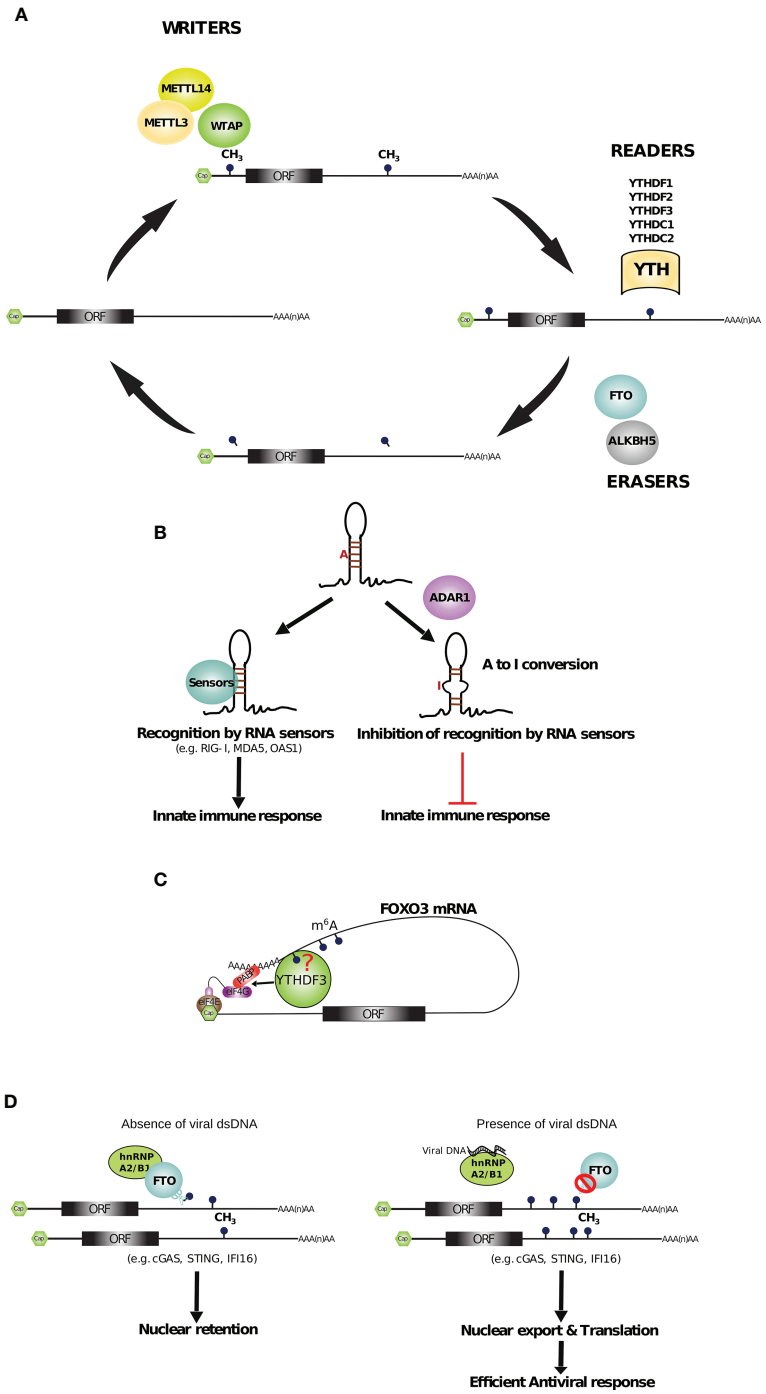

FIGURE 7 | RBPs mediated epitranscriptomic regulation of innate immunity. **(A)** m^{6}A modifications, elicited by methyltransferases (METTL3, METTL14 and WTAP), are read by YTH domain-containing proteins (YTHDF1-3, YTHDC 1-2) and reversed by the erasers (FTO and ALKBH5) to dynamically control the gene expression at the post-transcriptional level (349–351). **(B)** Recognition of endogenous dsRNAs by RNA sensors (e.g. RIG-I, MDA5 and OAS1) induces an innate immune response. However, A-to-I mediated base editing mediated by adenosine deaminase ADAR1 inhibits this process (352–354). **(C)** YTHDF3 promotes FOXO3 mRNA translation by binding the 5'UTR and circularizing the mRNA. The requirement of m^{6}A for YTHDF3 recruitment has not been elucidated yet (355). **(D)** On the left, hnRNPA2B1 interacts with FTO, a m^{6}A demethylase, to remove the m^{6}A modifications from hnRNPA2B1 mRNA targets. Thus, these mRNAs, important for the antiviral response, are retained into the nucleus. On the right, when viral DNA is sensed by hnRNPA2B1, the interaction with FTO is disrupted and hnRNPA2B1 targets, containing more m^{6}A modifications, are exported to the cytoplasm to be translated and to activate an efficient antiviral response (356, 357).

initiation factors. m^{6}A modifications thus lead to an increase of DC activation and function, promoting T-cell activation (360, 371, 374, 375),. YTHDF3, another reader of m^{6}A in RNAs has been shown to bind and promote translation of the transcription factor forkhead box protein O3 (FOXO3) RNA, a negative regulator of ISGs expression (355). By binding to the 5'UTR of FOXO3 transcript, YTHDF3 cooperates with PABP1 and eIF4G2 to stimulate its translation (see **Figure 7C**). Although YTHDF3 recognizes m^{6}A modified RNA targets to regulate their translation, its recruitment to FOXO3 mRNAs appears independent of METTL3 mediated m^{6}A addition. Nevertheless, the interaction depends on the hydrophobic pocket of YTHDF3 that is essential for m^{6}A recognition thus suggesting that other methyltransferases could be involved in m^{6}A addition on FOXO3 transcripts. Alternatively, YTHDF3 could interact with FOXO3 transcripts in a m^{6}A-independent manner, or recognise other types of methylated bases (such as m^{1}A). Thus, YTHDF3 participates indirectly to the negative control of antiviral responses by promoting translation of ISG inhibitors to limit the risk of unnecessary inflammation (355). Similarly, upon viral infections, the nuclear RNA-helicase DDX46 has been shown to recruit the m^{6}A demethylase protein ALKBH5 to the MAVS, Trif3 and Trif6 mRNAs inducing their nuclear retention to avoid their translation and prevent prolonged activation of the antiviral response (376). Dynamic m^{6}A modification is also involved in the antiviral response against DNA viruses. For instance, the viral DNA sensor hnRNPA2B1, in addition to its role in inducing the IFN signaling pathway, has been shown to interact with mRNAs coding for many innate immunity factors such as cGAS, STING and IFI16 (an ISG) (356, 357). In the absence of infection, hnRNPA2B1 interacts with the m^{6}A demethylase FTO to remove m^{6}A from hnRNPA2B1 targets and induce their nuclear retention. Upon viral DNA sensing, the interaction between FTO and hnRNPA2B1 is disrupted, leading to increase m^{6}A levels in hnRNPA2B1 target transcripts, therefore allowing their efficient nuclear export and translation to improve the antiviral response (**Figure 7D**).

Taken together, these results suggest that epitranscriptomics is a strategy used to prevent autoimmunity and balance the risk between an aberrant induction of innate response and self-tolerance (353, 362). However, more investigations are required to precisely apprehend the complex interplay between self-RNA and viral-RNA modifications, since factors involved in self-RNA disguise are not necessarily detrimental for viral RNA (and *vice versa*), suggesting that each of these factors is involved in several cellular mechanisms.

8 CONCLUSIONS AND PERSPECTIVES

Through their capacity to interact with specific RNA sequences, structural features or chemical modifications, RBPs orchestrate all steps of RNA metabolism from its synthesis, maturation and functional role, to its eventual decay. In the context of innate immunity, RBPs play multiple roles, acting at the first line of defense through their capacity to sense non-self RNAs and induce an immune response, being involved in the activation and effector functions of innate immune cells by finely tuning the amplitude and temporal control of gene expression, and finally acting as key effectors of the antiviral response through their capacity to destroy foreign RNAs. The activity of RBPs is tightly regulated by numerous mechanisms that include control of their subcellular localization, competition with other RBPs for their RNA substrate, or post-translational modifications that modulate their activity. Working in a collaborative network with signal transducers, epigenetic modifiers, and canonical trans-acting factors, RBPs play important roles in developing a global and complex gene regulatory network. Illustrating their importance in finely tuning the innate immune response, numerous human pathologies, such as autoimmune diseases, are associated to mutations in genes coding for RBPs [for a review see (377)]. Technical developments such as the RNA interactome capture (RIC) (31) and CLIP-seq have facilitated the functional identification of new RBPs and the characterization of their exact RNA binding sites. To date, more than 1000 human encoded proteins have been shown to display RNA-binding capacity (378) and the precise RNA target sites for several hundreds of these RBPs have been mapped (62). Nevertheless, we are still far from understanding precisely the numerous roles of RBPs and their mechanisms of action in the context of innate immunity. The rapid development of efficient gene editing technologies coupled with new protocols to quantitatively monitor gene expression at multiple levels (transcription and degradation rates, splicing and translation) in bulk and single-cells, as well as methods to quantitatively assess the binding dynamics of RBPs in single-molecule or transcriptome-wide assays opens the door for new and exciting discoveries in the field of RBPs and innate immunity.

AUTHOR CONTRIBUTIONS

AG and ER determined the scope and focus of the review with feedback from AK and MW. AG drafted the manuscript with contributions from ER and MW. AK generated most figures with help from AG and ER. All authors contributed to the article and approved the submitted version.

FUNDING

Work in our laboratory is supported by the European Research Council (ERC-StG-LS6-805500) under the European Union's Horizon 2020 research and innovation programs; ATIP-Avenir program; Fondation FINOVI; Agence Nationale des Recherches sur le SIDA et les Hépatites Virales (ANRS-ECTZ3306) and Agence Nationale de la Recherche (ANR-20-CE15-0025).

ACKNOWLEDGMENTS

We would like to thank Geneviève Fourel for critical reading of the manuscript. We also would like to thank the members of the RNA metabolism in immunity and infection's group for many fruitful discussions.

REFERENCES

1. Swamy M, Jamora C, Havran W, Hayday A. Epithelial Decision Makers: In Search of the "Epimmunome". *Nat Immunol* (2010) 11:656–65. doi: 10.1038/ni.1905
2. Kaye PM. Stromal Cell Responses in Infection. *Stromal Immunol Adv Exp Med Biol* (2018) 14:23–36. doi: 10.1007/978-3-319-78127-3_2
3. Sato A, Iwasaki A. Induction of Antiviral Immunity Requires Toll-Like Receptor Signaling in Both Stromal and Dendritic Cell Compartments. *PNAS* (2004) 101:16274–9. doi: 10.1073/pnas.0406268101
4. Constant DA, Nice TJ, Rauch I. Innate Immune Sensing by Epithelial Barriers. *Curr Opin Immunol* (2021) 73:1–8. doi: 10.1016/j.coi.2021.07.014
5. Cabeza-Cabrerizo M, Cardoso A, Minutti CM, Pereira da Costa M, Reis e Sousa C. Dendritic Cells Revisited. *Annu Rev Immunol* (2021) 39:131–66. doi: 10.1146/annurev-immunol-061020-053707
6. Durbin JE, Fernandez-Sesma A, Lee CK, Rao TD, Frey AB, Moran TM, et al. Type I Ifn Modulates Innate and Specific Antiviral Immunity. *J Immunol* (2000) 164:4220–8. doi: 10.4049/jimmunol.164.8.4220
7. Kohlmeier JE, Cookenham T, Roberts AD, Miller SC, Woodland DL. Type I Interferons Regulate Cytolytic Activity of Memory Cd8+ T Cells in the Lung Airways During Respiratory Virus Challenge. *Immunity* (2010) 33:96–105. doi: 10.1016/j.immuni.2010.06.016
8. Bianchi ME. Damps, Pamps and Alarmins: All We Need to Know About Danger. *J Leukocyte Biol* (2007) 81:1–5. doi: 10.1189/jlb.0306164
9. Thompson MR, Kaminski JJ, Kurt-Jones EA, Fitzgerald KA. Pattern Recognition Receptors and the Innate Immune Response to Viral Infection. *Viruses* (2011) 3:920–40. doi: 10.3390/v3060920
10. Schiller M, Parcina M, Heyder P, Foermer S, Ostrop J, Leo A, et al. Induction of Type I Ifn Is a Physiological Immune Reaction to Apoptotic Cell-Derived Membrane Microparticles. *J Immunol* (2012) 189:1747–56. doi: 10.4049/jimmunol.1100631
11. Gokhale NS, Smith JR, Van Gelder RD, Savan R. RNA Regulatory Mechanisms That Control Antiviral Innate Immunity. *Immunol Rev* (2021) 304:imr.13019. doi: 10.1111/imr.13019
12. Takeuchi O, Akira S. Pattern Recognition Receptors and Inflammation. *Cell* (2010) 140:805–20. doi: 10.1016/j.cell.2010.01.022
13. Chovatiya R, Medzhitov R. Stress, Inflammation, and Defense of Homeostasis. *Mol Cell* (2014) 54:281–8. doi: 10.1016/j.molcel.2014.03.030
14. Fan J, Ishmael FT, Fang X, Myers A, Cheadle C, Huang SK, et al. Chemokine Transcripts as Targets of the RNA-Binding Protein HuR in Human Airway Epithelium. *J Immunol* (2011) 186:2482–94. doi: 10.4049/jimmunol.0903634
15. Lin JX, Leonard WJ. Fine-Tuning Cytokine Signals. *Annu Rev Immunol* (2019) 37:295–324. doi: 10.1146/annurev-immunol-042718-041447
16. Cavaillon JM. Pro- Versus Anti-Inflammatory Cytokines: Myth or Reality. *Cell Mol Biol (Noisy-Le-Grand France)* (2001) 47:695–702.
17. Guo H, Callaway JB, Ting JPY. Inflammasomes: Mechanism of Action, Role in Disease, and Therapeutics. *Nat Med* (2015) 21:677–87. doi: 10.1038/nm.3893
18. Pietras EM. Inflammation: A Key Regulator of Hematopoietic Stem Cell Fate in Health and Disease. *Blood* (2017) 130:1693–8. doi: 10.1182/blood-2017-06-780882
19. Smale ST. Transcriptional Regulation in the Innate Immune System. *Curr Opin Immunol* (2012) 24:51–7. doi: 10.1016/j.coi.2011.12.008
20. Medzhitov R, Horng T. Transcriptional Control of the Inflammatory Response. *Nat Rev Immunol* (2009) 9:692–703. doi: 10.1038/nri2634
21. Carpenter S, Ricci EP, Mercier BC, Moore MJ, Fitzgerald KA. Post-Transcriptional Regulation of Gene Expression in Innate Immunity. *Nat Rev Immunol* (2014) 14:361–76. doi: 10.1038/nri3682
22. Anderson P. Post-Transcriptional Regulons Coordinate the Initiation and Resolution of Inflammation. *Nat Rev Immunol* (2010) 12:24–35. doi: 10.1038/nri2685
23. Rauscher R, Ignatova Z. Tuning Innate Immunity by Translation. *Biochem Soc Trans* (2015) 43:1247–52. doi: 10.1042/BST20150166
24. García-Mauriño SM, Rivero-Rodríguez F, Velázquez-Cruz A, Hernández-Vellisca M, Díaz-Quintana A, de la Rosa MA, et al. RNA Binding Protein Regulation and Cross-Talk in the Control of AU-Rich mRNA Fate. *Front Mol Biosci* (2017) 4:71. doi: 10.3389/fmolb.2017.00071
25. Turner M, Díaz-Muñoz MD. RNA-Binding Proteins Control Gene Expression and Cell Fate in the Immune System. *Nat Immunol* (2018) 19:120–9. doi: 10.1038/s41590-017-0028-4
26. Kafasla P, Skliris A, Kontoyiannis DL. Post-Transcriptional Coordination of Immunological Responses by RNA-Binding Proteins. *Nat Immunol* (2014) 15:492–502. doi: 10.1038/ni.2884
27. Gerstberger S, Hafner M, Tuschl T. A Census of Human RNA-Binding Proteins. *Nat Rev Genet* (2014) 15:829–45. doi: 10.1038/nrg3813
28. Hudson WH, Ortlund EA. The Structure, Function and Evolution of Proteins That Bind DNA and RNA. *Nat Rev Mol Cell Biol* (2014) 15:749–60. doi: 10.1038/nrm3884
29. Re A, Joshi T, Kulberkyte E, Morris Q, Workman CT. RNA–Protein Interactions: An Overview. In: Gorodkin J and Ruzzo WL, editors. *RNA Sequence, Structure, and Function: Computational and Bioinformatic Methods*, vol. 1097. Totowa, NJ: Humana Press (2014). p. 491–521. doi: 10.1007/978-1-62703-709-9
30. Hentze MW, Castello A, Schwarzl T, Preiss T. A Brave New World of RNA-Binding Proteins. *Nat Rev Mol Cell Biol* (2018) 19:327–41. doi: 10.1038/nrm.2017.130
31. Garcia-Moreno M, Noerenberg M, Ni S, Järvelin AI, González-Almela E, Lenz CE, et al. System-Wide Profiling of RNA-Binding Proteins Uncovers Key Regulators of Virus Infection. *Mol Cell* (2019) 74:196–211.e11. doi: 10.1016/j.molcel.2019.01.017
32. Liepelt A, Naarmann-de Vries IS, Simons N, Eichelbaum K, Föhr S, Archer SK, et al. Identification of RNA-Binding Proteins in Macrophages by Interactome Capture. *Mol Cell Proteomics* (2016) 15:2699–714. doi: 10.1074/mcp.M115.056564
33. Schmidt N, Lareau CA, Keshishian H, Ganskih S, Schneider C, Hennig T, et al. The Sars-Cov-2 RNA–Protein Interactome in Infected Human Cells. *Nat Microbiol* (2021) 6:339–53. doi: 10.1038/s41564-020-00846-z
34. Kamel W, Noerenberg M, Cerikan B, Chen H, Järvelin AI, Kammoun M, et al. Global Analysis of Protein-RNA Interactions in Sars-Cov-2-Infected Cells Reveals Key Regulators of Infection. *Mol Cell* (2021) 81:2851–67.e7. doi: 10.1016/j.molcel.2021.05.023
35. Ramanathan M, Porter DF, Khavari PA. Methods to Study RNA–protein Interactions. *Nat Methods* (2019) 16:225–34. doi: 10.1038/s41592-019-0330-1
36. Zhang C, Darnell RB. Mapping *In Vivo* Protein-RNA Interactions at Single-Nucleotide Resolution From Hits-Clip Data. *Nat Biotechnol* (2011) 29:607–14. doi: 10.1038/nbt.1873
37. Wheeler EC, Van Nostrand EL, Yeo GW. Advances and Challenges in the Detection of Transcriptome-Wide Protein– RNA Interactions. *WIREs RNA* (2018) 9:e1436. doi: 10.1002/wrna.1436
38. Liu ZR, Wilkie AM, Clemens MJ, Smith CW. Detection of Double-Stranded RNA-Protein Interactions by Methylene Blue-Mediated Photo-Crosslinking. *RNA* (1996) 2:611–21.
39. Ricci EP, Kucukural A, Cenik C, Mercier BC, Singh G, Heyer EE, et al. Staufen1 Senses Overall Transcript Secondary Structure to Regulate Translation. *Nat Struct Mol Biol* (2014) 21:26–35. doi: 10.1038/nsmb.2739
40. Urdaneta EC, Beckmann BM. Fast and Unbiased Purification of RNA-Protein Complexes After UV Cross-Linking. *Methods* (2020) 178:72–82. doi: 10.1016/j.ymeth.2019.09.013
41. Jensen KB, Darnell RB. Clip: Crosslinking and Immunoprecipitation of *In Vivo* RNA Targets of RNA-Binding Proteins. *Methods Mol Biol (Clifton NJ)* (2008) 488:85–98. doi: 10.1007/978-1-60327-475-3_6
42. Beckmann BM. RNA Interactome Capture in Yeast. *Methods* (2017) 118-119:82–92. doi: 10.1016/j.ymeth.2016.12.008
43. Hafner M, Landthaler M, Burger L, Khorshid M, Hausser J, Berninger P, et al. Transcriptome-Wide Identification of RNA-Binding Protein and MicroRNA Target Sites by PAR-CLIP. *Cell* (2010) 141:129–41. doi: 10.1016/j.cell.2010.03.009
44. Liu ZR, Sargueil B, Smith CW. Methylene Blue-Mediated Cross-Linking of Proteins to Double-Stranded RNA. *Methods Enzymol* (2000) 318:22–33. doi: 10.1016/S0076-6879(00)18041-3
45. Singh G, Ricci EP, Moore MJ. Ripit-Seq: A High-Throughput Approach for Footprinting RNA:Protein Complexes. *Methods* (2014) 65:320–32. doi: 10.1016/j.ymeth.2013.09.013

46. Woodward L, Gangras P, Singh G. Identification of Footprints of RNA: Protein Complexes *via* RNA Immunoprecipitation in Tandem Followed by Sequencing (Ripit-Seq). *J Visual Experiments* (2019) 59913:e59913. doi: 10.3791/59913
47. Patton RD, Sanjeev M, Woodward LA, Mabin JW, Bundschuh R, Singh G. Chemical Crosslinking Enhances RNA Immunoprecipitation for Efficient Identification of Binding Sites of Proteins That Photo-Crosslink Poorly With RNA. *RNA* (2020) 26:1216–33. doi: 10.1261/rna.074856.120
48. Yi Z, Singh G. Ripit-Seq: A Tandem Immunoprecipitation Approach to Reveal Global Binding Landscape of Multisubunit Ribonucleoproteins. *Methods Enzymol* (2021) 655:401–25. doi: 10.1016/bs.mie.2021.03.019
49. Singh G, Kucukural A, Cenik C, Leszyk J, Shaffer S, Weng Z, et al. The Cellular Ejc Interactome Reveals Higher-Order Mrnp Structure and an Ejc-Sr Protein Nexus. *Cell* (2012) 151:750–64. doi: 10.1016/j.cell.2012.10.007
50. Castello A, Horos R, Strein C, Fischer B, Eichelbaum K, Steinmetz LM, et al. System-Wide Identification of RNA-Binding Proteins by Interactome Capture. *Nat Protoc* (2013) 8:491–500. doi: 10.1038/nprot.2013.020
51. Perez-Perri JI, Rogell B, Schwarzl T, Stein F, Zhou Y, Rettel M, et al. Discovery of RNA-Binding Proteins and Characterization of Their Dynamic Responses by Enhanced RNA Interactome Capture. *Nat Commun* (2018) 9:4408. doi: 10.1038/s41467-018-06557-8
52. McHugh CA, Guttman M. RAP-MS: A Method to Identify Proteins That Interact Directly With a Specific RNA Molecule in Cells. *Methods Mol Biol* (2018) 1649:473–88. doi: 10.1007/978-1-4939-7213-5_31
53. Castello A, Fischer B, Eichelbaum K, Horos R, Beckmann B, Strein C, et al. Insights Into RNA Biology From an Atlas of Mammalian mRNA-Binding Proteins. *Cell* (2012) 149:1393–406. doi: 10.1016/j.cell.2012.04.031
54. Castello A, Horos R, Strein C, Fischer B, Eichelbaum K, Steinmetz LM, et al. Comprehensive Identification of RNA-Binding Proteins by RNA Interactome Capture. *Methods Mol Biol* (2016) 1358:131–9. doi: 10.1007/978-1-4939-3067-8_8
55. Bantscheff M, Lemeer S, Savitski MM, Kuster B. Quantitative Mass Spectrometry in Proteomics: Critical Review Update From 2007 to the Present. *Anal Bioanal Chem* (2012) 404:939–65. doi: 10.1007/s00216-012-6203-4
56. Grandi P, Bantscheff M. Advanced Proteomics Approaches to Unravel Protein Homeostasis. *Drug Discov Today: Technol* (2019) 31:99–108. doi: 10.1016/j.ddtec.2019.02.001
57. de Vries S, Benes V, Naarmann-de Vries IS, Rücklé C, Zarnack K, Marx G, et al. P23 Acts as Functional Rbp in the Macrophage Inflammation Response. *Front Mol Biosci* (2021) 8:625608. doi: 10.3389/fmolb.2021.625608
58. Ule J. CLIP Identifies Nova-Regulated RNA Networks in the Brain. *Science* (2003) 302:1212–5. doi: 10.1126/science.1090095
59. Huppertz I, Attig J, D'Ambrogio A, Easton LE, Sibley CR, Sugimoto Y, et al. Iclip: Protein–RNA Interactions at Nucleotide Resolution. *Methods* (2014) 65:274–87. doi: 10.1016/j.ymeth.2013.10.011
60. Van Nostrand EL, Pratt GA, Shishkin AA, Gelboin-Burkhart C, Fang MY, Sundararaman B, et al. Robust Transcriptome-Wide Discovery of RNA-Binding Protein Binding Sites With Enhanced Clip (Eclip). *Nat Methods* (2016) 13:508–14. doi: 10.1038/nmeth.3810
61. Heyl F, Maticzka D, Uhl M, Backofen R. Galaxy Clip-Explorer: A Web Server for Clip-Seq Data Analysis. *GigaScience* (2020) 9:giaa108. doi: 10.1093/gigascience/giaa108
62. Van Nostrand EL, Freese P, Pratt GA, Wang X, Wei X, Xiao R, et al. A Large-Scale Binding and Functional Map of Human RNA-Binding Proteins. *Nature* (2020) 583:711–9. doi: 10.1038/s41586-020-2077-3
63. Sharma D, Zagore LL, Brister MM, Ye X, Crespo-Hernández CE, Licatalosi DD, et al. The Kinetic Landscape of an RNA-Binding Protein in Cells. *Nature* (2021) 591:152–6. doi: 10.1038/s41586-021-03222-x
64. Uehata T, Takeuchi O. RNA Recognition and Immunity—Innate Immune Sensing and Its Posttranscriptional Regulation Mechanisms. *Cells* (2020) 9:1701. doi: 10.3390/cells9071701
65. Hardy MP, Audemard Ă, Migneault F, Feghaly A, Brochu S, Gendron P, et al. Apoptotic Endothelial Cells Release Small Extracellular Vesicles Loaded With Immunostimulatory Viral-Like RNAs. *Sci Rep* (2019) 9:7203. doi: 10.1038/s41598-019-43591-y
66. Nabet BY, Qiu Y, Shabason JE, Wu TJ, Yoon T, Kim BC, et al. Exosome RNA Unshielding Couples Stromal Activation to Pattern Recognition Receptor Signaling in Cancer. *Cell* (2017) 170:352–66.e13. doi: 10.1016/j.cell.2017.06.031
67. Alexopoulou L, Czopik Holt A, Medzhitov R, Flavell RA. Recognition of double-strandedRNA and Activation of NF-Kbby Toll-Like Receptor 3. *Nature* (2001) 413:732–8. doi: 10.1038/35099560
68. Leonard JN, Ghirlando R, Askins J, Bell JK, Margulies DH, Davies DR, et al. The TLR3 Signaling Complex Forms by Cooperative Receptor Dimerization. *Proc Natl Acad Sci* (2008) 105:258–63. doi: 10.1073/pnas.0710779105
69. Tatematsu M, Nishikawa F, Seya T, Matsumoto M. Toll-Like Receptor 3 Recognizes Incomplete Stem Structures in Single-Stranded Viral RNA. *Nat Commun* (2013) 4:1833. doi: 10.1038/ncomms2857
70. Heil F. Species-Specific Recognition of Single-Stranded RNA *via* Toll-Like Receptor 7 and 8. *Science* (2004) 303:1526–9. doi: 10.1126/science.1093620
71. Greulich W, Wagner M, Gaidt MM, Stafford C, Cheng Y, Linder A, et al. TLR8 Is a Sensor of RNAse T2 Degradation Products. *Cell* (2019) 179:1264–75.e13. doi: 10.1016/j.cell.2019.11.001
72. Diebold SS. Innate Antiviral Responses by Means of TLR7-Mediated Recognition of Single-Stranded RNA. *Science* (2004) 303:1529–31. doi: 10.1126/science.1093616
73. Tanji H, Ohto U, Shibata T, Taoka M, Yamauchi Y, Isobe T, et al. Toll-Like Receptor 8 Senses Degradation Products of Single-Stranded RNA. *Nat Struct Mol Biol* (2015) 22:109–15. doi: 10.1038/nsmb.2943
74. Cavassani KA, Ishii M, Wen H, Schaller MA, Lincoln PM, Lukacs NW, et al. TLR3 Is an Endogenous Sensor of Tissue Necrosis During Acute Inflammatory Events. *J Exp Med* (2008) 205:2609–21. doi: 10.1084/jem.20081370
75. Rehwinkel J, Gack MU. RIG-I-Like Receptors: Their Regulation and Roles in RNA Sensing. *Nat Rev Immunol* (2020) 20:537–51. doi: 10.1038/s41577-020-0288-3
76. He WT, Wan H, Hu L, Chen P, Wang X, Huang Z, et al. Gasdermin D Is an Executor of Pyroptosis and Required for Interleukin-1β Secretion. *Cell Res* (2015) 25:1285–98. doi: 10.1038/cr.2015.139
77. Stogerer T, Stager S. Innate Immune Sensing by Cells of the Adaptive Immune System. *Front Immunol* (2020) 11:1081. doi: 10.3389/fimmu.2020.01081
78. Wang Y, Yuan S, Jia X, Ge Y, Ling T, Nie M, et al. Mitochondria-Localised ZNFX1 Functions as a dsRNA Sensor to Initiate Antiviral Responses Through MAVS. *Nat Cell Biol* (2019) 21:1346–56. doi: 10.1038/s41556-019-0416-0
79. Mahony R, Broadbent L, Maier-Moore JS, Power UF, Jefferies CA. The RNA Binding Protein La/SS-B Promotes RIG-I-Mediated Type I and Type III IFN Responses Following Sendai Viral Infection. *Sci Rep* (2017) 7:14537. doi: 10.1038/s41598-017-15197-9
80. Wickenhagen A, Sugrue E, Lytras S, Kuchi S, Noerenberg M, Turnbull ML, et al. A Prenylated Dsrna Sensor Protects Against Severe Covid-19. *Science* (2021) 374:eabj3624. doi: 10.1126/science.abj3624
81. Hung T, Pratt GA, Sundararaman B, Townsend MJ, Chaivorapol C, Bhangale T, et al. The Ro60 Autoantigen Binds Endogenous Retroelements and Regulates Inflammatory Gene Expression. *Science* (2015) 350:455–9. doi: 10.1126/science.aac7442
82. Lee S, Karki R, Wang Y, Nguyen LN, Kalathur RC, Kanneganti TD. Aim2 Forms a Complex With Pyrin and Zbp1 to Drive Panoptosis and Host Defence. *Nature* (2021) 597:415–9. doi: 10.1038/s41586-021-03875-8
83. Jiao H, Wachsmuth L, Kumari S, Schwarzer R, Lin J, Eren RO, et al. Z-Nucleic-Acid Sensing Triggers ZBP1-Dependent Necroptosis and Inflammation. *Nature* (2020) 580:391–5. doi: 10.1038/s41586-020-2129-8
84. Zhang T, Yin C, Boyd DF, Quarato G, Ingram JP, Shubina M, et al. Influenza Virus Z-Rnas Induce Zbp1-Mediated Necroptosis. *Cell* (2020) 180:1115–29.e13. doi: 10.1016/j.cell.2020.02.050
85. Thomas PG, Shubina M, Balachandran S. ZBP1/DAI-Dependent Cell Death Pathways in Influenza A Virus Immunity and Pathogenesis (Springer Berlin Heidelberg). *Curr Topics Microbiol Immunol* (2019) 1–23. doi: 10.1007/82_2019_90
86. Zhang Z, Ohto U, Shibata T, Krayukhina E, Taoka M, Yamauchi Y, et al. Structural Analysis Reveals That Toll-Like Receptor 7 Is a Dual Receptor for

Guanosine and Single-Stranded RNA. *Immunity* (2016) 45:737–48. doi: 10.1016/j.immuni.2016.09.011
87. Ostendorf T, Zillinger T, Andryka K, Schlee-Guimaraes TM, Schmitz S, Marx S, et al. Immune Sensing of Synthetic, Bacterial, and Protozoan RNA by Toll-Like Receptor 8 Requires Coordinated Processing by RNase T2 and RNase 2. *Immunity* (2020) 52:591–605.e6. doi: 10.1016/j.immuni.2020.03.009
88. Liu K, Sato R, Shibata T, Hiranuma R, Reuter T, Fukui R, et al. Skewed Endosomal RNA Responses From Tlr7 to Tlr3 in RNAse T2-Deficient Macrophages. *Int Immunol* (2021) 33:479–90. doi: 10.1093/intimm/dxab033
89. Zhang Z, Ohto U, Shibata T, Taoka M, Yamauchi Y, Sato R, et al. Structural Analyses of Toll-Like Receptor 7 Reveal Detailed RNA Sequence Specificity and Recognition Mechanism of Agonistic Ligands. *Cell Rep* (2018) 25:3371–81.e5. doi: 10.1016/j.celrep.2018.11.081
90. Shibata T, Taoka M, Saitoh SI, Yamauchi Y, Motoi Y, Komine M, et al. Nucleosides Drive Histiocytosis in SLC29A3 Disorders by Activating TLR7. *Immunology* (2019). doi: 10.1101/2019.12.16.877357
91. Haroche J, Cohen-Aubart F, Rollins BJ, Donadieu J, Charlotte F, Idbaih A, et al. Histiocytoses: Emerging Neoplasia Behind Inflammation. *Lancet Oncol* (2017) 18:e113–25. doi: 10.1016/S1470-2045(17)30031-1
92. Pichlmair A, Schulz O, Tan CP, Naslund TI, Liljestrom P, Weber F, et al. RIG-I-Mediated Antiviral Responses to Single-Stranded RNA Bearing 5'-Phosphates. *Science* (2006) 314:997–1001. doi: 10.1126/science.1132998
93. Goubau D, Schlee M, Deddouche S, Pruijssers AJ, Zillinger T, Goldeck M, et al. Antiviral Immunity *via* RIG-I-Mediated Recognition of RNA Bearing 5'-Diphosphates. *Nature* (2014) 514:372–5. doi: 10.1038/nature13590
94. Hornung V, Ellegast J, Kim S, Brzózka K, Jung A, Kato H, et al. 5'-Triphosphate RNA Is the Ligand for RIG-I. *Science* (2006) 314:994–7. doi: 10.1126/science.1132505
95. Schuberth-Wagner C, Ludwig J, Bruder AK, Herzner AM, Zillinger T, Goldeck M, et al. A Conserved Histidine in the RNA Sensor RIG-I Controls Immune Tolerance to N1-2'o-Methylated Self Rna. *Immunity* (2015) 43:41–51. doi: 10.1016/j.immuni.2015.06.015
96. Kato H, Takeuchi O, Sato S, Yoneyama M, Yamamoto M, Matsui K, et al. Differential Roles of MDA5 and RIG-I Helicases in the Recognition of RNA Viruses. *Nature* (2006) 441:101–5. doi: 10.1038/nature04734
97. Pichlmair A, Schulz O, Tan CP, Rehwinkel J, Kato H, Takeuchi O, et al. Activation of MDA5 Requires Higher-Order RNA Structures Generated During Virus Infection. *JVI* (2009) 83:10761–9. doi: 10.1128/JVI.00770-09
98. Kato H, Takeuchi O, Mikamo-Satoh E, Hirai R, Kawai T, Matsushita K, et al. Length-Dependent Recognition of Double-Stranded Ribonucleic Acids by Retinoic Acid–Inducible Gene-I and Melanoma Differentiation–Associated Gene 5. *J Exp Med* (2008) 205:1601–10. doi: 10.1084/jem.20080091
99. Runge S, Sparrer KMJ, Lässig C, Hembach K, Baum A, García-Sastre A, et al. *In Vivo* Ligands of MDA5 and RIG-I in Measles Virus-Infected Cells. *PloS Pathog* (2014) 10:e1004081. doi: 10.1371/journal.ppat.1004081
100. Berke IC, Modis Y. MDA5 Cooperatively Forms Dimers and ATP-Sensitive Filaments Upon Binding Double-Stranded RNA: MDA5 Forms Dimers and Filaments on Binding dsRNA. *EMBO J* (2012) 31:1714–26. doi: 10.1038/emboj.2012.19
101. Peisley A, Lin C, Wu B, Orme-Johnson M, Liu M, Walz T, et al. Cooperative Assembly and Dynamic Disassembly of MDA5 Filaments for Viral dsRNA Recognition. *Proc Natl Acad Sci* (2011) 108:21010–5. doi: 10.1073/pnas.1113651108
102. Venkataraman T, Valdes M, Elsby R, Kakuta S, Caceres G, Saijo S, et al. Loss of DExD/H Box RNA Helicase LGP2 Manifests Disparate Antiviral Responses. *J Immunol* (2007) 178:6444–55. doi: 10.4049/jimmunol.178.10.6444
103. Broz P, Dixit VM. Inflammasomes: Mechanism of Assembly, Regulation and Signalling. *Nat Rev Immunol* (2016) 16:407–20. doi: 10.1038/nri.2016.58
104. Bauernfried S, Scherr MJ, Pichlmair A, Duderstadt KE, Hornung V. Human NLRP1 Is a Sensor for Double-Stranded RNA. *Science* (2021) 371:eabd0811. doi: 10.1126/science.abd0811
105. Vavassori S, Chou J, Faletti LE, Haunerdinger V, Opitz L, Joset P, et al. Multisystem Inflammation and Susceptibility to Viral Infections in Human ZNFX1 Deficiency. *J Allergy Clin Immunol* (2021) 148:381–93. doi: 10.1016/j.jaci.2021.03.045. S0091674921006138.
106. Miao Z, Tidu A, Eriani G, Martin F. Secondary Structure of the Sars-Cov-2 5'-Utr. *RNA Biol* (2021) 18:447–56. doi: 10.1080/15476286.2020.1814556
107. Skrivergaard S, Jensen MS, Rolander TB, Nguyen TBN, Bundgaard A, Nejsum LN, et al. The Cellular Localization of the P42 and P46 Oligoadenylate Synthetase 1 Isoforms and Their Impact on Mitochondrial Respiration. *Viruses* (2019) 11:1122. doi: 10.3390/v11121122
108. Bisbal C, Silverman RH. Diverse Functions of Rnase L and Implications in Pathology. *Biochimie* (2007) 89:789–98. doi: 10.1016/j.biochi.2007.02.006
109. Cao L, Liu S, Li Y, Yang G, Luo Y, Li S, et al. The Nuclear Matrix Protein Safa Surveils Viral RNA and Facilitates Immunity by Activating Antiviral Enhancers and Super-Enhancers. *Cell Host Microbe* (2019) 26:369–84.e8. doi: 10.1016/j.chom.2019.08.010
110. Liu G, Gack MU. Distinct and Orchestrated Functions of RNA Sensors in Innate Immunity. *Immunity* (2020) 53:26–42. doi: 10.1016/j.immuni.2020.03.017
111. Zhang Z, Kim T, Bao M, Facchinetti V, Jung SY, Ghaffari AA, et al. Ddx1, Ddx21, and Dhx36 Helicases Form a Complex With the Adaptor Molecule Trif to Sense DsRNA in Dendritic Cells. *Immunity* (2011) 34:866–78. doi: 10.1016/j.immuni.2011.03.027
112. Zhang Z, Yuan B, Lu N, Facchinetti V, Liu YJ. Dhx9 Pairs With Ips-1 to Sense Double-Stranded RNA in Myeloid Dendritic Cells. *J Immunol (Baltimore Md: 1950)* (2011) 187:4501–8. doi: 10.4049/jimmunol.1101307
113. Mitoma H, Hanabuchi S, Kim T, Bao M, Zhang Z, Sugimoto N, et al. The Dhx33 RNA Helicase Senses Cytosolic RNA and Activates the Nlrp3 Inflammasome. *Immunity* (2013) 39:123–35. doi: 10.1016/j.immuni.2013.07.001
114. Zhu S, Ding S, Wang P, Wei Z, Pan W, Palm NW, et al. Nlrp9b Inflammasome Restricts Rotavirus Infection in Intestinal Epithelial Cells. *Nature* (2017) 546:667–70. doi: 10.1038/nature22967
115. Oshiumi H, Sakai K, Matsumoto M, Seya T. Dead/h Box 3 (Ddx3) Helicase Binds the Rig-I Adaptor Ips-1 to Up-Regulate Ifn-Beta-Inducing Potential. *Eur J Immunol* (2010) 40:940–8. doi: 10.1002/eji.200940203
116. Miyashita M, Oshiumi H, Matsumoto M, Seya T. Ddx60, a Dexd/H Box Helicase, Is a Novel Antiviral Factor Promoting Rig-I-Like Receptor-Mediated Signaling. *Mol Cell Biol* (2011) 31:3802–19. doi: 10.1128/MCB.01368-10
117. Kumar H, Kawai T, Kato H, Sato S, Takahashi K, Coban C, et al. Essential Role of IPS-1 in Innate Immune Responses Against RNA Viruses. *J Exp Med* (2006) 203:1795–803. doi: 10.1084/jem.20060792
118. Poeck H, Bscheider M, Gross O, Finger K, Roth S, Rebsamen M, et al. Recognition of RNA Virus by RIG-I Results in Activation of CARD9 and Inflammasome Signaling for Interleukin 1β Production. *Nat Immunol* (2010) 11:63–9. doi: 10.1038/ni.1824
119. Rudin CM, Thompson CB. Transcriptional Activation of Short Interspersed Elements by Dna-Damaging Agents. *Genes Chromosomes Cancer* (2001) 30:64–71. doi: 10.1002/1098-2264(2000)9999:9999<::AID-GCC1066>3.0.CO;2-F
120. Liu WM, Chu WM, Choudary PV, Schmid CW. Cell Stress and Translational Inhibitors Transiently Increase the Abundance of Mammalian Sine Transcripts. *Nucleic Acids Res* (1995) 23:1758–65. doi: 10.1093/nar/23.10.1758
121. Russanova VR, Driscoll CT, Howard BH. Adenovirus Type 2 Preferentially Stimulates Polymerase Iii Transcription of Alu Elements by Relieving Repression: A Potential Role for Chromatin. *Mol Cell Biol* (1995) 15:4282–90. doi: 10.1128/MCB.15.8.4282
122. Panning B, Smiley JR. Activation of RNA Polymerase Iii Transcription of Human Alu Repetitive Elements by Adenovirus Type 5: Requirement for the Elb 58-Kilodalton Protein and the Products of E4 Open Reading Frames 3 and 6. *Mol Cell Biol* (1993) 13:14. doi: 10.1128/mcb.13.6.3231-3244.1993
123. Lander ES, Linton LM, Birren B, Nusbaum C, Zody MC, Baldwin J, et al. Initial Sequencing and Analysis of the Human Genome. *Nature* (2001) 409:860–921. doi: 10.1038/35057062
124. Venter JC, Adams MD, Myers EW, Li PW, Mural RJ, Sutton GG, et al. The Sequence of the Human Genome. *THE Hum Genome* (2001) 291:50. doi: 10.1126/science.1058040
125. Deininger P. Alu Elements: Know the Sines. *Genome Biol* (2011) 12:236. doi: 10.1186/gb-2011-12-12-236

126. Panning B, Smiley JR. Regulation of Cellular Genes Transduced by Herpes Simplex Virus. *J Virol* (1989) 63:1929–37. doi: 10.1128/jvi.63.5.1929-1937.1989
127. Chattopadhyay P, Srinivasa Vasudevan J, Pandey R. Noncoding RNAs: Modulators and Modulatable Players During Infection-Induced Stress Response. *Briefings Funct Genomics* (2021) 20:28–41. doi: 10.1093/bfgp/elaa026
128. Clancy RM, Alvarez D, Komissarova E, Barrat FJ, Swartz J, Buyon JP. Ro60-Associated Single-Stranded RNA Links Inflammation With Fetal Cardiac Fibrosis *via* Ligation of Tlrs: A Novel Pathway to Autoimmune-Associated Heart Block. *J Immunol* (2010) 184:2148–55. doi: 10.4049/jimmunol.0902248
129. Yulug IG, Yulug A, Fisher EM. The Frequency and Position of Alu Repeats in Cdnas, as Determined by Database Searching. *Genomics* (1995) 27:544–8. doi: 10.1006/geno.1995.1090
130. Herbert A. Z-Dna and Z-RNA in Human Disease. *Commun Biol* (2019) 2:10. doi: 10.1038/s42003-018-0237-x
131. Nichols PJ, Bevers S, Henen M, Kieft JS, Vicens Q, Vögeli B. Recognition of Non-Cpg Repeats in Alu and Ribosomal Rnas by the Z-RNA Binding Domain of Adar1 Induces a-Z Junctions. *Nat Commun* (2021) 12:793. doi: 10.1038/s41467-021-21039-0
132. Chung H, Calis JJ, Wu X, Sun T, Yu Y, Sarbanes SL, et al. Human Adar1 Prevents Endogenous RNA From Triggering Translational Shutdown. *Cell* (2018) 172:811–24.e14. doi: 10.1016/j.cell.2017.12.038
133. Ahmad S, Mu X, Yang F, Greenwald E, Park JW, Jacob E, et al. Breaching Self-Tolerance to Alu Duplex RNA Underlies Mda5-Mediated Inflammation. *Cell* (2018) 172:797–810.e13. doi: 10.1016/j.cell.2017.12.016
134. Karki R, Sundaram B, Sharma BR, Lee S, Malireddi RS, Nguyen LN, et al. Adar1 Restricts Zbp1-Mediated Immune Response and Panoptosis to Promote Tumorigenesis. *Cell Rep* (2021) 37:109858. doi: 10.1016/j.celrep.2021.109858
135. Chiang JJ, Sparrer KMJ, van Gent M, Lässig C, Huang T, Osterrieder N, et al. Viral Unmasking of Cellular 5s Rrna Pseudogene Transcripts Induces Rig-I-Mediated Immunity. *Nat Immunol* (2018) 19:53–62. doi: 10.1038/s41590-017-0005-y
136. Rigby RE, Webb LM, Mackenzie KJ, Li Y, Leitch A, Reijns MAM, et al. RNA: DNA Hybrids Are a Novel Molecular Pattern Sensed by TLR9. *EMBO J* (2014) 33:542–58. doi: 10.1002/embj.201386117
137. Sun L, Wu J, Du F, Chen X, Chen ZJ. Cyclic GMP-AMP Synthase Is a Cytosolic DNA Sensor That Activates the Type I Interferon Pathway. *Science* (2013) 339:786–91. doi: 10.1126/science.1232458
138. Mankan AK, Schmidt T, Chauhan D, Goldeck M, Höning K, Gaidt M, et al. Cytosolic RNA:DNA Hybrids Activate the Cgas–Sting Axis. *EMBO J* (2014) 33:2937–46. doi: 10.15252/embj.201488726
139. Lee YN, Nechushtan H, Figov N, Razin E. The Function of Lysyl-tRNA Synthetase and Ap4A as Signaling Regulators of MITF Activity in Fc-RI-Activated Mast Cells. *Immunity* (2018) 20:145–51. doi: 10.1016/S1074-7613(04)00020-2
140. Park SG, Kim HJ, Min YH, Choi EC, Shin YK, Park BJ, et al. Human Lysyl-Trna Synthetase Is Secreted to Trigger Proinflammatory Response. *PNAS* (2005) 102:6356–61. doi: 10.1073/pnas.0500226102
141. Yannay-Cohen N, Carmi-Levy I, Kay G, Yang CM, Han JM, Kemeny DM, et al. LysRS Serves as a Key Signaling Molecule in the Immune Response by Regulating Gene Expression. *Mol Cell* (2009) 34:603–11. doi: 10.1016/j.molcel.2009.05.019
142. Guerra J, Valadao AL, Vlachakis D, Polak K, Vila IK, Taffoni C, et al. Lysyl-tRNA Synthetase Produces Diadenosine Tetraphosphate to Curb STING-Dependent Inflammation. *Sci Adv* (2020) 6:eaax3333. doi: 10.1126/sciadv.aax3333
143. Wang ET, Sandberg R, Luo S, Khrebtukova I, Zhang L, Mayr C, et al. Alternative Isoform Regulation in Human Tissue Transcriptomes. *Nature* (2008) 456:470–6. doi: 10.1038/nature07509
144. Kim MS, Pinto SM, Getnet D, Nirujogi RS, Manda SS, Chaerkady R, et al. A Draft Map of the Human Proteome. *Nature* (2014) 509:575–81. doi: 10.1038/nature13302
145. Mele M, Ferreira PG, Reverter F, DeLuca DS, Monlong J, Sammeth M, et al. The Human Transcriptome Across Tissues and Individuals. *Science* (2015) 348:660–5. doi: 10.1126/science.aaa0355
146. Ule J, Blencowe BJ. Alternative Splicing Regulatory Networks: Functions, Mechanisms, and Evolution. *Mol Cell* (2019) 76:329–45. doi: 10.1016/j.molcel.2019.09.017
147. Wang Y, Liu J, Huang B, Xu YM, Li J, Huang LF, et al. Mechanism of Alternative Splicing and Its Regulation. *Biomed Rep* (2015) 3:152–8. doi: 10.3892/br.2014.407
148. Rogers TF, Palmer DH, Wright AE. Sex-Specific Selection Drives the Evolution of Alternative Splicing in Birds. *Mol Biol Evol* (2020) 12:519–30. doi: 10.1093/molbev/msaa242
149. Baralle FE, Giudice J. Alternative Splicing as a Regulator of Development and Tissue Identity. *Nat Rev Mol Cell Biol* (2017) 18:437–51. doi: 10.1038/nrm.2017.27
150. Yabas M, Elliott H, Hoyne G. The Role of Alternative Splicing in the Control of Immune Homeostasis and Cellular Differentiation. *IJMS* (2015) 17:3. doi: 10.3390/ijms17010003
151. Ergun A, Doran G, Costello JC, Paik HH, Collins JJ, Mathis D, et al. Differential Splicing Across Immune System Lineages. *Proc Natl Acad Sci* (2013) 110:14324–9. doi: 10.1073/pnas.1311839110
152. Martinez NM, Lynch KW. Control of Alternative Splicing in Immune Responses: Many Regulators, Many Predictions, Much Still to Learn. *Immunol Rev* (2013) 253:216–36. doi: 10.1111/imr.12047
153. Robinson EK, Jagannatha P, Covarrubias S, Cattle M, Smaliy V, Safavi R, et al. Inflammation Drives Alternative First Exon Usage to Regulate Immune Genes Including a Novel Iron-Regulated Isoform of Aim2. *eLife* (2021) 10:e69431. doi: 10.7554/eLife.69431
154. Lee FFY, Davidson K, Harris C, McClendon J, Janssen WJ, Alper S. Nf-κb Mediates Lipopolysaccharide-Induced Alternative Pre-Mrna Splicing of Myd88 in Mouse Macrophages. *J Biol Chem* (2020) 295:6236–48. doi: 10.1074/jbc.RA119.011495
155. Pai AA, Baharian G, Pagé Sabourin A, Brinkworth JF, Nédélec Y, Foley JW, et al. Widespread Shortening of 3' Untranslated Regions and Increased Exon Inclusion Are Evolutionarily Conserved Features of Innate Immune Responses to Infection. *PloS Genet* (2016) 12:e1006338. doi: 10.1371/journal.pgen.1006338
156. Janssens S, Burns K, Vercammen E, Tschopp J, Beyaert R. MyD88$_s$, a Splice Variant of MyD88, Differentially Modulates NF-κb- and AP-1-Dependent Gene Expression. *FEBS Lett* (2003) 548:103–7. doi: 10.1016/S0014-5793(03)00747-6
157. Rao N, Nguyen S, Ngo K, Fung-Leung WP. A Novel Splice Variant of Interleukin-1 Receptor (IL-1r)-Associated Kinase 1 Plays a Negative Regulatory Role in Toll/IL-1r-Induced Inflammatory Signaling. *MCB* (2005) 25:6521–32. doi: 10.1128/MCB.25.15.6521-6532.2005
158. Gray P, Michelsen KS, Sirois CM, Lowe E, Shimada K, Crother TR, et al. Identification of a Novel Human MD-2 Splice Variant That Negatively Regulates Lipopolysaccharide-Induced TLR4 Signaling. *J Immunol* (2010) 184:6359–66. doi: 10.4049/jimmunol.0903543
159. Tumurkhuu G, Dagvadorj J, Jones HD, Chen S, Shimada K, Crother TR, et al. Alternatively Spliced Myeloid Differentiation Protein-2 Inhibits Tlr4-Mediated Lung Inflammation. *J Immunol* (2015) 194:1686–94. doi: 10.4049/jimmunol.1402123
160. Seo JW, Yang EJ, Kim SH, Choi IH. An Inhibitory Alternative Splice Isoform of Toll-Like Receptor 3 Is Induced by Type I Interferons in Human Astrocyte Cell Lines. *BMB Rep* (2015) 48:696–701. doi: 10.5483/BMBRep.2015.48.12.106
161. Crocker PR, Paulson JC, Varki A. Siglecs and Their Roles in the Immune System. *Nat Rev Immunol* (2007) 7:255–66. doi: 10.1038/nri2056
162. Ali SR, Fong JJ, Carlin AF, Busch TD, Linden R, Angata T, et al. Siglec-5 and Siglec-14 Are Polymorphic Paired Receptors That Modulate Neutrophil and Amnion Signaling Responses to Group B Streptococcus. *J Exp Med* (2014) 211:1231–42. doi: 10.1084/jem.20131853
163. Chen GY, Brown NK, Wu W, Khedri Z, Yu H, Chen X, et al. Broad and Direct Interaction Between Tlr and Siglec Families of Pattern Recognition Receptors and Its Regulation by Neu1. *eLife* (2014) 3:e04066. doi: 10.7554/eLife.04066
164. Huang PCJ, Low PY, Wang I, Hsu STD, Angata T. Soluble Siglec-14 Glycan-Recognition Protein Is Generated by Alternative Splicing and Suppresses Myeloid Inflammatory Responses. *J Biol Chem* (2018) 293:19645–58. doi: 10.1074/jbc.RA118.005676

165. Takeda K, Akira S. TLR Signaling Pathways. *Semin Immunol* (2004) 16:3–9. doi: 10.1016/j.smim.2003.10.003
166. O'Neill LAJ, Bowie AG. The Family of Five: Tir-Domain-Containing Adaptors in Toll-Like Receptor Signalling. *Nat Rev Immunol* (2007) 7:353–64. doi: 10.1038/nri2079
167. Janssens S, Burns K, Tschopp J, Beyaert R. Regulation of Interleukin-1- and Lipopolysaccharide-Induced Nf-κB Activation by Alternative Splicing of Myd88. *Curr Biol* (2002) 12:467–71. doi: 10.1016/S0960-9822(02)00712-1
168. Burns K, Janssens S, Brissoni B, Olivos N, Beyaert R, Tschopp J. Inhibition of Interleukin 1 Receptor/Toll-Like Receptor Signaling Through the Alternatively Spliced, Short Form of Myd88 Is Due to Its Failure to Recruit Irak-4. *J Exp Med* (2003) 197:263–8. doi: 10.1084/jem.20021790
169. De Arras L, Alper S. Limiting of the Innate Immune Response by SF3A-Dependent Control of MyD88 Alternative mRNA Splicing. *PloS Genet* (2013) 9:e1003855. doi: 10.1371/journal.pgen.1003855
170. O'Connor BP, Danhorn T, De Arras L, Flatley BR, Marcus RA, Farias-Hesson E, et al. Regulation of Toll-Like Receptor Signaling by the SF3a mRNA Splicing Complex. *PloS Genet* (2015) 11:e1004932. doi: 10.1371/journal.pgen.1004932
171. West KO, Scott HM, Torres-Odio S, West AP, Patrick KL, Watson RO. The Splicing Factor hnRNP M Is a Critical Regulator of Innate Immune Gene Expression in Macrophages. *Cell Rep* (2019) 29:1594–1609.e5. doi: 10.1016/j.celrep.2019.09.078
172. Haque N, Ouda R, Chen C, Ozato K, Hogg JR. ZFR Coordinates Crosstalk Between RNA Decay and Transcription in Innate Immunity. *Nat Commun* (2018) 9:1145. doi: 10.1038/s41467-018-03326-5
173. De Arras L, Laws R, Leach SM, Pontis K, Freedman JH, Schwartz DA, et al. Comparative Genomics RNAi Screen Identifies Eftud2 as a Novel Regulator of Innate Immunity. *Genetics* (2014) 197:485–96. doi: 10.1534/genetics.113.160499
174. Iwasaki A. A Virological View of Innate Immune Recognition. *Annu Rev Microbiol* (2012) 66:177–96. doi: 10.1146/annurev-micro-092611-150203
175. Yang E, Li MMH. All About the RNA: Interferon-Stimulated Genes That Interfere With Viral RNA Processes. *Front Immunol* (2020) 11:605024. doi: 10.3389/fimmu.2020.605024
176. Crosse KM, Monson EA, Beard MR, Helbig KJ. Interferon-Stimulated Genes as Enhancers of Antiviral Innate Immune Signaling. *J Innate Immun* (2018) 10:85–93. doi: 10.1159/000484258
177. Wagner AR, Scott HM, West KO, Vail KJ, Fitzsimons TC, Coleman AK, et al. Global Transcriptomics Uncovers Distinct Contributions From Splicing Regulatory Proteins to the Macrophage Innate Immune Response. *Front Immunol* (2021) 12:656885. doi: 10.3389/fimmu.2021.656885
178. Beyer AL, Christensen ME, Walker BW, LeStourgeon WM. Identification and Characterization of the Packaging Proteins of Core 40S hnRNP Particles. *Cell* (1977) 11:127–38. doi: 10.1016/0092-8674(77)90323-3
179. Eekelen CA, Riemen T, Venrooij WJ. Specificity in the Interaction of Hnrna and Mrna With Proteins as Revealed by *In Vivo* Cross Linking. *FEBS Lett* (1981) 130:223–6. doi: 10.1016/0014-5793(81)81125-8
180. Ford LP, Suh JM, Wright WE, Shay JW. Heterogeneous Nuclear Ribonucleoproteins C1 and C2 Associate With the RNA Component of Human Telomerase. *Mol Cell Biol* (2000) 20:9084–91. doi: 10.1128/MCB.20.23.9084-9091.2000
181. Moumen A, Masterson P, O'Connor MJ, Jackson SP. hnRNP K: An HDM2 Target and Transcriptional Coactivator of P53 in Response to DNA Damage. *Cell* (2005) 123:1065–78. doi: 10.1016/j.cell.2005.09.032
182. Gautrey H, Jackson C, Dittrich AL, Browell D, Lennard T, Tyson-Capper A. SRSF3 and hnRNP H1 Regulate a Splicing Hotspot of *HER2* in Breast Cancer Cells. *RNA Biol* (2015) 12:1139–51. doi: 10.1080/15476286.2015.1076610
183. Loh TJ, Moon H, Cho S, Jang H, Liu YC, Tai H, et al. CD44 Alternative Splicing and hnRNP A1 Expression Are Associated With the Metastasis of Breast Cancer. *Oncol Rep* (2015) 34:1231–8. doi: 10.3892/or.2015.4110
184. Meagher MJ, Schumacher JM, Lee K, Holdcraft RW, Edelhoff S, Disteche C, et al. Identification of ZFR, an Ancient and Highly Conserved Murine Chromosome-Associated Zinc Finger Protein. *Gene* (1999) 228:197–211. doi: 10.1016/S0378-1119(98)00615-5
185. Stanek D, Fox AH. Nuclear Bodies: News Insights Into Structure and Function. *Curr Opin Cell Biol* (2017) 46:94–101. doi: 10.1016/j.ceb.2017.05.001
186. Machyna M, Kehr S, Straube K, Kappei D, Buchholz F, Butter F, et al. The Coilin Interactome Identifies Hundreds of Small Noncoding Rnas That Traffic Through Cajal Bodies. *Mol Cell* (2014) 56:389–99. doi: 10.1016/j.molcel.2014.10.004
187. Xu H, Pillai RS, Azzouz TN, Shpargel KB, Kambach C, Hebert MD, et al. The C-Terminal Domain of Coilin Interacts With Sm Proteins and U Snrnps. *Chromosoma* (2005) 114:155–66. doi: 10.1007/s00412-005-0003-y
188. Lemm I, Girard C, Kuhn AN, Watkins NJ, Schneider M, Bordonné R, et al. Ongoing U Snrnp Biogenesis Is Required for the Integrity of Cajal Bodies. *Mol Biol Cell* (2006) 17:3221–31. doi: 10.1091/mbc.e06-03-0247
189. Lee S, Lee TA, Lee E, Kang S, Park A, Kim SW, et al. Identification of a Subnuclear Body Involved in Sequence-Specific Cytokine RNA Processing. *Nat Commun* (2015) 6:5791. doi: 10.1038/ncomms6791
190. Lee S, Park B. InSAC: A Novel Sub-Nuclear Body Essential for Interleukin-6 and -10 RNA Processing and Stability. *BMB Rep* (2015) 48:239–40. doi: 10.5483/BMBRep.2015.48.5.060
191. Gruber AJ, Zavolan M. Alternative Cleavage and Polyadenylation in Health and Disease. *Nat Rev Genet* (2019) 20:599–614. doi: 10.1038/s41576-019-0145-z
192. Hoque M, Ji Z, Zheng D, Luo W, Li W, You B, et al. Analysis of Alternative Cleavage and Polyadenylation by 3' Region Extraction and Deep Sequencing. *Nat Methods* (2013) 10:133–9. doi: 10.1038/nmeth.2288
193. Zhu H. Hu Proteins Regulate Polyadenylation by Blocking Sites Containing U-Rich Sequences*. *J Biol Chem* (2007) 282:8. doi: 10.1074/jbc.M609349200
194. Miura P, Shenker S, Andreu-Agullo C, Westholm JO, Lai EC. Widespread and Extensive Lengthening of 39 Utrs in the Mammalian Brain. *Genome Res* (2013) 23:812–25. doi: 10.1101/gr.146886.112
195. Stevenson B, Iseli C, Beutler B, Jongeneel C. Use of Transcriptome Data to Unravel the Fine Structure of Genes Involved in Sepsis. *J Infect Dis* (2003) 187:S308–14. doi: 10.1086/374755
196. Jia X, Yuan S, Wang Y, Fu Y, Ge Y, Ge Y, et al. The Role of Alternative Polyadenylation in the Antiviral Innate Immune Response. *Nat Commun* (2017) 8:14605. doi: 10.1038/ncomms14605
197. Shell SA, Hesse C, Morris SM, Milcarek C. Elevated Levels of the 64-Kda Cleavage Stimulatory Factor (Cstf-64) in Lipopolysaccharide-Stimulated Macrophages Influence Gene Expression and Induce Alternative Poly(a) Site Selection. *J Biol Chem* (2005) 280:39950–61. doi: 10.1074/jbc.M508848200
198. Chen KW, Demarco B, Ramos S, Heilig R, Goris M, Grayczyk JP, et al. Ripk1 Activates Distinct Gasdermins in Macrophages and Neutrophils Upon Pathogen Blockade of Innate Immune Signaling. *Proc Natl Acad Sci* (2021) 118:e2101189118. doi: 10.1073/pnas.2101189118
199. Szappanos D, Tschismarov R, Perlot T, Westermayer S, Fischer K, Platanitis E, et al. The RNA Helicase Ddx3x Is an Essential Mediator of Innate Antimicrobial Immunity. *PloS Pathog* (2018) 14:e1007397. doi: 10.1371/journal.ppat.1007397
200. Peng Q, O'Loughlin JL, Humphrey MB. Dok3 Negatively Regulates Lps Responses and Endotoxin Tolerance. *PloS One* (2012) 7:e39967. doi: 10.1371/journal.pone.0039967
201. Marsters S, Sheridan J, Pitti R, Huang A, Skubatch M, Baldwin D, et al. A Novel Receptor for Apo2l/Trail Contains a Truncated Death Domain. *Curr Biol* (1997) 7:1003–6. doi: 10.1016/S0960-9822(06)00422-2
202. Gitlin AD, Heger K, Schubert AF, Reja R, Yan D, Pham VC, et al. Integration of Innate Immune Signalling by Caspase-8 Cleavage of N4bp1. *Nature* (2020) 587:275–80. doi: 10.1038/s41586-020-2796-5
203. Ingolia NT, Ghaemmaghami S, Newman JRS, Weissman JS. Genome-Wide Analysis in Vivo of Translation With Nucleotide Resolution Using Ribosome Profiling. *Science* (2009) 324:218–23. doi: 10.1126/science.1168978
204. Beck A. Structure, Tissue Distribution and Genomic Organization of the Murine RRM-Type RNA Binding Proteins TIA-1 and TIAR. *Nucleic Acids Res* (1996) 24:3829–35. doi: 10.1093/nar/24.19.3829
205. Tian Q, Streuli M, Saito H, Schlossman SF, Anderson P. A Polyadenylate Binding Protein Localized to the Granules of Cytolytic Lymphocytes Induces DNA Fragmentation in Target Cells. *Cell* (1991) 11:629–39. doi: 10.1016/0092-8674(91)90536-8
206. Kawakami A, Tian Q, Duan X, Streuli M, Schlossman SF, Anderson P. Identification and Functional Characterization of a TIA-1-Related

Nucleolysin. *Proc Natl Acad Sci* (1992) 89:8681–5. doi: 10.1073/pnas.89.18.8681
207. Kedersha NL, Gupta M, Li W, Miller I, Anderson P. RNA-Binding Proteins TIA-1 and TIAR Link the Phosphorylation of eIF-2 to the Assembly of Mammalian Stress Granules. *J Cell Biol* (1999) 147:11. doi: 10.1083/jcb.147.7.1431
208. Anderson P, Kedersha N. Stress Granules: The Tao of RNA Triage. *Trends Biochem Sci* (2008) 33:141–50. doi: 10.1016/j.tibs.2007.12.003
209. Gueydan C, Droogmans L, Chalon P, Huez G, Caput D, Kruys V. Identification of TIAR as a Protein Binding to the Translational Regulatory AU-Rich Element of Tumor Necrosis Factor α mRNA. *J Biol Chem* (1999) 274:2322–6. doi: 10.1074/jbc.274.4.2322
210. Piecyk M, Wax S, Beck AR, Kedersha N, Gupta M, Maritim B, et al. TIA-1 Is a Translational Silencer That Selectively Regulates the Expression of TNF-α. *EMBO J* (2000) 19:4154–63. doi: 10.1093/emboj/19.15.4154
211. Naz S, Battu S, Khan RA, Afroz S, Giddaluru J, Vishwakarma SK, et al. Activation of Integrated Stress Response Pathway Regulates Il-1β Production Through Posttranscriptional and Translational Reprogramming in Macrophages. *Eur J Immunol* (2019) 49:277–89. doi: 10.1002/eji.201847513
212. Loflin P, Chen CYA, Shyu AB. Unraveling a Cytoplasmic Role for hnRNP D in the *In Vivo* mRNA Destabilization Directed by the AU-Rich Element. *Genes Dev* (1999) 13:1884–97. doi: 10.1101/gad.13.14.1884
213. Mukhopadhyay R, Jia J, Arif A, Ray PS, Fox PL. The GAIT System: A Gatekeeper of Inflammatory Gene Expression. *Trends Biochem Sci* (2009) 8:324–31. doi: 10.1016/j.tibs.2009.03.004
214. Ban N, Beckmann R, Cate JHD, Dinman JD, Dragon F, Ellis SR, et al. A New System for Naming Ribosomal Proteins. *Curr Opin Struct Biol* (2014) 24:165–9. doi: 10.1016/j.sbi.2014.01.002
215. Mazumder B, Sampath P, Seshadri V, Maitra RK, DiCorleto PE, Fox PL. Regulated Release of L13a From the 60S Ribosomal Subunit as A Mechanism of Transcript-Specific Translational Control. *Cell* (2003) 12:187–98. doi: 10.1016/S0092-8674(03)00773-6
216. Yao P, Potdar AA, Ray PS, Eswarappa SM, Flagg AC, Willard B, et al. The HILDA Complex Coordinates a Conditional Switch in the 3'-Untranslated Region of the VEGFA mRNA. *PloS Biol* (2013) 11:e1001635. doi: 10.1371/journal.pbio.1001635
217. Arif A, Yao P, Terenzi F, Jia J, Ray PS, Fox PL. The GAIT Translational Control System: GAIT System. *WIREs RNA* (2018) 9:e1441. doi: 10.1002/wrna.1441
218. Arif A, Jia J, Willard B, Li X, Fox PL. Multisite Phosphorylation of S6K1 Directs a Kinase Phospho-Code That Determines Substrate Selection. *Mol Cell* (2019) 73:446–57.e6. doi: 10.1016/j.molcel.2018.11.017
219. Poddar D, Basu A, Baldwin WM, Kondratov RV, Barik S, Mazumder B. An Extraribosomal Function of Ribosomal Protein L13a in Macrophages Resolves Inflammation. *J Immunol* (2013) 14:3600–12. doi: 10.4049/jimmunol.1201933
220. Kapasi P, Chaudhuri S, Vyas K, Baus D, Komar AA, Fox PL, et al. L13a Blocks 48s Assembly: Role of a General Initiation Factor in mRNA-Specific Translational Control. *Mol Cell* (2007) 14:113–26. doi: 10.1016/j.molcel.2006.11.028
221. Chaudhuri S, Vyas K, Kapasi P, Komar AA, Dinman JD, Barik S, et al. Human Ribosomal Protein L13a Is Dispensable for Canonical Ribosome Function But Indispensable for Efficient rRNA Methylation. *RNA* (2007) 15:2224–37. doi: 10.1261/rna.694007
222. Poddar D, Kaur R, Baldwin WM, Mazumder B. L13a-Dependent Translational Control in Macrophages Limits the Pathogenesis of Colitis. *Cell Mol Immunol* (2016) 13:816–27. doi: 10.1038/cmi.2015.53
223. Basu A, Poddar D, Robinet P, Smith JD, Febbraio M, Iii WMB, et al. Ribosomal Protein L13a Deficiency in Macrophages Promotes Atherosclerosis by Limiting Translation Control-Dependent Retardation of Inflammation. *ATVB* (2014) 10:533–42. doi: 10.1161/ATVBAHA.113.302573
224. Ray PS, Fox PL. A Post-Transcriptional Pathway Represses Monocyte VEGF-A Expression and Angiogenic Activity. *EMBO J* (2007) 26:3360–72. doi: 10.1038/sj.emboj.7601774
225. Ray PS, Jia J, Yao P, Majumder M, Hatzoglou M, Fox PL. A Stress-Responsive RNA Switch Regulates VEGFA Expression. *Nature* (2009) 457:915–9. doi: 10.1038/nature07598
226. Schoggins JW, Wilson SJ, Panis M, Murphy MY, Jones CT, Bieniasz P, et al. A Diverse Range of Gene Products Are Effectors of the Type I Interferon Antiviral Response. *Nature* (2011) 472:481–5. doi: 10.1038/nature09907
227. Li MM, MacDonald MR, Rice CM. To Translate, or Not to Translate: Viral and Host mRNA Regulation by Interferon-Stimulated Genes. *Trends Cell Biol* (2015) 25:320–9. doi: 10.1016/j.tcb.2015.02.001
228. Manche L, Green SR, Schmedt C, Mathews MB. Interactions Between Double-Stranded RNA Regulators and the Protein Kinase DAI. *Mol Cell Biol* (1992) 12:5238–48. doi: 10.1128/MCB.12.11.5238
229. McCormick C, Khaperskyy DA. Translation Inhibition and Stress Granules in the Antiviral Immune Response. *Nat Rev Immunol* (2017) 17:647–60. doi: 10.1038/nri.2017.63
230. Eiermann N, Haneke K, Sun Z, Stoecklin G, Ruggieri A. Dance With the Devil: Stress Granules and Signaling in Antiviral Responses. *Viruses* (2020) 12:E984. doi: 10.3390/v12090984
231. Reineke LC, Kedersha N, Langereis MA, van Kuppeveld FJM, Lloyd RE. Stress Granules Regulate Double-Stranded RNA-Dependent Protein Kinase Activation Through a Complex Containing G3bp1 and Caprin1. *mBio* (2015) 6:e02486. doi: 10.1128/mBio.02486-14
232. Law LMJ, Razooky BS, Li MMH, You S, Jurado A, Rice CM, et al. Zap's Stress Granule Localization Is Correlated With Its Antiviral Activity and Induced by Virus Replication. *PloS Pathog* (2019) 15:e1007798. doi: 10.1371/journal.ppat.1007798
233. Williams GD, Gokhale NS, Snider DL, Horner SM. The mRNA Cap 2'- *O* -Methyltransferase CMTR1 Regulates the Expression of Certain Interferon-Stimulated Genes. *mSphere* (2020) 5:e00202–20. doi: 10.1128/mSphere.00202-20
234. Diamond MS. Ifit1: A Dual Sensor and Effector Molecule That Detects Non-2'-O Methylated Viral RNA and Inhibits Its Translation. *Cytokine Growth Factor Rev* (2014) 25:543–50. doi: 10.1016/j.cytogfr.2014.05.002
235. Welsby I, Hutin D, Gueydan C, Kruys V, Rongvaux A, Leo O. PARP12, an Interferon-Stimulated Gene Involved in the Control of Protein Translation and Inflammation. *J Biol Chem* (2014) 289:26642–57. doi: 10.1074/jbc.M114.589515
236. Leung A, Vyas S, Rood J, Bhutkar A, Sharp P, Chang P. Poly(ADP-Ribose) Regulates Stress Responses and MicroRNA Activity in the Cytoplasm. *Mol Cell* (2011) 42:489–99. doi: 10.1016/j.molcel.2011.04.015
237. Espert L, Degols G, Gongora C, Blondel D, Williams BR, Silverman RH, et al. ISG20, a New Interferon-Induced RNase Specific for Single-Stranded RNA, Defines an Alternative Antiviral Pathway Against RNA Genomic Viruses. *J Biol Chem* (2003) 278:16151–8. doi: 10.1074/jbc.M209628200
238. Liu Y, Nie H, Mao R, Mitra B, Cai D, Yan R, et al. Interferon-Inducible Ribonuclease ISG20 Inhibits Hepatitis B Virus Replication Through Directly Binding to the Epsilon Stem-Loop Structure of Viral RNA. *PloS Pathog* (2017) 13:e1006296. doi: 10.1371/journal.ppat.1006296
239. Wu N, Nguyen XN, Wang L, Appourchaux R, Zhang C, Panthu B, et al. The Interferon Stimulated Gene 20 Protein (ISG20) Is an Innate Defense Antiviral Factor That Discriminates Self Versus Non-Self Translation. *PloS Pathog* (2019) 15:e1008093. doi: 10.1371/journal.ppat.1008093
240. Zhu Y, Wang X, Goff SP, Gao G. Translational Repression Precedes and Is Required for ZAP-Mediated mRNA Decay: ZAP-Mediated Translational Repression Versus mRNA Decay. *EMBO J* (2012) 31:4236–46. doi: 10.1038/emboj.2012.271
241. Zhu Y, Chen G, Lv F, Wang X, Ji X, Xu Y, et al. Zinc-Finger Antiviral Protein Inhibits HIV-1 Infection by Selectively Targeting Multiply Spliced Viral mRNAs for Degradation. *Proc Natl Acad Sci* (2011) 108:15834–9. doi: 10.1073/pnas.1101676108
242. Kmiec D, Lista MJ, Ficarelli M, Swanson CM. Neil SJD. S-Farnesylation Is Essential for Antiviral Activity of the Long Zap Isoform Against RNA Viruses With Diverse Replication Strategies. *PloS Pathog* (2021) 17:e1009726. doi: 10.1371/journal.ppat.1009726
243. Kmiec D, Nchioua R, Sherrill-Mix S, Stürzel CM, Heusinger E, Braun E, et al. Cpg Frequency in the 5′ Third of the Env Gene Determines Sensitivity of Primary Hiv-1 Strains to the Zinc-Finger Antiviral Protein. *mBio* (2020) 11:e02903–19. doi: 10.1128/mBio.02903-19
244. Yoneyama M, Onomoto K, Jogi M, Akaboshi T, Fujita T. Viral RNA Detection by RIG-I-Like Receptors. *Curr Opin Immunol* (2015) 32:48–53. doi: 10.1016/j.coi.2014.12.012

245. Pichlmair A, Lassnig C, Eberle CA, Górna MW, Baumann CL, Burkard TR, et al. IFIT1 Is an Antiviral Protein That Recognizes 5'-Triphosphate RNA. *Nat Immunol* (2011) 12:624–30. doi: 10.1038/ni.2048
246. Abbas YM, Pichlmair A, Górna MW, Superti-Furga G, Nagar B. Structural Basis for Viral 5'-PPP-RNA Recognition by Human IFIT Proteins. *Nature* (2013) 494:60–4. doi: 10.1038/nature11783
247. Wang C, Pflugheber J, Sumpter R, Sodora DL, Hui D, Sen GC, et al. Alpha Interferon Induces Distinct Translational Control Programs To Suppress Hepatitis C Virus RNA Replication. *JVI* (2003) 77:3898–912. doi: 10.1128/JVI.77.7.3898-3912.2003
248. Kimura T, Katoh H, Kayama H, Saiga H, Okuyama M, Okamoto T, et al. Ifit1 Inhibits Japanese Encephalitis Virus Replication Through Binding to 5' Capped 2'-O Unmethylated RNA. *J Virol* (2013) 87:9997–10003. doi: 10.1128/JVI.00883-13
249. Roy B, Jacobson A. The Intimate Relationships of mRNA Decay and Translation. *Trends Genet* (2013) 29:691–9. doi: 10.1016/j.tig.2013.09.002
250. Radhakrishnan A, Green R. Connections Underlying Translation and mRNA Stability. *J Mol Biol* (2016) 428:3558–64. doi: 10.1016/j.jmb.2016.05.025
251. Schwede A, Ellis L, Luther J, Carrington M, Stoecklin G, Clayton C. A Role for Caf1 in mRNA Deadenylation and Decay in Trypanosomes and Human Cells. *Nucleic Acids Res* (2008) 36:3374–88. doi: 10.1093/nar/gkn108
252. Chen J, Chiang YC, Denis CL. CCR4, A 3'-5' Poly(A) RNA and ssDNA Exonuclease, Is the Catalytic Component of the Cytoplasmic Deadenylase. *EMBO J* (2002) 21:1414–26. doi: 10.1093/emboj/21.6.1414
253. She M, Decker CJ, Svergun DI, Round A, Chen N, Muhlrad D, et al. Structural Basis of Dcp2 Recognition and Activation by Dcp1. *Mol Cell* (2008) 29:337–49. doi: 10.1016/j.molcel.2008.01.002
254. Deshmukh MV, Jones BN, Quang-Dang DU, Flinders J, Floor SN, Kim C, et al. mRNA Decapping Is Promoted by an RNA-Binding Channel in Dcp2. *Mol Cell* (2008) 29:324–36. doi: 10.1016/j.molcel.2007.11.027
255. Muhlrad D, Decker CJ, Parker R. Deadenylation of the Unstable mRNA Encoded by the Yeast MFA2 Gene Leads to Decapping Followed by 5'–>3' Digestion of the Transcript. *Genes Dev* (1994) 13:855–66. doi: 10.1101/gad.8.7.855
256. Anderson JSJ, Parker R. The 3' to 5' Degradation of Yeast mRNAs Is a General Mechanism for mRNA Turnover that Requires the SKI2 DEVH Box Protein and 3' to 5' Exonucleases of the Exosome Complex. *EMBO J* (1998) 10:1497–506. doi: 10.1093/emboj/17.5.1497
257. Sheth U. Decapping and Decay of Messenger RNA Occur in Cytoplasmic Processing Bodies. *Science* (2003) 300:805–8. doi: 10.1126/science.1082320
258. Hubstenberger A, Courel M, Bénard M, Souquere S, Ernoult-Lange M, Chouaib R, et al. P-Body Purification Reveals the Condensation of Repressed mRNA Regulons. *Mol Cell* (2017) 68:144–57.e5. doi: 10.1016/j.molcel.2017.09.003
259. Courel M, Clément Y, Bossevain C, Foretek D, Vidal Cruchez O, Yi Z, et al. GC Content Shapes mRNA Storage and Decay in Human Cells. *eLife* (2019) 8:e49708. doi: 10.7554/eLife.49708
260. Tuck AC, Rankova A, Arpat AB, Liechti LA, Hess D, Iesmantavicius V, et al. Mammalian RNA Decay Pathways Are Highly Specialized and Widely Linked to Translation. *Mol Cell* (2020) 77:1222–36.e13. doi: 10.1016/j.molcel.2020.01.007
261. Wu Q, Medina SG, Kushawah G, DeVore ML, Castellano LA, Hand JM, et al. Translation Affects mRNA Stability in a Codon-Dependent Manner in Human Cells. *eLife* (2019) 8:e45396. doi: 10.7554/eLife.45396
262. Bicknell AA, Ricci EP. When mRNA Translation Meets Decay. *Biochem Soc Trans* (2017) 45:339–51. doi: 10.1042/BST20160243
263. Morris C, Cluet D, Ricci EP. Ribosome Dynamics and mRNA Turnover, a Complex Relationship Under Constant Cellular Scrutiny. *WIREs RNA* (2021) 12:e1658. doi: 10.1002/wrna.1658
264. Schoenberg DR. Mechanisms of Endonuclease-Mediated mRNA Decay: Endonuclease-Mediated mRNA Decay. *WIREs RNA* (2011) 2:582–600. doi: 10.1002/wrna.78
265. Bhatt D, Pandya-Jones A, Tong AJ, Barozzi I, Lissner M, Natoli G, et al. Transcript Dynamics of Proinflammatory Genes Revealed by Sequence Analysis of Subcellular RNA Fractions. *Cell* (2012) 150:279–90. doi: 10.1016/j.cell.2012.05.043
266. Rabani M, Levin JZ, Fan L, Adiconis X, Raychowdhury R, Garber M, et al. Metabolic Labeling of RNA Uncovers Principles of RNA Production and Degradation Dynamics in Mammalian Cells. *Nat Biotechnol* (2011) 29:436–42. doi: 10.1038/nbt.1861
267. Paulsen MT, Veloso A, Prasad J, Bedi K, Ljungman EA, Tsan YC, et al. Coordinated Regulation of Synthesis and Stability of RNA During the Acute Tnf-Induced Proinflammatory Response. *Proc Natl Acad Sci* (2013) 110:2240–5. doi: 10.1073/pnas.1219192110
268. Bergen V, Lange M, Peidli S, Wolf FA, Theis FJ. Generalizing RNA Velocity to Transient Cell States Through Dynamical Modeling. *Nat Biotechnol* (2020) 38:1408–14. doi: 10.1038/s41587-020-0591-3
269. Furlan M, Galeota E, Gaudio ND, Dassi E, Caselle M, de Pretis S, et al. Genome-Wide Dynamics of RNA Synthesis, Processing, and Degradation Without RNA Metabolic Labeling. *Genome Res* (2020) 30:1492–507. doi: 10.1101/gr.260984.120
270. Chen CYA, Shyu AB. AU-Rich Elements: Characterization and Importance in mRNA Degradation. *Trends Biochem Sci* (1995) 20:465–70. doi: 10.1016/S0968-0004(00)89102-1
271. Zubiaga AM, Belasco JG, Greenberg ME. The Nonamer Uuauuuauu Is the Key Au-Rich Sequence Motif That Mediates Mrna Degradation. *Mol Cell Biol* (1995) 15:2219–30. doi: 10.1128/MCB.15.4.2219
272. Lal A, Mazan-Mamczarz K, Kawai T, Yang X, Martindale JL, Gorospe M. Concurrent Versus Individual Binding of Hur and Auf1 to Common Labile Target Mrnas. *EMBO J* (2004) 23:3092–102. doi: 10.1038/sj.emboj.7600305
273. Hopkins TG, Mura M, Al-Ashtal HA, Lahr RM, Abd-Latip N, Sweeney K, et al. The RNA-Binding Protein Larp1 Is a Post-Transcriptional Regulator of Survival and Tumorigenesis in Ovarian Cancer. *Nucleic Acids Res* (2016) 44:1227–46. doi: 10.1093/nar/gkv1515
274. Wigington CP, Jung J, Rye EA, Belauret SL, Philpot AM, Feng Y, et al. Post-Transcriptional Regulation of Programmed Cell Death 4 (Pdcd4) Mrna by the RNA-Binding Proteins Human Antigen R (Hur) and T-Cell Intracellular Antigen 1 (Tia1). *J Biol Chem* (2015) 290:3468–87. doi: 10.1074/jbc.M114.631937
275. Dassi E. Handshakes and Fights: The Regulatory Interplay of RNA-Binding Proteins. *Front Mol Biosci* (2017) 4:67. doi: 10.3389/fmolb.2017.00067
276. Shaw G, Kamen R. A Conserved Au Sequence From the 3' Untranslated Region of Gm-Csf Mrna Mediates Selective Mrna Degradation. *Cell* (1986) 46:659–67. doi: 10.1016/0092-8674(86)90341-7
277. Caput D, Beutler B, Hartog K, Thayer R, Brown-Shimer S, Cerami A. Identification of a Common Nucleotide Sequence in the 3'-Untranslated Region of Mrna Molecules Specifying Inflammatory Mediators. *Proc Natl Acad Sci* (1986) 83:1670–4. doi: 10.1073/pnas.83.6.1670
278. Hao S, Baltimore D. The Stability of mRNA Influences the Temporal Order of the Induction of Genes Encoding Inflammatory Molecules. *Nat Immunol* (2009) 10:281–8. doi: 10.1038/ni.1699
279. Ivanov P, Anderson P. Post-Transcriptional Regulatory Networks in Immunity. *Immunol Rev* (2013) 253:253–72. doi: 10.1111/imr.12051
280. Lai WS, Stumpo DJ, Blackshear PJ. Rapid Insulin-Stimulated Accumulation of an mRNA Encoding a Proline-Rich Protein. *J Biol Chem* (1990) 265:16556–63. doi: 10.1016/S0021-9258(17)46259-4
281. Taylor GA, Lai WS, Oakey RJ, Seldin MF, Shows TB, Eddy RL, et al. The Human TTP Protein: Sequence, Alignment With Related Proteins, and Chromosomal Localization of the Mouse and Human Genes. *Nucl Acids Res* (1991) 19:3454–4. doi: 10.1093/nar/19.12.3454
282. Thompson MJ, Lai WS, Taylor GA, Blackshear PJ. Cloning and Characterization of Two Yeast Genes Encoding Members of the CCCH Class of Zinc Finger Proteins: Zinc Finger-Mediated Impairment of Cell Growth. *Gene* (1996) 174:225–33. doi: 10.1016/0378-1119(96)00084-4
283. Carballo E. Feedback Inhibition of Macrophage Tumor Necrosis Factor-Production by Tristetraprolin. *Science* (1998) 281:1001–5. doi: 10.1126/science.281.5379.1001
284. Lai WS, Carballo E, Thorn JM, Kennington EA, Blackshear PJ. Interactions of CCCH Zinc Finger Proteins With mRNA. *J Biol Chem* (2000) 275:17827–37. doi: 10.1074/jbc.M001696200
285. Carballo E, Lai WS, Blackshear PJ. Evidence That Tristetraprolin Is a Physiological Regulator of Granulocyte-Macrophage Colony-Stimulating Factor Messenger RNA Deadenylation and Stability. *Blood* (2000) 95:1891–9. doi: 10.1182/blood.V95.6.1891
286. Fabian MR, Frank F, Rouya C, Siddiqui N, Lai WS, Karetnikov A, et al. Structural Basis for the Recruitment of the Human CCR4–NOT Deadenylase

Complex by Tristetraprolin. *Nat Struct Mol Biol* (2013) 20:735–9. doi: 10.1038/nsmb.2572
287. Sun L, Stoecklin G, Van Way S, Hinkovska-Galcheva V, Guo RF, Anderson P, et al. Tristetraprolin (Ttp)-14-3-3 Complex Formation Protects Ttp From Dephosphorylation by Protein Phosphatase 2a and Stabilizes Tumor Necrosis Factor-Alpha mRNA. *J Biol Chem* (2007) 282:3766–77. doi: 10.1074/jbc.M607347200
288. Lykke-Andersen J, Wagner E. Recruitment and Activation of Mrna Decay Enzymes by Two Are-Mediated Decay Activation Domains in the Proteins Ttp and Brf-1. *Genes Dev* (2005) 19:351–61. doi: 10.1101/gad.1282305
289. Bulbrook D, Brazier H, Mahajan P, Kliszczak M, Fedorov O, Marchese F, et al. Tryptophan-Mediated Interactions Between Tristetraprolin and the Cnot9 Subunit Are Required for Ccr4-Not Deadenylase Complex Recruitment. *J Mol Biol* (2018) 430:722–36. doi: 10.1016/j.jmb.2017.12.018
290. Mino T, Murakawa Y, Fukao A, Vandenbon A, Wessels HH, Ori D, et al. Regnase-1 and Roquin Regulate a Common Element in Inflammatory mRNAs by Spatiotemporally Distinct Mechanisms. *Cell* (2015) 161:1058–73. doi: 10.1016/j.cell.2015.04.029
291. Maeda K, Akira S. Regulation of Mrna Stability by Ccch-Type Zinc-Finger Proteins in Immune Cells. *Int Immunol* (2017) 29:149–55. doi: 10.1093/intimm/dxx015
292. Fenger-Grøn M, Fillman C, Norrild B, Lykke-Andersen J. Multiple Processing Body Factors and the ARE Binding Protein TTP Activate mRNA Decapping. *Mol Cell* (2005) 20:905–15. doi: 10.1016/j.molcel.2005.10.031
293. Stoecklin G, Stubbs T, Kedersha N, Wax S, Rigby WF, Blackwell TK, et al. MK2-Induced Tristetraprolin:14-3-3 Complexes Prevent Stress Granule Association and ARE-mRNA Decay. *EMBO J* (2004) 23:1313–24. doi: 10.1038/sj.emboj.7600163
294. Tiedje C, Diaz-Muñoz MD, Trulley P, Ahlfors H, Laaß K, Blackshear PJ, et al. The RNA-Binding Protein TTP Is a Global Post-Transcriptional Regulator of Feedback Control in Inflammation. *Nucleic Acids Res* (2016) 44:gkw474. doi: 10.1093/nar/gkw474
295. Tiedje C, Ronkina N, Tehrani M, Dhamija S, Laass K, Holtmann H, et al. The P38/MK2-Driven Exchange Between Tristetraprolin and HuR Regulates AU–Rich Element–Dependent Translation. *PloS Genet* (2012) 8:e1002977. doi: 10.1371/journal.pgen.1002977
296. Schott J, Reitter S, Philipp J, Haneke K, Schäfer H, Stoecklin G. Translational Regulation of Specific mRNAs Controls Feedback Inhibition and Survival During Macrophage Activation. *PloS Genet* (2014) 10:e1004368. doi: 10.1371/journal.pgen.1004368
297. Sedlyarov V, Fallmann J, Ebner F, Huemer J, Sneezum L, Ivin M, et al. Tristetraprolin Binding Site Atlas in the Macrophage Transcriptome Reveals a Switch for Inflammation Resolution. *Mol Syst Biol* (2016) 12:868. doi: 10.15252/msb.20156628
298. Taylor GA, Carballo E, Lee DM, Lai WS, Thompson MJ, Patel DD, et al. A Pathogenetic Role for Tnfα in the Syndrome of Cachexia, Arthritis, and Autoimmunity Resulting From Tristetraprolin (TTP) Deficiency. *Tumor Necrosis Factor* (1996) 4:10. doi: 10.1016/S1074-7613(00)80411-2
299. Stoecklin G, Ming XF, Looser R, Moroni C. Somatic mRNA Turnover Mutants Implicate Tristetraprolin in the Interleukin-3 mRNA Degradation Pathway. *Mol Cell Biol* (2000) 20:3753–63. doi: 10.1128/MCB.20.11.3753-3763.2000
300. Stoecklin G, Lu M, Rattenbacher B, Moroni C. A Constitutive Decay Element Promotes Tumor Necrosis Factor Alpha Mrna Degradation *via* an Au-Rich Element-Independent Pathway. *Mol Cell Biol* (2003) 23:3506–15. doi: 10.1128/MCB.23.10.3506-3515.2003
301. Leppek K, Schott J, Reitter S, Poetz F, Hammond MC, Stoecklin G. Roquin Promotes Constitutive mRNA Decay *via* a Conserved Class of Stem-Loop Recognition Motifs. *Cell* (2013) 153:869–81. doi: 10.1016/j.cell.2013.04.016
302. Schaefer JS, Klein JR. Roquin—A Multifunctional Regulator of Immune Homeostasis. *Genes Immun* (2016) 17:79–84. doi: 10.1038/gene.2015.58
303. Moraes KC. Cug-Bp Binds to RNA Substrates and Recruits Parn Deadenylase. *RNA* (2006) 12:1084–91. doi: 10.1261/rna.59606
304. Antic S, Wolfinger MT, Skucha A, Hosiner S, Dorner S. General and MicroRNA-Mediated mRNA Degradation Occurs on Ribosome Complexes in Drosophila Cells. *Mol Cell Biol* (2015) 35:2309–20. doi: 10.1128/MCB.01346-14
305. Tat TT, Maroney PA, Chamnongpol S, Coller J, Nilsen TW. Cotranslational microRNA Mediated Messenger RNA Destabilization. *eLife* (2016) 5:e12880. doi: 10.7554/eLife.12880
306. Biasini A, Abdulkarim B, Pretis S, Tan JY, Arora R, Wischnewski H, et al. Translation Is Required for miRNA-Dependent Decay of Endogenous Transcripts. *EMBO J* (2021) 40:e104569. doi: 10.15252/embj.2020104569
307. Matsushita K, Takeuchi O, Standley DM, Kumagai Y, Kawagoe T, Miyake T, et al. Zc3h12a Is an RNase Essential for Controlling Immune Responses by Regulating mRNA Decay. *Nature* (2009) 458:1185–90. doi: 10.1038/nature07924
308. Uehata T, Takeuchi O. Post-Transcriptional Regulation of Immunological Responses by Regnase-1-Related Rnases. *Int Immunol* (2021) 33:dxab048. doi: 10.1093/intimm/dxab048
309. Mizgalska D, Węgrzyn P, Murzyn K, Kasza A, Koj A, Jura J, et al. Interleukin-1-Inducible MCPIP Protein Has Structural and Functional Properties of RNase and Participates in Degradation of IL-1β mRNA: MCPIP Protein as an RNase. *FEBS J* (2009) 276:7386–99. doi: 10.1111/j.1742-4658.2009.07452.x
310. Dobosz E, Wilamowski M, Lech M, Bugara B, Jura J, Potempa J, et al. MCPIP-1, Alias Regnase-1, Controls Epithelial Inflammation by Posttranscriptional Regulation of IL-8 Production. *J Innate Immun* (2016) 8:564–78. doi: 10.1159/000448038
311. Mino T, Iwai N, Endo M, Inoue K, Akaki K, Hia F, et al. Translation-Dependent Unwinding of Stem–Loops by UPF1 Licenses Regnase-1 to Degrade Inflammatory mRNAs. *Nucleic Acids Res* (2019) 47:8838–59. doi: 10.1093/nar/gkz628
312. Bartel DP. MicroRNAs: Target Recognition and Regulatory Functions. *Cell* (2009) 136:215–33. doi: 10.1016/j.cell.2009.01.002
313. Friedman RC, Farh KKH, Burge CB, Bartel DP. Most Mammalian mRNAs Are Conserved Targets of microRNAs. *Genome Res* (2008) 19:92–105. doi: 10.1101/gr.082701.108
314. Djuranovic S, Nahvi A, Green R. miRNA-Mediated Gene Silencing by Translational Repression Followed by mRNA Deadenylation and Decay. *Science* (2012) 336:237–40. doi: 10.1126/science.1215691
315. Alivernini S, Gremese E, McSharry C, Tolusso B, Ferraccioli G, McInnes IB, et al. MicroRNA-155—at the Critical Interface of Innate and Adaptive Immunity in Arthritis. *Front Immunol* (2018) 8:1932. doi: 10.3389/fimmu.2017.01932
316. O'Connell RM, Taganov KD, Boldin MP, Cheng G, Baltimore D. MicroRNA-155 Is Induced During the Macrophage Inflammatory Response. *Proc Natl Acad Sci* (2007) 104:1604–9. doi: 10.1073/pnas.0610731104
317. Xu H, Xu SJ, Xie SJ, Zhang Y, Yang JH, Zhang WQ, et al. MicroRNA-122 Supports Robust Innate Immunity in Hepatocytes by Targeting the RTKs/STAT3 Signaling Pathway. *eLife* (2019) 8:e41159. doi: 10.7554/eLife.41159
318. Quinn SR, Mangan NE, Caffrey BE, Gantier MP, Williams BR, Hertzog PJ, et al. The Role of Ets2 Transcription Factor in the Induction of Microrna-155 (Mir-155) by Lipopolysaccharide and Its Targeting by Interleukin-10. *J Biol Chem* (2014) 289:4316–25. doi: 10.1074/jbc.M113.522730
319. Seo G, Kincaid R, Phanaksri T, Burke J, Pare J, Cox J, et al. Reciprocal Inhibition Between Intracellular Antiviral Signaling and the RNAi Machinery in Mammalian Cells. *Cell Host Microbe* (2013) 14:435–45. doi: 10.1016/j.chom.2013.09.002
320. Backes S, Shapiro J, Sabin L, Pham A, Reyes I, Moss B, et al. Degradation of Host MicroRNAs by Poxvirus Poly(A) Polymerase Reveals Terminal RNA Methylation as a Protective Antiviral Mechanism. *Cell Host Microbe* (2012) 12:200–10. doi: 10.1016/j.chom.2012.05.019
321. Pegtel DM, Cosmopoulos K, Thorley-Lawson DA, van Eijndhoven MAJ, Hopmans ES, Lindenberg JL, et al. Functional Delivery of Viral miRNAs *via* Exosomes. *Proc Natl Acad Sci* (2010) 107:6328–33. doi: 10.1073/pnas.0914843107
322. Momen-Heravi F, Bala S, Kodys K, Szabo G. Exosomes Derived From Alcohol-Treated Hepatocytes Horizontally Transfer Liver Specific miRNA-122 and Sensitize Monocytes to LPS. *Sci Rep* (2015) 5:9991. doi: 10.1038/srep09991
323. Saha B, Momen-Heravi F, Kodys K, Szabo G. MicroRNA Cargo of Extracellular Vesicles From Alcohol-Exposed Monocytes Signals Naive Monocytes to Differentiate Into M2 Macrophages. *J Biol Chem* (2016) 291:149–59. doi: 10.1074/jbc.M115.694133

324. Montecalvo A, Larregina AT, Shufesky WJ, Beer Stolz D, Sullivan MLG, Karlsson JM, et al. Mechanism of Transfer of Functional microRNAs Between Mouse Dendritic Cells *via* Exosomes. *Blood* (2012) 119:756–66. doi: 10.1182/blood-2011-02-338004
325. Mittelbrunn M, Gutiérrez-Vázquez C, Villarroya-Beltri C, González S, Sánchez-Cabo F, González MÁ, et al. Unidirectional Transfer of microRNA-Loaded Exosomes From T Cells to Antigen-Presenting Cells. *Nat Commun* (2011) 2:282. doi: 10.1038/ncomms1285
326. Higa M, Oka M, Fujihara Y, Masuda K, Yoneda Y, Kishimoto T. Regulation of Inflammatory Responses by Dynamic Subcellular Localization of RNA-Binding Protein Arid5a. *Proc Natl Acad Sci* (2018) 115:E1214–20. doi: 10.1073/pnas.1719921115
327. Minoda Y, Saeki K, Aki D, Takaki H, Sanada T, Koga K, et al. A Novel Zinc finger Protein, ZCCHC11, Interacts With TIFA and Modulates TLR Signaling. *Biochem Biophys Res Commun* (2006) 10:1023–30. doi: 10.1016/j.bbrc.2006.04.006
328. Jones MR, Quinton LJ, Blahna MT, Neilson JR, Fu S, Ivanov AR, et al. Zcchc11-Dependent Uridylation of microRNA Directs Cytokine Expression. *Nat Cell Biol* (2009) 11:1157–63. doi: 10.1038/ncb1931
329. Li F, Hu DY, Liu S, Mahavadi S, Yen W, Murthy KS, et al. RNA-Binding Protein HuR Regulates RGS4 mRNA Stability in Rabbit Colonic Smooth Muscle Cells. *Am J Physiology-Cell Physiol* (2010) 299:C1418–29. doi: 10.1152/ajpcell.00093.2010
330. Fan XC, Steitz JA. HNS, a Nuclear-Cytoplasmic Shuttling Sequence in HuR. *Proc Natl Acad Sci* (1998) 95:15293–8. doi: 10.1073/pnas.95.26.15293
331. Scheiba RM, de Opakua AI, Díaz-Quintana A, Martínez-Cruz LA, Martínez-Chantar ML, Díaz-Moreno I. The C-Terminal RNA Binding Motif of HuR Is a Multi-Functional Domain Leading to HuR Oligomerization. *RNA Biol* (2014) 11:13. doi: 10.1080/15476286.2014.996069
332. Herdy B, Karonitsch T, Vladimer GI, Tan CS, Stukalov A, Trefzer C, et al. The RNA-Binding Protein Hur/Elavl1 Regulates Ifn-β Mrna Abundance and the Type I Ifn Response: Innate Immunity. *Eur J Immunol* (2015) 45:1500–11. doi: 10.1002/eji.201444979
333. Rothamel K, Arcos S, Kim B, Reasoner C, Lisy S, Mukherjee N, et al. Elavl1 Primarily Couples Mrna Stability With the 3′ Utrs of Interferon-Stimulated Genes. *Cell Rep* (2021) 35:109178. doi: 10.1016/j.celrep.2021.109178
334. Sueyoshi T, Kawasaki T, Kitai Y, Ori D, Akira S, Kawai T. Hu Antigen R Regulates Antiviral Innate Immune Responses Through the Stabilization of Mrna for Polo-Like Kinase 2. *J Immunol* (2018) 200:3814–24. doi: 10.4049/jimmunol.1701282
335. Mancino A, Natoli G. Specificity and Function of Irf Family Transcription Factors: Insights From Genomics. *J Interferon Cytokine Res* (2016) 36:462–9. doi: 10.1089/jir.2016.0004
336. Mukherjee N. Integrative Regulatory Mapping Indicates That the RNA-Binding Protein HuR Couples Pre-mRNA Processing and mRNA Stability. *Mol Cell* (2011) 13:327–39. doi: 10.1016/j.molcel.2011.06.007
337. Ku Y, Park JH, Cho R, Lee Y, Park HM, Kim M, et al. Noncanonical Immune Response to the Inhibition of DNA Methylation by Staufen1 *via* Stabilization of Endogenous Retrovirus RNAs. *Proc Natl Acad Sci USA* (2021) 118: e2016289118. doi: 10.1073/pnas.2016289118
338. Ye C, Yu Z, Xiong Y, Wang Y, Ruan Y, Guo Y, et al. STAU1 Binds to IBDV Genomic Double-Stranded RNA and Promotes Viral Replication *via* Attenuation of MDA5-Dependent β Interferon Induction. *FASEB J* (2019) 33:286–300. doi: 10.1096/fj.201800062RR
339. Minervini CF, Parciante E, Impera L, Anelli L, Zagaria A, Specchia G, et al. Epitranscriptomics in Normal and Malignant Hematopoiesis. *IJMS* (2020) 21:6578. doi: 10.3390/ijms21186578
340. Tajaddod M, Jantsch MF, Licht K. The Dynamic Epitranscriptome: A to I Editing Modulates Genetic Information. *Chromosoma* (2016) 125:51–63. doi: 10.1007/s00412-015-0526-9
341. Helm M, Motorin Y. Detecting RNA Modifications in the Epitranscriptome: Predict and Validate. *Nat Rev Genet* (2017) 18:275–91. doi: 10.1038/nrg.2016.169
342. Kumar S, Mohapatra T. Deciphering Epitranscriptome: Modification of Mrna Bases Provides a New Perspective for Post-Transcriptional Regulation of Gene Expression. *Front Cell Dev Biol* (2021) 9:628415. doi: 10.3389/fcell.2021.628415
343. Nachtergaele S, He C. Chemical Modifications in the Life of an mRNA Transcript. *Annu Rev Genet* (2018) 52:349–72. doi: 10.1146/annurev-genet-120417-031522
344. Liu N, Pan T. N6-Methyladenosine–Encoded Epitranscriptomics. *Nat Struct Mol Biol* (2016) 23:98–102. doi: 10.1038/nsmb.3162
345. Solomon O, Di Segni A, Cesarkas K, Porath HT, Marcu-Malina V, Mizrahi O, et al. RNA Editing by Adar1 Leads to Context-Dependent Transcriptome-Wide Changes in RNA Secondary Structure. *Nat Commun* (2017) 8:1440. doi: 10.1038/s41467-017-01458-8
346. Nishikura K. A-To-I Editing of Coding and Non-Coding Rnas by Adars. *Nat Rev Mol Cell Biol* (2016) 17:83–96. doi: 10.1038/nrm.2015.4
347. Gray MW, Charette M. Pseudouridine in RNA: What, Where, How, and Why. *IUBMB Life (International Union Biochem Mol Biol: Life)* (2000) 49:341–51. doi: 10.1080/152165400410182
348. Mannion N, Greenwood SM, Young R, Cox S, Brindle J, Read D, et al. The RNA-Editing Enzyme ADAR1 Controls Innate Immune Responses to RNA. *Cell Rep* (2014) 9:1482–94. doi: 10.1016/j.celrep.2014.10.041
349. Yoshinaga M, Takeuchi O. Post-Transcriptional Control of Immune Responses and Its Potential Application. *Clin Trans Immunol* (2019) 8: e1063. doi: 10.1002/cti2.1063
350. Jing FY, Zhou LM, Ning YJ, Wang XJ, Zhu YM. The Biological Function, Mechanism, and Clinical Significance of M6a RNA Modifications in Head and Neck Carcinoma: A Systematic Review. *Front Cell Dev Biol* (2021) 9:683254. doi: 10.3389/fcell.2021.683254
351. Baquero-Perez B, Geers D, Díez J. From a to M6a: The Emerging Viral Epitranscriptome. *Viruses* (2021) 13:1049. doi: 10.3390/v13061049
352. Liddicoat BJ, Piskol R, Chalk AM, Ramaswami G, Higuchi M, Hartner JC, et al. RNA Editing by Adar1 Prevents Mda5 Sensing of Endogenous Dsrna as Nonself. *Science* (2015) 349:1115–20. doi: 10.1126/science.aac7049
353. Lamers MM, van den Hoogen BG, Haagmans BL. ADAR1: "Editor-In-Chief" of Cytoplasmic Innate Immunity. *Front Immunol* (2019) 10:1763. doi: 10.3389/fimmu.2019.01763
354. Schlee M, Hartmann G. Discriminating Self From Non-Self in Nucleic Acid Sensing. *Nat Rev Immunol* (2016) 16:566–80. doi: 10.1038/nri.2016.78
355. Zhang Y, Wang X, Zhang X, Wang J, Ma Y, Zhang L, et al. RNA-Binding Protein YTHDF3 Suppresses Interferon-Dependent Antiviral Responses by Promoting FOXO3 Translation. *Proc Natl Acad Sci USA* (2019) 116:976–81. doi: 10.1073/pnas.1812536116
356. Zhang X, Flavell RA, Li HB. Hnrnpa2b1: A Nuclear Dna Sensor in Antiviral Immunity. *Cell Res* (2019) 29:879–80. doi: 10.1038/s41422-019-0226-8
357. Wang L, Wen M, Cao X. Nuclear Hnrnpa2b1 Initiates and Amplifies the Innate Immune Response to Dna Viruses. *Sci (New York NY)* (2019) 365: eaav0758. doi: 10.1126/science.aav0758
358. Yang Y, Hsu PJ, Chen YS, Yang YG. Dynamic Transcriptomic M6a Decoration: Writers, Erasers, Readers and Functions in RNA Metabolism. *Cell Res* (2018) 28:616–24. doi: 10.1038/s41422-018-0040-8
359. Lee H, Bao S, Qian Y, Geula S, Leslie J, Zhang C, et al. Stage-Specific Requirement for Mettl3 -Dependent M 6 A mRNA Methylation During Haematopoietic Stem Cell Differentiation. *Nat Cell Biol* (2019) 1:700–9. doi: 10.1038/s41556-019-0318-1
360. Eisenberg E, Levanon EY. A-To-I RNA Editing — Immune Protector and Transcriptome Diversifier. *Nat Rev Genet* (2018) 19:473–90. doi: 10.1038/s41576-018-0006-1
361. Sadeq S, Al-Hashimi S, Cusack CM, Werner A. Endogenous Double-Stranded RNA. *Non-Coding RNA* (2021) 7:15. doi: 10.3390/ncrna7010015
362. Barak M, Porath HT, Finkelstein G, Knisbacher BA, Buchumenski I, Roth SH, et al. Purifying Selection of Long dsRNA Is the First Line of Defense Against False Activation of Innate Immunity. *Genome Biol* (2020) 21:26. doi: 10.1186/s13059-020-1937-3
363. Rice GI, Kasher PR, Forte GMA, Mannion NM, Greenwood SM, Szynkiewicz M, et al. Mutations in Adar1 Cause Aicardi-Goutières Syndrome Associated With a Type I Interferon Signature. *Nat Genet* (2012) 44:1243–8. doi: 10.1038/ng.2414
364. Pujantell M, Franco S, Galván-Femenía I, Badia R, Castellví M, Garcia-Vidal E, et al. ADAR1 Affects HCV Infection by Modulating Innate Immune Response. *Antiviral Res* (2018) 156:116–27. doi: 10.1016/j.antiviral.2018.05.012

365. Nie Y, Hammond GL, Yang JH. Double-Stranded RNA Deaminase Adar1 Increases Host Susceptibility to Virus Infection. *J Virol* (2007) 81:917–23. doi: 10.1128/JVI.01527-06
366. Zhou S, Yang C, Zhao F, Huang Y, Lin Y, Huang C, et al. Double-Stranded RNA Deaminase Adar1 Promotes the Zika Virus Replication by Inhibiting the Activation of Protein Kinase Pkr. *J Biol Chem* (2019) 294:18168–80. doi: 10.1074/jbc.RA119.009113
367. Clerzius G, Gélinas JF, Daher A, Bonnet M, Meurs EF, Gatignol A. Adar1 Interacts With Pkr During Human Immunodeficiency Virus Infection of Lymphocytes and Contributes to Viral Replication. *J Virol* (2009) 83:10119–28. doi: 10.1128/JVI.02457-08
368. Toth AM, Li Z, Cattaneo R, Samuel CE. RNA-Specific Adenosine Deaminase Adar1 Suppresses Measles Virus-Induced Apoptosis and Activation of Protein Kinase Pkr. *J Biol Chem* (2009) 284:29350–6. doi: 10.1074/jbc.M109.045146
369. Nallagatla SR, Toroney R, Bevilacqua PC. A Brilliant Disguise for Self RNA: 5'-End and Internal Modifications of Primary Transcripts Suppress Elements of Innate Immunity. *RNA Biol* (2008) 5:140–4. doi: 10.4161/rna.5.3.6839
370. Vogel OA, Han J, Liang CY, Manicassamy S, Perez JT, Manicassamy B. The P150 Isoform of Adar1 Blocks Sustained Rlr Signaling and Apoptosis During Influenza Virus Infection. *PloS Pathog* (2020) 16:e1008842. doi: 10.1371/journal.ppat.1008842
371. Karikó K, Buckstein M, Ni H, Weissman D. Suppression of RNA Recognition by Toll-Like Receptors: The Impact of Nucleoside Modification and the Evolutionary Origin of RNA. *Immunity* (2005) 23:165–75. doi: 10.1016/j.immuni.2005.06.008
372. Chen YG, Chen R, Ahmad S, Verma R, Kasturi SP, Amaya L, et al. N6-Methyladenosine Modification Controls Circular RNA Immunity. *Mol Cell* (2019) 76:96–109.e9. doi: 10.1016/j.molcel.2019.07.016
373. Bokar JA, Shambaugh ME, Polayes D, Matera AG, Rottman FM. Purification and cDNA Cloning of the AdoMet-Binding Subunit of the Human mRNA (N6-Adenosine)-Methyltransferase. *RNA* (1997) 3:1233–47.
374. Wang H, Hu X, Huang M, Liu J, Gu Y, Ma L, et al. Mettl3-Mediated mRNA M6a Methylation Promotes Dendritic Cell Activation. *Nat Commun* (2019) 10:1898. doi: 10.1038/s41467-019-09903-6
375. Wang X. N6-Methyladenosine Modulates Messenger RNA Translation Efficiency. *Cell* (2015) 13:1388–99. doi: 10.1016/j.cell.2015.05.014
376. Zheng Q, Hou J, Zhou Y, Li Z, Cao X. The RNA Helicase Ddx46 Inhibits Innate Immunity by Entrapping M6a-Demethylated Antiviral Transcripts in the Nucleus. *Nat Immunol* (2017) 18:1094–103. doi: 10.1038/ni.3830
377. Yoshinaga M, Takeuchi O. RNA Binding Proteins in the Control of Autoimmune Diseases. *Immunol Med* (2019) 42:53–64. doi: 10.1080/25785826.2019.1655192
378. Quattrone A, Dassi E. The Architecture of the Human RNA-Binding Protein Regulatory Network. *iScience* (2019) 21:706–19. doi: 10.1016/j.isci.2019.10.058

Conflict of Interest: The authors declare that the research was conducted in the absence of any commercial or financial relationships that could be construed as a potential conflict of interest.

Publisher's Note: All claims expressed in this article are solely those of the authors and do not necessarily represent those of their affiliated organizations, or those of the publisher, the editors and the reviewers. Any product that may be evaluated in this article, or claim that may be made by its manufacturer, is not guaranteed or endorsed by the publisher.

frontiers in Immunology

ORIGINAL RESEARCH
published: 11 February 2022
doi: 10.3389/fimmu.2022.752215

Inactivation of AUF1 in Myeloid Cells Protects From Allergic Airway and Tumor Infiltration and Impairs the Adenosine-Induced Polarization of Pro-Angiogenic Macrophages

Sofia Gargani[1,2†], Niki Lourou[1,2†], Christina Arapatzi[1], Dimitris Tzanos[1], Marania Saridaki[1], Esmeralda Dushku[2], Margarita Chatzimike[1], Nikolaos D. Sidiropoulos[2], Margarita Andreadou[1], Vasileios Ntafis[1], Pantelis Hatzis[1], Vassiliki Kostourou[1] and Dimitris L. Kontoyiannis[1,2]*

[1] Biomedical Sciences Research Centre "Alexander Fleming", Institute of Fundamental Biomedical Research, Vari, Greece, [2] Department of Genetics, Development and Molecular Biology, School of Biology, Aristotle University of Thessaloniki, Thessaloniki, Greece

The four isoforms of the RNA-binding protein hnRNPD/AUF1 have been proposed to limit the use of inflammatory mRNAs in innate immune cells. Mice engineered to lack AUF1s in all tissues are sensitive to acute inflammatory assaults; however, they also manifest complex degenerations obscuring assessment of AUF1s' roles in innate immune cells. Here, we restricted a debilitating AUF1 mutation to the mouse myeloid lineage and performed disease-oriented phenotypic analyses to assess the requirement of AUF1s in variable contexts of innate immune reactivity. Contrary to the whole-body mutants, the myeloid mutants of AUF1s did not show differences in their susceptibility to cytokine storms occurring during endotoxemia; neither in type-I cell-mediated reactions driving intestinal inflammation by chemical irritants. Instead, they were resistant to allergic airway inflammation and displayed reductions in inflammatory infiltrates and an altered T-helper balance. The *ex-vivo* analysis of macrophages revealed that the loss of AUF1s had a minimal effect on their proinflammatory gene expression. Moreover, AUF1s were dispensable for the classical polarization of cultured macrophages by LPS & IFNγ correlating with the unchanged response of mutant mice to systemic and intestinal inflammation. Notably, AUF1s were also dispensable for the alternative polarization of macrophages by IL4, TGFβ and IL10, known to be engaged in allergic reactions. In contrast, they were required to switch proinflammatory macrophages towards a pro-angiogenic phenotype induced by adenosine receptor signals. Congruent to this, the myeloid mutants of AUF1 displayed lower levels of vascular remodeling factors in exudates from allergen exposed lungs; were unable to support the growth and inflammatory infiltration of transplanted melanoma tumors; and failed to vascularize inert grafts unless supplemented with angiogenic factors. Mechanistically, adenosine receptor signals enhanced the association of AUF1s with the *Vegfa, Il12b, and Tnf* mRNAs to

OPEN ACCESS

Edited by:
Osamu Takeuchi, Kyoto University, Japan

Reviewed by:
Robert Schneider, NYU Grossman School of Medicine, United States
Gary Brewer, Rutgers, The State University of New Jersey, United States
Manuel Daniel Díaz-Muñoz, INSERM Toulouse Institute for Infectious and Inflammatory Diseases, France

***Correspondence:**
Dimitris L. Kontoyiannis
dkontoyiannis@bio.auth.gr; kontoyiannis@fleming.gr

†These authors have contributed equally to this work

Specialty section:
This article was submitted to Molecular Innate Immunity, a section of the journal Frontiers in Immunology

Received: *02 August 2021*
Accepted: *21 January 2022*
Published: *11 February 2022*

Citation:
Gargani S, Lourou N, Arapatzi C, Tzanos D, Saridaki M, Dushku E, Chatzimike M, Sidiropoulos ND, Andreadou M, Ntafis V, Hatzis P, Kostourou V and Kontoyiannis DL (2022) Inactivation of AUF1 in Myeloid Cells Protects From Allergic Airway and Tumor Infiltration and Impairs the Adenosine-Induced Polarization of Pro-Angiogenic Macrophages. Front. Immunol. 13:752215. doi: 10.3389/fimmu.2022.752215

differentially regulate and facilitate the pro-angiogenic switch. Our data collectively demonstrates that AUF1s do not act as general anti-inflammatory factors in innate immune cells but have more specialized roles in regulons allowing specific innate immune cell transitions to support tissue infiltration and remodeling processes.

Keywords: inflammation, innate immunity, post-transcriptional regulation, RNA-binding proteins, animal models

INTRODUCTION

Heterogeneous nuclear ribonucleoprotein D (hnRNP D), commonly known as AU-rich element-binding factor 1 (AUF1), is an RNA-binding protein (RBP) presented in eukaryotic cells as four protein isoform members (p37, p40, p42 & p47) (1). These arise from the alternative splicing of a single pre-mRNA transcript and share two non-identical RNA-recognition motifs and a glutamine rich sequence proximal to their C-terminus. All AUF1 members can bind RNA as monomers or oligomers and localize in nuclear and cytoplasmic compartments, albeit to a variable extent (1–3).

As their name implies, AUF1 members were amongst the first RBPs identified biochemically to bind to regulatory RNA elements rich in Adenylate/Uridylate motifs (AU-Rich Elements, AREs) (4). Such elements are commonly found in the untranslated termini of mRNAs encoding immune regulators, growth signalers, and death controllers (5). Furthermore, early findings in macrophage cell lines suggested AUF1 members are post-translationally modified by immune signals to promote the degradation of pro-inflammatory mRNAs such as those encoding TNF, IL-1β, IL-3, IL-6, IL-10, GM-CSF (6–8), iNOS (9), and the NFkB regulators (10). As such, they were predicted to act in concert to other RBPs active in innate immune cells (e.g. Zfp36, Regnase-1, Roquins 1&2, TIA-1), which impede the use of inflammatory mRNAs, and whose genetic ablation in mice predisposes to acute and chronic inflammatory pathologies (4, 11–14).

Indeed, the first reports on mice deficient in AUF1s demonstrated their increased susceptibility to acute inflammatory assaults and spontaneous dermatitis upon aging (15, 16). The appearance of these phenotypes correlated to augmentations in elicited cytokine storms connecting to the increased stability of related mRNAs in immune cells. However, subsequent reports revealed these inflammatory occurrences were not due to *bona fide* aberrations in inflammation control. Instead, they seem to be triggered by tissue degenerations resulting either from their premature senescence due to involvement of AUF1 in telomere maintenance (17); or from distortion of critical developmental programs organized by AUF1 (affecting e.g. growth, myogenesis and muscle regeneration) (18–20). Notably, the fundamental roles of AUF1 in controlling aging or development were linked to the activation of key mRNAs, thus deviating from the original supposition of its action as an instructor of ARE-mediated suppression (15, 20).

Indeed, it is now clear that AUF1 members can both positively and negatively affect mRNA stability, initiation of translation, editing and even transcription (21). Comprehensive studies assessing the interactions of AUF1s revealed a relaxed stringency in their affinities for AU- to U- and GU-rich motifs (22). These studies also showed that AUF1 members do not bind only to coding but also non-coding RNAs to aid their maturation, target-loading, and function (23). The current biochemical and molecular information on AUF1s point to an indirect *modus operandi* in RNA regulation which entails changes in local RNA structures, cooperative binding with other RBPs and miRNAs or competition with other *trans*-factors (14, 21).

Still, the original findings connecting AUF1s to ARE-containing inflammatory mRNAs suggest their cell-intrinsic involvement in the regulation of innate immunity. In that context, the complex molecular activities of AUF1s could contribute to the outstanding functional heterogeneity of innate immune cells which arises due to plasticity in response to the ever-changing signals of inflamed tissues. For example, macrophages adapt to varying microenvironments and acquire a spectrum of functional phenotypes to support host defense to infection and tissue damage, different types of T-helper mediated immunity, homeostasis, and tissue vascularization and regeneration (24–27). However, the complexity of aberrations observed in whole-body AUF1 knockouts precludes judgment on the direct involvement of AUF on innate immune responses.

In this report, we identified contexts of inflammatory reactions where innate immunity was affected by the dysfunction of AUF1s. To do so, we employed a mouse system where the expression of all of AUF1 isoforms was explicitly debilitated in the myeloid lineage. Using a disease-oriented phenotypic approach, we demonstrate that AUF1s do not act as general deactivators of inflammatory responses. Instead, they are required for specific contexts of cellular immunity; and for specialized phenotypic transitions of innate immune cells, which in turn support such inflammatory contexts.

RESULTS

The Susceptibility of Mice With a Germline Deletion of *hnRNPD's* Exons 3 and 4 Differs From The Susceptibility of Mice With a Myeloid Deletion

Our original strategy entailed targeting exons 3 and 4 of the *hnRNPD* gene to debilitate the RRMs present in all four AUF1 isoforms. Mutant $hnRNPD^{flx3,4/flx3,4}$ mice containing functional *hnRNPD* alleles amenable to loxP-mediated recombination (**Figure S1A**), were derived *via* gene-targeting manipulations

of embryonic stem cells, germline removal of antibiotic selection cassettes and inbreeding to a C57Bl6/J background for 12 generations. To generate a mutant *hnRNPD*$^{\Delta x3,4}$ allele, we crossed *hnRNPD*$^{flx3,4/+}$ mice to a mouse line expressing germline-active Cre recombinase. Subsequently, *hnRNPD*$^{\Delta x3,4/+}$ mice were intercrossed to yield homozygous *hnRNPD*$^{\Delta x3,4/\Delta x3,4}$ mice. Examination of the F2 progenies at post-natal day 10 (P10) revealed a skew in mendelian segregation relating to a 30% loss in the *hnRNPD*$^{\Delta x3,4/\Delta x3,4}$ genotype (**Figure S1B**). However, *hnRNPD*$^{\Delta x3,4/\Delta x3,4}$ embryos were properly detected till the embryonic day E14.5, suggesting that their post-natal loss was not due to early embryonic lethality. Moreover, the majority of *hnRNPD*$^{\Delta x3,4/\Delta x3,4}$ mice identified post birth displayed a delay in weight gain (**Figure S1C**), and 50% succumbed during the two months of age (**Figure S1D**). The remaining that survived to adulthood displayed fertility issues and perished progressively past the 6-months of age. The analyses of AUF1-encoding mRNAs and proteins in extracts from *hnRNPD*$^{+/+}$, and *hnRNPD*$^{\Delta x3,4/\Delta x3,4}$ mouse embryonic fibroblasts (MEFs) indicated the near-complete loss of all isoforms (**Figure 1A**). Thus, the genetic removal of exons 3 and 4 did not yield an RRM deficient mutein but instead led to the diminished synthesis of AUF1s.

To identify whether AUF1s have specific functions in innate immune cells, we restricted the *Δx3,4* mutation in the mouse myeloid linage *via* crossing the *hnRNPD*$^{flx3,4/flx3,4}$ mice to a *LysMCre*$^{+}$ line. Contrary to whole-body mutants, *LysMCre*$^{+}$ *hnRNPD*$^{flx3,4/flx3,4}$ mice (termed hereafter as *M-hnRNPD*$^{\Delta x3,4}$ or *M-Δx3,4* mice) appeared phenotypically normal through a 12-month observation period. As in the case of *hnRNPDΔ*$^{x3,4/\Delta x3,4}$ MEFs, the reduction of AUF1 proteins in *M-hnRNPD*$^{\Delta x3,4}$ mice was verified in bone marrow-derived (BMDMs), thioglycolate-elicited peritoneal (TEMPs) macrophages and peritoneal Gr1^{+} polymorphonuclear cells (PMNs) but not in other myeloid derivatives like e.g. Siglec-F^{+} peritoneal eosinophils (**Figure 1B** and **Figure S1E**).

Published data on obligatory AUF1 deficient mice demonstrated their increased susceptibility to the systemic administration of lipopolysaccharides (LPS; endotoxins) from Gram-negative bacteria. LPS activates the canonical TLR4 pathway in immune and non-immune cells triggering an excessive cytokine storm (15). This leads to a variety of cytokine-induced danger signals in tissues and changes in physiology. Depending on the LPS dose, such changes range from hypothermia to systemic organ failure and lethality. To test whether our *mutant* mice responded to endotoxemia in an exaggerated manner, we challenged them first with a low dose of LPS (4mg/kg) and monitored changes in body temperature. In *hnRNPD*$^{+/+}$ mice, this dose elicited a temperature drop till the 4th hour post treatment which then recovered by the 6th hour (**Figure 1C**). Under the same conditions, the hypothermic response of *hnRNPD*$^{\Delta x3,4/\Delta x3,4}$ mice verified their enhanced susceptibility. The drop in their body temperature was not transient but continued past the 4th hour leading to a moribund state which necessitated the termination of the experiment. Surprisingly, the hypothermic response of *M-hnRNPD*$^{\Delta x3,4}$ mice to the same treatment was as transient as in the case of their control and of *hnRNPD*$^{+/+}$ mice **(Figure 1D).** Similarly, the susceptibility of *M-hnRNPD*$^{\Delta x3,4}$ mice to higher doses of LPS prolonging hypothermia (12mg/kg) or leading to sub-lethality (20mg/kg) was comparable to that of their corresponding controls (**Figure 1D**).

The different response of the whole-body to the myeloid mutants could reflect changes in the spectrum of inflammatory mediators elicited by LPS. To address this, we measured 10 prototypical mediators in the sera of all mice challenged with the low dose of LPS for 90mins (**Figure 1E**). Eight of these mediators (TNF, IL6, IL12b, IL1β, IL10, and the chemokines CCL2, 17&22) were detected in a similar range between the different control groups; whereas two (TGFβ1 & CXCL1) showed intergroup variations and were thus excluded from further comparisons.

In our analysis we noted selective quantitative differences between the mutants. *hnRNPD*$^{\Delta x3,4/\Delta x3,4}$ mice possessed higher pro-inflammatory IL1β, whereas this was not observed in *M-hnRNPD*$^{\Delta x3,4}$ mice. The secretion of IL1β is elicited by inflammasomes which can sense signals from degenerating tissues (28, 29). Given the previous foreground on AUF1s control over senescent or homeostatic programs (17), the exacerbated response of the whole-body mutants to LPS might be a secondary consequence of inflammatory tissue degenerations enhanced by the loss of such programs in afflicted tissues.

Notably, the sera from the challenged *M-hnRNPD*$^{\Delta x3,4}$ mice revealed augmentations in pro-inflammatory TNF and IL12b. The mRNAs encoding these cytokines are subject to ARE-mediated control, and their augmented presence connects to the enhanced LPS-response of mouse mutants lacking other ARE-BPs like *Zfp36/TTP*, *TIA1*, or *Elavl1/HuR* (4, 11). Unlike those mutants, the *M-hnRNPD*$^{\Delta x3,4}$ mice did not display an exacerbated response to LPS despite the presence of higher TNF and IL12b; whereas the quantity of these cytokines was not altered in *hnRNPD*$^{\Delta x3,4/\Delta x3,4}$ mice. These observations may be taken to suggest that (a) AUF1s have a more limited role upon the secretion of TNF and IL12b which may be masked by the pleiotropic events underlying the response of the whole-body knockouts, and (b) the activities of TNF and IL12b in our myeloid mutants could be compensated due to the effects of AUF1s' loss upon other myeloid-derived effectors or inhibitors acting downstream of these cytokines.

Myeloid AUF1 Is Dispensable for Pro-Inflammatory and Type I Immune Reactions Facilitating the Development of Chemically-Induced Intestinal Inflammation

The invariable, yet puzzling, systemic response of our myeloid AUF1 mutants to endotoxin prompted us to screen them for more restricted, cell-mediated and organ specific inflammatory responses. We started with two well-established models of intestinal inflammation elicited by chemical irritants. In the first model, inflammation in the colon is induced by the addition of dextran sodium sulfate (DSS) in the drinking water of mice for 7

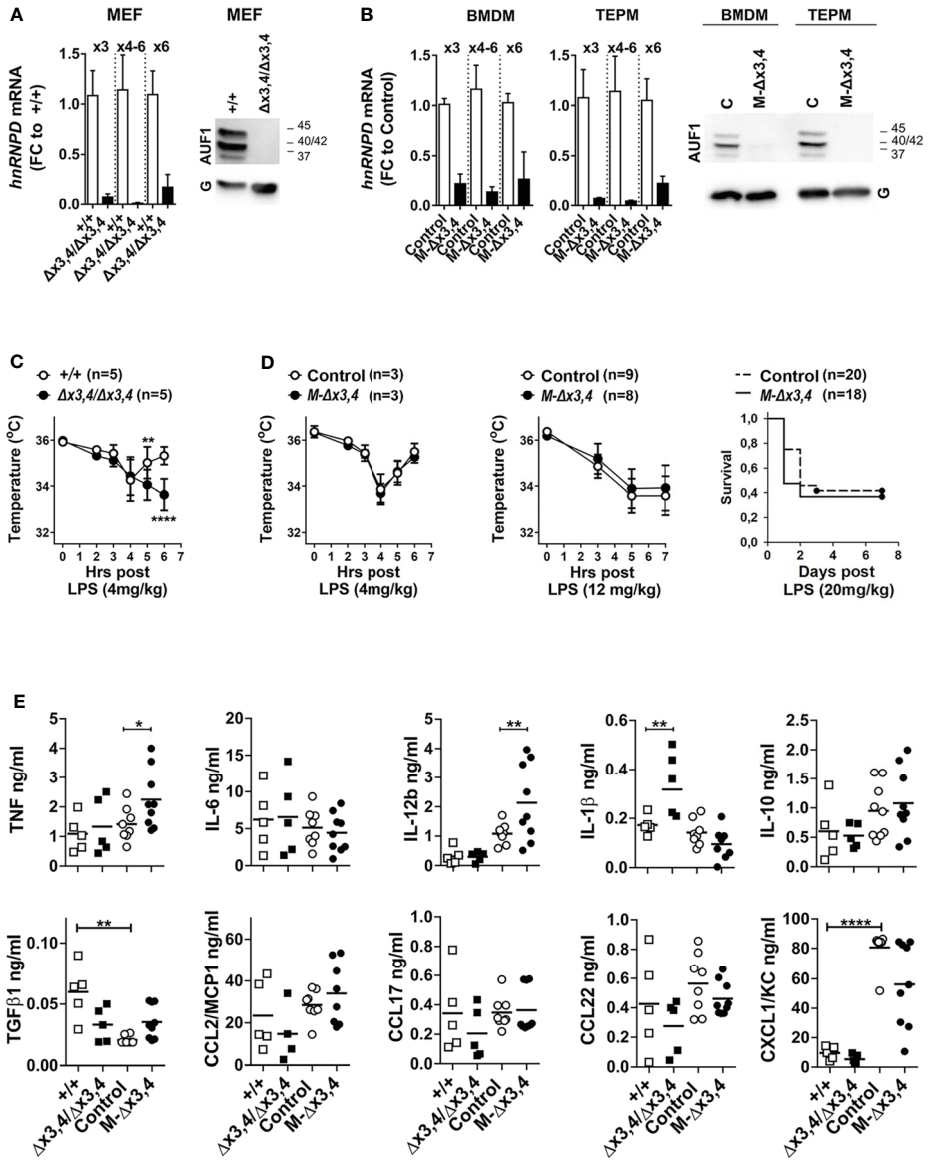

FIGURE 1 | Whole-body and myeloid mutants of AUF1s differ in their responses to endotoxemia. Detection of *hnRNPD* mRNAs containing exons (x) 3 to 6 *via* qRT-PCR; and of AUF1 protein isoforms *via* immunoblots in extracts from **(A)** *hnRNPD*$^{+/+}$, and *hnRNPD*$^{\Delta x3,4/\Delta x3,4}$ mouse embryonic fibroblasts (MEFs)**;** and **(B)** bone-marrow derived (BMDM) and thioglycolate-elicited peritoneal macrophages from control and *LysMCre*$^{+}$*hnRNPD*$^{flx3,4/flx3,4}$ *(M-Δx3,4)* mice. Bar graphs show mean fold change values (± SD) relative to the corresponding controls. Representative immunoblots indicate signals detected by an anti-AUF1 antibody or GAPDH (G) for quantitation. **(C)** Body temperature measurements of control and hnRNPD$^{\Delta x3,4/\Delta x3,4}$ mice at the indicated time-points post the intraperitoneal administration of the indicated does of LPS. **(D)** Body temperature and Survival measurements of control and *M-Δx3,4* mice at the indicated time-points post the intraperitoneal administration of the indicated doses of LPS. Line graphs depict mean temperature values (± SD); or Kaplan-Maier percentile cumulative survival. n denotes number of mice per group. **(E)** Detection of inflammatory mediators in the sera from control, whole body (n=5/genotype) and myeloid mutant mice (n=8-9/genotype) 90mins post administration of 4mg/Kg LPS. Scatter plots indicate individual and mean protein values (line) as detected *via* cytometric bead arrays. For graphs in **(A, C–E)** (*,**,****) denote p values ≤ 0.05, ≤ 0.01 or 0.00001 respectively as determined *via* One-Way ANOVA.

days (30). This disrupts the colonic epithelial barrier allowing entry of commensal bacterial antigens and activation of underlying innate immune cells. The inflammatory stimulus is subsequently removed to allow for the resolution of inflammation and the restitution of the epithelium. Clinical symptoms (i.e. weight loss, diarrhea and bloody stools) were monitored daily for 15 days after the initial exposure to DSS, with endoscopic evaluation of the colon on day 8 and histological assessment on days 3, 6 and 13 representing the initiation, peak and restitution phases, respectively. The evaluation of the clinical and endoscopic parameters revealed that the disease activity of the *M-hnRNPD*$^{\Delta x3,4}$ mice, was indistinguishable from that in the

controls (**Figures 2A, B**). Similarly, the histological assessment verified that the inflammatory, degenerative and restitution phases in the afflicted colons progressed invariably between mutant and control groups (**Figure 2C**). To test whether *M-hnRNPD*$^{\Delta x3,4}$ mice could be differentiated *via* the cytokine variations we detected in their LPS response, we sought for disturbances in IL1β, TNF, IL6 & IL10 that are commonly engaged in systemic and mucosal inflammation. However, we failed to detect any statistical

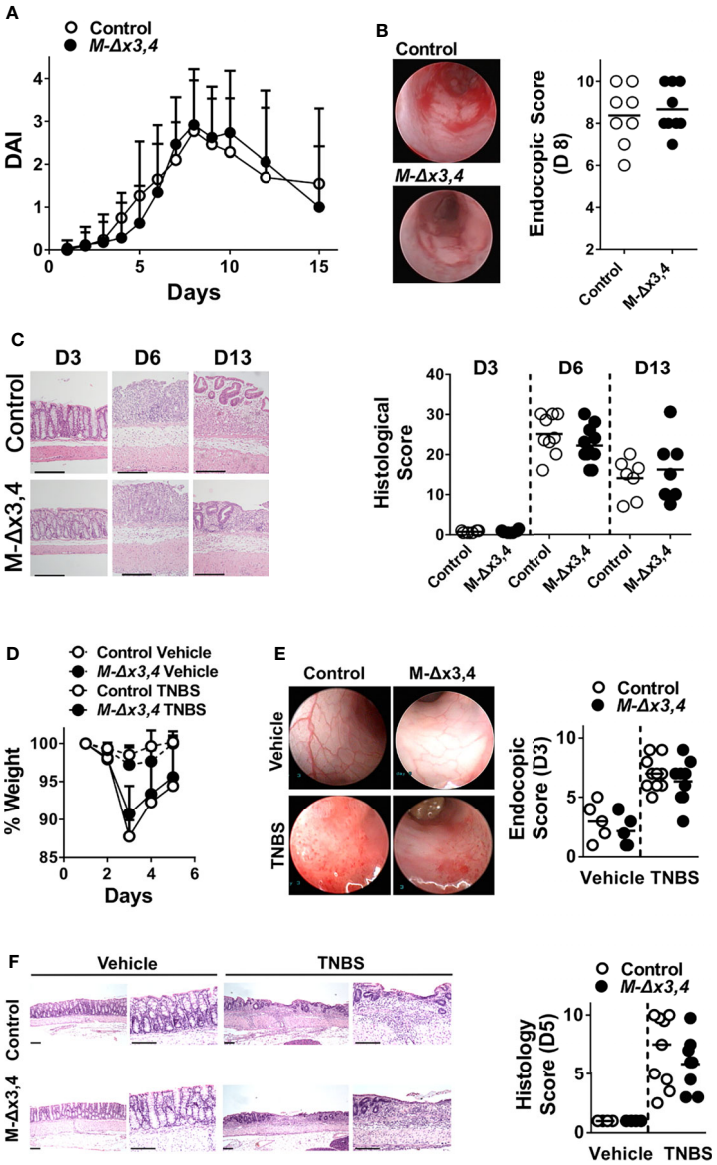

FIGURE 2 | The ablation of AUF1 functions in myeloid cells does not affect the initiation nor the progression of chemically-induced intestinal inflammation. **(A)** Macroscopic Disease Activity Index (DAI) of control and *M-Δx3,4* mice after treated with DSS for seven days. Line graphs depict mean values (± SD; n_i=20-28/group/genotype). **(B)** Representative photographs (left) and Scores (right) derived from the endoscopic evaluation of control and *M-Δx3,4* colons on the 8th day of the DSS protocol. **(C)** *Left.* Histology of colonic tissue (left) from control and *M-Δx3,4* mice on days 3, 6 and 13 of the DSS protocol. Shown are representative photomicrographs of paraffin-embedded sections stained with H&E. Such sections were used for the evaluation of mean histological scores (*Right*) from 8-11 mice/genotype/timepoint). **(D)** Whole body-weight measurements of control and *M-Δx3,4* mice sensitized with TNBS and challenged intrarectally either with ethanol vehicle or TNBS. Line graphs depict mean weight values (± SD) from n=5-9 mice/group/genotype **(E)** Representative photographs (left) and Scores (right) derived from the endoscopic evaluation of control and *M-Δx3,4* colons from mice treated with ethanol vehicle (n=5/genotype) on TNBS (n=9-10/genotype) for 3 days. **(F)** *Left.* Histology of colonic tissue (left) from control and *M-Δx3,4* mice on day 5 of the TNBS protocol. Shown are representative photomicrographs of paraffin-embedded sections stained with H&E. Such sections were used for the evaluation of mean histological scores (*Right*) from Vehicle treated (n=5/genotype), on TNBS treated (n=9-10/genotype) mice. For **(B–F)**, Scatter plots indicate individual and mean protein values (line). The lack of statistical significance was tested *via* One-Way ANOVA.

differences in the secretion of these cytokines by colonic explants isolated from mice on the 13th day of the challenge (**Figure S2**). In the second model, colitis was induced by the haptenating agent 2,4,6-trinitrobenzene sulfonic acid (TNBS). This model is more complex because it relies on Type I adaptive immune responses encompassing the functions of Th1 T-helper subsets (31). Yet, innate immunity is paramount in this model as some form of clinical disease can occur even in the absence of lymphocytes. For the model, TNBS in ethanol was administered intrarectally in mice 7 days after a peripheral skin pre-sensitization, whereas a parallel group received only the ethanol vehicle (32). Weight changes were monitored for 5 days after administration of TNBS (**Figure 2D**), with parallel endoscopic evaluation on day 3 (**Figure 2E**) followed by histopathology at day 5 (**Figure 2F**). The kinetics of weight loss and recovery, the endoscopic scoring and the histological analysis of afflicted colonic tissue were nearly identical in control and *M-hnRNPD*$^{\Delta x3,4}$ mice (**Figure 2E**).

Collectively our data indicate that myeloid AUF1s are dispensable for the proinflammatory and Type I cell-mediated immune reactions which facilitate intestinal inflammation in models of chemically-induced colitis.

Myeloid AUF1 Is Required for the Development of Allergic Airway Inflammation

Next, we screened for changes in Type II cell-mediated responses such as those observed in allergy and hypersensitivity reactions (33). To do so we explored an animal model of human asthma where lung inflammation is elicited post the systemic sensitization of mice to Ovalbumin (OVA) and subsequent to a local challenge with aerosolized OVA. This leads to a skewed Th2 response, the production of OVA-specific IgE, the elicitation of eosinophilic lung inflammation, and airway obstruction. In this model, immunoregulatory innate immune cells promote the recruitment of eosinophils and lymphocytes; and sustain the Th2 feedback loop while counteracting pro-inflammatory, neutrophilic and Th1 responses.

Relative to mice challenged with PBS, both Control and *M-hnRNPD*$^{\Delta x3,4}$ mice challenged with OVA mounted the allergic response. However, the lungs of challenged *M-hnRNPD*$^{\Delta x3,4}$ mice displayed less peribronchial (PBI) and perivascular (PVI) inflammation, reduced fibrosis, and decreased bronchial mucus metaplasia relative to the lungs of control mice (**Figures 3A, B**). This correlated with a significant reduction in OVA-specific IgE in the sera of *M-hnRNPD*$^{\Delta x3,4}$ mice (**Figure 3C**) and a dramatic decrease in cells infiltrating their Bronchioalveolar Fluid (BALF; **Figure 3D**). Flow cytometric analysis of BALF exudates from the *M-hnRNPD*$^{\Delta x3,4}$ lungs revealed that this numeric reduction was not only restricted to eosinophils but extended to all central myeloid and lymphoid infiltrates (**Figure 3E** and **Figure S3**).

The assessment of BALFs for T-helper 2 lymphokines (**Figure 3F**) revealed a significant reduction of IL-4 in the lungs of challenged *M-hnRNPD*$^{\Delta x3,4}$ mice whereas other lymphokines engaged in the allergic response were either augmented (e.g. IL-5, IL-13) or remained unchanged (e.g. IL-9). However, we detected significant elevations in the Th1-lymphokine IFNγ and of pro-inflammatory TNF. Together, our data indicate that the loss of AUF1s functions in myeloid cells restricts the progression of allergic airway infiltration and skews T-helper functions.

AUF1 Is Dispensable for Macrophage Activation and Central Polarization Programs

The resistance of *M-hnRNPD*$^{\Delta x3,4}$ mice to allergic airway inflammation as opposed to their normotypic response to endotoxemia and colitis, suggested that in innate cells, AUF1 does not act as an anti-inflammatory factor. Instead it appears to be engaged in signal-induced programs balancing cell-mediated immune reactions.

To gain further insight into this, we focused our subsequent analyses on macrophages as a prototypical innate-immune subset. Given the prior connection of AUF1s to pro-inflammatory control, we sought for comprehensive changes in RNA expression incurred by the loss of this RBP in macrophages activated by the predominant TLR4 ligand -i.e., LPS- for 4hrs. We decided to assess only mature mRNAs associated with the response without considering immature, fragmented and non-coding RNAs. To do so, we used 3′ end sequencing of transcripts (Quantseq) and performed our analysis on transcript rather than on gene level. Our search for changes (with a log2 Fold Change of 1 and p value<0.05) between the profiles of *M-hnRNPD*$^{\Delta x3,4}$ and control BMDMs showed an unexpectedly small number of differentially expressed transcripts (424 transcripts corresponding to 204 genes) **(Figure 4A** and **Table S1).** Moreover, 2/3 of the transcripts appeared as downregulated in AUF1-deficient macrophages **(Figure 4B),** contrasting the original hypothesis on AUF1s' as primary decay-promoting factors. By inspecting the dataset for changes in *hnRNPD* RNAs we verified the reduction of three RNA isoforms; and in three RNAs derived from Nonsense-mediated decay (NMD) **(Figures 4A, C)**. Notably, the RNAs of other isoforms including that of the larger p45 **(Figure 4C)** were poorly expressed in macrophages suggesting the predominance of the p37, p40 & p42 isoforms in these cells.

To explore further the biological consequences of these differences in macrophage activation, we performed functional analysis using WebGestalt (2019). Ten weighted terms were identified as significant with an FDR<0.05 **(Figure 4D)**. As expected, the term "negative regulation of gene expression" was significantly enriched in the dataset and included RNA regulators involved in nuclear and cytoplasmic events besides *hnRNPD* (e.g. *Elavl1, Eif4a3, hnRNPs A2/B1* & *U, Pum1*). This implied that AUF1s may act in the apex of several regulons for RNA control. However, these regulons did not connect to changes in cytokines. Rather they connected to (a) metabolic changes such as those relating to nitrogen containing biomolecules or ATP; (b) negative effects of stress in protein modification or use and (c) extracellular signals transmitted by biotic stimuli such as those produced by the same or other cells.

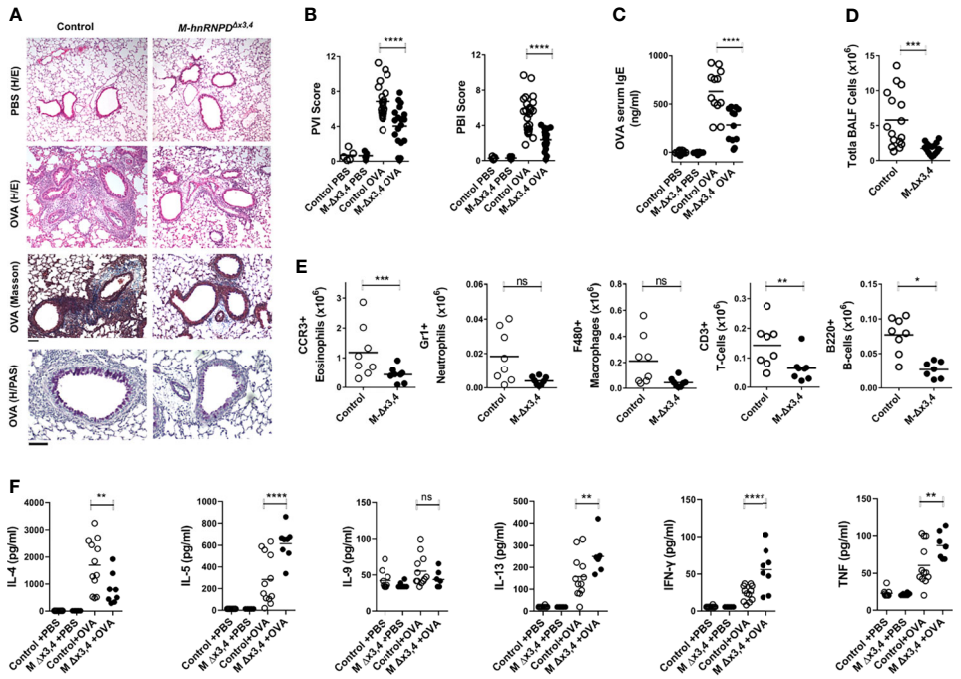

FIGURE 3 | The ablation of AUF1s functions in myeloid cells attenuates the development of allergic-airway inflammation. **(A)** Representative histology of lung tissue from control and *M-Δx3,4* mice at the endpoint of treatment with aerosolized Ovalbumin (OVA). Photomicrographs of paraffin-embedded sections stained with Hematoxylin & Eosin (H&E) for the generic assessment of pathological features of peribronchial and perivascular inflammation in mice treated either with OVA or PBS vehicle; as well as Masson trichrome for fibrosis and Periodic Acid Schiff (PAS) for bronchial mucus metaplasia in OVA challenged mice. Scale bar corresponds to 50μm. **(B)** Estimation of Perivascular (PVI) and Peribronchial (PVI) Inflammation Score in Control and *M-Δx3,4* mice. Scatter plots indicate individual values and means (lines) derived from the scoring of H&E stained sections derived from n=17-22 mice/genotype. **(C)** Quantitation of total anti-OVA IgE in the sera of control and *M-Δx3,4* mice challenged with OVA or PBS vehicle. Scatter plots indicate individual values and means (lines) as assessed *via* ELISA of sera from n=11 mice/genotype. **(D)** Endpoint quantitation of total cell numbers in BALF from Control and *M-Δx3,4* mice treated with OVA. Scatter plots indicate individual values and means (lines) as assessed *via* coulter counting of BALFs from n=15-17 mice/genotype. **(E)** Absolute quantitation of distinct cellular subsets in the BALF of Control and *M-Δx3,4* mice treated with OVA. Scatter plots indicate individual values and means (lines) as assessed *via* the flow cytometric analysis of BALFs from n=8 mice/genotypeanalyzed *via* the gating strategy indicated in **Figure S3**. **(F)** Detection of T-helper lymphokines in the BALFs from control and *M-Δx3,4* mice challenged with OVA or PBS vehicle. Scatter plots indicate individual and mean protein values (line) as detected *via* cytometric bead arrays. For graphs in **(B–F)** (ns, *, **, ***, ****) denote p values > 0.05, ≤0.05, ≤0.001, ≤0.0001, ≤0.00001 respectively as determined *via* One-Way ANOVA.

We postulated that AUF1s may regulate innate immune responses depending upon signal-induced changes in cellular metabolism as in those inducing the wide spectrum of polarized macrophage phenotypes. Extremes of this spectrum can be elicited *in vitro* through different signaling combinations supporting either the classical pro-inflammatory phenotype (M1-like); or a multitude of alternative phenotypes (M2-like; M2a,b,c,d) (34). M1-like macrophages are driven by Toll-like receptor (TLR) and interferon signals and use Nitric Oxide Synthase 2 (NOS2) to metabolize arginine to nitric oxide (NO) which can be further metabolized to downstream reactive nitrogen species. Functionally, they mount pro-inflammatory type-I and Type III immune responses against bacteria, intracellular pathogens, and tumor cells and support pathologic tissue damage like in sepsis and IBD and cellular transformation if uncontrolled. Differently, the major subset of M2 macrophages is driven by IL-4 (and/or IL13; M2a) and use Arginase 1 (ARG1) to hydrolyze arginine to urea and ornithine for the support of polyamine and proline synthesis. Functionally, M2 macrophages inhibit M1-like pro-inflammatory responses, promote vascular remodeling, tissue regeneration and helminth control; but also support pathologic Type II immune responses (e.g., as in allergy), tumor vascularization and growth (35, 36).

In response to signals promoting a classical M1 phenotype (i.e., LPS+IFNγ) the total levels of *hnRNPD* transcripts were reduced (**Figure 4E**). Still, M1 polarized *M-hnRNPD*$^{\Delta x3,4}$ BMDMs secreted TNF, IL6, IL12, IL10 and expressed the Nos2 and several chemokine mRNAs at levels comparable to control macrophages and only under the specific signaling regime (**Figure 4F** and **Figure S4**). Intriguingly, and in response to the M2-promoting cytokine IL-4, *hnRNPD* transcripts were also reduced (**Figure 4E**); and *M-hnRNPD*$^{\Delta x3,4}$ BMDMs elevated properly the characteristic *Arg1, Mrc1, Retnla/Fizz1, Chi3l3/Ym1* mRNAs whereas M1 markers remained silent **(Figure 4F** and **Figure S4).**

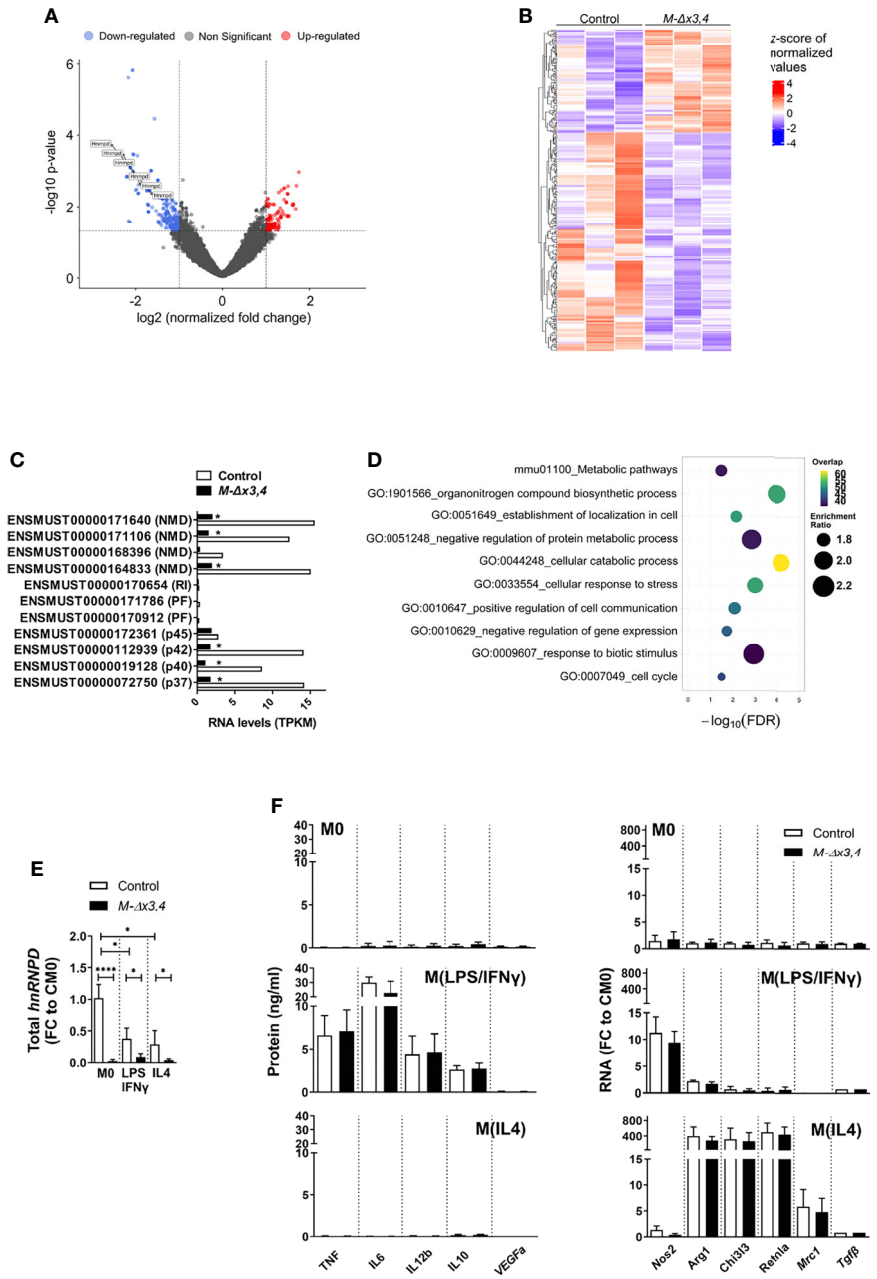

FIGURE 4 | Macrophages lacking AUF1 functions display minimal changes in their activation programs and properly acquire M1- and M2a- like phenotypes *in vitro*. **(A)** Volcano plot depicting the distribution of the adjusted P values (-Log10 (adjusted P value) and the fold changes (Log2 FC) of mRNA transcripts differing between control and *M-Δx3,4* BMDMs treated with LPS for 4hrs and analyzed *via* 3'end sequencing. Significantly upregulated and downregulated transcripts are indicated by color. **(B)** Heatmap depicting the extend of significant changes in the levels of transcripts differing between 3 samples of LPS treated control and *M-Δx3,4* BMDMs. **(C)** Quantitation of *hnRNPD* RNA isoforms as derived from sequencing analyses of activated control and *M-Δx3,4* BMDMs. Bar graphs depict mean values of Transcripts Per Kilobase Million (TPKM) of ENSEMBL annotated RNAs for the p37,40,42 & 45 isoforms of AUF1; other protein coding fragments (PF); retained intron transcripts (RI); or RNAs yielded *via* NMD. (*) asterisks denote statistical significance as per the bioinformatic analyses of the datasets. **(D)** Functional classification of differential expressed transcripts as identified *via* Webgestalt (2019). Bubble plots indicate the enrichment scores and overlap of the functional categories. **(E)** Quantitation of total hnRNPD mRNA in Control and *M-Δx3,4* BMDMs (n=5) in a resting state (M0), following exposure to LPS+INFγ, or IL4. Bar graphs denote mean fold changes (FC ± SD) in exon 3 containing mRNAs relative to resting control values (CM0) as assessed *via* qRT-PCR. **(F)** Quantitation of factors marking the classical or the alternative polarization of macrophages in control and *M-Δx3,4* BMDMs (n=10) either in a resting state (M0), following exposure to LPS+IFNγ, or IL4. Bar graphs denote mean values (± SD) of secreted proteins assessed *via* Cytometric bead arrays; or mean fold changes (FC) in mRNAs relative to resting control values (CM0) as assessed *via* qRT-PCR. In all bar graphs, (*, ****) denote p values ≤0.05 or ≤0.00001 respectively as determined *via* unpaired Student's t-test.

Together, our *ex vivo* data indicate that AUF1s may not be required to establish central macrophage activation and M1 or M2a-like polarization programs. However, their connection to regulatory catabolic programs may be linked instead to their requirement for transition between programs occurring in other polarization settings.

AUF1s Is Required for the Adenosine-Induced Transition of Pro-Inflammatory Macrophages Towards a Pro-Angiogenic Phenotype

In vivo, M1- and M2- like macrophages co-exist in inflammatory settings, and their plasticity allows them to switch their phenotype in response to microenvironment derived cues. Apart from the highly polarized macrophages induced by LPS ± IFNγ or IL4, several different alternative subsets have been described *in vitro.* These subsets presumably mimic phenotypes switching in response to particular tissue signals that block one phenotype for another to occur (25, 37). For example, when LPS-primed macrophages are exposed to the combination of homeostatic TGFβ and anti-inflammatory IL10 they "deactivate" proinflammatory mediators and acquire an M2-like identity (also known as M2c) (38). In response to TGFβ and IL10, the expression of *hnRNPD* mRNAs was as low as in the case of macrophages treated with LPS; still, LPS-activated *M-hnRNPD*$^{\Delta x3,4}$ BMDMs reduced their secretion of TNF, IL-6 and IL-12 while upregulating the M2-associated mRNAs of *Arg1, Chi3l3* and *Retnla* (**Figure 5A**) in a manner similar to control macrophages.

Another macrophage switching effect is observed, when the M1 macrophages are exposed to purinergic signals stimulated by adenosines (described loosely as M2d) (39). Adenosines bind to A2A receptors to suppress pro-inflammatory mediators while enhancing the expression of M2 markers; but also augment the expression of vascular remodeling factors like VEGFα and one of its downstream regulators, Thrombospondin-1 encoded by the *Thbs1* mRNA (40, 41). To explore the response of LPS-activated macrophages to adenosines, we used the specific adenosine A2A receptor agonist, CGS-21680 (CGS). In control BMDMs primed with LPS, CGS suppressed the expression of TNF, IL-12b and IL10 but not of M1-related chemokines; induced the secretion of VEGF and the expression *Arg1, Chil3l3, Retnla and the Thbs1* mRNAs; and -strikingly- augmented the expression of *hnRNPD* transcripts (**Figure 5B** and **Figure S5**). On the contrary, *M-hnRNPD*$^{\Delta x3,4}$ BMDMs exposed to LPS+CGS failed to downregulate specifically TNF and IL12 and were unable to augment properly VEGFα and the, *Thbs1* and *Arg1* mRNAs (**Figure 5B** and **Figure S5**).

The compromised expression of VEGFα & Thrombospondin as opposed to the enhanced TNF by *M-hnRNPD*$^{\Delta x3,4}$ BMDMs suggested that AUF1s may be involved in the macrophage specific support of vascular permeability of inflamed tissues. Indeed, we noted that the reduction of *hnRNPD* expressing cells in the BALF of OVA challenged *M-hnRNPD*$^{\Delta x3,4}$ mice related to comparable reductions in the *Vegfa* and *Thbs1* mRNAs (**Figure 5C**).

Three pieces of evidence suggested that AUF1s control selective transcripts rather than adenosine receptor signaling. First, the induction of *Chil3l3 and Retnla* mRNAs and the reduction of secreted IL10 in *M-hnRNPD*$^{\Delta x3,4}$ BMDMs were comparable to those in control macrophages (**Figure 5B**) Second, the expression of the *Adora2a* mRNA encoding the A2A receptor was enhanced 150-fold in both control and AUF1 lacking macrophages exposed LPS+CGS and 50-fold in those treated with LPS whereas it was only minimally affected by other macrophage signals (**Figure 5D**). Similarly, the loss of AUF1s did not affect the macrophage expression of *Adora2b* mRNA encoding the A2B receptor that may act synergistically to A2A and which was exclusively enhanced 5-fold by LPS+CGS (**Figure 5D**). Finally, the examination of downstream PKA activity which is commonly activated by LPS and LPS+CGS signals was not significantly altered by the loss of AUF1s (**Figure S6**).

These data indicate that AUF1s are required downstream of adenosine signalers to control specific transcripts during the switch of pro-inflammatory macrophages to those supporting vascular remodeling.

The Loss of AUF1s in Myeloid Cells Inhibits Neo-Vascularization and Immune Infiltration of Tumors

M2-like pro-angiogenic macrophages usually appear as tumor-associated infiltrates (TAMs) to support tumor angiogenesis and growth (42). To connect the functions of myeloid AUF1s to tumor growth we used the model of B16 melanoma tumors transplanted subcutaneously in the flanks of syngeneic mice. Contrary to tumors in control mice, the tumors in *M-hnRNPD*$^{\Delta x3,4}$ mice grew to smaller volumes at the endpoint (**Figure 6A**), posing difficulties in their comparative evaluation of vessel density. In an effort to gain insight on tumor vascularization, we selected whose volume was proximal to the lower range of control tumor volumes compare their vessel density as marked by endothelial marker, CD31 (PECAM). As shown in **Figure 6B**, a reducing trend in the number of CD31^{+} vessels were observed in the tumors from *M-hnRNPD*$^{\Delta x3,4}$ mice but their low number precluded statistical validation. To gain indirect insight we assessed the inflammatory infiltration of all tumors following dissociation and analyses of their immune infiltrates *via* flow cytometry. The percentage of total immune CD45+ tumor infiltrates in *M-hnRNPD*$^{\Delta x3,4}$ mice was reduced 4-fold relative those in the tumors of control mice indicating a possible defect in tumor vasculature impeding immune infiltration (**Figure 6C**). We also noted reductions amongst the myeloid CD45+ cells expressing high levels of Gr1+ which includes neutrophils and myeloid-derived suppressive cells; and on CD11b+ Gr1 negative subsets suggesting limitations in the general myeloid influx.

To get a direct answer as to whether the loss of AUF1s in myeloid cells limits their effect on blood vessels, we exploited an *in vivo* angiogenic model measuring neovascularization directly (43). In this model, inert biomaterials in a sponge-like form were engrafted subcutaneously in the flanks of mice and were injected either with PBS or recombinant VEGFα every 2 days. At the

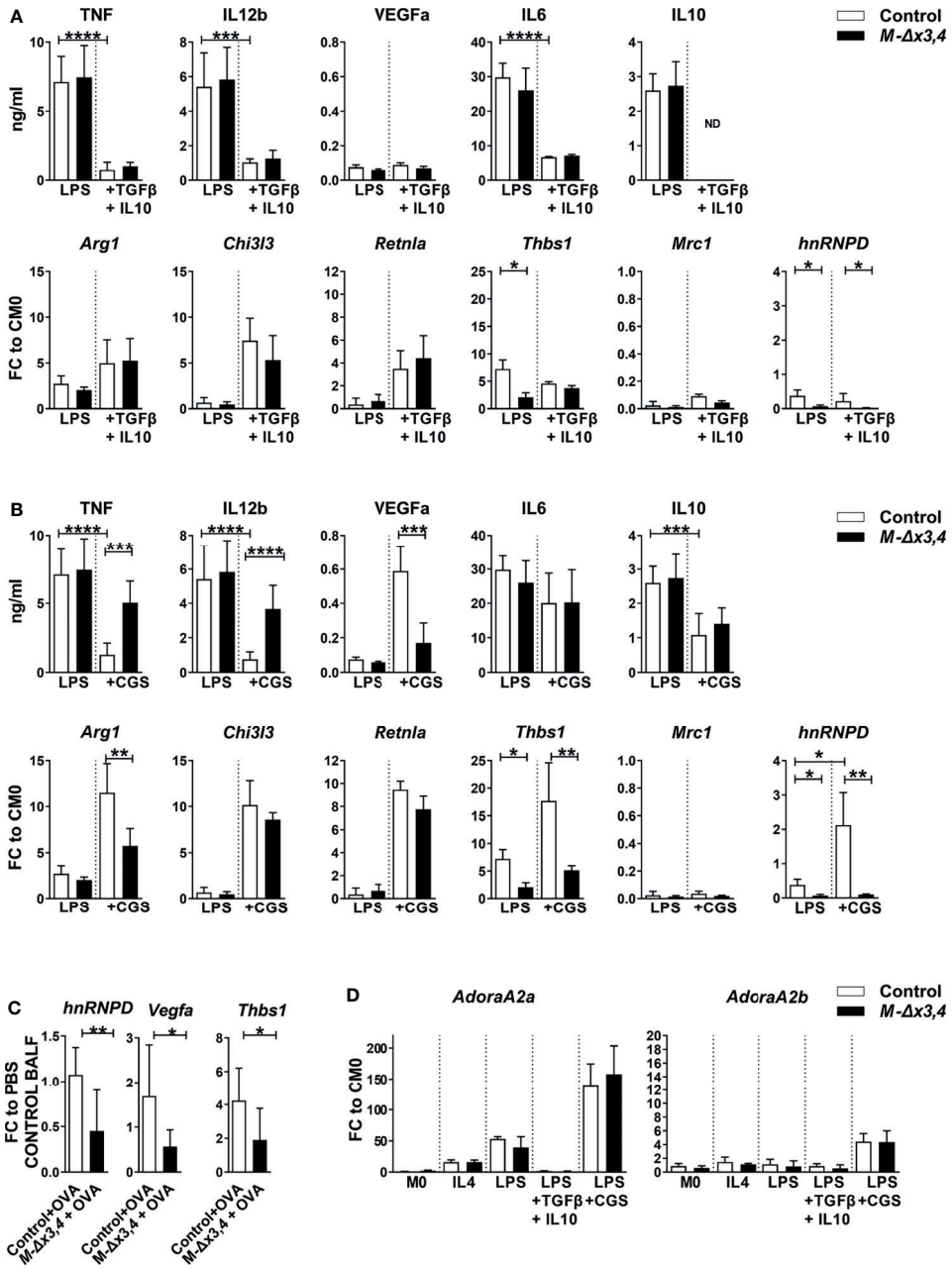

FIGURE 5 | Macrophages lacking AUF1s functions show defects in their transitions in response to adenosine receptor signals but not in response to TGFβ and IL10. Quantitation of factors marking the classical or the alternative polarization of macrophages as well as detection of *hnRNPD* expression in response to **(A)** the combination of TGFβ+IL10 and; **(B)** adenosine A2A receptor agonist (CGS) in LPS-activated control and *M-hnRNPD*$^{\Delta x3,4}$ BMDMs (n=10). Bar graphs denote mean values (± SD) of secreted proteins assessed *via* Cytometric bead arrays; or mean fold changes (FC) in mRNAs relative to resting control values (CM0) as assessed *via* qRT-PCR. **(C)** Detection of *hnRNPD*, *Vegfa* and *Thbs1* mRNAs in BALF cells from OVA-treated samples (n=5-6) relative to untreated (PBS) values as assessed *via* q RT-PCR. **(D)** Quantitation of *Adora2a* and *Adora2b* mRNAs in control and *M-hnRNPD*$^{\Delta x3,4}$ BMDMs (n=10) in response to the indicated signals. Bar graphs denote mean values (± SD) or mean fold changes (FC) in mRNAs relative to resting control values (CM0) as assessed *via* qRT-PCR (*, **, ***, ****) denote p values ≤0.05, ≤0.001, ≤0.0001, ≤0.00001 respectively as determined *via* unpaired Student's t-test.

14th day sponges were excised and processed for the immunohistochemical enumeration of blood vessels using the endothelial marker endomucin. As demonstrated in **Figure 6D**, the vessel density of PBS-treated sponges engrafted in *M-hnRNPD*$^{\Delta x3,4}$ mice was nearly half of those in the grafts of control mice. In contrast, the VEGFα-treated sponges possessed an equally elevated blood vessel density in both the grafts in control and mutant mice.

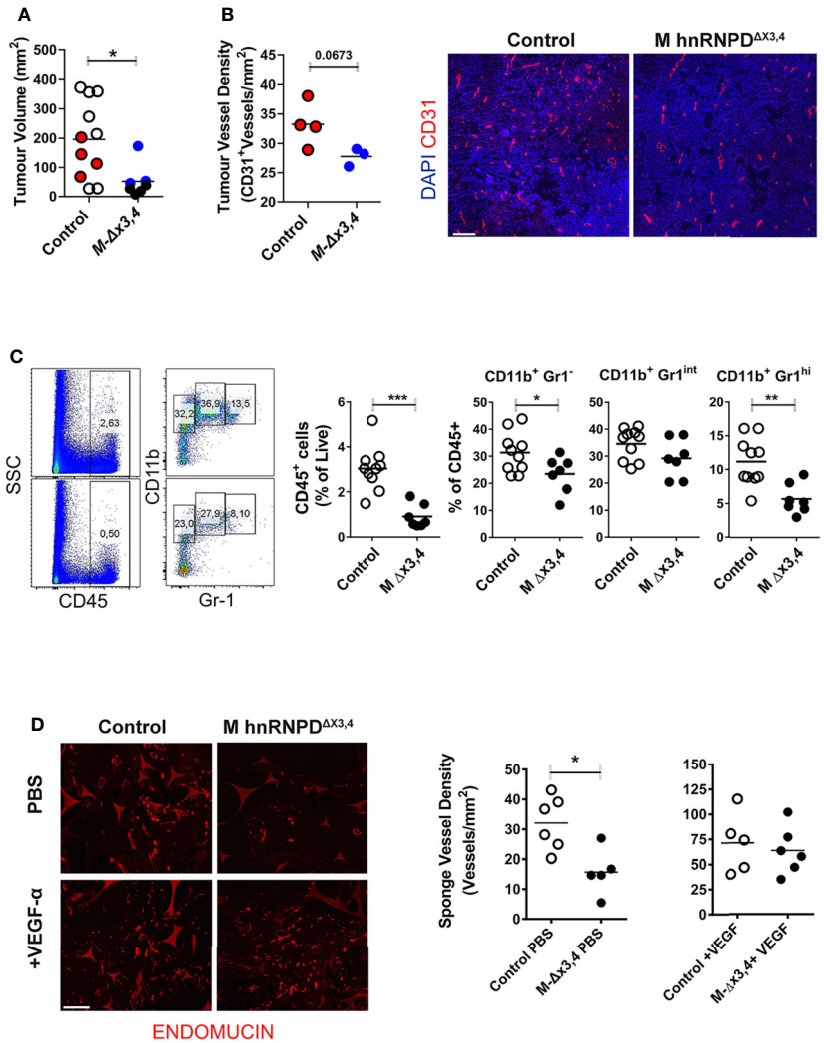

FIGURE 6 | The ablation of AUF1 functions in myeloid cells attenuates tumor infiltration and the vascularization of inert grafts. **(A)** Endpoint quantitation of subcutaneous B16F0 tumor sizes of control and *M-hnRNPD*$^{\Delta x3,4}$ mice. Scatter plots indicate individual values and means (lines) of tumor volumes, n=10 mice/per genotype. Colored circles indicate samples that were selected for the analysis in tumor vessels density. **(B)** Graphs (left) denote mean values (± SD) of blood vessels per mm2 of midline section of B16 tumor following immunofluorescent staining of midline with endothelial marker CD31 and counterstained *via* DAPI as indicated in the representative photomicrographs (right). **(C)** Quantification of the percentage of live total CD45+ cells and subgated myeloid cells detected *via* CD11b/Gr-1 expression infiltrating B16-tumors of control and *M-hnRNPD*$^{\Delta x3,4}$ mice as analyzed *via* flow cytometry analysis. Representative dot plots (*right*) and scatter plots (*left*) depicting individual values and means (lines) from n=11 mice/per genotype. **(D)** Endomucin staining patterns of midline sections of engraphed sponges (left) and quantitation of microvessel density in sponges from control and *M-hnRNPD*$^{\Delta x3,4}$ mice 14 days post administration of PBS or recombinant VEGF. Graphs denote mean values (± SD) of blood vessels per mm2 of midline sponge section of n=6 mice/genotype. In all graphs (*, **, ***) denote p values ≤0.05, ≤0.001 or ≤0.0001 respectively as determined *via* unpaired students t-test (on **A**) or One-Way ANOVA **(B–D)**.

Divergent AUF1-Mediated Control Upon Its Macrophage Targets

Our analysis on macrophages suggested that AUF1s may affect a transcript specific regulon to facilitate the functional switch from the pro-inflammatory to the pro-angiogenic state. To gain insight on how AUF1s modulate such transcripts, we focused on those that appear as most affected by the loss of AUF1s' functions, namely the *Tnf, Il12b, Vegfa and Thbs1* mRNAs (44). First, we immunoprecipitated AUF1-containing RNPs (RIP) from cytoplasmic extracts of resting, LPS or LPS+CGS treated BMDMs for 4hrs using a specific antibody recognizing all four AUF1 isoforms. To estimate background, we performed parallel immunoprecipitations with an isotype-matched antibody. The efficiency of the RIP was monitored using immunoblots for the AUF1 proteins as antibody-bound (e.g. **Figure S7A**). Subsequently, the RNA content of the RNPs was analyzed *via* qRT-PCR and values were normalized to the levels of expression of each mRNA (**Figure 7A**). Enrichments above 2-fold were

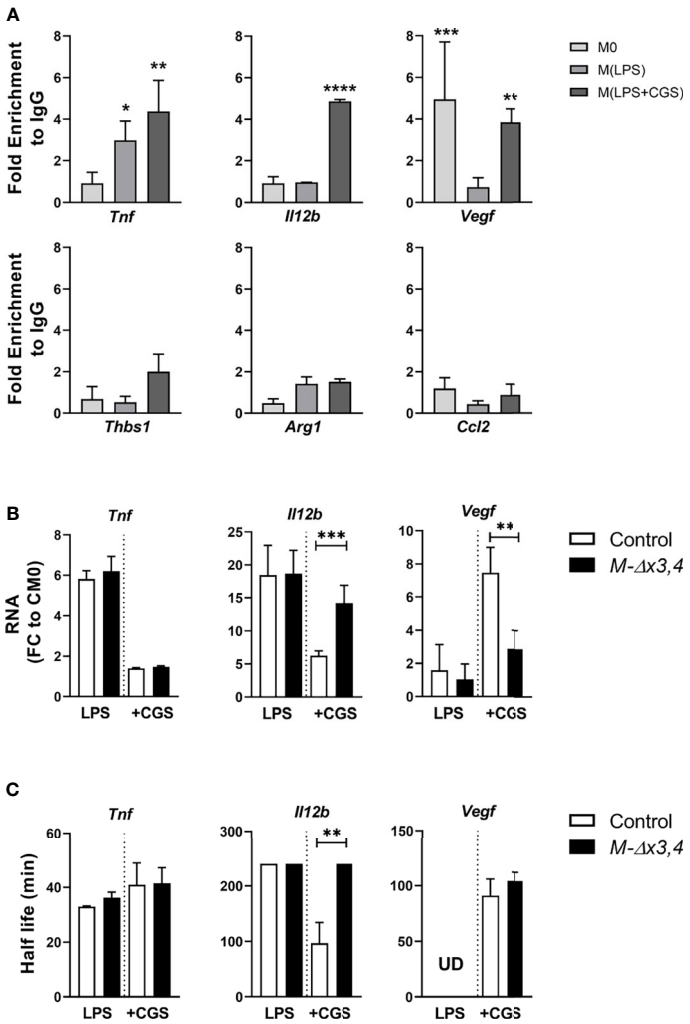

FIGURE 7 | Adenosines promote the binding of AUF1 upon selective transcripts leading to their differential control. **(A)** qRT-PCR detection of selected mRNAs tested to IP with anti-AUF1 in control BMDMs activated with LPS or LPS+CGS compared to untreated (M0). Enrichment of each mRNA in AUF1-IP samples compared with its abundance in IgG-IPs and normalized to mRNA expression levels. Enrichments above two-fold were considered significant. **(B)** Expression levels of mRNAs bound by AUF1 were measured in extracts from BMDMs activated with LPS or LPS+CGS. **(C)** The half-lives ($t_{1/2}$) of *Tnf*, *Il-12b* and *Vegf* mRNA were quantified by measuring the time required for reducing transcript levels to 50% of their original abundance after adding actinomycin as in **Figure S7B**. Graphs depict mean values ± SD. Note that half-lives in *Il-12b* mRNAs under LPS or under LPS+CGS in the mutants lack variation since they exceed monitoring times and as such were assigned a common maximal value. In all cases, data were analyzed by two tailed, unpaired Student's t test. *p ≤ 0.05, **p ≤ 0.01 ***p ≤ 0.001, ****p ≤ 0.0001.

considered as significant. This analysis demonstrated that AUF1: RNPs associate only with the *Vegfa* mRNA in resting macrophages; with the *Tnf* mRNA in LPS stimulated macrophages; and most strongly with the *Il12b*, *Vegfa* and *Tnf* mRNAs in adenosine-stimulated macrophages. In contrast we did not observe associations with the *Ccl2* mRNA which we used as a relevant control; neither with the *Thbs1* mRNA indicating that its reduction could be due to the loss of eliciting VEGF (45).

Further comparison of the levels of these mRNAs in extracts from Control BMDMs revealed that CGS suppressed the LPS-induced expression of the *Il12b* mRNA whilst augmenting that of the *Vegfa* mRNA; yet it failed do so in *M-hnRNPD*$^{\Delta x3,4}$ macrophages (**Figure 7B**). These data correlated to the differences we observed in the secretion of IL12b and VEGF by these cells **(Figure 5B)**. Notably, and in contrast to its protein (**Figure 5B**), the *Tnf* mRNA was properly suppressed by CGS in both control and *M-hnRNPD*$^{\Delta x3,4}$ BMDMs (**Figure 7B**). We postulate that AUF1s either control the translation of the *Tnf* mRNA or the post-translational release of the TNF protein.

The analysis of the decay of these mRNAs following the arrest of their transcription by Actinomycin D was most revealing (**Figures 7C**, **S7B**). CGS had a potent destabilizing effect upon the *il12b* mRNA which was ablated in the absence of AUF1s. In contrast the decay of the *Vegfa* mRNA was not affected by the loss of AUF1s suggesting that AUF1s are required for its nuclear synthesis as promoted by CGS. Finally, the decay of the *Tnf*

mRNA was not affected neither by the loss of AUF1s nor by CGS. Taken together these data indicate that AUF1s are involved in various transcript specific RNPs that respond to adenosine signaling which independently promote mRNA decay (e.g. *Il12b* mRNA), nuclear synthesis (e.g. *Vegfa* mRNA) or translation (e.g. *Tnf* mRNA).

DISCUSSION

In this study, we sought for changes to inflammatory responses caused by the loss of AUF1s in innate immune cells. To abrogate the functions of all protein-coding AUF1 isoforms in the mouse, we used gene targeting to render two exons 3 and 4 of the murine *hnRNPD* gene as conditionally removable. Hypothetically, this removal could lead to splicing events joining exons 1 or 2 to exon 5 and the synthesis of RRM-inactive AUF1 muteins. Instead, removing exons 3 and 4 reduced the expression of all coding RNA and proteins to near undetectable values. This effect was not due to aberrations imposed by our targeting strategy on the *hnRNPD* locus since mice carrying the non-recombined, loxP-flanked, alleles expressed the AUF1 proteins appropriately. Instead, we hypothesize that the diminution of *hnRNPD* transcripts could result from their decay as incorrectly spliced variants similar to *hnRNPD* variants degraded by Nonsense-mediated-decay (46).

The gross phenotypic characteristics of our germline $hnRNPD^{\Delta x3,4}$ mice resembled those of whole body *hnRNPD* null mice; as did their enhanced sensitivity to endotoxemia. In contrast, in mice where *Δx3,4* mutation was restricted in descendants of the myeloid lineage and mostly monocytes, macrophages, and polymorphonuclear cells did not phenocopy the endotoxic response of whole-body mutants. It is, therefore, likely that the enhanced endotoxic response of whole-body mutants does not pertain to dysfunctions within inflammatory cells but rather from enhanced tissue degenerations imposed by AUF1's control over cellular senescence or development (17). This is supported further by the high levels of serum IL1β observed in endotoxic $hnRNPD^{\Delta x3,4}$ and *hnRNPD* null mice [**Figure 1E** & (17)]. The secretion of IL1β is elicited *via* inflammasomes which are in turn activated by danger and senescent signals. Moreover, the activation of inflammasomes can support a specialized form of cell death called pyroptosis which can feedback to enhance the damaging response (28, 29).

In our analysis, we did not find any evidence for impediments in the differentiation of macrophages and polymorphonuclear cells in the myeloid mutants of AUF1s. Although we cannot exclude such a possibility, the proper response of these mice to endotoxemia, which requires emergency hematopoiesis (47, 48) supports the notion that AUF1s may not be essential for the ontogeny of myeloid descendants. On the other hand, our analyses on the sera of LPS-challenged myeloid mutants revealed counteracting augmentations (e.g. in pro-inflammatory TNF & IL12b that could result in altered cellular reactivities. To reveal such activities, we selected to challenge myeloid mutants for Type I or Type II cell-mediated reactions controlled either by pro-inflammatory or immunoregulatory circuits. For the assessment of pro-inflammatory and Type I cellular reactions we chose challenges inducing intestinal inflammation. The lamina propria underlying the intestinal epithelium contains many phagocytic macrophages supporting local homeostasis and microbiome balance (49). In Inflammatory Bowel Diseases (IBD), neutrophils and monocytes/macrophages are massively recruited from the blood to the lamina propria. Neutrophils have differential roles in IBD (50); whereas macrophages become polarized towards an "M1-like" state which uncontrollably release inflammatory cytokines, promote intestinal barrier damage, enhance Th1 and Th17 T-cell responses (51) and cannot be counteracted by anti-inflammatory "M2-like" macrophages expressing and responding to IL10 and TGFβ or primed by regulatory T-cell subsets (52). Currently, there is sufficient evidence on the dysfunction of "ARE-binding proteins" in supporting IBD (30). Moreover, a connection between mutations in the human *hnRNPD* gene and Crohn's Disease has been revealed from studies on monozygotic twins (53). In light of the above, the indifferent response of the myeloid AUF1 mutants to DSS and TNBS induced colitis was exceptionally noteworthy. These results should be interpreted cautiously concerning human disease since these chemical models mimic only some of its aspects. However, they provide first proof of the dispensability of AUF1s in the functioning of proinflammatory macrophages in chronic intestinal inflammation.

The combination of our data on endotoxemia and colitis suggests that AUF1s have redundant roles in the activation and cytokine-induced deactivation of classical "M1-like" macrophages. This redundancy was also apparent in our *ex vivo* assays. Our holistic analyses on LPS stimulated macrophages revealed only specialized changes in mRNAs devoid of alterations in cytokine mRNAs. Moreover, the loss of AUF1 functions did not debilitate the end polarization of "M1-like" macrophages *via* LPS and IFNγ; neither did their transition towards a deactivated "M2c-like" phenotypes by IL10 and TGFβ. These contradict earlier studies in human and mouse cell lines pointing to AUF1s control over the use of pro-inflammatory mRNAs by these signals. We hypothesize that methodological differences and the use of transformed cellular settings account for this contradiction.

Unlike the responses in endotoxemia and intestinal inflammation, allergic airway inflammation entails more complex innate immune reactivities. Several studies demonstrated a positive correlation between the presence of macrophages and enhanced eosinophilic inflammation using allergic models in mouse and humans (54, 55). These studies have already revealed the active role of alternatively activated macrophages -particularly those induced by IL4 and/or IL13 - in the exacerbation of Th2/Th9-driven inflammation (56). The fact that myeloid AUF1 mutants display a strong reduction in allergic airway inflammation and IL4 in their BALF could connect to the loss of such "M2-like" functionalities. To that end, we were surprised to find that cultured macrophages lacking AUF1 could be properly polarized towards an "M2a-like" phenotype by IL-4.

Arguably, the augmented presence of IFNγ in the BALF of allergen challenged myeloid AUF1 mutants could connect to an enhanced Th1 response supported by innate cells expressing high levels of IL12. These responses could have an opposing effect upon eosinophilic inflammation favoring neutrophil infiltration. However, such a switch was not detected in our mutants. Instead, all types of infiltrates were diminished in the allergen exposed myeloid AUF1 mutants. Such a phenotype could arise from aberrations in vascular remodeling, as exemplified in allergen exposed mice treated with anti-VEGF antibodies (57). Increased expression of VEGF is a common feature in the BALF of asthmatic patients, whereas its overexpression in the murine lung induces an asthma-like phenotype with features including vascular remodeling, mucus metaplasia, and augmented Th2 inflammation. VEGF is produced by infiltrating cells and the resident tissue, which includes alveolar macrophages and required for the infiltration of inflammatory cells in allergic airway inflammation (58).

The reduced number of VEGF-expressing infiltrates in the BALF of our myeloid mutants posits that their defective infiltrating response to allergen relates to defects in vascular permeability promoted by specialized alternative macrophage subsets. Since our focus was on immunocellular events, we did not look for changes in the responses of lung endothelia. However, our hypothesis was further supported by our tumor data, where the positive effect of M2-like, pro-angiogenic tumor-associated macrophages (TAMs) is well established (59). The myeloid loss of AUF1 compromised the growth of transplanted B16 melanomas correlating with reduced infiltration of TAMs (and TILs; data not shown)-despite the fact that tumor cells can produce part of the VEGF required for their vascularization. The poor growth of tumors in the setting of myeloid AUF1 deficiency prohibited the proper statistical evaluation of impediments in their vascularization or remodeling. However, these became apparent in the myeloid mutants failing to vascularize an inert graft; and the rescuing response of exogenously added VEGF. Moreover, we hypothesize that the defective VEGF response of myeloid-AUF1 mutants may also connect to their invariable susceptibility to LPS despite the presence of high TNF and IL12b. Vascular permeability and leakiness are critical events in endotoxemia, and VEGF blockade has a beneficial effect against it (60, 61).

Our *in vivo* observations correlate with the inability of AUF1 lacking macrophages to switch towards a pro-angiogenic phenotype (denoted by some as M2d) at least by adenosine receptor signals. Extracellularly, adenosines are generated by the surface enzymes CD73 and CD39. They transmit their signals through the surface G-coupled A2AR receptors and the cAMP/CEBP pathway (62). The importance of CD73 and CD39 activities against lung injury and for tumor growth is well documented. The lack of these enzymes -and hence of adenosines- provides susceptibility to allergic airway inflammation (63) and adenosine signaling has emerged as therapeutic target (64, 65). Concerning their functions in macrophages, adenosines were originally identified anti-inflammatory agents. It was later shown that they can promote the switch of activated macrophages towards an angiogenic phenotype expressing VEGF and independently of IL4 signaling (40), hence connecting to the *in vivo* functions of adenosine-generating enzymes. Our study connects the deranged activities of adenosine-induced pro-angiogenic macrophages incurred by the loss of AUF1s to the susceptibility of the mutant mice to airway and tumor infiltration. The full characterization of such cells in a disease setting and at a single cell level is currently lacking. However, their future identification holds promise for their exploitation in disease treatment *via* cellular ablation or addition strategies.

In macrophages, the expression of AUF1s was augmented by the agonistic activation of A2AR; and is needed to suppress TNF and IL12 whilst supporting the *de novo* expression of VEGF and Thrombospondin indicating the complex involvement of AUF1-controlled regulons in the pro-angiogenic switch. Notably, other "M2-like" mRNAs (e.g. *Il10*, *Retnla, Chi3l3*) were regulated by A2AR signals but independently of AUF1s. Moreover, TLRs and A2ARs signals remained unaffected by the loss of AUF1s. These suggested that AUF1s act in a transcript-selective fashion and downstream of A2AR signaling. Indeed, and to the limits of our analysis on pre-defined marker RNAs, only the *Tnf*, *Vegfa* and *Il12b* mRNAs were identified to associate with AUF1-containing ribonucleocomplexes. Most intriguingly, the type of regulation imposed by AUF1 on these mRNAs indicated three different types of regulons for RNA control: activation of mRNA biogenesis (*Vegfa*), activation of protein synthesis or release (*Tnf*) and mRNA degradation (*Il12b*). Given the pleiotropy AUF1s molecular activities on RNAs this is not so unprecedented. However, the confinement of its activities in selective cellular subsets -like in the case of pro-angiogenic macrophages- is noteworthy; especially considering propositions on its functional overlap with other factors (e.g. *Zfp36/TTP* and *Elavl1/HuR*) whose immune mutations have more profound effects (4, 11). Our genomic data revealed changes in RBP transcripts affected by the loss of AUF1s. Such changes could have functional consequences in the control of AUF1-regulons; or compensate for AUF1s loss in specific cellular contexts. Irrespective however of the cross-relationships affecting RNAs, the paradigm of AUF1 indicates that RBPs may control the selective diversification of cellular subtypes rather than affect RNA use in all.

MATERIALS AND METHODS

Mice and Study Approvals

The targeting of the *hnRNPD* locus in murine ES cells was performed by Regeneron Pharmaceuticals using their proprietary *Velocigene recombineering* technology (66). Modifications included the flanking of exons 3 and 4 with loxP sites; the inclusion of and FRT-flanked neomycin resistance gene for selection proximal to the loxP of exon 3. These ES cells were integrated onto blastocysts from C57Bl6/J mice. Derivative mice where then crossed to mice expressing a germline encoded

Flipase gene to remove the neomycin cassette and yield mice containing the *hnRNPD*^{flx3,4} allele. To generate a mutant hnRNPD$^{\Delta x3,4}$ allele, hnRNPD$^{flx3,4/+}$ mice were crossed to a mouse line expressing germline-active Cre recombinase (67). Subsequently, hnRNPD$^{\Delta x3,4/+}$ mice were intercrossed to yield homozygous hnRNPD$^{\Delta x3,4/\Delta x3,4}$ mice. For the myeloid restriction of the mutation *hnRNPD*$^{flx3,4/flx3,4}$ mice were crossed to the *LysM-MCre*$^{+}$ line. All mouse lines were maintained in a C57BL/6J background and in the animal facilities of the Biomedical Sciences Research Center (BSRC) "Alexander Fleming" under specific-pathogen free conditions. All experiments were performed with 8 to 16 weeks old mice and in accordance to the recommendations of the BSRC's Institutional Committee for Protocol Evaluation, the Veterinary Authorities of the Prefecture of Attika, the national legislation and the European Union Directive 63/2010. Protocols were approved by the Veterinary Authorities of the Prefecture of Attika (licenses # 4376/2014, 262781-22/04/2020, 26497-13/01/2020, 6197-21/11/2017, 4401-5/7/2016, 2823-13/06/2018, 531-13/2/2019, 26488-13/01/2020).

LPS-Induced Endotoxemia

Mice 6- to 8-week-old were injected intraperitoneally (i.p.) with the indicated amount of LPS (LPS from *Salmonella enterica* serotype enteritidis; Sigma-Aldich, L6011). Core body temperature and survival were monitored through a period of 7 days to determine mice sensitivity to endotoxemia. For measurement of inflammatory mediators, *hnRNPD*$^{\Delta x3,4/\Delta x3,4}$ and *hnRNPD*$^{\Delta x3,4}$ mice were injected i.p. with LPS at 4mg/kg of body weight. Sera were collected 90 minutes later by cardiac puncture and cytokines were quantified using LEGENDplex™ Mouse Th Macrophage Panel (Biolegend, Cat. No.740846).

DSS Induced Colitis

Mice 6- to 8-week-old were fed ad libitum for one cycle with water containing 2% (wt/vol) DSS (MW 40,000 kDa; MP Biomedicals Inc.) for 7 days followed by 8 days with regular water without DSS (68). Mice were monitored daily for changes in body weight, stool consistency and rectal bleeding. These values were used to calculate the Disease Activity Index (DAI). Endoscopy was performed using Coloview endoscopic system (Karl Storz, Germany) at day 8. Colonic inflammation was scored according to MEICS (Murine Endoscopic Index of Colitis Severity) as described (69). Mice were sacrificed at indicated time points or at the end of the protocol for the isolation of colonic tissue. Histological scoring was performed on hematoxylin and eosin (H&E) stained colon sections as previously described (70). Scores of inflammation and epithelial damage were summed to produce the overall histological score. All histological assessments were performed in a blinded fashion, by two independent investigators.

TNBS Induced Colitis

Mice 6- to 8-week-old were pre-sensitized applying TNBS solution (1% w/v in acetone and olive oil solution 4:1) epidermally at day -7. On day 0, mice were inoculated intrarectally with 100μl TNBS solution (2.5% w/v in absolute ethanol). Weight loss was daily monitored from day 0 to 4. Endoscopy was performed the 3rd day when severe symptoms peaked as described above (32).

Allergic Airway Inflammation

Airway inflammation was induced by ovalbumin (OVA-sensitization) as previously described (54). Briefly, sex matched mice were pre-sensitized on days 0 and 15 *via* intraperitoneal injection of 10μg chicken egg-derived OVA (Sigma Aldich, A5503) mixed with 1mg of aluminum hydroxide (Alum) as an adjuvant dissolved in 300 μl phosphate buffered saline (PBS) on day 0 and 15. Subsequently, mice inhaled 1% OVA aerosol for 30 min/day from day 21 to 25. At the end point, bronchoalveolar lavage fluid (BALF) was collected from the lungs by gently washing airway lumina with 0.5 mM EDTA in PBS *via* a tracheal cannula. BALF cells were analyzed by flow cytometry (strategy of analysis is presented in **Figure S3**), while supernatants were used for cytokines analysis using the LEGENDplex™ Mouse Th Cytokine Panel (Biolegend, 741044). To determine the effectiveness of the immunization, anti-OVA IgE levels were measured in the serum of PBS and OVA challenged mice using Anti-Ovalbumin IgE Elisa Kit (Cayman, 500840), according to the manufacturer's instructions. Lungs were collected, fixed in 10% formalin (VWR, 9713.500) and proceeded for histopathological examination. General morphology and inflammation were examined in H&E, Periodic acid Schiff (PAS)-H&E, and Trichrome Masson stained lung sections. Perivascular (PVI) and peribronchiolar (PBI) inflammation were assessed using a four-tier score system (0=none, 1=mild, 2=moderate, 3=severe, 4=tissue destruction) with an increment of 0.5 if the inflammation fell between two integers.

B16 Tumor Model

Mice were injected subcutaneously in the flank with 10^6 B16-F0 melanoma cells in 100ul PBS. Tumors were grown for 14 days. Post-mortem volume was determined using all 3 dimensions ($m1 \times m2 \times m3 \times \pi/6$). To prepare Single cell suspensions, tumor tissues were gently removed, cut into small pieces and incubated with 50 μg/ml Collagenase/Dispase (Roche, 10269638001) and 200 Units/ml DNAse I (Sigma-Aldrich, D5025) in RPMI 1640 (Gibco, 31870025) for 30 min at 37°C. Enzymatic dissociation was stopped with 10% FBS. Cells were washed with PBS and stained with the anti-mCD45, anti-mCD11, anti-mGr1, anti-mCD3 and anti-CD45R/B220 flow cytometry antibodies to identify immune subsets infiltrated in tumors. FACS analysis strategy is presented in Fig 6B.

Subcutaneous Angiogenesis Assay

Growth factor induced angiogenesis assay was performed as described previously (43). Briefly, subcutaneously implanted sponges of 1 cm^3 size were injected with 100μl of either PBS alone (as negative control) or PBS containing 10 ng/ml^{-1} VEGF (VEGF 164, R&D,493-MV), every 2 days. Sponges were excised, and paraffin embedded after 14 days.

Histological Analysis and Immunohistochemistry

For immunohistochemistry, all tissues were embedded in paraffin blocks. Thick sections (4μm) of embedded colon and lung tissues were stained with H&E. PAS staining and Masson trichrome were performed with standard protocols to determine fibrosis and mucus secretion in lung tissues. Blood vessels were identified by immunofluorescence staining using primary antibody against Endomucin antibody [santa cruz, sc65498/V.7C7.1] followed by secondary anti-rat 546 Alexa (A11081) and vessel density was calculated as the number of blood vessels per mm^2 of sponge section area using ImageJ software. Representative images were obtained on a Nikon ECLIPSE E200 microscope with a Nikon Digital Sight DS-5M digital camera.

Cell Isolation and Culture

Bone Marrow Derived Macrophages (BMDMs) were isolated from tibiae and femora of 6-8 week-old mice. Isolation was performed as previously described by Warren and Vogel (1985) and then differentiated to Bone Marrow Derived Macrophages in RPMI 1640 medium (Gibco, 31870-025) supplemented with 5% FBS (Gibco, 31870-025), 1% penicillin/streptomycin (Gibco, 15140122), 1% L-glutamine (Gibco, 25030024) and 10% L-medium (produced by L929 cells) incubated for 10 days at 37° C with 5% CO_2. Exudate macrophages, neutrophils and eosinophils were isolated from mice 48 or 72 hours upon intraperitoneal injection of 1 ml Brewer thioglycollate medium (4%; Becton-Dickinson).

Cell Treatments

BMDMs were activated with LPS (100 ng/ml, *Salmonella* enterica *enteritidis*; Sigma L6011), IFN-γ (10 ng/ml, Peprotech 315-05), IL-4 (10ng/ml, Peprotech 214-14), CGS (10μM, Sigma, 21680), IL-10 (10ng/ml, Peprotech, 210-10) and/or TGFβ1 (10 ng/ml, Cell-signaling, 231LC) for 24 hours.

Flow Cytometry Analysis and Sorting

For surface Single cell suspensions were prepared from either *in vivo* or *in vitro* experiments. For surface antigens, staining was performed using standard procedures. Antibodies were from BD Biosciences CD11b (M1/70); CD34 (RAM34); CD4 (H129.19); CD8 (H129.19), siclecF (E50-2440); eBioscience (F4/80), (CD16/32 (93), ScaI (D7), Biolegend GR1 (RB6-865), CD11C (N418); CD3e (145-2C11), CD206 (CO68C2), CCR3 (144505), Zombie NIR; B220 (RA3-6B2), Lin (mouse lineage panel, BD Pharmigen-559971). Cell viability was assessed by Propidium Iodide Staining. Cells were detected using FACSCantoII flow cytometer. Data were analyzed using FACSDIVA (V.6; BD Biosciences) and V10; Treestar, FlowJo).

Immunoblotting and ELISAs

The cells were lysed in ice-cold lysis buffer (50 mM Tris-HCl, pH 7.4, 150 mM NaCl, 1 mM EDTA, 0.25% SDS, 10% Glycerol, 1% NP-40 and one tablet of complete protease inhibitors) for 15 min on ice. Lysates were analyzed on SDS-polyacrylamide gels (SDS-PAGE; 12-14%), along with protein molecular weight markers (Nippon MWP03, Fermentas, Thermo Scientific, SM0431) and blotted onto nitrocellulose membrane (GE Healthcare). After blocking with 5% milk in TBS-Tween 20 buffer, membranes were incubated with primary and HRP-conjugated secondary antibodies (Biotech, anti-rabbit HRP 1030-05 or anti-mouse HRP 4050-05) signals were visualized by enhanced chemiluminescence (ECL, GE Healthcare) using films or a ChemiDocTMXRS+ System with Image LabTM software. Primary antibodies used: anti-AUF1 (milipore, 07-260) and anti-GAPDH (Ambion, 6C5). Cell culture Supernatants or serum were analyzed *via* specific ELISA kits of TNFa, IL-10, IL-6, VEGF, IL12 (Peprotech 900-K54, 900-K53, 900-K50, 900-K99), IL-1b (Thermo-Fisher, 88-7013-88), Anti-Ovalbumin IgE (Cayman 500840) or cytometric bead-based assay panels following manufacturer's instructions Legendplex Panels (Biolegend, Cat. No.741044 and 740846). Protein levels were normalized to cell number using crystal violet staining.

Ribonucleoprotein Immunoprecipitation

BMDMs were stimulated with LPS or LPS and CGS for 4 hours. Cells were harvested and lysed in 300μl lysis buffer containing 100 mM KCl, 25 mM EDTA, 5 mM MgCl2, 10 mM HEPES, 0.5% NP40, 2 mM DTT, 0.2%, protease inhibitors cocktails, Vanadyl Ribonucleoside Complex (Invitrogen) and 100 U/ml RNAse OUT (Invitrogen). A small quantity of samples was kept aside as Input (total cytosolic) for Western Blot analysis and for total cytosolic RNA (RNA-input). Antibody uncoated beads (protein G), (Dynabeads™ Protein G Immunoprecipitation kit, ThermoFisher), were washed and maintained in 600 μl of NT-2 buffer (50 mM Tris, pH 7.4, 150 mM NaCl, 1 mM MgCl2, and 0.05% NP40). For IP, 400 μl of cell lysate were loaded onto the beads and incubated overnight on a rotary at 4°C. Subsequently, beads were washed four times with NT-2 buffer, one of which contained 0.7M urea and finally resuspended in NT2 buffer. Fifteen microliters of the total volume of samples were removed for immunoblot verification while the remaining volume was used for RNA isolation *via* TRI reagent. For immunoblotting, polyclonal anti-AUF1 antibody (Millipore 07-260) and a IP conformation-specific secondary antibody (anti-mouse IgG -HRP-conjugated Veriblot for IP Detection Reagent, Abcam, ab131366) were used.

RNA Stability Assay

Stability of the mRNAs of interest was assessed by the addition of RNA polymerase II inhibitor, actinomycin D (10 μg/ml, Sigma) into cell culture for a period of 240 min. Total RNA was isolated at the indicated time points using TRI reagent and quantified using qRT-PCR. The half-live of transcripts was calculated using a fitted exponential curve. High undetermined values are arbitrarily defined.

RNA Isolation and Analysis

Total RNAs were extracted from cells using TRI Reagent (MRC, TR 118) according to the manufacturer's protocol. For cDNA synthesis 0.5-2μg of total RNA was reverse transcribed using MMLV-RT (Promega, M1705) and Oligo dT (NEB, S1316S) at 37°C for 1h. qRT-PCR was performed using EvaGreen SsoFast

mix (Bio-Rad, Hercules, CA, USA, 172-5201) on a RotorGene 6000 machine (Corbett Research, Qiagen). Relative mRNA expression was normalized to β2-microglobulin (B2M) and calculated as the difference between the test values and the control values assigned as 1, using Bio-Rad RelQuant (Bio-Rad). Primers are listed in **Supplementary Materials.**

Sequencing Analysis and Bioinformatics

RNA Total RNA in expansion phase was collected using TRI Reagent (Invitrogen, Life technologies). RNA was extracted according to the manufacturer's instructions and resuspended in 30μls of nuclease free water. Total RNA was quantitated using the NanoDrop ND1000 Spectrophotometer. Samples were diluted accordingly to a mean concentration of approximately 150 ng/μl, on an area of 235.0 and their quality assessed on a Bioanalyzer (Agilent Technologies) using the Agilent RNA 6000 Nano Kit reagents and protocol (Agilent Technologies). Sequencing libraries were prepared by using the QuantSeq 3' mRNA-Seq Library Prep Kit FWD (QuantSeq-LEXOGEN™, Vienna, Austria) and RNA-seq libraries were sequenced on an Ion Proton PI™ V2 chips, an IIon Proton™ System. Library preparation and alignment strategies are provided in **Supplementary Material**. Mapped sequences Quant-Seq BAM files were analyzed on a transcript level base with the Bioconductor package metaseqR2 (71) v.1.3.14 which has built-in support for Quant-Seq data. Differential expression analysis for the contrasts MΔχ3,4 versus Control was performed using DESeq2, edgeR, NOISeq, limma, NBPSeq, ABSSeq and DSS algorithms and a combined meta-analysis procedure by the PANDORA algorithm implemented in metaseqR2. 3' UTR areas (and their corresponding transcripts) presenting a PANDORA p-value less than 0.05 and an absolute fold change (for each contrast) greater than 1 in log2 scale were considered as differentially expressed. Categorical enrichment analysis of differentially expressed transcripts was implemented with WebGestaltR6 version 0.4.4 R package. The method that was used was the Over-Representation Analysis (ORA) against the Biological Process functional database of Gene Ontology and Kyoto Encyclopedia of Genes Genomes (KEGG) pathways and the terms retrieved were identified at a significance level of FDR ≤ 0.05. Multiple testing adjustment was carried out with the Benjamini-Hochberg procedure. All data extracted from sequencing datasets and gene sets were plotted in R (v.4.1.0) using ggplot27 (v.3.3.5) package. Z-scores were calculated as a derivative of the normalized counts.

Statistics

Statistical analysis was performed on Graphpad Prism 6.01 (Graphpad Software). Statistical significance was determined using unpaired Student's t-test or One Way Anova when comparing three or more groups. Survival analysis was performed using Kaplan-Meier statistics. Results with a P-value 0.05 considered to be statistically significant.

DATA AVAILABILITY STATEMENT

The datasets for this study have been deposited in Gene Expression Omnibus (GEO) with the accession numbers GSE181222.

ETHICS STATEMENT

The animal study was reviewed and approved by Veterinary Authorities of the Prefecture of Attika, Greece.

AUTHOR CONTRIBUTIONS

DLK and SG designed and supervised the study. Most the *in vivo* experiments were performed by NL and SG assisted by MS and MA. Tumor and vascularization assays were performed by SG and VK. Endoscopic measurements were performed by VN. Macrophage experiments were performed by SG, NL, ED and NS. RIPs were performed by MC and SG. Sequencing experiments were overviewed by PH, and bioinformatic analyses was performed by DT. Data interpretation and presentation was performed by DK, SG, and NL Manuscript was written and edited by DK and SG with support from ED. All authors contributed to the article and approved the submitted version.

FUNDING

We acknowledge support of this work by projects InfrafrontierGR/Phenotypos (MIS 5002135) and Strategic Development of the Biomedical Research Institute Alexander Fleming (MIS 5002562), which are implemented under the Actions Reinforcement of the Research and Innovation Infrastructure and Action for the Strategic Development on the Research and Technological Sector respectively, funded by the Operational Programme Competitiveness, Entrepreneurship and Innovation (NSRF 2014-2020) and co-financed by Greece and the European Union (European Regional Development Fund). We also acknowledge support by ARISTEIA-I project No. 1096 PREcISE, funded by the Operational Programme Education and Lifelong Learning (NSRF 2007-2013) and co-financed by Greece and the European Union (European Social Fund). This research is also supported by Greece and the European Union (European Social Fund-ESF) through the Operational Programme «Human Resources Development, Education and Lifelong Learning 2014-2020» (project MIS 5069605) and NSRF 2014-2020, European Regional Development Fund, Operational Programme "Competitiveness, Entrepreneurship and Innovation 2014-2020 (EPAnEK)" (MIS 5032782).

ACKNOWLEDGMENTS

The authors would like to thank: Aris Economides and Regeneron Pharmaceutical for their generous provision of ES cells generated *via* their proprietary Velocigene™ technology to possess the modifications in the *hnRNPD* locus; current and past members of the Transgenics Facility of BSRC "Alexander Fleming" and particularly Maria Alexiou and Kostas Bozonelos for the generation of the mutant mice; Vaggelis Harokopos from the Genomics Facility of BSRC "Alexander Fleming", for performing Quant Seq analysis and Panagiotis Moulos for help

with the bioinformatics analyses. Fotis Ioakeimidis for help with the tumor experiments, Sofia Grammenoudi and Kleopatra Dagla for help in flow cytometry; Meropi Gennadi for support in histopathology; and the InfrafrontierGR Infrastructure for animal housing, transgenic generation and phenotyping.

SUPPLEMENTARY MATERIAL

The Supplementary Material for this article can be found online at: https://www.frontiersin.org/articles/10.3389/fimmu.2022.752215/full#supplementary-material

REFERENCES

1. Wagner BJ, DeMaria CT, Sun Y, Wilson GM, Brewer G. Structure and Genomic Organization of the Human AUF1 Gene: Alternative pre-mRNA Splicing Generates Four Protein Isoforms. *Genomics* (1998) 48(2):195–202. doi: 10.1006/geno.1997.5142
2. Wilson GM, Sun Y, Lu H, Brewer G. Assembly of AUF1 Oligomers on U-Rich RNA Targets by Sequential Dimer Association. *J Biol Chem* (1999) 274 (47):33374–81. doi: 10.1074/jbc.274.47.33374
3. Zucconi BE, Ballin JD, Brewer BY, Ross CR, Huang J, Toth EA, et al. Alternatively Expressed Domains of AU-Rich Element RNA-Binding Protein 1 (AUF1) Regulate RNA-Binding Affinity, RNA-Induced Protein Oligomerization, and the Local Conformation of Bound RNA Ligands. *J Biol Chem* (2010) 285(50):39127–39. doi: 10.1074/jbc.M110.180182
4. Lourou N, Gavriilidis M, Kontoyiannis DL. Lessons From Studying the AU-Rich Elements in Chronic Inflammation and Autoimmunity. *J Autoimmun* (2019) 104:102334. doi: 10.1016/j.jaut.2019.102334
5. Diaz-Munoz MD, Turner M. Uncovering the Role of RNA-Binding Proteins in Gene Expression in the Immune System. *Front Immunol* (2018) 9:1094. doi: 10.3389/fimmu.2018.01094
6. Sarkar S, Han J, Sinsimer KS, Liao B, Foster RL, Brewer G, et al. RNA-Binding Protein AUF1 Regulates Lipopolysaccharide-Induced IL10 Expression by Activating IkappaB Kinase Complex in Monocytes. *Mol Cell Biol* (2011) 31 (4):602–15. doi: 10.1128/MCB.00835-10
7. Buzby JS, Lee SM, Van Winkle P, DeMaria CT, Brewer G, Cairo MS. Increased Granulocyte-Macrophage Colony-Stimulating Factor mRNA Instability in Cord Versus Adult Mononuclear Cells is Translation-Dependent and Associated With Increased Levels of A + U-Rich Element Binding Factor. *Blood* (1996) 88(8):2889–97. doi: 10.1182/blood.V88.8.2889.bloodjournal8882889
8. Wang XY, Hoyle PE, McCubrey JA. Characterization of Proteins Binding the 3' Regulatory Region of the IL-3 Gene in IL-3-Dependent and Autocrine-Transformed Hematopoietic Cells. *Leukemia* (1998) 12(4):520–31. doi: 10.1038/sj.leu.2400975
9. Pautz A, Linker K, Altenhofer S, Heil S, Schmidt N, Art J, et al. Similar Regulation of Human Inducible Nitric-Oxide Synthase Expression by Different Isoforms of the RNA-Binding Protein AUF1. *J Biol Chem* (2009) 284(5):2755–66. doi: 10.1074/jbc.M809314200
10. Nyati KK, Masuda K, Zaman MM, Dubey PK, Millrine D, Chalise JP, et al. TLR4-Induced NF-kappaB and MAPK Signaling Regulate the IL-6 mRNA Stabilizing Protein Arid5a. *Nucleic Acids Res* (2017) 45(5):2687–703. doi: 10.1093/nar/gkx064
11. Kafasla P, Skliris A, Kontoyiannis DL. Post-Transcriptional Coordination of Immunological Responses by RNA-Binding Proteins. *Nat Immunol* (2014) 15 (6):492–502. doi: 10.1038/ni.2884
12. Garcia-Maurino SM, Rivero-Rodriguez F, Velazquez-Cruz A, Hernandez-Vellisca M, Diaz-Quintana A, de la Rosa MA, et al. RNA Binding Protein Regulation and Cross-Talk in the Control of AU-Rich mRNA Fate. *Front Mol Biosci* (2017) 4:71. doi: 10.3389/fmolb.2017.00071
13. Akira S, Maeda K. Control of RNA Stability in Immunity. *Annu Rev Immunol* (2021) 39:481–509. doi: 10.1146/annurev-immunol-101819-075147
14. Zucconi BE, Wilson GM. Assembly of Functional Ribonucleoprotein Complexes by AU-Rich Element RNA-Binding Protein 1 (AUF1) Requires Base-Dependent and -Independent RNA Contacts. *J Biol Chem* (2013) 288 (39):28034–48. doi: 10.1074/jbc.M113.489559
15. Lu JY, Sadri N, Schneider RJ. Endotoxic Shock in AUF1 Knockout Mice Mediated by Failure to Degrade Proinflammatory Cytokine mRNAs. *Genes Dev* (2006) 20(22):3174–84. doi: 10.1101/gad.1467606
16. Sadri N, Schneider RJ. Auf1/Hnrnpd-Deficient Mice Develop Pruritic Inflammatory Skin Disease. *J Invest Dermatol* (2009) 129(3):657–70. doi: 10.1038/jid.2008.298
17. Pont AR, Sadri N, Hsiao SJ, Smith S, Schneider RJ. mRNA Decay Factor AUF1 Maintains Normal Aging, Telomere Maintenance, and Suppression of Senescence by Activation of Telomerase Transcription. *Mol Cell* (2012) 47 (1):5–15. doi: 10.1016/j.molcel.2012.04.019
18. Panda AC, Abdelmohsen K, Yoon JH, Martindale JL, Yang X, Curtis J, et al. RNA-Binding Protein AUF1 Promotes Myogenesis by Regulating MEF2C Expression Levels. *Mol Cell Biol* (2014) 34(16):3106–19. doi: 10.1128/MCB.00423-14
19. Abbadi D, Yang M, Chenette DM, Andrews JJ, Schneider RJ. Muscle Development and Regeneration Controlled by AUF1-Mediated Stage-Specific Degradation of Fate-Determining Checkpoint mRNAs. *Proc Natl Acad Sci USA* (2019) 116(23):11285–90. doi: 10.1073/pnas.1901165116
20. Chenette DM, Cadwallader AB, Antwine TL, Larkin LC, Wang J, Olwin BB, et al. Targeted mRNA Decay by RNA Binding Protein AUF1 Regulates Adult Muscle Stem Cell Fate, Promoting Skeletal Muscle Integrity. *Cell Rep* (2016) 16(5):1379–90. doi: 10.1016/j.celrep.2016.06.095
21. White EJ, Matsangos AE, Wilson GM. AUF1 Regulation of Coding and Noncoding RNA. *Wiley Interdiscip Rev RNA* (2017) 8(2):10. doi: 10.1002/wrna.1393
22. Yoon JH, De S, Srikantan S, Abdelmohsen K, Grammatikakis I, Kim J, et al. PAR-CLIP Analysis Uncovers AUF1 Impact on Target RNA Fate and Genome Integrity. *Nat Commun* (2014) 5:5248. doi: 10.1038/ncomms6248
23. Min KW, Jo MH, Shin S, Davila S, Zealy RW, Kang SI, et al. AUF1 Facilitates microRNA-Mediated Gene Silencing. *Nucleic Acids Res* (2017) 45(10):6064–73. doi: 10.1093/nar/gkx149
24. Mantovani A, Biswas SK, Galdiero MR, Sica A, Locati M. Macrophage Plasticity and Polarization in Tissue Repair and Remodelling. *J Pathol* (2013) 229(2):176–85. doi: 10.1002/path.4133
25. Murray PJ. Macrophage Polarization. *Annu Rev Physiol* (2017) 79:541–66. doi: 10.1146/annurev-physiol-022516-034339
26. Lawrence T, Natoli G. Transcriptional Regulation of Macrophage Polarization: Enabling Diversity With Identity. *Nat Rev Immunol* (2011) 11 (11):750–61. doi: 10.1038/nri3088
27. Wynn TA, Vannella KM. Macrophages in Tissue Repair, Regeneration, and Fibrosis. *Immunity* (2016) 44(3):450–62. doi: 10.1016/j.immuni.2016.02.015
28. Broz P, Dixit VM. Inflammasomes: Mechanism of Assembly, Regulation and Signalling. *Nat Rev Immunol* (2016) 16(7):407–20. doi: 10.1038/nri.2016.58
29. Acosta JC, Banito A, Wuestefeld T, Georgilis A, Janich P, Morton JP, et al. A Complex Secretory Program Orchestrated by the Inflammasome Controls Paracrine Senescence. *Nat Cell Biol* (2013) 15(8):978–90. doi: 10.1038/ncb2784
30. Christodoulou-Vafeiadou E, Ioakeimidis F, Andreadou M, Giagkas G, Stamatakis G, Reczko M, et al. Divergent Innate and Epithelial Functions of the RNA-Binding Protein HuR in Intestinal Inflammation. *Front Immunol* (2018) 9:2732. doi: 10.3389/fimmu.2018.02732
31. Antoniou E, Margonis GA, Angelou A, Pikouli A, Argiri P, Karavokyros I, et al. The TNBS-Induced Colitis Animal Model: An Overview. *Ann Med Surg (Lond)* (2016) 11:9–15. doi: 10.1016/j.amsu.2016.07.019
32. Wirtz S, Neufert C, Weigmann B, Neurath MF. Chemically Induced Mouse Models of Intestinal Inflammation. *Nat Protoc* (2007) 2(3):541–6. doi: 10.1038/nprot.2007.41
33. Balhara J, Gounni AS. The Alveolar Macrophages in Asthma: A Double-Edged Sword. *Mucosal Immunol* (2012) 5(6):605–9. doi: 10.1038/mi.2012.74
34. Murray PJ, Allen JE, Biswas SK, Fisher EA, Gilroy DW, Goerdt S, et al. Macrophage Activation and Polarization: Nomenclature and Experimental Guidelines. *Immunity* (2014) 41(1):14–20. doi: 10.1016/j.immuni.2014.06.008
35. Sica A, Mantovani A. Macrophage Plasticity and Polarization: *In Vivo* Veritas. *J Clin Invest* (2012) 122(3):787–95. doi: 10.1172/JCI59643
36. Locati M, Curtale G, Mantovani A. Diversity, Mechanisms, and Significance of Macrophage Plasticity. *Annu Rev Pathol* (2020) 15:123–47. doi: 10.1146/annurev-pathmechdis-012418-012718

37. Murray PJ, Wynn TA. Protective and Pathogenic Functions of Macrophage Subsets. *Nat Rev Immunol* (2011) 11(11):723–37. doi: 10.1038/nri3073
38. Martinez FO, Sica A, Mantovani A, Locati M. Macrophage Activation and Polarization. *Front Biosci* (2008) 13:453–61. doi: 10.2741/2692
39. Csoka B, Selmeczy Z, Koscso B, Nemeth ZH, Pacher P, Murray PJ, et al. Adenosine Promotes Alternative Macrophage Activation *via* A2A and A2B Receptors. *FASEB J* (2012) 26(1):376–86. doi: 10.1096/fj.11-190934
40. Ferrante CJ, Pinhal-Enfield G, Elson G, Cronstein BN, Hasko G, Outram S, et al. The Adenosine-Dependent Angiogenic Switch of Macrophages to an M2-Like Phenotype is Independent of Interleukin-4 Receptor Alpha (IL-4Ralpha) Signaling. *Inflammation* (2013) 36(4):921–31. doi: 10.1007/s10753-013-9621-3
41. Pinhal-Enfield G, Ramanathan M, Hasko G, Vogel SN, Salzman AL, Boons GJ, et al. An Angiogenic Switch in Macrophages Involving Synergy Between Toll-Like Receptors 2, 4, 7, and 9 and Adenosine A(2A) Receptors. *Am J Pathol* (2003) 163(2):711–21. doi: 10.1016/S0002-9440(10)63698-X
42. Caux C, Ramos RN, Prendergast GC, Bendriss-Vermare N, Menetrier-Caux C. A Milestone Review on How Macrophages Affect Tumor Growth. *Cancer Res* (2016) 76(22):6439–42. doi: 10.1158/0008-5472.CAN-16-2631
43. Pedrosa AR, Bodrug N, Gomez-Escudero J, Carter EP, Reynolds LE, Georgiou PN, et al. Tumor Angiogenesis Is Differentially Regulated by Phosphorylation of Endothelial Cell Focal Adhesion Kinase Tyrosines-397 and -861. *Cancer Res* (2019) 79(17):4371–86. doi: 10.1158/0008-5472.CAN-18-3934
44. Fordham JB, Hua J, Morwood SR, Schewitz-Bowers LP, Copland DA, Dick AD, et al. Environmental Conditioning in the Control of Macrophage Thrombospondin-1 Production. *Sci Rep* (2012) 2:512. doi: 10.1038/srep00512
45. Resovi A, Pinessi D, Chiorino G, Taraboletti G. Current Understanding of the Thrombospondin-1 Interactome. *Matrix Biol* (2014) 37:83–91. doi: 10.1016/j.matbio.2014.01.012
46. Banihashemi L, Wilson GM, Das N, Brewer G. Upf1/Upf2 Regulation of 3' Untranslated Region Splice Variants of AUF1 Links Nonsense-Mediated and a+U-Rich Element-Mediated mRNA Decay. *Mol Cell Biol* (2006) 26 (23):8743–54. doi: 10.1128/MCB.02251-05
47. Skirecki T, Kawiak J, Machaj E, Pojda Z, Wasilewska D, Czubak J, et al. Early Severe Impairment of Hematopoietic Stem and Progenitor Cells From the Bone Marrow Caused by CLP Sepsis and Endotoxemia in a Humanized Mice Model. *Stem Cell Res Ther* (2015) 6:142. doi: 10.1186/s13287-015-0135-9
48. Baou M, Norton JD, Murphy JJ. AU-Rich RNA Binding Proteins in Hematopoiesis and Leukemogenesis. *Blood* (2011) 118(22):5732–40. doi: 10.1182/blood-2011-07-347237
49. Wang J, Linnenbrink M, Kunzel S, Fernandes R, Nadeau MJ, Rosenstiel P, et al. Dietary History Contributes to Enterotype-Like Clustering and Functional Metagenomic Content in the Intestinal Microbiome of Wild Mice. *Proc Natl Acad Sci USA* (2014) 111(26):E2703–10. doi: 10.1073/pnas.1402342111
50. Wera O, Lancellotti P, Oury C. The Dual Role of Neutrophils in Inflammatory Bowel Diseases. *J Clin Med* (2016) 5(12):118. doi: 10.3390/jcm5120118
51. Backert I, Koralov SB, Wirtz S, Kitowski V, Billmeier U, Martini E, et al. STAT3 Activation in Th17 and Th22 Cells Controls IL-22-Mediated Epithelial Host Defense During Infectious Colitis. *J Immunol* (2014) 193 (7):3779–91. doi: 10.4049/jimmunol.1303076
52. Rahabi M, Jacquemin G, Prat M, Meunier E, AlaEddine M, Bertrand B, et al. Divergent Roles for Macrophage C-Type Lectin Receptors, Dectin-1 and Mannose Receptors, in the Intestinal Inflammatory Response. *Cell Rep* (2020) 30(13):4386–98 e5. doi: 10.1016/j.celrep.2020.03.018
53. Prakash T, Veerappa A, N BR. Complex Interaction Between HNRNPD Mutations and Risk Polymorphisms is Associated With Discordant Crohn's Disease in Monozygotic Twins. *Autoimmunity* (2017) 50(5):275–6. doi: 10.1080/08916934.2017.1300883
54. Moon KA, Kim SY, Kim TB, Yun ES, Park CS, Cho YS, et al. Allergen-Induced CD11b+ CD11c(int) CCR3+ Macrophages in the Lung Promote Eosinophilic Airway Inflammation in a Mouse Asthma Model. *Int Immunol* (2007) 19 (12):1371–81. doi: 10.1093/intimm/dxm108
55. Barrett NA, Austen KF. Innate Cells and T Helper 2 Cell Immunity in Airway Inflammation. *Immunity* (2009) 31(3):425–37. doi: 10.1016/j.immuni.2009.08.014
56. Lambrecht BN, Hammad H, Fahy JV. The Cytokines of Asthma. *Immunity* (2019) 50(4):975–91. doi: 10.1016/j.immuni.2019.03.018
57. Turkeli A, Yilmaz O, Karaman M, Kanik ET, Firinci F, Inan S, et al. Anti-VEGF Treatment Suppresses Remodeling Factors and Restores Epithelial Barrier Function Through the E-Cadherin/Beta-Catenin Signaling Axis in Experimental Asthma Models. *Exp Ther Med* (2021) 22(1):689. doi: 10.3892/etm.2021.10121
58. Song C, Ma H, Yao C, Tao X, Gan H. Alveolar Macrophage-Derived Vascular Endothelial Growth Factor Contributes to Allergic Airway Inflammation in a Mouse Asthma Model. *Scand J Immunol* (2012) 75(6):599–605. doi: 10.1111/j.1365-3083.2012.02693.x
59. Gocheva V, Wang HW, Gadea BB, Shree T, Hunter KE, Garfall AL, et al. IL-4 Induces Cathepsin Protease Activity in Tumor-Associated Macrophages to Promote Cancer Growth and Invasion. *Genes Dev* (2010) 24(3):241–55. doi: 10.1101/gad.1874010
60. Yano K, Liaw PC, Mullington JM, Shih SC, Okada H, Bodyak N, et al. Vascular Endothelial Growth Factor is an Important Determinant of Sepsis Morbidity and Mortality. *J Exp Med* (2006) 203(6):1447–58. doi: 10.1084/jem.20060375
61. Jeong SJ, Han SH, Kim CO, Choi JY, Kim JM. Anti-Vascular Endothelial Growth Factor Antibody Attenuates Inflammation and Decreases Mortality in an Experimental Model of Severe Sepsis. *Crit Care* (2013) 17(3):R97. doi: 10.1186/cc12742
62. Cekic C, Linden J. Purinergic Regulation of the Immune System. *Nat Rev Immunol* (2016) 16(3):177–92. doi: 10.1038/nri.2016.4
63. Caiazzo E, Cerqua I, Riemma MA, Turiello R, Ialenti A, Schrader J, et al. Exacerbation of Allergic Airway Inflammation in Mice Lacking ECTO-5'-Nucleotidase (Cd73). *Front Pharmacol* (2020) 11:589343. doi: 10.3389/fphar.2020.589343
64. Caruso M, Varani K, Tringali G, Polosa R. Adenosine and Adenosine Receptors: Their Contribution to Airway Inflammation and Therapeutic Potential in Asthma. *Curr Med Chem* (2009) 16(29):3875–85. doi: 10.2174/092986709789178055
65. Cicala C, Ialenti A. Adenosine Signaling in Airways: Toward a Promising Antiasthmatic Approach. *Eur J Pharmacol* (2013) 714(1-3):522–5. doi: 10.1016/j.ejphar.2013.06.033
66. Economides AN, Carpenter LR, Rudge JS, Wong V, Koehler-Stec EM, Hartnett C, et al. Cytokine Traps: Multi-Component, High-Affinity Blockers of Cytokine Action. *Nat Med* (2003) 9(1):47–52. doi: 10.1038/nm811
67. Schwenk F, Baron U, Rajewsky K. A Cre-Transgenic Mouse Strain for the Ubiquitous Deletion of loxP-Flanked Gene Segments Including Deletion in Germ Cells. *Nucleic Acids Res* (1995) 23(24):5080–1. doi: 10.1093/nar/23.24.5080
68. Yiakouvaki A, Dimitriou M, Karakasiliotis I, Eftychi C, Theocharis S, Kontoyiannis DL. Myeloid Cell Expression of the RNA-Binding Protein HuR Protects Mice From Pathologic Inflammation and Colorectal Carcinogenesis. *J Clin Invest* (2012) 122(1):48–61. doi: 10.1172/JCI45021
69. Gutierrez Becker B, Arcadu F, Thalhammer A, Gamez Serna C, Feehan O, Drawnel F, et al. Training and Deploying a Deep Learning Model for Endoscopic Severity Grading in Ulcerative Colitis Using Multicenter Clinical Trial Data. *Ther Adv Gastrointest Endosc* (2021) 14:2631774521990623. doi: 10.1177/2631774521990623
70. Maines LW, Fitzpatrick LR, French KJ, Zhuang Y, Xia Z, Keller SN, et al. Suppression of Ulcerative Colitis in Mice by Orally Available Inhibitors of Sphingosine Kinase. *Dig Dis Sci* (2008) 53(4):997–1012. doi: 10.1007/s10620-007-0133-6
71. Fanidis D, Moulos P. Integrative, Normalization-Insusceptible Statistical Analysis of RNA-Seq Data, With Improved Differential Expression and Unbiased Downstream Functional Analysis. *Brief Bioinform* (2021) 22(3): bbaa156. doi: 10.1093/bib/bbaa156

Conflict of Interest: The authors declare that the research was conducted in the absence of any commercial or financial relationships that could be construed as a potential conflict of interest.

Publisher's Note: All claims expressed in this article are solely those of the authors and do not necessarily represent those of their affiliated organizations, or those of the publisher, the editors and the reviewers. Any product that may be evaluated in this article, or claim that may be made by its manufacturer, is not guaranteed or endorsed by the publisher.

frontiers in Immunology

MINI REVIEW
published: 18 February 2022
doi: 10.3389/fimmu.2022.839762

Cooperation of RNA-Binding Proteins – a Focus on Roquin Function in T Cells

Gesine Behrens[1] *and Vigo Heissmeyer*[1,2]*

[1] Institute for Immunology, Biomedical Center (BMC), Faculty of Medicine, Ludwig-Maximilians-Universität in Munich, Planegg-Martinsried, Germany, [2] Research Unit Molecular Immune Regulation, Helmholtz Zentrum München, Munich, Germany

Post-transcriptional gene regulation by RNA-binding proteins (RBPs) is important in the prevention of inflammatory and autoimmune diseases. With respect to T cell activation and differentiation, the RBPs Roquin-1/2 and Regnase-1 play pivotal roles by inducing degradation and/or translational silencing of target mRNAs. These targets encode important proinflammatory mediators and thus Roquin and Regnase-1 functions dampen cellular programs that can lead to inflammation and autoimmune disease. Recent findings demonstrate direct physical interaction of both RBPs. Here, we propose that cooperativity of *trans*-acting factors may be more generally used to reinforce the regulatory impact on selected targets and promote specific cell fate decisions. We develop this concept for Roquin and Regnase-1 function in resting and activated T cells and discuss the involvement in autoimmunity as well as how the therapeutic potential can be used in anti-tumor therapies.

Keywords: RNA-binding proteins, Roquin, Regnase-1, post-transcriptional gene regulation, cooperativity, autoimmunity, tumor immunity

OPEN ACCESS

Edited by:
Osamu Takeuchi,
Kyoto University, Japan

Reviewed by:
Pavel Kovarik,
University of Vienna, Austria

***Correspondence:**
Vigo Heissmeyer
vigo.heissmeyer@med.uni-muenchen.de

Specialty section:
This article was submitted to Molecular Innate Immunity, a section of the journal Frontiers in Immunology

Received: *20 December 2021*
Accepted: *31 January 2022*
Published: *18 February 2022*

Citation:
Behrens G and Heissmeyer V (2022) Cooperation of RNA-Binding Proteins – a Focus on Roquin Function in T Cells. Front. Immunol. 13:839762. doi: 10.3389/fimmu.2022.839762

INTRODUCTION

In response to infections, our immune system first involves innate and then adaptive immune cells to clear pathogens. Lymphocytes recognize foreign structures derived from pathogens through their antigen receptors. One main purpose of antigen receptor signal transduction is to elicit specific changes in gene expression, which turn on selective differentiation programs. This is, for example, true for mature T cells recognizing antigen on antigen-presenting cells (APCs) in secondary lymphoid organs. As part of the adaptive immune response, T cells reprogram their metabolism, enter and progress in the cell cycle and commit to differentiation programs that lead to specific effector or memory functions. T cell receptor (TCR) signal transduction causes epigenetic changes and induces *de novo* transcription of mRNAs, whose expression can subsequently be controlled by numerous post-transcriptional regulatory mechanisms (1, 2). Transcription factors typically recognize DNA *cis*-elements in promoter regions of coding genes and recruit RNA polymerase II to initiate transcription from downstream transcription start sites. Similar to transcription factors recognizing DNA *cis*-elements of individual or composite binding sites, RNA-binding proteins (RBPs) are *trans*-acting factors recognizing *cis*-elements, which are mainly localized in 5' or 3'-untranslated regions (UTR) of mRNAs, but can also be found in introns or in coding sequences.

Again, such *cis*-element can be composed of binding sites for one or even several RBPs to function as a regulatory unit. The site-specific recognition then induces RBP-dependent types of post-transcriptional gene regulation. Prominent *cis*-elements for RBPs are adenylate-uridylate rich elements (AREs) or stem-loop (SL) structures (3–6). Besides RBPs, miRNAs are also important *trans*-acting factors involved in post-transcriptional gene regulation. miRNAs are a class of short (~22 nt) non-coding RNAs that, together with Argonaute (Ago) proteins, form the so-called miRISC complex, which recognizes sequence-specific sites in the 3′-UTR of their target mRNAs *via* base-pairing (7). Post-transcriptional regulation can affect nuclear pre-mRNAs and regulate processing, modification and export of mRNAs. On mature mRNAs in the cytoplasm, post-transcriptional regulation can have stabilizing effects or induce degradation as well as enhance or inhibit protein translation (8, 9). Dysregulation of gene expression in lymphocytes can cause inappropriate immune responses and lead to the development of autoimmunity or immunodeficiencies (10).

COOPERATIVITY OF TRANSCRIPTION FACTORS IN RESPONSE TO T CELL ACTIVATION

Decades of research focusing on the regulation of transcription in T lymphocytes have uncovered a high degree of cooperation between transcription factors. For example, induced transcription of the gene encoding the cytokine interleukin (IL)-2 requires TCR engagement and costimulation, since the *Il2* gene contains a composite *cis*-element in the promoter. This *cis*-element requires the coinciding binding of NFAT, AP-1 and NF-κB, which are induced only during productive activation of T cells through both signals (11, 12). In fact, T cells can become anergic or exhausted if TCR stimulation triggers NFAT-dependent gene expression programs in the absence of AP-1 (13–16). In T cells, a physical interaction on composite DNA *cis*-elements has been observed for NFAT and AP-1 during productive T cell activation (17). On the other hand, alternative ternary complex formation of NFAT and Foxp3 was observed during Treg differentiation and function (18).

These well-investigated examples on the regulation of transcription illustrate how a limited set of *trans*-acting factors can, by engaging in a few different combinatorial activities that have been selected in evolution, allow for a number of fine-tuned, alternative and even opposing cell fate decisions.

COOPERATIVITY OF *TRANS*-ACTING FACTORS INVOLVED IN POST-TRANSCRIPTIONAL GENE REGULATION

Cooperativity in gene regulation can be observed when two or more factors function together and depend on each other to reach full regulatory impact. The main types of cooperativity in post-transcriptional gene regulation are: Physical cooperativity between different RBPs binding to the same *cis*-element where either both RBPs bind to the RNA of the *cis*-element at the same or at different binding sites or by forming a complex in which just one RBP binds directly to the RNA (**Figure 1A**), functional cooperativity by binding to different *cis*-elements on the same mRNA molecule (**Figure 1B**), or cooperativity due to changes in binding site accessibility, meaning that one *trans*-acting factor induces a redistribution within different conformational states of an RNA, thereby facilitating the access to binding sites for other *trans*-acting factors (**Figure 1C**) (19–25).

In the past, studies in the field of post-transcriptional gene regulation typically focused on the monocausal regulation performed by a single *trans*-acting factor recognizing a defined *cis*-element. However, based on the circumstantial evidence listed below we propose that cooperativity is an important aspect of post-transcriptional gene regulation, in general and in T cells.

1. The mRNAs of key proteins involved in cell fate decisions (e.g. regulators of transcription and signal transduction) are often unstable, contain long 3'-UTRs with multiple binding sites for several different *trans*-acting factors and show regulation by overlapping sets of post-transcriptional regulators. In line with this, T cell activation results in expression of transcripts with shorter 3′-UTRs due to usage of upstream polyadenylation sites, pointing to activation-dependent regulation due to altered 3′-UTR binding sites (26–28).

2. The high number of approximately 1200 canonical RBPs harboring a defined RNA-binding domain (RBD) and non-canonical RBPs without defined RBDs in human or mouse primary CD4+ T cells suggests an unexplored complexity of post-transcriptional gene regulation (29).

3. A recent study in human cell lines estimated an average of 22,000 3'UTR-located binding sites for each RBP (22), supporting the idea that most 3' UTRs provide binding sites for several RBPs and/or miRNAs. The inducible T cell co-stimulator (ICOS), which encodes a costimulatory receptor that is essential for T cell help to B cells during the germinal center reaction, is a good example for a transcript regulated by different *trans*-acting factors. It responded to regulation by Roquin, Regnase-1, miRNAs and Wtap/m6A during the activation of murine T cells (29, 30).

Further evidence for the importance of cooperative post-transcriptional gene regulation in T cells comes from miRNA studies describing that several miRNAs which bind simultaneously to the same target mRNA molecule exerted stronger repression of the target mRNA than independent actions of each miRNA. In T cells, such functional cooperativity of miR-99a and miR-150 was involved in the repression of the mTOR mRNA promoting the conversion into iTreg cells (31).

Moreover, several publications have involved the Roquin-1 protein in physical or functional interactions with other post-transcriptional regulators of *ICOS* mRNA (32–34). Roquin was proposed to engage in physical interactions with Ago2 and miR-146a and thereby enable profound regulation of ICOS (33). A physical interaction of Roquin-1 with Nufip2 was identified in a

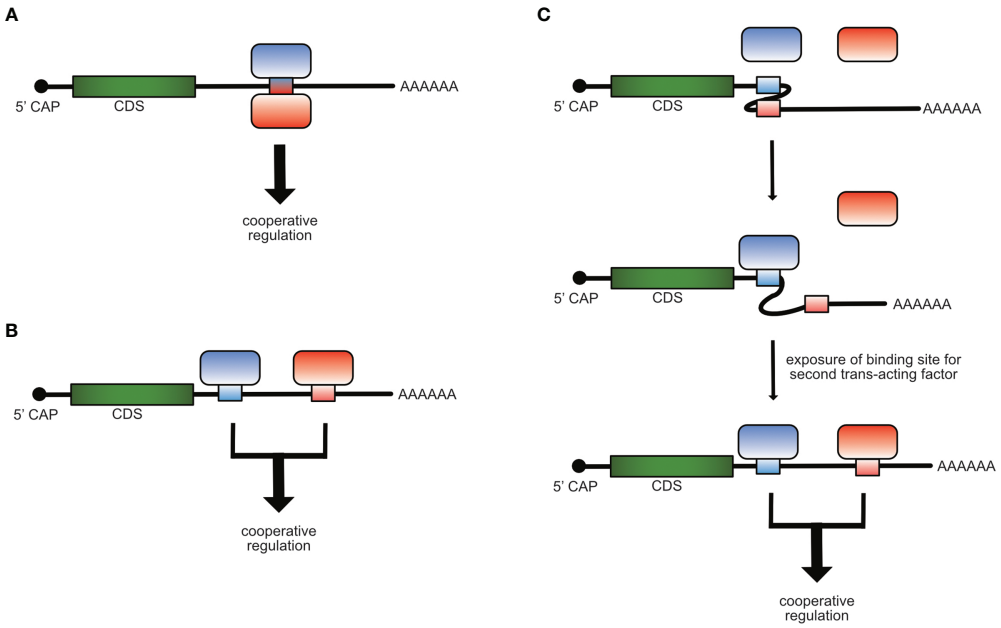

FIGURE 1 | Mechanisms of cooperative post-transcriptional gene regulation of mRNAs. Cooperativity of RBPs can occur by binding of two trans-acting factors to the same *cis*-element **(A)**, to different *cis*-elements **(B)** on the same mRNA molecule or when the binding of one trans-acting factor induces a structural re-arrangement in the mRNA, which allows the access and binding of the second **(C)**.

siRNA screen for Roquin-1 cofactors and Nufip2 was shown to strengthen RNA-binding of Roquin-1 to tandem SL structures *in vitro* (32). More recently, overexpression of Celf1 or Igf2bp3 proteins were suggested to counteract Roquin-mediated repression of ICOS (29). Although these examples suggest intriguing cooperations, it is still unclear how the reported effects can be explained mechanistically. Moreover, the proposed interactions have not been substantiated by genetic proof *in vivo*.

In this review, we will focus on the RBP Roquin-1 and its interaction with Regnase-1, in which we showcase the importance of cooperativity of RBPs in T cells.

SIMILARITIES IN ROQUIN-1 AND REGNASE-1 FUNCTIONS

Several recent papers have addressed a potential functional interdependence of Roquin and Regnase RBPs. Roquin-1, its redundantly-functioning paralog Roquin-2, as well as Regnase-1 are important regulators of T cell activation and differentiation (35–40). These proteins exhibit striking similarities in the following aspects:

1.) In addition to the ROQ RNA-binding domain (RBD) that specifies the binding of Roquin-1 and Roquin-2 to RNA (33, 41–44) and the PIN domain that enables Regnase-1 endoribonuclease function (45), all proteins harbor one CCCH zinc finger (46).

2.) Roquin-1, Roquin-2 and Regnase-1 are all cleaved by the paracaspase MALT1 in response to TCR stimulation (36, 38).

3.) Roquin-1, Roquin-2 and Regnase-1 have an overlapping set of mRNA targets including *Icos*, *cRel*, *Il6*, *Nfkbid* and also *Zc3h12a*, the Regnase-1 encoding mRNA (36, 38, 45, 47).

4.) Global mapping of binding sites of overexpressed Regnase-1 crosslinked to cellular mRNAs revealed comparable sequence determinants of Roquin-recognized SLs as defined by the constitutive decay element (CDE) (3, 47).

5.) Roquin-1 and Regnase-1 have been found to induce post-transcriptional repression through rapid mRNA degradation as well as translational silencing (3, 38, 45, 48–50).

6.) Mice with T cell-specific deletions of the Roquin-1/2 encoding genes, *Rc3h1* and *Rc3h2* (DKO), or the Regnase-1 encoding gene *Zc3h12a* (KO) develop comparable phenotypes characterized by spontaneous activation of $CD4^+$ and $CD8^+$ T cells and accumulation of Tfh and GC B cells (30, 38, 40).

7.) Mice harboring a single point mutation in the *Rc3h1* gene that exchanges methionine 199 to arginine (M199R) in the Roquin-1 protein develop a severe systemic lupus erythematosus-like (SLE-like) phenotype, showing deregulation of the immune system and production of anti-nuclear antibodies (ANAs), a phenotype which can be also found in the Regnase-1 KO mouse (38, 39, 45).

This striking resemblance in Roquin-1 and Regnase-1 protein functions as well as mouse model phenotypes led to the hypothesis that these two proteins may have a cooperative function. Indeed, initial data with reporter assays using overexpressed RBPs showed impaired regulation of a CDE-containing TNF 3′-UTR fragment in the absence of one or the other, supporting the idea of cooperativity (36).

DISCREPANCIES AND CHALLENGES OF ROQUIN AND REGNASE-1 FUNCTIONAL INTERDEPENDENCE

The proposed concept of cooperation (36, 51) has been questioned (46, 47), since Roquin and Regnase-1 RBPs also exhibit extensive differences:

On the mechanistic level, Roquin has been found to mediate degradation of its target mRNAs through the recruitment of the deadenylation machinery (3, 52) or through interactions with enhancers of decapping (50, 53). Regnase-1 harbors an intrinsic endonuclease activity, which requires Upf1 function and other factors involved in nonsense-mediated decay (NMD) (47, 54). Cellular localization studies revealed a close association of Regnase-1 with the ER and co-fractionation with translating ribosomes. Due to target expression kinetics, Regnase-1 was proposed to selectively regulate translationally active mRNAs in the early phase after LPS stimulation of fibroblasts. In contrast, Roquin localizes in P bodies and induces mRNA decay rather in fractions of polysome gradients that contain translationally inactive mRNAs and in the late phase of the innate immune response (47). These differences have led to the concept of an entirely compartmentalized function in which Roquin-1 and Regnase-1 regulate an overlapping set of target mRNAs *via* a common SL at different times, in different subcellular locations and through different mechanisms (46, 47).

A first approach of genetically combining the *sanroque* alleles with conditional ablation of Regnase-1 encoding alleles in T cells suggested non-redundant functions of both RBPs (55), however, this study did not discriminate T cell-intrinsic against known contributions of T cell-extrinsic functions of Roquin-1 (30, 56). The notion of more distinct functions was further supported by genetic inactivation of Regnase-1 in adoptively transferred tumor-antigen-specific cytotoxic T cells. In these experiments, Regnase-1 was shown to be a key regulator of T cell survival and metabolism. The inactivation of Regnase-1 encoding alleles by sgRNA/Cas9 targeting resulted in a profound improvement of anti-tumor responses (57, 58), while aspects of $CD8^+$ T cell biology had not been studied for Roquin-1, yet.

COOPERATIVE FUNCTIONS OF ROQUIN AND REGNASE-1 IN T CELLS

Addressing the controversy about cooperativity or compartmentalization, the existence and importance of cooperative functions of Roquin-1 and Regnase-1 proteins in T cells has received strong support from our recent study, especially through reconstitution and complementation assays, the definition of structure/function-relationships and through the genetic disruption of physical interaction (30).

Reconstitution and Functional Complementation

Reconstitution experiments overexpressing Roquin-1 or Regnase-1 in Roquin-1/2 DKO or Regnase-1 KO $CD4^+$ T cells confirmed cooperative functions, since in the absence of Regnase-1, Roquin-1 showed a partial impairment in the ability to suppress ICOS expression and vice versa Regnase-1 overexpression did not downregulate ICOS in Roquin-deficient T cells (30). Also the regulation of endogenous Regnase-1 expression fully depended on cooperation, since ectopic Regnase-1 expression in Roquin-deficient T cells did not affect expression of *Zc3h12a* mRNA and Regnase-1 protein. Correspondingly, Regnase-1 protein was highly upregulated in Roquin-1/2 DKO T cells, reflecting that despite high endogenous Regnase-1 expression, the protein cannot complement for the loss of Roquin-1 and Roquin-2 function (30, 36). On the other hand, overexpression of other Regnase family members i.e. Regnase-2, Regnase-3 and Regnase-4 in Regnase-1 KO cells suppressed ICOS expression equally well and complemented for Regnase-1 loss-of-function. While the mRNAs encoding for ICOS and even more for Regnase-1 were cooperatively regulated, the *Tnfrsf4* mRNA encoding for Ox40 was not. Intriguingly, the MALT1-cleavage fragment of Roquin-1 (aa1-510), which was shown to be inactive in the regulation of the *Tnfrsf4* mRNA, retained a residual function to cooperatively repress *ICOS* or *Zc3h12a* mRNA in reconstitution experiments (3, 30, 36, 53).

The Molecular Basis of Cooperation

A prerequisite for cooperativity is colocalization and proximity within the cell. Behrens et al., therefore confirmed colocalization of Roquin-1 and Regnase-1 in P bodies, verified their proximity *via* NanoBret assays and proved formation of a stable binary protein complex at a submicromolar affinity (KD=417nM) using Biacore measurements. Finally, a CDE-like SL (nt 194–212) of the *Zc3h12a* mRNA (59) was specifically bound by Roquin-1 and increasing Regnase-1 levels induced a supershift, indicating the formation of a ternary complex and cooperative binding of both RBPs on the same SL. Of note, whether Regnase-1 also binds to the RNA or only to Roquin-1 without directly contacting the RNA is not clear, yet. For interaction and cooperative target regulation with Regnase-1, the HEPN-ROQ domains of Roquin-1 were sufficient. The introduction of mutations on the surface of the ROQ domain defined the interaction surface, and intriguingly, the amino acid M199 was part of this binding site. Accordingly, mutations that impaired interaction of Roquin-1 and Regnase-1 also reduced the suppression of the cooperatively regulated targets *ICOS* and *Zc3h12a* in *in vitro* reconstitution experiments (30). However, a full mechanistic understanding how cooperative regulation of target mRNAs by Roquin and Regnase-1 is achieved, remains elusive and has to be part of future studies.

Genetic Proof of Cooperative Regulation

The final proof of concept was achieved by the generation of mice harboring mutations, which were shown to interfere with Roquin-1 and Regnase-1 cooperation in *in vitro* studies. These mice developed a severe autoimmune phenotype with an increase in activated $CD4^+$ and $CD8^+$ T cells, accumulation of Tfh and GC B cells as well as the production of ANAs and showed a striking resemblance with *sanroque* mice (30). The interaction of Roquin and Regnase-1 in the repression of

cooperative targets therefore proved to be essential for the prevention of autoimmune disease.

PERSPECTIVES

The advantage of two trans-acting factors cooperating is to focus an enhanced regulatory impact on a defined set of targets. We think that in such a cooperation Roquin rather contributes the specificity of RNA-binding, while Regnase-1 may exert the strong post-transcriptional repression.

Cooperativity of two *trans*-acting factors depends on the respective expression levels and post-translational regulations as well as on the hierarchies of affinities and binding properties of interactions. Knowing and integrating these determinants may allow us to understand cooperative regulation of specific targets but not of others. From *in vitro* binding studies it appears that the RBD containing protein fragment of Roquin-1 has a higher affinity for CDE-like elements than the Regnase-1 fragment, whose binding was much more sensitive to nonspecific competitor RNA (30). An assessment of quantitative aspects in primary T cells and, considering heterogeneity, favorably on the single cell level, is challenging. However, these considerations can inspire novel approaches and help us to adjust the directions of future research. Future studies should for example focus on *cis*-element-encoded features, which define a cooperative target. Which other targets show cooperative regulation? By which post-transcriptional mechanism do Roquin and Regnase-1 suppress expression of their cooperatively regulated targets? Does it involve mechanisms of deadenylation or decapping which have been involved in Roquin-mediated target regulation (3, 50, 52), does it employ endonucleolytic cleavage, a main function of Regnase-1 (45)? Or can cooperative targets also be translationally silenced, a recently involved function that was ascribed to Roquin as well as Regnase-1 for certain targets (48, 49)? Does ternary complex formation of Roquin and Regnase-1 on RNA recruit effector molecules from individual or all of these mechanisms or even enable new interactions? It is likely that cooperative target regulation does not involve a prototypic Roquin-dependent post-transcriptional mechanism, since the amino-terminal MALT1 cleavage product of Roquin-1 (aa1-510) is sufficient to repress *Zc3h12a*/Regnase-1 and is also partially active to repress ICOS (30).

One intriguing aspect of Roquin/Regnase-1 cooperation is that, on the one hand, this mechanism controls T cell activity, and on the other hand, it is prominently involved in the repression of the *Zc3h12a* mRNA, which encodes the Regnase-1 protein itself. Thereby, this RBP interaction prevents autoimmunity but at the same time precisely adjusts Regnase-1 expression, which may also confer an evolutionary advantage potentially related to the toxicity that can be observed in overexpression studies of Regnase-1 (48, 60).

An important consideration is the kinetics of cooperation before, during and after TCR signal transduction (**Figure 2**). A recent report has now uncovered a previously unrecognized constitutive MALT1 protease activity, which is dampened through MALT1 interactions with TRAF6 through a so-far elusive mechanism. In this study the absence of TRAF6 or mutations in MALT1 impairing the interaction with TRAF6, enhanced the T cell activation independent protease activity of MALT1 and caused flagrant autoimmunity in mice (61). Reflecting constitutive MALT1 activity, Roquin-1 and Roquin-2 exhibit more constitutive cleavage by MALT1 than Regnase-1 in naive mature T cells (30). These findings lead to the question whether already naive T cells require Roquin cooperation with Regnase-1 to prevent autoimmunity. In line with this, Regnase-1 protein strongly increased prior to T cell activation, if Roquin function was genetically inactivated in naive T cells (30). Therefore, negative autoregulation of Regnase-1 levels as well as regulation of other cooperatively regulated targets are likely to occur prior to TCR-dependent activation of T cells, when Roquin expression levels are moderate and both, full-length as well as the truncated proteins are present, and only low levels of Regnase-1 full-length protein are expressed.

During TCR activation, when Roquin protein levels increase (30, 32), but are subject to MALT1 cleavage, no regulation of Roquin "only" targets occurs, for which the abundance of full-length Roquin is mandatory. In contrast, even in the absence of full-length Roquin the *Zc3h12a* mRNA could be suppressed by the Roquin-1 (aa1-510) MALT1 cleavage fragment when low amounts of induced and newly synthesized full-length Regnase-1 become available. This might reflect an important safe-guard mechanism which protects cells from overshooting Regnase-1 levels. Finally, upon removal of TCR signals, when Roquin and Regnase-1 re-appear in their full-length forms, they can switch off expression of cooperatively as well as Roquin and Regnase-1 independently regulated targets, efficiently stopping expression of pro-inflammatory mediators by several different modes of repression (30).

The *trans*-acting factors Roquin-1 and Regnase-1 were recently shown to be promising targets for therapeutic approaches. Despite experimental differences of either employing sgRNA-mediated inactivation of Regnase-1 or Roquin-1 or introducing point mutations, which disrupt the interaction of both RBPs, all studies report increased proliferation and persistence of the tumor-antigen-specific $CD8^+$ T cells or CAR T cells in the tumor as well as efficient inhibition of tumor growth (30, 57, 58, 62). It is currently not clear whether these beneficial effects result from several different contributions from Roquin and Regnase-1 loss-of-function in addition to or only from cooperative regulation of targets. Importantly, inactivation of either Roquin-1 and Roquin-2 or Regnase-1 in T cells showed a similar enhancement but gradually different impacts on glycolysis and oxidative phosphorylation or on the proliferation and persistence of T cells as well as their effector functions (30). Moreover, the effect of Regnase-1 inactivation was specifically attributed to survival and proliferation, which depended on BATF expression (57). Consistent with such function, BATF3 was recently shown to prevent contraction in the pool-size of activated and differentiated effector $CD8^+$ T cells as well as to be important for the development of memory (63). In contrast, gene editing to inactivate Roquin-1 boosted the proliferation of tumor-antigen-

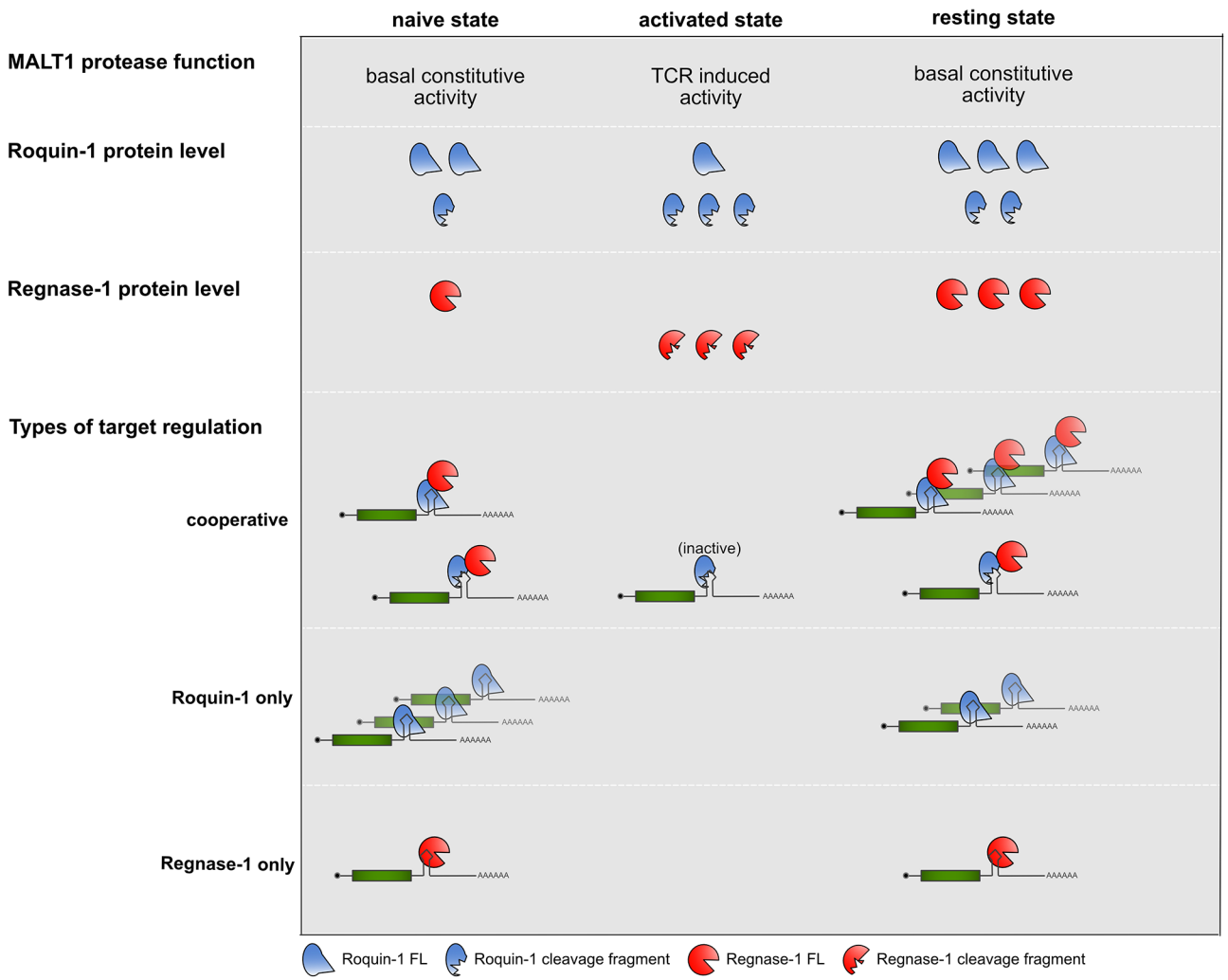

FIGURE 2 | Summary of MALT1 protease function, Roquin-1 and Regnase-1 protein levels and types of target regulations in the different states of CD4$^+$ T cells.

specific CD8$^+$ T cells in a similar tumor setting, but this effect specifically required expression of the Roquin target IRF4 (36, 62). Determining the phenotype of tumor-antigen-specific CD8$^+$ T cells with impaired Roquin-1/Regnase-1 interaction in the tumor we found that these cells showed greatly reduced expression of the exhaustion markers CD101, PD1 and Tox (30). Although, we have not yet identified or verified the cooperatively post-transcriptionally regulated targets that cause this phenotype, a very recent publication now presented an exciting connection of these findings: CAR T cells were shown to acquire enhanced functions in respect to expansion, persistence and memory formation through retroviral overexpression of BATF. Intriguingly, the physical interaction of BATF with the IRF4 transcription factor was essential for the improvement of anti-tumor responses and prevention of exhaustion in the tumor-specific CAR T cells (64). Together, these findings point at very promising new targets for improving immunotherapies. They also suggest cooperative gene regulation as a concept that can be exploited to achieve higher efficacy of adoptive T cell therapies, which is urgently needed to improve and expand treatment options for cancer patients.

AUTHOR CONTRIBUTIONS

All authors listed have made a substantial, direct, and intellectual contribution to the work, and approved it for publication.

FUNDING

The work was supported by the German Research Foundation grants SPP 1935-273941853, SFB-TRR 338/12021-452881907 (project C02), SFB 1054-210592381 (project A03) as well as

HE3359/7-1 (432656284) and HE3359/8-1 (444891219) as well as grants from the Wilhelm Sander (2018.082.2), Fritz Thyssen (Az.10.16.1.021.MN), Else Kröner-Fresenius (2015_A158) and Krebshilfe (70113538) Foundations.

ACKNOWLEDGMENTS

We would like to thank all members from our lab for critical reading and useful comments on the manuscript.

REFERENCES

1. Conley JM, Gallagher MP, Berg LJ. T Cells and Gene Regulation: The Switching On and Turning Up of Genes After T Cell Receptor Stimulation in CD8 T Cells. *Front Immunol* (2016) 7:3389. doi: 10.3389/fimmu.2016.00076
2. Turner M. Is Transcription the Dominant Force During Dynamic Changes in Gene Expression? *Adv Exp Med Biol* (2011) 780:1–13. doi: 10.1007/978-1-4419-5632-3_1
3. Leppek K, Schott J, Reitter S, Poetz F, Hammond MC, Stoecklin G. Roquin Promotes Constitutive mRNA Decay *via* a Conserved Class of Stem-Loop Recognition Motifs. *Cell* (2013) 153(4):869–81. doi: 10.1016/j.cell.2013.04.016
4. Janowski R, Heinz GA, Schlundt A, Wommelsdorf N, Brenner S, Gruber AR, et al. Roquin Recognizes a non-Canonical Hexaloop Structure in the 3′-UTR of *Ox40*. *Nat Commun* (2016) 7:11032. doi: 10.1038/ncomms11032
5. Chen CY, Shyu AB. AU-Rich Elements: Characterization and Importance in mRNA Degradation. *Trends Biochem Sci* (1995) 20:465–70. doi: 10.1016/S0968-0004(00)89102-1
6. Bakheet T, Williams BR, Khabar KS. ARED 3.0: The Large and Diverse AU-Rich Transcriptome. *Nucleic Acids Res* (2006) 34:D111–4. doi: 10.1093/nar/gkj052
7. Baumjohann D, Ansel KM. MicroRNA-Mediated Regulation of T Helper Cell Differentiation and Plasticity. *Nat Rev Immunol* (2013) 13(9):666–78. doi: 10.1038/nri3494
8. Corbett AH. Post-Transcriptional Regulation of Gene Expression and Human Disease. *Curr Opin Cell Biol* (2018) 52:96–104. doi: 10.1016/j.ceb.2018.02.011
9. Velazquez-Cruz A, Banos-Jaime B, Diaz-Quintana A, de la Rosa MA, Diaz-Moreno I. Post-Translational Control of RNA-Binding Proteins and Disease-Related Dysregulation. *Front Mol Biosci* (2021) 8:3389. doi: 10.3389/fmolb.2021.658852
10. Salerno F, Turner M, Wolkers MC. Dynamic Post-Transcriptional Events Governing CD8(+) T Cell Homeostasis and Effector Function. *Trends Immunol* (2020) 41(3):240–54. doi: 10.1016/j.it.2020.01.001
11. Rothenberg EV, Ward SB. A Dynamic Assembly of Diverse Transcription Factors Integrates Activation and Cell-Type Information for Interleukin 2 Gene Regulation. *Proc Natl Acad Sci USA* (1996) 93(18):9358–65. doi: 10.1073/pnas.93.18.9358
12. Zhou XY, Yashiro-Ohtani Y, Nakahira M, Park WR, Abe R, Hamaoka T, et al. Molecular Mechanisms Underlying Differential Contribution of CD28 Versus non-CD28 Costimulatory Molecules to IL-2 Promoter Activation. *J Immunol* (2002) 168(8):3847–54. doi: 10.4049/jimmunol.168.8.3847
13. Heissmeyer V, Macian F, Im SH, Varma R, Feske S, Venuprasad K, et al. Calcineurin Imposes T Cell Unresponsiveness Through Targeted Proteolysis of Signaling Proteins. *Nat Immunol* (2004) 5(3):255–65. doi: 10.1038/ni1047
14. Hogan PG. Calcium-NFAT Transcriptional Signalling in T Cell Activation and T Cell Exhaustion. *Cell Calcium* (2017) 63:66–9. doi: 10.1016/j.ceca.2017.01.014
15. Macian F, Garcia-Cozar F, Im SH, Horton HF, Byrne MC, Rao A. Transcriptional Mechanisms Underlying Lymphocyte Tolerance. *Cell* (2002) 109(6):719–31. doi: 10.1016/s0092-8674(02)00767-5
16. Martinez GJ, Pereira RM, Aijo T, Kim EY, Marangoni F, Pipkin ME, et al. The Transcription Factor NFAT Promotes Exhaustion of Activated CD8(+) T Cells. *Immunity* (2015) 42(2):265–78. doi: 10.1016/j.immuni.2015.01.006
17. Chen L, Glover JN, Hogan PG, Rao A, Harrison SC. Structure of the DNA-Binding Domains From NFAT, Fos and Jun Bound Specifically to DNA. *Nature* (1998) 392(6671):42–8. doi: 10.1038/32100
18. Wu Y, Borde M, Heissmeyer V, Feuerer M, Lapan AD, Stroud JC, et al. FOXP3 Controls Regulatory T Cell Function Through Cooperation With NFAT. *Cell* (2006) 126(2):375–87. doi: 10.1016/j.cell.2006.05.042
19. Dassi E. Handshakes and Fights: The Regulatory Interplay of RNA-Binding Proteins. *Front Mol Biosci*. (2017) 4:67. doi: 10.3389/fmolb.2017.00067
20. HafezQorani S, Lafzi A, de Bruin RG, van Zonneveld AJ, van der Veer EP, Son YA, et al. Modeling the Combined Effect of RNA-Binding Proteins and microRNAs in Post-Transcriptional Regulation. *Nucleic Acids Res* (2016) 44(9):e83. doi: 10.1093/nar/gkw048
21. Kedde M, van Kouwenhove M, Zwart W, Oude Vrielink JA, Elkon R, Agami R. A Pumilio-Induced RNA Structure Switch in P27-3' UTR Controls miR-221 and miR-222 Accessibility. *Nat Cell Biol* (2010) 12(10):1014–20. doi: 10.1038/ncb2105
22. Kim S, Kim S, Chang HR, Kim D, Park J, Son N, et al. The Regulatory Impact of RNA-Binding Proteins on microRNA Targeting. *Nat Commun* (2021) 12(1):5057. doi: 10.1038/s41467-021-25078-5
23. Kumar R, Poria DK, Ray PS. RNA-Binding Proteins La and HuR Cooperatively Modulate Translation Repression of PDCD4 mRNA. *J Biol Chem* (2021) 296:100154. doi: 10.1074/jbc.RA120.014894
24. Lin YH, Bundschuh R. RNA Structure Generates Natural Cooperativity Between Single-Stranded RNA Binding Proteins Targeting 5' and 3'utrs. *Nucleic Acids Res* (2015) 43(2):1160–9. doi: 10.1093/nar/gku1320
25. Wu X, Chesoni S, Rondeau G, Tempesta C, Patel R, Charles S, et al. Combinatorial mRNA Binding by AUF1 and Argonaute 2 Controls Decay of Selected Target mRNAs. *Nucleic Acids Res* (2013) 41(4):2644–58. doi: 10.1093/nar/gks1453
26. Friedel CC, Dolken L, Ruzsics Z, Koszinowski UH, Zimmer R. Conserved Principles of Mammalian Transcriptional Regulation Revealed by RNA Half-Life. *Nucleic Acids Res* (2009) 37(17):e115. doi: 10.1093/nar/gkp542
27. Sandberg R, Neilson JR, Sarma A, Sharp PA, Burge CB. Proliferating Cells Express mRNAs With Shortened 3' Untranslated Regions and Fewer microRNA Target Sites. *Science* (2008) 320(5883):1643–7. doi: 10.1126/science.1155390
28. Turner M, Galloway A, Vigorito E. Noncoding RNA and its Associated Proteins as Regulatory Elements of the Immune System. *Nat Immunol* (2014) 15(6):484–91. doi: 10.1038/ni.2887
29. Hoefig KP, Reim A, Gallus C, Wong EH, Behrens G, Conrad C, et al. Defining the RBPome of Primary T Helper Cells to Elucidate Higher-Order Roquin-Mediated mRNA Regulation. *Nat Commun* (2021) 12(1):5208. doi: 10.1038/s41467-021-25345-5
30. Behrens G, Edelmann SL, Raj T, Kronbeck N, Monecke T, Davydova E, et al. Disrupting Roquin-1 Interaction With Regnase-1 Induces Autoimmunity and Enhances Antitumor Responses. *Nat Immunol* (2021) 22(12):1563–76. doi: 10.1038/s41590-021-01064-3
31. Warth SC, Hoefig KP, Hiekel A, Schallenberg S, Jovanovic K, Klein L, et al. Induced miR-99a Expression Represses Mtor Cooperatively With miR-150 to Promote Regulatory T-Cell Differentiation. *EMBO J* (2015) 34(9):1195–213. doi: 10.15252/embj.201489589
32. Rehage N, Davydova E, Conrad C, Behrens G, Maiser A, Stehklein JE, et al. Binding of NUFIP2 to Roquin Promotes Recognition and Regulation of ICOS mRNA. *Nat Commun* (2018) 9(1):299. doi: 10.1038/s41467-017-02582-1
33. Srivastava M, Duan G, Kershaw NJ, Athanasopoulos V, Yeo JH, Ose T, et al. Roquin Binds microRNA-146a and Argonaute2 to Regulate microRNA Homeostasis. *Nat Commun* (2015) 6:6253. doi: 10.1038/ncomms7253
34. Yu D, Tan AH, Hu X, Athanasopoulos V, Simpson N, Silva DG, et al. Roquin Represses Autoimmunity by Limiting Inducible T-Cell Co-Stimulator Messenger RNA. *Nature* (2007) 450(7167):299–303. doi: 10.1038/nature06253
35. Essig K, Hu D, Guimaraes JC, Alterauge D, Edelmann S, Raj T, et al. Roquin Suppresses the PI3K-mTOR Signaling Pathway to Inhibit T Helper Cell Differentiation and Conversion of Treg to Tfr Cells. *Immunity* (2017) 47(6):1067–82.e1012. doi: 10.1016/j.immuni.2017.11.008
36. Jeltsch KM, Hu D, Brenner S, Zoller J, Heinz GA, Nagel D, et al. Cleavage of Roquin and Regnase-1 by the Paracaspase MALT1 Releases Their Cooperatively Repressed Targets to Promote T(H)17 Differentiation. *Nat Immunol* (2014) 15(11):1079–89. doi: 10.1038/ni.3008

37. Linterman MA, Rigby RJ, Wong R, Silva D, Withers D, Anderson G, et al. Roquin Differentiates the Specialized Functions of Duplicated T Cell Costimulatory ReceptorGenes CD28 and ICOS. *Immunity* (2009) 30 (2):228–41. doi: 10.1016/j.immuni.2008.12.015
38. Uehata T, Iwasaki H, Vandenbon A, Matsushita K, Hernandez-Cuellar E, Kuniyoshi K, et al. Malt1-Induced Cleavage of Regnase-1 in CD4(+) Helper T Cells Regulates Immune Activation. *Cell* (2013) 153(5):1036–49. doi: 10.1016/j.cell.2013.04.034
39. Vinuesa CG, Cook MC, Angelucci C, Athanasopoulos V, Rui L, Hill KM, et al. A RING-Type Ubiquitin Ligase Family Member Required to Repress Follicular Helper T Cells and Autoimmunity. *Nature* (2005) 435(7041):452–8. doi: 10.1038/nature03555
40. Vogel KU, Edelmann SL, Jeltsch KM, Bertossi A, Heger K, Heinz GA, et al. Roquin Paralogs 1 and 2 Redundantly Repress the Icos and Ox40 Costimulator mRNAs and Control Follicular Helper T Cell Differentiation. *Immunity* (2013) 38(4):655–68. doi: 10.1016/j.immuni.2012.12.004
41. Murakawa Y, Hinz M, Mothes J, Schuetz A, Uhl M, Wyler E, et al. RC3H1 Post-Transcriptionally Regulates A20 mRNA and Modulates the Activity of the IKK/NF-kappaB Pathway. *Nat Commun* (2015) 6:7367. doi: 10.1038/ncomms8367
42. Sakurai S, Ohto U, Shimizu T. Structure of Human Roquin-2 and its Complex With Constitutive-Decay Element RNA. *Acta Crystallogr F Struct Biol Commun* (2015) 71(Pt 8):1048–54. doi: 10.1107/S2053230X15011887
43. Schlundt A, Heinz GA, Janowski R, Geerlof A, Stehle R, Heissmeyer V, et al. Structural Basis for RNA Recognition in Roquin-Mediated Post-Transcriptional Gene Regulation. *Nat Struct Mol Biol* (2014) 21(8):671–8. doi: 10.1038/nsmb.2855
44. Tan D, Zhou M, Kiledjian M, Tong L. The ROQ Domain of Roquin Recognizes mRNA Constitutive-Decay Element and Double-Stranded RNA. *Nat Struct Mol Biol* (2014) 21(8):679–85. doi: 10.1038/nsmb.2857
45. Matsushita K, Takeuchi O, Standley DM, Kumagai Y, Kawagoe T, Miyake T, et al. Zc3h12a is an RNase Essential for Controlling Immune Responses by Regulating mRNA Decay. *Nature* (2009) 458(7242):1185–90. doi: 10.1038/nature07924
46. Fu M, Blackshear PJ. RNA-Binding Proteins in Immune Regulation: A Focus on CCCH Zinc Finger Proteins. *Nat Rev Immunol* (2017) 17(2):130–43. doi: 10.1038/nri.2016.129
47. Mino T, Murakawa Y, Fukao A, Vandenbon A, Wessels HH, Ori D, et al. Regnase-1 and Roquin Regulate a Common Element in Inflammatory mRNAs by Spatiotemporally Distinct Mechanisms. *Cell* (2015) 161 (5):1058–73. doi: 10.1016/j.cell.2015.04.029
48. Behrens G, Winzen R, Rehage N, Dorrie A, Barsch M, Hoffmann A, et al. A Translational Silencing Function of MCPIP1/Regnase-1 Specified by the Target Site Context. *Nucleic Acids Res* (2018) 46(8):4256–70. doi: 10.1093/nar/gky106
49. Essig K, Kronbeck N, Guimaraes JC, Lohs C, Schlundt A, Hoffmann A, et al. Roquin Targets mRNAs in a 3'-UTR-Specific Manner by Different Modes of Regulation. *Nat Commun* (2018) 9(1):3810. doi: 10.1038/s41467-018-06184-3
50. Glasmacher E, Hoefig KP, Vogel KU, Rath N, Du L, Wolf C, et al. Roquin Binds Inducible Costimulator mRNA and Effectors of mRNA Decay to Induce microRNA-Independent Post-Transcriptional Repression. *Nat Immunol* (2010) 11(8):725–33. doi: 10.1038/ni.1902
51. Jeltsch KM, Heissmeyer V. Regulation of T Cell Signaling and Autoimmunity by RNA-Binding Proteins. *Curr Opin Immunol* (2016) 39:127–35. doi: 10.1016/j.coi.2016.01.011
52. Sgromo A, Raisch T, Bawankar P, Bhandari D, Chen Y, Kuzuoglu-Ozturk D, et al. A CAF40-Binding Motif Facilitates Recruitment of the CCR4-NOT Complex to mRNAs Targeted by Drosophila Roquin. *Nat Commun* (2017) 8:14307. doi: 10.1038/ncomms14307
53. Tavernier SJ, Athanasopoulos V, Verloo P, Behrens G, Staal J, Bogaert DJ, et al. A Human Immune Dysregulation Syndrome Characterized by Severe Hyperinflammation With a Homozygous Nonsense Roquin-1 Mutation. *Nat Commun* (2019) 10(1):4779. doi: 10.1038/s41467-019-12704-6
54. Mino T, Iwai N, Endo M, Inoue K, Akaki K, Hia F, et al. Translation-Dependent Unwinding of Stem-Loops by UPF1 Licenses Regnase-1 to Degrade Inflammatory mRNAs. *Nucleic Acids Res* (2019) 47(16):8838–59. doi: 10.1093/nar/gkz628
55. Cui X, Mino T, Yoshinaga M, Nakatsuka Y, Hia F, Yamasoba D, et al. Regnase-1 and Roquin Nonredundantly Regulate Th1 Differentiation Causing Cardiac Inflammation and Fibrosis. *J Immunol* (2017) 199(12):4066–77. doi: 10.4049/jimmunol.1701211
56. Bertossi A, Aichinger M, Sansonetti P, Lech M, Neff F, Pal M, et al. Loss of Roquin Induces Early Death and Immune Deregulation But Not Autoimmunity. *J Exp Med* (2011) 208(9):1749–56. doi: 10.1084/jem.20110578
57. Wei J, Long L, Zheng W, Dhungana Y, Lim SA, Guy C, et al. Targeting REGNASE-1 Programs Long-Lived Effector T Cells for Cancer Therapy. *Nature* (2019) 576(7787):471–6. doi: 10.1038/s41586-019-1821-z
58. Zheng W, Wei J, Zebley CC, Jones LL, Dhungana Y, Wang YD, et al. Regnase-1 Suppresses TCF-1+ Precursor Exhausted T-Cell Formation to Limit CAR-T-Cell Responses Against ALL. *Blood* (2021) 138(2):122–35. doi: 10.1182/blood.2020009309
59. Iwasaki H, Takeuchi O, Teraguchi S, Matsushita K, Uehata T, Kuniyoshi K, et al. The IkappaB Kinase Complex Regulates the Stability of Cytokine-Encoding mRNA Induced by TLR-IL-1R by Controlling Degradation of Regnase-1. *Nat Immunol* (2011) 12(12):1167–75. doi: 10.1038/ni.2137
60. Zhou L, Azfer A, Niu J, Graham S, Choudhury M, Adamski FM, et al. Monocyte Chemoattractant Protein-1 Induces a Novel Transcription Factor That Causes Cardiac Myocyte Apoptosis and Ventricular Dysfunction. *Circ Res* (2006) 98(9):1177–85. doi: 10.1161/01.RES.0000220106.64661.71
61. O'Neill TJ, Seeholzer T, Gewies A, Gehring T, Giesert F, Hamp I, et al. TRAF6 Prevents Fatal Inflammation by Homeostatic Suppression of MALT1 Protease. *Sci Immunol* (2021) 6(65):eabh2095. doi: 10.1126/sciimmunol.abh2095
62. Zhao H, Liu Y, Wang L, Jin G, Zhao X, Xu J, et al. Genome-Wide Fitness Gene Identification Reveals Roquin as a Potent Suppressor of CD8 T Cell Expansion and Anti-Tumor Immunity. *Cell Rep* (2021) 37(10):110083. doi: 10.1016/j.celrep.2021.110083
63. Ataide MA, Komander K, Knöpper, Peters AE, Wu H, Eickhoff S, et al. BATF3 Programs $CD8^+$ T Cell Memory. *Nat Immunol* (2020) 21:1397–407. doi: 10.1038/s41590-020-0786-2
64. Seo H, González-Avalos E, Zhang W, Ramchandani P, Yang C, Lio C-WJ, et al. BATF and IRF4 Cooperate to Counter Exhaustion in Tumor-Infiltrating CAR T Cells. *Nat Immunol* (2021) 22:983–95. doi: 10.1038/s41590-021-00964-8

Conflict of Interest: The authors declare that the research was conducted in the absence of any commercial or financial relationships that could be construed as a potential conflict of interest.

Publisher's Note: All claims expressed in this article are solely those of the authors and do not necessarily represent those of their affiliated organizations, or those of the publisher, the editors and the reviewers. Any product that may be evaluated in this article, or claim that may be made by its manufacturer, is not guaranteed or endorsed by the publisher.

frontiers | Frontiers in Immunology

ORIGINAL RESEARCH
published: 07 April 2022
doi: 10.3389/fimmu.2022.793582

RNA 2'-O-Methyltransferase Fibrillarin Facilitates Virus Entry Into Macrophages Through Inhibiting Type I Interferon Response

Panpan Li[1†], *Yang Liu*[1*†], *Renjie Song*[1], *Lu Zhao*[1], *Jiang Yang*[1], *Fengjiao Lu*[1] *and Xuetao Cao*[1,2*]

[1] Department of Immunology, Institute of Basic Medical Sciences, Peking Union Medical College, Chinese Academy of Medical Sciences, Beijing, China, [2] Institute of Immunology, College of Life Sciences, Nankai University, Tianjin, China

Type I interferons (IFN-I) play crucial roles in antiviral immune responses through inducing multiple antiviral interferon stimulated genes (ISGs). RNA modifications are emerging as critical post-transcriptional regulators of gene expression programs, which affect diverse biological processes. 2'-O-methylation (Nm) is one of the most common types of RNA modifications found in several kinds of RNA. However, the function and underlying mechanism of Nm modification in regulating viral infection and innate immunity are largely unknown. Here we found that 2'-O-methyladenosine (Am) on poly A+ RNA was increased in virus infected-macrophages. Functional screening identified RNA 2'-O-methyltransferase Fibrillarin (FBL) in facilitating viral infection. Down-regulation of FBL inhibited viral infection through blocking virus entry into macrophages. Furthermore, knockdown of FBL could reduce viral entry by increasing ISGs expression through IFN-I signaling. These results indicated that FBL-mediated Nm modifications of RNA may avoid the innate immune recognition, thereby maintain immune homeostasis. Once FBL is down-regulated, the decreased Nm modifications of RNA in macrophages may act as "non-self" RNA and be recognized by RNA sensor interferon induced with helicase C domain 1 (MDA5), leading to innate immune activation by inducing the expression of IFN-I and ISGs. Therefore, our finding reveals a new role of FBL and its mediated RNA Nm modifications in facilitating viral infection and inhibiting innate immune response, adding mechanistic insight to the RNA modifications in infection and immunity.

Keywords: RNA 2'-O-methylation, fibrillarin, viral infection, type I interferon, innate immunity, macrophages

OPEN ACCESS

Edited by:
Osamu Takeuchi,
Kyoto University, Japan

Reviewed by:
Hansjörg Hauser,
Helmholtz Association of German Research Centers (HZ), Germany
Takashi Mino,
Kyoto University, Japan

***Correspondence:**
Yang Liu
yliu@immunol.org
Xuetao Cao
caoxt@immunol.org

[†]*These authors have contributed equally to this work*

Specialty section:
This article was submitted to Molecular Innate Immunity, a section of the journal Frontiers in Immunology

Received: *12 October 2021*
Accepted: *15 March 2022*
Published: *07 April 2022*

Citation:
Li P, Liu Y, Song R, Zhao L, Yang J, Lu F and Cao X (2022) RNA 2'-O-Methyltransferase Fibrillarin Facilitates Virus Entry Into Macrophages Through Inhibiting Type I Interferon Response. Front. Immunol. 13:793582. doi: 10.3389/fimmu.2022.793582

INTRODUCTION

Innate immune response plays an essential role in host defenses against viral infection. Innate immune cells express kinds of pattern recognition receptors (PRRs) to identify pathogen associated molecular patterns (PAMPs) from the invading viruses, such as "non-self" viral RNAs and DNAs, which can activate the host innate immune response for the elimination of invading virus (1–3). The inducible IFN-I plays key role in establishing and modulating host defense against viral infection

through inducing the expression of interferon stimulated genes (ISGs) *via* Janus kinase (JAK)-signal transducer and activator of transcription (STAT) signaling pathway (1, 3). In the interaction between viruses and the host, the immune cells can regulate gene expressions in response to the pathogen infection at multiple epigenetic levels, including histone modifications, DNA modifications, RNA modifications, and non-coding RNAs, etc. (4–6). Among those epigenetic modifiers, RNA modifications in regulating immunity and infection attract much attention (7), while most studies mainly focused on N^6-methyladenosine (m^6A) (8–11). We previously revealed that m^6A RNA modification–mediated down-regulation of the α-ketoglutarate dehydrogenase-itaconate pathway and cellular metabolism rewiring inhibit viral replication in macrophages (8). However, whether other types of RNA modifications also participate in viral infection or innate immunity remains largely unknown.

RNA 2'-O methylation (Nm) is one of the most common types of RNA modifications that are found in ribosomal RNAs (rRNAs), transfer RNAs, small nucleolar RNAs and also in messenger RNAs (mRNAs) (6). Nm modifications are formed in 2'-OH group of RNA riboses and respectively named as 2'-O-methyladenosine (Am), 2'-O-methylguanosine (Gm), 2'-O-methylcytidine (Cm) and 2'-O-methyluridine (Um). Nm endows nucleotides with greater hydrophobicity and affects RNA molecules in a variety of ways including the structure, stability and interaction of RNA, so as to regulate various cellular processes such as translation (6, 12–14). Research on the biological functions of Nm became possible until high-throughput sequencing methods of Nm residues have been developed, especially for low abundant mRNA (15, 16). The Nm modifications of mRNA 5'cap, precisely on the first and sometimes second cap-proximal nucleotides, are shown to serve as a "self-RNA" signal to prevent PRRs from recognizing self mRNA (17, 18). 2'-O-methylation sequencing (Nm-Seq) confirm that Nm modifications are present not only in the 5'cap of the mRNA, but also in the interior of some mRNAs (15). However, the physiological functions of Nm modifications in immune cells are still unknown.

Fibrillarin (FBL) is a 34 kDa nucleolar RNA 2'-O-methyltransferase and a highly conserved protein, which is located in the dense fibrillar component of the nucleolus (19). FBL mainly catalyzes Nm modifications on rRNA under the guidance of BOX C/D small nucleolar RNAs (snoRNAs) (19). Previous studies on FBL mainly focused on tumors. For instance, FBL contributes to tumorigenesis and is associated with poor survival in patients with breast cancer (20). Targeting FBL shows great potential correlation to an improved survival rate at low expression in breast cancer patients and association with p53, due to its pivotal role in ribosome biogenesis (21). Besides, FBL knockdown enhances the resistance in *C. elegans* against bacterial pathogens independent of the major innate immunity mediators (22). FBL also contributes to the long-distance transport of plant viruses in plants (23, 24). However, whether FBL-catalyzed Nm modifications regulate innate immunity is unclear.

By functional screening of eight RNA 2'-O-methyltransferases, in this study we found that FBL inhibits innate immune response by suppressing the expression of IFN-I and ISGs in macrophages, which can promote virus entry into macrophages to facilitate viral infection.

MATERIALS AND METHODS

Mice and Cells

C57BL/6 mice (6-8 weeks old) were from Institute of Laboratory Animal Science, Chinese Academy of Medical Sciences (Beijing). The interferon-α/β receptor 1 (IFNAR1)-deficient (*Ifnar1*$^{-/-}$) mice (6-8 weeks old) were obtained from Jackson Laboratory. All mice were bred and maintained under specific-pathogen-free conditions. All animal experiments were performed according to the National Institutes of Health Guide for the Care and Use of Laboratory Animals, with the approval of the Animals Care and Use Committees of the Institute of Laboratory Animal Sciences of Chinese Academy of Medical Sciences (ACUC-A01-2021-040).

Mouse peritoneal macrophages were obtained as previously described (8, 25). The RAW264.7, A549 and HEK293T cell lines were obtained from American Type Culture Collection (ATCC) and cultured as required. We generated FBL-knockdown RAW264.7 cells by a CRISPR-Cas9 gene-editing system with short guide RNA sequence-containing plasmid targeting specific sequences in the genome (5'-GGAGGTCGAGGTCGAGGCGG-3' and 5'-GCTGCCAGCTTGGAGCGGAA-3'). We used PCR followed by sequencing and immunoblotting to determine the knockdown efficiency. *MAVS*$^{-/-}$ A549 cells and *MDA5*$^{-/-}$ A549 cells were also generated by a CRISPR-Cas9 approach.

Plasmids, Reagents, and Pathogens

FBL full-length sequences were obtained from mouse peritoneal macrophage cDNA and then cloned into pcDNA™4/myc-His A. Vesicular Stomatitis Virus (VSV) and herpes simplex virus type 1 (HSV-1) viruses were used as described previously (25).

Adenosine (132283), 2'-O-Methyladenosine (591363), Cytidine (119085), 2'-O-Methylcytidine (391517), Guanosine (979688), 2'-O-Methylguanosine hydrate (329290), Uridine (399796), 6-chloropurine riboside (455573), 2'-O-Methyluridine (488001) were obtained from J&K Scientific Ltd.

Western Blot

These assays were performed as described previously (8). VSV-G (ab183497) antibody was obtained from Abcam. FBL (16021-1-AP), Beta Actin (66009-1-Ig) antibodies were from Proteintech. Myc-tag (2278S), RIG-I (3743S), STAT1 (14994S), P-STAT1 (9167S), IRF3 (4302S), P-IRF3 (4947S) antibodies were from Cell Signal Technology. GAPDH (M171-3) antibody was obtained from MBL International Corporation.

RNA Extraction and Quantitative RT-PCR

Total RNA was extracted by TRIZOL reagent (Invitrogen) according to the manufacturer's instructions. RNA was reversed-transcribed using the Reverse Transcription System from Toyobo (FSQ 301). Then cDNA was amplified by real-

time PCR and analyzed as described previously (8). The primer sequences for qPCR analysis are listed in **Supplementary Table 1**.

Transfection

RAW264.7 and A549 cells were transfected with Lipofectamine™ 3000 Transfection Reagent (L3000015, Thermo) or LipoMax DNA Transfection Reagent (32012, SUDGEN) for 48 h according to the manufacturer's instructions.

RNA Interference

Small interfering RNAs (siRNAs) were transfected into the mouse peritoneal macrophages and A549 cell lines with Lipofectamine™ RNAiMAX Transfection Reagent (13778150, Thermo) for 48 h following the manufacturer's instructions. After 48h, the cells were harvested or infected with virus for corresponding hours. siRNAs were designed and synthesized by RiboBio (**Supplementary Table 2**). The efficiency of interference was determined by qPCR or Western blot.

Construction of Inducible *Fbl* Knockout (*Fbl*-iKO) RAW 264.7 Cells

RAW264.7 cells with inducible expression of Cas9 by Cre-loxP system (iKO RAW264.7 cell) were conducted. In these cells, genome was inserted with Cas9 sequence and before cas9 sequence there was transcriptional termination sequences with LoxP sites at both ends (**Supplementary Figure 4D**). When iKO RAW264.7 cells were infected with lentivirus expressing Cyclization Recombination Enzyme (Cre), Cas9 expression was then induced by Cre. We constructed *Fbl*-iKO RAW264.7 cells which stably expressed *Fbl* sgRNA based on above iKO RAW264.7 cells. When *Fbl*-iKO cell line was infected with this lentivirus, Cas9 expression first induced and then the transient knockout of *Fbl* with *Fbl* sgRNA induced.

ELISA

The concentrations of IFN-β and IFN-α in the supernatants were determined with VeriKine Mouse IFN Beta ELISA Kit (42400, PBL Interferon Source) and VeriKine Mouse IFN Alpha ELISA Kit (42120, PBL Interferon Source) according to the manufacturer's instructions.

Virus Binding and Entry Assays

For virus-binding assays, mouse peritoneal macrophages were transfected with the indicated siRNAs for 48 h and then infected with VSV (MOI=3) for 30min on the ice. Cells were washed 6 times with ice-cold PBS supplemented with 2% bovine serum albumin to remove unbound virions. Then cells were lysed and RNA was extracted. Bound virions were quantified as viral RNA (vRNA) levels *via* qRT–PCR. For virus-entry assays, mouse peritoneal macrophages transfected with the indicated siRNAs for 48 h and then infected with VSV (MOI=3) for 30min in 4°C. After 6 washes with ice-cold PBS and 2% BSA, pre-warmed 37°C medium supplemented with 2% FBS and 15 mM NH_4Cl was added to cells. Cells were incubated at 37°C for 1 h to allow the virus to enter cells. Then cells were chilled on ice and incubated with 500 ng/ml proteinase K in PBS at 4 °C for 2h to remove residual plasma-membrane-bound virions. After 6 additional washes with ice-cold PBS and 2% bovine serum albumin. Then cells were lysed and RNA was extracted. And vRNA levels were quantified *via* qRT–PCR.

Poly A+ RNA Purification

Poly A+ RNA was purified from total RNA with polyA tail purification using Dynabeads™ mRNA Purification Kit (61006, Thermo). The remaining rRNAs were further removed using NEB Next® rRNA Depletion Kit (E6310L) from New England BioLabs (NEB).

Relative Quantification of RNA Modifications by LC-HRMS

1~2ug isolated mRNA or total RNA were digested into single nucleosides by 1U nuclease P1 (N8630, Sigma) in 50 μl buffer containing 10mM ammonium acetate, pH 5.3 at 37°C for 12 h, followed by 42°C for 12 h, then mixed with 2 μl 1M ammonium bicarbonate, pH8.3, added 1U Bacterial Alkaline Phosphatase (18011015, Thermo) in a final reaction volume of 100 μl adjusted with water, and incubated at 37°C for 12 h. 100ul chloroform was added to the reaction solution, 80ul supernatant was extracted by centrifugation after vortexing, and 20ul 6-chloropurine riboside (50ug/ml) was added and mixed. High performance liquid chromatography (HPLC) was modified slightly of the published procedures (26). Briefly, the nucleosides were separated with Hypersil GOLD aQ 3-μm column (150-mm length × 2.1-mm inner diameter, pore size 120 Å, particle size 3 μm, Thermo), and then detected by Triple TOF 5600 Mass Spectrometer (AB SCIEX) or Orbitrap Fusion Tribrid Mass Spectrometer (Thermo). The column was equilibrated to 37°C with 0.1% formic acid in HPLC-grade water at a flow rate of 0.4 ml/min for at least 20 min. 10μl of the solution was injected into LC-MS. Mobile phase A was 0.1% formic acid aqueous solution and mobile phase B was 0.1% formic acid acetonitrile solution. The solvent gradient was described in **Supplementary Table 3**. The chromatographic profiles were obtained by high resolution mass spectrum with full scan mode.

2'-O-Methylation Sequencing

2'-O-methylation sequencing (Nm-Seq) was performed by CloudSeq Biotech Inc. (Shanghai, China) by following the published procedures with slight modification (15). Briefly, the RNA samples were fragmented at 95°C for 5 min with RNA Fragmentation Reagents (Thermo). RNA fragments were 3'-end repaired using Antarctic phosphatase (NEB) at 37°C for 30 min. Then, repaired RNA samples were oxidized/eliminated using 10 mM $NaIO_4$ (Sigma) in 200 mM lysine-HCl buffer (pH 8.5, Sigma-Aldrich) in a total volume of 40 μl at 37°C for 30 min. The reaction was quenched by ethylene glycol, samples were further dephosphorylated by Shrimp Alkaline Phosphatase (NEB) at 37°C for 30 min. Eight cycles of oxidation-elimination-dephosphorylation were performed. A final round of oxidation/elimination reaction was performed, excluding dephosphorylation. Then, purified RNA samples were 5'phosphorylated by T4 polynucleotide kinase 3' phosphatase minus (NEB) at 37 °C for 60 min. Libraries were constructed from treated RNA fragments and untreated input fragments

using NEBNext Small RNA Library Prep Set for Illumina (NEB). Sequencing was carried out on Illumina HiSeq4000 according to the manufacturer's instructions.

Raw data was generated after sequencing, image analysis, base calling and quality filtering on Illumina HiSeq4000 sequencer. Firstly, Q30 was used to perform quality control. After adaptor-trimming and low quality reads removing by cutadapt (v1.9.1) software (27), high quality clean reads were generated. Then these clean reads were aligned to reference genome (mm10) using bowtie2 (v2.2.4) software (28) with end-to-end mode. Raw 2'-O-methylation counts and coverage counts were calculated by bedtools (v2.24) software and in-house scripts, then 2'-O-methylation-ratio (defined as: count/coverage) and 2'-O-methylation-fc (defined as: 2'-O-methylation-ratio/Input-2'-O-methylation-ratio) were also calculated. 2'-O-methylation sites were annotated with gene information by bedtools software. And the 2'-O-methylation sites were visualized in IGV (v2.64) software (29). Sequence motifs on Nm peaks were identified by HOMER (30).

RNA High Throughput Sequencing

Briefly, total RNA was used for removing the rRNAs with NEBNext rRNA Depletion Kit (NEB) following the manufacturer's instructions. RNA libraries were constructed by using NEBNext® Ultra™ II Directional RNA Library Prep Kit (NEB) according to the manufacturer's instructions. RNA high throughput sequencing (RNA-Seq) was performed by Cloud-Seq Biotech (Shanghai, China). Two independent biological replicates were performed for RNA-seq.

Statistical Analysis

Data are expressed as the mean ± standard error of the mean (SEM) from at least three independent triplicated experiments. The number of individuals and repeated experiments are stated in each figure legend. All data was analyzed using the GraphPad Prism software version 8.4.2. The statistical significance of comparisons between two groups was determined with Two-tailed unpaired Student's *t* test. The relative gene expression data was acquired using the $2^{\Delta\Delta CT}$ method. *P*-value: ns, $P > 0.05$; *, $P \leq 0.05$; **, $P \leq 0.01$; ***, $P \leq 0.001$; ****, $P \leq 0.0001$.

RESULTS

Increased Am Modification on Poly A+ RNA in Macrophages Upon Viral Infection

In order to identify RNA modifications that regulate virus infection or innate immunity, we used high resolution mass spectrometry to observe the changed types of RNA modifications in RAW264.7 macrophages induced by VSV infection. To prevent rRNA modifications from interfering with the detection of low RNA modification level on mRNA, we optimized the poly A+ RNA purification method by adding a rRNA removal step, and the rRNA residue in this optimized method was much lower than the traditional purification method of Oligo dT beads (**Figure 1A**). We found that the level of Am was increased on poly A+ RNA of RAW264.7 macrophages after VSV infection, while Am level in total RNA remained unchanged after VSV infection (**Figures 1B, C** and **Supplementary Figures 1A, B**).

Am is one type of Nm modifications. To provide functional insights into whether mRNAs carrying Nm modification in macrophages are linked to antiviral innate immunity, we performed transcriptome-wide Nm-seq on the poly A+ RNA of RAW264.7 macrophages with or without VSV infection. We identified 6808 Nm sites (fold change (FC)≥4), 5643 of which had a minimal Nm-seq count of ten reads. Next, Gene Ontology (GO) analyses of these methylated genes were performed and showed that the significantly enriched methylated genes were as follows: translation and RNA process for molecular function (MF); extracellular exosome, nucleus and cytoplasm for cell compartment (CC); RNA and nucleotide binding, protein binding for biological process (BP) (**Figure 1D** and **Supplementary Table 4**). The most dramatic BP was binding, especially binding of RNA and nucleotide, suggesting that mRNA Nm modifications might play an important role in the nucleus, including RNA splicing and processing. Most of the Nm peaks were apparently positioned in coding DNA sequence (CDS), which was consistent with the other reported Nm-seq result (15) (**Figure 1E**). An unbiased search for common motifs enriched in segments around Nm peak summits was performed. The most significantly enriched motifs were slightly changed after VSV infection (**Figure 1F**), which may be due to the differences in the relative abundance of different RNAs before and after viral infection. Interestingly, we found that the Nm modifications are changed on the mRNA of a large number of genes related to viral infection (**Figure 1G** and **Supplementary Table 5**). These results of GO and KEGG analysis suggested that Nm RNA modifications may be involved in regulating virus infection and antiviral innate immunity.

Functional Screening Identifies RNA 2'-O-Methyltransferase FBL to Facilitate Viral Infection

Then we focused on identifying which RNA 2'-O-methyltransferase may participate in regulating viral infection. Through performing functional screening of eight Nm associated enzymes (FTSJ1, FTSJ2, FTSJ3, FBL, CMTR1, CMTR2, MRM1, MRM3) *via* siRNAs-mediated knockdown, we found that knockdown of FBL inhibited VSV infection of mouse peritoneal macrophages, down-regulation of FTSJ1 promoted VSV infection in mouse peritoneal macrophages, and the effects of different siRNA of other enzymes were inconsistent or had no significant effects on VSV infection (**Figure 2A** and **Supplementary Figures 2A, B**). FBL is an essential nucleolar protein that participates in pre-rRNA methylation and processing, and also is an extremely well-conserved protein during the evolution from archaea to human (19). We found that FBL was the highest expressed RNA 2'-O-methyltransferase in mouse peritoneal macrophages (**Supplementary Figure 3A**). We retrieved gene expression omnibus (GEO) dataset GDS4185 which contains FBL mRNA expression data of isolated CD4+ T

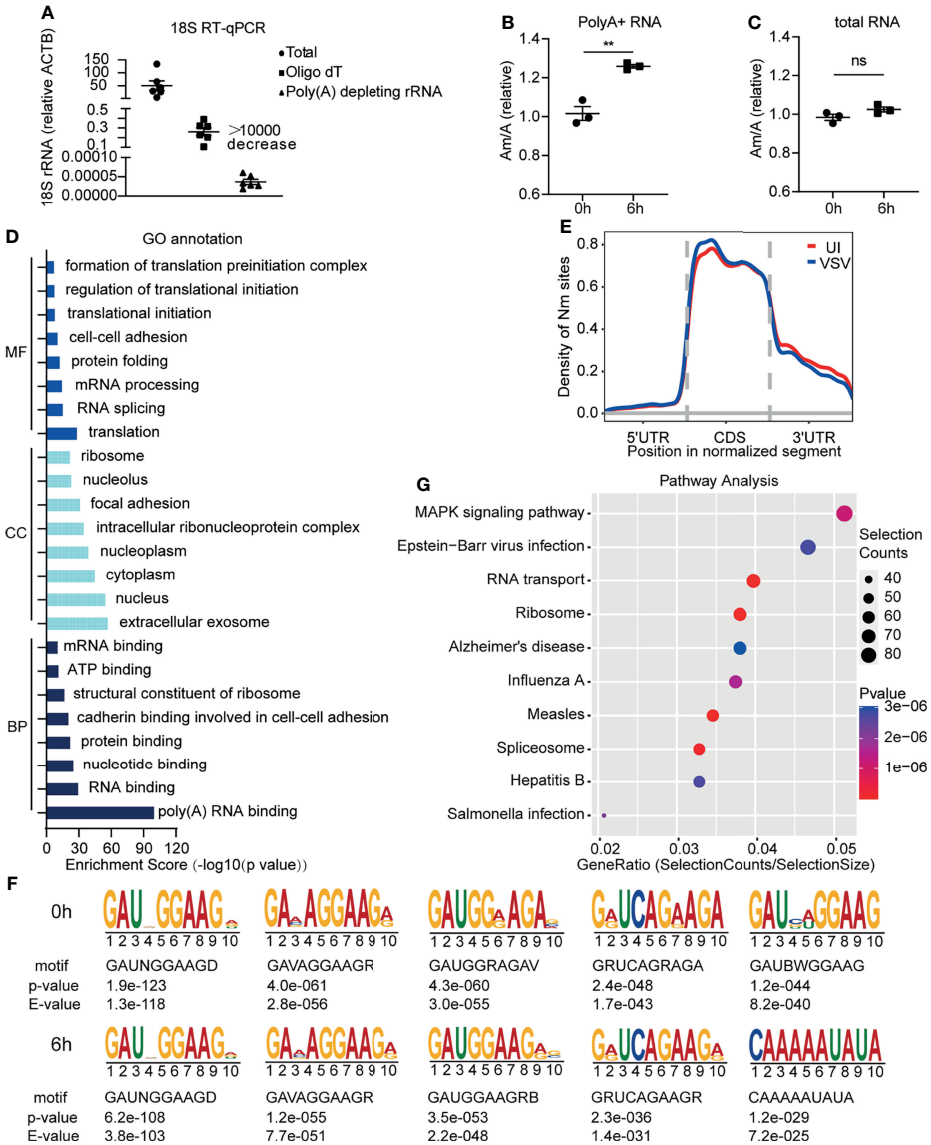

FIGURE 1 | Increased Am modification on poly A+ RNA in macrophages upon viral infection. **(A)** Determination of poly A+ RNA purity through RT-qPCR with primers specific to 18S rRNA and *Actb*. Total, total RNA; Oligo dT, poly A+ purified by Oligo dT beads; Poly A+ depleting rRNA, poly A+ purified by Oligo dT beads and rRNA depleting kit (n=6); **(B)** Quantification of the Am/A ratio in poly A+ RNA of RAW264.7 cells with or without VSV infection (n=3). 0h, RNA from RAW264.7 cells; 6h, RNA from RAW264.7 cells infected with VSV (MOI=1) for 6 h; **(C)** Quantification of the Am/A ratio in total RNA of RAW264.7 cells with or without VSV infection (n=3). 0h, RNA from RAW264.7 cells; 6h, RNA from RAW264.7 cells infected with VSV (MOI=1) for 6 h; **(D)** GO terms of MF, CC, BP for Nm-methylated transcripts of RAW264.7 at the steady state; MF, Molecular function; CC, Cell Compartment; BP, Biological process; **(E)** Metagene profile of Nm sites distribution along a normalized mRNA transcript; **(F)** Sequence logo of enriched motifs behind Nm sites identified by HOMER; **(G)** KEGG pathway enrichment for Nm up-regulated genes after viral infection. UI, poly A+ RNA from RAW264.7 cells; VSV, poly A+ RNA from RAW264.7 cells infected with VSV (MOI=1) for 6 h. All data are mean ± SEM of biologically independent samples.ns, not significant, $^{**}P < 0.01$, two-tailed unpaired Student's *t* test.

cells and CD19+ B cells from the blood of Systemic Lupus Erythematosus (SLE) patients and healthy controls. We found that FBL expressions in CD19+ B cells and CD4+ T cells of SLE patients were lower than that of healthy controls (**Supplementary Figures 3B, C**), suggesting that FBL may play an immunomodulatory role. FBL was reported that mainly catalyzes Nm modifications on rRNA under the guidance of BOX C/D snoRNAs (19). However, whether FBL regulates immune response is largely unknown. This inspired us to investigate the role of FBL in infection and innate immunity.

Furthermore, we observed that siRNA-mediated knockdown of FBL decreased VSV protein expression and VSV titers in cell supernatant (**Figures 2B–D**). Because FBL deficiency induces lethality (31), FBL knockout monoclonal cell lines and *Fbl*$^{-/-}$ mice

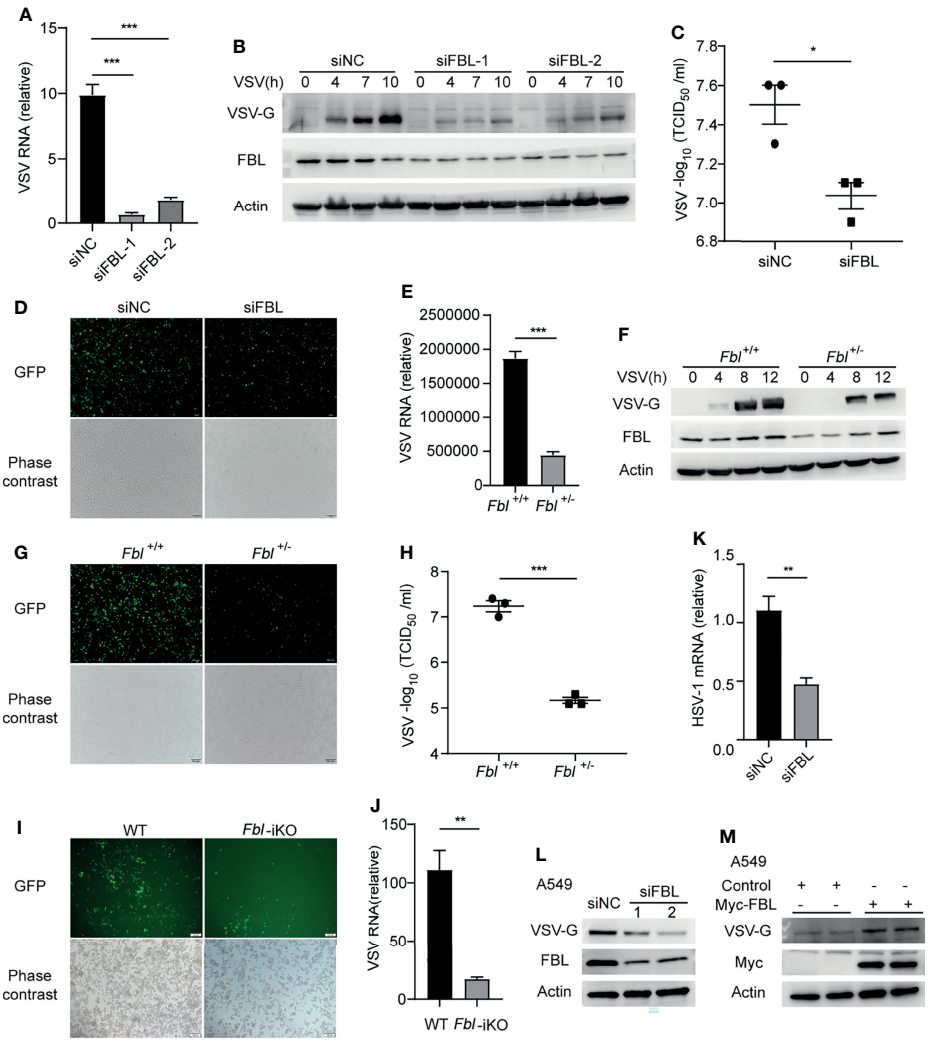

FIGURE 2 | RNA 2′-O-methyltransferase FBL facilitates viral infection. **(A)** RT-qPCR of VSV RNA in mouse peritoneal macrophages transfected with the indicated siRNAs for 48 h and then infected with VSV (MOI=3) for 10 h (n=3); **(B)** Western blot of VSV-G protein in mouse peritoneal macrophages transfected with the indicated siRNAs for 48 h and then infected with VSV (MOI=3) for 0, 4, 7, 10 h (n=3); **(C)** VSV titers by median tissue culture infectious dose ($TCID_{50}$) assay in supernatants of peritoneal macrophages transfected with the indicated siRNAs for 48 h and then infected with VSV for 12 h (n=3); **(D)** Fluorescence microscopy images of mouse peritoneal macrophages transfected with the indicated siRNAs for 48 h and then infected with GFP-VSV (MOI=5) for 8 h. Scale bar, 100 μm (n=3); **(E)** RT-qPCR of VSV RNA in WT and *Fbl*$^{+/-}$ RAW264.7 cells infected with GFP-VSV for 8 h (n=4); **(F)** Western blot of VSV-G levels in WT and *Fbl*$^{+/-}$ RAW264.7 cells infected with GFP-VSV for 0, 4, 8, 12 h (n=3); **(G)** Fluorescence microscopy images of WT and *Fbl*$^{+/-}$ RAW264.7 cells infected with GFP-VSV for 8 h. Scale bar, 100 μm (n=3); **(H)** VSV titers by $TCID_{50}$ assay in supernatants of WT and *Fbl*$^{+/-}$ RAW264.7 cells infected with GFP-VSV for 12 h (n=3); **(I)** Fluorescence microscopy images of WT and *Fbl*-iKO RAW264.7 cells infected with GFP-VSV for 16 h. Scale bar, 100 μm (n=3); **(J)** RT-qPCR of VSV RNA in WT and *Fbl*-iKO RAW264.7 cells infected with GFP-VSV for 8 h (n=3); **(K)** qRT-PCR of HSV-1 RNA in mouse peritoneal macrophages transfected with the indicated siRNAs for 48 h and then infected with HSV-1 for 10 h (n=4); **(L)** Western blot of VSV-G protein in A549 cells transfected with the indicated siRNAs (siFBL-1 and siFBL-2) for 48 h and then infected with VSV (MOI=0.5) for 8 h (n=3); **(M)** Western blot of VSV-G protein in A549 cells transfected with empty vector or FBL expression vector for 48 h and then infected with VSV (MOI=0.5) for 8 h (n=3). All data are mean ± SEM of biologically independent samples. *$P < 0.05$, **$P < 0.01$, ***$P < 0.001$, two-tailed unpaired Student's *t* test.

cannot be obtained. We generated FBL-knockdown RAW264.7 cells by CRISPR-Cas9 gene-editing systems (**Supplementary Figures 4A–C**), and these *Fbl*$^{+/-}$ RAW264.7 cells also showed decreased intracellular virus production upon infection of recombinant green fluorescent protein-expressing VSV (GFP-VSV) (**Figures 2E–H**). We further verified that FBL promoted VSV infection by *Fbl*-iKO RAW264.7 cells (**Figures 2I, J; Supplementary Figures 4D–F**). Besides, knockdown of FBL significantly inhibited the infection of DNA virus HSV-1 in mouse peritoneal macrophages (**Figure 2K**), in addition to RNA virus VSV. Consistently, knockdown of FBL inhibited VSV infection while overexpression of FBL facilitated VSV infection in human A549 cells (**Figures 2L, M**). These results demonstrate that FBL facilitates viral infection.

FBL Facilitates VSV Entry Into Macrophages at the Early Stage of Infection

IFN-I and ISGs play important roles in antiviral innate immunity. However, the mRNA and protein expressions of IFN-α and IFN-β, as well as the activation of IFN-I signaling pathway in FBL-knockdown mouse peritoneal macrophages were not increased than that in the control cells during VSV infection (**Figures 3A–C**). Besides, we found that FBL knockdown did not affect the viability of mouse peritoneal macrophages (**Figures 3D, E**). FBL knockdown significantly inhibited the VSV protein expression in the early stage of infection (**Figure 3C**). Therefore, we hypothesize that FBL may affect the early stages of the VSV life cycle. To test this idea, we performed VSV binding and entry assays in mouse peritoneal macrophages and found that FBL knockdown did not affect VSV binding, but inhibited VSV entry into mouse peritoneal macrophages (**Figures 3F, G**).

FBL Inhibits the Expression of ISGs in Macrophages Under Steady State

It was reported that low density lipoprotein receptor (LDLR) and other members of this receptor family serve as VSV receptors on host cells (32, 33). We found that knockdown of FBL did not influence the expression of LDLR (**Figure 4A**). Therefore, FBL-promoted VSV entry into macrophages in the early stage of VSV infection was not due to the regulation of LDLR expression in macrophages.

In order to investigate the underlying mechanism of FBL in facilitating VSV entry into macrophages, we performed RNA-seq

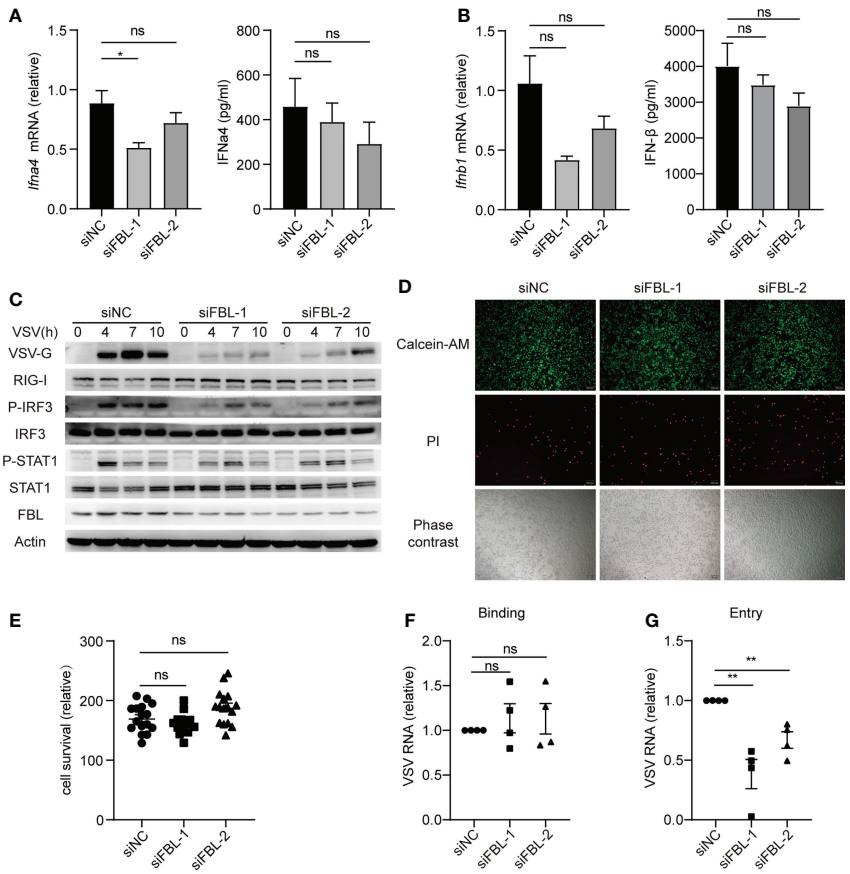

FIGURE 3 | FBL facilitates VSV entry into macrophages at the early stage of infection. **(A)** qRT-PCR of *Ifnα4* mRNA and ELISA of IFNα4 protein level in mouse peritoneal macrophages transfected with the indicated siRNAs for 48 h and then infected with VSV for 10 h (n=3); **(B)** qRT-PCR of *Ifnb1* mRNA and ELISA of IFNβ protein level in mouse peritoneal macrophages transfected with the indicated siRNAs for 48 h and then infected with VSV for 10 h (n=3); **(C)** Western blot of innate signaling activation in mouse peritoneal macrophages transfected with the indicated siRNAs for 48 h and then infected with VSV for 0, 4, 7, 10 h; **(D)** Mouse peritoneal macrophages were transfected with the indicated siRNAs for 48 h then to test cell activity and cytotoxicity by fluorescence microscopy images. Scale bar, 100 μm (n=4); **(E)** Calcein/PI cell activity and cytotoxicity assay kit to test cell survival (n=4, repeated four times); **(F)** Mouse peritoneal macrophages transfected with the indicated siRNAs for 48 h and then infected with VSV for 30 min on the ice, then bound virions were quantified as viral RNA (vRNA) levels *via* qRT-PCR (n=4); **(G)** Mouse peritoneal macrophages transfected with the indicated siRNAs for 48 h and then infected with VSV for 30min in 4°C (n=4). After removal of unbound virus, the temperature was increased to 37°C for 1 h to allow internalization. Then quantify vRNA levels *via* qRT–PCR. Data are mean ± SEM of biologically independent samples. ns, not significant, $^{*}P < 0.05$, $^{**}P < 0.01$, two-tailed unpaired Student's *t* test.

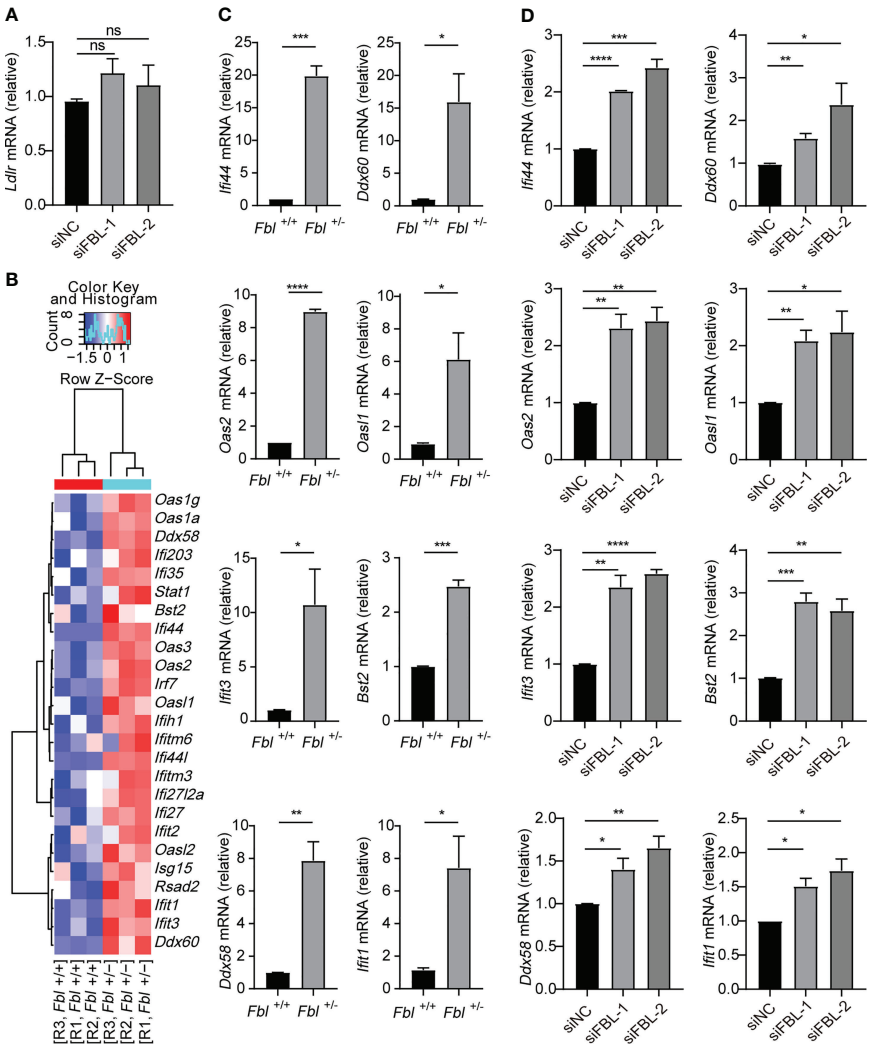

FIGURE 4 | FBL inhibits the expression of ISGs in macrophages. **(A)** qRT-PCR analysis of *Ldlr* mRNA in mouse peritoneal macrophages transfected with the indicated siRNAs for 48 h (n=3); **(B)** Hotmap showing normalized transcript expression levels of immune-associated genes in WT and *Fbl*$^{+/-}$ RAW264.7 cells (n=3); **(C)** qRT-PCR analysis of *Ifi44*, *Oas2*, *Ifit3*, *Ddx58*, *Ddx60*, *Oasl1*, *Bst2*, *Ifit1* mRNA in WT and *Fbl*$^{+/-}$ RAW264.7 cells (n=3); **(D)** qRT-PCR analysis of *Ifi44*, *Oas2*, *Ifit3*, *Ddx58*, *Ddx60*, *Oasl1*, *Bst2*, *Ifit1* mRNA in mouse peritoneal macrophages transfected with the indicated siRNAs for 48 h (n=3). Data are mean ± SEM of biologically independent samples. ns, not significant, **P*<0.05, ***P*<0.01, ****P*<0.001, *****P*<0.0001, two-tailed unpaired Student's *t* test.

and found that mRNA expressions of many ISGs were up-regulated in *Fbl*$^{+/-}$ RAW264.7 cells at the steady state without viral infection (**Figure 4B** and **Supplementary Table 6**). Quantitative reverse transcription PCR (qRT-PCR) analysis also confirmed that the mRNA expressions of *Ifi44*, *Oas2*, *Ifit3*, *Ddx58*, *Ddx60*, *Oasl1*, *Bst2*, *Ifit1* were up-regulated in *Fbl*$^{+/-}$ RAW264.7 cells (**Figure 4C**). Besides, siRNA-mediated knockdown of FBL in mouse peritoneal macrophages also increased the expressions of above ISGs at the steady state (**Figure 4D**).

Therefore, FBL may act as an immunosuppressive factor under physiological conditions. FBL knockdown leads to increased expression of antiviral immune genes, thus inhibiting VSV entry into the "antiviral primed-macrophages".

Knockdown of FBL Reduces Viral Entry by Increasing ISGs Expression Through IFN-I Signaling

IFN-I induces the expression of ISGs through interferon-α/β receptor (IFNAR)-JAK-STAT signaling pathway (1, 3). Whether FBL regulates these antiviral immune genes through IFN-I signaling? In *Ifnar1*$^{-/-}$ mouse macrophages, knockdown of FBL could not promote ISGs expression (**Figure 5A**). Meanwhile, we found that FBL knockdown did not affect VSV entry into *Ifnar1*$^{-/-}$ mouse peritoneal macrophages anymore (**Figure 5B**). Besides, down-regulation of FBL did not regulate the expression of ISGs directly in macrophages when stimulated with enough IFN-β (**Supplementary Figures 5A, B**). Thus, FBL facilitates

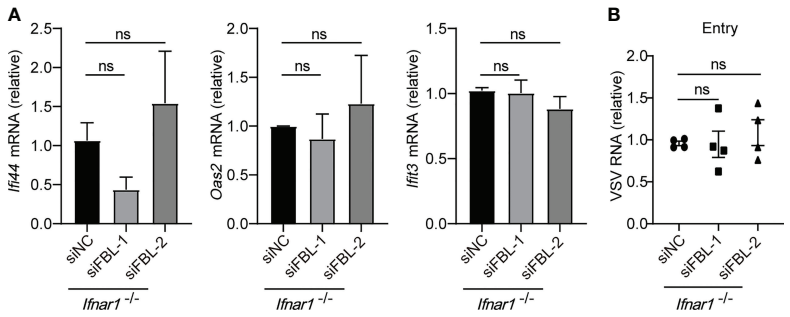

FIGURE 5 | Knockdown of FBL reduces viral entry by increasing ISGs expression through IFN-I signaling. **(A)** qRT-PCR analysis of *Ifi44*, *Oas2*, *Ifit3* mRNA in *Ifnar1*$^{-/-}$ mouse peritoneal macrophages transfected with the indicated siRNAs for 48 h (n=3); **(B)** VSV RNA levels in *Ifnar1*$^{-/-}$ peritoneal macrophages transfected with the indicated siRNAs for 48 h and then infected with VSV for 30 min in 4°C. After removal of unbound virus, the temperature was increased to 37°C to allow internalization. Then quantify VSV RNA levels *via* qRT-PCR (n=4). Data are mean ± SEM of biologically independent samples. ns, not significant, two-tailed unpaired Student's *t* test.

VSV entry into macrophages depending on the impairment of IFN-I signaling pathway.

FBL-Mediated RNA 2'-O Methylation Suppresses Innate Immune Activation and IFN-I Expression

FBL usually catalyzes the formation of Nm modifications on rRNA under the guidance of BOX C/D snoRNAs (6). A recent study reported that FBL and two box C/D snoRNAs (U51 and U32A) lead to Nm modification in the protein-coding region of peroxidasin (Pxdn) mRNA (13). This enlightened us that FBL may facilitate VSV entry by catalyzing Nm modification on poly A+ mRNA and rRNA broadly. We further proved this hypothesis by finding that the levels of Am modification were decreased on poly A+ RNA of *Fbl*$^{+/-}$ RAW264.7 macrophages compared to wide type cells **(Figure 6A)**. As rRNA is the most abundant type of RNA (80 to 85% of total RNA). We also measured Nm modifications in total RNA, and found that the levels of Am, Gm were decreased on total RNA of *Fbl*$^{+/-}$ RAW264.7 macrophages compared to wide type macrophages **(Figure 6B)**. While overexpression of mouse FBL led to increased Nm levels in *Fbl*$^{+/-}$ RAW264.7 cells **(Figure 6C)**. These results showed that FBL catalyzes the formation of Nm modifications directly.

Nm modification of capped mRNA has been reported as a molecular signature for the distinction of self and nonself mRNA by RNA sensor MDA5 (17, 18). Specifically, West Nile virus mutant (E218A) that lacks 2'-O-methyltransferase activity was recognized and attenuated in wild-type primary cells and mice, but was pathogenic in the absence of IFN-I signaling (17). The induction of IFN-I by coronavirus mutants lacking 2'-O-methyltransferase was dependent on the cytoplasmic RNA sensor MDA5 (18). Based on the relationship between FBL and Nm, we speculated that the lower Nm modification levels on host self RNA of the FBL knockdown macrophages could be recognized as "non-self" RNA by PRRs, so as to activate the innate immune response and subsequently amplify the downstream signals of IFN-I in macrophages. Then, our results showed that both the mRNA expressions of IFN-β and anti-viral immune signaling activation were increased in FBL knockdown macrophages (**Figures 6D–G**). Besides, in *MAVS*-deficient A549 cells, down-regulation of FBL did not increase the expression of IFN-I and ISGs compared with that in wild-type A549 cells (**Figure 6H**). These imply that the sensor upstream of MAVS might initiate the IFN-I signal in FBL-deficient cells.

FBL Deficiency Increases IFN-I Signaling and ISGs Expression Through RNA Sensor MDA5

Based on the blocking effect of MAVS in FBL-mediated suppression of IFN-I signaling and ISGs expression, we next explored the RNA sensor RIG-I and MDA5, respectively. We found that down-regulation of FBL still inhibited VSV entry into *Rig-i*$^{-/-}$ mouse peritoneal macrophages **(Figure 7A)**. While, knockdown of FBL did not affect VSV entry process in *MDA5*$^{-/-}$ A549 cells **(Figure 7B)**. Besides, knockdown of FBL could not inhibit the expression of ISGs any longer when loss of MDA5 rather than RIG-I under steady state **(Figures 7C, D)**.

Taken together, our results indicate that FBL directly catalyzes the formation of Nm RNA modifications. Lower expression of FBL leads to decreased Nm modification levels on host RNA, which may be recognized as "non-self" RNAs by MDA5, thus promoting the expression of IFN-I at the steady state, and then induces the expression of antiviral ISGs, such as IFIT1, OAS2, IFIT3 and so on. This "Primed immune activated state" in macrophages, upon FBL is inhibited during viral infection, contributes to blockade of the viral entry **(Figure 8)**.

DISCUSSION

Viruses use host factors to complete the life cycles. Multiple host proteins inhibit the viral infection process by targeting different stages of the viral life cycle (34). RNA modifications regulate gene expressions to effect immunity and infection (7). We previously revealed that m^{6}A RNA modification inhibits viral

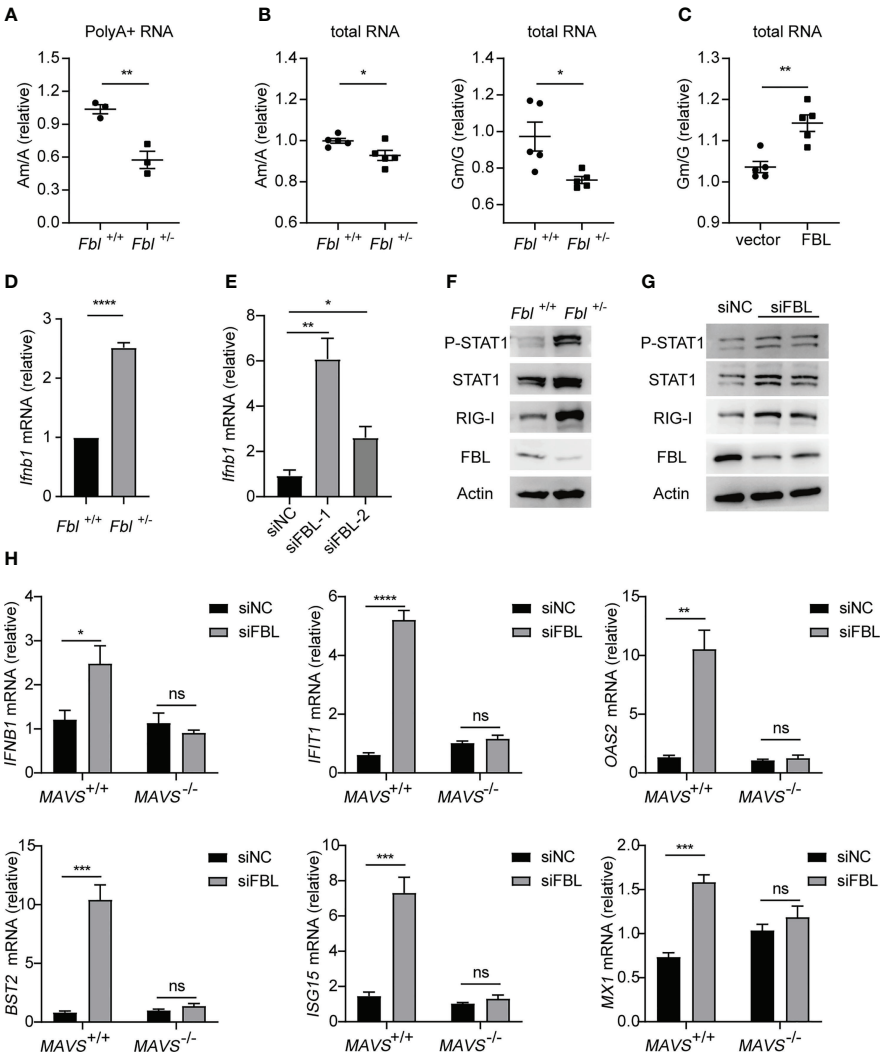

FIGURE 6 | FBL-mediated RNA 2'-O methylation suppresses IFN-I expression and signaling in macrophages. **(A)** Quantification of the Am/A ratio in poly A+ RNA of WT and *Fbl*$^{+/-}$ RAW264.7 cells (n=3); **(B)** Quantification of the Am/A and Gm/G ratio in total RNA of WT and *Fbl*$^{+/-}$ RAW264.7 cells (n=5); **(C)** Quantification of the Am/A, Cm/C, Gm/G ratio in total RNA of *Fbl*$^{+/-}$ RAW264.7 cells transfected with empty vector and vector encoding mouse FBL for 30 h (n=5); **(D)** qRT-PCR analysis of *Ifnb1* mRNA in WT and *Fbl*$^{+/-}$ RAW264.7 cells (n=3); **(E)** qRT-PCR analysis of *Ifnb1* mRNA in mouse peritoneal macrophages transfected with the indicated siRNAs for 48 h (n=3); **(F)** Western blot of interferon signaling in WT and *Fbl*$^{+/-}$ RAW264.7 cells; **(G)** Western blot of interferon signaling in mouse peritoneal macrophages transfected with the indicated siRNAs for 48 h; **(H)** qRT-PCR analysis of *IFNB1*, *IFIT1*, *OAS2*, *BST2*, *ISG15*, *MX1* mRNA in *MAVS*$^{+/+}$ and *MAVS*$^{-/-}$ A549 cells transfected with the indicated siRNAs for 48 h (n=4). All data are mean ± SEM of biologically independent samples. ns, not significant, **P*<0.05, ***P*<0.01, ****P* < 0.001, *****P*<0.0001, two-tailed unpaired Student's *t* test.

replication through down-regulating the α-ketoglutarate dehydrogenase-itaconate pathway and reprogramming cellular metabolism (8). Here we found that Nm RNA modification and RNA 2'-O-methyltransferase FBL also regulate viral infection.

FBL affects ribosome heterogeneity by regulating ribose methylation of rRNA to regulate translation, and plays an important role in the process of cell proliferation, senescence, tumor genesis and development (35). It has been reported that FBL regulates bacterial infection, independent of the p38 MAPK pathway, autophagy, or ubiquitin-proteasome (22). FBL is related to human diseases. The GEO dataset GDS4185 shows that FBL expressions in CD19+ B cells and CD4+ T cells of SLE patients are lower than that of healthy controls. Besides, FBL is highly expressed in a variety of tumors and has potential as a therapeutic target for tumors (21). Whether the abnormal expression of FBL in SLE and various tumors related to its immunosuppressive function need further investigations.

We wonder which process of VSV life cycle (that is binding, entry, uncoating, biosynthesis, assembly maturation and release) that FBL takes effect. In the VSV entry assay (**Figure 3G**), the low-temperature conditions (VSV could not undergo the normal process of life cycle) inhibited the VSV's life cycle and only

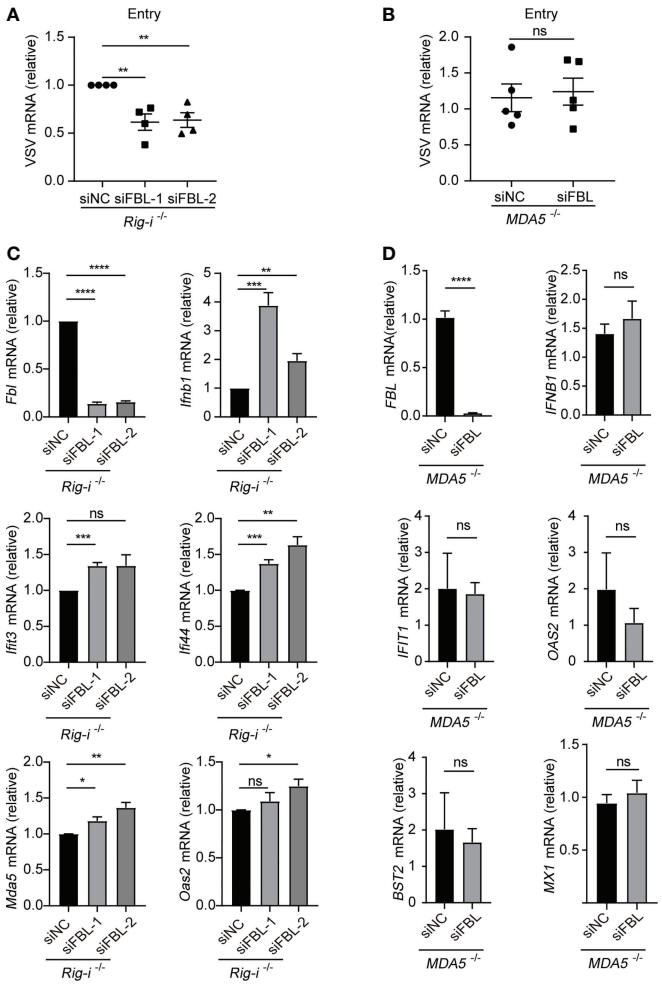

FIGURE 7 | FBL deficiency increases IFN-I signaling and ISGs expression *via* RNA sensor MDA5 **(A)** VSV RNA levels in *Rig-i*$^{-/-}$ mouse peritoneal macrophages transfected with the indicated siRNAs for 48 h and then infected with VSV for 30 min in 4°C. After removal of unbound virus, the temperature was increased to 37 °C to allow internalization. Then quantify VSV RNA levels *via* qRT-PCR (n=4); **(B)** VSV RNA levels in *MDA5*$^{-/-}$ A549 cells transfected with the indicated siRNAs for 48 h and then infected with VSV for 30 min in 4°C. After removal of unbound virus, the temperature was increased to 37 °C to allow internalization. Then quantify VSV RNA levels *via* qRT-PCR (n=5); **(C)** qRT-PCR analysis of *Fbl*, *Ifnb1*, *Ifit3*, *Ifi44*, *Mda5*, *Oas2* mRNA in *Rig-i*$^{-/-}$ mouse peritoneal macrophages transfected with the indicated siRNAs for 48 h (n=3); **(D)** qRT-PCR analysis of *FBL*, *IFNB1*, *IFIT1*, *OAS2*, *BST2*, *MX1* mRNA in *MDA5*$^{-/-}$ A549 cells transfected with the indicated siRNAs for 48 h (n=6). Data are mean ± SEM of biologically independent samples. ns, not significant, **P*<0.05, ***P*<0.01, ****P*<0.001, *****P*<0.0001, two-tailed unpaired Student's *t* test.

allowed VSV to enter mouse peritoneal macrophages slowly. However, under normal culture condition (37°C) (**Figure 2**), when VSV infected mouse macrophages, VSV could rapidly proliferate in the cells. Firstly, VSV binding analysis proved that FBL did not affect VSV binding to the macrophages. Secondly, the entry experiment showed that FBL affected VSV entry process. Therefore, fewer viruses can enter FBL-knockdown macrophages in the initial stage of infection.

In FBL-deficient immune cells, which PRR misidentifies self RNA with reduced Nm modifications as "non-self" RNA to activate the immune signaling pathway still needs further investigations. For RNA-sensing in the cytoplasm, RIG-I monitors the uncapped 5'-ends of RNA molecules (36). The carboxy-terminal domain (CTD) has a pocket binding specifically to 5'-PPP or 5'-PP groups and also contacts the unmethylated 2'-O group of the first nucleotide (36). Besides, 5'-Capped mRNA with Nm modifications could not be sensed by MDA5 (17, 18). In *MAVS*-deficient A549 cells, down-regulation of FBL cannot increase the expression of IFN-I and ISGs, implying that the RNA sensor upstream of MAVS might account for the activation of IFN-I signal in FBL-deficient macrophages. Our results further showed that MDA5 is the RNA sensor responsible for the activation of IFN signal induced by FBL deficiency.

Our results reveal that FBL inhibits the expression of IFN-I and ISGs by suppressing the innate immune activation, which promotes virus entry and further viral infection in macrophages. In sum, we propose the following working model of FBL in viral

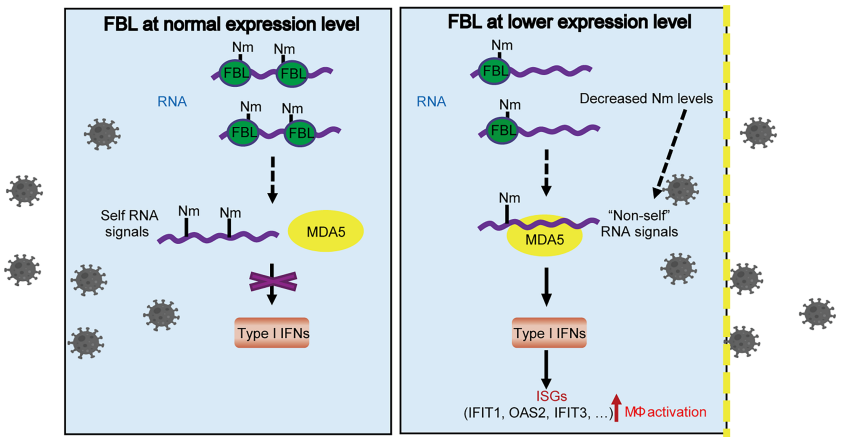

FIGURE 8 | A proposed model for FBL-mediated RNA 2′-O methylation in promoting viral entry into macrophages by inhibiting MDA5-mediated IFN-I and ISGs expression. FBL directly catalyzes the formation of Nm RNA modifications. When FBL is expressed at a low level, the RNA with decreased Nm modification levels may be recognized as "non-self" RNAs by MDA5, which promotes the expression of IFN-I at the steady state, and then induces the expression of antiviral ISGs, such as IFIT1, OAS2, IFIT3 and so on. This "Primed immune activated state" in macrophages, upon FBL is inhibited in response to viral infection, contributes to blockade of the viral entry.

infection and immunity. FBL directly catalyzes the formation of Nm RNA modifications. When FBL is at low expression level, the reduced Nm modification may be recognized as "non-self" RNA by MDA5, which activates innate immune response and promotes the IFN-I expression thus widely increasing the expression of antiviral ISGs, such as IFIT1, OAS2, IFIT3 and so on. Our findings also indicate the possible role of FBL in homeostasis maintenance by preventing autoinflammation. This study may provide a potential target for the control of infectious diseases and autoimmune diseases.

DATA AVAILABILITY STATEMENT

The datasets presented in this study can be found in online repositories. The names of the repository/repositories and accession number(s) can be found below: https://www.ncbi.nlm.nih.gov/geo/, GSE185660 and https://www.ncbi.nlm.nih.gov/geo/, GSE185661.

ETHICS STATEMENT

The animal study was reviewed and approved by the Animals Care and Use Committees of the Institute of Laboratory Animal Sciences of Chinese Academy of Medical Sciences (ACUC-A01-2021-040).

AUTHOR CONTRIBUTIONS

XC designed the experimental approach and supervised the study. PL, YL, RS, LZ, JY, and FL performed experiments. PL, YL, and XC analyzed data and wrote the paper. All authors contributed to the article and approved the submitted version.

FUNDING

This work was supported by grants from the National Natural Science Foundation of China (81788101, 82071793), and the Chinese Academy of Medical Sciences Innovation Fund for Medical Sciences (2021-I2M-1-017).

ACKNOWLEDGMENTS

We thank members of our laboratory for helpful discussion.

SUPPLEMENTARY MATERIAL

The Supplementary Material for this article can be found online at: https://www.frontiersin.org/articles/10.3389/fimmu.2022.793582/full#supplementary-material

Supplementary Figure 1 | Increased Am modification levls on poly A+ RNA in macrophages upon viral infection **(A)** Quantification of the Am/G, Am/C and Am/U ratio in poly A+ RNA of RAW264.7 cells with or without VSV infection (n=3); **(B)** Quantification of the Am/G, Am/C and Am/U ratio in total RNA of RAW264.7 cells with or without VSV infection (n=3). 0h, RNA from RAW264.7 cells; 6h, RNA from RAW264.7 cells infected with VSV (MOI=1) for 6 h. All data are mean ± SEM of biologically independent samples. ns, not significant, $^{*}P<0.05$, $^{**}P<0.01$, two-tailed unpaired Student's t test.

Supplementary Figure 2 | RNAi screening of RNA 2′-O-methyltransferases in regulation of viral infection in macrophages **(A)** qRT-PCR of VSV RNA in mouse peritoneal macrophages transfected with the corresponding siRNA for 48h then

infected with VSV (MOI=3) for 10 h (n=3). **(B)** qRT-PCR analysis mRNA expressions of *Ftsj1*, *Ftsj2*, *Ftsj3*, *Fbl*, *Cmtr1*, *Cmtr2*, *Mrm1*, *Mrm3* in mouse peritoneal macrophages transfected with the corresponding siRNA for 48 h (n =3). All data are mean ± SEM of biologically independent samples. ***P*<0.01, ****P*<0.001, *****P*<0.0001, two-tailed unpaired Student's t test.

Supplementary Figure 3 | Expression of FBL in mouse macrophages and human disease **(A)** qRT-PCR analysis mRNA expressions of *Ftsj1*, *Ftsj2*, *Ftsj3*, *Fbl*, *Cmtr1*, *Cmtr2*, *Mrm1*, *Mrm3* in mouse peritoneal macrophages under steady state (n=3). Data are mean ± SEM of biologically independent samples; **(B)** FBL and FTSJ1 expression levels in CD19+ B cells of SLE patients (n=9) and healthy controls(n=14). Data are mean ± SEM resourced from GEO dataset GDS4185; **(C)** FBL and FTSJ1 expression levels in CD4+ T cells of SLE patients (n=9) and healthy controls (n=14). Data are mean ± SEM resourced from GEO dataset GDS4185. ns, not significant, **P*<0.05, ***P*<0.01, two-tailed unpaired Student's t test.

Supplementary Figure 4 | RNA 2′-O-methyltransferase FBL facilitates viral infection **(A)** CRISPR/Cas9 strategy used to knockout the second to fifth exon of Fbl in mouse macrophage cell line; **(B)** Verification of FBL deletion in *Fbl*$^{+/-}$ RAW264.7 cells by PCR followed by DNA gel electrophoresis; **(C)** Verification of FBL deletion in *Fbl*$^{+/-}$ RAW264.7 cells by Western blot; **(D)** Schematic diagram of the gene elements driving the expression of Cas9; **(E)** RT-qPCR of FBL sgRNA in WT (n=3) and *Fbl*-iKO RAW264.7 cells (n=5); (F) Western blot of FBL levels in WT and *Fbl*-iKO RAW264.7 cells. All data are mean ± SEM of biologically independent samples. ***P*<0.01, two-tailed unpaired Student's t test.

Supplementary Figure 5 | RNA 2′-O-methyltransferase FBL does not regulate the expression of ISGs directly **(A)** qRT-PCR analysis of Ifi44, Oas2, Ifit3, Ddx58, Ddx60, Oasl1, Bst2, Ifit1 mRNA in mouse peritoneal macrophages transfected with the indicated siRNAs for 48 h (n=3), then treated with 500pg/ml IFNβ for 4 h; **(B)** qRT-PCR analysis of Ifi44, Oas2, Ifit3, Ddx58, Ddx60, Oasl1, Bst2, Ifit1 mRNA in WT and *Fbl*$^{+/-}$ RAW264.7 cells (n=9) stimulated with 500pg/ml IFNβ for 4 h. Data are mean ± SEM of biologically independent samples. ns, not significant, **P*<0.05, ***P*<0.01, *****P*<0.0001, two-tailed unpaired Student's t test.

Supplementary Table 1 | Primers used for qRT-PCR.

Supplementary Table 2 | siRNA sequences used for RNA interference.

Supplementary Table 3 | Gradient elution procedure.

Supplementary Table 4 | Methylated_sites in mRNA of RAW264.7 cells.

Supplementary Table 5 | Up-regulated Nm sites after VSV infection.

Supplementary Table 6 | mRNA Expression Profiling in *Fbl*$^{+/+}$ and *Fbl*$^{+/-}$ RAW264.7 cells.

REFERENCES

1. Schoggins JW. Recent Advances in Antiviral Interferon-Stimulated Gene Biology. *F1000Research* (2018) 7(1):309. doi: 10.12688/f1000research.12450.1
2. Cao X. Self-Regulation and Cross-Regulation of Pattern-Recognition Receptor Signalling in Health and Disease. *Nat Rev Immunol* (2016) 16 (1):35–50. doi: 10.1038/nri.2015.8
3. Chen K, Liu J, Cao X. Regulation of Type I Interferon Signaling in Immunity and Inflammation: A Comprehensive Review. *J Autoimmun* (2017) 83(1):1–11. doi: 10.1016/j.jaut.2017.03.008
4. Zhao BS, Roundtree IA, He C. Post-Transcriptional Gene Regulation by mRNA Modifications. *Nat Rev Mol Cell Biol* (2017) 18(1):31–42. doi: 10.1038/nrm.2016.132
5. Zhang Q, Cao X. Epigenetic Regulation of the Innate Immune Response to Infection. *Nat Rev Immunol* (2019) 19(1):417–32. doi: 10.1038/s41577-019-0151-6
6. Ayadi L, Galvanin A, Pichot F, Marchand V, Motorin Y. RNA Ribose Methylation (2'-O-Methylation): Occurrence, Biosynthesis and Biological Functions. *Biochim Biophys Acta Gene Regul Mech* (2019) 1862(3):253–69. doi: 10.1016/j.bbagrm.2018.11.009
7. He C. Special Issue on Regulating the Central Dogma. *Biochemistry* (2019) 58 (5):295–6. doi: 10.1021/acs.biochem.9b00059
8. Liu Y, You Y, Lu Z, Yang J, Li P, Liu L, et al. N (6)-Methyladenosine RNA Modification-Mediated Cellular Metabolism Rewiring Inhibits Viral Replication. *Science* (2019) 365(6458):1171–6. doi: 10.1126/science.aax4468
9. Winkler R, Gillis E, Lasman L, Safra M, Geula S, Soyris C, et al. M(6)A Modification Controls the Innate Immune Response to Infection by Targeting Type I Interferons. *Nat Immunol* (2019) 20(2):173–82. doi: 10.1038/s41590-018-0275-z
10. Wang L, Wen M, Cao X. Nuclear Hnrnpa2b1 Initiates and Amplifies the Innate Immune Response to DNA Viruses. *Science* (2019) 365(6454): eaav0758. doi: 10.1126/science.aav0758
11. Zheng Q, Hou J, Zhou Y, Li Z, Cao X. The RNA Helicase DDX46 Inhibits Innate Immunity by Entrapping M(6)A-Demethylated Antiviral Transcripts in the Nucleus. *Nat Immunol* (2017) 18(10):1094–103. doi: 10.1038/ni.3830
12. Choi J, Indrisiunaite G, DeMirci H, Ieong KW, Wang J, Petrov A, et al. 2'-O-Methylation in mRNA Disrupts tRNA Decoding During Translation Elongation. *Nat Struct Mol Biol* (2018) 25(3):208–16. doi: 10.1038/s41594-018-0030-z
13. Elliott BA, Ho HT, Ranganathan SV, Vangaveti S, Ilkayeva O, Abou Assi H, et al. Modification of Messenger RNA by 2'-O-Methylation Regulates Gene Expression *In Vivo*. *Nat Commun* (2019) 10(1):3401. doi: 10.1038/s41467-019-11375-7
14. Dimitrova DG, Teysset L, Carre C. RNA 2'-O-Methylation (Nm) Modification in Human Diseases. *Genes (Basel)* (2019) 10(2):117. doi: 10.3390/genes10020117
15. Dai Q, Moshitch-Moshkovitz S, Han D, Kol N, Amariglio N, Rechavi G, et al. Nm-Seq Maps 2'-O-Methylation Sites in Human mRNA With Base Precision. *Nat Methods* (2017) 14(7):695–8. doi: 10.1038/nmeth.4294
16. Hsu PJ, Fei Q, Dai Q, Shi H, Dominissini D, Ma L, et al. Single Base Resolution Mapping of 2'-O-Methylation Sites in Human mRNA and in 3' Terminal Ends of Small RNAs. *Methods* (2019) 156(1):85–90. doi: 10.1016/j.ymeth.2018.11.007
17. Daffis S, Szretter KJ, Schriewer J, Li J, Youn S, Errett J, et al. 2'-O Methylation of the Viral mRNA Cap Evades Host Restriction by IFIT Family Members. *Nature* (2010) 468(7322):452–6. doi: 10.1038/nature09489
18. Zust R, Cervantes-Barragan L, Habjan M, Maier R, Neuman BW, Ziebuhr J, et al. Ribose 2'-O-Methylation Provides a Molecular Signature for the Distinction of Self and Non-Self mRNA Dependent on the RNA Sensor Mda5. *Nat Immunol* (2011) 12(2):137–43. doi: 10.1038/ni.1979
19. Rodriguez-Corona U, Sobol M, Rodriguez-Zapata LC, Hozak P, Castano E. Fibrillarin From Archaea to Human. *Biol Cell* (2015) 107(6):159–74. doi: 10.1111/boc.201400077
20. Marcel V, Ghayad SE, Belin S, Therizols G, Morel AP, Solano-Gonzalez E, et al. P53 Acts as a Safeguard of Translational Control by Regulating Fibrillarin and rRNA Methylation in Cancer. *Cancer Cell* (2013) 24(3):318–30. doi: 10.1016/j.ccr.2013.08.013
21. El Hassouni B, Sarkisjan D, Vos JC, Giovannetti E, Peters GJ. Targeting the Ribosome Biogenesis Key Molecule Fibrillarin to Avoid Chemoresistance. *Curr Med Chem* (2019) 26(33):6020–32. doi: 10.2174/0929867326666181203133332
22. Tiku V, Kew C, Mehrotra P, Ganesan R, Robinson N, Antebi A. Nucleolar Fibrillarin is an Evolutionarily Conserved Regulator of Bacterial Pathogen Resistance. *Nat Commun* (2018) 9(1):3607. doi: 10.1038/s41467-018-06051-1
23. Chang CH, Hsu FC, Lee SC, Lo YS, Wang JD, Shaw J, et al. The Nucleolar Fibrillarin Protein Is Required for Helper Virus-Independent Long-Distance Trafficking of a Subviral Satellite RNA in Plants. *Plant Cell* (2016) 28 (10):2586–602. doi: 10.1105/tpc.16.00071
24. Canetta E, Kim SH, Kalinina NO, Shaw J, Adya AK, Gillespie T, et al. A Plant Virus Movement Protein Forms Ringlike Complexes With the Major Nucleolar Protein, Fibrillarin, *In Vitro*. *J Mol Biol* (2008) 376(4):932–7. doi: 10.1016/j.jmb.2007.12.039

25. Wang P, Xu J, Wang Y, Cao X. An Interferon-Independent lncRNA Promotes Viral Replication by Modulating Cellular Metabolism. *Science* (2017) 358 (6366):1051–5. doi: 10.1126/science.aao0409
26. Su D, Chan CT, Gu C, Lim KS, Chionh YH, McBee ME, et al. Quantitative Analysis of Ribonucleoside Modifications in tRNA by HPLC-Coupled Mass Spectrometry. *Nat Protoc* (2014) 9(4):828–41. doi: 10.1038/nprot.2014.047
27. Martin M. Cutadapt Removes Adapter Sequences From High-Throughput Sequencing Reads. *EMBnetjournal* (2011) 17(1):1138–43. doi: 10.14806/ej.17.1.200
28. Langmead B, Salzberg SL. Fast Gapped-Read Alignment With Bowtie 2. *Nat Methods* (2012) 9(4):357–9. doi: 10.1038/nmeth.1923
29. Thorvaldsdottir H, Robinson JT, Mesirov JP. Integrative Genomics Viewer (IGV): High-Performance Genomics Data Visualization and Exploration. *Brief Bioinform* (2013) 14(2):178–92. doi: 10.1093/bib/bbs017
30. Bailey TL. DREME: Motif Discovery in Transcription Factor ChIP-Seq Data. *Bioinformatics* (2011) 27(12):1653–9. doi: 10.1093/bioinformatics/btr261
31. Newton K, Petfalski E, Tollervey D, Caceres JF. Fibrillarin is Essential for Early Development and Required for Accumulation of an Intron-Encoded Small Nucleolar RNA in the Mouse. *Mol Cell Biol* (2003) 23(23):8519–27. doi: 10.1128/mcb.23.23.8519-8527.2003
32. Nikolic J, Belot L, Raux H, Legrand P, Gaudin Y, Albertini AA. Structural Basis for the Recognition of LDL-Receptor Family Members by VSV Glycoprotein. *Nat Commun* (2018) 9(1):1029. doi: 10.1038/s41467-018-03432-4
33. Finkelshtein D, Werman A, Novick D, Barak S, Rubinstein M. LDL Receptor and its Family Members Serve as the Cellular Receptors for Vesicular Stomatitis Virus. *Proc Natl Acad Sci USA* (2013) 110(18):7306–11. doi: 10.1073/pnas.1214441110
34. Dawson AR, Wilson GM, Coon JJ, Mehle A. Post-Translation Regulation of Influenza Virus Replication. *Annu Rev Virol* (2020) 7(1):167–87. doi: 10.1146/annurev-virology-010320-070410
35. Shubina MY, Musinova YR, Sheval EV. Proliferation, Cancer, and Aging-Novel Functions of the Nucleolar Methyltransferase Fibrillarin? *Cell Biol Int* (2018) 42(11):1463–6. doi: 10.1002/cbin.11044
36. Rehwinkel J, Gack MU. RIG-I-Like Receptors: Their Regulation and Roles in RNA Sensing. *Nat Rev Immunol* (2020) 20(9):537–51. doi: 10.1038/s41577-020-0288-3

Conflict of Interest: The authors declare that the research was conducted in the absence of any commercial or financial relationships that could be construed as a potential conflict of interest.

Publisher's Note: All claims expressed in this article are solely those of the authors and do not necessarily represent those of their affiliated organizations, or those of the publisher, the editors and the reviewers. Any product that may be evaluated in this article, or claim that may be made by its manufacturer, is not guaranteed or endorsed by the publisher.

Advantages of publishing in Frontiers

OPEN ACCESS
Articles are free to read for greatest visibility and readership

FAST PUBLICATION
Around 90 days from submission to decision

HIGH QUALITY PEER-REVIEW
Rigorous, collaborative, and constructive peer-review

TRANSPARENT PEER-REVIEW
Editors and reviewers acknowledged by name on published articles

Frontiers
Avenue du Tribunal-Fédéral 34
1005 Lausanne | Switzerland

Visit us: www.frontiersin.org
Contact us: frontiersin.org/about/contact

REPRODUCIBILITY OF RESEARCH
Support open data and methods to enhance research reproducibility

DIGITAL PUBLISHING
Articles designed for optimal readership across devices

FOLLOW US
@frontiersin

IMPACT METRICS
Advanced article metrics track visibility across digital media

EXTENSIVE PROMOTION
Marketing and promotion of impactful research

LOOP RESEARCH NETWORK
Our network increases your article's readership